

AD-A222 517

NPS-61-90-004

NAVAL POSTGRADUATE SCHOOL
Monterey, California



APR 1990
CO

**VANDENBERG BOUNDARY LAYER SURVEY (VBLS)
FINAL REPORT - RESULTS**

by

C. E. Skupniewicz, R. F. Kamada, and L. McKay

April 1990

Final Report for Period
January 1988 - December 1988

Approved for public release; distribution unlimited

Prepared for: U.S. Air Force, Space Division
Los Angeles, California 90009

90 10 1990

NAVAL POSTGRADUATE SCHOOL
Monterey, California


Rear Admiral R. W. West
Superintendent

Provost H. Shull


The work reported herein was supported in part by U. S. Air
Force Space Division, Los Angeles, California.

Reproduction of all or part of this report is authorized.


Principal author for this report was


R. F. Kamada, Adjunct Research
Professor of Physics

Approved by:


R. Woehler, Chairman
Department of Physics

Released by:


G. E. Schacher, Dean of
Faculty and Graduate Studies

REPORT DOCUMENTATION PAGE

1a REPORT SECURITY CLASSIFICATION unclassified		1b RESTRICTIVE MARKINGS none	
2a SECURITY CLASSIFICATION AUTHORITY none		3 DISTRIBUTION AVAILABILITY OF REPORT approved for public release; distribution unlimited	
2b DECLASSIFICATION/DOWNGRADING SCHEDULE none			
4 PERFORMING ORGANIZATION REPORT NUMBER(S) NPS-61-90-004		5 MONITORING ORGANIZATION REPORT NUMBER(S)	
6a NAME OF PERFORMING ORGANIZATION Naval Postgraduate School	6b OFFICE SYMBOL (if applicable) PH	7a NAME OF MONITORING ORGANIZATION Aerospace Corporation	
6c ADDRESS (City, State, and ZIP Code) Monterey, CA. 93943-5000		7b ADDRESS (City, State, and ZIP Code) Los Angeles, CA. 90009	
8a NAME OF FUNDING SPONSORING ORGANIZATION USAF Space Division	8b OFFICE SYMBOL (if applicable) SD/CLFR	9 PROCUREMENT INSTRUMENT IDENTIFICATION NUMBER MIPR# FY76168800350	
8c ADDRESS (City, State, and ZIP Code) Los Angeles, CA. 90009		10 SOURCE OF FUNDING NUMBERS	
		PROGRAM ELEMENT NO	TASK NO
		PROJECT NO	WORK UNIT ACCESSION NO
11 TITLE (Include Security Classification) Vandenberg Boundary Layer Survey Final Report			
12 PERSONAL AUTHOR(S) C.E. Skupniewicz, R.F. Kamada, and L. McKay			
13a TYPE OF REPORT technical	13b TIME COVERED FROM 9-87 TO 1-89	14 DATE OF REPORT (Year, Month, Day) 90,05,01	15 PAGE COUNT 341
16 SUPPLEMENTARY NOTES			
17 COSAT CODES		18 SUBJECT TERMS (Continue on reverse if necessary and identify by block number)	
FIELD	GROUP	SUB-GROUP	
		atmosphere, boundary-layer, diffusion, complex terrain, SODAR, turbulence	
19 ABSTRACT (Continue on reverse if necessary and identify by block number) VBLS consisted of a set of three experiments at Vandenberg AFB, Calif. during 1988 to study characteristics of the atmospheric boundary layer over complex terrain during sea breeze conditions. This report consists of two sections. The section labelled as "Results" contains an analysis and interpretation of data. The "Appendix" section contains details of measurement techniques and a variety of charts and tables summarizing and supplementing the data set. Results indicate that characteristic surface roughness lengths range from .01 to .19 m, not accounting for large scale topography. The surface heat flux was not a strong function of location, and primarily depended on solar insolation as described by time and cloud cover. The base was divided into four regions based on topography, and probabilities of boundary layer depth was examined for its dependence upon terrain height and slope, boundary layer stability, and			
20 DISTRIBUTION STATEMENT OF ABSTRACT <input checked="" type="checkbox"/> UNCLASSIFIED UNLIMITED <input type="checkbox"/> LIMITS AS FOLLOWS <input type="checkbox"/> DTIC USERS		21 ABSTRACT SECURITY CLASSIFICATION unclassified	
22a NAME OF RESPONDER AND ADDRESS C.E. Skupniewicz		22b TELEPHONE (Include Area Code) (408) 646 2451	22c OFFICE SYMBOL PH

SECURITY CLASSIFICATION OF THIS PAGE(When Data Entered)

inversion strength. Terrain height was most important. Large variations in boundary layer characteristics near the stratus edge were also observed.

Accession For

NTIS GRA&I	<input checked="" type="checkbox"/>
DTIC TAB	<input type="checkbox"/>
Unannounced	<input type="checkbox"/>
Justification	

By _____

Date _____

Pages _____

A-1



DD Form 1473 (BACK)
S/N 0102-014-6601

SECURITY CLASSIFICATION OF THIS PAGE(When Data Entered)

TABLE OF CONTENTS

I. INTRODUCTION	page 2
II. DATA DESCRIPTION (GENERAL)	3
III. MEASUREMENT TECHNIQUE (GENERAL)	6
IV. BACKGROUND METEOROLOGY (SUMMARY)	10
V. RAWINSONDE COMPARISON	16
VI. DASS SHADOWGRAPH INTERPRETATIONS	24
VII. VBLS TRANSECTS - REGIONAL ANALYSIS	30
.1 SURFACE ROUGHNESS	31
.2 SURFACE HEAT FLUX	34
.3 WIND DIRECTION	38
.4 WIND SPEED	42
.5 VERTICAL WIND SHEAR	44
.6 BOUNDARY LAYER TURBULENCE	51
.7 BOUNDARY LAYER DRAG COEFFICIENT	54
VIII. VBLS TRANSECTS - STRATUS FRONT ANALYSIS	58
.1 INTRODUCTION	58
.2 STRATUS EFFECTS ON BOUNDARY LAYER HEIGHTS	59
.3 STRATUS EFFECTS ON VERTICAL WIND SHEAR	65
IX. PREDICTION OF BOUNDARY LAYER HEIGHTS	70
.1 INTRODUCTION	70
.2 DESCRIPTION OF METHODS	70
.3 CORRELATION ANALYSIS	76
.4 ABL HEIGHT CONTOURS	80
X. CONCLUSIONS	90
XI. BIBLIOGRAPHY	97
APPENDIX A. DATA DESCRIPTIONS AND MEASUREMENT TECHNIQUES (SPECIFICS)	99
APPENDIX B. BACKGROUND METEOROLOGY (CHARTS AND MAPS)	104
APPENDIX C. RAWINSONDE SUMMARY	301
APPENDIX D. TRANSECT SUMMARY	312
APPENDIX E. BASE AVERAGE WINDS	328
APPENDIX F. STRATUS EDGE BOUNDARIES	333
APPENDIX BIBLIOGRAPHY	339

I. INTRODUCTION

This report summarizes a series of field experiments performed at Vandenberg AFB, California (VBG) during 1988 by the Environmental Physics Group at the Naval Postgraduate School, Monterey, Calif. under contract to USAF Space Division, Los Angeles, Calif. MIPR# FY76168800350. The report is addressed to the VBG flow and diffusion modeling community, and therefore basic understanding of boundary layer turbulence principles is assumed.

The primary purpose of VBLS was to measure the atmospheric boundary layer at a wide variety of locations both on and off the base in order to parameterize boundary layer variability, and to provide a comprehensive data set for use in flow and/or diffusion model initialization or validation. The primary model parameters targeted for evaluation in this study are boundary layer height (Z_i), wind flow, turbulence, and shear. Quantities of special interest are surface heat and momentum fluxes. All of these quantities are critical elements of model prediction. Current operational models at VBG assume a constant Z_i derived from the most recent rawinsonde launch. They determine wind flow either from the nearest surface tower (OBDG) or from a single rawinsonde

measurement (REEDM). The soon to be installed MACHWIND uses rawinsonde and tower data to initialize its profiles. All models use diffusion estimates based on 1) 12 ft wind speed, 2) 12 ft horizontal turbulence intensity, and 3) 6-54 ft temperature differences obtained from the tower nearest the release site. We will offer suggestions for 1) improved Z_i prediction, and 2) realistic boundary layer averaged speed and turbulence estimates.

Other topics of interest at VBG may be partially addressed from these data and analysis. These issues include marine stratus characteristics and low level wind shear which can affect flight operations or missile launches.

II. DATA DESCRIPTION (GENERAL)

The data consists of a) doppler acoustic SODAR (DASS) measurements from a trailer mounted system which give boundary layer heights, winds, and turbulence, along with corresponding surface layer measurements of mean wind, temperature, humidity, pressure, stress, and heat flux, b) DASS measurements from the three permanent VBG facilities, c) quality controlled tower measurements from the VBG Winds System, d) hourly averaged wind and temperatures from over thirty off-base sites ranging from Santa Barbara to Santa Maria, e) rawinsonde data from VBG and the NPS portable rawinsonde system, f) synoptic weather charts, and g) stratus

edge boundaries derived from satellite photos. A schematic of the NPS mobile laboratory is shown in fig. 1. A complete description of the equipment and measurement techniques is supplied in Appendix A.

VBLS was conducted in three phases; May 18-20, July 26-29, and October 18-21. All three phases were conducted under sea breeze conditions during daylight hours. The following generalizations may be made about the experiments.

- * Phase I was dominated by clear sky conditions, but the sea breeze was obviously influenced by a cold front passage on early May 17 and later synoptic changes.
- * Phase II was strongly influenced by the stratus front which advanced and receded each day.
- * Phase III was a relatively quiescent time period, with light winds and progressively thickening stratus. Oct 20 was the most quiet, and stratus remained to inland distances of at least 10 miles for the entire day.

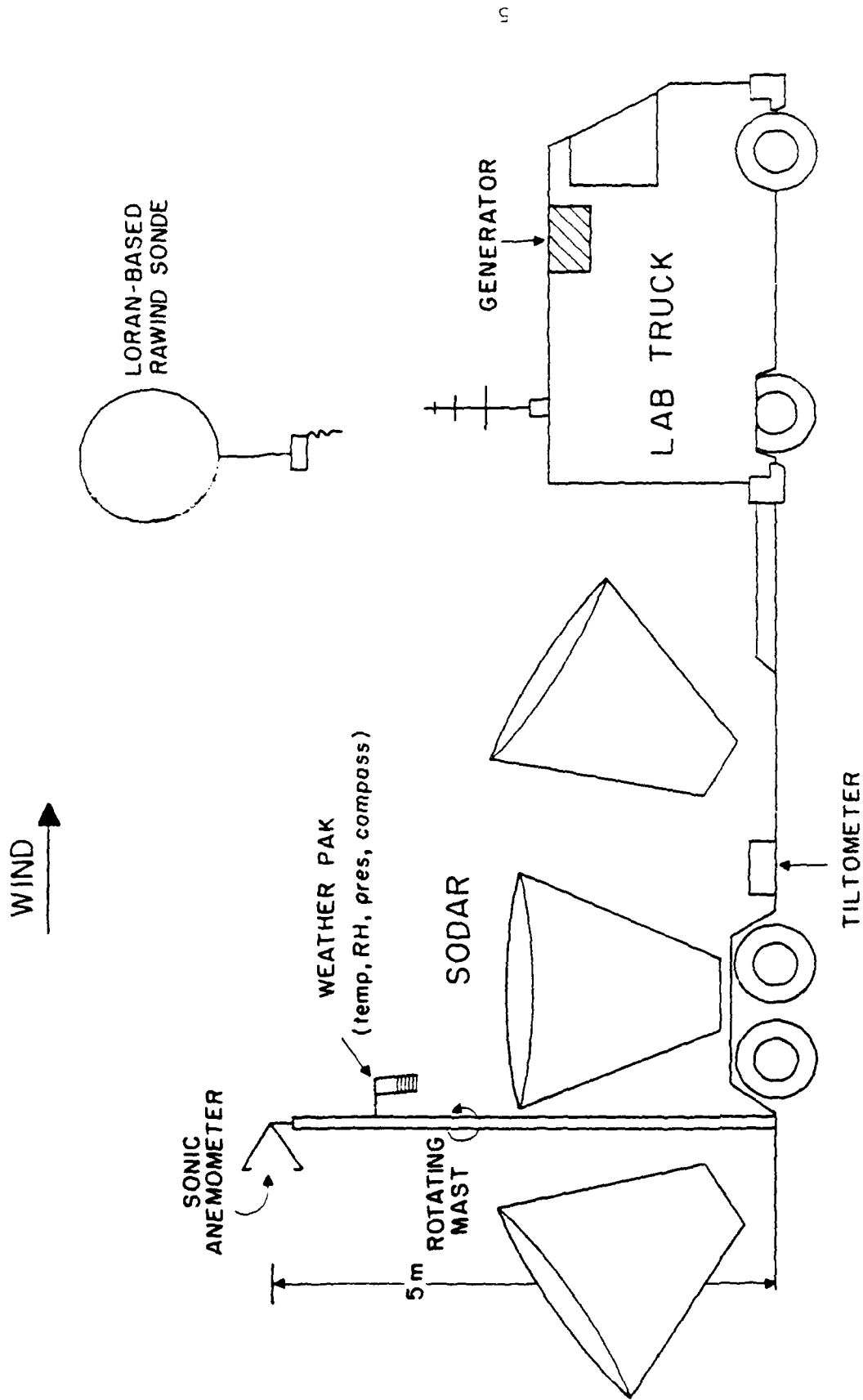


Fig. 1 Schematic of NPS mobile boundary layer laboratory.

III. MEASUREMENT TECHNIQUE (GENERAL)

The fundamental strategy for VBLS was to survey a "representative" set of locations on the base and the surrounding area from Jalama Beach (south) to the Los Alamos Valley (north) to Mail Rd. (15 km east of Lompoc). Two major constraints limited the implementation of the approach. First, navigable roads were required. Some of the most interesting and important areas of the base were simply inaccessible. Second, the need to sample many locations made each sample shorter than optimal for statistical confidence. We address this issue later in the report.

The survey consisted of a series of transects, i.e., a group of short samples measured at locations which were roughly equally spaced along an appropriate road through a section of the domain. When possible, the transects were designed to follow the mean wind direction in order to spatially integrate the results over the area type. Each sample was typically 10-15 min. in length, and the spacing between locations was typically 2-4 km. The total time of a transect ranged from 1-4 hrs. Over the 3 phases of VBLS, 200 measurements were made at 98 different locations. Fig. 2 shows these locations, the permanent towers, the DASS sites, and the rawinsonde locations used in VBLS. Fig. 3 displays the transects performed on each day of the experiment. Due to time and distance constraints, each day's sampling was

VBLS DATA SITES

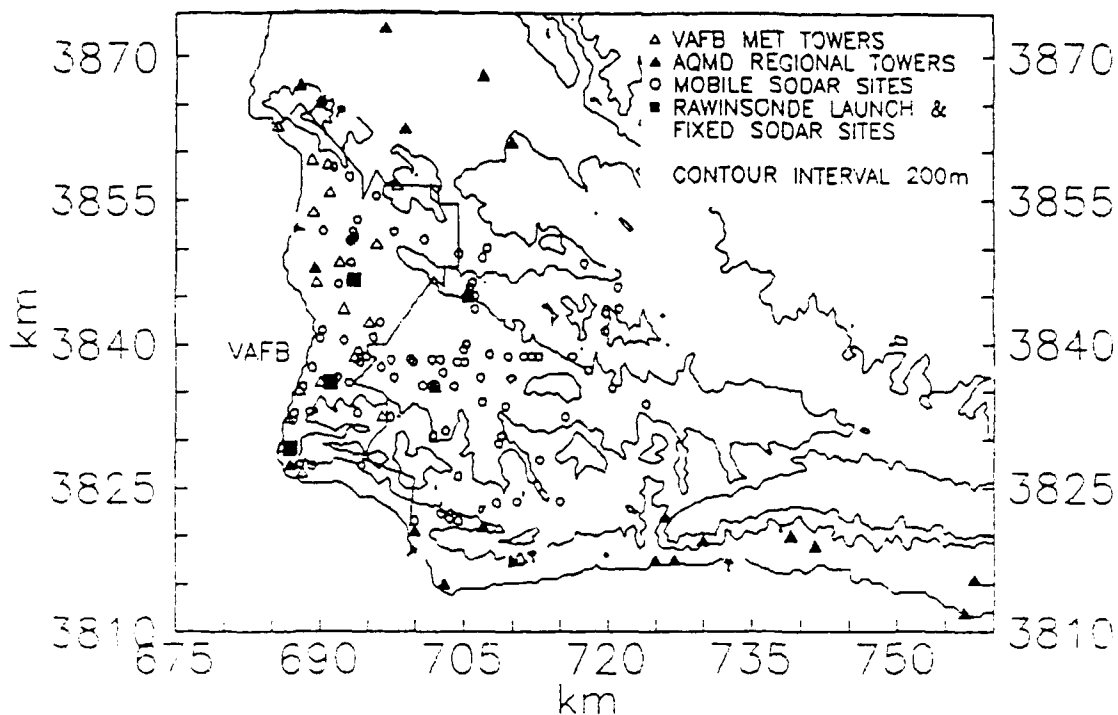


Fig. 2 Composite of all measurement locations sampled during VBLS. Coordinates are in UTMS. An approximate conversion to spherical coordinates is $\text{latitude} = .0903 \times \text{longitude} = 128 - ((Y + 30) / 97.2)$. Only VBG towers with 12 ft level winds are shown. Only Santa Barbara Air Quality Control District (AQCD) towers used for this analysis are shown.

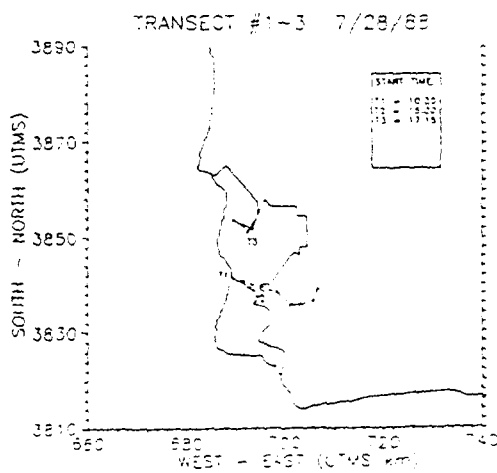
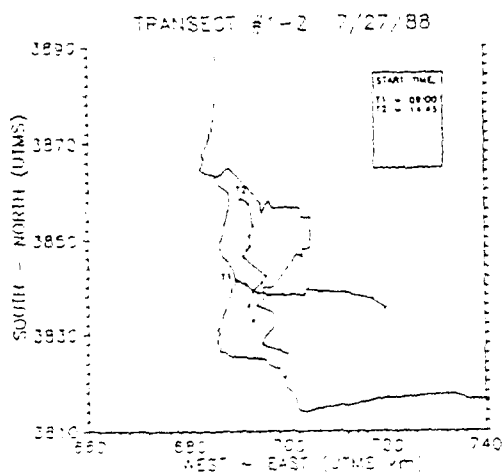
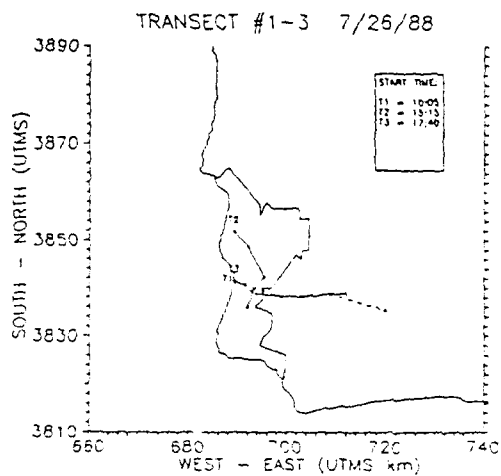
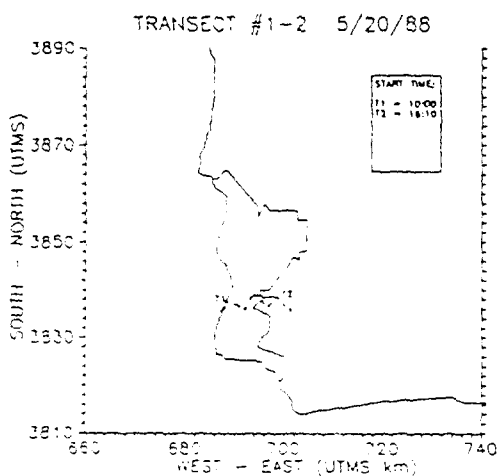
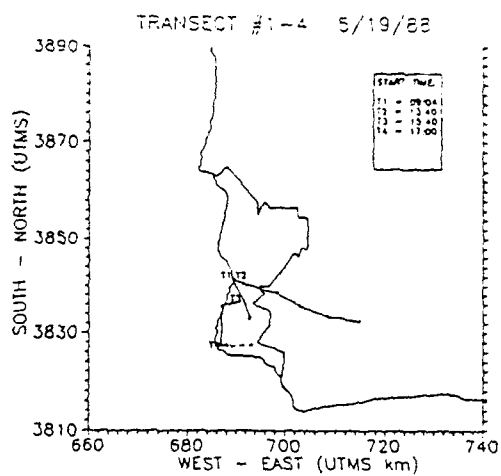
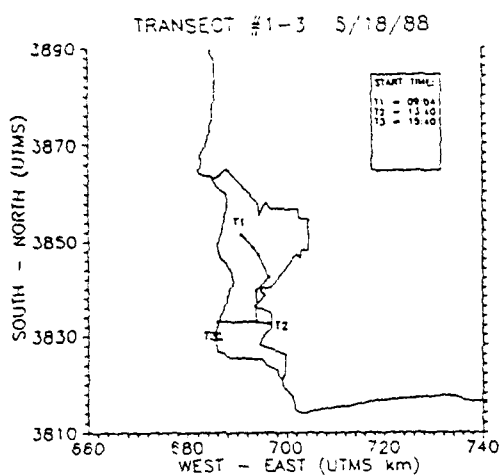
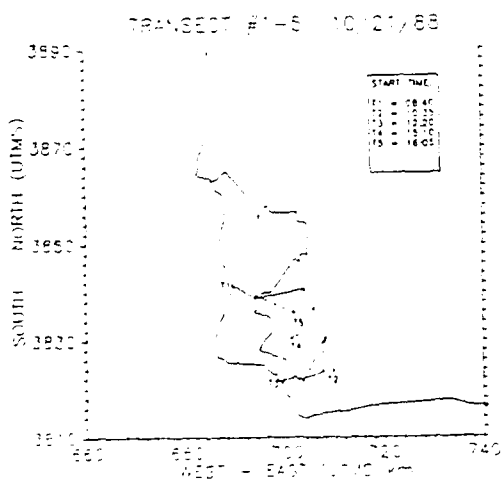
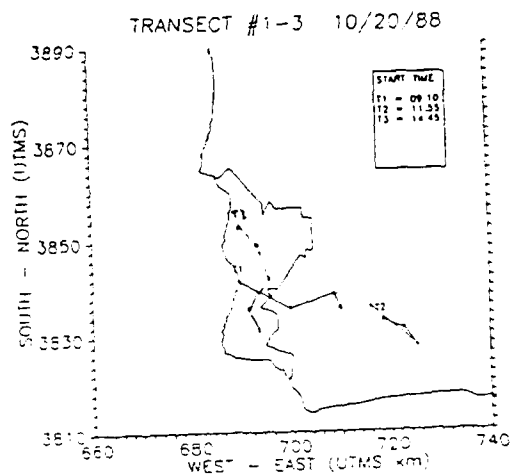
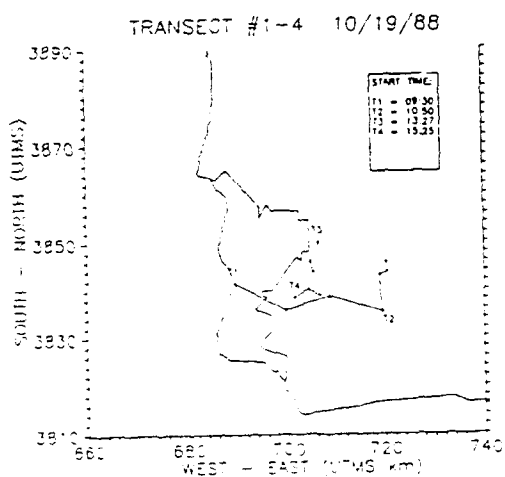
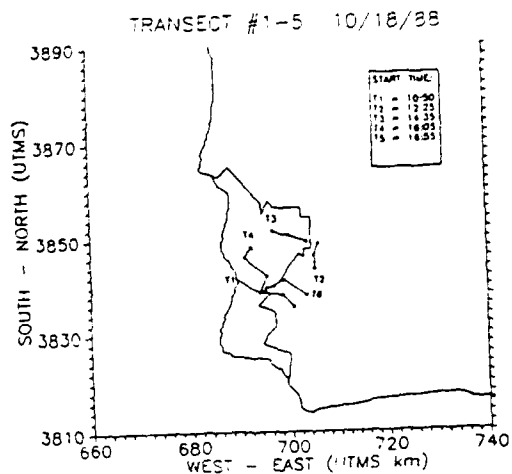
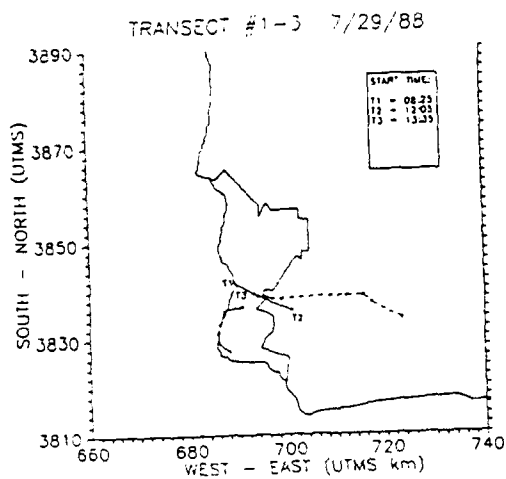


Fig. 3 Daily transect routes for VBLs. Times are in PDT. Some solitary sample locations may not be shown.



restricted to only a portion of the total domain of interest. The Lompoc Valley was sampled most often because of its special importance to the community of Lompoc. Other areas, such as Jalama Rd., were sampled much less frequently.

IV. BACKGROUND METEOROLOGY (SUMMARY)

Before discussing survey results, we first examine standard weather information products available to the weather detachment at VBG. In the following we discuss a range of scales and make some rather qualitative statements related to the observations. Appendix B supplies all the charts and maps from which these generalities are inferred, along with a detailed day by day discussion of these data.

We chose the standard 500 mb chart to gauge the synoptic scale forcing. The spring experiment took place under a moderate but weakening northwest pressure gradient following the passage of a trough, the fall measurements took place under a moderate and constant northeast gradient at the leading edge of a ridge, and the summer experiment had weak flows from a veering gradient which rotated through 360 degrees in 4 days. The size of the overall sea breeze "cell" varies seasonally in both horizontal and vertical dimensions. Therefore, the 500 mb level may be above the cell during the spring or fall, but within the cell during the summer. Fig. 4

shows 12Z rawinsonde winds for May. After the uniformly strong winds following the trough passage, the sea breeze return flow is apparent to about 5000 m. The wind profile through the return flow region is highly variable between observations. During July, this confused region extended to well above 7000 m, which explains the variable flow at 500 mb.

The surface pressure fields clearly showed the trough passage described above during phase I. The first day was under the influence of a weakening synoptic low pressure system, as evidenced by an unusually N-S pressure gradient, but the midday temperature contours paralleled the coast as in a sea breeze circulation. The resulting flow at VBG had characteristics of both a sea breeze and a passing cold front. The rest of the experiment had no significant synoptic weather system influence observable at the surface.

Although the patterns of pressure, wind, and temperature were similar in all the remaining days, there was a significant seasonal dependence on the coastal pressure gradient. Namely, the spring and fall pressure gradients were much weaker than the summer gradients. This resulted in higher sea breeze related wind speeds at many stations during the summer, especially at inland locations. (This was not true for VBG, however.) The midday temperature gradients on a regional scale were quite similar for all days. We are therefore reminded that although these temperature contrasts

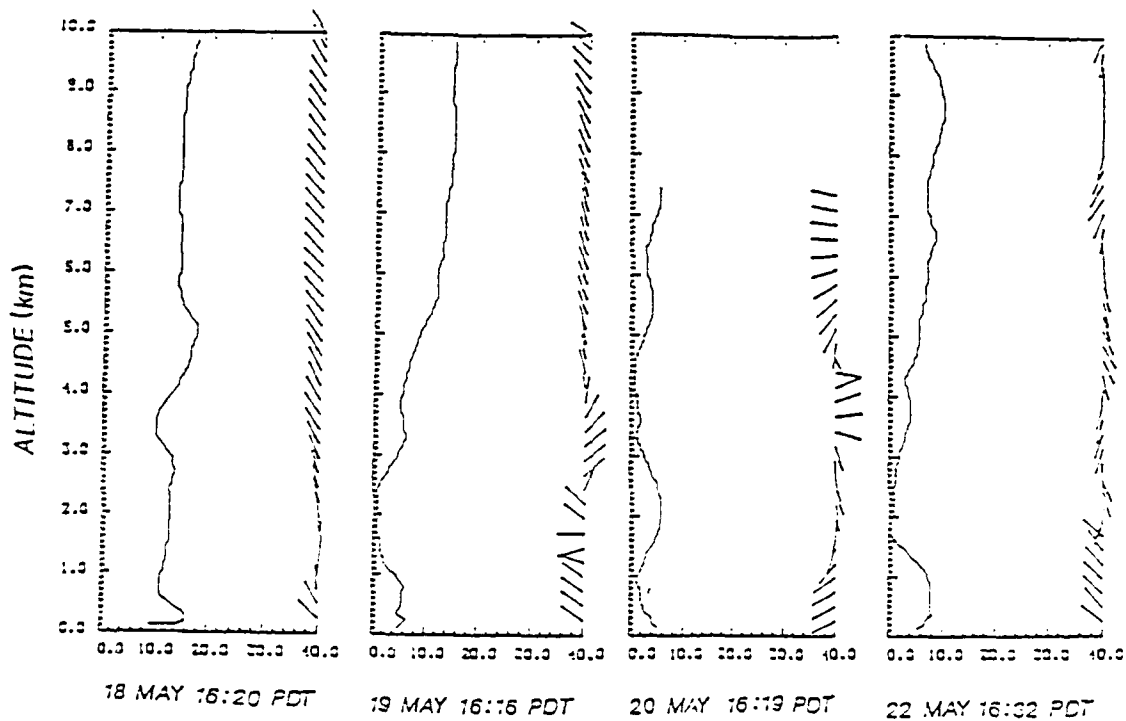


Fig. 4 Rawinsonde derived wind profiles at 12Z measured during Phase I of VBLS. Wind speeds are in m/s.

drive the sea breeze, pressure gradients result from mass adjustments on a regional/synoptic scale. Since the days are significantly shorter and nights cooler in the fall, a regional/synoptic (monsoonal) scale pressure gradient was not allowed to develop for those cases. The reasons are less clear in the spring, since the days of May were comparable in length to the July days.

A major stratus deck was a daily visitor to VBG during the July and October experiments. Discussion of some effects of the stratus on wind and boundary layer heights are presented in section VIII. A summary of the stratus edge position during VBLS is given in Appendix E.

The regional wind flow was obtained from hourly averages of 12 ft winds at towers maintained by the Santa Barbara Air Quality Management District. These were scattered over an area from Santa Maria to Santa Barbara. The "typical" regional wind field is described in more detail in Appendix B, but the general features are outlined here. One major feature is that winds normal to the coast occur near midday and veer with time. The midday winds are therefore from the west to northwest for coastal areas north of Pt. Concepcion and south to southwest in the Santa Barbara Channel. Another repeated observation is anomalous strong northerly winds at Pt. Arguello. This was verified by a second tower (as opposed to Tower 301, described in Kamada et al. 1989), and shown to

often persist through the night. A third major feature is a wind reversal from on to offshore along the Santa Barbara Channel coast near dusk. The start of the sea breeze usually brings coast perpendicular southerlies during midday, but offshore northerly winds are at least as common as variable winds at 1900 LDT.

Kamada et al. (1989) classified the surface flow field at VBG into 10 categories. Based on 12 ft hourly averages of the base tower network, most flows observed during VBLS could be classified in this manner. In general, two rather rapid transitions in flow direction could be defined for each day, with somewhat stationary flow in between.

The passage of the sea breeze front is the obvious first transition. This is not usually apparent in the widely spaced hourly average flow fields presented in Appendix B. Those maps that did happen to catch the event usually showed coast-perpendicular winds, and a convergence zone in some instances. Adjustment to the midday flow pattern occurred rather rapidly, however. The midday pattern was generally characterized by a uniform flow direction at most towers ranging from 240 to 320, depending upon the day, with the following characteristics; a) backed (west) winds in the valleys, b) veered (north) directions at the high points, and c) veered, stronger winds at Pt. Arguello. When the mean direction is less than 270, item c) changes to d) backed winds at Pt. Arguello. Wind

speeds, on the other hand, changed constantly throughout the day, as one would expect in a sea breeze system. In the Kamada et al. (1989) scheme, the midday flow pattern described above could be classified as Moderate Southwesterly, Weak Westerly, or Summer Northwesterly, depending upon the particular day.

The second transition occurs near dusk, and is marked by a sudden veering from the midday pattern to the "evening pattern" (see Appendix B), and is clearly visible in the data. This transition is not associated with a sudden speed change as is common with the sea breeze front. The reason for this transition is not as well understood as the sea breeze front, but is probably due to Coriolis turning combined with a decoupling of boundary layer from surface flow due to the neutral stratification (see Mizzi and Pielke 1984). The evening pattern ranged widely during VBLS. Evening Northerlies were the rule during July, while spring and fall periods showed mixtures of Stagnation and Nocturnal Easterly Drainage. Early morning flow was seasonally dependent in that the "evening pattern" persisted through the night during the summer experiment, with some minor exceptions. For the spring and fall experiments, early morning winds varied widely and could not be considered stationary on most days.

V. RAWINSONDE COMPARISON

Since the standard ascents at VBG are at 0 and 12Z, we wish to know how representative these data are for other times. Thus, for winds, we simply interpolated between the two ascents at hourly intervals and compared with actual values observed. The method used was to linearly interpolate the u and v components for each hour, then reform the vector. Table 1 shows the results for winds above and below the inversion for several time series. Level 6 (above the inversion) is shown for all 3 phases. Because of missing data within the boundary layer during 0 or 12Z ascents, only a few time series could be examined below the inversion. Those were at level 1 (50-100m) during phase I, and level 3 (200-400m) during phase II.

As expected, interpolation of low level winds (50-100 m, May) from two soundings a day produced bad results. Undoubtedly, diurnal variability as well as spatial separation in the launch locations contribute to the disagreement.

The 200-400m layer interpolations also fail for a majority of the days. Though spatial separation is less important than for the lower layer because the boundary layer becomes more homogeneous with height, the diurnal variability is not reduced, and the presence of the inversion somewhere

INTERPOLATED RAWINDSONDE TIME SERIES

- * hourly values are interpolated between "stars"
- * intermediate observations are in paranthesis

SPEED (50-100M) [m/s]

5-18-88 12Z>				14.9	14.8	14.8	14.8	14.8	14.9	14.9	15.0
				*					(8.6)		
15.2	15.3	15.5	15.7	15.9	15.2	14.5	13.8	13.1	12.4	11.7	11.1
(14.2)				*			miss				
10.5	9.8	9.2	8.7	8.2	7.9	7.6	7.3	7.0	6.8	6.5	6.3
				*					(1.8)		
6.1	5.9	5.8	5.7	5.6	5.2	4.7	4.2	3.8	3.3	3.0	2.6
				*		(2.7)					
2.4	2.2	2.2	2.4	2.6	2.3	2.0	1.8	1.8	1.8	2.0	2.2
				*					(1.4)		
2.6	2.9	3.3	3.7	4.1	<5-21-88 0Z						
				*							

DIRECTION (50-100M) [deg]

5-18-88 12Z>				347	344	342	339	337	334	332	330
				*					(342)		
327	325	322	320	318	319	320	322	323	325	327	329
(347)				*			miss				
332	335	338	341	345	343	340	338	335	332	328	325
				*					(43)		
321	317	313	308	304	306	309	313	317	323	330	339
				*		(352)					
350	3	17	30	41	33	22	9	355	340	327	317
				*					(63)		
308	302	297	293	290	<5-21-88 0Z						
				*							

SPEED (BL-2000M)

5-18-88 12Z>				15.5	15.2	14.8	14.5	14.2	13.9	13.6	13.3
				*					(14.3)		
13.1	12.8	12.5	12.3	12.1	11.6	11.1	10.7	10.4	10.1	9.8	9.6
(13.3)				*			(14.6)				
9.5	9.4	9.4	9.5	9.6	8.7	7.9	7.0	6.2	5.4	4.6	3.9
				*					(4.3)		
3.3	2.8	2.6	2.6	3.0	2.6	2.3	2.0	1.7	1.4	1.2	1.0
				*		(3.9)					
1.0	1.1	1.2	1.5	1.7	1.4	1.1	0.9	0.8	0.8	1.0	1.3
				*					(0.6)		
1.6	2.0	2.3	2.7	3.0	<5-21-88 0Z						
				*							

DIRECTION (BL-2000M)

		5-18-88	12Z>	13	12	10	9	8	7	5	4
				*					(15)		
2	1	359	357	356	359	2	6	9	13	18	22
	(4)			*			(360)				
27	31	36	41	45	44	42	39	36	32	27	20
				*					(123)		
10	355	336	317	300	302	305	310	316	324	336	352
				*		(302)					
12	31	47	58	65	72	83	99	124	151	171	183
				*					(121)		
191	196	200	203	205	<5-21-88 0Z						
				*							

SPEED (200-400M)

		7-26-12Z>	4.2	4.0	3.9	3.8	3.7	3.6	3.5	3.5
			*				miss			(0.7)
3.4	3.4	3.4	3.4	3.4	3.2	3.0	2.9	2.7	2.5	2.2
		(3.7)		*			(3.0)			(3.1)
2.0	1.9	1.7	1.5	1.4	1.4	1.4	1.5	1.6	1.7	1.9
				*				(1.4)		(1.8)
2.1	2.2	2.4	2.6	2.7	2.5	2.3	2.1	1.9	1.8	1.6
				*			(1.8)			(3.4)
1.5	1.4	1.4	1.5	1.5	<7-28-88 12Z					
				*						

DIRECTION (200-400M)

		7-26-88	12Z>	344	341	338	334	331	327	324	320
				*				miss			(301)
315	311	307	303	300	301	301	302	303	304	306	307
		(300)		*			(297)				(338)
309	311	313	316	316	307	299	291	283	276	270	266
				*				(8)			(302)
261	258	254	252	250	253	257	261	266	270	279	287
				*			(25)				(358)
296	305	315	325	332	<7-28-88 12Z						
				*							

SPEED (BL-2000M)

				7-26-88 12Z>	4.5	4.3	4.2	4.0	3.8	3.7	3.5	3.4
					*				miss			(4.9)
3.2	3.1	2.9	2.8	2.7	2.7	2.8	2.9	2.9	3.0	3.1	3.2	
		(2.5)		*			(4.6)					(6.4)
3.3	3.4	3.4	3.5	3.5	3.4	3.3	3.3	3.4	3.6	3.8	4.1	
				*				(1.2)				(2.2)
4.4	4.7	5.1	5.5	5.8	5.6	5.4	5.2	5.0	4.9	4.7	4.6	
				*			(7.0)					(7.8)
4.5	4.5	4.4	4.4	4.5	<7-28-88 12Z							
				*								

DIRECTION (BL-2000M)

				7-26-88 12Z>	41	41	40	39	39	38	37	36
					*							(27)
35	34	33	32	31	33	35	37	39	41	42	44	
		(31)		*			(349)					(4)
45	47	48	49	48	40	32	23	14	6	359	353	
				*				(34)				(3)
347	343	339	335	333	336	339	342	346	349	353	357	
				*			(339)					(356)
1	5	10	14	18	<7-28-88 12Z							
				*								

SPEED (BL-2000M)

				10-18-88 12Z>	3.6	3.4	3.1	2.9	2.7	2.5	2.3	2.1
					*							
1.9	1.7	1.5	1.4	1.3	1.3	1.4	1.6	1.9	2.2	2.6	2.9	
		(1.2)		*								
3.3	3.6	4.0	4.4	4.7	4.9	5.2	5.4	5.7	6.0	6.4	6.7	
				*					(6.5)			
7.0	7.4	7.7	8.1	8.5	8.1	7.5	6.9	6.4	5.8	5.3	4.8	
			(8.1)	*	(8.1)							
4.3	3.9	3.5	3.2	3.1	3.1	3.2	3.4	3.7	4.1	4.6	5.1	
				miss					(2.2)			
5.6	6.2	6.7	7.3	7.9	8.4	7.9	7.5	7.1	6.7	6.3	5.9	
	(4.7)			*								
5.5	5.1	4.7	4.2	3.8	3.3	2.9	2.5	2.1	1.9	1.7	1.6	
				*				(3.6)				
1.7	1.9	2.2	2.5	2.9	<10-21-88 12Z							
	(2.3)			*								

DIRECTION (BL-2000M)

			10-18-88 12Z>	9	11	12	14	16	19	22	26
				*							
30	36	42	50	60	46	30	17	8	1	356	352
		(90)		*							
349	346	344	343	342	346	349	353	356	359	1	3
				*					(2)		
5	7	9	10	12	12	13	15	18	21	25	29
			(20)	*	(12)						
35	42	50	60	71	83	95	106	114	122	128	133
				miss					(123)		
136	140	142	145	147	148	148	148	148	148	149	149
	(133)			*							
149	150	150	150	151	148	143	137	128	117	103	86
				*				(112)			
69	55	44	36	30	<10-21-88 12Z						
	(46)			*							

within this altitude zone can radically change the mean wind vector.

Winds above the boundary layer, on the other hand, are more closely matched both for speed and direction. This is particularly interesting, since the 0 and 12 Z launches were often alternated between the north and south base facilities, and the intermediate rawinsondes were made from widely varying locations around the base. Even though there was considerable variability between the 0 and 12 Z values (especially for the Phase I and III time series), our interpolations do a fairly good job of prediction. This implies that any intrinsic time scale for the variability must be significantly larger than 24 hours. But the presence of the variability mandates rawinsonde observations at shorter intervals when forecasts of releases in the above boundary layer zone are required.

Boundary layer heights were specified by the base of the first inversion as estimated from the potential temperature and humidity profiles. Fig. 5 shows two examples of the inversion layer base and top, and fig. 6 plots these values for VBLS. The observations are widely scattered, in part due to the variable launch locations.

The following generalizations can be made. The May ascents showed the lowest heights on average (inversion bases near 100 m), followed by the July data (300-400 m), and then

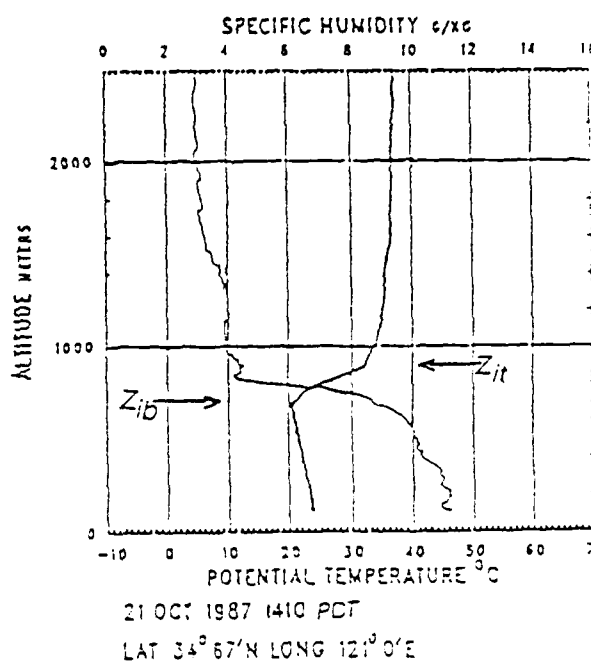
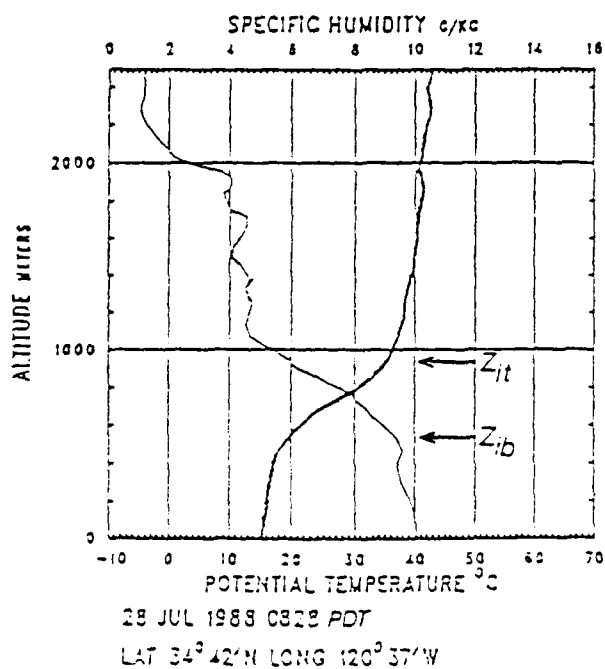


Fig. 5 Two examples of rawinsonde thermodynamic boundary layer profiles and the definition of the inversion layer bottom, Z_{ib} , and top, Z_{it} , for these cases. Heavy solid line is potential temperature. Light solid line is specific humidity.

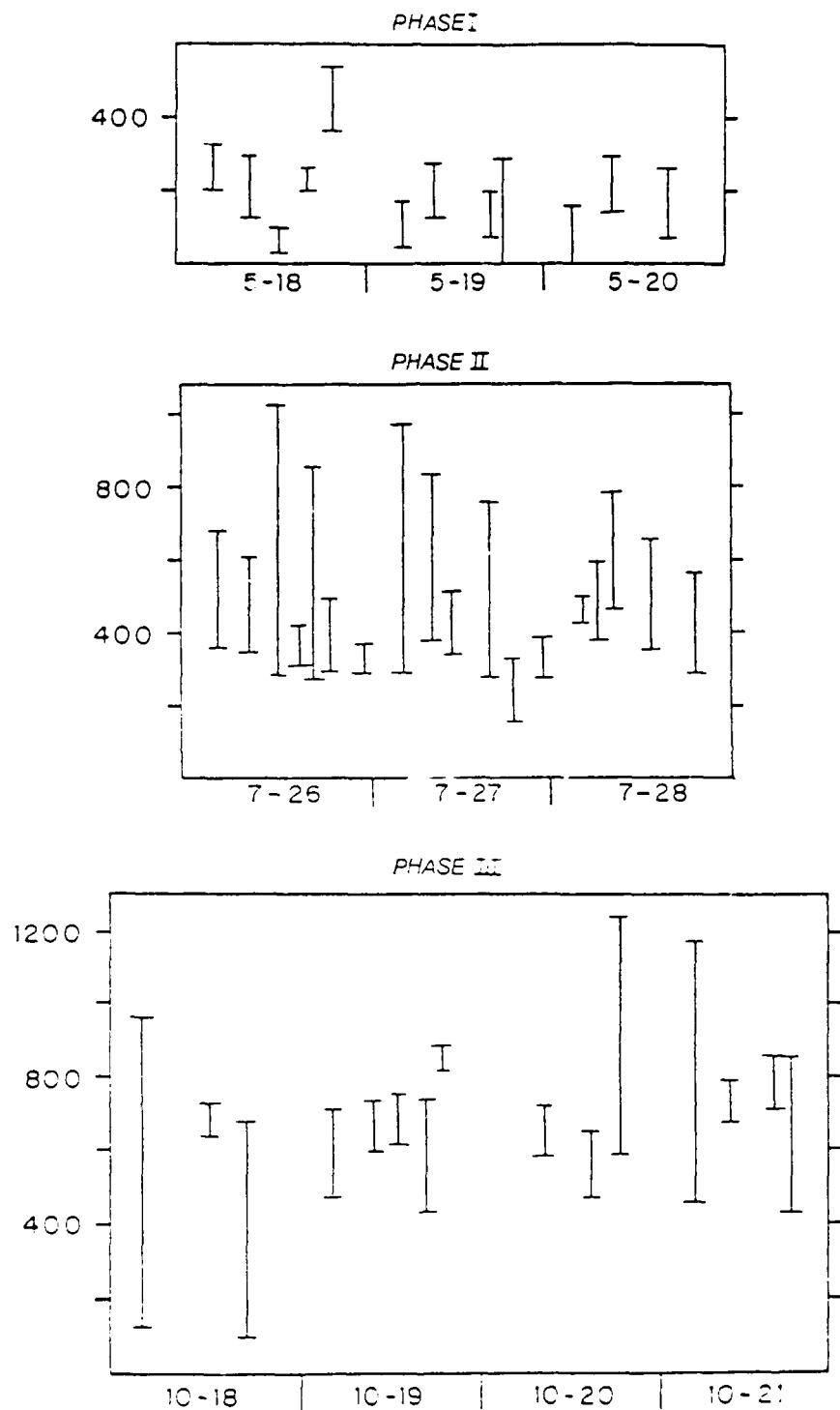


Fig. 6 Inversion layer heights determined from rawinsonde derived thermodynamic profiles. Vertical lines range from Zib to Zit. See Appendix C for numerical values and launch locations.

the October sondes (400-600 m). While some of the low May inversions were due to early morning surface based cooling, others were associated with a very low surface fog in stable onshore flow. For these fog cases, a uniform wind profile often extended to much higher altitudes, which suggests that the actual mixing layer (as would be used in a diffusion model) was higher than the thermodynamic profile would suggest. The top of the inversion layer was often much higher than the bottom, which suggests that the idealized thin "capping inversion" may often not be present in complex terrain.

VI. DASS SHADOWGRAPH INTERPRETATIONS

All the DASSes used during VBLS were monostatic triaxial systems. All DASS of this type measure sound energy scattered from temperature variations having scales close to the wavelength of the sound. The frequency used for all DASSes was 1600 Hz, which makes the relevant wavelength roughly 1/3 meter. In a turbulent atmosphere, the magnitude of temperature fluctuations correlates with the length scale of the fluctuation for a fairly broad range of scales, and the DASSes characteristic length scale resides within this range. A single parameter describes the strength of these fluctuations; the temperature structure function, C_T^2 . To a large degree, the strength of the DASS echo depends directly on C_T^2 for a turbulent atmosphere.

Temperature variation can also result from temperature stratification in non-turbulent conditions. In this case the echo strength depends on stability, such as measured by the gradient Richardson number.

Common sources of C_T^2 in the boundary layer are free convection (thermal plumes), forced convection (wind driven heat transfer at the surface), and turbulent mixing within an inversion. Large Richardson numbers occur within the inversion at the boundary layer top and within surface based inversions.

Proper interpretation of DASS data requires knowledge of the echo source. A few examples are shown in fig. 7. The first example shows a convective boundary layer under clear skies. Echoes are strong through the whole depth of the boundary layer, especially near the bottom and top where additional C_T^2 is produced by forced convection and turbulence near the inversion. The shadowgraph is characteristically "blotchy" due to the passage of large scale thermals. While the strong power returns allow good wind calculations through the whole depth of the boundary layer, the vectors often vary widely between 10 min records due to these thermals. Since the VBG DASS are all situated within a few km of the coast, such conditions will exist for onshore flow only at low wind speeds, or in Santa Ana (offshore)

SAMPLE VBG DASS SHADOWGRAPHS

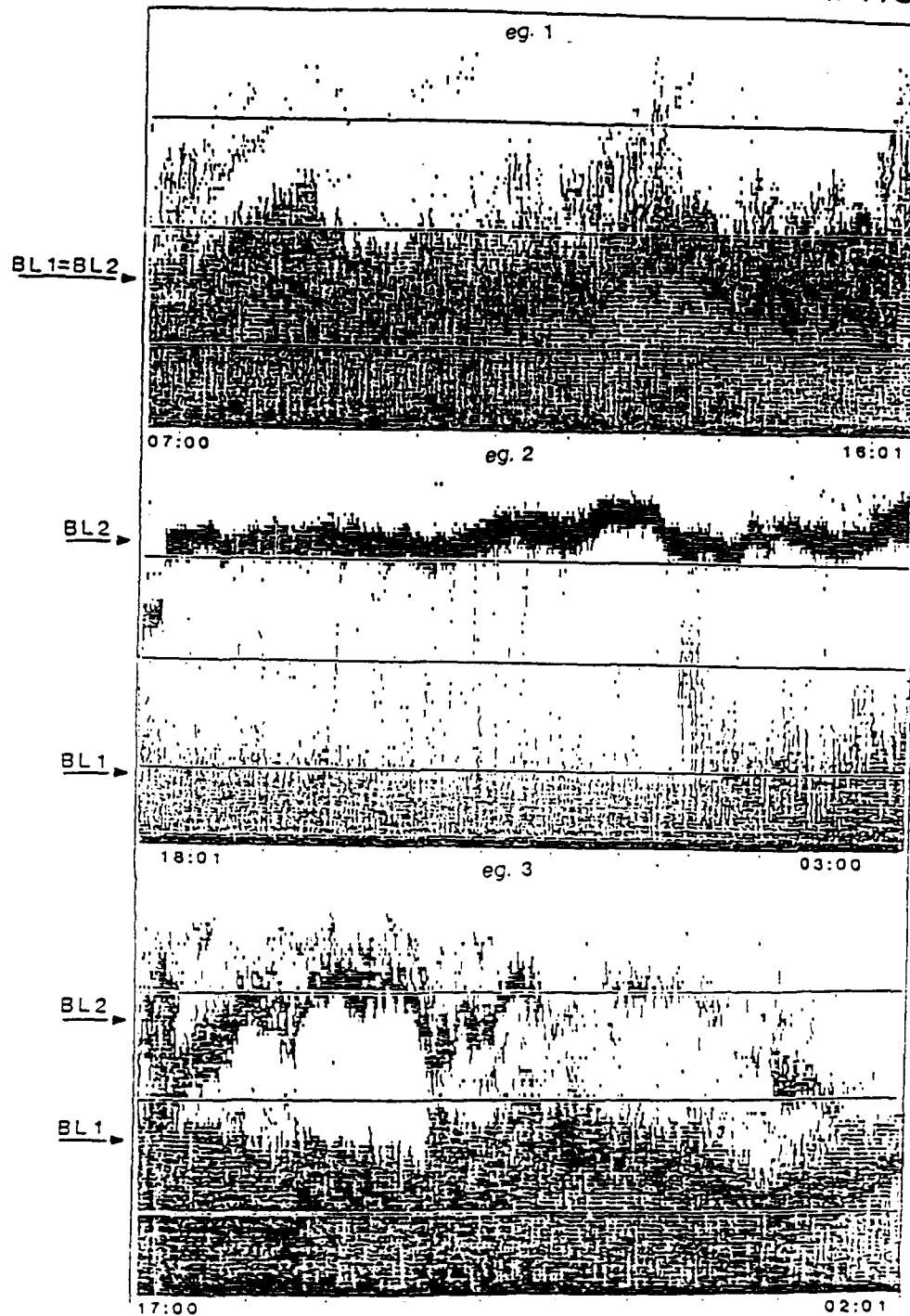


Fig. 7 Examples of DASS shadowgraphs from SLC6 SODAR and definition of BL1 and BL2 for these cases. Times are in PDT. Echo intensities have been corrected for spherical divergence.

conditions. Thus wind records will seem unreliable for such an onshore case, even though they reach relatively high altitudes. For these cases several 10 min records should be averaged to account for the passage of slow moving thermals.

Example 2 shows a stratus covered boundary layer. While echoes are strong at the inversion and very near the ground, most of the boundary layer is "quiet" in terms of temperature fluctuations. Stratus insulates the surface from either significant radiative heat loss or gain, and any C_T^2 near the surface results from forced convection due to wind blowing over a surface with only a slightly different temperature than the air. The near surface winds will be fairly consistent from record to record. The quiet region may have quite strong and turbulent winds, but because this region is also very uniform in temperature, winds may not be measurable. Winds from returns near the inversion may be measurable, but they may not be indicative of the general boundary layer flow due to large shears often present at this interface.

The third example shows a thermal mechanical internal boundary layer (TMIBL) under the "main" boundary layer inversion during clear skies and moderate to strong winds. The shadowgraph resembles the free convection case from the surface up to the top of the TMIBL, and the stratus case above the TMIBL. At VBG, TMIBLs result when cool marine air is advected over the sun-heated ground. Both free and forced

convection results and the height of the activity increases as the air moves inland, eventually reaching the top of the main boundary layer. The inland distance at which this equilibrium is reached depends on the surface heat flux and mechanical energy, integrated over the travel time of the air mass. Because the base DASSes are located near the ocean, this travel time is not long enough for equilibrium to be reached, except during very light winds. Winds within the TMIBL are easily computed by the DASS because of high C_T^2 , and are more consistent between records than the free convection case, due to smaller thermals and deeper forced convection near the surface.

The main problem for this case is identifying the true mixing depth for input to diffusion models. While the air above the TMIBL and below the "main" boundary layer top is less turbulent than within the TMIBL, the top of the TMIBL does not act as a lid to diffusion, and therefore the main boundary layer top should be specified as the mixing depth. Unfortunately, due to strong winds, the lack of stratus and added mixing at the inversion often reduces the strength of the echoes within the inversion. Thus, care must be taken to examine sufficiently long shadowgraph and wind records to define this height to not confuse a TMIBL top with a free convective boundary layer top. In general, a convective boundary layer develops rapidly in light winds after stratus burn off or when morning thermals first develop in clear

skies. However, its height will change slowly thereafter. TMIBLs are apparent under clear skies with stronger winds, and the height often changes dramatically with changes in wind speed or direction. A TMIBL may remain for a time after stratus has advected inland in the afternoon, due to residual surface heat.

Two boundary layer heights were defined based upon the average backscatter power profiles. Again, refer to the shadowgraphs of fig. 7 for the following discussion. We define a "boundary layer depth #1" (BL1) as the first level at which the backscattered power dropped to less than roughly 10% of its maximum near-surface value. The backscatter profile below this height could be quite complex, with several "ridges and valleys", so long as it was strong enough and continuous from the surface. We interpret "boundary layer depth #2" (BL2) as an inversion defined by the height of the largest and strongest echo layer above BL1. This is the height normally selected from shadowgraphs for boundary layer applications. If no elevated inversion was observed, then BL2=BL1.

Under stratus (e.g. 2), conditions are near-neutral and C_T^2 depends strongly on surface layer stability (z/L). Therefore, BL1 should be qualitatively related to z/L . BL2 most likely represents the sharp cloud top temperature gradient as shown by Neff (1988) for similar circumstances.

In sunny conditions, either very near the coast or cloud edge, BL1 can be thought of as the height of the TMIBL as in fig. 7, e.g. 3. In some convective clear sky cases, an elevated echo layer was often observed just above BL1. This layer may indicate the short term average range of the thin, sharp inversion interface which penetrates into the stratified air above. In this case, the height range BL2-BL1 may indicate the entrainment zone, and BL1 would be considered the appropriate mixing depth for diffusion models.

VII. VBLS TRANSECTS - REGIONAL ANALYSIS

One fundamental strategy for VBLS was to group areas of the base and surrounding countryside by topography. Based on this factor and data availability, we divided the VBG area into 4 regions defined as

<u>REGION</u>	<u>BOUNDARIES</u>	<u>TERRAIN</u>
North Base	Los Alamos Valley (N)	flat to rolling
(NB)	Base boundary (E)	elevated mesa
	Lompoc Valley (S)	with groups of trees
	Ocean (W)	and buildings

Lompoc	valley "walls" (N/S)	flat, gently sloping
Valley	City of Lompoc (E)	flood plain with low
(LV)	Ocean (W)	cut agricultural fields
South	Lompoc Valley (N)	mountains (0-600 m),
Base	Base boundary (E)	long grass vegetation
(SB)	Ocean (S/W)	
East	Los Alamos Valley (N)	mountains (0-600 m),
Hills	Mail Rd. (E)	trees and long grass
(EH)	Base Boundary (W)	vegetation
	Jalama Rd. (S)	

All of these regions, except the Lompoc Valley, encompass varying terrain. Hence, we do not contend that they are in any sense homogeneous. Still, by sampling a wide variety of locations within each region we can place bounds on some important quantities.

VII.1 SURFACE ROUGHNESS

For each transect through a region, we averaged vertical momentum flux, u_*^2 , and the total (latent and sensible) heat flux, H , as derived from direct covariance calculations using the sonic anemometer over all locations visited during that transect. Each value was weighted by its respective sampling

time. These spatially averaged values were then used to calculate roughness lengths with surface layer similarity. To do so, we employ

$$L = - T u_{\star}^3 / (k g H) , \quad (7.1)$$

as the Monin-Obukhov length,

$$z_0 = z \text{ EXP}(k u(z) / u_{\star} + p(z/L)) , \quad (7.2)$$

as the surface roughness length, where

$$\begin{aligned} p(z/L) = & 2 \ln((1 + x) / 2) \\ & + \ln((1 + x^2) / 2) \\ & - 2 \tan^{-1}(x) + \pi / 2 , \text{ and} \end{aligned} \quad (7.3)$$

$$x = (1 - 16 z/L)^{1/4} , \quad (7.4)$$

for the unstable surface layer (Paulson, 1970).

The results for z_0 are shown in fig. 8 and they generally agree with other published values for the ground cover type of each respective region. As expected, the Lompoc Valley has the lowest values while the East Hills were roughest. Because the measurements were made at 5 m, this roughness measure is representative of only a few hundred meters of terrain upwind of the anemometer. Therefore, values in the

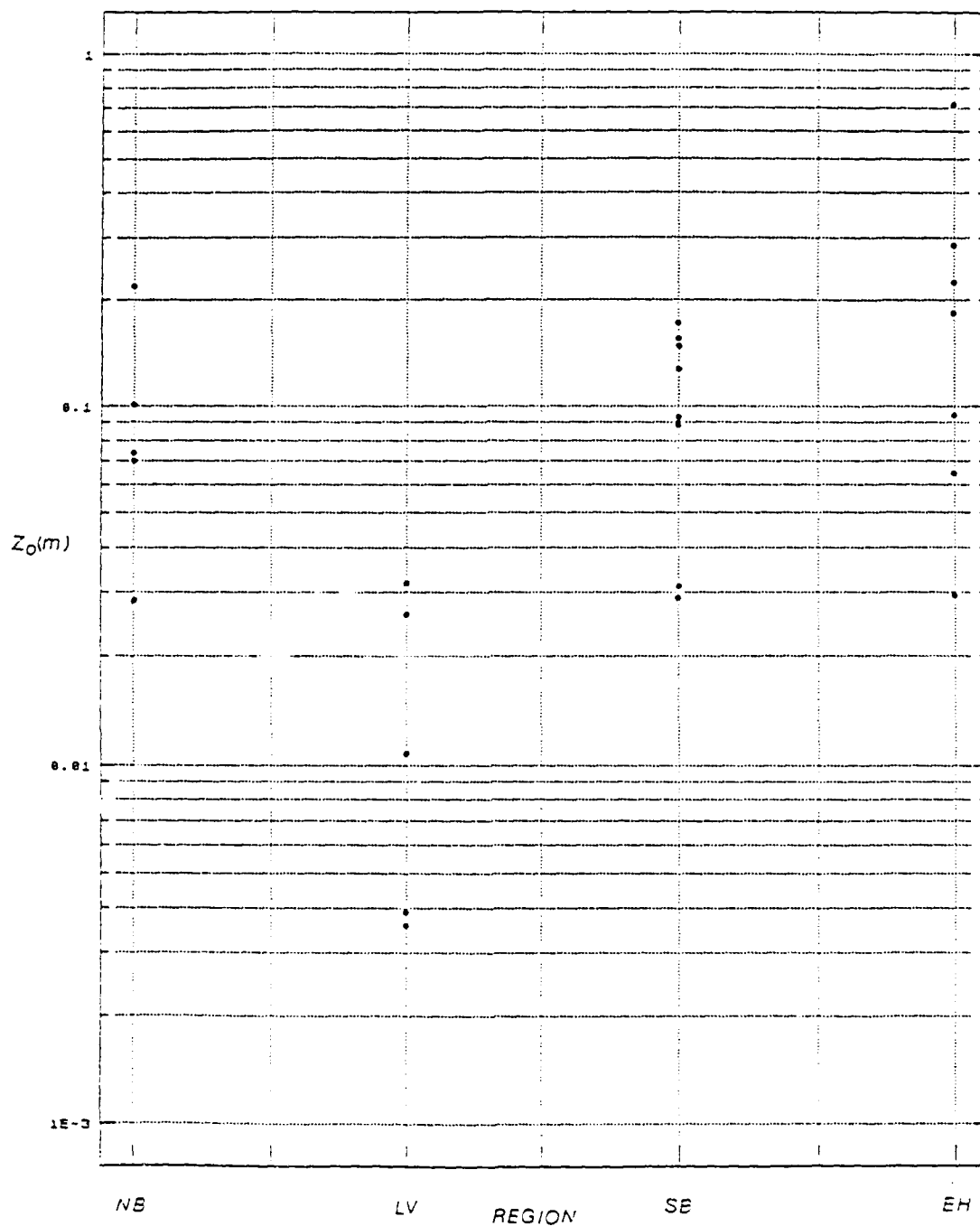


Fig. 8 Surface roughness lengths measured during VBLs and segregated by region. Each sample is an average of all locations sampled during a single transect through the region. Direct eddy correlation measurements were made with a sonic anemometer mounted at 5 m.

South Base and East Hills are less than we would expect for mountainous terrain. The net effect of the mountains on fluxes would only be seen by measurements from very high platforms such as aircraft. Near the surface, the effect of mountains is to create local maxima or minima of stress and heat flux which are seen as increased scatter. By averaging between locations we have roughly removed this effect. As "typical" values, we recommend using the medians, which are

North Base	.073 m
Lompoc Valley	.011 m
South Base	.108 m
East Hills	.186 m .

VII.2 SURFACE HEAT FLUX

Surface heat flux depends mainly on solar insolation and the heat absorbing characteristics of the surface cover (albedo, moisture content, etc.). A diurnal signal due to solar heating is evident in the regional averages of heat flux (see fig. 9). When no clouds were present, the May data could not be differentiated from July, but October was clearly lower for a given time of day. This coincides with the fact that the length of the solar day during phase I was almost identical to that of phase II, while the October days were significantly shorter. Stratus cover significantly reduced

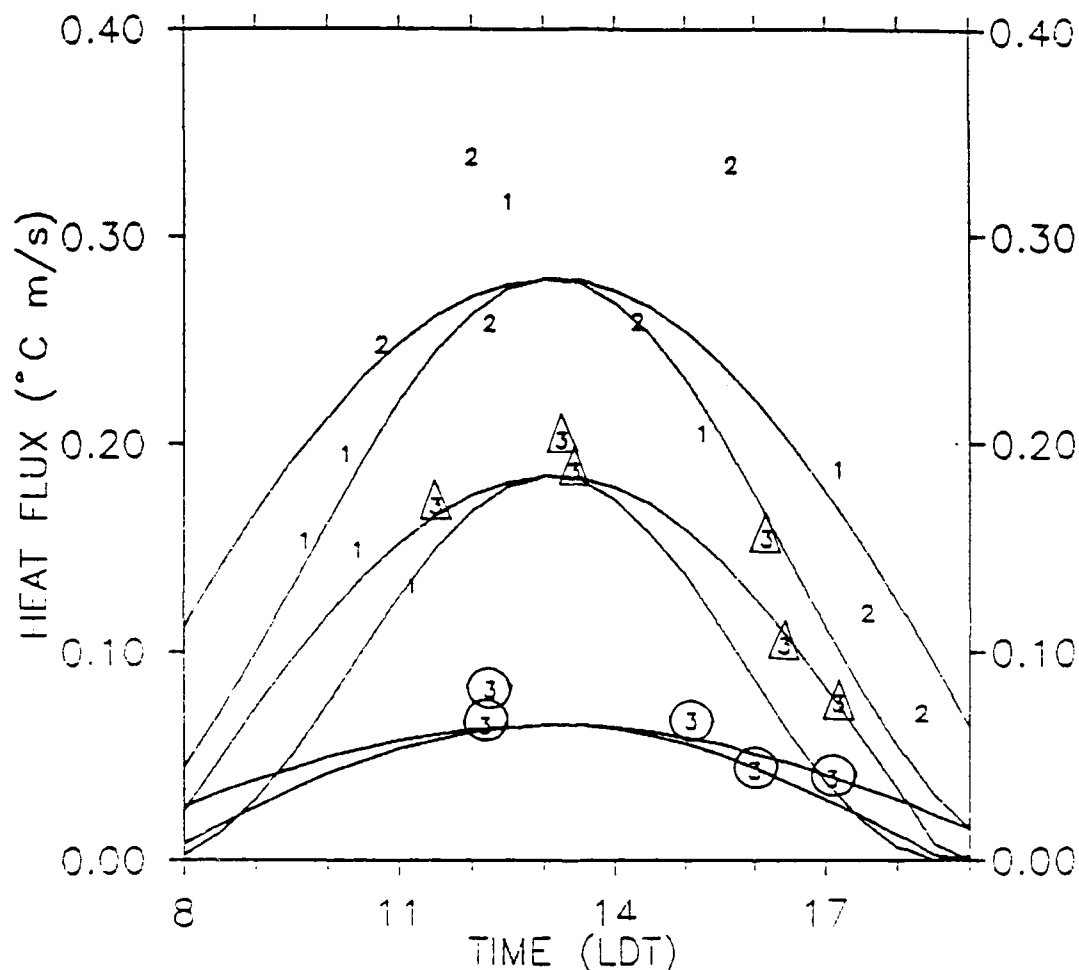


Fig. 9 Surface heat flux as a function of time and VBLS measurement period, where label 1 is 18-20 May, 2 is 26-29 July, 3 is 18-21 October, 1988. Circles are total stratus cloud cover cases, triangles are October clear sky cases, and no symbols are May/July clear sky cases. Lines are COS (broad) and COS2 (narrow) empirical fits of these data for (upper) May/July sunny data, (middle) October sunny data, and (lower) cloud covered data.

the heat flux, as evidenced by fig. 9. We have approximated the heat fluxes observed with cosine and cosine-squared functions by 1) fixing the solar day length as 1/2 the wavelength, and 2) matching the approximate maximum value to the amplitude. The results in fig. 9 indicate that the \cos^2 form is more appropriate for May and July, while the COS form is more representative of the October data. We also speculate on a single fit for the sparse stratus cover data, but most likely the amplitude is a function of the cloud thickness. The approximations are

$$H = .28 \cos^2((t - 13.1) / 13.83) \pi), \quad (7.1)$$

(no clds , May/Jul) , [6.2 < t < 20]

$$H = .19 \cos((t - 13.1) / 11.1) \pi), \quad (7.2)$$

(no clds , Oct) , [8.0 < t < 18.6]

$$H = .065 \cos((t - 13.1) / 13.83) \pi), \quad (7.3)$$

(clds , May/Jul) , [6.2 < t < 20]

$$H = .065 \cos((t - 13.1) / 11.1) \pi), \quad (7.4)$$

(clds , Oct) , [8.0 < t < 18.6]

where H is in degC*m/s and t is time in hours PDT. Fig. 10 plots the same data with the region identified by the label. While the data is sparse, there is no clear reason to differentiate results based upon region. Morning values do

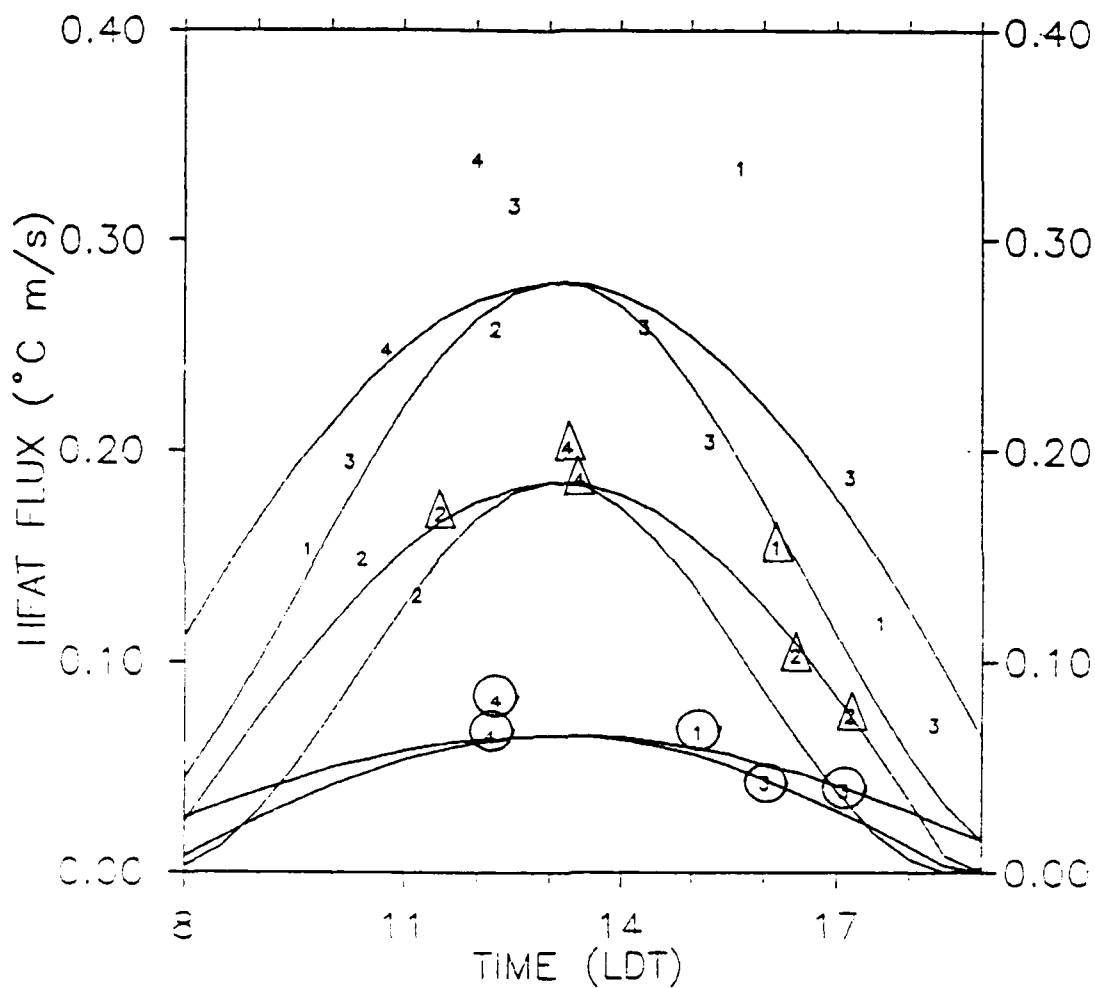


Fig. 10 Same as fig. 9, except labels represent VBG topographic region, where label 1 is North Base, 2 is Lompoc Valley, 3 is South Base, and 4 is East Hills.

tend to be somewhat lower than their afternoon counterparts, and this may be due to the fact that we have assumed a constant Bowen ratio (sensible/latent heat flux), when in fact morning dew may significantly reduce the ratio.

VIII.3 WIND DIRECTION

The variability of the wind direction was a major objective of VBLS. For the following analysis we have averaged all wind values through the depth of the boundary layer for each location. We only consider times when the sea breeze front has passed all VBG towers; in other words, the first transition (section IV) has occurred and the wind flow pattern is well established. Lastly, we calculate the vector difference between the boundary layer wind direction and the average wind direction at 12 ft across the base. (Appendix D lists the base averaged winds for each day.) The resulting direction difference histograms are plotted by region in fig. 11. We've taken the liberty of assuming a Gaussian shape to these data and have plotted the corresponding probability density functions in fig. 12 with the corresponding statistics listed below.

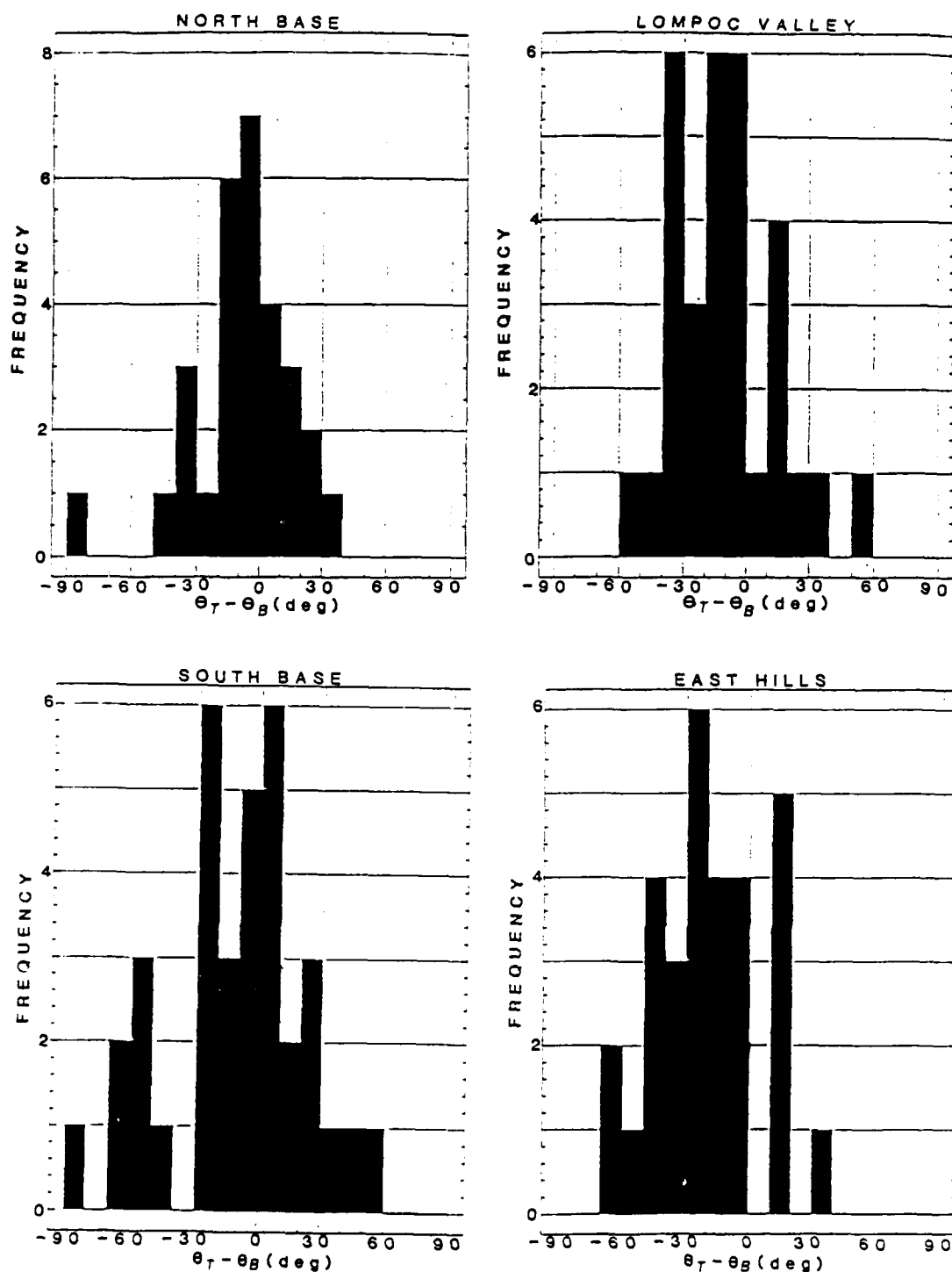


Fig. 11 Difference between the mobile SODAR measured boundary layer average wind direction (T) and the VBG tower network average 12 ft wind direction (B). Each observation represents the average value at a measurement location.

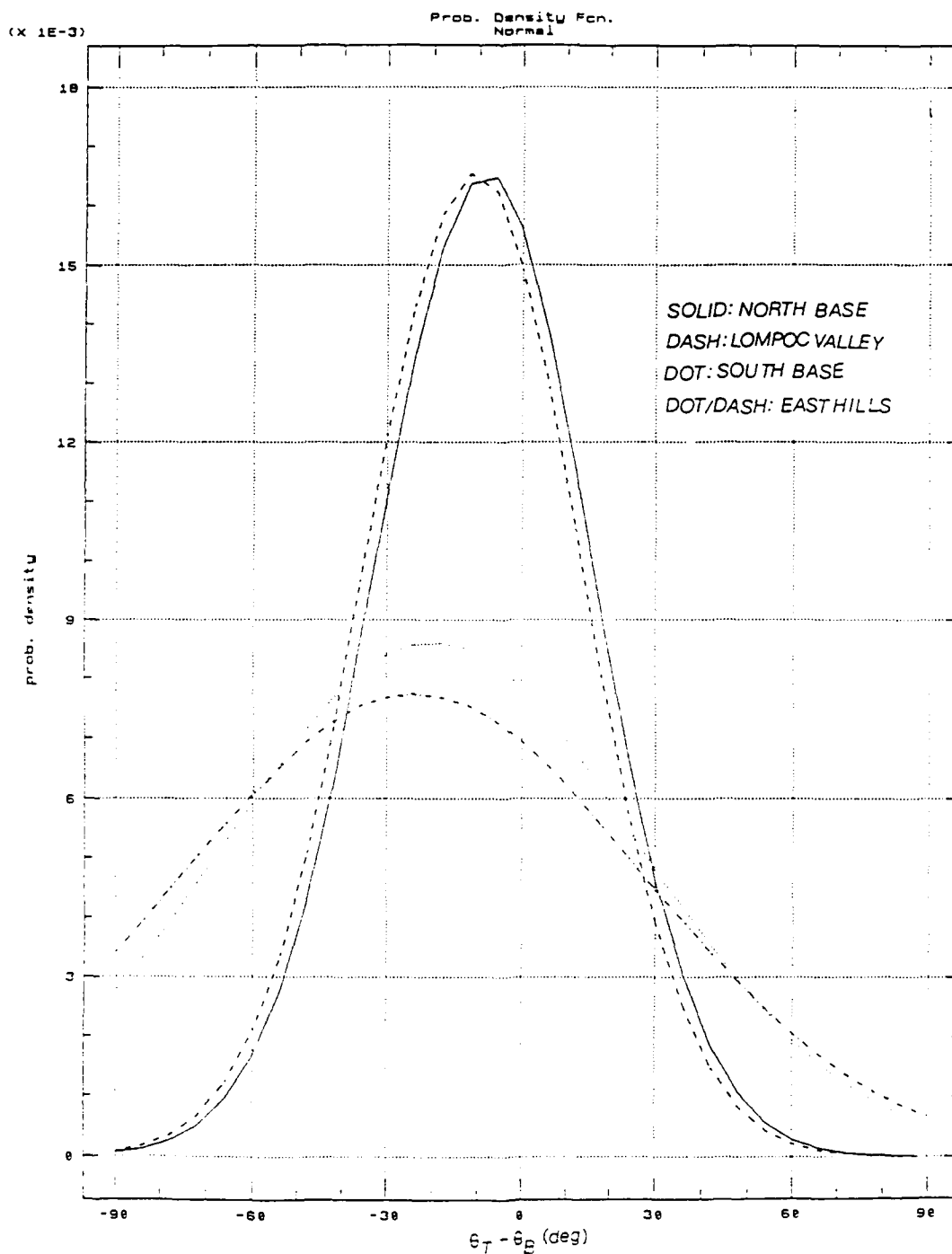


Fig. 12 Probability densition function representation of the data in fig. 11. Normal distributions were assumed. NB is North Base, LV is Lompoc Valley, SB is South Base, and EH is East Hills.

<u>REGION</u>	<u>BIAS</u>	<u>STD. DEV.</u>	<u>CHISQUARE</u>	<u>SIG. LEVEL</u>
NB	-8.4 deg	24.1 deg	.83	.36
LV	-10.9	24.1	.92	.34
SB	-19.9	46.4	2.67	.45
EH	-24.0	51.6	8.83	.03

The reliability of the fits is poor for the South Base and East Hills regions, but the data tend to fall into two groups. The North Base and Lompoc Valley statistics are similar, while the South Base and East Hills have larger bias and standard deviation.

If we compare the North Base / Lompoc Valley standard deviations with the values for the VBG towers in Appendix D, we see that they are similar. This implies that the VBG tower network does a realistic job in describing wind direction variability across the base. More importantly, this shows that the variability observed near the surface is similar to the variability of the flow through the depth of the boundary layer.

Based on the histogram, the bias in the South Base data appears to be induced by the large negative outlying values, but the East Hills bias does seem genuine. Certainly the relative standard deviations seem realistic. The huge variability in the mountains suggests that once a plume enters

this type of terrain, it may be impossible to predict its trajectory with a reasonable degree of confidence.

VII.4 WIND SPEED

In a similar manner to wind direction, we calculated the ratio of the vector averaged boundary layer wind speed observed at each location to the base average. Since this average used only 12 ft base sensors, we expect the speed ratio to be larger than unity in most cases. Fig. 13 plots histograms for each respective region, and there is a tendency for some to be bimodal.

The high wind speed mode is similar in all regions (1.5 - 2.0), except the Lompoc Valley where it is surprisingly large (2.5 - 3.0). This is most likely the result of the "funnel effect" which is noticeable in other ocean facing valleys such as the Sacramento delta.

For each case, there are a significant number of observations near or below unity. The East Hills low wind speed mode is actually stronger than the high wind speed mode. One plausible explanation is that each region may have local areas of convergence where boundary layer averaged horizontal wind speeds are significantly reduced. It would be logical to

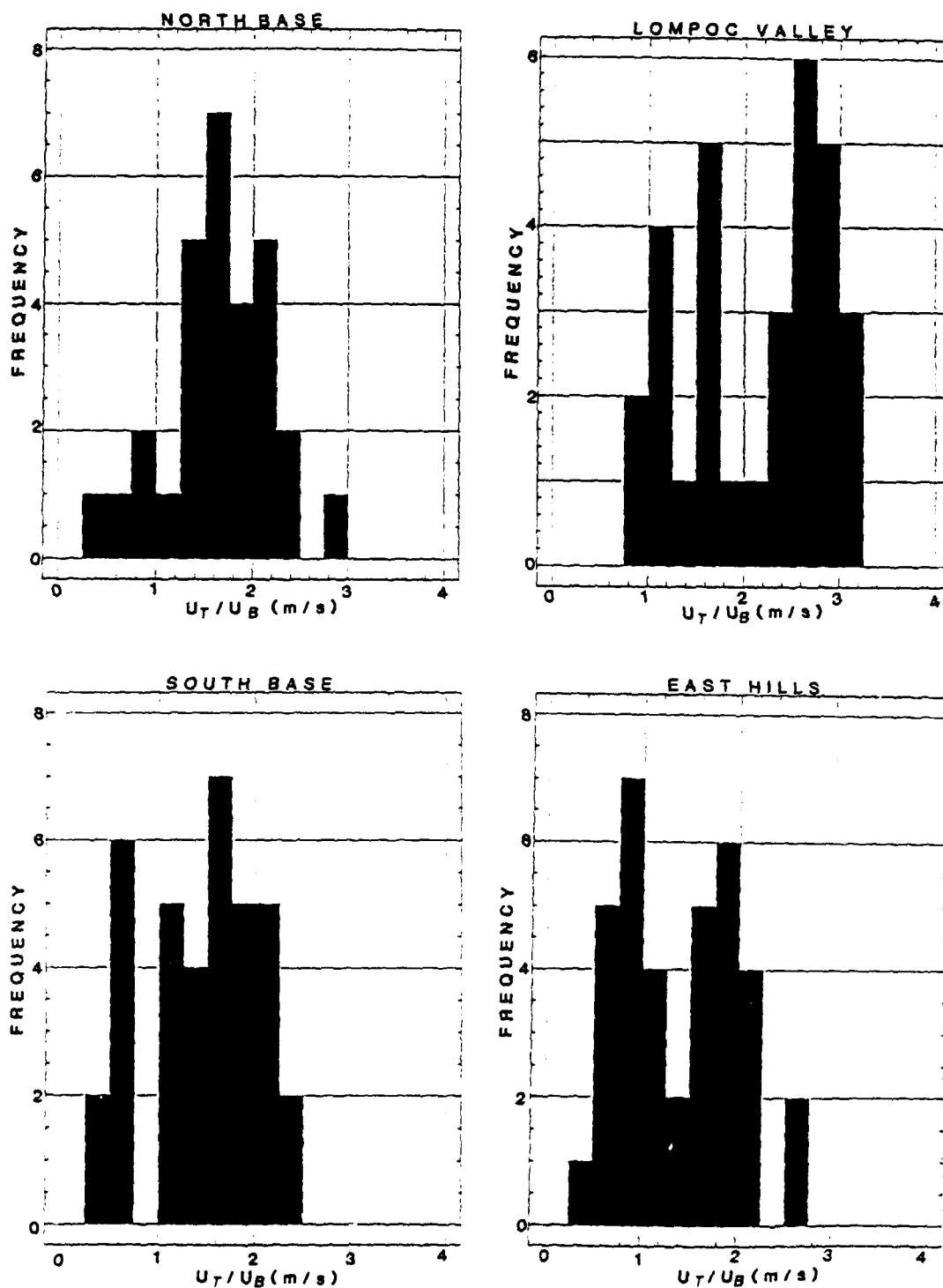


Fig. 13 Ratio of the mobile SODAR measured boundary layer average wind speed (T) to the VBG tower network average 12 ft wind speed (B).

find these "chimneys" in sunny mountainous regions such as the East Hills.

VII.5 VERTICAL WIND SHEAR

The change in the wind with increasing altitude within the boundary layer is important for diffusion predictions and also for launch or flight operations. The SODAR readily provides measurements of vertical wind shear in the boundary layer. For the data we have decomposed each vector, assumed a linear change of each component with height, then regressed through all available points within the free boundary layer. We define the following quantities,

$$C = 100[-du/dz \cos(D) + dv/dz \sin(D)]/U, \quad (7.5)$$

$$S = 100[-du/dz \sin(D) - dv/dz \cos(D)]/U, \quad (7.6)$$

where C is a measure of the directional clocking with height, and S is a measure of the speed increase with height (speedup). u and v are vector wind components in absolute coordinates and D is the wind direction. We normalize the shear by U, the mean wind speed through the shear layer. We also arbitrarily define the shear through a 100 m depth, since it is not apparent that shear should scale with any unique

length (such as BL2) for these data. If $S=0$, a value of $C=1$ represents a change of 60 degrees through 100 m. Likewise, if $C=0$ a value of $S=1$ represents a change from .5U to 1.5U over 100 m.

We are primarily interested in how often wind shears are large. Figs. 14+15 plot the cumulative distribution function of the absolute value of C and S for each region. 50% of all data have C or S values of .4 or less, and all regions appear similar for low shear values. At higher values of C , all regions are similar, except South Base which has a relatively high probability of experiencing a large directional shear within the boundary layer. As to the incidence of high speed shear, the ranking appears to be 1) East Hills or South Base, 2) North Base, and 3) Lompoc Valley.

When the regions are combined, the histograms of C and S are remarkably similar (see fig. 16). These data do not have a normal distribution. This is demonstrated in fig. 17, where we have attempted to fit a Gaussian function to the clocking data. The combined distributions are also quite symmetric, as is generally the case for individual regions.

No independent parameters do an adequate job of predicting these shearing quantities. The following table summarizes the partial correlations for some logical candidates

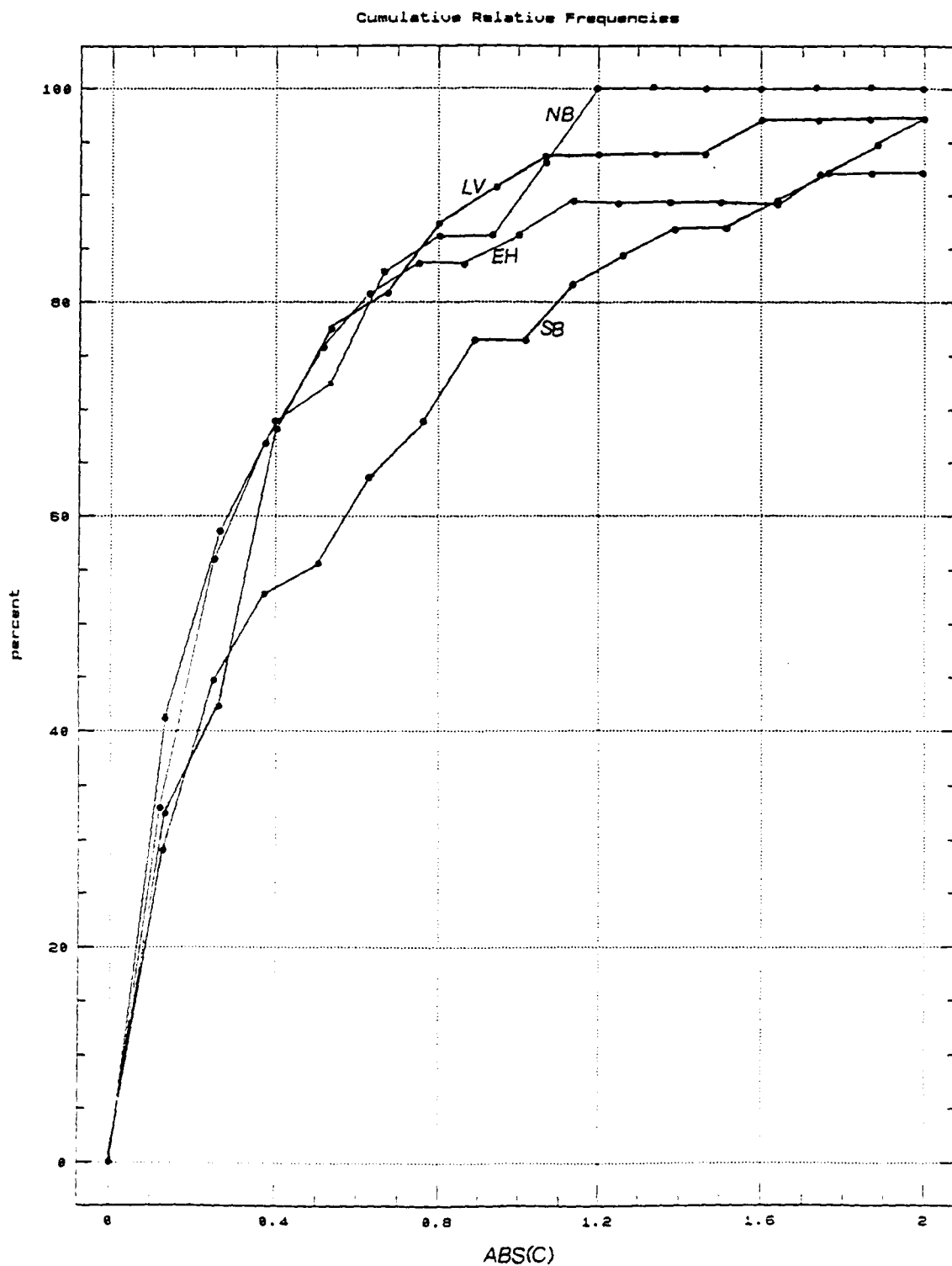


Fig. 14 Cumulative relative frequency (CRF) of the clocking parameter magnitude segregated by VBG region. CRF represents the probability of experiencing wind shear below a selected value.

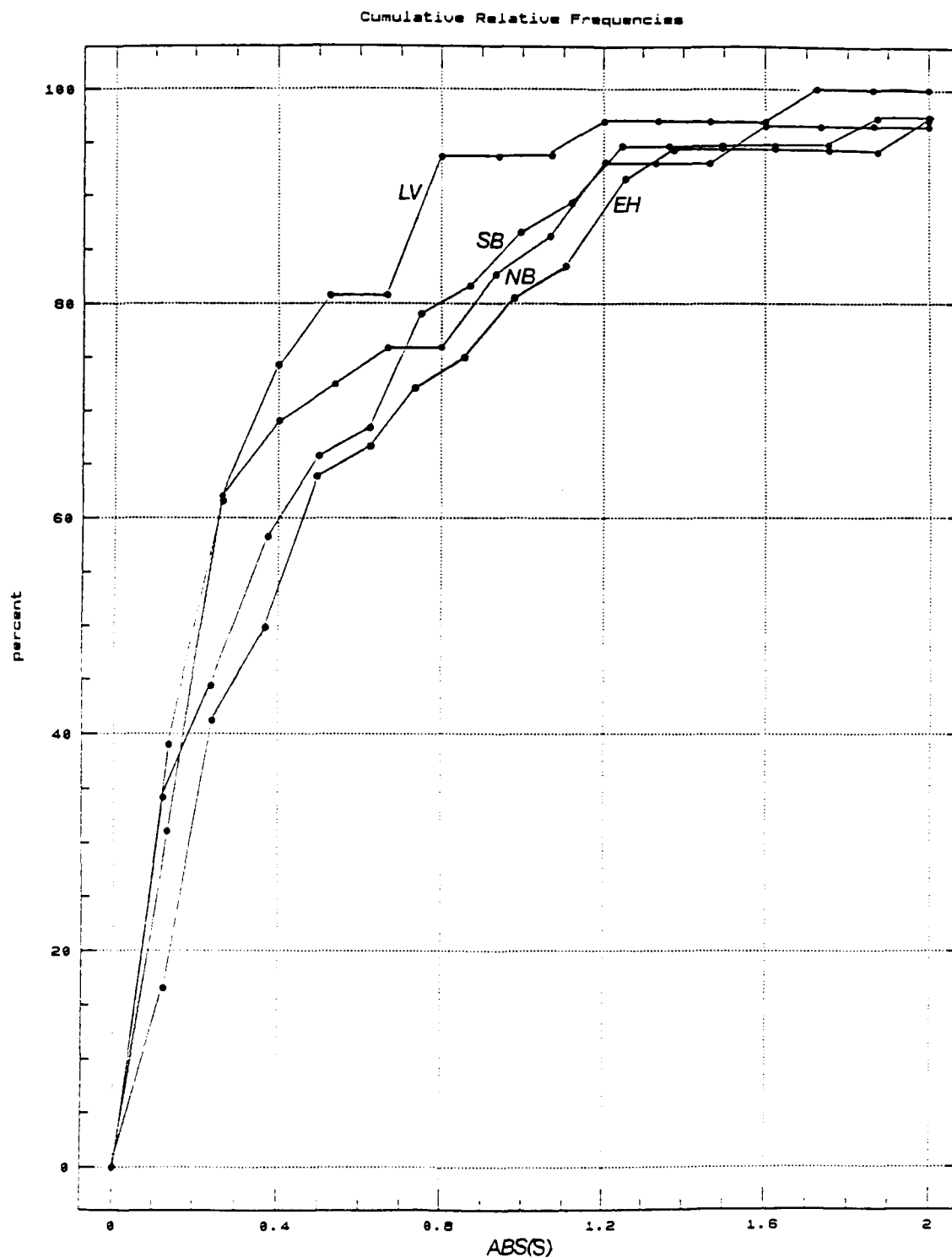


Fig. 15 Cumulative relative frequency of the speed up parameter magnitude segregated by VBG region.

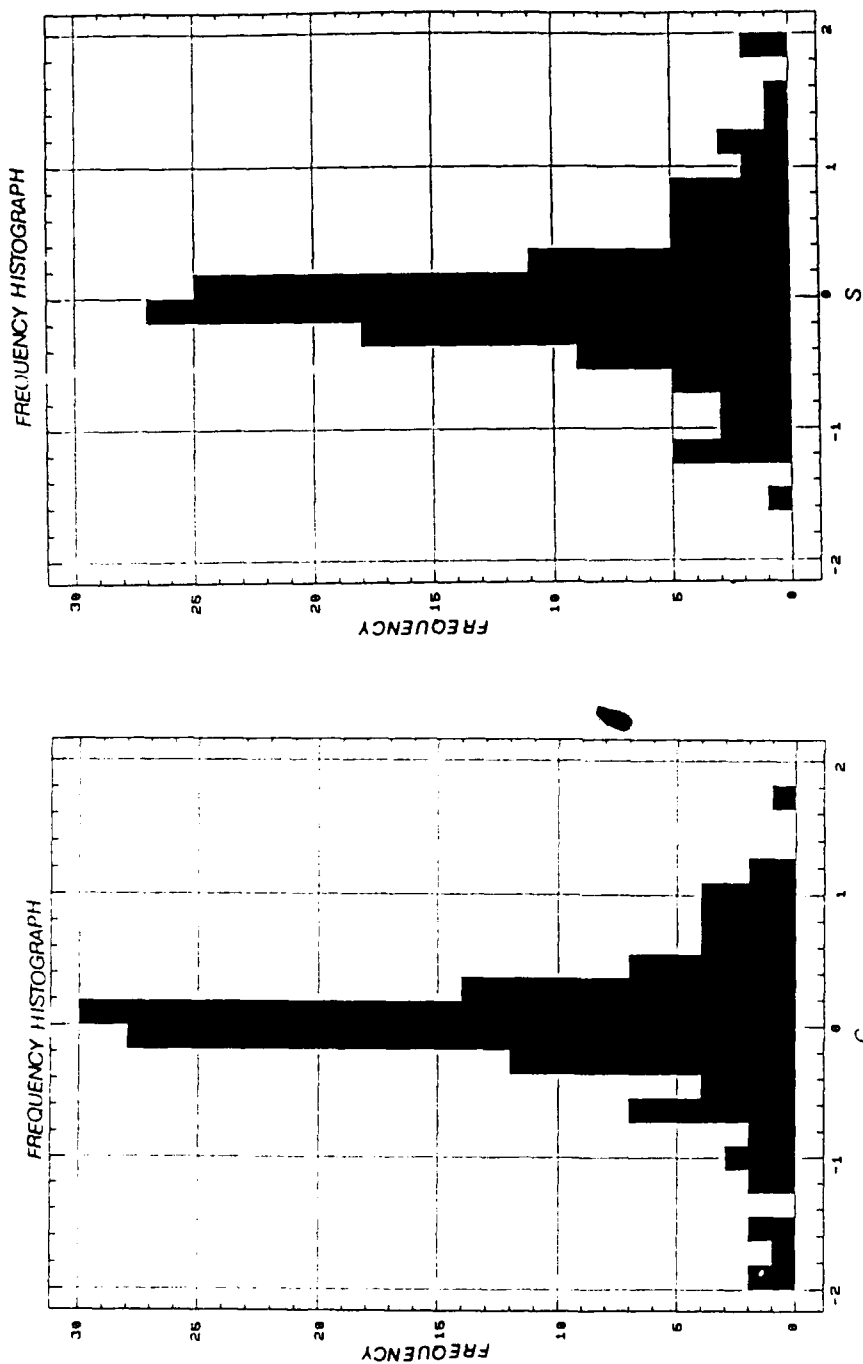


Fig. 16 Histograms of the boundary layer average clocking parameter, C , and the speed up parameter, S , for all data. Positive values of C indicate that the wind direction veers with height. Positive values of S represent a wind speed increase with height.

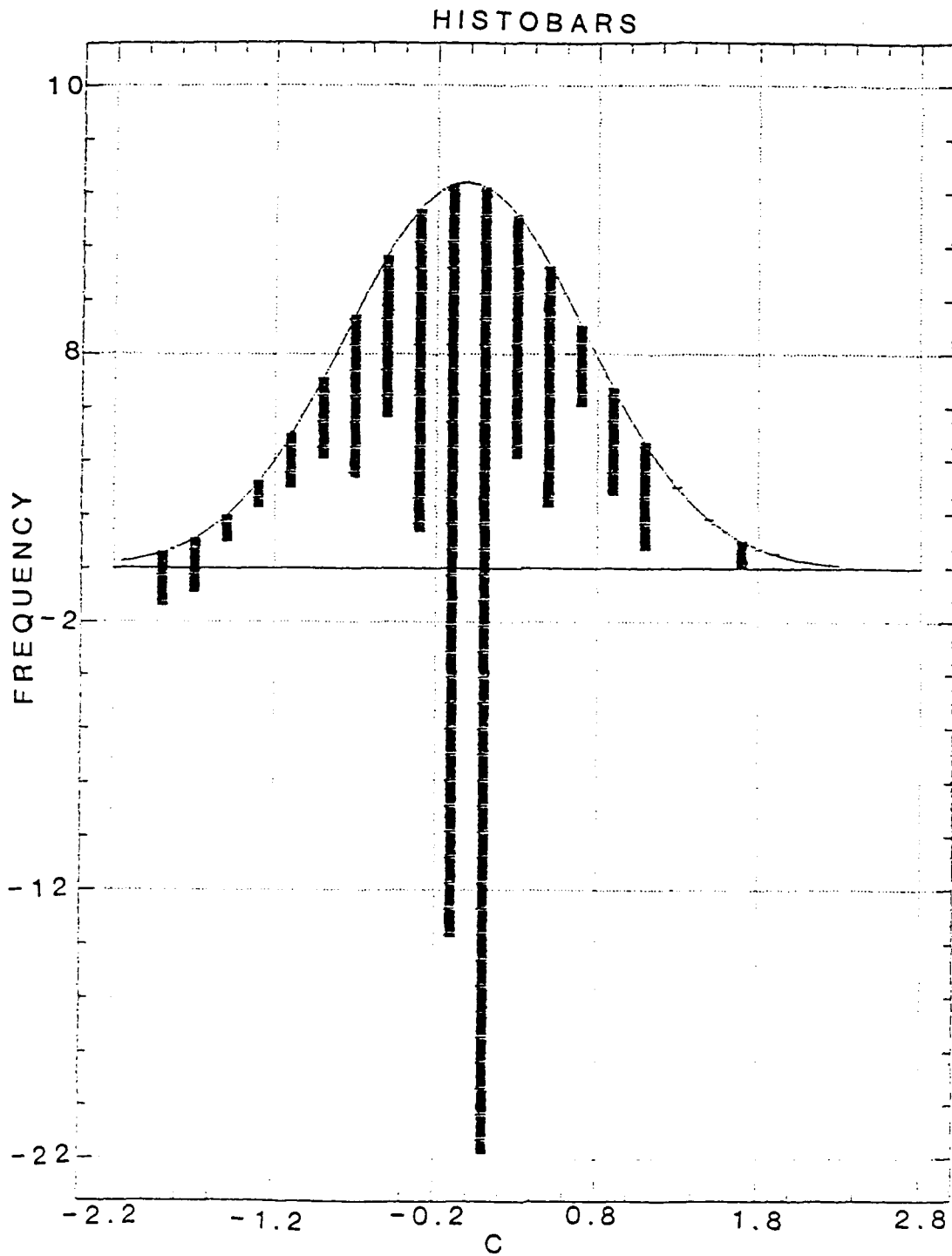


Fig. 17 The departure of the clocking variable frequency from an assumed normal distribution. Histobars are the same as in fig 16.

	C	S
C	1.000	.219
S	.219	1.000
sigma v	.100	.035
sigma w	.134	.067
U_t / U_b	-.176	.084
$D_t - D_b$.269	-.165
cloud cover	-.009	.163
BL1	-.094	-.023
BL2	-.035	-.122
z_0	.224	-.156
L	-.083	.011
BL1/L	.029	.052
BL2/L	-.012	-.051

where sigma v,w are averages through the mid-boundary layer (see next section), $D_t - D_b$ is the direction difference used in section VII.3, U_t / U_b is the speed ratio used in section VII.4, and L is the Monin Obukhov length. Correlations below approximately .2 should be considered negligible. Considering the similar shapes of the C and S distributions, the correlation between variables is very small. Neither shear measure correlates with boundary layer height or stability. It should not be surprising to see some correlation with the direction difference, and this could possibly be used as a predictor. It is encouraging to see modest correlation with

z_0 , which in this case is the average roughness measured at each location (as opposed to the regional averages of section VII.1). The implication is that higher than average stress at the surface translates into clocking of the wind direction and, to a lesser degree, a decrease in wind speed with height.

VII.6 BOUNDARY LAYER TURBULENCE

In a convective boundary layer, both σ_v and σ_w scale with w_* , the convective scaling velocity, defined as

$$w_* = ((g / T) H Z_i)^{1/3} . \quad (7.7)$$

Near the top or bottom of the boundary layer, the variances are also a function of the relative height, z/Z_i , and possibly other quantities. But from roughly .2 to .8 Z_i , the scaling has been shown to be fairly constant over flat terrain, i.e.,

$$(\sigma_v^2)^{1/2} / w_* = K_1 , \quad (7.8)$$

$$(\sigma_w^2)^{1/2} / w_* = K_2 , \quad (7.9)$$

where the constants K_1 and K_2 are about the same for the Minnesota data (Kaimal et al. 1976) and range from .5 to .7. We will use the median value of .6 for comparative purposes.

Recall that the 5 minute base averaging time acts to filter out low frequency energy. This is not a severe limitation in the surface layer, but significant energy can be lost at higher altitudes. While we cannot explicitly correct for this loss, we can adjust the flat terrain benchmark based on Hojstrup's (1981) spectral similarity relationships in the convective boundary layer as follows,

$$(w'^2)^{1/2} / w_* = (v'^2)^{1/2} / w_* = .6 (1 + Z_i / U T)^{-1/3}, \quad (7.10)$$

where T is the averaging time, 5 minutes in this case. For example, a 500 m boundary layer and 5 m/s wind speed results in a correction factor of .91.

Histograms of the ratio of the observed vertical turbulence versus that expected for flat terrain are shown in fig. 18. In general, both North and South Base show a broad range of values centered near unity, while the Lompoc Valley and East Hills show a preference for turbulence at 50 - 80 % of flat terrain values. Finkelstein et al. (1986) compared a variety of SODAR systems against the Boulder Atmospheric Observatory and found that, although scatter was large, the Radian Corp. SODAR (used in VBLS) did an adequate job of estimating vertical turbulence during daylight hours. If anything, the Radian tended to overestimate low values of vertical turbulence. Therefore, the lower than expected

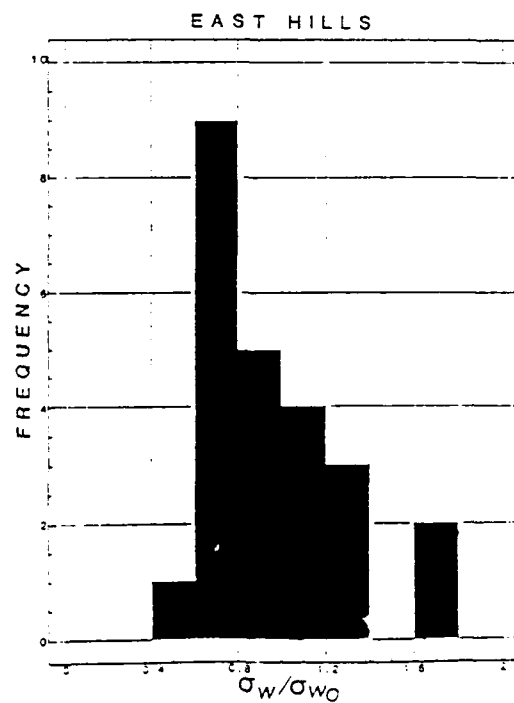
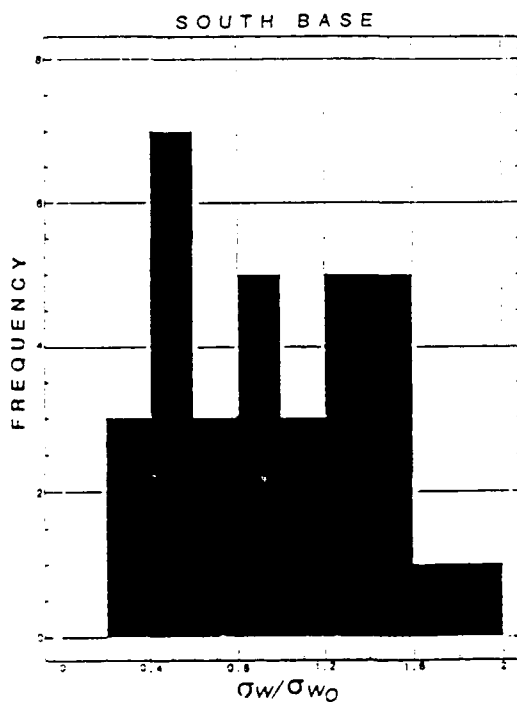


Fig. 18 The ratio of the measured boundary layer average vertical turbulence to that assumed for flat terrain ($.6 w^*$). Only data from $.1 Z_i$ to $.8 Z_i$ was used in the average. w^* was calculated using the regional estimates of heat flux and z_0 , and the local measure of the boundary layer height.

turbulence in the Lompoc Valley and East Hills should be considered significant.

Horizontal turbulence is shown in fig. 19 and all regions showed significantly lower values (40 %) than for flat terrain. To our knowledge, no comprehensive evaluation of SODAR-derived lateral turbulence has been reported in refereed literature. We can only speculate that the small values and scatter compared to vertical turbulence suggest problems with the Radian's estimation of lateral turbulence. Unfortunately, we do not have enough simultaneously recorded data to evaluate the base DASS'es estimates of turbulence.

VII.7 BOUNDARY LAYER DRAG COEFFICIENT

The surface roughness results of section VII.1 are applicable only for the generic surface cover found in each region (i.e. long grass, trees, etc.). In order to evaluate the effect of the larger scale terrain features, a technique sometimes employed in complex terrain is to define a geostrophic drag coefficient (i.e. Garratt, 1977),

$$C_g = u_{*t}^2 / U_g^2 , \quad (7.11)$$

where U_g is the geostrophic wind speed, and u_{*t} is the effective friction velocity (i.e. measured high in the boundary layer). Typical values range from .001 for flat

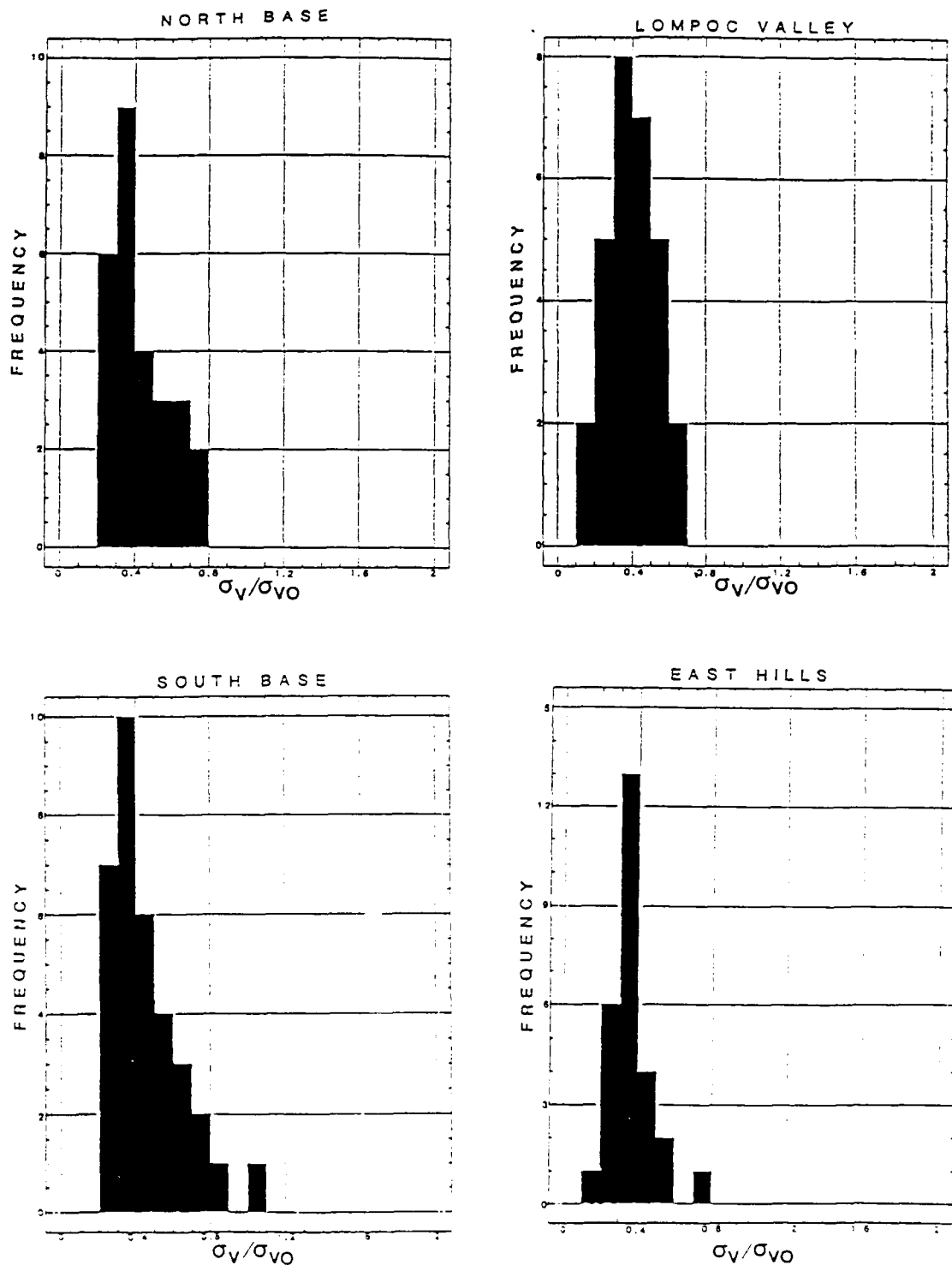


Fig. 19 The ratio of the measured boundary layer average cross wind turbulence to that assumed for flat terrain (.6 w*).

surfaces to 3 for "average" mountains. We will define a boundary layer drag coefficient,

$$C_{BL} = u_*^2 / U^2 , \quad (7.12)$$

where u_* is our 5 m (low level) measure of friction velocity and U is the mean velocity through the boundary layer. Unlike the geostrophic wind, the boundary layer speed is affected by the underlying terrain (both surface type and large scale terrain features). C_{BL} is, therefore, a crude measure of the momentum transfer coefficient for varying types of large scale terrain, with the surface roughness effects removed in a first order sense. Fig. 20 shows results for the four regions which generally agree with their corresponding "degree of hilliness". North Base is most confusing in that two peaks are observed. Clearly, other factors influence the mean boundary layer wind speed, but based on these results, we suggest the following values:

REGION	C_{BL}
NB	.0020 +- .0012
LV	.0018 +- .0010
SB	.0022 +- .0020
EH	.0032 +- .0010

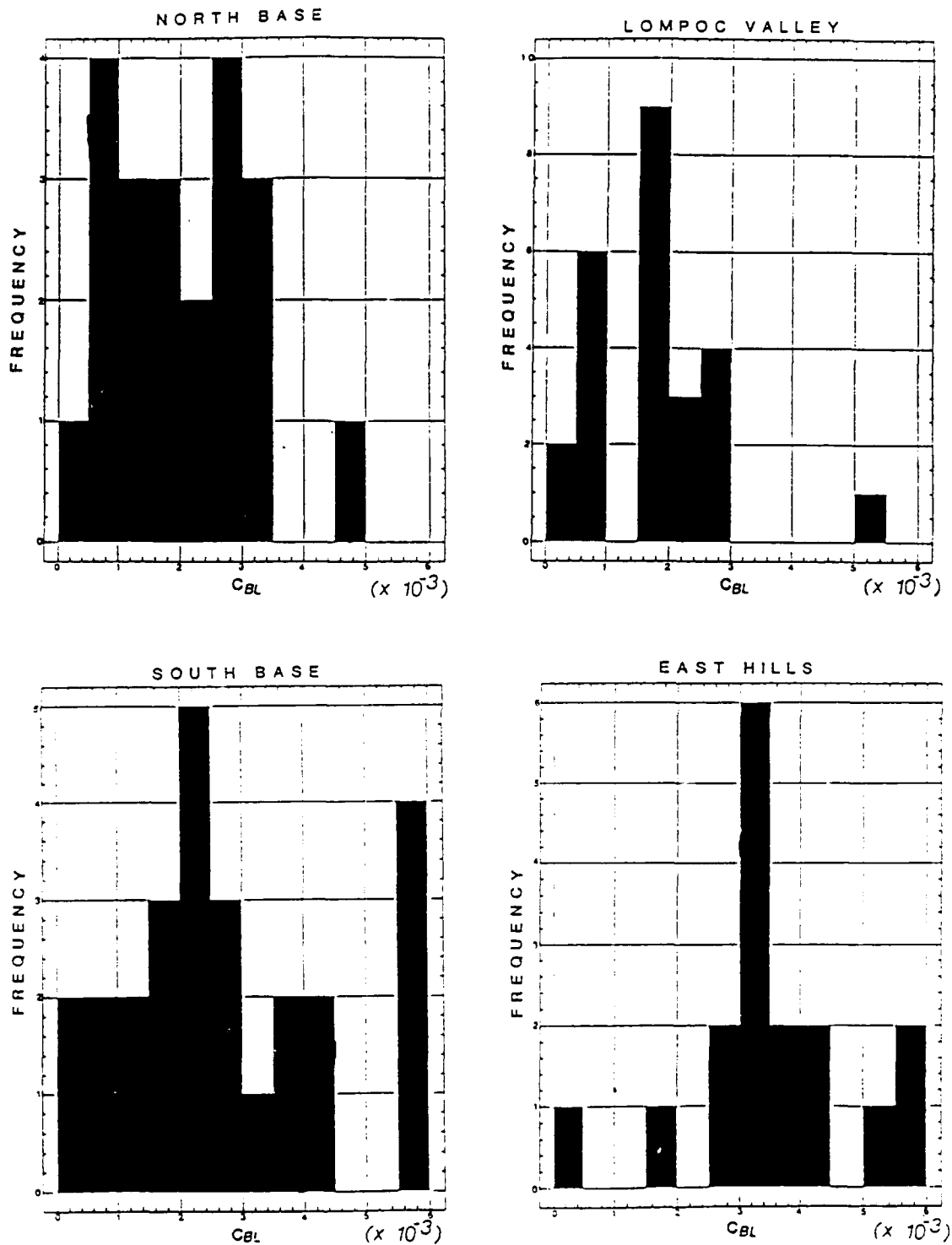


Fig. 20 Regional histograms of the boundary layer drag coefficient. the local value of u^* was obtained by applying surface layer similarity to the local 5 m measure of wind speed, using the regional estimates of heat flux and z_0 .

One potentially useful application of these simplistic results would be the prediction of boundary layer wind speeds based on surface speeds. Using the average z_0 and H values from the above sections, z/L and u_* can be estimated, and the above relationship will predict the average boundary layer wind speed.

VIII VBLS TRANSECTS - STRATUS FRONT ANALYSIS

VIII.1 INTRODUCTION

This section describes a unique subset of the data collected during the experiment; transects of the marine stratus cloud edge. As mentioned earlier, a semi-permanent stratus deck of considerable size was located in the eastern Pacific during the July and October phases of VBLS. Stratus coverage ranged from 0 to 100% during various periods of the experiment. As is typical for California, maximum coverage occurred at night. Solar heating gradually "lifted" the stratus base during the morning hours until a "burn-off" occurred which proceeded rapidly from east to west. This burn-off was often well correlated with the passage of the sea breeze front which increased boundary layer mixing. After the initial burn-off the orientation of the stratus edge stabilized, and its location relative to the coast would stay fairly fixed until late afternoon when the stratus would move progressively inland. As is common, on several occasions the

edge stabilized several miles inland and at right angles to the Lompoc Valley. Since this valley tends to channel flow to the west-northwest, this scenario offered a good opportunity to transect the stratus edge with the mobile SODAR and observe boundary layer changes across this type of front.

VIII.1 STRATUS EFFECTS ON BOUNDARY LAYER HEIGHTS

In the following discussion we have normalized the boundary layer height observed at the mobile SODAR by the mean of BL2 observed at the most "marine-like" of the 3 permanent SODAR, SLC6. This SODAR is located .5 km from the ocean and about 10 km south of the valley mouth. While there are 2 other SODAR significantly closer to the valley, they are several km inland. Moreover, BL2 is not always traceable at these sites and often shows a diurnal behavior absent at the southern location.

We transected the cloud edge on four separate occasions. All four occurred during July 88, a period of no synoptic scale activity. Unfortunately, only transect C (see below) has "good" spacing between observations near the edge, but some important characteristics can be seen from all four transects. Sampling more locations on a transect increased the total transect time, and likewise increased instationarity. It is difficult to "measure" instationarity, but a relevant quantity may be wind at a fixed location in the

valley. The following table lists transect beginning and ending times and winds at WT009 which was along the transect and always cloud covered during these transects.

<u>Transect</u>	<u>Date</u>	<u>Time(LDT)</u>	<u>Speed(m/s)</u>	<u>Dir(deg)</u>
Start A	7-26	1005	3.2	305
End A		1205	3.8	312
Start B		1740	3.0	302
End B		1900	2.8	306
Start C	7-27	900	1.4	302
End C		1305	4.1	308
Start D	7-28	1030	1.5	306
End D		1255	3.8	314

It is clear that the wind direction remains fairly constant, but the speed does not. While we have no fixed measure of the heat flux, it is safe to assume that its value is also constantly changing. This inherent instationarity should be considered when interpreting the results described below.

Fig. 21 shows the evolution of BL1 and BL2 as a function of distance from the edge. The edge was fairly well-defined for all transects, with a change from total to no cloud cover occurring within about .5 km. For this study, the edge is defined as 50% cloud cover. Fig. 21 shows that BL1 rapidly adjusts to near the height of BL2 at the cloud edge. This is not surprising, since the small potential temperature gradient

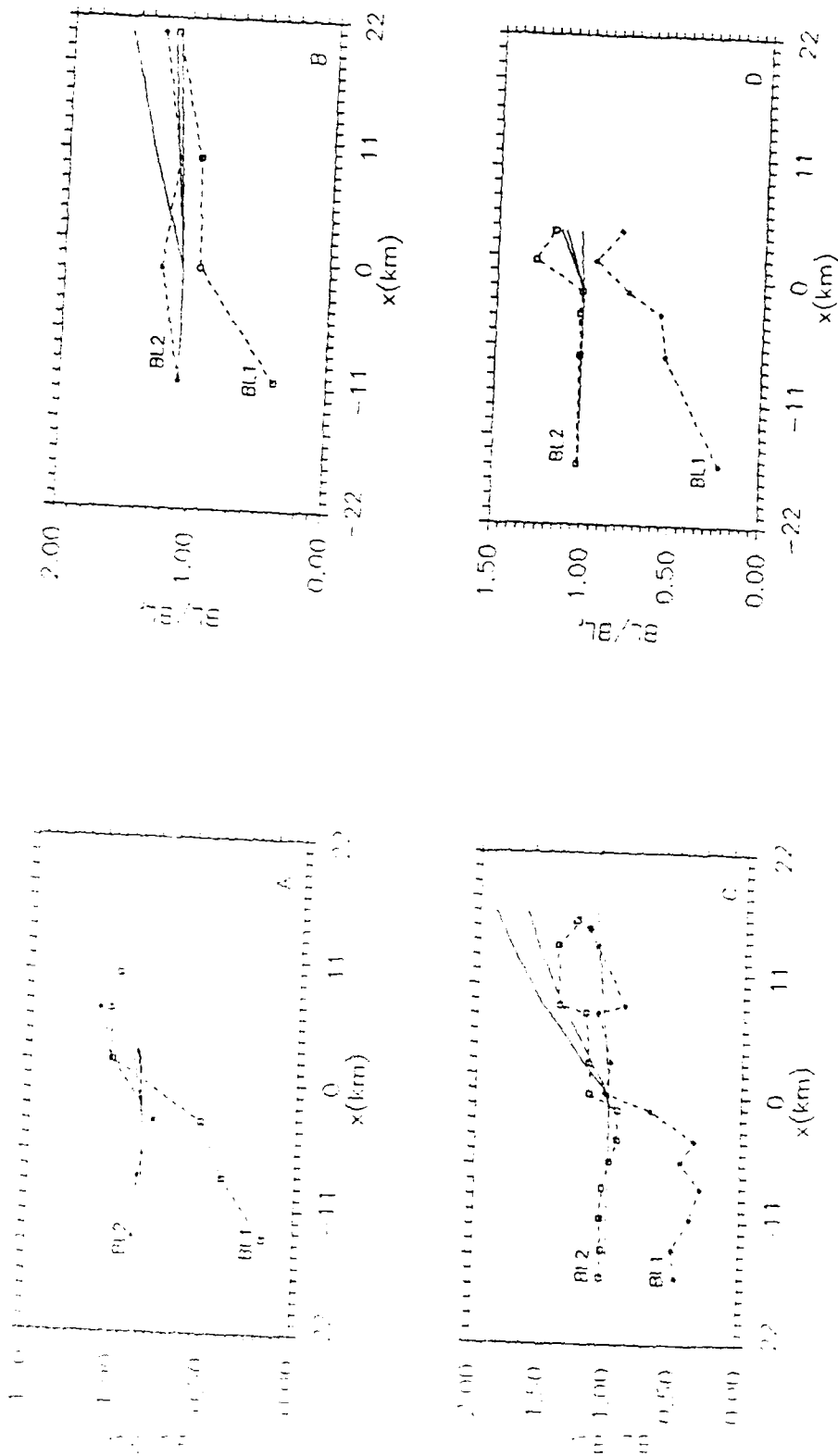


Fig. 21. Transition of boundary layer height across the cloud edge boundary. Negative x is under stratus. Data are dashed lines. Solid lines are the Venkatram model with (upper line) free boundary layer lapse rate, (middle line) above inversion layer, and (lower line) within inversion layer lapse rates.

within the boundary layer offers little resistance to thermal plumes. Likewise, BL2 also grows in the sun, first rapidly and then at a slower rate.

As a physical model for the growth of BL2, we consider the energy balance approach for an TMIBL presented by Venkatram (1979). If a constant heat flux is assumed on the sunny side of the front, then

$$h^2(x) = h^2(0) + 2xH/[G(1-2F)U], \quad (8.1)$$

where $h(x)$ is the boundary layer height at distance x from the cloud edge, H is the surface heat flux ($\text{degC}\cdot\text{m/s}$), G is the potential temperature gradient in the "stable" upwind flow, F is an entrainment factor, and U is the mean boundary layer speed. We use $F=1/7$, as suggested by both Tennekes and Venkatram, who also states that results are relatively insensitive to this parameter. We used a 900 LST sounding at the mouth of the valley to determine G for 3 layers; within the marine boundary (but above the surface layer), within the marine inversion layer, and between the inversion top and 2000 m. The last of these layers should be the value used, but we include the other two in order to test the sensitivity of this parameter. We averaged the cloudy side BL2 observations to define $h(0)$, and averaged the sunny side surface heat flux observations to define H .

As seen in fig. 21, the model underpredicts the growth of BL2 for most cases, even when using the unrealistic lower limit for G. All the transects suggest that this rapid growth may be a very local phenomenon, and transect C suggests that this simple model may work adequately for longer distances from the edge. Transects A, C, and D together suggest that there may be a complimentary depression in the boundary layer on the cloud side of the front.

These features should not be surprising, if the cloud front is considered as a miniature cold front. The differential heat flux would naturally create a baroclinic zone within the boundary layer. Given the semi-permanent nature of the stratus deck, a thermal wind component parallelling the front may induce a secondary circulation producing sinking motion on the cold side and enhance the rising tendency on the warm side of the front. The thermal wind should be observed as a backing in the mean boundary layer wind direction from the cold to the warm side. As with larger scale fronts, an increase in speed should be realized near the front. Fig. 22 shows the difference between the boundary layer average wind direction observed at the mobile SODAR and the average surface wind direction observed simultaneously at 21 towers in the vicinity of the valley. It is clear that there is considerable variability between and within transects, but in each case there is backing for distances less than roughly 5 km from the front. Fig. 22 also

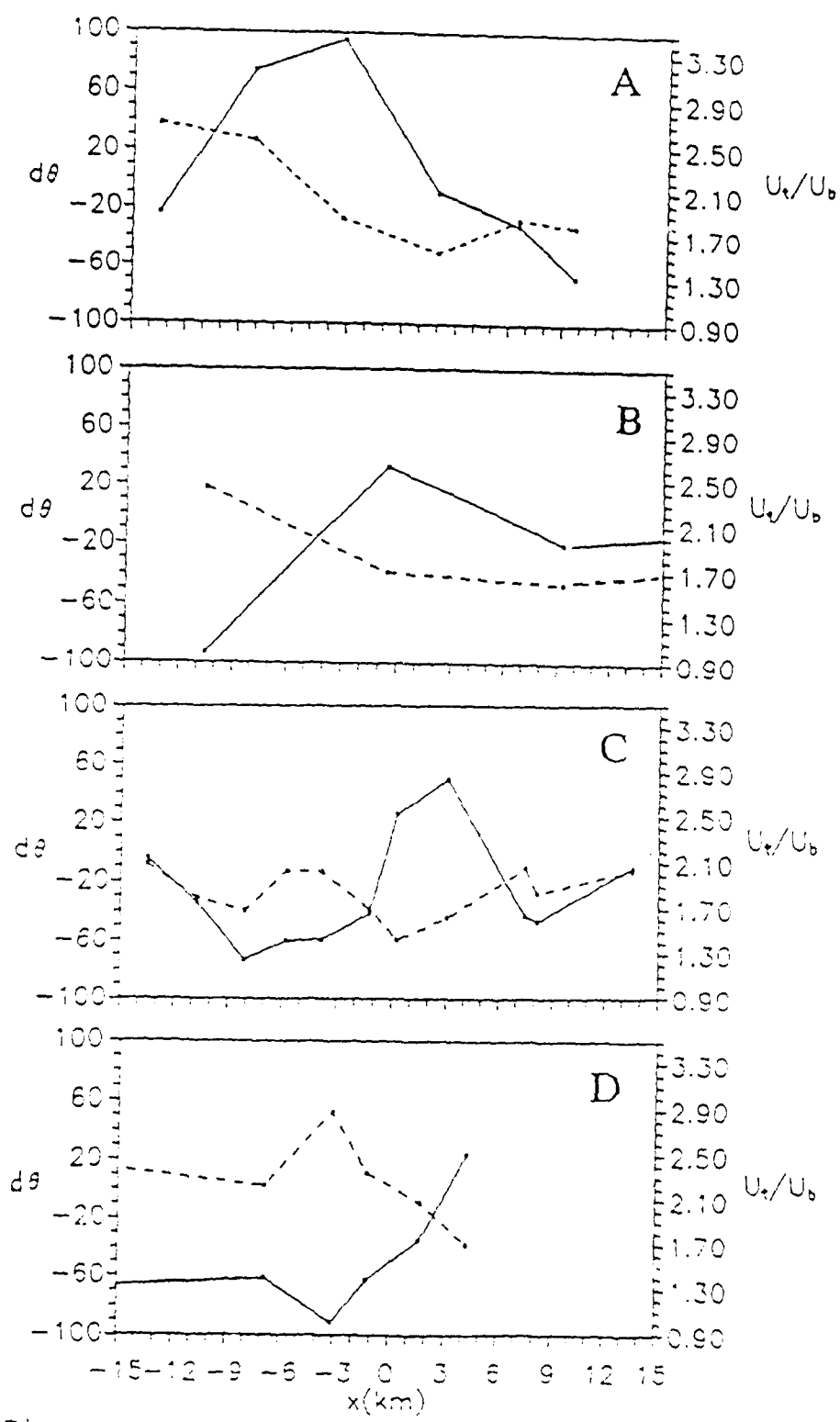


Fig. 22. Horizontal variations in (dashed) wind direction difference and (solid) speed ratio across the stratus front.

shows the ratio of the boundary layer wind speed observed at the trailer versus the simultaneous surface speeds averaged from the 21 towers. The ratio always exceeds unity, and there is an enhancement near the front. The location of that enhancement relative to the front is not consistent between transects, but does appear to correlate with areas where the directional difference is decreasing with x . This is also consistent with the above concept, assuming the thermal wind vector adds to the boundary layer wind vector.

VIII.2 STRATUS EFFECTS ON VERTICAL WIND SHEAR

If a baroclinic zone is present within the boundary layer, it could reduce the well-mixed nature of the boundary layer. This effect may be observed as vertical wind shear. Fig. 23 plots the clocking and speedup variables described in section VII.5 versus distance from the edge for all cases. Speedup scatters about zero, while there appears to be a distinct preference for clocking with height on the cloudy side of the front. Remember that the overall distribution of the shear variables was symmetric, with no preference for either positive or negative clocking values.

Wyngaard (1985) proposed a method of estimating vertical profiles of scalars or wind for the baroclinic case, with no

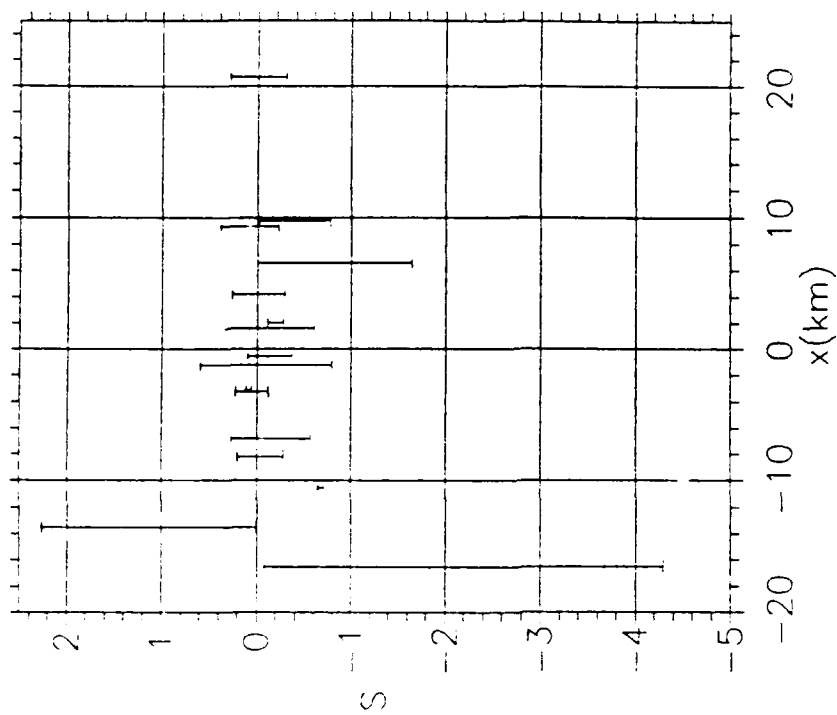
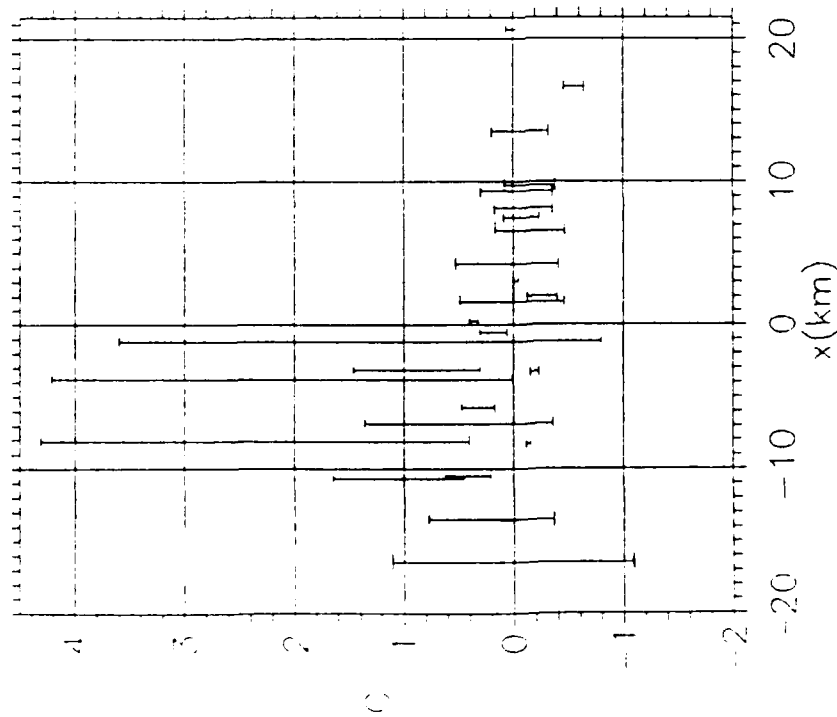


Fig. 23. Boundary layer clocking, C , and speedup, S , across the stratus front. Vertical lines are maximum to minimum span for a given location based on 5 min averages.

advection or rate change contributions. If we invert his results, we find that,

$$dU_g/dz = dU/dz - (fZ_i/w^*)dV/dz, \quad (8.2)$$

$$dV_g/dz = (fZ_i/w^*)dU/dz + dV/dz, \quad (8.3)$$

$$\text{with } dU_g/dz = (-g/fT)dT/dy, \quad (8.4)$$

$$\text{and } dV_g/dz = (g/fT)dT/dx, \quad (8.5)$$

where the geostrophic wind shear is defined within the boundary layer. U and V are aligned with the mean wind, ergo dU/dz and dV/dz are simply dimensional forms of our clocking and speedup parameters. fZ_i/w^* is the ratio of the convective to Coriolis time scales. This ratio was on the order of .1 for all 4 transects. The main disadvantage in using Wyngaard's solution for this study is assuming steady state. Therefore, results can only be considered qualitative.

Fig. 24 plots the horizontal temperature gradients derived from eq. 8.5 for transect C, and for the composite data set. Because of the low values of fZ_i/w^* , the horizontal temperature gradients mirror the clocking and speedup parameters to a large degree. On average, the temperature gradients are both positive, as expected. As with the clocking parameter there is an average enhancement in dT/dx on

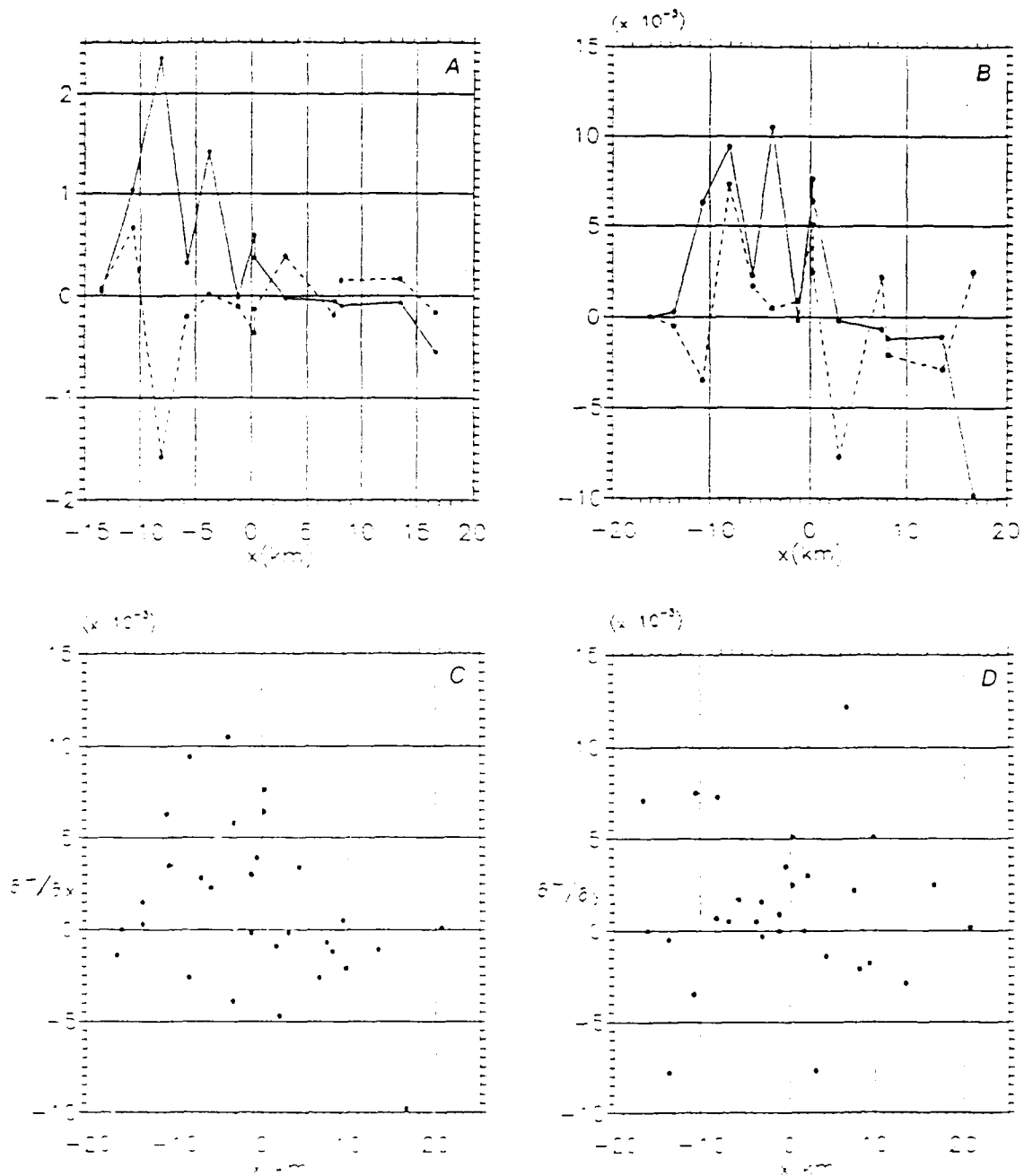


Fig. 24. a) Clocking (solid line), and speedup, (dashed) for transect C. b) Horizontal temperature gradient for transect C where dT/dx is solid and dT/dy is dashed. c,d) Horizontal temperature gradients for composite data set.

the cold side of the front. An eyeball average of the points on the cloudy side would give an "effective" boundary layer temperature gradient of $0.06 \text{ deg C} \cdot \text{km}^{-1}$ on the cold side of the front. There is an indication that once past the front, dT/dx may be slightly negative. There is too much scatter in dT/dy to discern a trend.

The main difficulty with this explanation of the wind shear lies in the position of the wind shear relative to the edge. We are presently in the process of using a numerical model to simulate the cloud edge effect, and preliminary results indicate the region of maximum vertical directional wind shear should occur within the first few kilometers on the sunny side of the front, i.e. in the region of maximum baroclinicity. This placement of the baroclinic zone has been supported by our surface temperature measurements. With regards to wind shear, these results are contrary to our findings, and we are currently examining other mechanisms for the observed wind shear under the clouds.

IX. PREDICTION OF BOUNDARY LAYER HEIGHTS

IX.1 INTRODUCTION

Inversion height is a key factor in diffusion as well as general boundary layer behavior. However, in VBG's complex terrain, inversion height estimates remain very problematic. The simple inversion rise models of Zeman and Tennekes (1977), Venkatram (1977), or Kamada (1988) do not apply here because they depend on horizontally homogeneous terrain or a single land/water interface. Fully non-linear, 3-D, non-hydrostatic, prognostic windflow modeling is a remedy which is years from operational use. Meanwhile, for convenience, some diagnostic flow/diffusion models assume that atmospheric boundary layer (ABL) inversions are either flat or terrain parallel. Though this may set the range across daytime and nocturnal conditions, we wondered whether stability or other measures could improve on such estimates. Thus, we developed five simple inversion height algorithms of the terrain following type and compared them with daytime data from the three VBG DASSes (SODARs) and our own mobile SODAR.

IX.2 DESCRIPTION OF METHODS

All five inversion height methods start with the same objective analysis based on data from the fixed VBG SODARs. The methods are: 1) a pure objective analysis which yields an inversion height estimate, Z_i , 2) a fixed but optimized "terrain-followingness" coefficient, C , such that the local

inversion height, $Z_i = Z_{i0} + hC$, where h is terrain height above sea level and Z_{i0} is a reference inversion height taken from a sodar or high resolution sonde (Endlich, 1984), 3) a C varying with a supra-ABL inversion stability parameter, (Z_{i0}/G_1) , where G_1 refers to the lapse rate within the capping/marine subsidence inversion, 4) a C varying with bulk ABL stability, Z_{i0}/L , where L is Obukhov length, and 5) a force balance criterion, w/N , (where w is the vertical velocity component of the local wind speed and N is the Brunt-Vaisala frequency). In 5) inversion displacement is determined by a balance between w along the nearest upwind slope and the overall supra-ABL stability. Sondes and/or towers are needed in addition to SODAR data to implement schemes 3) - 5).

The objective analysis employed the usual inverse distance square method,

$$Z_{io}(x, y) = \frac{\sum_{k=1}^n \frac{Z_{io,k}}{\sum_{j=1}^n \frac{R_{ij}^2}{R_{ij}^2}}}{\sum_{k=1}^n \frac{1}{\sum_{j=1}^n \frac{R_{ij}^2}{R_{ij}^2}}} \quad (9.1)$$

However, the distance, $r_i = \sqrt{(x - x_i)^2 + (y - y_i)^2}$, was modified by the aspect ratio, A^2 , of the local terrain height contours surrounding each SODAR site, so that

$$R_i = (A - ((A^2 - 1)/A) \sin \theta) r_i \quad (9.2)$$

where θ is the angle of the minor aspect with respect to the site direction. In effect this "ovalizes" each SODAR's

circle of influence according to the terrain.

Methods 3 and 4 invoke ad hoc expressions with empirical coefficients. The idea in method 3 is that small values of Z_i / G_o less than 1000 indicate a low, stable, nocturnal ABL. Strong stability tends to suppress the vertical mixing needed to couple the surface momentum stress and heat fluxes to the rest of the ABL. Thus, the contour of the top of the stable ABL has less tendency to follow the underlying terrain. On the other hand, higher values suggest a range from convective, clear ABLs with $C \sim 0.6 - 1.2$, down to low, quiescent, likely stratus covered ABLs with C less than 0.6. With the caveat that our data did not include stable cases, we still found by inspecting an array of values that optimal correlations resulted for method 3 from the simple form (see fig.25),

$$Z_i = Z_o + (\log(Z_i / G_o) / a_3 - b_3) h_3, \quad (9.3)$$

where $a_3 = 3.0$, and $b_3 = 0.4$.

Similarly, method 4 assumes that C is large when the bulk ABL stability parameter, Z_i / L_o , is negative and small when positive. Under convective conditions ($L < 0$), Z_i is strongly influenced by local thermals which mix ABL air into the capping inversion aloft. As convection increases, the thermals assume large vertical/horizontal aspect ratios. Figure 26 suggests that near zero (neutral conditions) we expect C to drop rapidly through the range, 0.7 to 0.3. Since kL (where $k \sim 0.4$ is von Karman's constant) defines the height from the surface at which momentum flux drops below

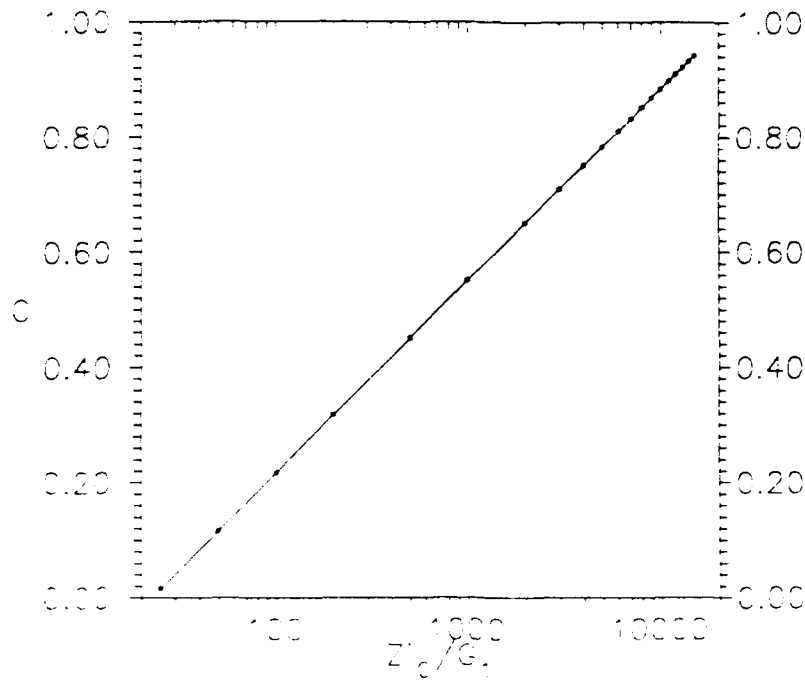


Fig. 25 Assumed behavior of C in method 3 using the supra-ABL stability parameter, Z_i/G .

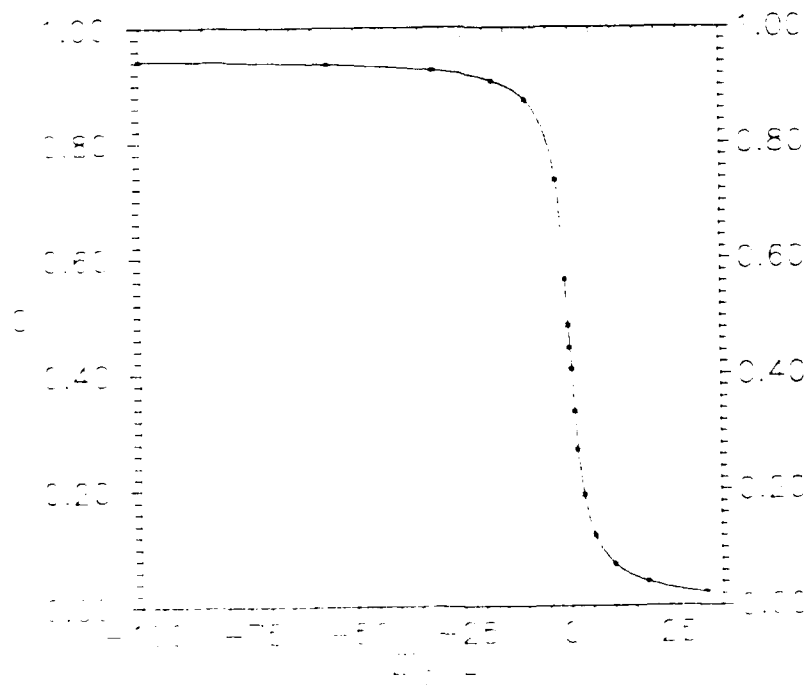


Fig. 26 Assumed behavior of C in method 4 using the bulk ABL stability parameter, Z_i/L .

the heat flux, method 4 argues that local surface fluxes also influence inversion contours.

The modeling expression must be necessarily somewhat complex because of the assumed sigmoid nature of the curve. Thus, we used,

$$Z_i = Z_{i_o} + a_4 - (b_4/\pi) \tan^{-1} (d_4 + e_4 * Z_{i_o}/L) , \quad (9.4)$$

where $a_4 = 0.475$, $b_4 = 0.95$, $d_4 = 0.1$, and $e_4 = 0.4$.

By contrast method 3 argues that inversion strength has more bearing on terrain followingness than surface condition. However, Z_{i_o}/L correlates with inversion strength. Highly negative values suggest moderate capping inversions, near zero values suggest stronger inversions, and highly positive values indicate a strong surface based inversion. However, method 4, has the advantage that it can be assessed with surface towers and a non-local SODAR or rawinsonde.

Although we do not have enough data to confirm the following effect, method 4 also may mimic an effect often seen in the lee of Tranquillon Ridge. The ridge rises east from Pt. Arguello to an average height of ~ 350m, while the strong regional subsidence inversion typically caps the mixed layer at heights of 400-600m. With this geometry, moderate winds will cause a leeside bora jet which draws down the inversion. The enhanced stress will drastically increase L and cause C to drop quickly, resulting in a lowered inversion. Of course, the method cannot model the downwind hydraulic jump which occurs at higher speeds.

Method 5 assumes a force balance similar to the critical streamline idea (see Hunt et al. 1979), except that this method does not require stable flow. That is, the vertical component of the bulk ABL wind, U , as it moves upslope from low-lying terrain, is assumed to be $w = U \sin \phi$, where ϕ is the nearest upstream slope angle. Meanwhile, the incurred negative buoyancy opposes the ABL's vertical motion. Thus, assuming zero acceleration, hydrostaticity, and constant lapse rate, the force balance is roughly,

$$w \frac{dw}{dz} = g \frac{\Delta \theta}{T_o} \quad (9.5)$$

If we assume that the bulk ABL vertical velocity reaches zero at an inversion deformation height, Δz , then integration leads immediately to

$$\Delta z = w \left(\frac{T_o}{g G_o} \right) = w/N \quad (9.6)$$

Here, we picture the rising ABL as lifting rather than penetrating the air mass above. Hence, unlike method 3, G_o^2 refers here to the bulk lapse rate of the entire layer above the ABL. In this way, method 5 combines a local dynamical measure, $U \sin \phi$, with the horizontally more extensive, G_o^2 . This mimics 3-D modeling results from Han et al. (1982) which show that the height and shape of the ABL in complex terrain depends on wind direction.

Methods 4 and 5 are also qualitatively consistent with changes expected across the chronic, local, stratus front discussed in section VIII. That is, the mild instability under stratus increases dramatically near the front, allowing

the inversion to become more terrain following, as in method 4. The local pressure gradient caused by the surface heating difference also induces a speedup reflected in method 5.

IX.3 CORRELATION ANALYSIS

Correlation coefficient, r , normalized root mean square error, RMSE, normalized mean bias, MB, and a confidence interval of \pm two standard deviations were used to optimize and compare our estimates with results from our mobile SODAR data. Normally, the sonic anemometer is used for heat flux and stress values. However, sonic readings were unreliable during some periods, due to baseline drift. Yet, we could still assume free convection for the mid-to-lower SODAR range gates. As discussed above, heat flux and thus L was estimated from the SODAR returns during those instances.

As shown in Table 1, each method improves on objective analysis by statistically significant increments (> 2 sigma confidence interval), with method 2 (terrain parallel) and method 3 (supra-ABL stability) correlating best with mobile sodar data. Method 4 (bulk ABL stability) lags slightly, but the difference is statistically insignificant. This may be due partly to the limited sample size (600 points) and the unavoidable degradation of the SODAR returns under a chronic stratus deck as indicated by the RMSEs. This points to the fact that though longer sampling times would have helped stabilize L , this would further limit the sample size as well as terrain coverage. Data noise probably also limited the

total r values. The small positive mean bias which remained after calibration between mobile and fixed sodars may stem from instrumentation differences or possibly shadowgraph interpretation differences. However, recalibration by the apparent bias invariably tended to degrade correlations.

METHOD	r	MB	+/-2 σ	RMSE
1) $Z_i + \frac{h^2}{Z_i}$ (based on $1/r$ obj. analysis)	.360	.078	.074	.422
2) $Z_i + h$.711	.140	.043	.397
3) $Z_i + [\log(Z_i/G) / 3 - .4]h$.711	.139	.043	.393
4) $Z_i + [.475 - (.95/\pi) * \tan^{-1}(0.1 + 0.4*(Z_i/L))]h$.702	.140	.050	.404
5) $Z_i + w/N$.503	.096	.064	.420

Table 1. Statistical Comparison of five terrain following inversion height algorithms.

Individual statistics were obtained for each fixed SODAR and for all possible combinations. However, those presented above are based on just the two northern SODARs 1 and 2. Correlations were significantly lower when SODAR 3 (located at the tip of Pt. Arguello) was included. This and results from previous studies (Kamada et al. 1989) suggest that very local dynamics operate at this site. For example, we find that the presence of Tranquillon Ridge tends to channel the typically northwesterly flow, causing high inversions and

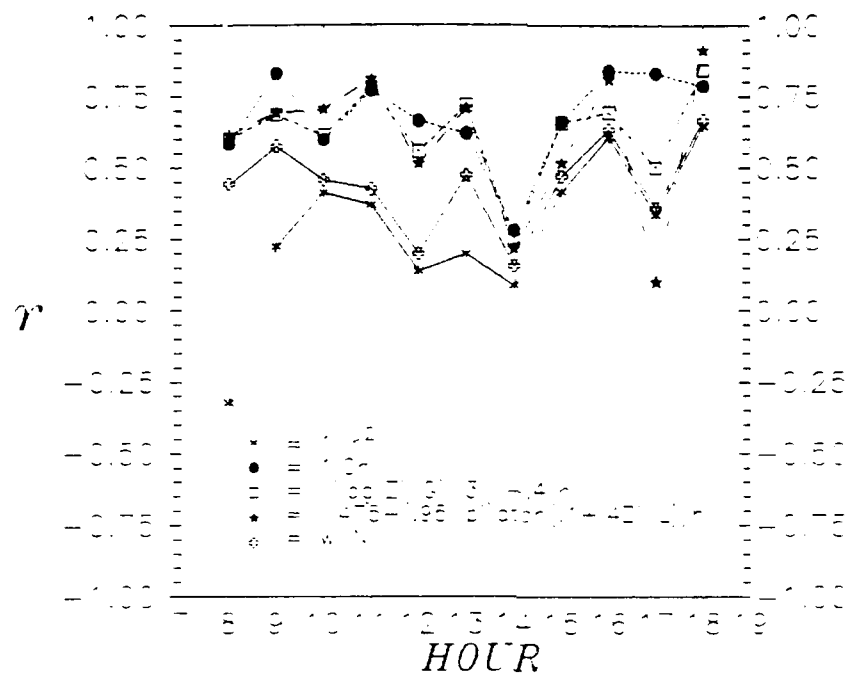


Fig. 27 Hourly correlation coefficients for the five methods

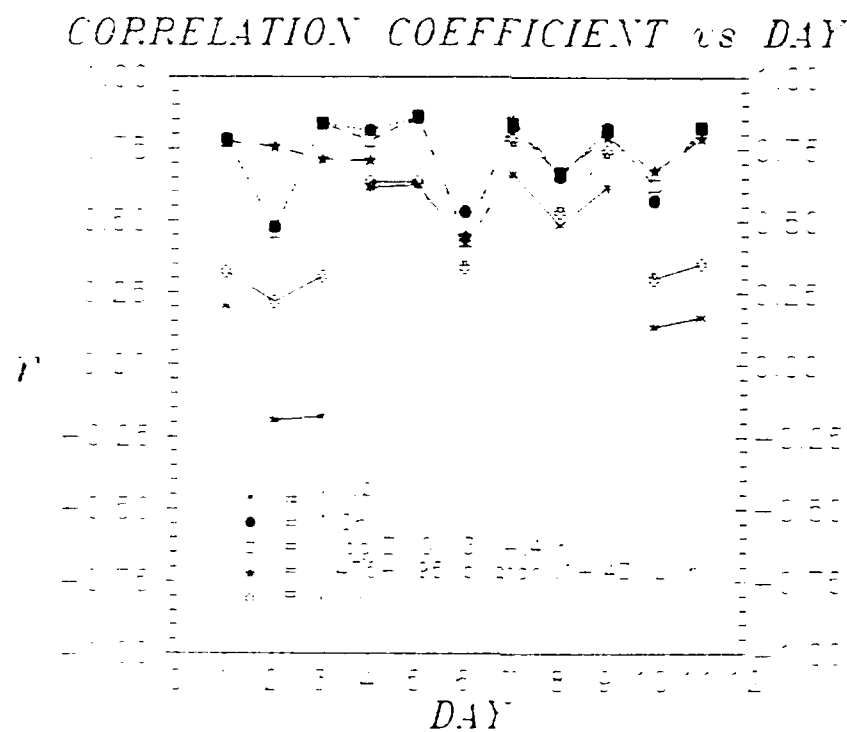


Fig. 28 Daily correlation coefficients for the five methods

chronically northerly winds over the SODAR site.

The diurnal and daily correlations in figs. 27 and 28 show that the algorithms generally improve upon the objectively analyzed estimates. In fact very large improvements over objective analysis occurred during morning hours, while the objective analysis scores rise in the later afternoon to close the gap. The mobile sodar began most morning transects from the Ocean Park site at the mouth of the Lompoc Valley near sea level, while the two sites serving as a basis for the objective analysis were situated to the north and south at elevations of 100 and 112m, respectively. Thus, the terrain height difference, together with funneling into the mouth of the valley, may have caused the anti-correlation with objective analysis seen in hour 8. While many morning measurements were taken within 10km of the coastal SODAR, we tended to visit some of the more distant inland sites around mid-day. This may explain why the objective analysis scores are low during this period. It is promising to note that the other methods maintain improved scores during this period.

Methods 2, 3, and 5 show significant improvements over objective analysis at all hours, while relative scores vary more with method 4, due to local variations in L. Method 5 appears generally less adept, though still a significant improvement over objective analysis. In judging method 5, note that it is the only method which was not data tuned, since it is a physical rather than semi-ad hoc expression.

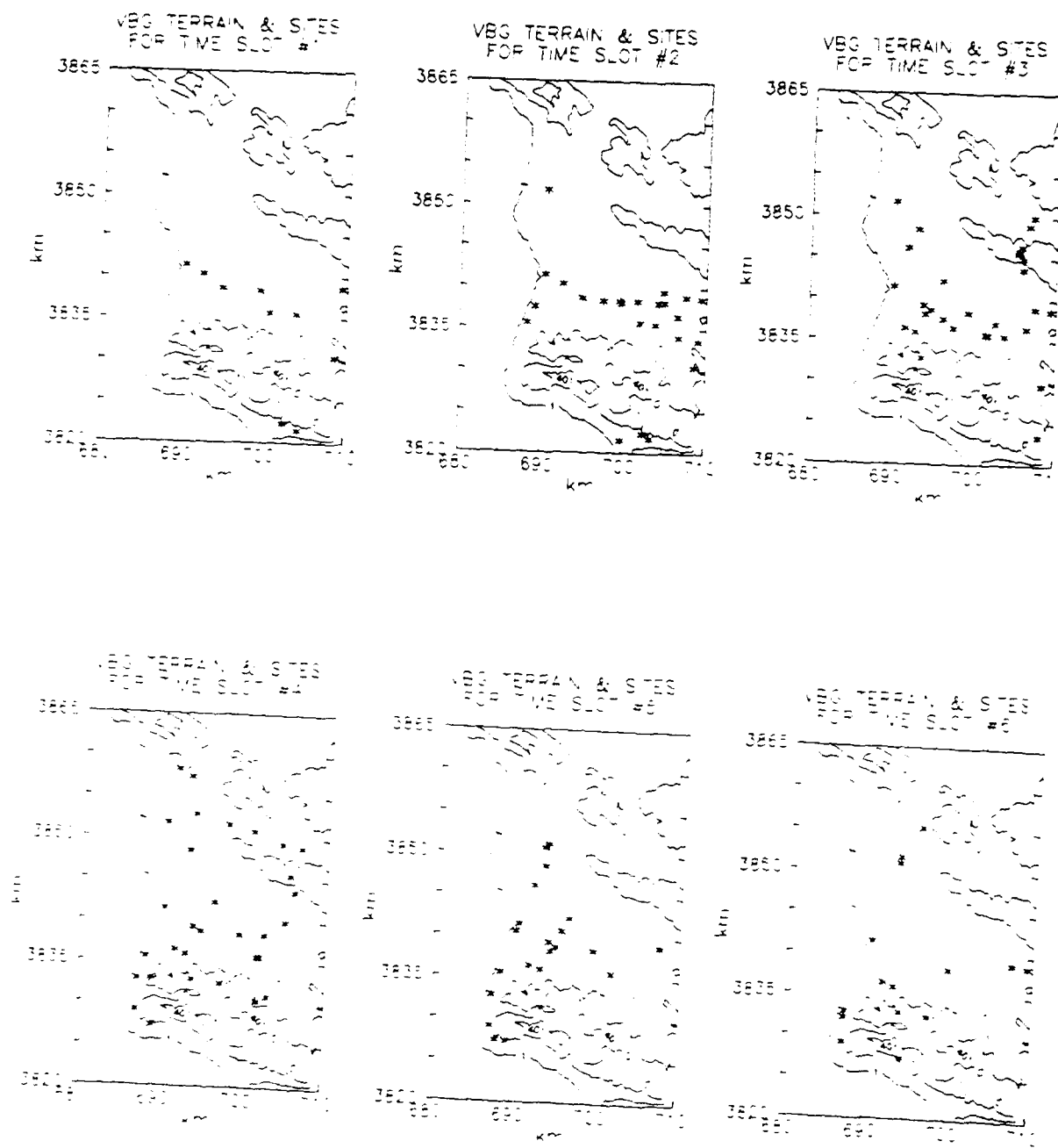
Figure 28 shows on a daily basis that the algorithms

outperform pure objective analysis, except for method 5 on day 6 of the July period. We note that the synoptic situation for days 2 and 3 was complex, with easterlies during the pre-seabreeze period and northerlies ~ 10:00. On day 3 the usual mid-morning westerly seabreeze did not appear until 13:00. Meanwhile, mid-day southwesterlies were seen at the mouth of the valley. This suggests that the seabreeze gradually overcame a strong opposing easterly. Opposing easterlies tend to drive inland advected marine inversions toward the surface, as seen in the day 3 SODAR and rawinsonde data. Certainly, objective analysis from the near-coastal SODARs cannot diagnose this condition. Thus, it is significant to note that the simple algorithms in methods 2 - 4 maintain reasonable data correlations during this period. Again, in the day by day comparison, methods 2, 3, and 4 appear quite competitive overall and statistically indistinguishable, while method 5 clearly lags the others.

IX.4 ABL HEIGHT CONTOURS

As a different comparison method, inversion height patterns were determined by normalizing heights and grouping data within an initial pre-seabreeze period and five later, equi-spaced segments of "seabreeze time". Hence, period 2 begins as mean coastal winds exceeded 2 m/s, while period 6 ends at 19:30, shortly following the last van records.

Unlike seabreeze initiation, the 19:30 cutoff is simply arbitrary but convenient, since the wind data do not show a temporally distinct seabreeze cutoff. Within each period, we normalized heights by the coastal SODAR 2 height multiplied by

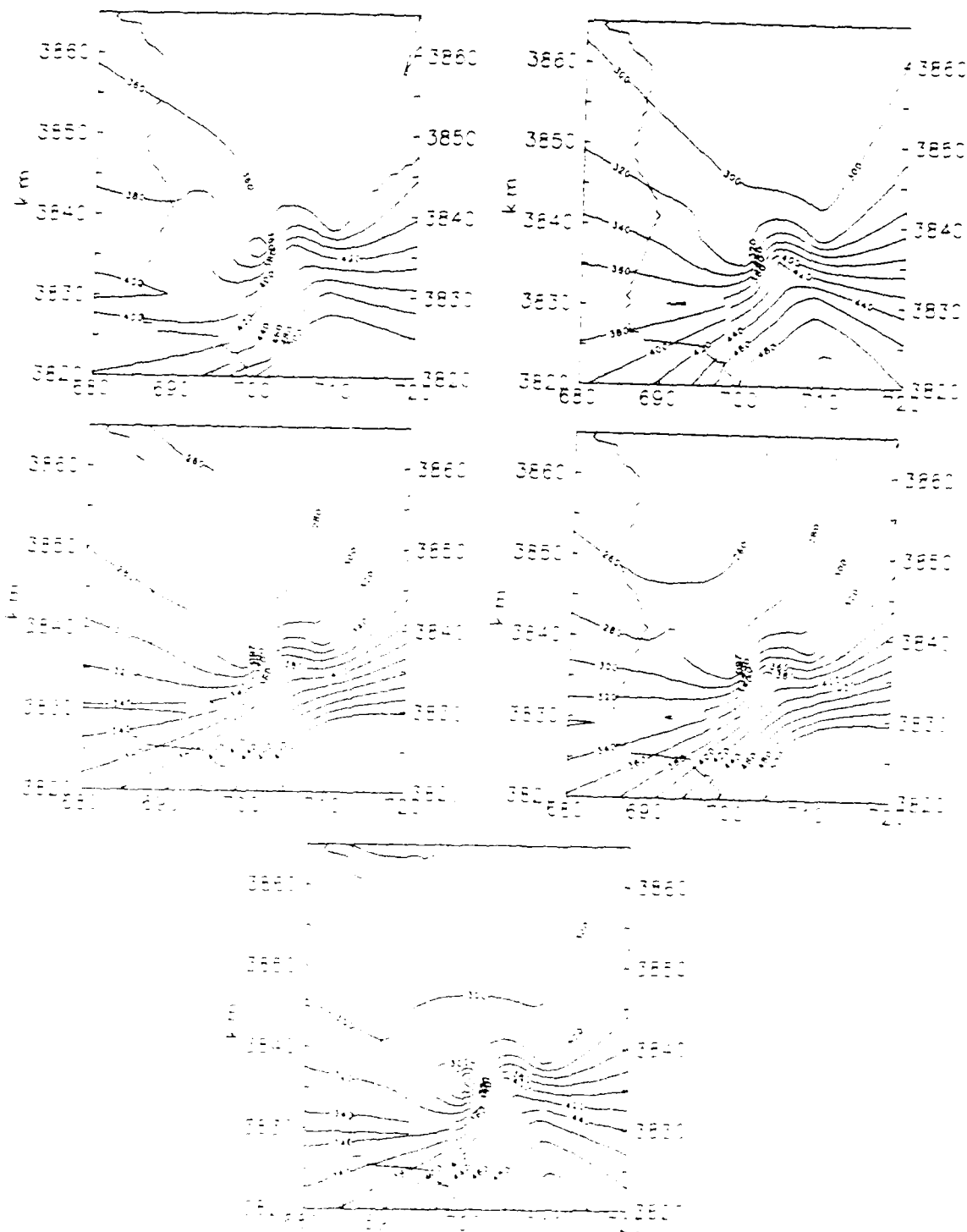


Figs. 29a - e. Terrain map and sampling sites during seabreeze periods 1 - 6. Contours in meters msl.

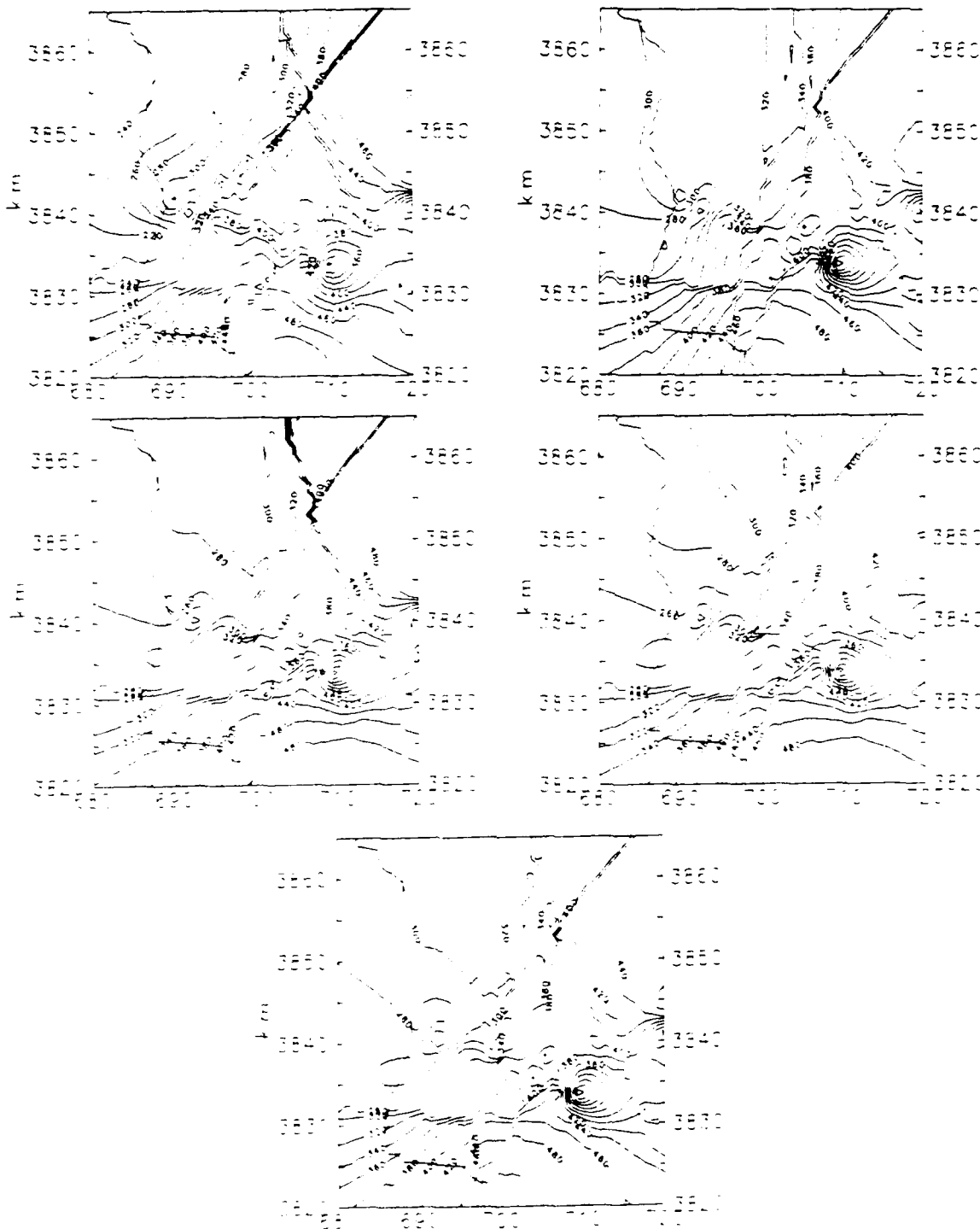
the period averaged SODAR 2 height. We also period averaged all co-located values. However, the spatial sampling density was probably insufficient to validly interpret the resulting contours as typical of the domain. Yet, since estimates were computed for the same times and locations as the mobile SODAR sites, they may be used to compare different methods with data. Figures, 29a - e, show the mobile SODAR sampling sites during seabreeze periods 1 - 6.

In figs. 30 - 35 we have omitted the expectedly dull contours derived from objective analysis. However, the figures displayed do show that methods 2 - 5 retain the general features suggested in the data. However, method 4 (bulk ABL stability) sometimes seems to add new features or markedly accentuate existing ones. It manages to retain a fairly high correlation by also capturing smaller existing features more often than the other methods. Conversely, method 5 (force balance) tends to mildly dampen existing features, but otherwise does general patterns surprisingly well. The strictly terrain parallel method 2 appears to coincide very slightly better with the data than the other methods. However, we cannot say that it is clearly superior.

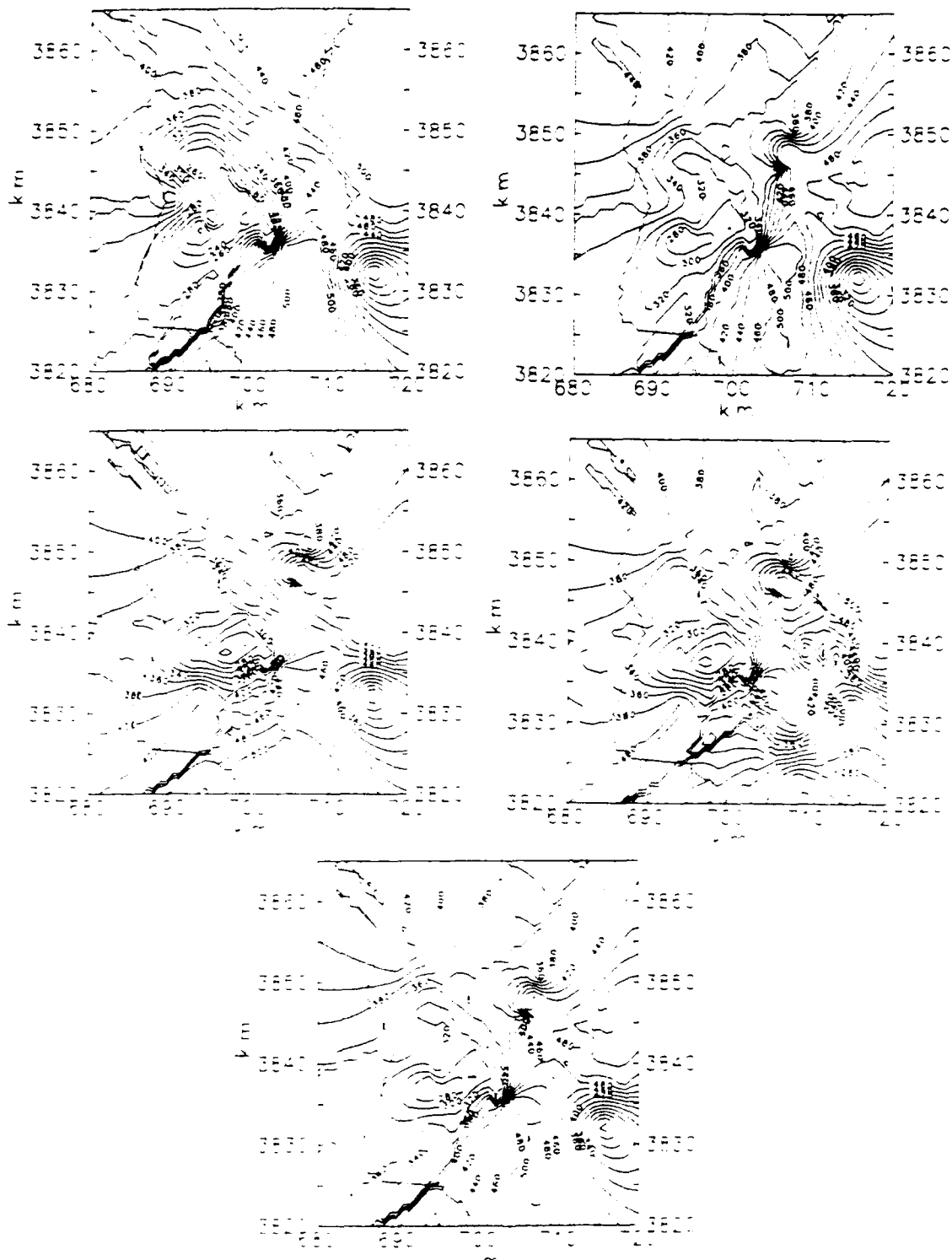
Without regarding the displayed smaller scale features too seriously, we note that the data based figures: 30a - 35a, together show some generally characteristic features. 1) The northwest to southeast inversion height gradient, apparently indicated during the pre-seabreeze period, gradually reverses itself over the course of the day to a



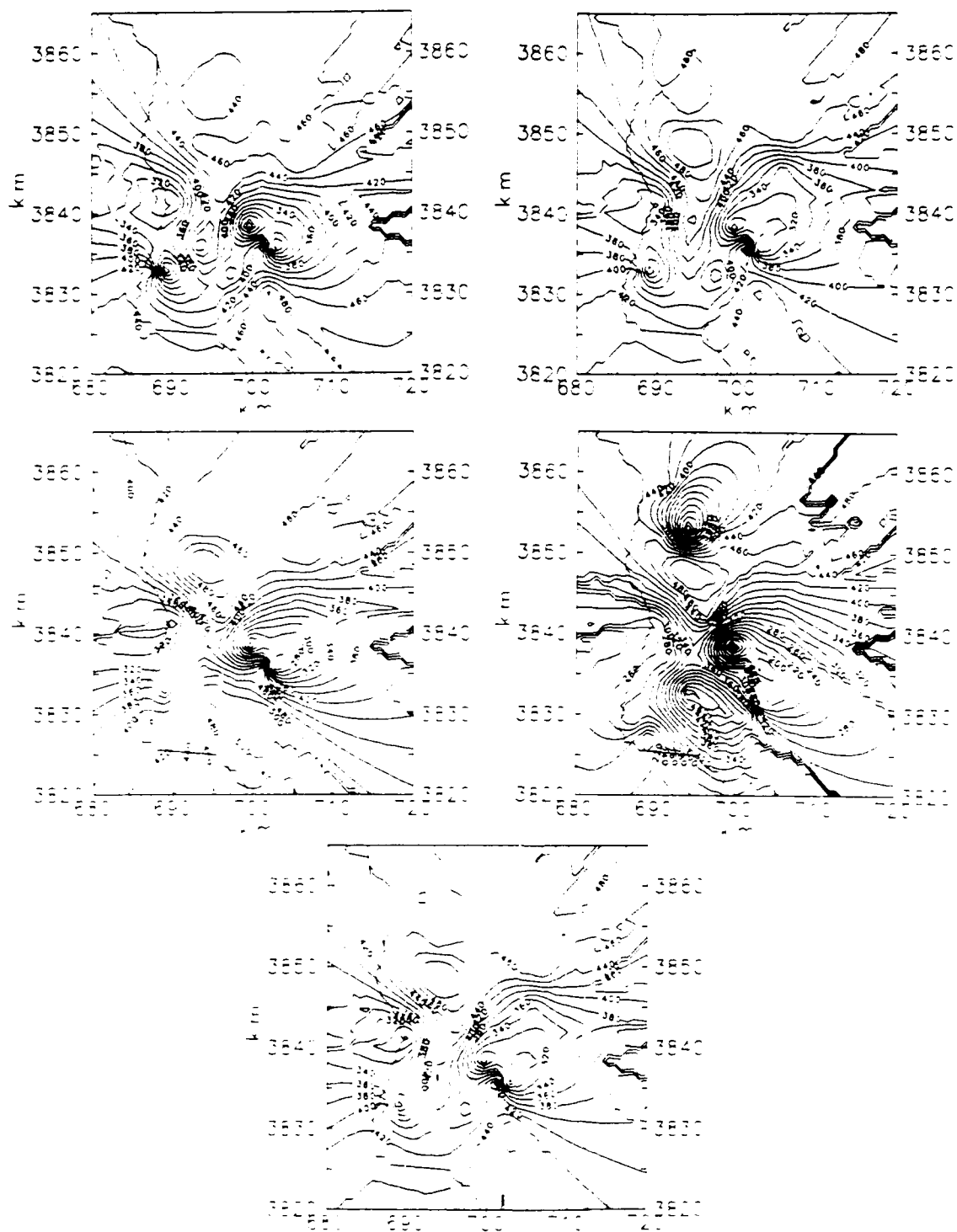
Figs. 30a - e. Sample inversion height contours (in meters msl) during pre-seabreeze period 1, from mobile + fixed SODAR data and also from methods 2 - 5 (plus fixed SODAR data). Order is left to right and top to bottom:



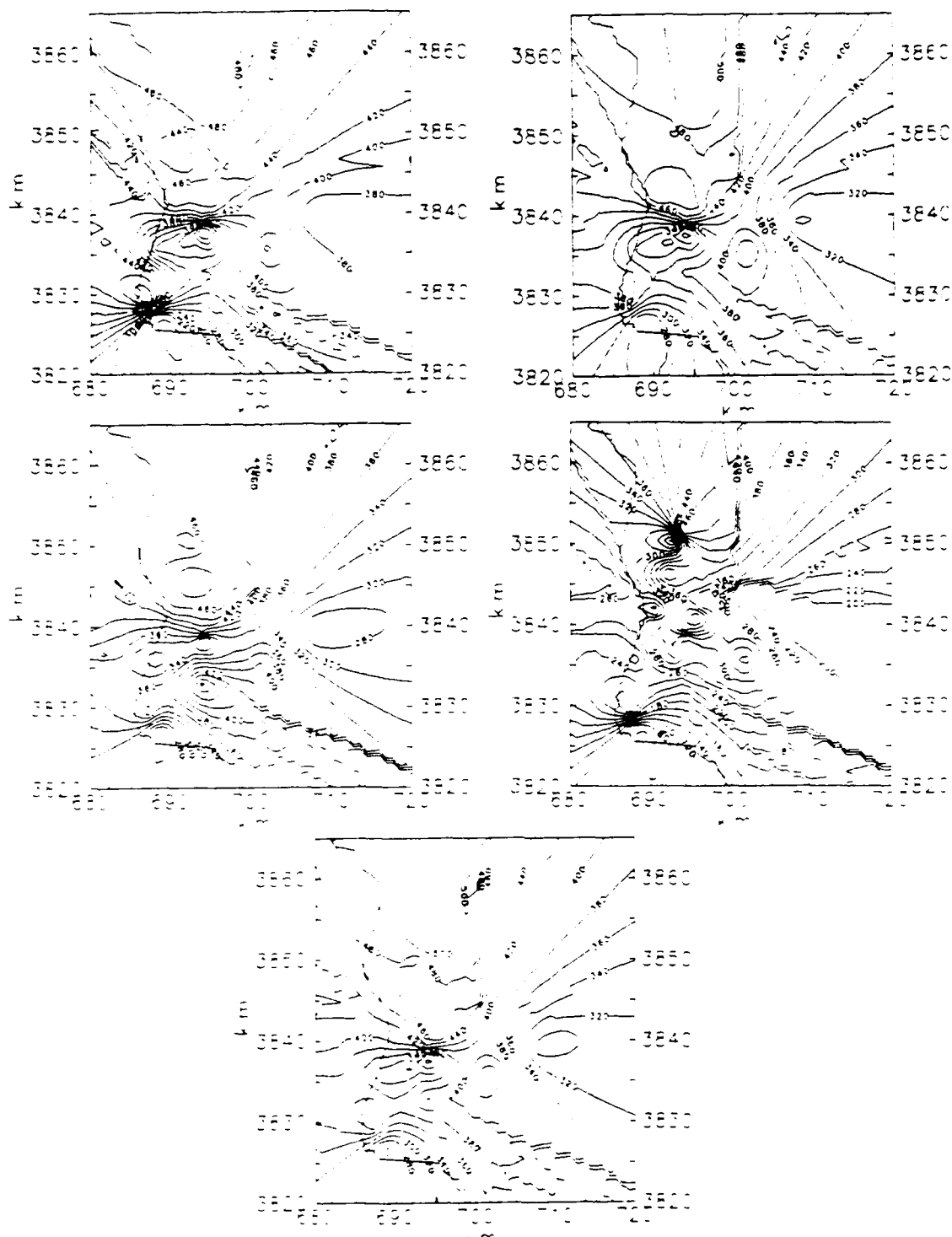
Figs. 31a - e. Sample inversion height contours (in meters msl) during seabreeze period 2, from mobile + fixed SODAR data and also from methods 2 - 5 (plus fixed SODAR data). Order is left to right and top to bottom:



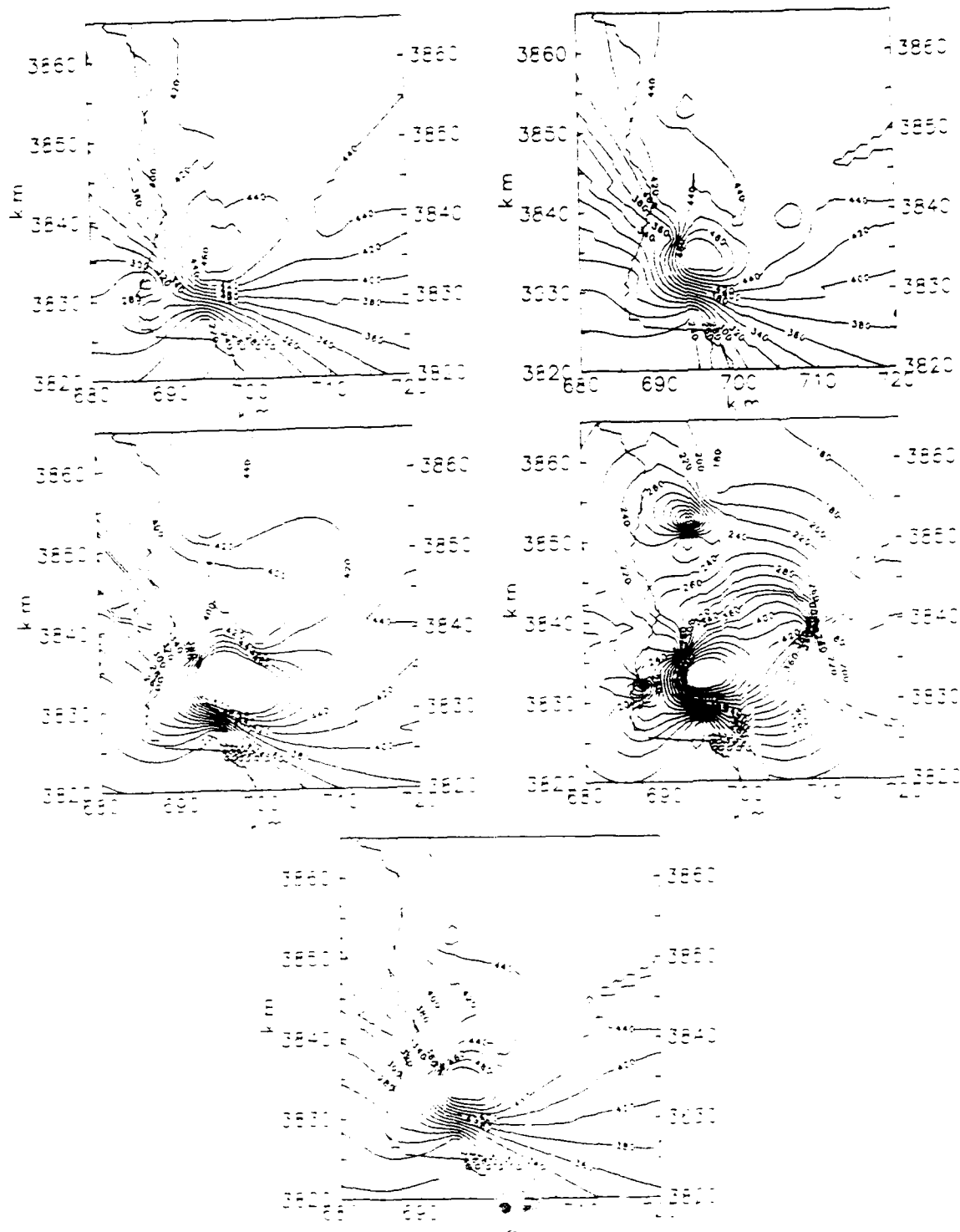
Figs. 32a - e. Sample inversion height contours (in meters msl) during seabreeze period 3, from mobile + fixed SODAR data and also from methods 2 - 5 (plus fixed SODAR data). Order is left to right and top to bottom:



Figs. 33a - e. Sample inversion height contours (in meters msl) during seabreeze period 4, from mobile + fixed SODAR data and also from methods 2 - 5 (plus fixed SODAR data). Order is left to right and top to bottom:



Figs. 34a - e. Sample inversion height contours (in meters msl) during seabreeze period 5, from mobile + fixed SODAR data and also from methods 2 - 5 (plus fixed SODAR data). Order is left to right and top to bottom:



Figs. 35a - e. Sample inversion height contours (in meters msl) during seabreeze period 6, from mobile + fixed SODAR data and also from methods 2 - 5 (plus fixed SODAR data). Order is left to right and top to bottom:

southwest to northeast gradient. Preliminary larger scale (200km x 200km) modeling by Yamada and Bunker (personal communication) also shows this afternoon gradient, presumably due to strong upslope flow toward the high Sierra Madre ridge northeast of Vandenberg. Kamada and Mikkelsen's (1990) analytical results show in general that the magnitude of thermal forcing increases with the square of the horizontal scale. Thus, the presence of the Sierra Madre ridge (in excess of 100km from Vandenberg) causes the local flow to be very much a mixture of seabreeze and upslope forcings. However, for convenience we will continue to refer to the local circulation as the seabreeze.

2) The strong initial west to east gradient undergoes a mild reversal in period 5. This coincides with suggestions, seen in periods 2 - 4, of an inland moving subsidence zone which trails the seabreeze front. By period 6 the inland heating has ended and this effect disappears. 3) As expected, much more structure appears during the strong inland heating periods, 2 - 5, than in periods 1 or 6. This may indicate local, terrain/coastline altered, convergence/subsidence zones. However, it may also be an artifact of the sparsity of data during the pre- and late seabreeze periods.

X. CONCLUSIONS

The VBLS series of experiments resulted in a set of surface and boundary layer measurements which can be used to initialize or validate both operational and research oriented flow and diffusion models for VBG. The data covers a fairly wide range of sea breeze dominated conditions; 3 seasons with strong to negligible synoptic influence, southwest to northwest mean flow directions, and total to nonexistent stratus cover.

Rawinsonde comparisons showed that 0 and 12 Z ascents do an adequate job of observing winds between the boundary layer top and 2000 m, since changes occur on a longer than diurnal time scale. Estimation of the boundary layer height from rawinsonde thermodynamic profiles is very location dependent, and sometimes misleading.

Characteristic VBG DASS shadowgraphs were discussed in terms of interpreting boundary layer heights and observed wind profiles. Stratus cover or the presence of a TMIBL can make selection of a boundary layer height difficult.

It is preferable to use DASS shadowgraphs and wind profiles in concert with rawinsonde data when estimating boundary layer

heights for input to flow or diffusion models. We suggest the following technique:

- a) correlate the latest rawinsonde thermodynamic profile with the local DASS shadowgraph. Identify the echo feature which best represents the mixing layer using the guidelines suggested in section VI.
- b) If possible, trace that echo feature to the current time. If the feature is not traceable, evaluate the current shadowgraph using knowledge of changes in stratus cover, ground fog, surface inversions, or boundary layer winds.

The VBG region was divided into 4 regions of grossly similar terrain. Traditional roughness lengths which depended primarily upon the surface cover for each region were determined. Heat flux was shown to be primarily a function of the solar insolation and an empirical formula was proposed. For flow or diffusion model input, we strongly suggest basing heat flux on measurements of solar insolation as opposed to tower temperature differences. This would require added pyranometers at both coastal and inland sites due to the strong dependence on stratus cover. Estimates of the absorption characteristics of the ground could be parameterized.

Wind speed and directional variability were shown to be a function of region. The wind direction variability across North Base and the Lompoc Valley was similar to the variability measured by the VBG base tower network. Variability was greater in the South Base and East Hills. Wind speeds were similar in all regions except the Lompoc Valley, where they were roughly 50% higher. For medium range (5-50 km) diffusion, we suggest using the spatial variability between towers as a measure of the "hazardous corridor" instead of the local (release site) standard deviation of the surface wind direction. This corridor could be adjusted based on knowledge of the region in which the plume is travelling.

Vertical wind shears of speed and direction were not a function of region. The degree of shear was not normally distributed. Even though the distribution of directional shear was very similar to the speed, they were not strongly correlated to each other. There was correlation with boundary layer wind direction difference (from the base average), and the local measure of roughness length.

On average, vertical boundary layer turbulence was generally similar to that predicted for the flat terrain case in the North and South Base regions, but there was a large amount of scatter. Unexpectedly, vertical turbulence in the Lompoc Valley and East Hills was less than flat terrain

predictions. For daytime medium range diffusion model applications, we suggest basing turbulence intensities of DASS measurements of vertical turbulence through the middle part of the boundary layer. We also suggest installing at least one DASS at a sunny inland location.

A boundary layer drag coefficient was defined which could be used for predicting boundary layer average wind speeds above a surface observation.

A variety of boundary layer height parameterizations were examined. All cases showed the importance of including terrain height in the formulation. A technique using the bulk boundary layer stability was found to be marginally superior, and can be applied at VBG with current meteorological information and terrain information.

Measurements of the transition in the atmospheric boundary layer during flow from a stratus covered ABL to clear sky conditions indicate that a rapid increase in boundary layer height occurs on the sunny side of the boundary which may be accompanied by a decrease on the cloudy side. A simple TMIBL rise model does not account for the sudden growth near the stratus transition. It appears that mass adjustments occur which are consistent with baroclinicity within the boundary layer. A trend from veered to backed mean boundary layer wind direction occurs as the front is transected from cold to warm.

Acceleration occurs in the vicinity of the front, but its location relative to the front is variable. Measurements of the vertical wind shear are also consistent with Wyngaard's theory of the unmixed nature of the boundary layer in the presence of a baroclinic zone, but the placement of this zone is contradicted by surface temperature measurements and modeling results. Based on these effects and the dramatic influence of stratus on heat flux (and therefore boundary layer turbulence), more research should be directed toward cloud edge effects. Realistic diffusion models should include the stratus edge as a required input and adjust flow and diffusion accordingly.

The inversion height prediction methods examined here under sea breeze conditions all show strong correlations with data. Though an objective analysis based solely on the two coastal SODARs was included in each method, the more complex methods all earn correlation scores distinctly superior to pure objective analysis. The small correlation differences among methods 2 - 4 are not statistically significant, while method 5 appears clearly inferior. Methods 2 - 4 maintained fairly high correlations with the mobile SODAR measurements, even when their objectively analyzed components exhibited relatively poor correlations during inland excursions and one period of unusual flow. From these preliminary results, it seems that the simple terrain parallel assumption in method 2 is at least as suitable as more complex assumptions during

non-winter daytime hours for the Vandenberg region. The pattern recognition involved in the contour comparison technique also shows a slight advantage with method 2. Moreover, we find that method 5 retains a fair degree of coincidence, while method 4 tends to accentuate existing features or even introduce new ones. Thus, we suggest that the simpler methods, 2 or 3, be employed in diagnostic flow models.

In general, the terrain followingness coefficient methods simply alter some reference Z_i measurement. This allows for the possibility of some improvement in the inversion height diagnosis by capturing a portion of the Eulerian time change. That is, in lieu of a coeval upwind measurement, we could use an upwind measurement lagged backward in time by an amount equal to the distance to the site of interest, divided by the mean local wind speed. We would then assume that the Lagrangian advective changes were included in the alterations used in methods such as 4 and 5. In this vein, Method 4 can also be refined slightly to account for downstream stability changes. If we assume that changes in L affect the inversion within a convective turnover time of kZ_i/w , then Z_i will change at a downwind distance, kUZ_i/w . Previous analytic work (Kamada, 1988) suggests that the minimum velocity for an entraining eddy is $\sim 2w$. This implies a $k \sim 0.5$. Hence, for typical convective ABL values,

the site measurements required to implement method 4 should really be applied to downwind distances on the order of 1km.

XI. BIBLIOGRAPHY

- Endlich, R.M., 1984: Wind Energy Estimates by Use of a Diagnostic Model. *Bound.-Layer Meteor.*, **30**, 375-386.
- Finkelstein, P.L., J.C. Kaimal, J.E. Gaynor, M.E. Graves, and T.J. Lockhart, 1986: Comparison of Wind Monitoring Systems. Part II: Doppler Sodars. *J. Atmos. and Ocean. Tech.*, **3**, 594-604.
- Garratt, J.R., 1977: Review of Drag Coefficients over Oceans and Continents. *Mon. Wea. Rev.*, **105**, 915-929.
- Han, Y.J., Ueyoshi, K., and Deardorff, J.W., 1980: Numerical Study of Terrain-Induced Mesoscale Motions in a Mixed Layer. *J. Atmos. Sci.*, **39**, 2464-2476.
- Hojstrup, J., 1982: Velocity Spectra in the Unstable Boundary Layer. *J. Atmos. Sci.*, **39**, 2239-2248.
- Hunt, J.C.R., Britter, R.E., Puttock, J.S., 1979: Mathematical Models of Dispersion of Air Pollution around Buildings and Hills. *Mathematical Modeling of Turbulent Diffusion in the Environment*, Academic Press, New York, 145-200.
- Kaimal, J.C., D.A. Haugen, O.R. Cote, S.J. Caughey, and C.J. Readings, 1976: Turbulence Structure of the Convective Boundary Layer. *J. Atmos. Sci.*, **33**, 2152-2169.
- Kamada, R.F., 1988: A Fractal Interfacial Entrainment Model for Dry Convective Boundary Layers. Part I: Model Description. *J. Atmos. Sci.*, **45**, 2365-2374.
- Kamada, R.F., C.E. Skupniewicz, J.W. Glendening, G.E. Schacher, T. Mikkelsen, S.T. Nielsen, I. Troen, S. Larsen, E. Takle, L. Ly, and J. Griffin, 1989: Vandenberg Meteorology and Plume Dispersion Handbook for Boundary Layer Releases. Naval Postgraduate School Technical Report, NPS61-89-004, 450 pp.
- Mizzi, A.P., and R.A. Pielke, 1984: A Numerical Study of the Mesoscale Atmospheric Circulation Observed During a Coastal Upwelling Event on August 23, 1972. Part I: Sensitivity Studies. *Mon. Wea. Rev.*, **112**, 76-90.
- Neff, W. D., 1988: Observations of Complex Terrain Flows using Acoustic Sounders: Echo Interpretation. *Boundary-Layer Meteor.*, **42**, 207-228.
- Paulson, C.A., 1970: The Mathematical Representation of Wind Speed and Temperature Profiles in the Unstable Atmospheric Surface Layer. *J. Appl. Meteorol.*, **9**, 857-861.
- Skupniewicz, C.E., Kamada, R.F., and McKay, L., 1990: Measurements of the ABL Across a Stratus to Clear Sky Boundary under Seabreeze Conditions. *Proc. of the 9th Conference on Turbulence and Diffusion, Roskilde, Denmark*.
- Venkatram, A., 1977: A Model of Internal Boundary-Layer Development. *Boundary-Layer Meteor.*, **11**, 419-437.

Wyngaard, J.C., 1985: Structure of the Planetary Boundary Layer and Implications for its Modeling. *J. Climate Appl. Meteor.*, **24**, 1131-1142.

**VANDENBERG AIR FORCE BASE BOUNDARY LAYER EXPERIMENT (VBLS)
FINAL REPORT - APPENDIX**

C. E. Skupniewicz, R. Kanada, and L. McKay
Environmental Physics Group, Naval Postgraduate School
Monterey, Calif. 93943-5000

**APPENDIX A. DATA DESCRIPTION AND MEASUREMENT TECHNIQUES
(SPECIFICS)**

The following text details equipment and analysis techniques summarized in the associated report "VBLS Final Report - Results".

The SODAR is a combination of Radian Echosnde electronics and RemTech antennas. Transducers are 200 W JBL speakers and the operating frequency is 1600 Hz. As with most SODARs, the standard outputs are 3 dimensional mean and turbulent winds, and range-square-corrected backscattered power from which mixing depths and inversion heights may be inferred. A tiltmeter mounted on the antenna frame supplied the true zenith direction, and boundary layer heights and winds were corrected accordingly. A compass supplied corrections for true wind direction. Maximum range is, of course, a function of atmospheric conditions and background noise. In a cloud free marine boundary layer during a typical California summer day the system has no problem retrieving data through the whole depth of the boundary layer with an averaging time of 5 minutes and vertical resolution of 25 m. The introduction of a marine stratus deck usually causes some range degradation. Typically, wind data under stratus was contiguous from the surface up to

about 200 m (depending upon the surface heating and wind), a mid-boundary layer data gap was observed, and above that a few wind values within the cloud top inversion were recoverable. For some cases, stratus complicated the selection of boundary layer heights based on backscattered power. Clouds which were busily entraining air sometimes produced 2 layers of high backscatter. During light wind conditions, multiple stable layers occasionally produce many echo layers within the clouds. (These problems are not unique to our SODAR, and will be encountered to some degree with any acoustical system under stratus cover.) Automobile noise was only a problem when it was more or less continuous. A few passing vehicles were easily filtered out by the system.

Surface fluxes of momentum and heat were obtained using eddy correlation with a Kaijo Denki Dat-300 sonic anemometer sampling at 6 hz and mounted above the SODAR on a telescoping mast at 5 m. The need to navigate trees and elevated wiring limited the measurement height/antenna height aspect ratio to 2X. The low measurement height also meant that flux measurements represented a fairly limited local area, say a few hundred meters upwind of the sensor. To perform a measurement, a site was selected with a homogeneous upwind fetch of at least .5 km. The anemometer was rotated to within 30 degrees of the mean wind direction to avoid sensor support contamination, as in Grant and

Watkins (1989). Also, only time series where the trailer/mast was upwind of the towing vehicle were considered. The time series were first screened for stationarity in wind speed and direction, then fluxes were calculated using the covariance method. As is common practice, the mean vertical velocity was assumed to be unity and wind vector coordinates were rotated appropriately to minimize the effects of sensor tilt. Schotanus et al. (1983) has shown that Kaijo Denki measured heat fluxes are artificially low, due to humidity and velocity fluctuations along the path of the temperature measurement with errors typically 10-20%. Their suggested Bowen ratio correction techniques were implemented. Then by definition,

$$H = w'T_v' , \quad (A1)$$

$$u_*^2 = -u'w' , \quad (A2)$$

where H is the total (sensible and latent) heat flux and u_* is the friction velocity.

Due to instrument drift, values of H calculated from the sonic were sometimes unavailable. In order to fill these gaps, and to increase statistical confidence, we averaged H with a value determined independently from the SODAR power returns. That value was derived as follows. We consider only sunny/clear sky cases for which we assume free convection over the altitude band $-L$ to $.8 Z_i$. Since we did

not know L explicitly for all cases, and since L requires longer time averaging than was the case for most location visits, we chose 65 m as the lower altitude limit. This height was greater than $.1 Z_i$ for 95% of the data and larger than $-L$ for 90% of the regional averages of L . Over this region of free convection, Wyngaard et al. (1971) show that

$$C_T^2 = K_1 H^{4/3} z^{-4/3} (T/g)^{2/3} \quad (A3)$$

where K_1 is a constant. A good assumption which relates the range-squared corrected power return from the SODAR is

$$C_T^2 = K_2 P e^{2az} . \quad (A4)$$

Here K_2 is a system constant, P is the power, and a is the absorption coefficient for sound which we assumed to be .002 based on 50% relative humidity and 1600 Hz. From these equations we calculated values proportional to the heat flux averaged over the free convection layer. We then calibrated these values against the sonic for locations where both instruments were operating and the terrain was flat and uniform. The resulting calibrations were then applied to all of the clear sky cases.

Selecting an appropriate averaging time is always a difficult task, particularly in convective conditions.

Because heat and momentum flux scale with z (Kaimal et al. 1972), the low measurement height allows for very little low frequency contribution to the cospectra. Still, we need to average long enough to account for the passage of many boundary layer scale eddies. For low ($z < 20$ m) measurements and convective conditions, Wyngaard (1973) argues for averaging times of at least 1 hr for stress. For this paper, we require surface heat fluxes, which need significantly less averaging than stress in order to achieve the same degree of accuracy. Wyngaard estimated that heat flux need be averaged only 1/8 as long as stress. But these estimates were based upon the Kansas data. The addition of instationarity due to sea breeze and complex terrain further complicates our selection of averaging time. We were also forced to compromise between obtaining a large number of SODAR samples at many locations (as mandated by the experiment objectives) and using a longer averaging time. Our solution was to extend the concept of "effective" fluxes of heat by averaging short records at multiple locations to account for inhomogeneity between sites. The first step was to select a base time series length which was long enough to capture most of the covariance spectra. We selected 5 minutes, which should conservatively capture at least 90% of the flux for a wind speed of 5 m/s (Panofsky and Dutton, 1984). We then averaged all 5 minute values for each visit to a particular location. Those averages and the total averaging time are supplied in Appendix D. The "Regional

Analysis" section of "VBLS Final Report - Results" we extended this idea one more step and averaged between locations. This technique suffers in assuming that we are randomly sampling eddies which are independent of our location. However, it does attack the inhomogeneity problem, which can be severe for low measurement heights.

APPENDIX B. BACKGROUND METEOROLOGICAL (CHARTS AND MAPS)

The major features for each day of VBLS are described by stepping through a range of scales from synoptic meteorology to local flow fields. Days 1-3 are 18-20 May 1988, days 4-7 are 26-29 July 1988, and days 8-11 are 18-21 October, 1988. A summary of these observations is presented in "VBLS Experiment Final Report - Results".

500 mb Analysis

The 500 mb surface heights (m) are shown as solid lines. The isotherms (deg C) are shown as dashed lines.

Day 1. A fast moving trough passed through California and VBG was under veering northwest flow all day.

Day 2. At 500 LST the northwest pressure gradient was still present and only slightly less than day 1, but by 1600 the gradient had weakened significantly.

Day 3. The weak northwest gradient remained. Also, temperatures had remained about the same for all of days 1-3.

Day 4. Note that the isoline intervals have decreased from those used for days 1-3. VBG was under a veering southwest gradient flow, with slowly decreasing temperatures at 500 mb.

Day 5. The gradient continued to veer and by 1700 LST was northwest. The temperatures bottomed out and were a few degrees cooler than day 4.

Day 6. Temperatures begin to rise as a high approaches from the west. Gradients over VBG continue to veer and were due north by 1700.

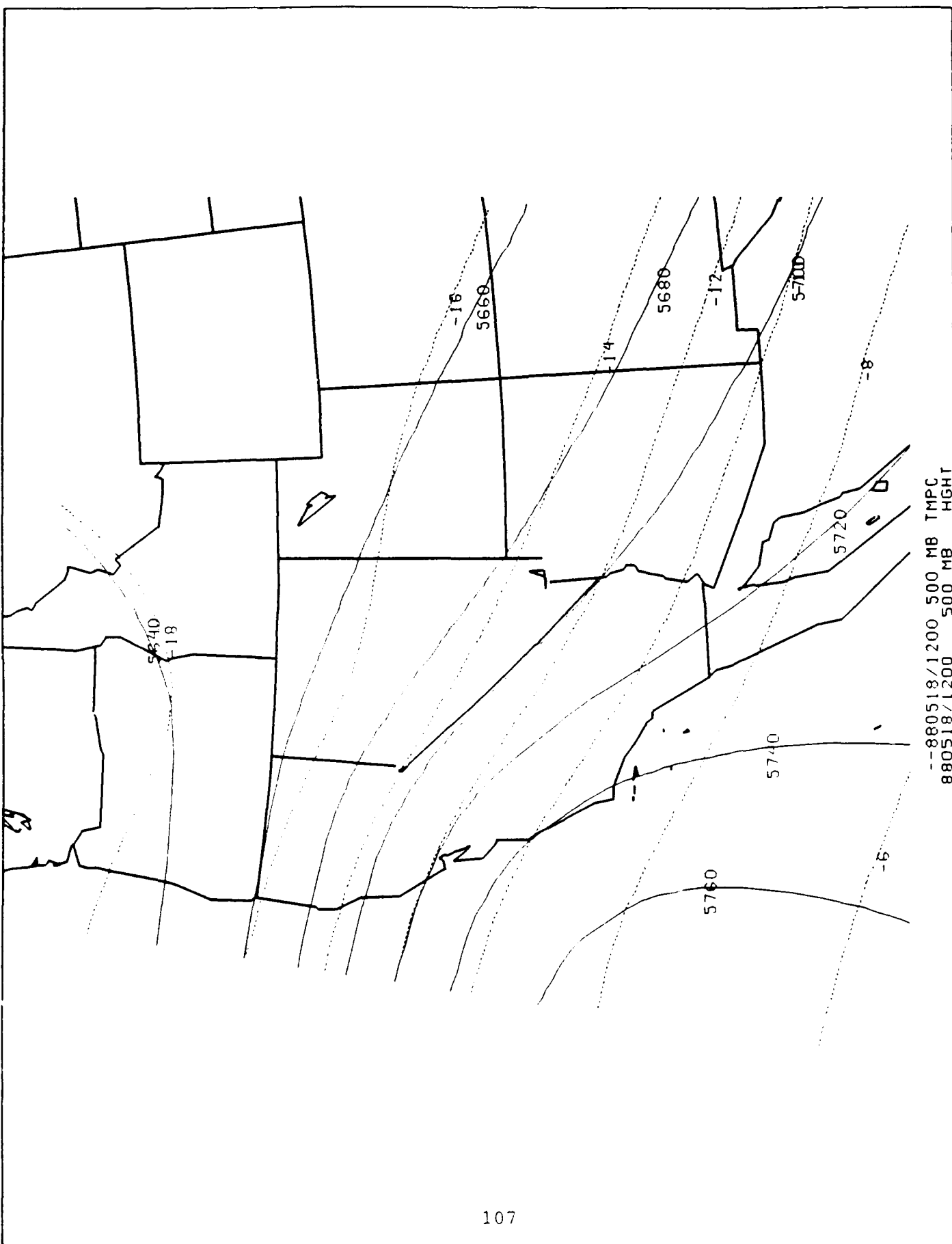
Day 7. The rotation of the flow since day 4 was completed, as a northeasterly was again present over VBG.

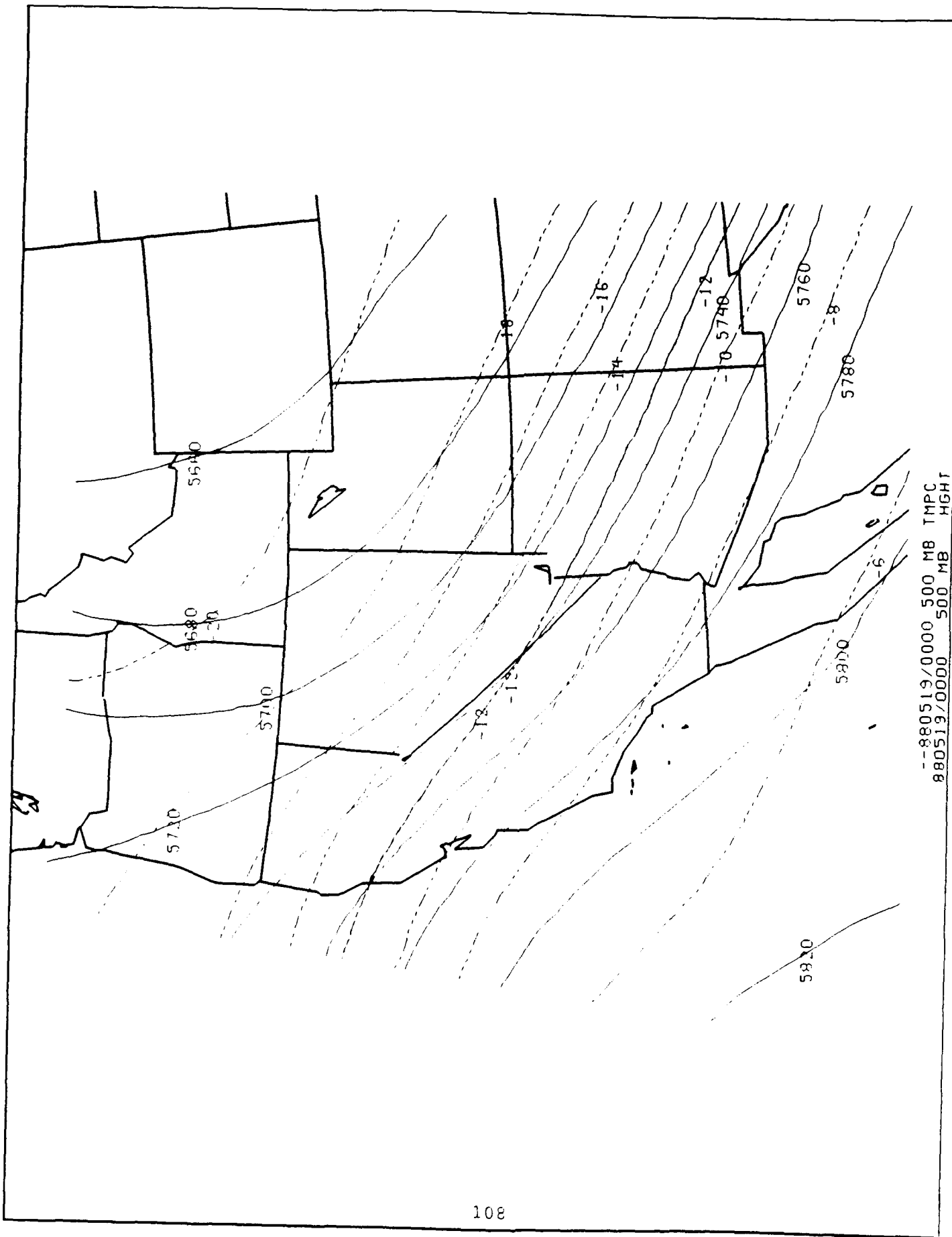
Day 8. Note that the isoline intervals have been increased from days 4-7. VBG is under the influence of high pressure west of San Francisco, with a fairly strong northeasterly gradient flow.

Day 9. The high migrates a bit to the north, but flow and temperature over VBG remain unchanged.

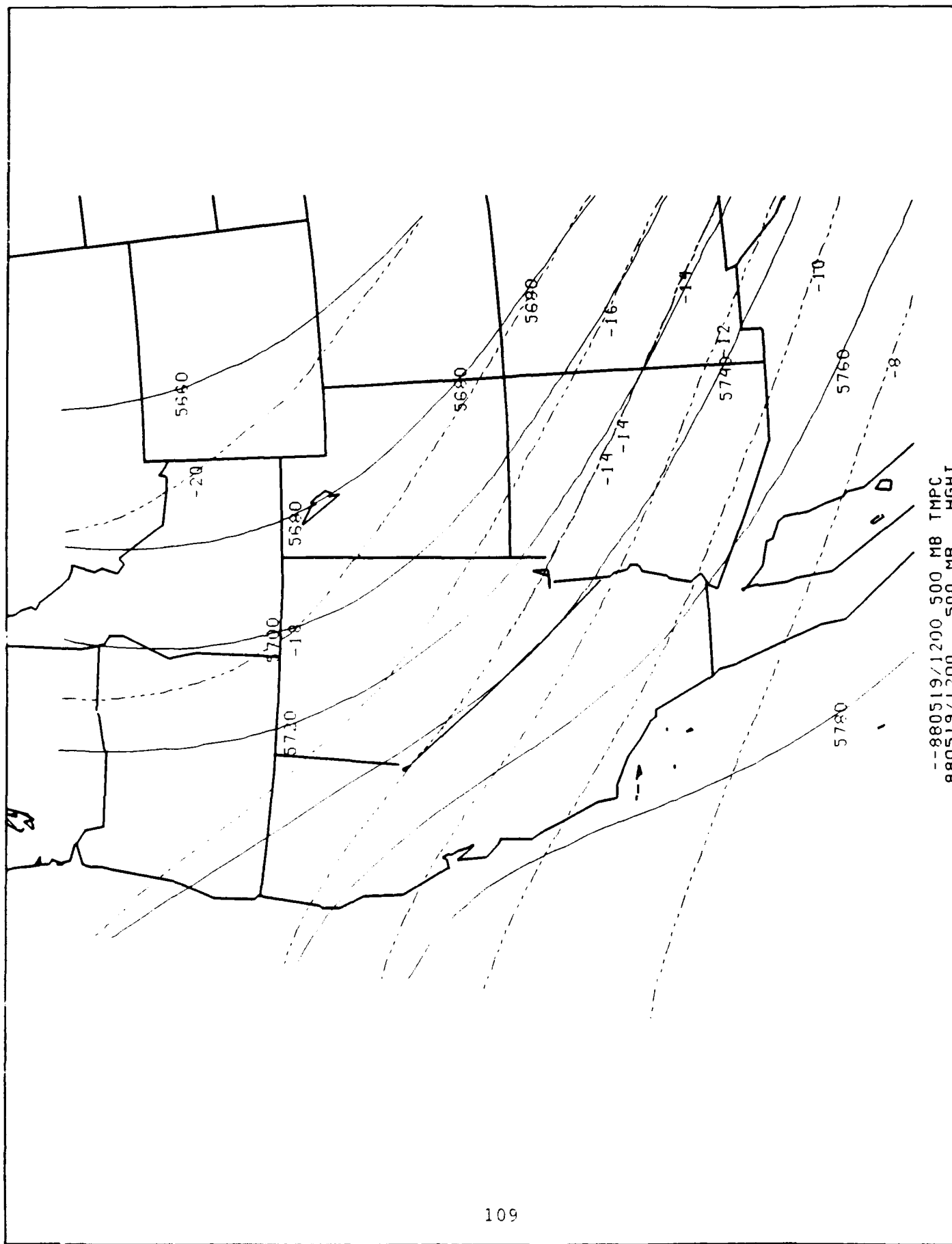
Day 10. Temperature rises and flow veers as the high appears to slide to the northeast.

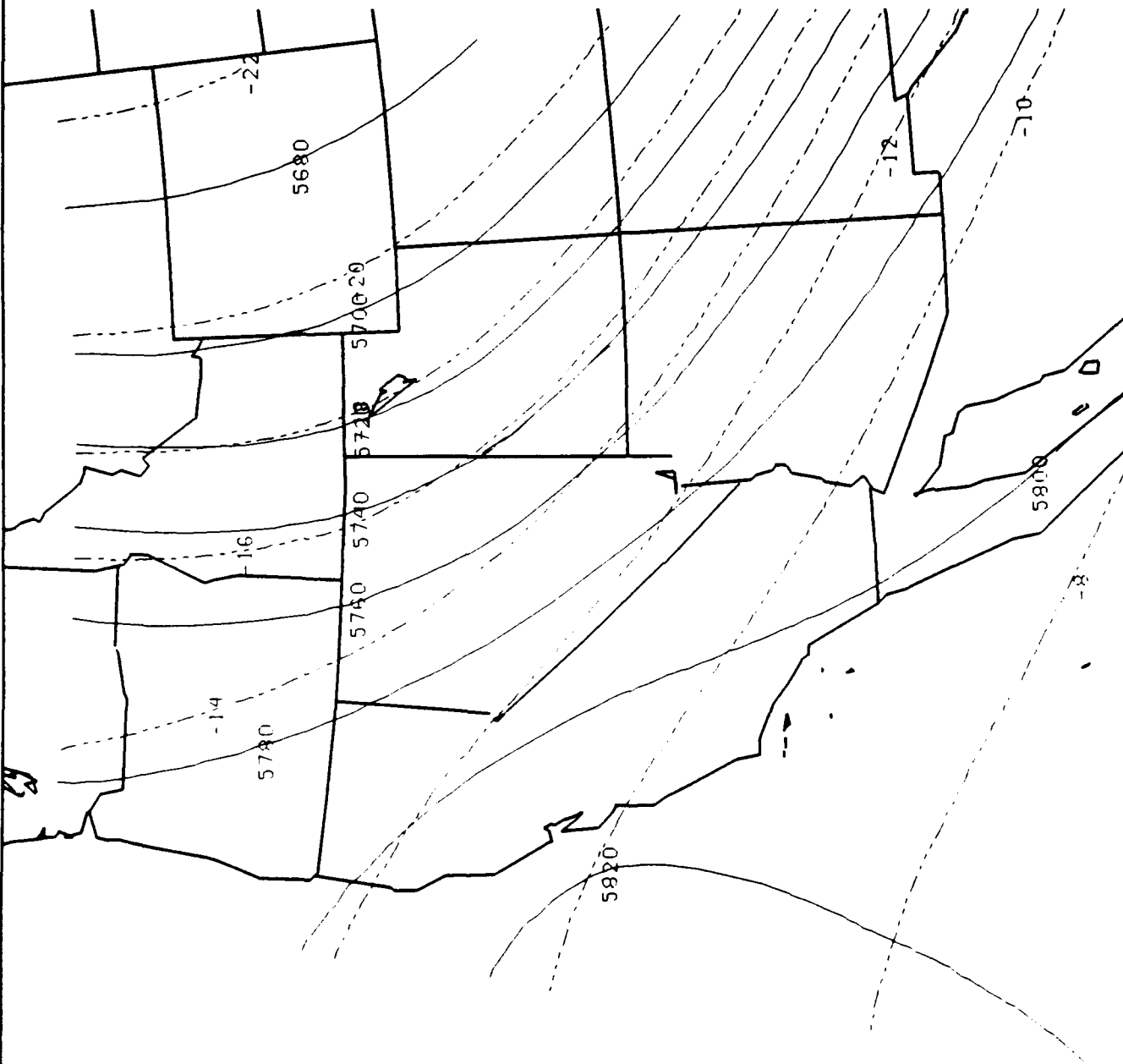
Day 11. Conditions at 500 mb are not significantly changed from day 10.



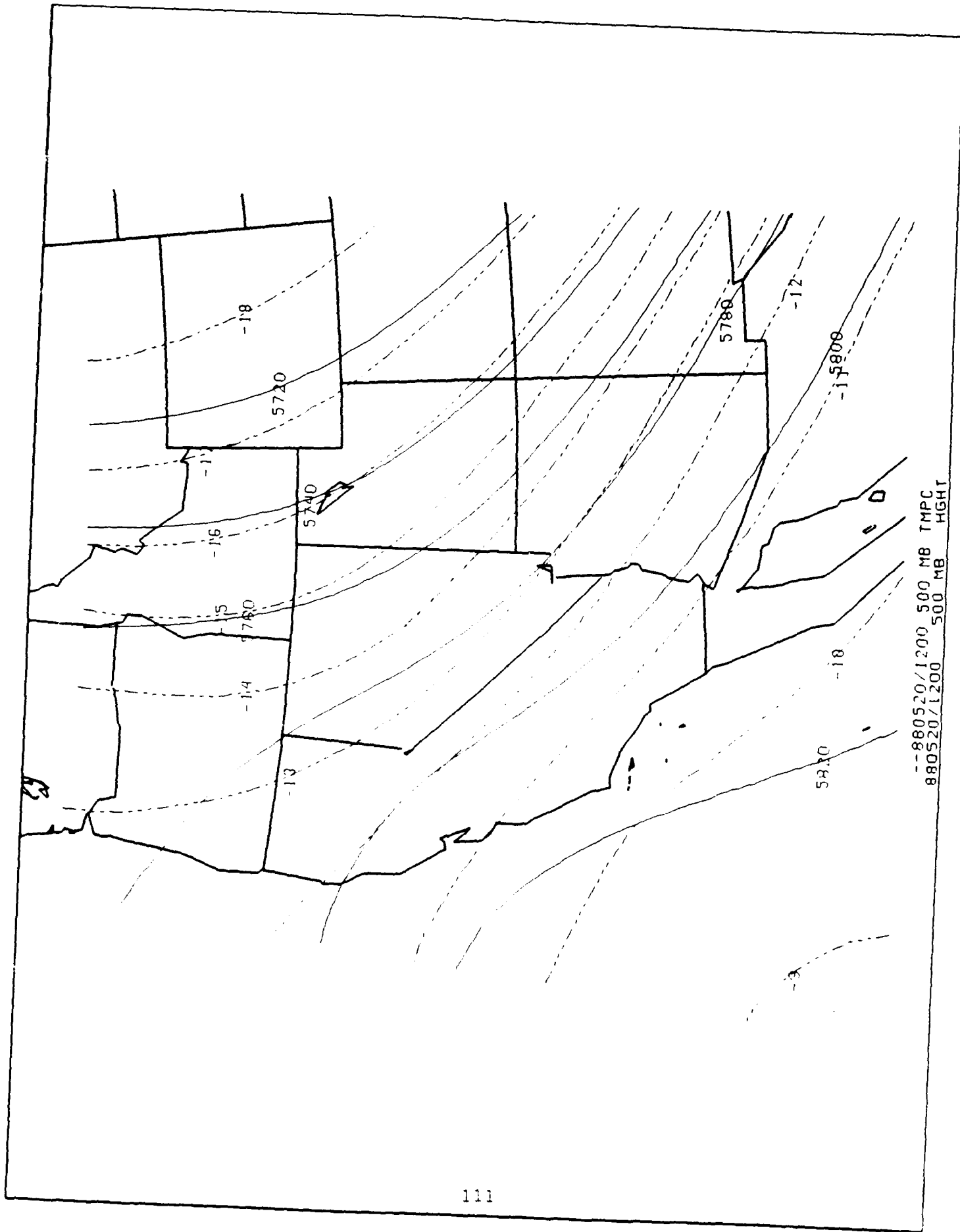


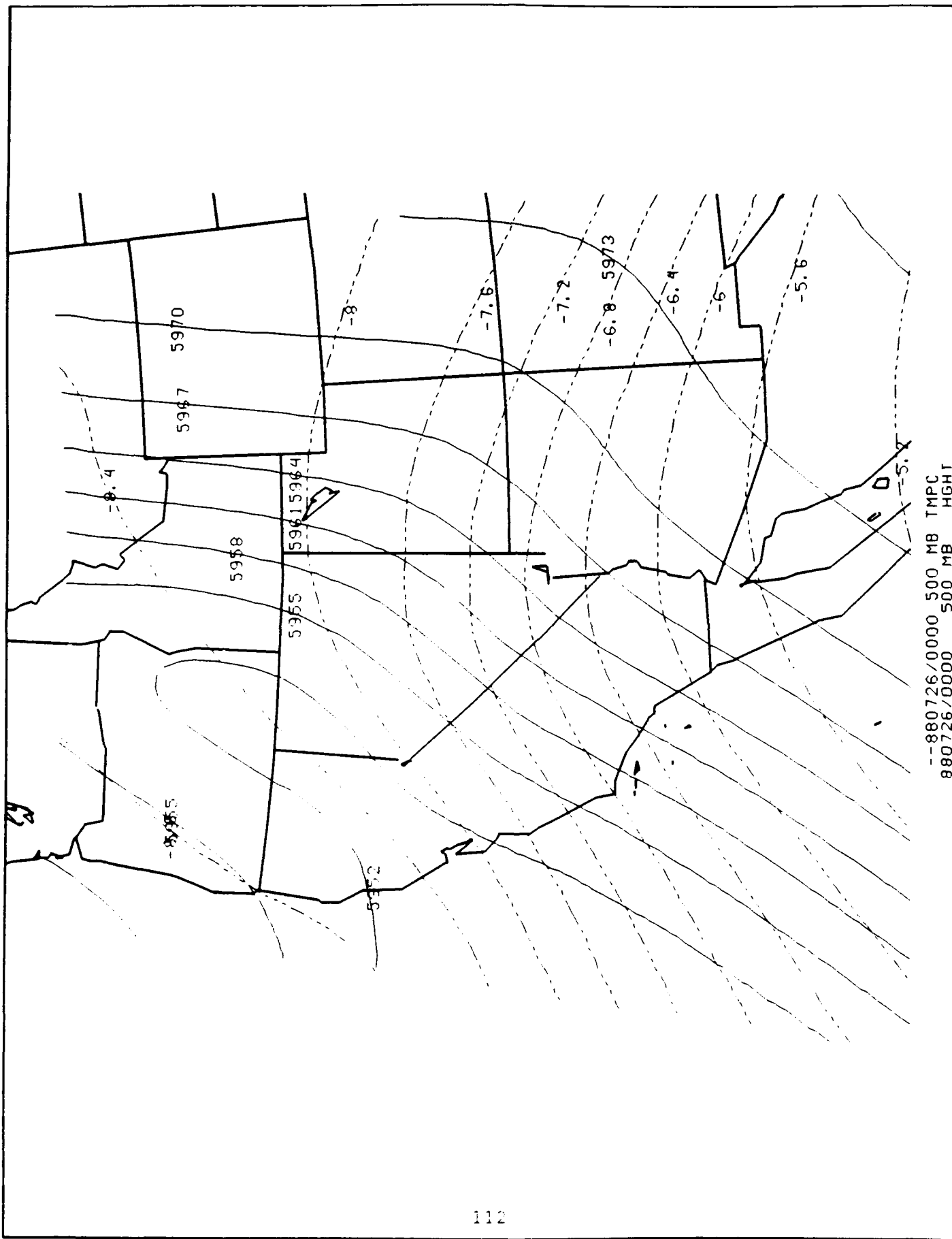
--880519/0000 500 MB TMPC
880519/0000 500 MB HGT



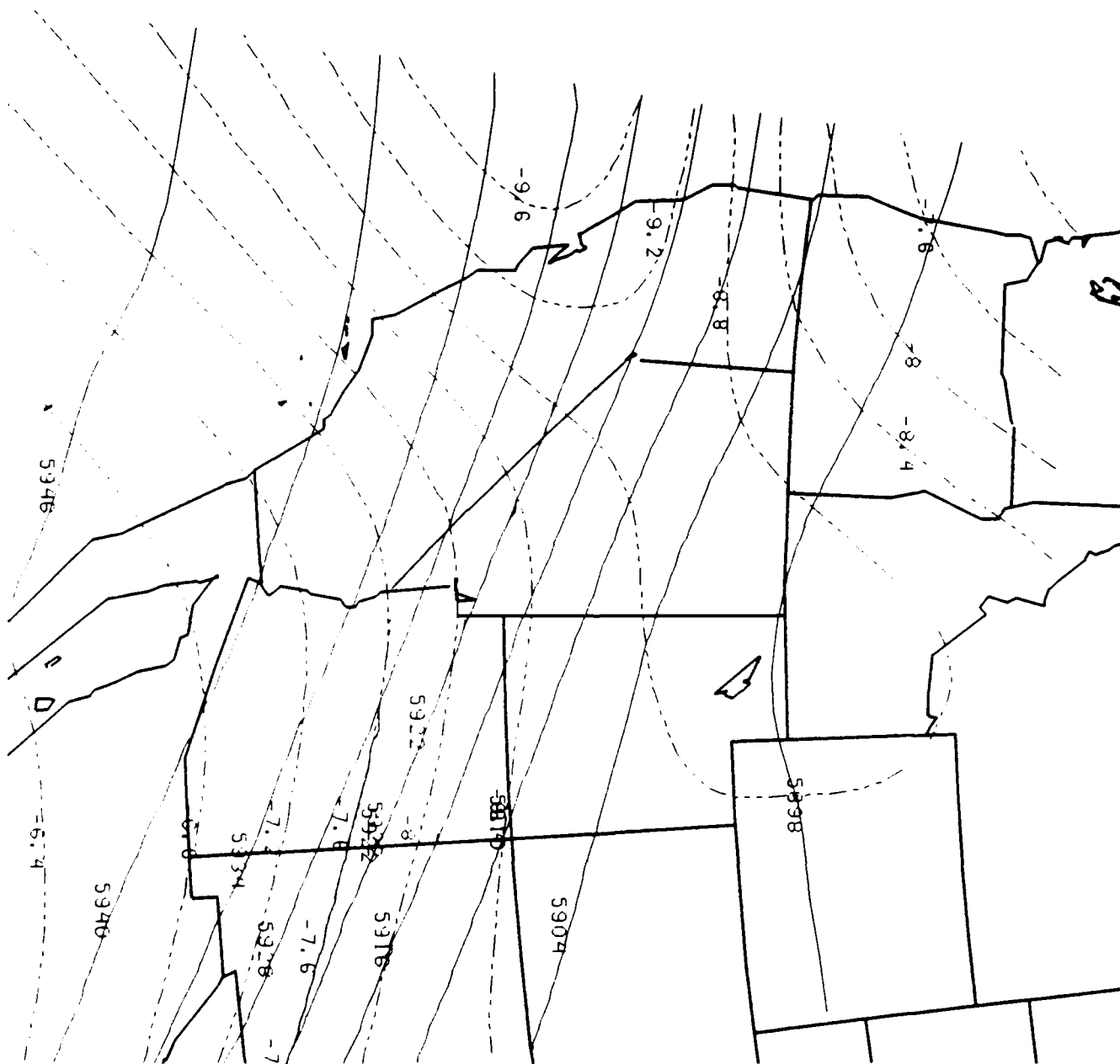


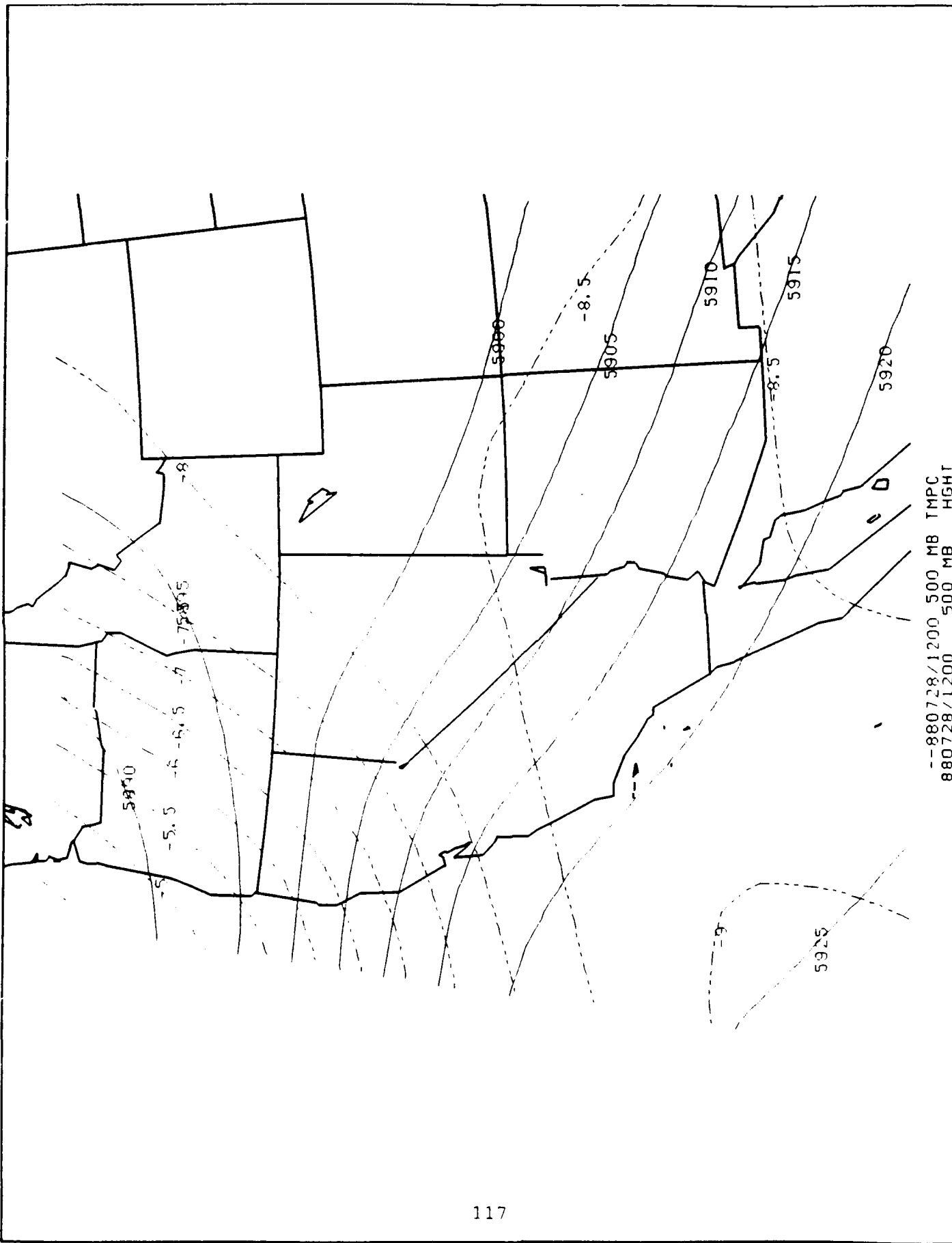
--880520/0000 500 MB TMPC
880520/0000 500 MB HGT

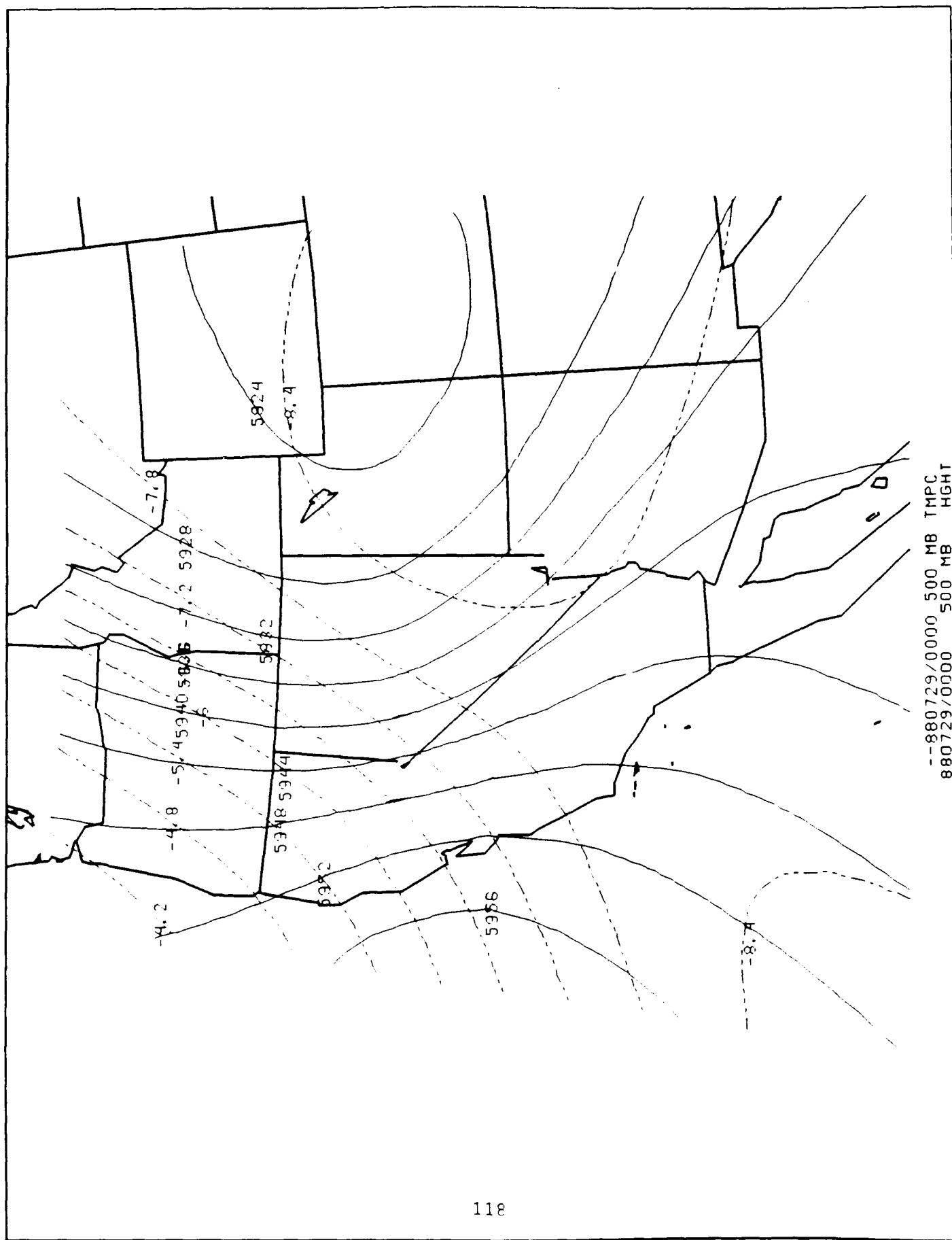


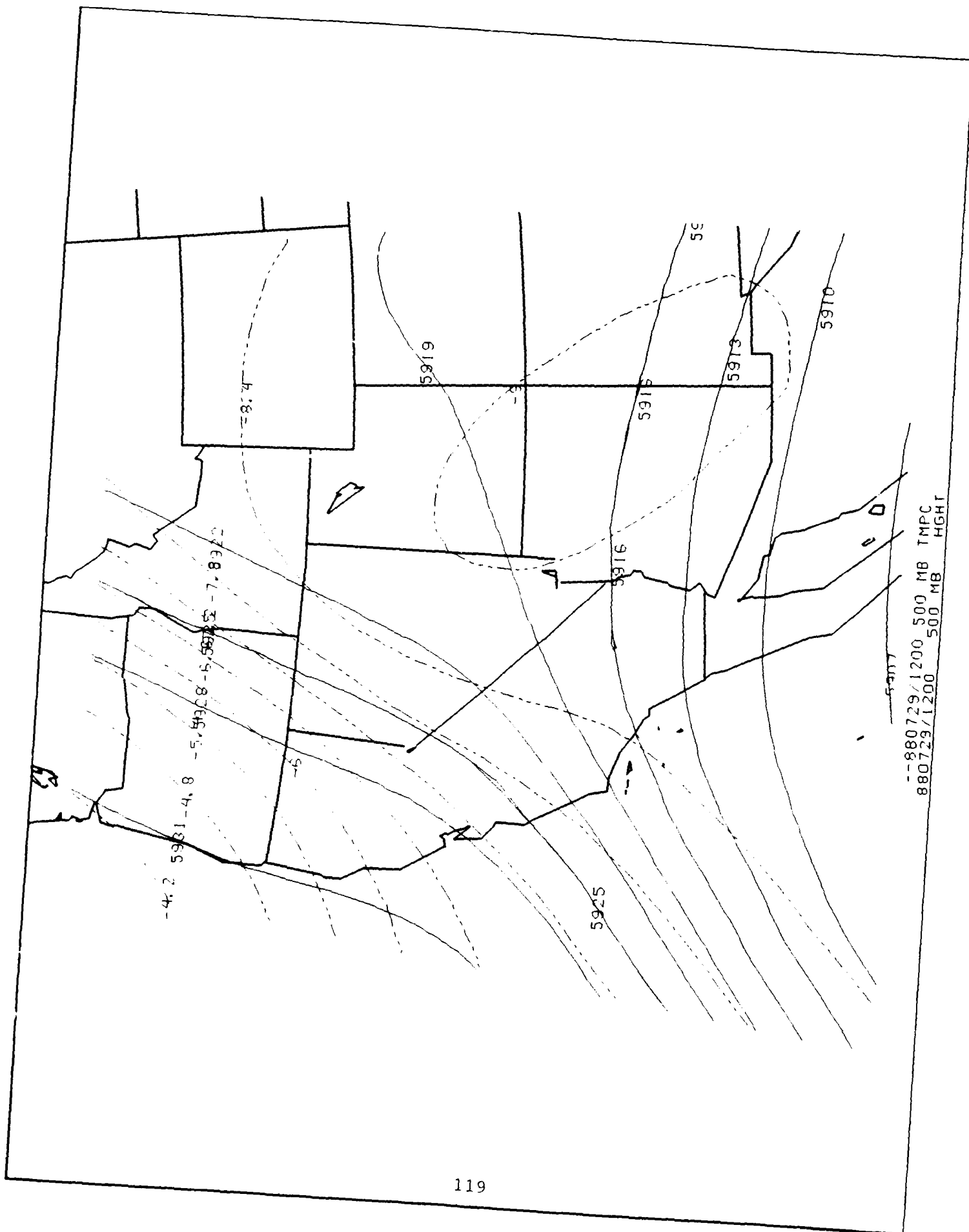


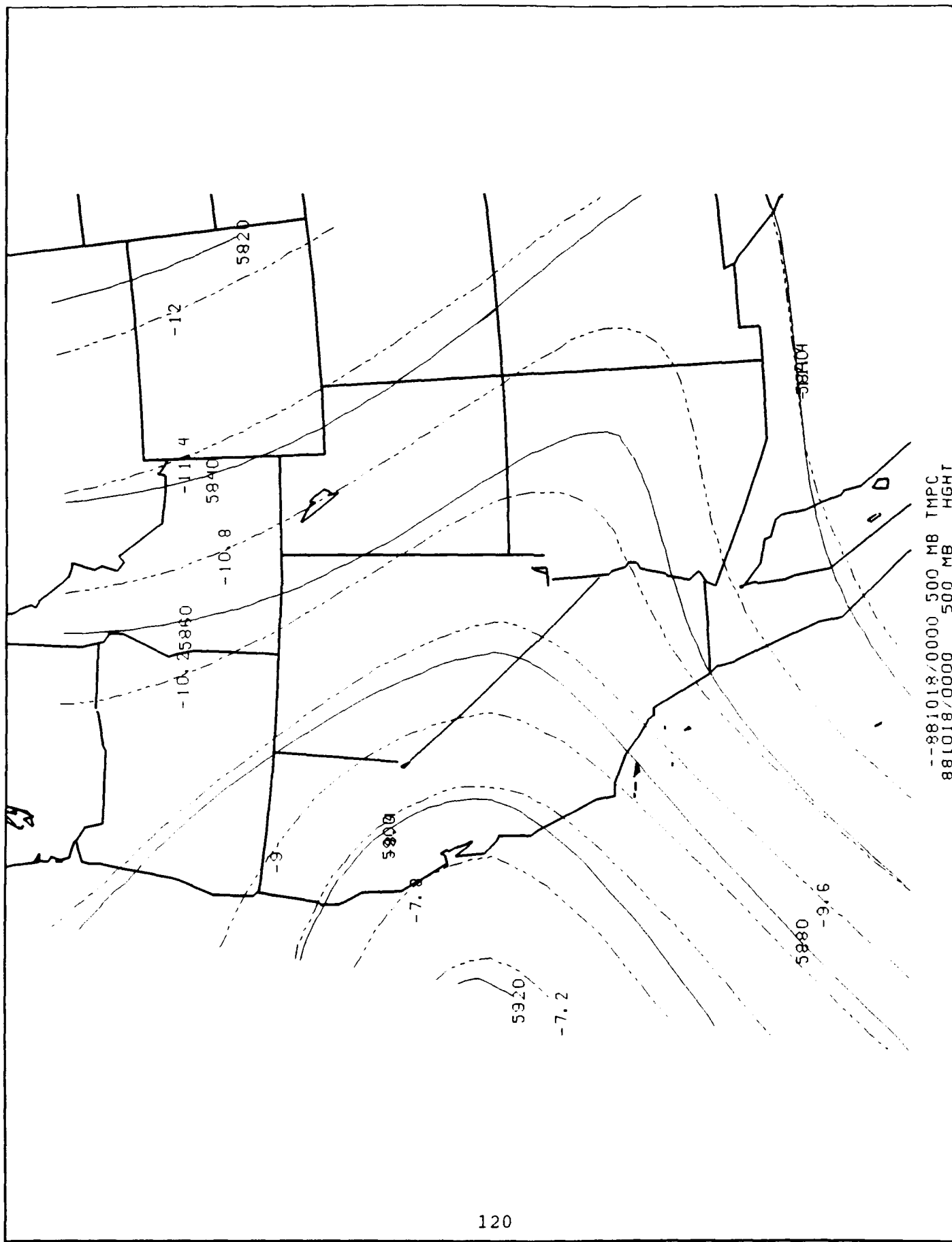
--880728 0000 500 MB TNP
 880728 0000 500 MB HGT

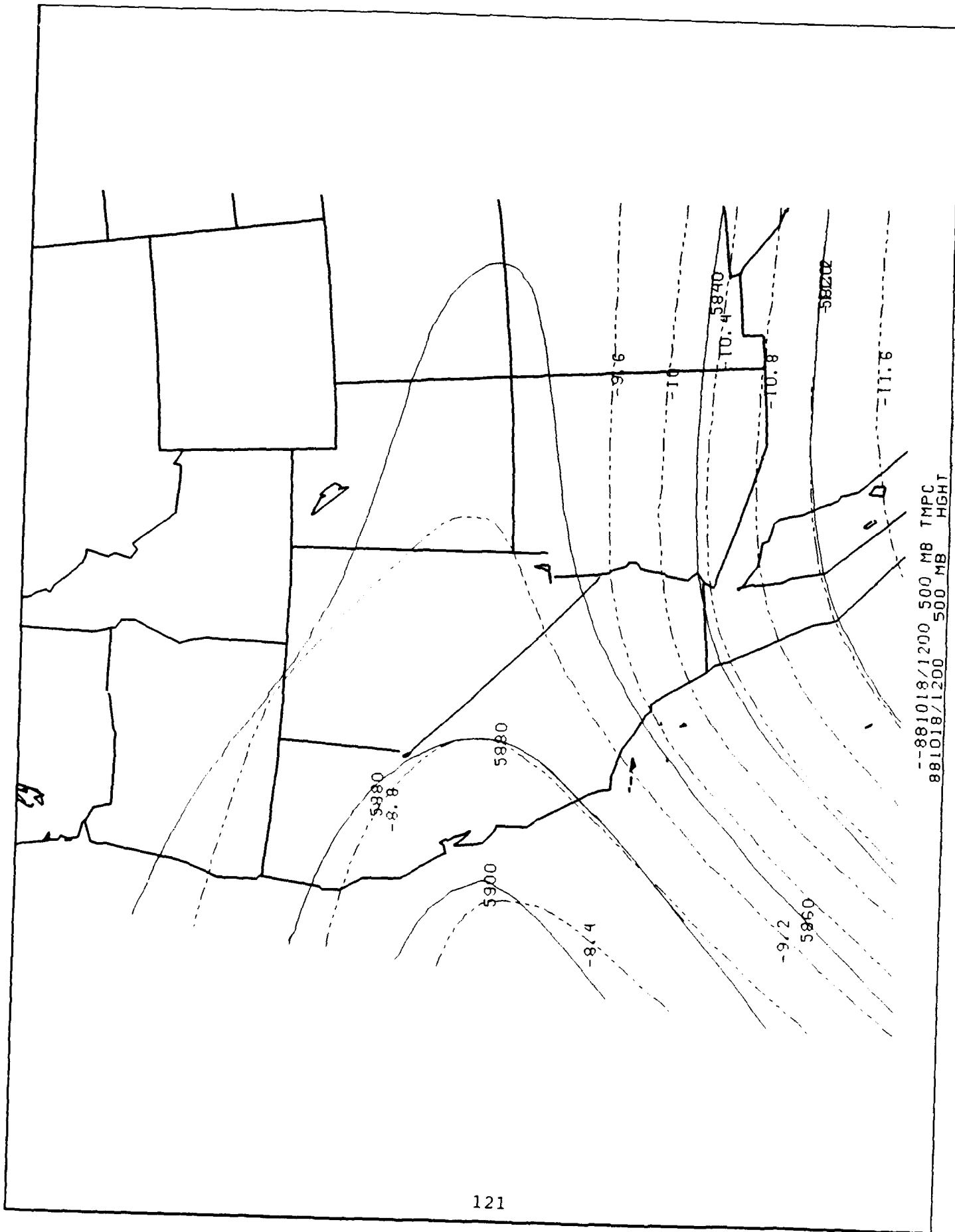


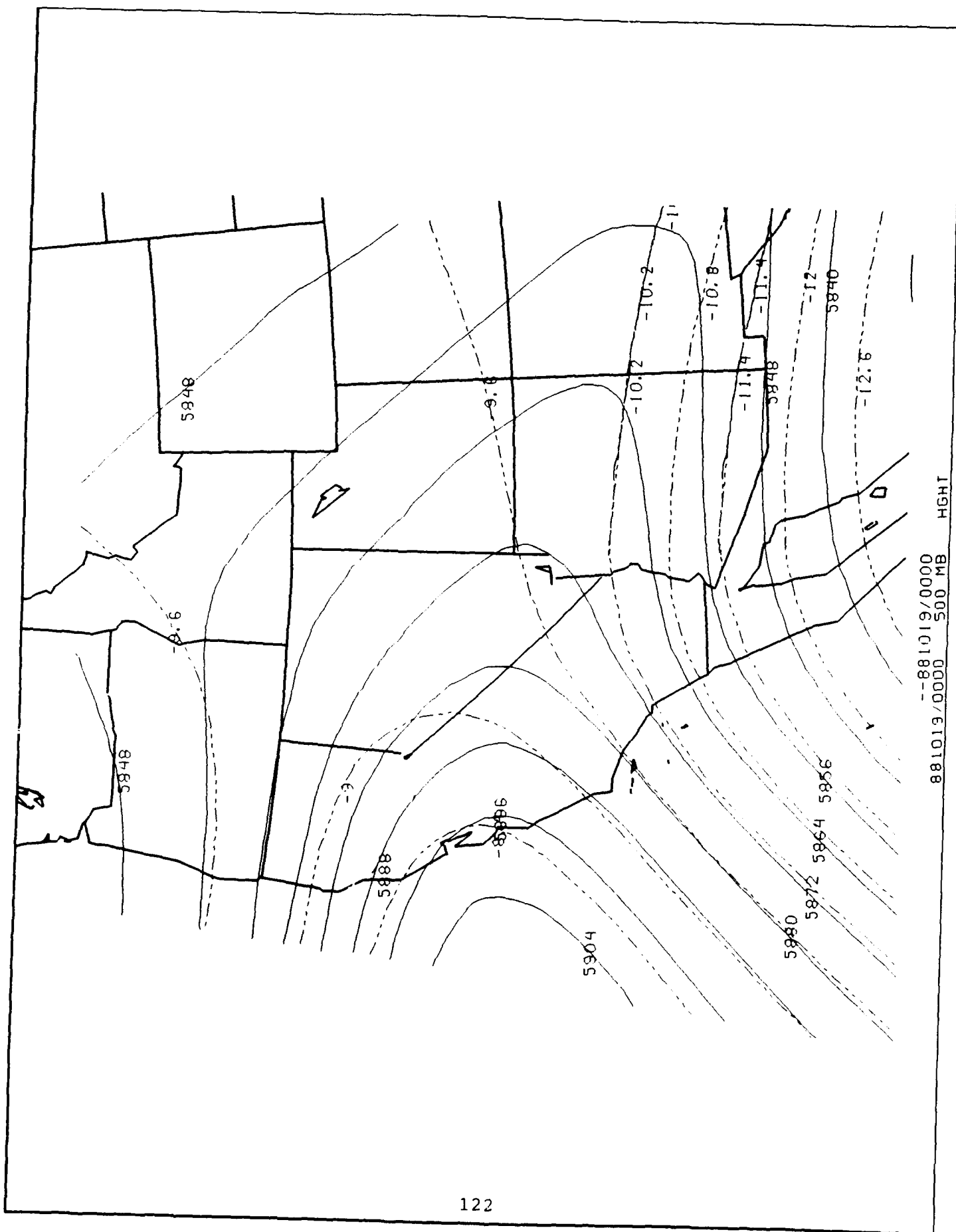


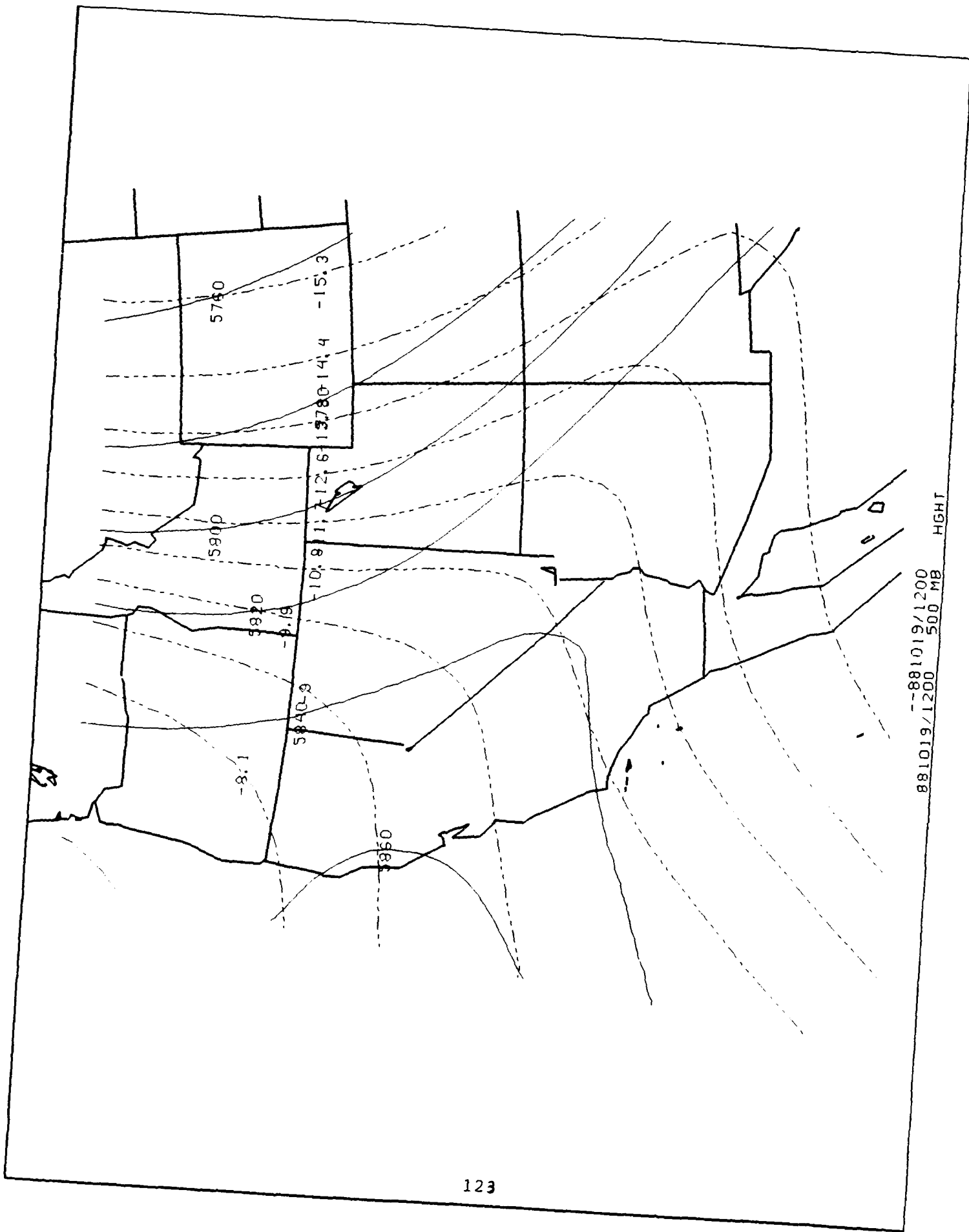




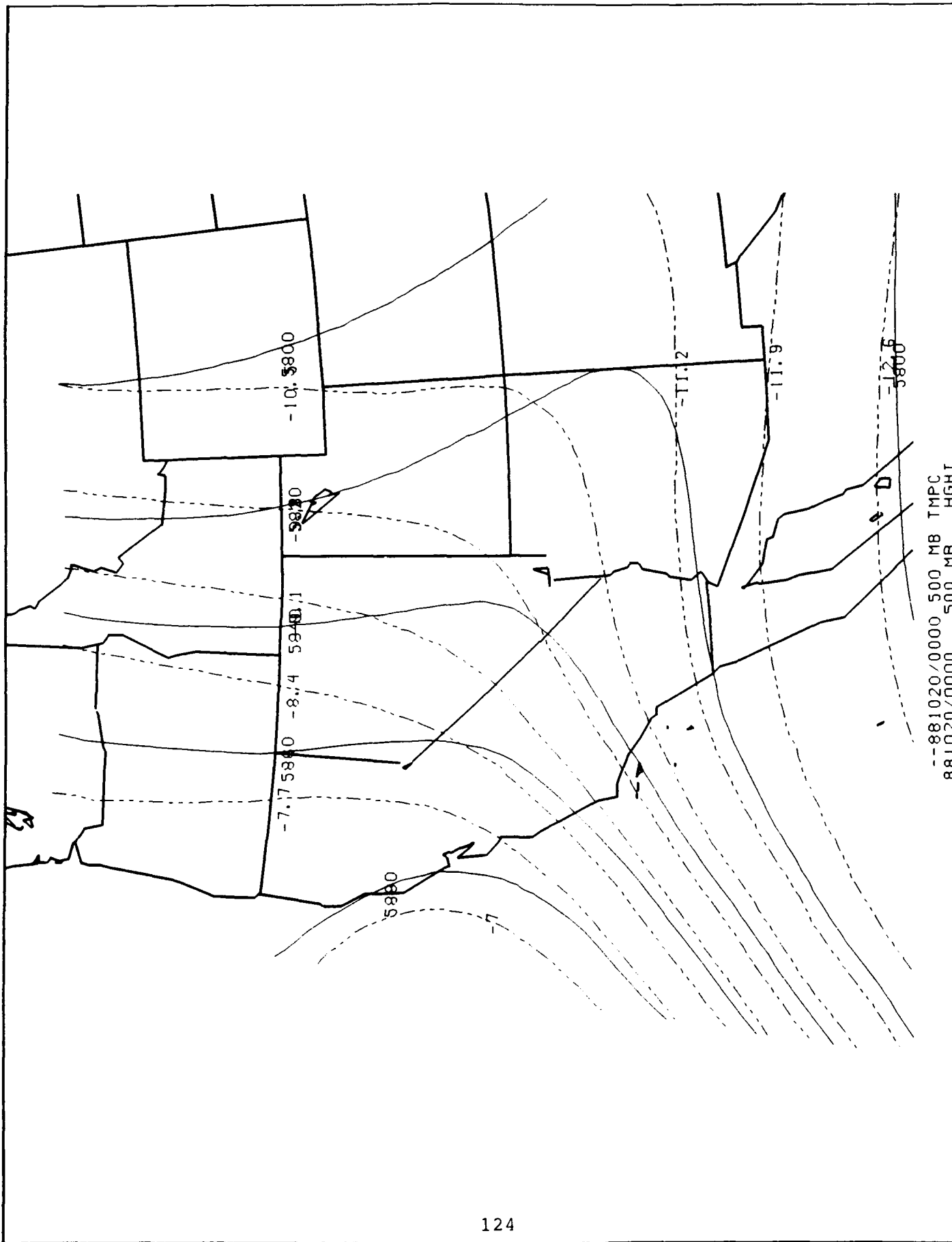


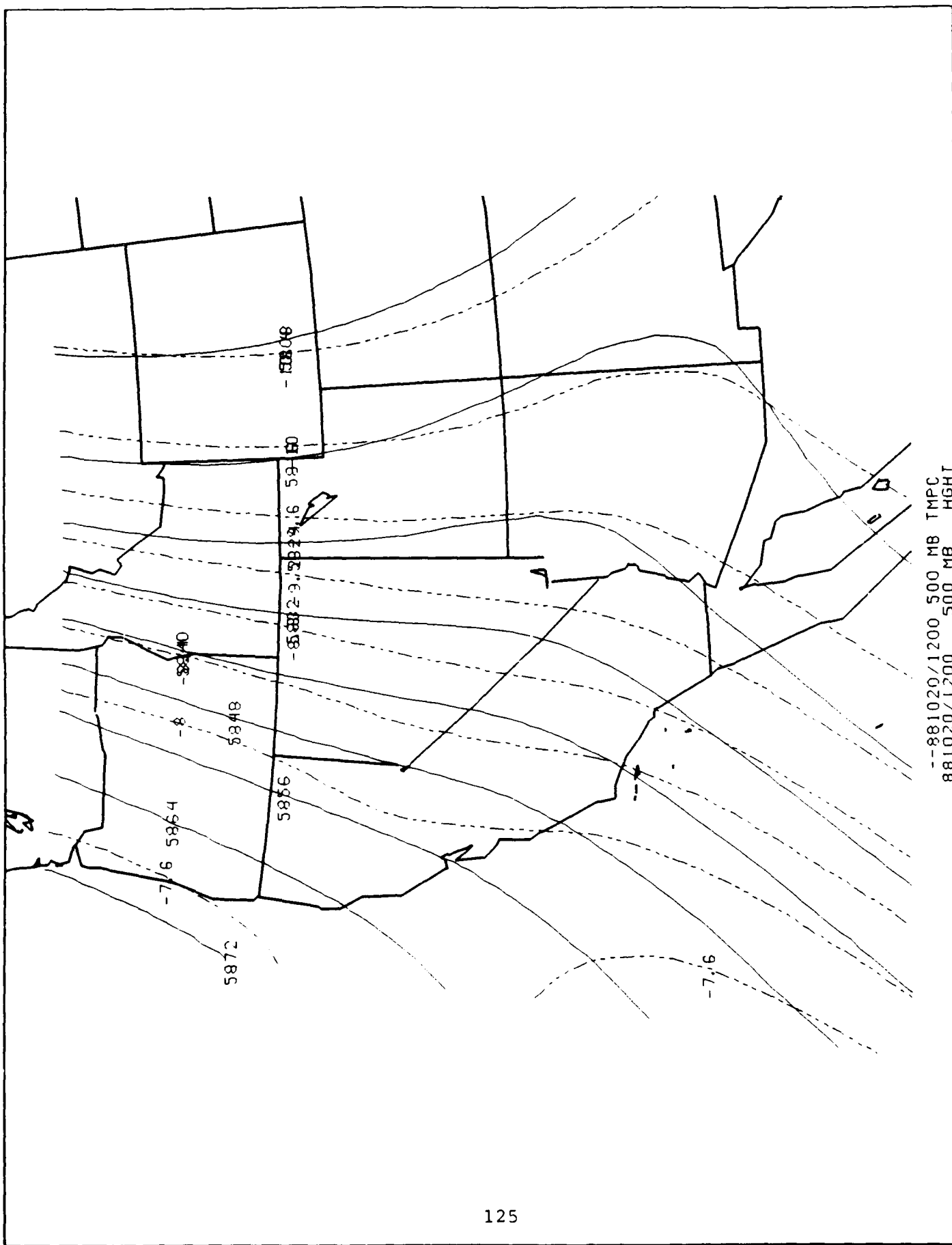






881019/1200 500 MB HGT





Surface Synoptics and Stratus Cloud Deck

The surface isobars (mb) are shown as solid lines. The isotherms (deg C) are shown as dashed lines. Wind barbs are in m/s. An example of a visible GOES image is shown for each phase of VBLS.

Day 1. The spring experiment started with passage of an upper level cold front, resulting in unusually strong northerly winds and clear conditions. The charts 0Z, 5-18 through 0Z, 5-19 show brisk northerly winds throughout the central valley and northern coastal areas of California produced by a N-S pressure gradient. The gradient never appears to reach S. California, however, where winds are much more variable. It is clear from the temperature contours that diurnal heating in the southern inland valley and desert regions is intense and swamps any cold air advection from the frontal passage. This is undoubtedly a primary cause for the cold front breakup.

Days 2-3. The major pressure and temperature gradients on a regional scale are in a line from N. California southeast to the Utah/Arizona border, reflecting a cold continental air mass over the N. Rocky Mtn. states. To a lesser degree, temperature gradients align with the coast in C. and S. California, but the pressure gradient is weak and less organized. Remnants of the day 1 weather system produced a moderate pressure gradient and northerly winds in the valleys to the east of Los Angeles on day 2. Coastal midday sea breeze winds could be considered typical for spring over most of California; northwest in direction at and to the north of VBG and west/southwest directions in S. California. No significant fog bank was observed anywhere near California during any of the spring experiment days as is evident from the satellite images.

Day 4. During all of the summer experimental days, the main synoptic feature influencing VBG was the thermal low centered roughly over the Mohave Desert. The isotherms roughly parallel the isobars in the coastal zone. Winds were generally NW at VBG and in the San Joaquin Valley, but fairly light. Southwest winds in S. California were quite strong, and crossed the isotherm/isobars at nearly right angles. The satellite photo shows a large stratus bank extending from the tip of Baja to north of San Francisco and 1000 km to the west. The Santa Barbara Channel cleared out during the day, but completely filled back in at night.

Day 5. Similar to day 4, except that the NW flow along the central coast was stronger. Also, a second thermal low developed over N. California. The fog bank remained intact.

Day 6. The southern low has moved a bit to the north. While there is still some cross isobar flow into the low in the S. California area, it is weaker, and more stations record along isobar northwesterly flow. The northern edge of the fog bank has migrated significantly to the south over the last day, and was 100 km north of VBG at 1700 LST.

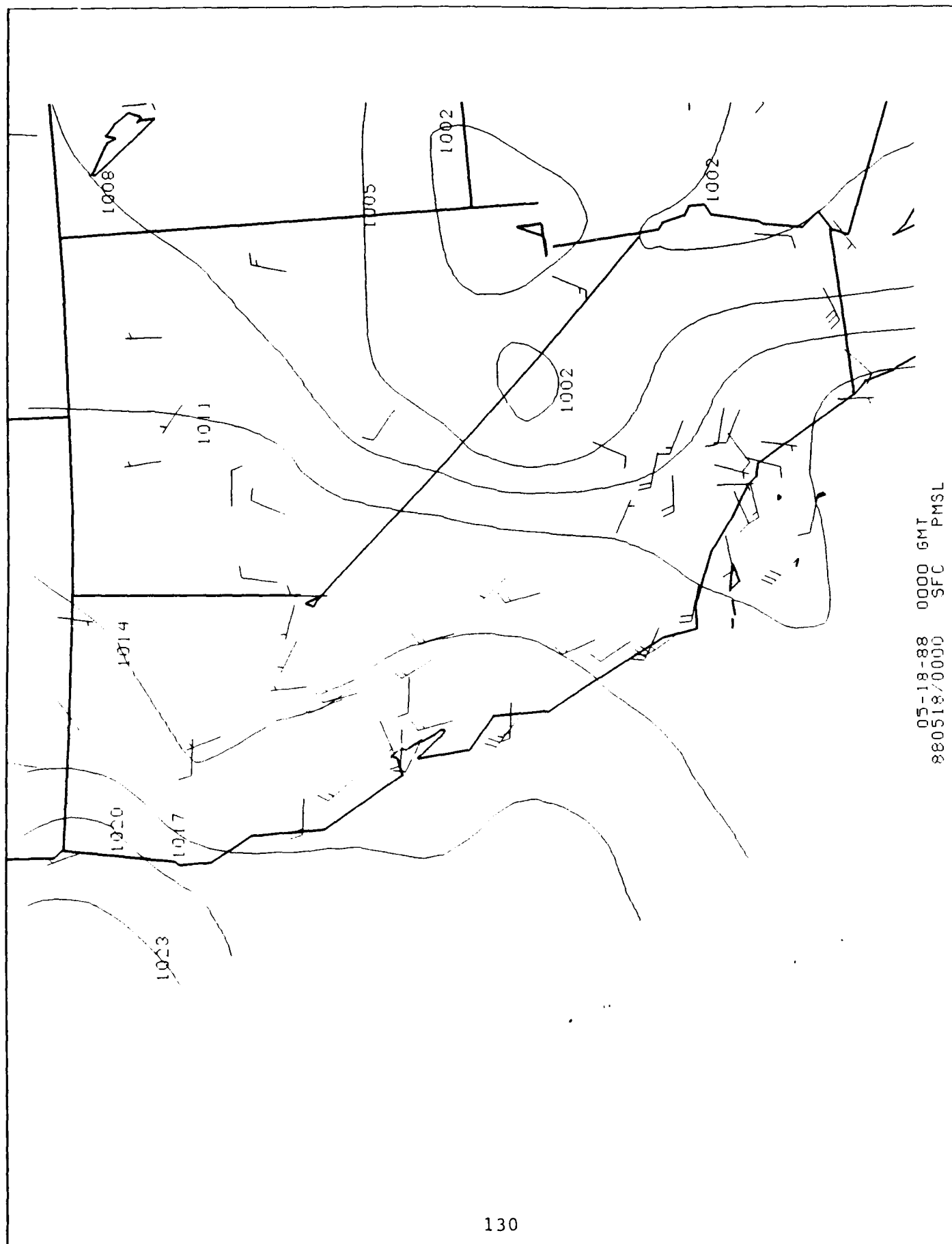
Day 7. Pressure, temperature, and wind patterns were roughly the same as day 6, but coastal winds are slightly weaker on average due to a strengthening of the fog bank which reappears along central and northern California. Inland penetration of stratus is relatively deep at many coastal sites, including VBG.

Day 8. The fall experiment was characterized by the 2 thermal lows described above, but pressure gradients along the coast were significantly weaker than during summer. This is somewhat surprising, since the thermal gradient was comparable to the summer scenario. The strongest coastal winds on this day were in the San Francisco Bay region, with VBG marking the transition from C. California northwesterly to S. California southwesterly flow. The stratus deck was from San Francisco to the Mexico border. S. California had unusually persistent fog on this day.

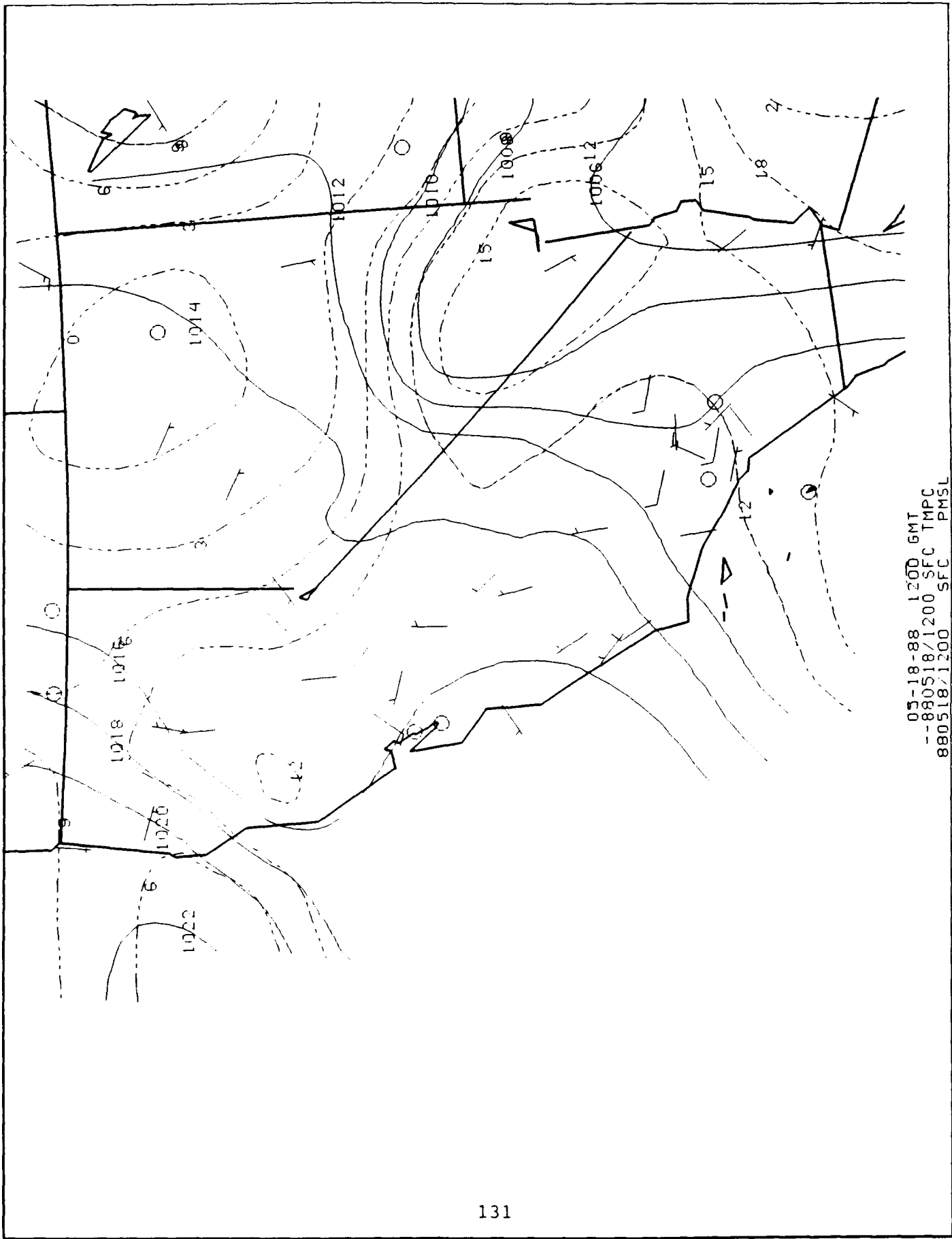
Day 9. Temperatures were lower along most of the C. California coast on this day. Pressure patterns were the same as for day 8. Winds were northwesterly at most stations in S. California. The fog bank migrated slightly (200 km) to the south, but VBG was still solidly in the fog.

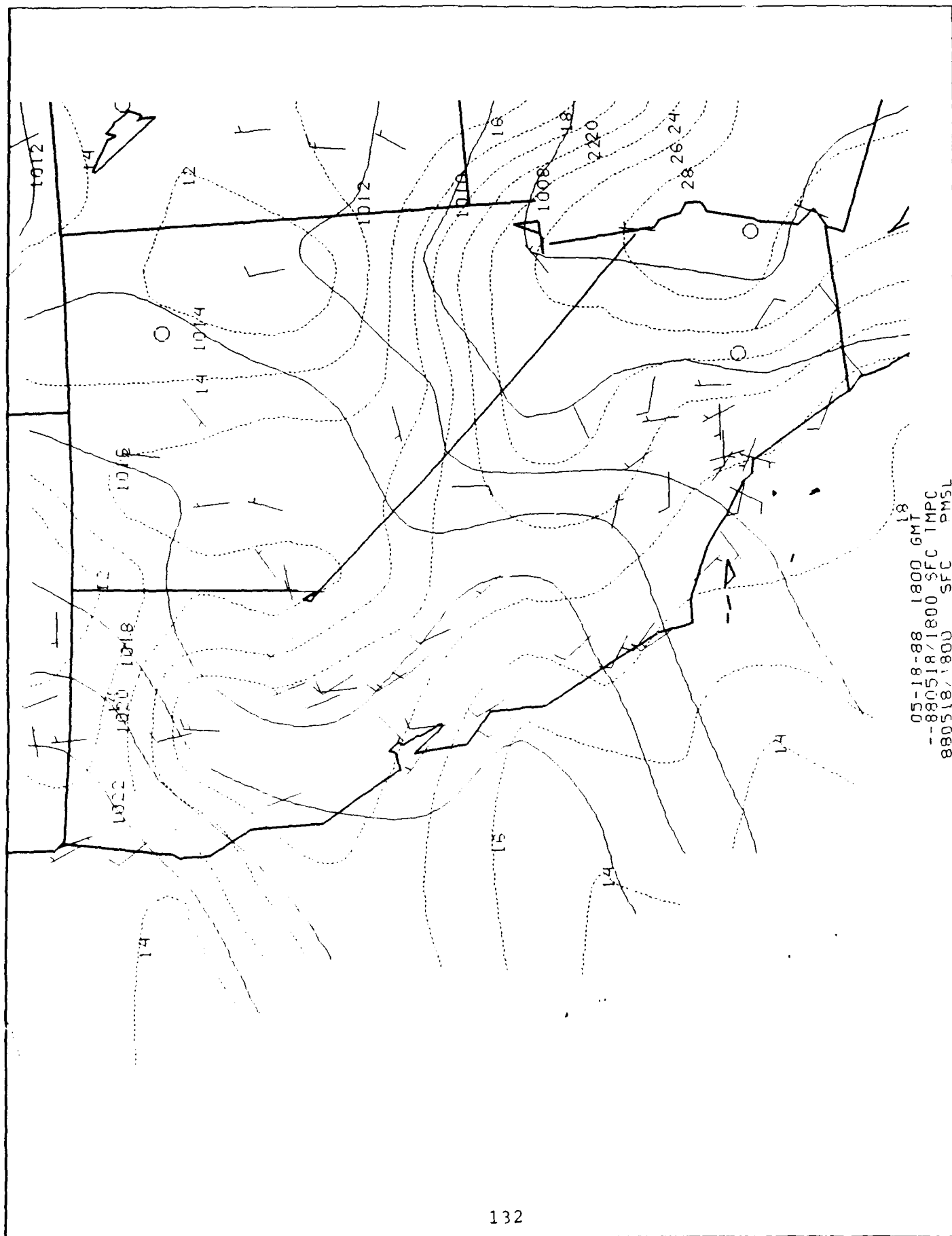
Day 10. A weak coastal pressure gradient coupled with light winds over most of the California coast and valley regions. The stratus bank was significantly larger than the previous day, reaching from C. Baja to N. California. The Santa Barbara Channel never cleared on this day, and this was the foggiest day at VBG during the VBLS period.

Day 11. The stratus bank was the same size as on the previous day, but the Santa Barbara Channel did partially clear during midday.

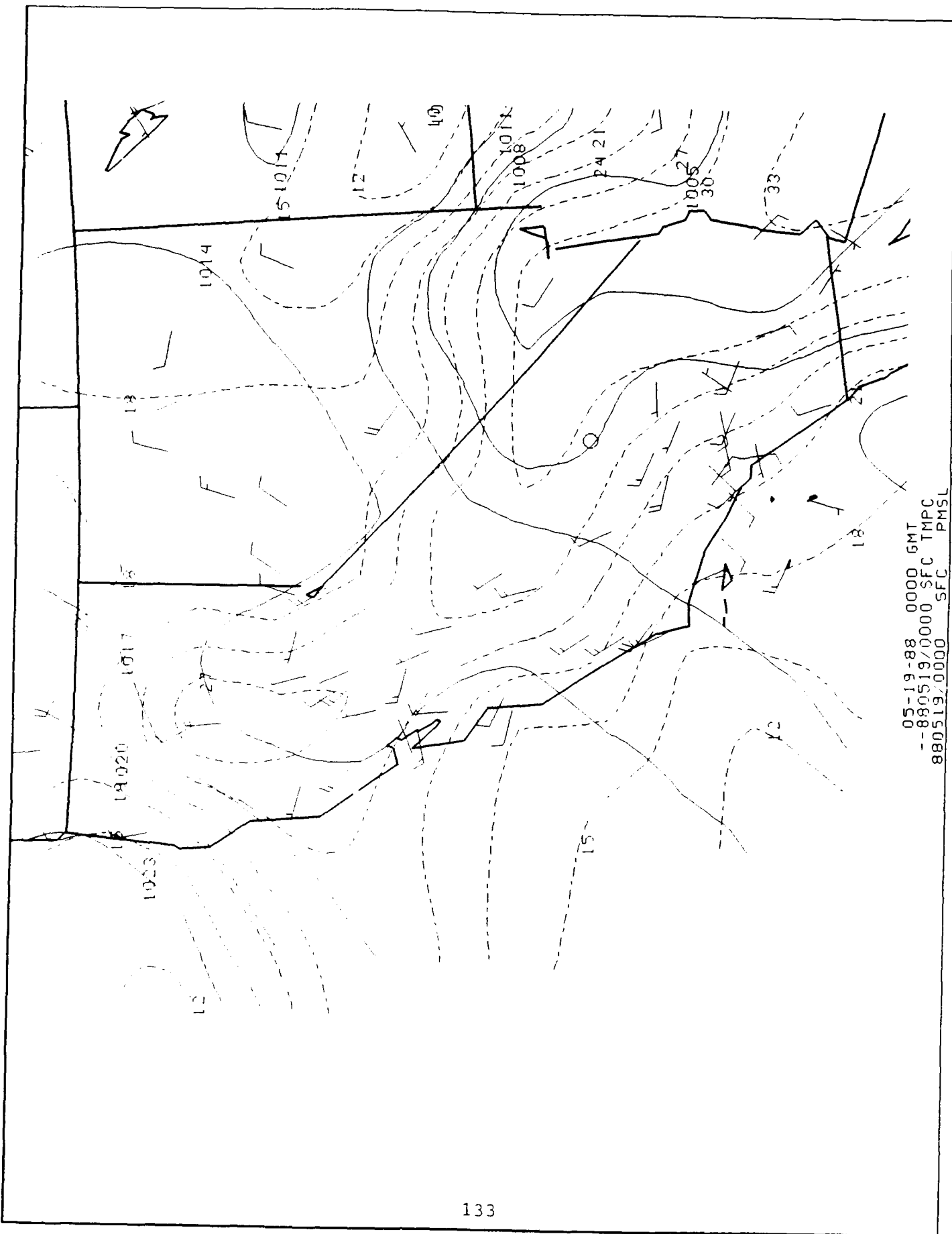


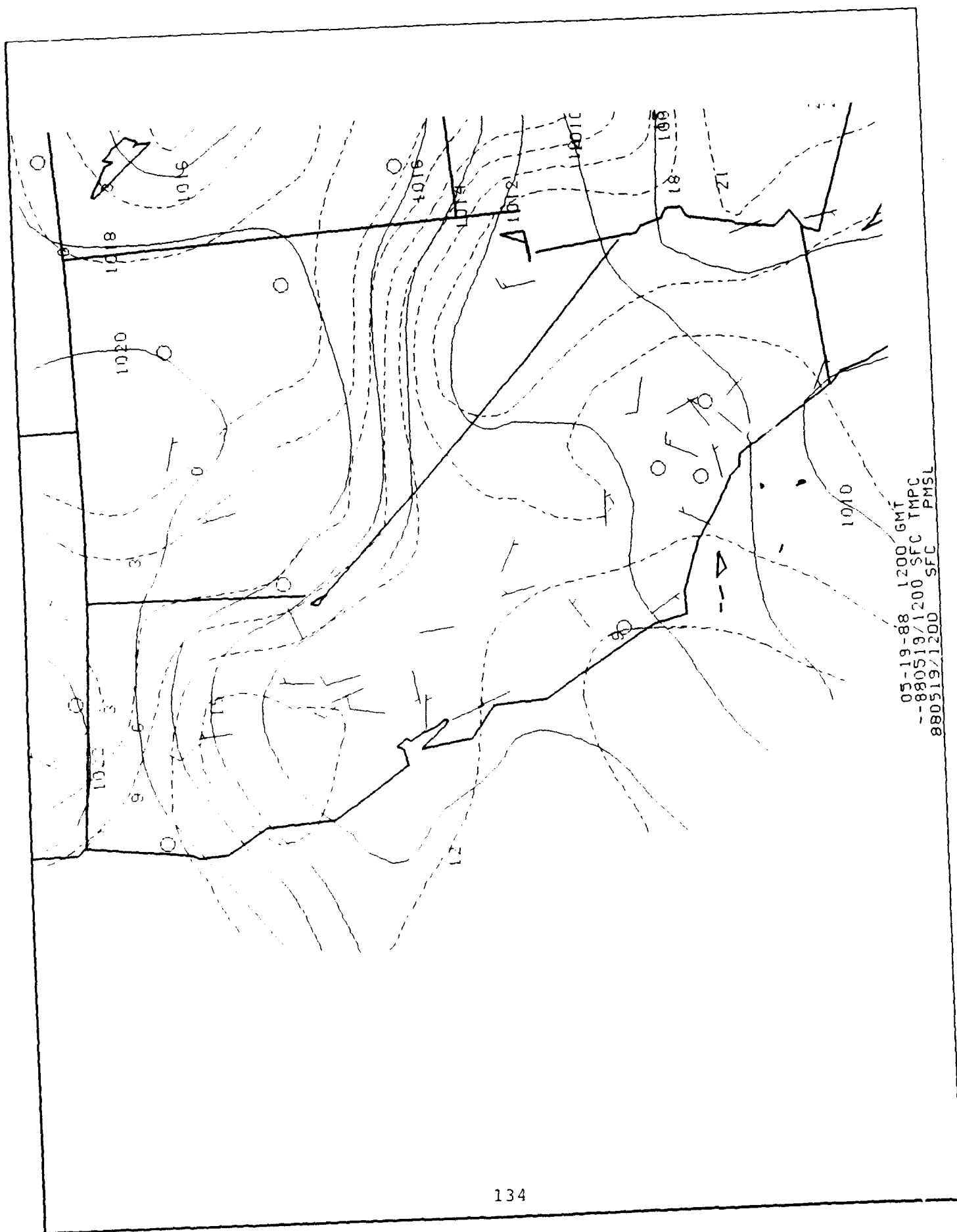
05-18-88 0000 GMT
880518/0000 SFC PMSL

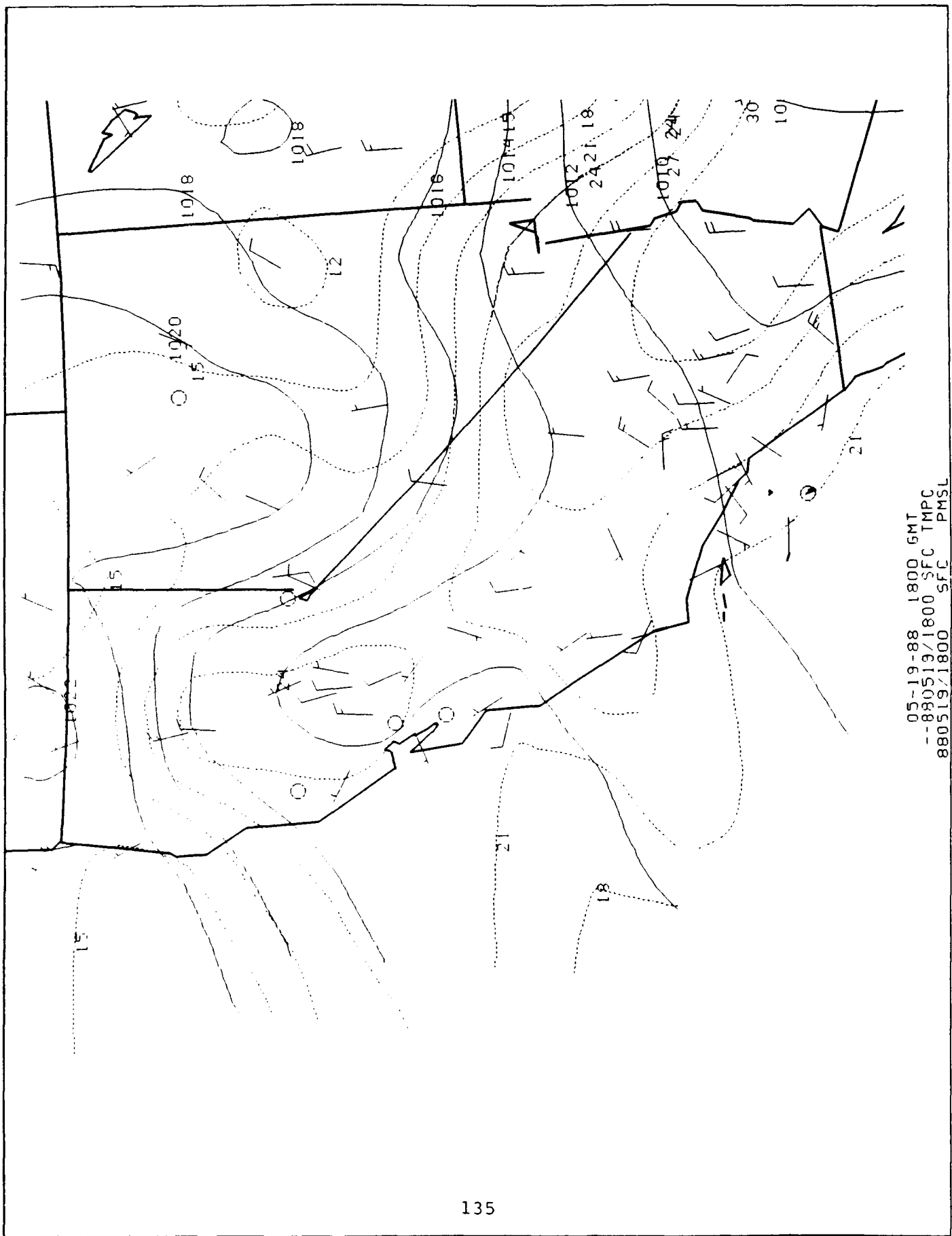


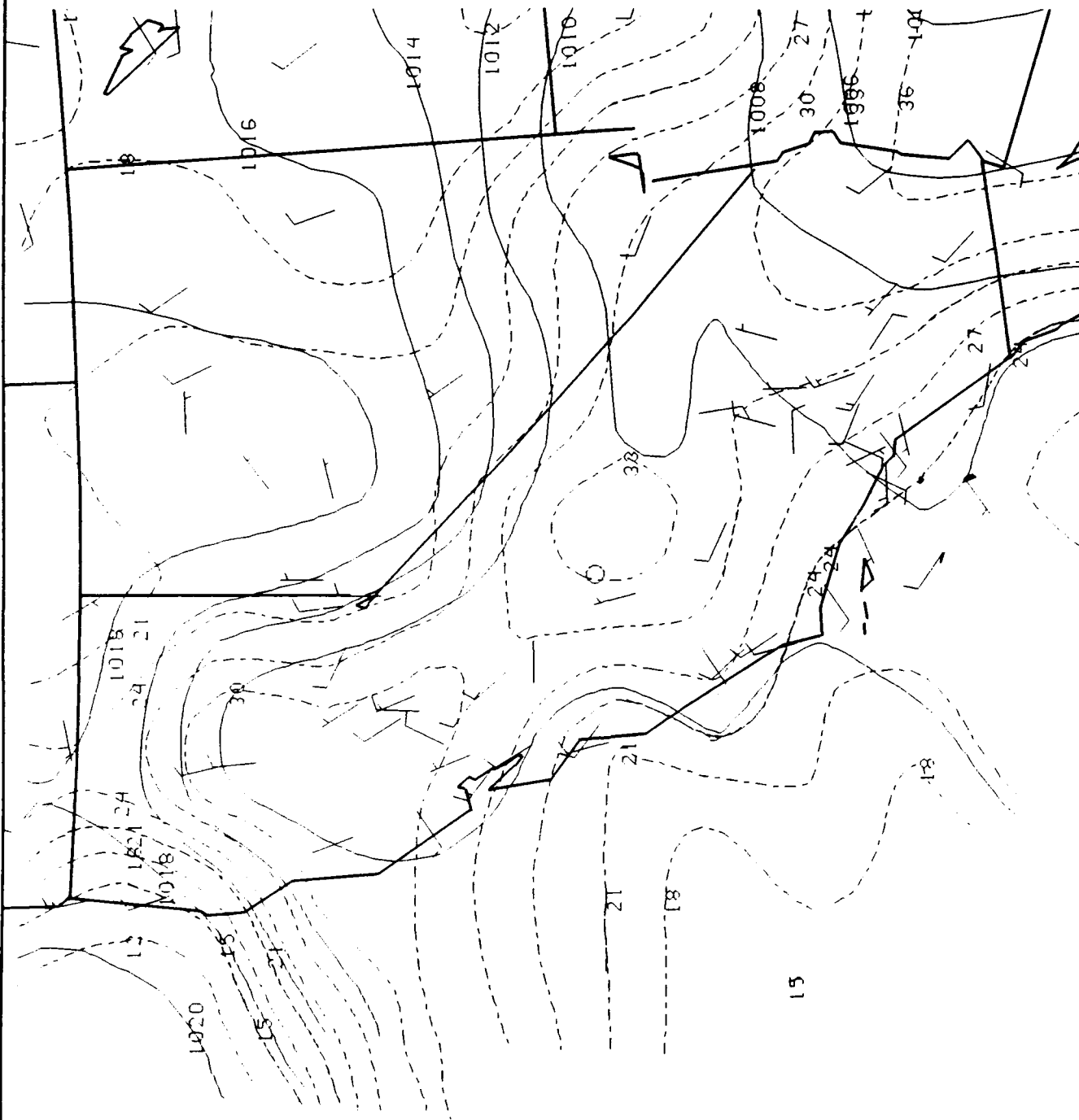


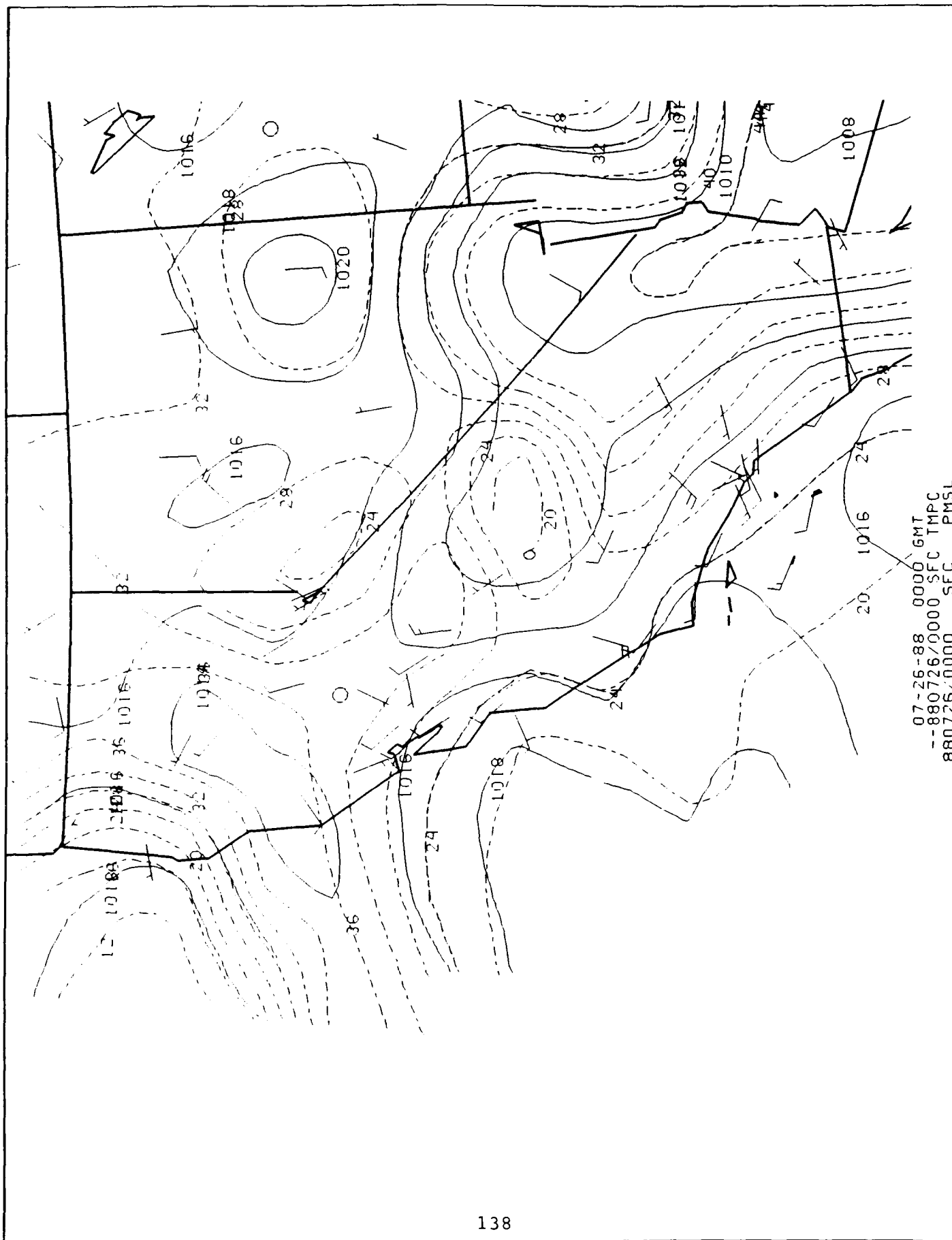
05-18-88 1800 GMT
--880518/1800 SFC 1MPC
880518/1800 SFC 1MPC



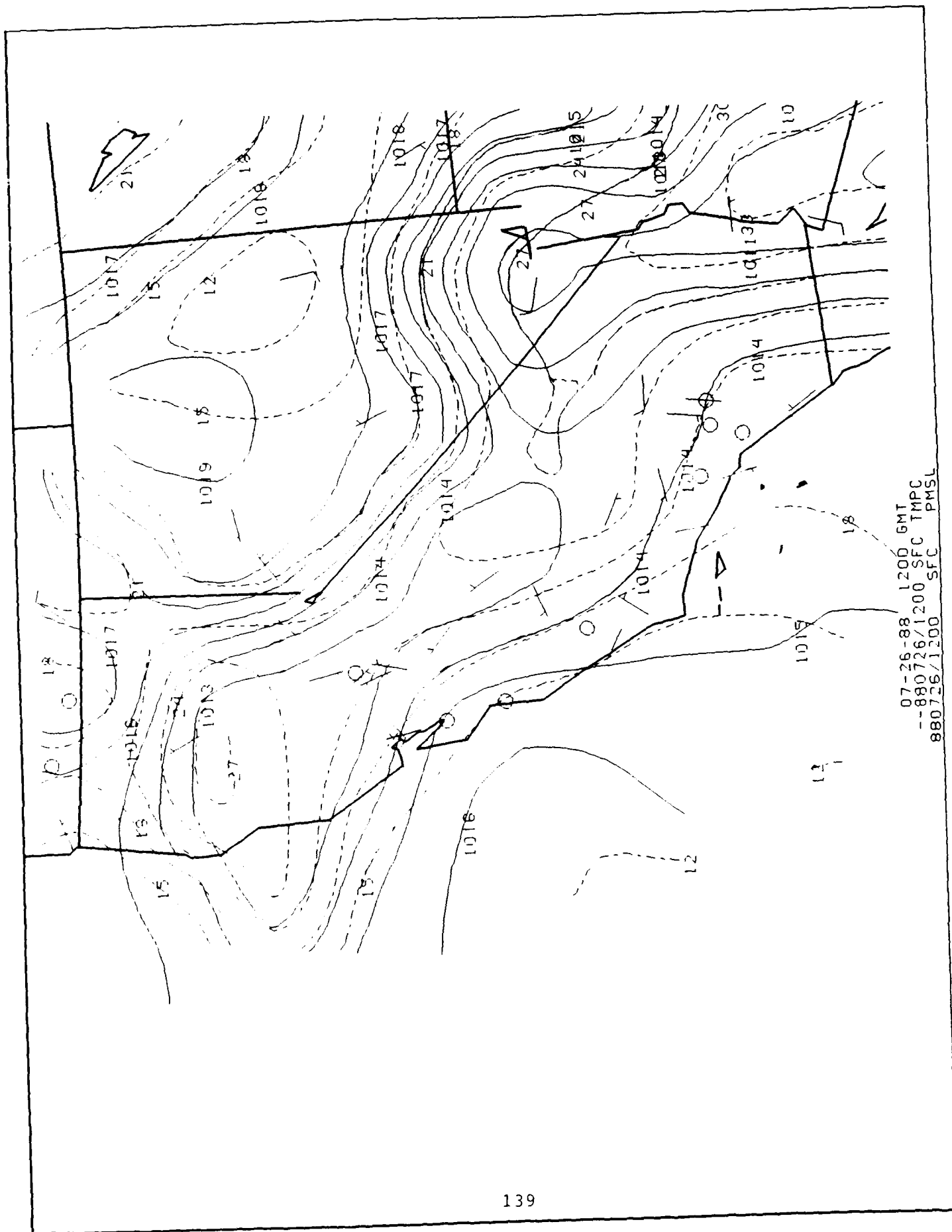


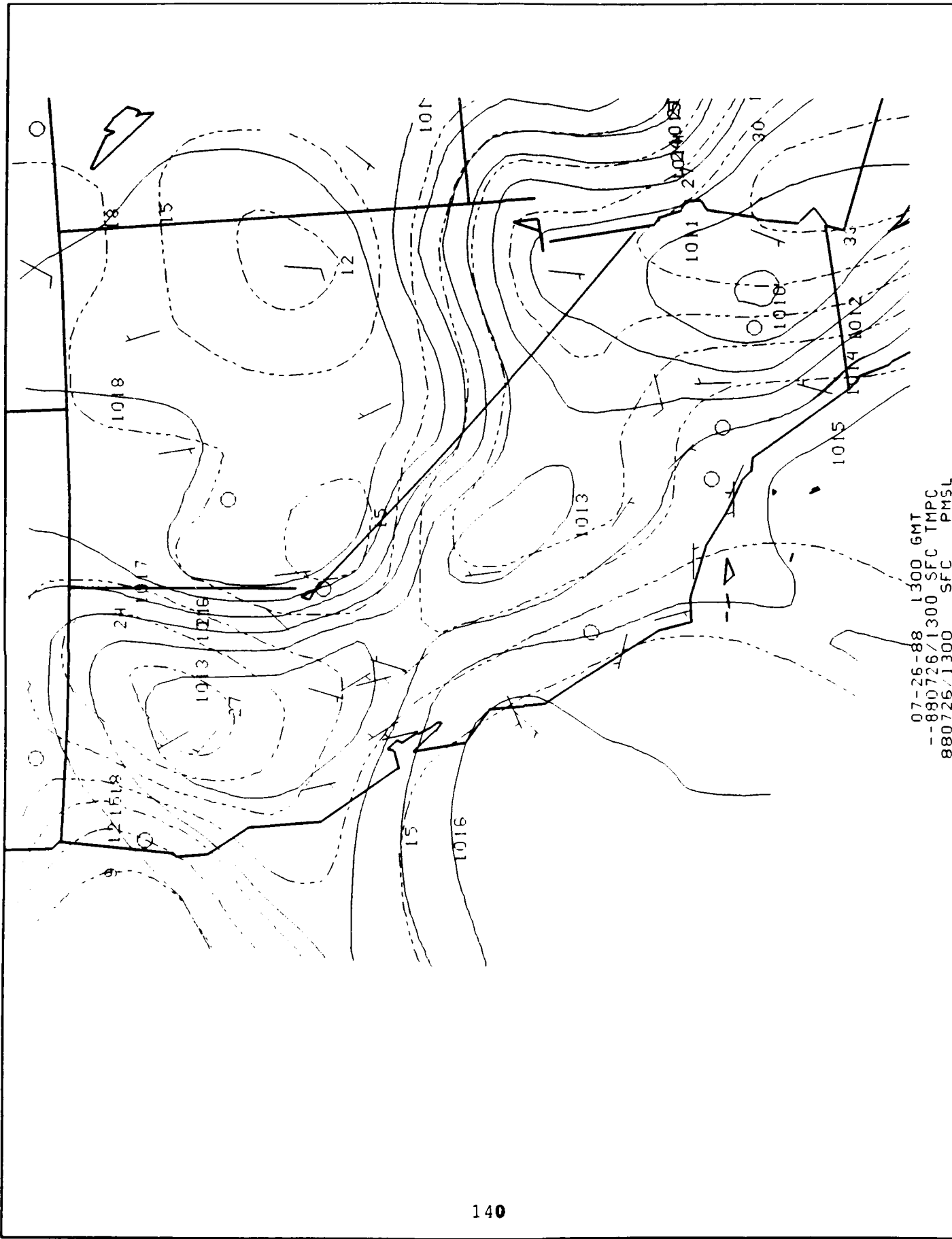


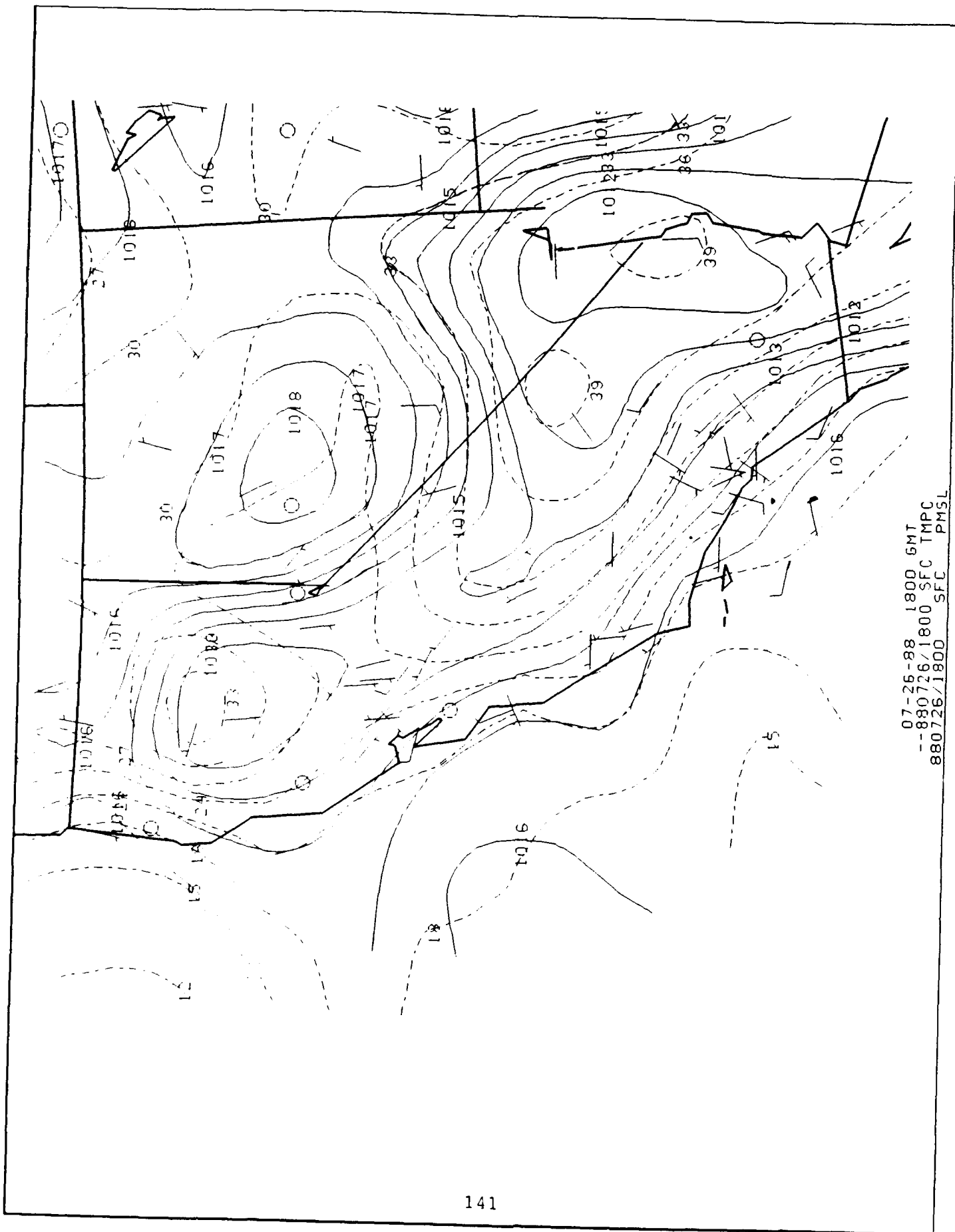


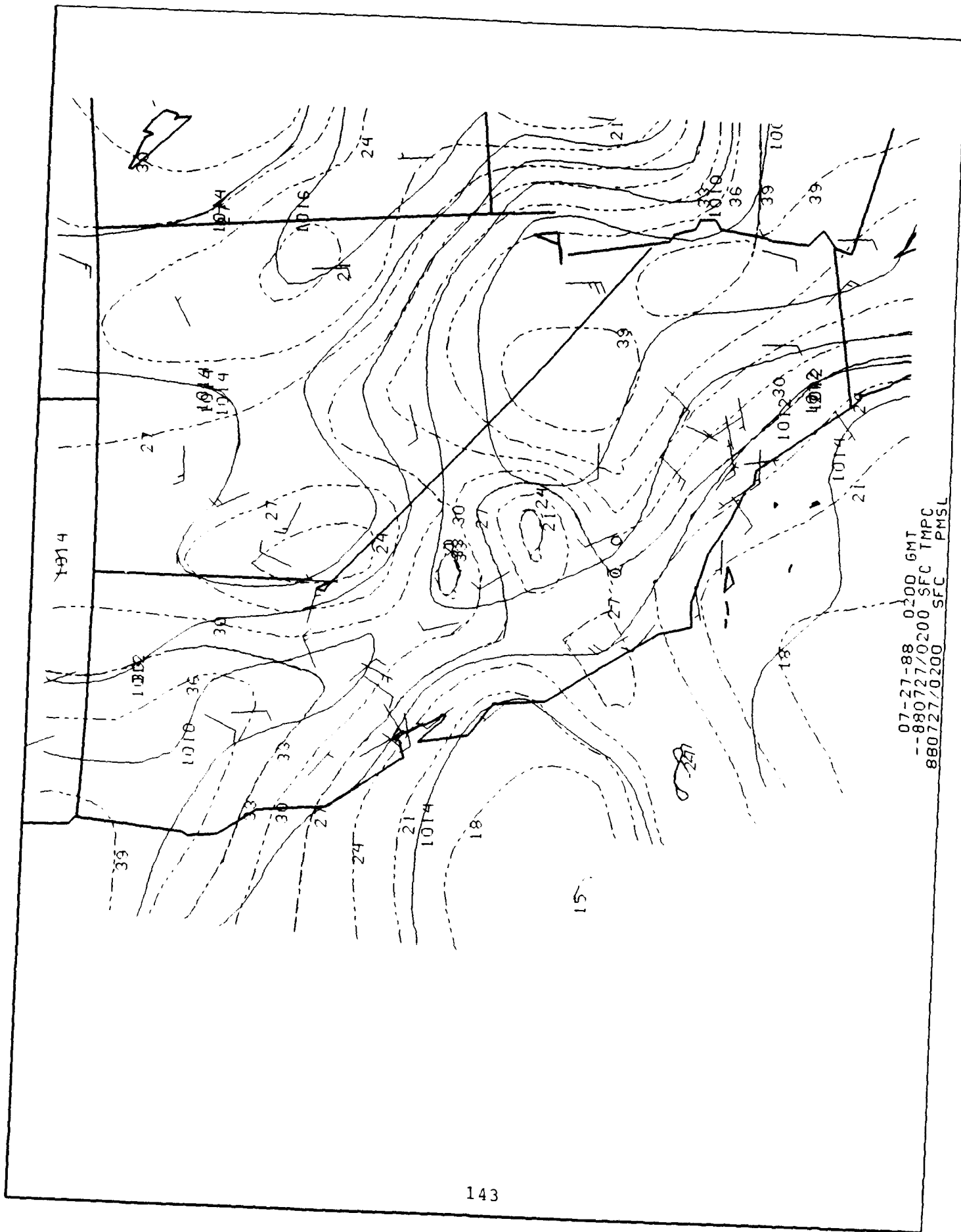


07-26-88 0000 GMT
 --880726/0000 SFC TMPC
 880726/0000 SFC PMSL

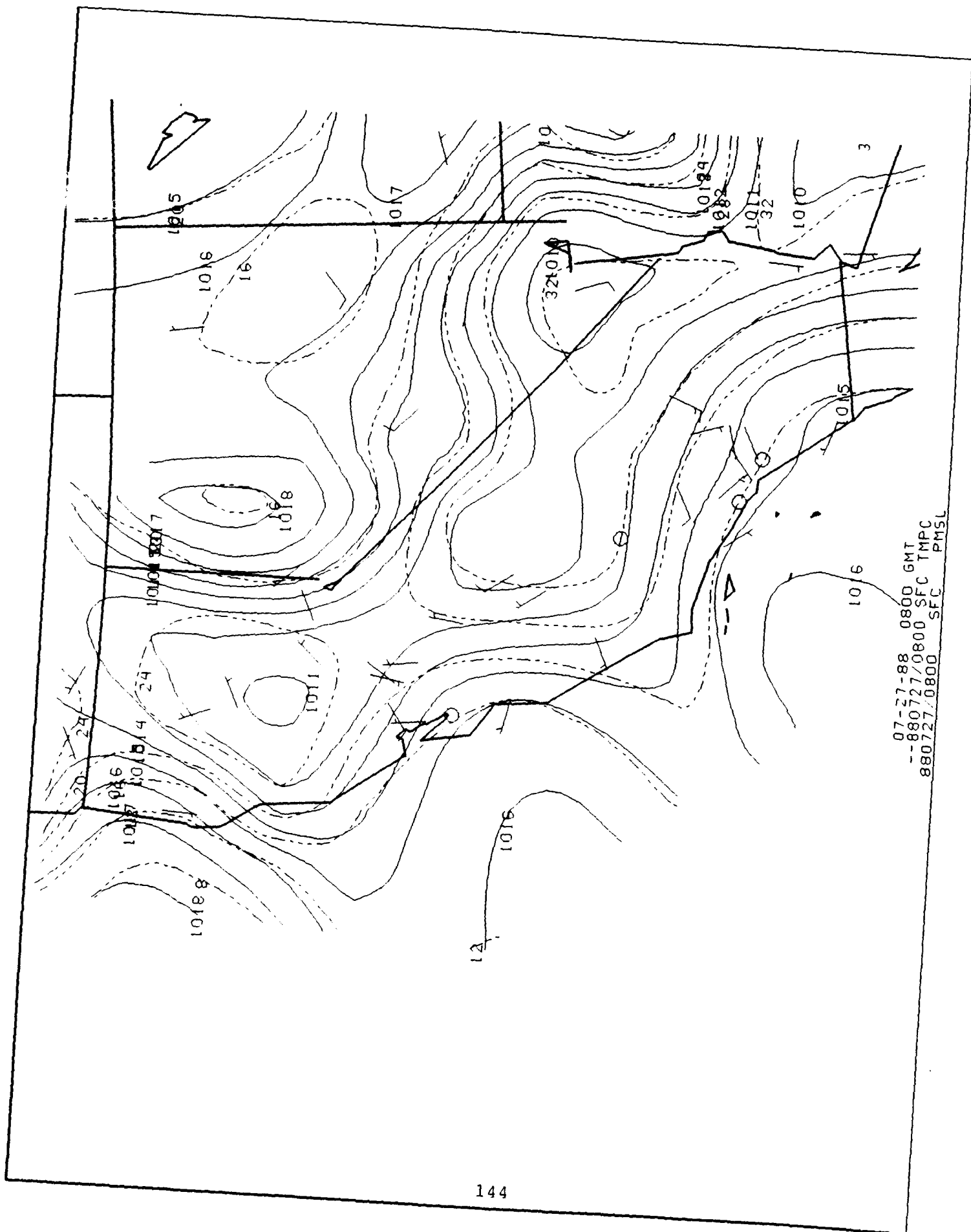


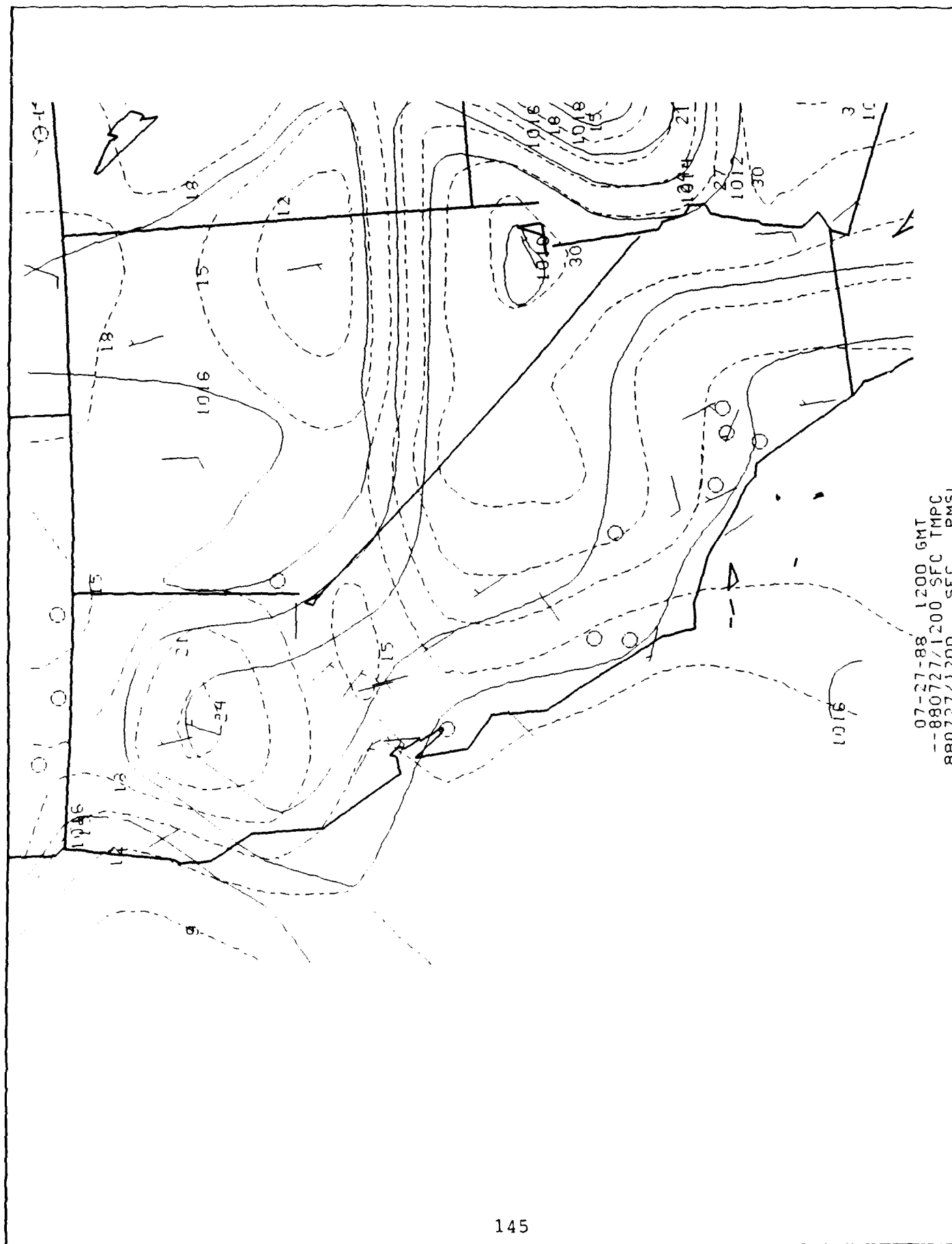


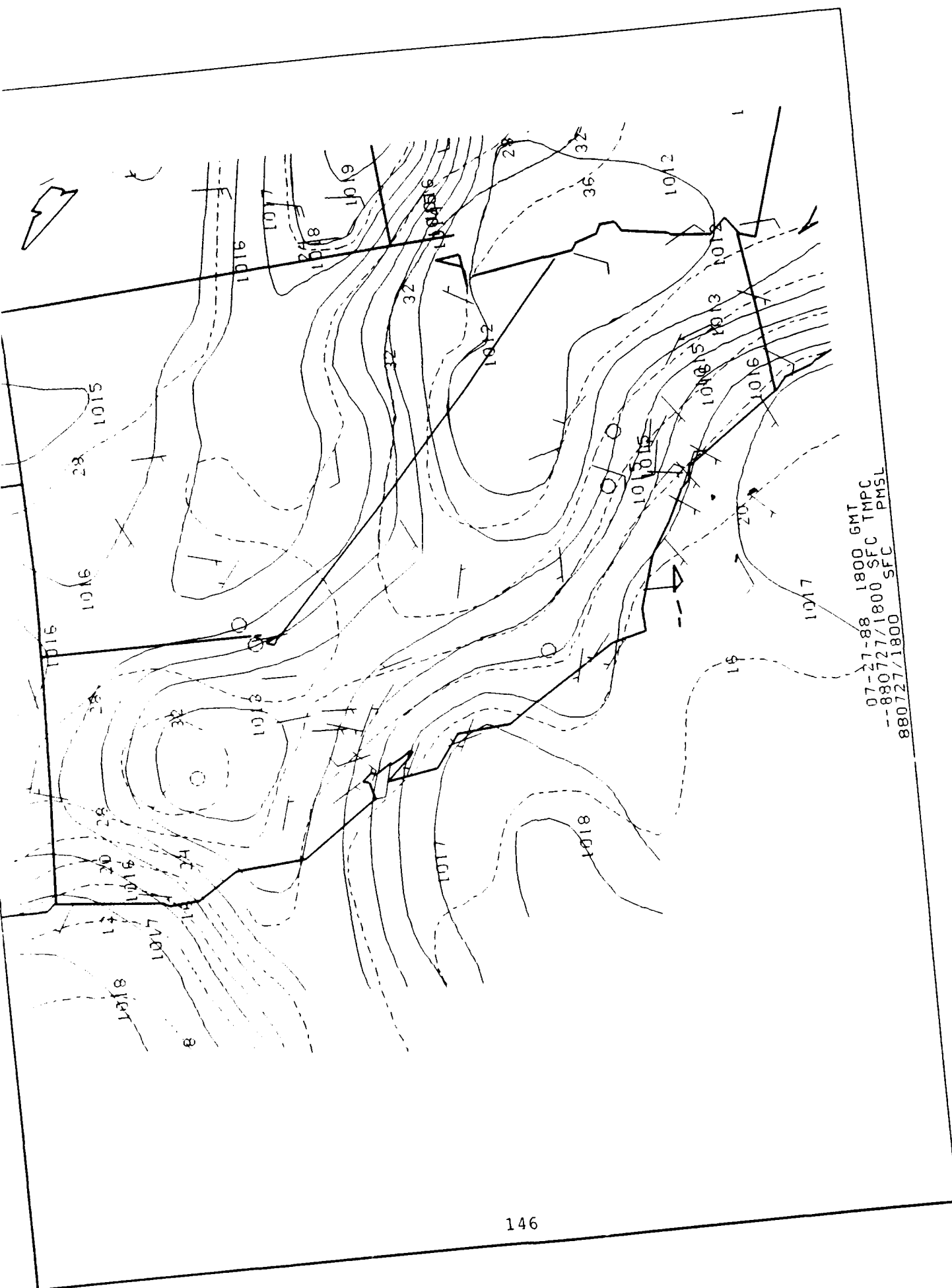


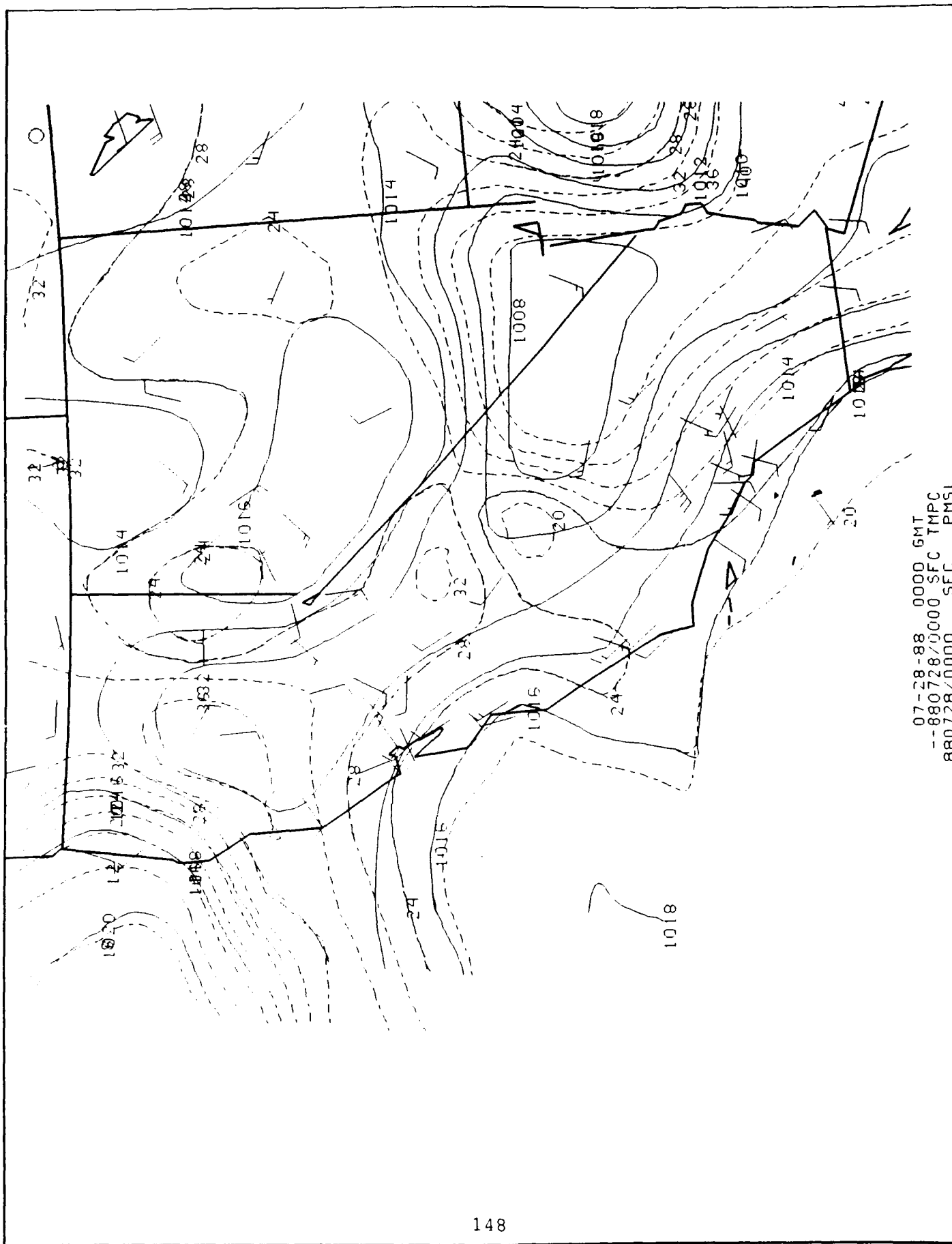


07-27-88 0200 GMT
 --880727/0200 SFC TMPC
 880727/0200 SFC PMSL

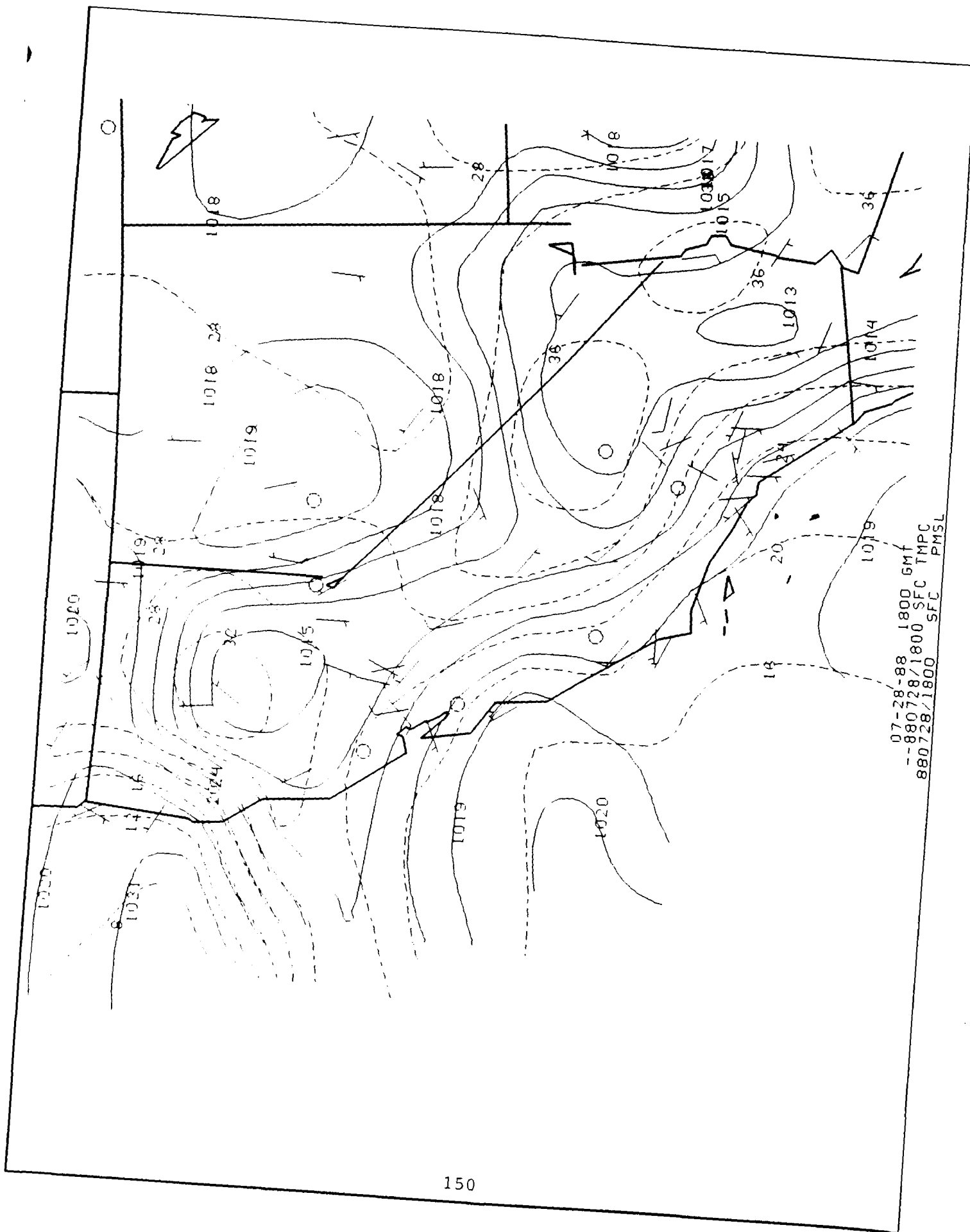


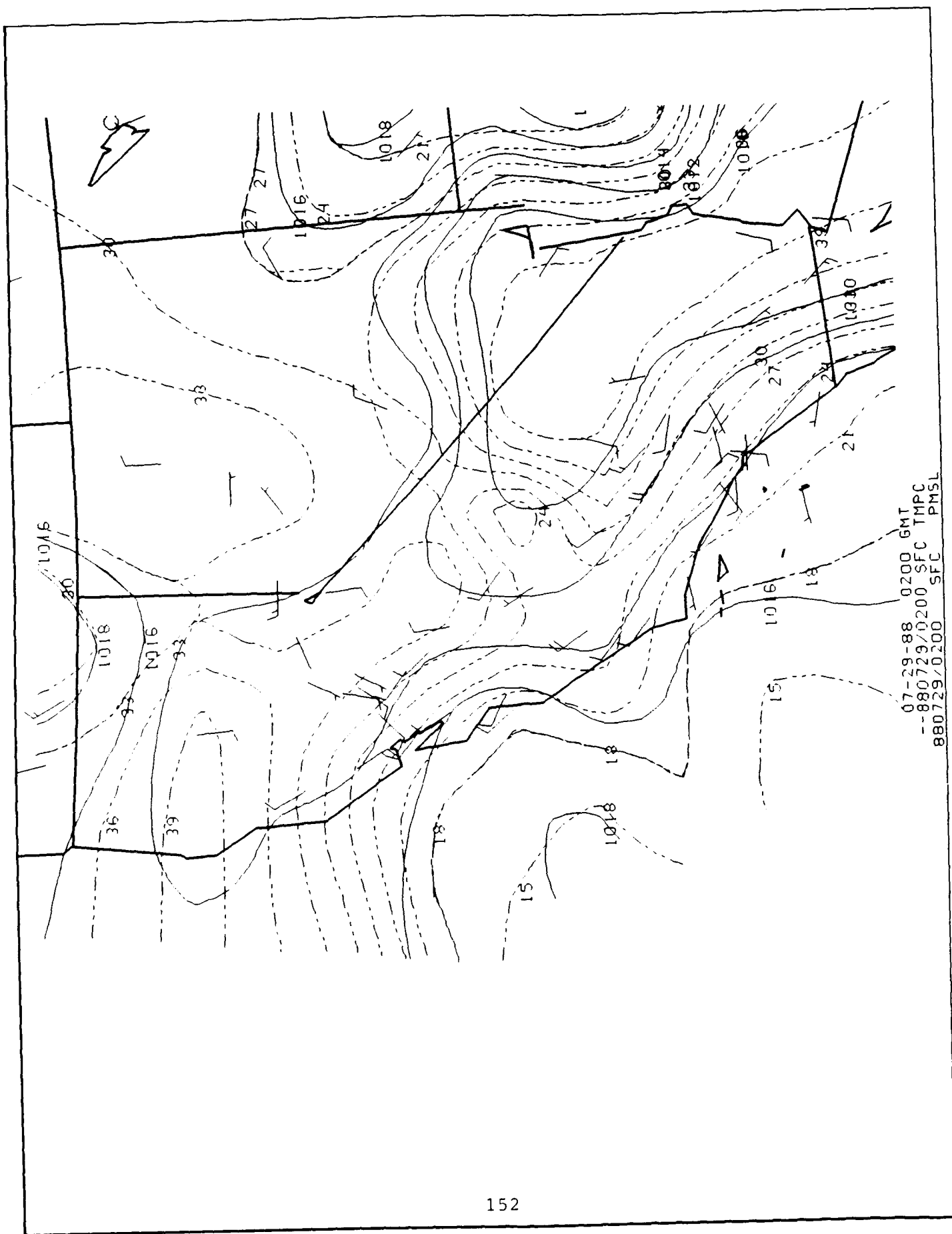


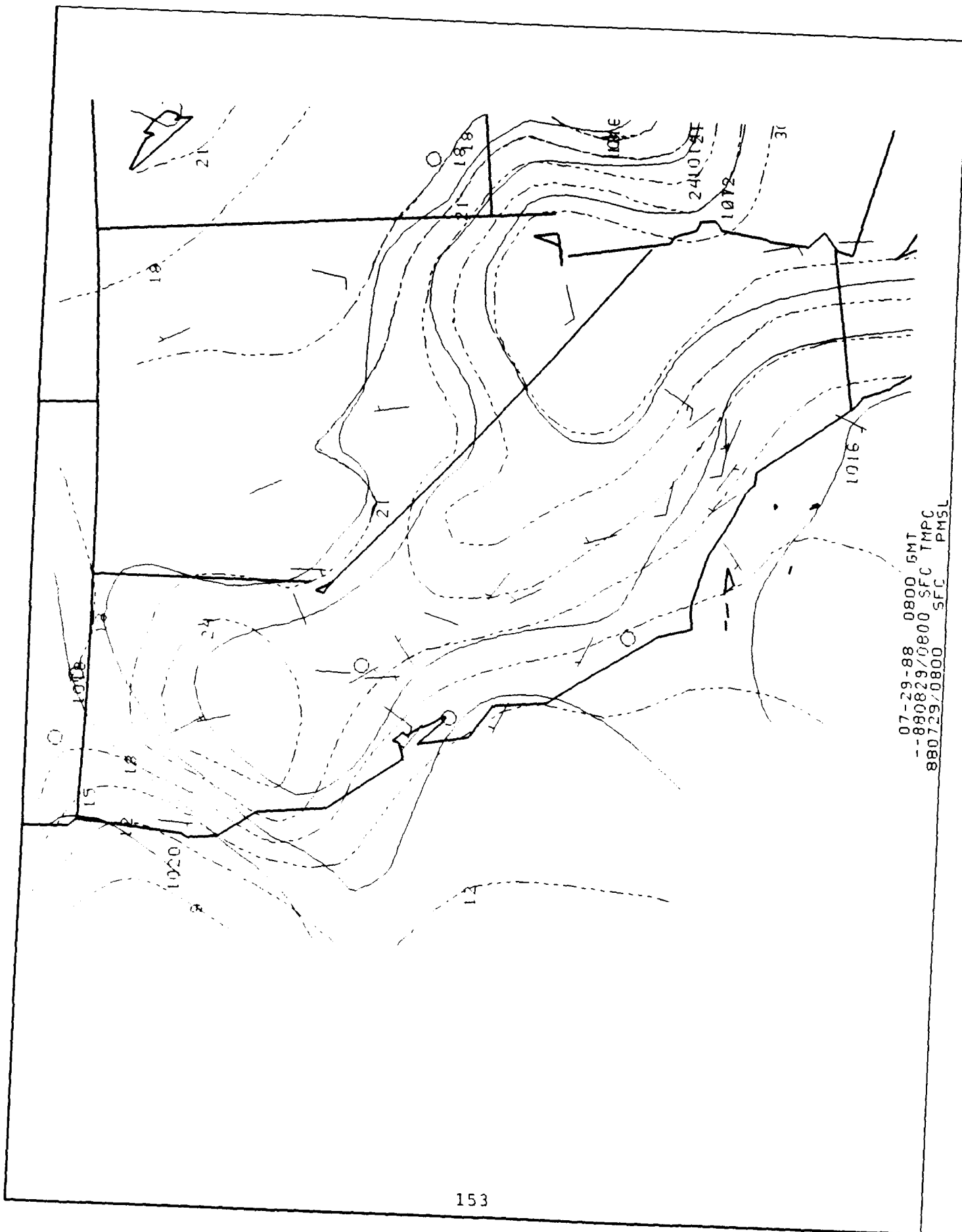




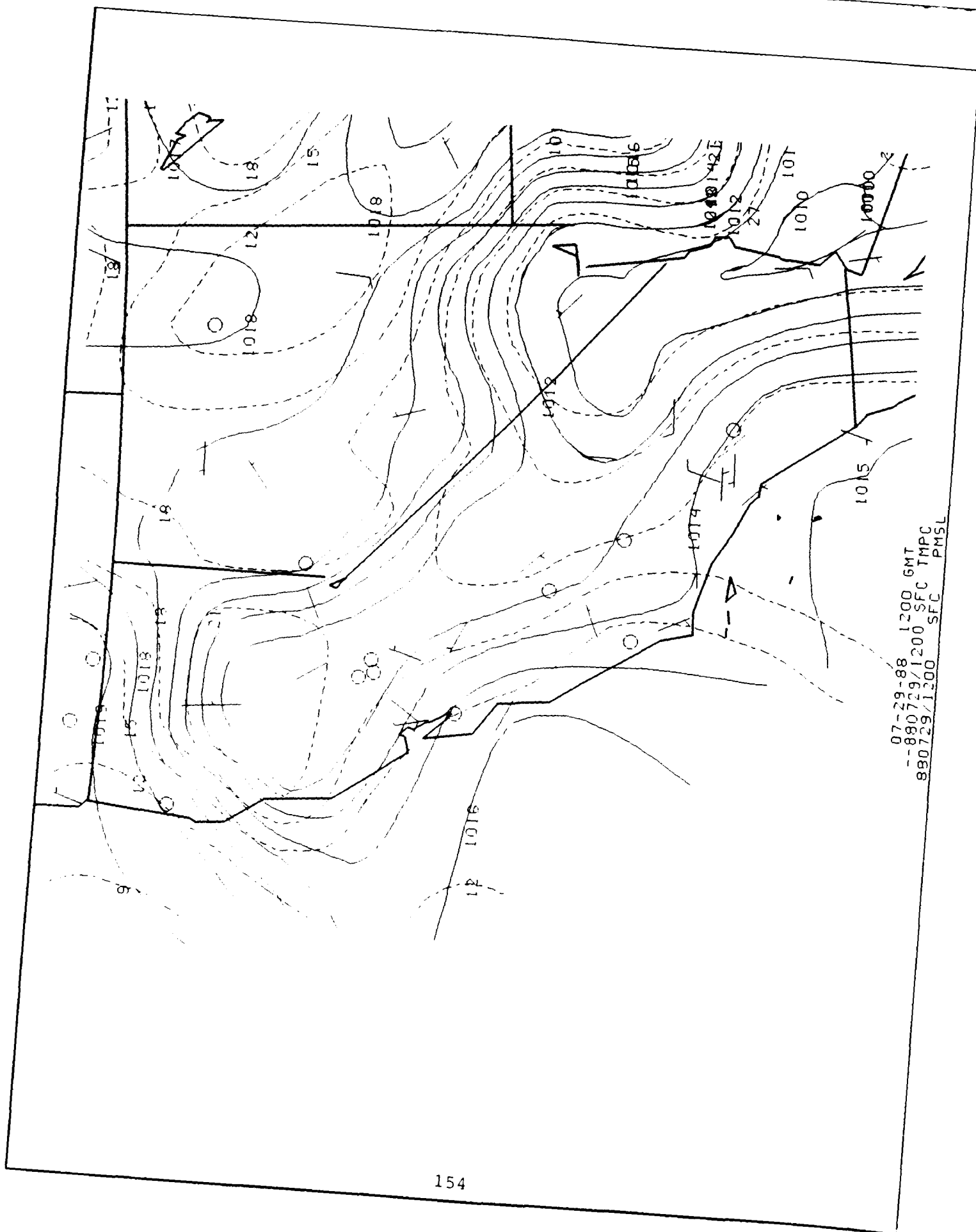
07-28-88 0000 GMT
 --880728/0000 SFC TMPC
 880728/0000 SFC PMSL

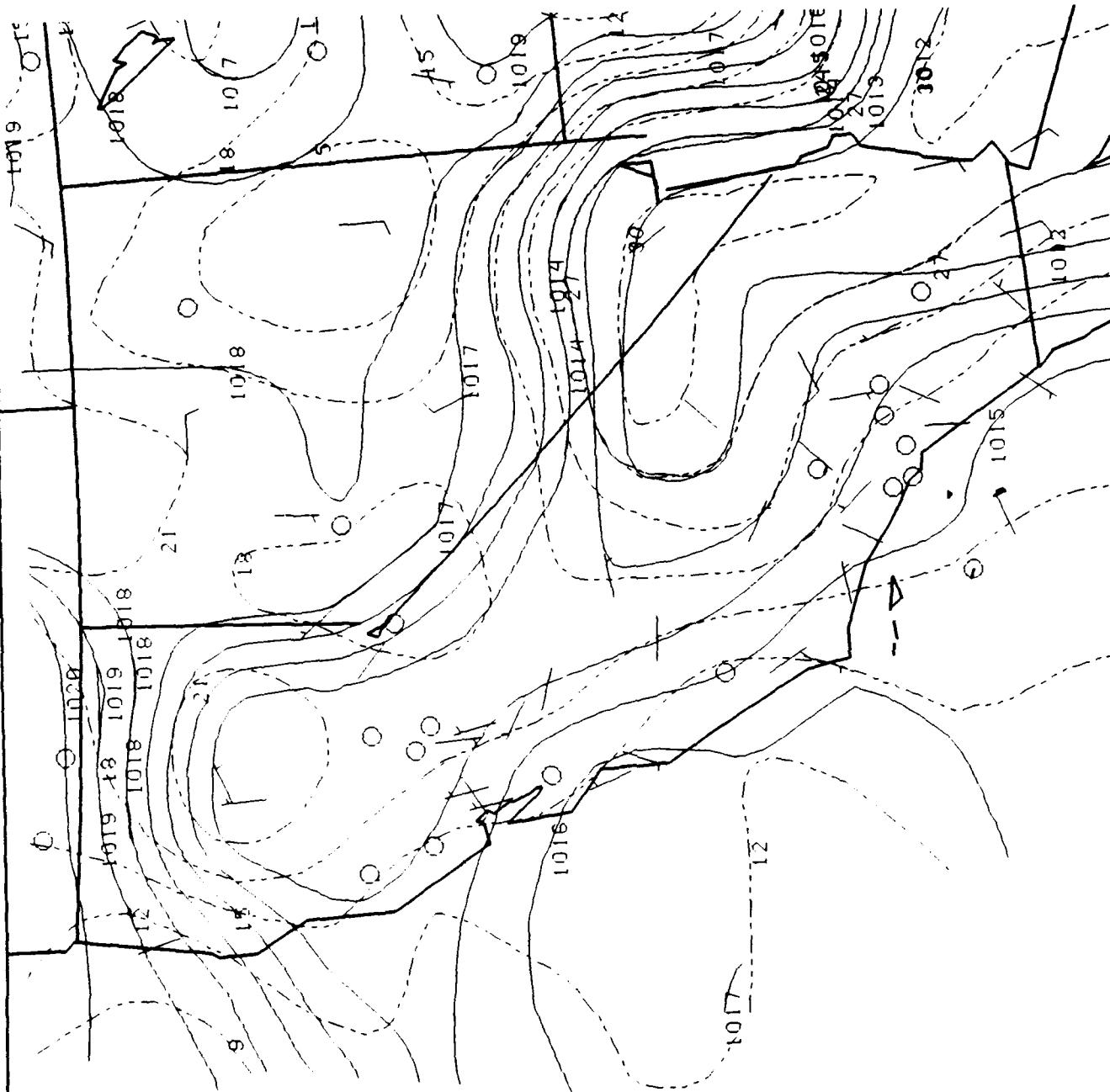




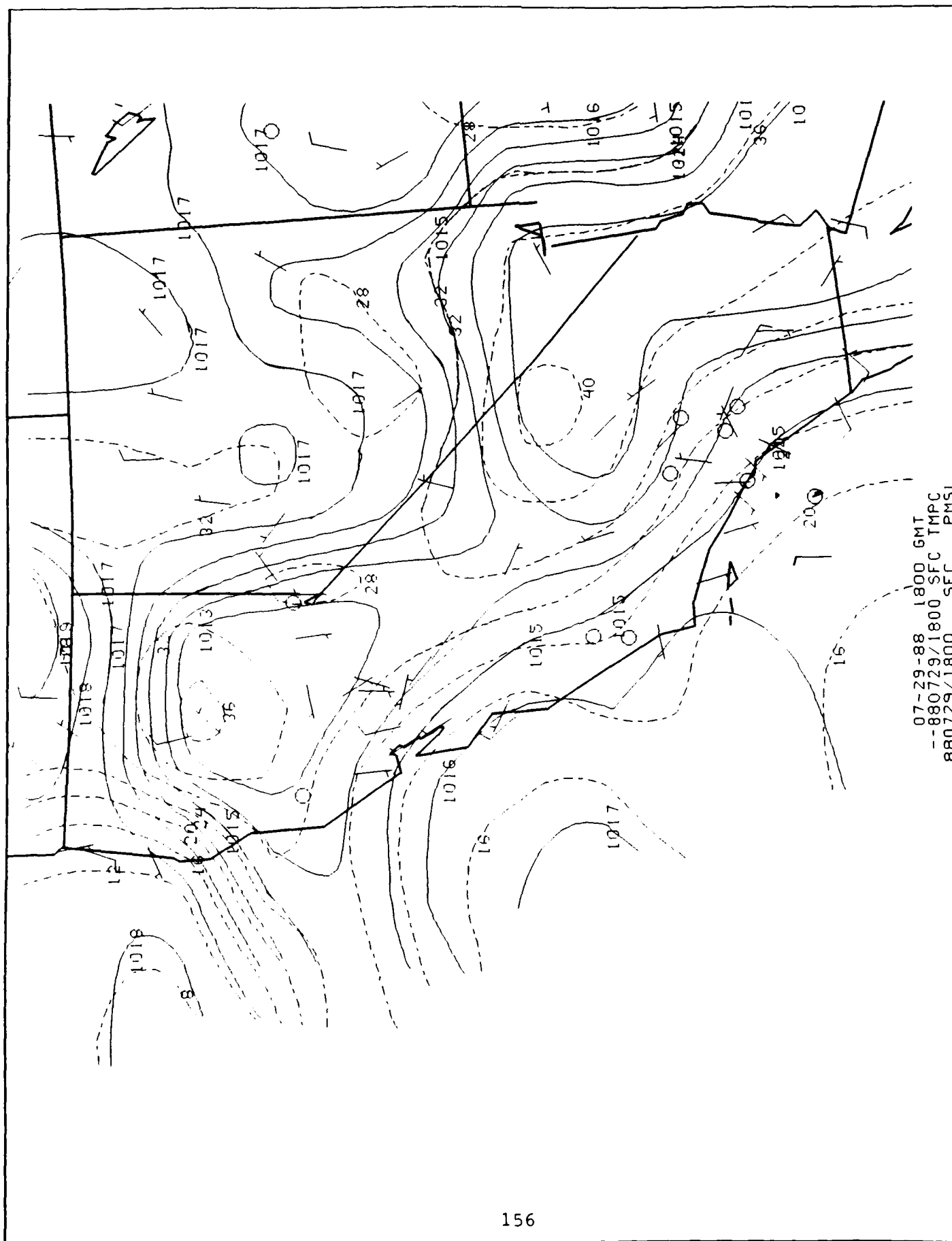


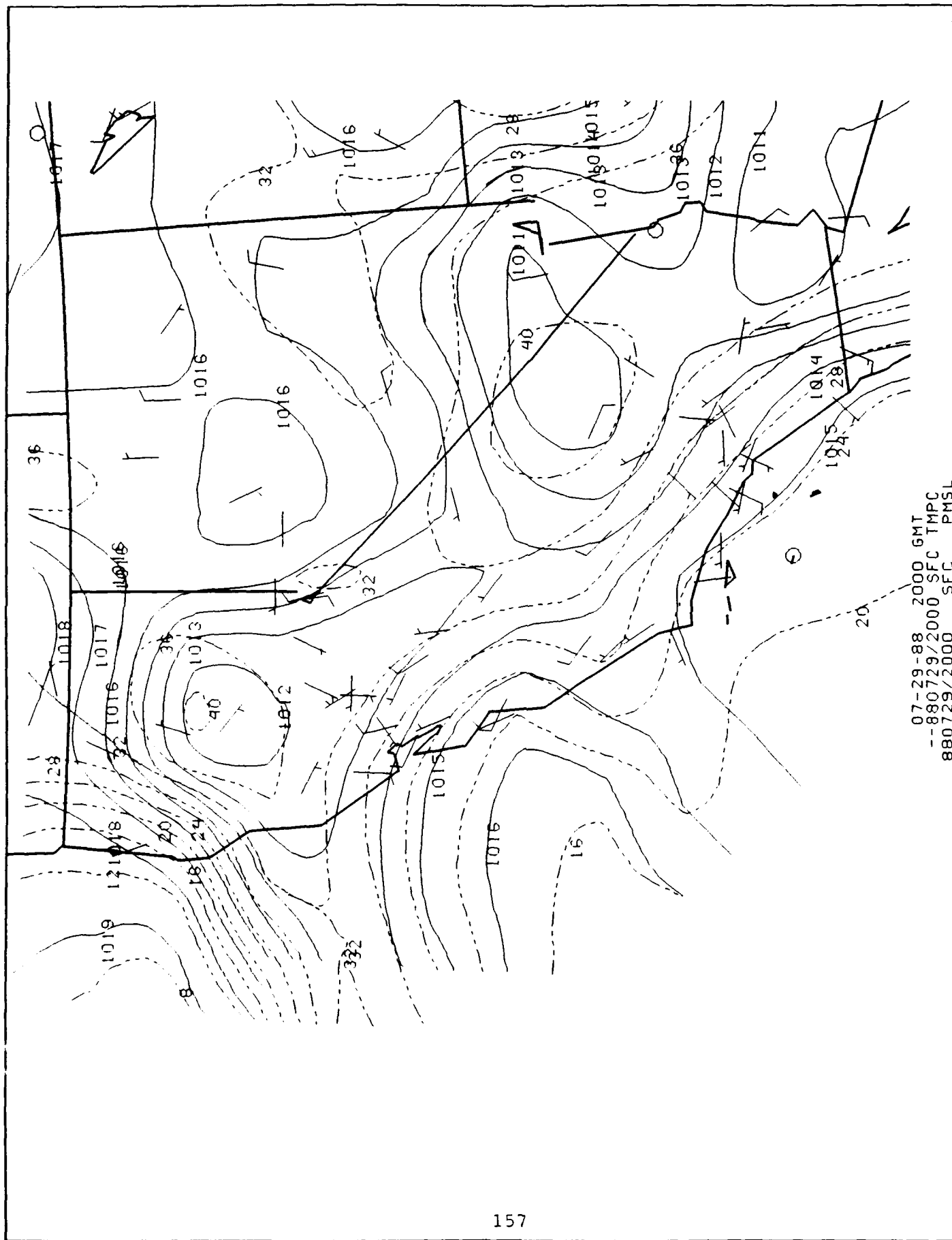
07-29-88 0800 GMT
--880829/0800 SFC TMPC
880729/0800 SFC PMSL

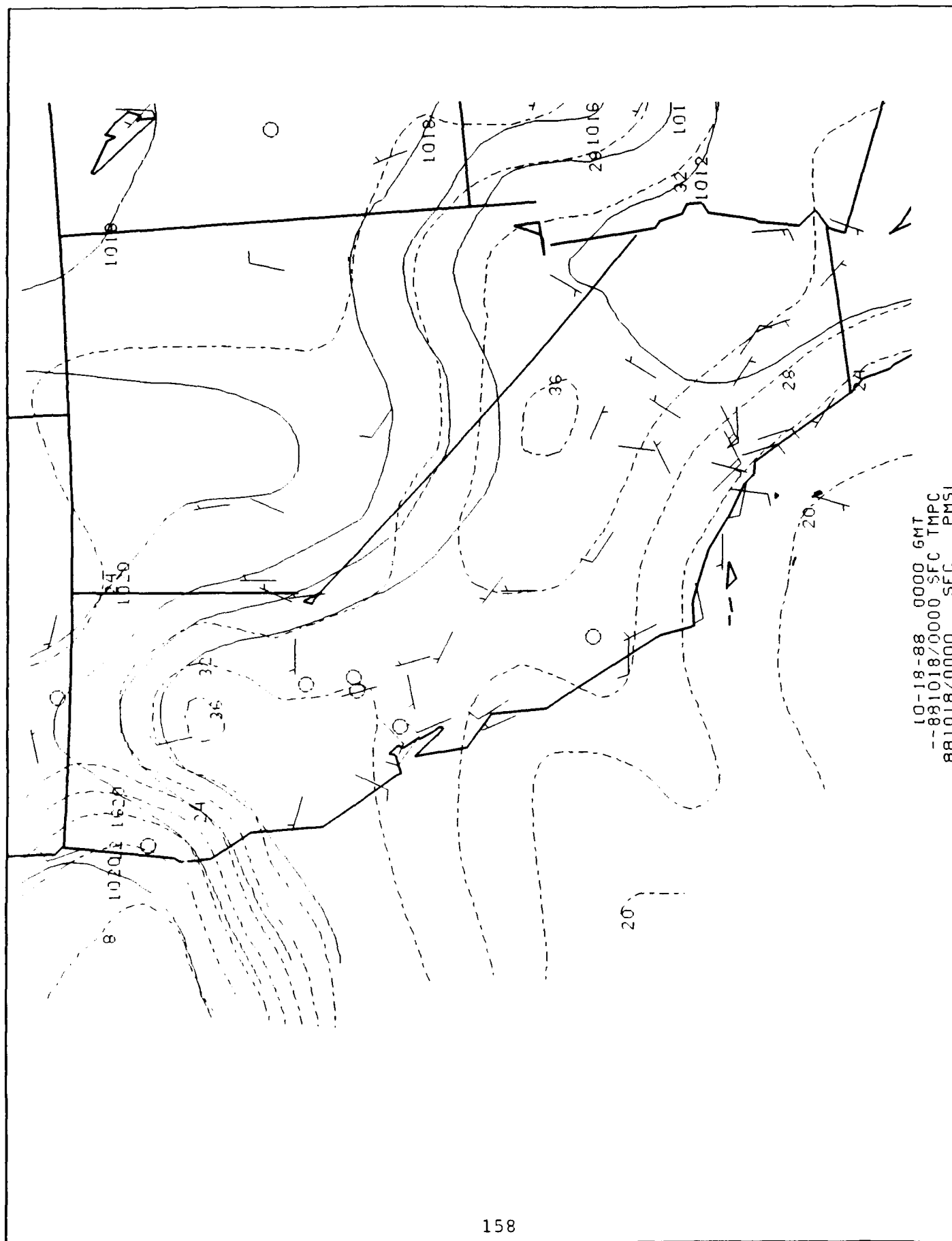


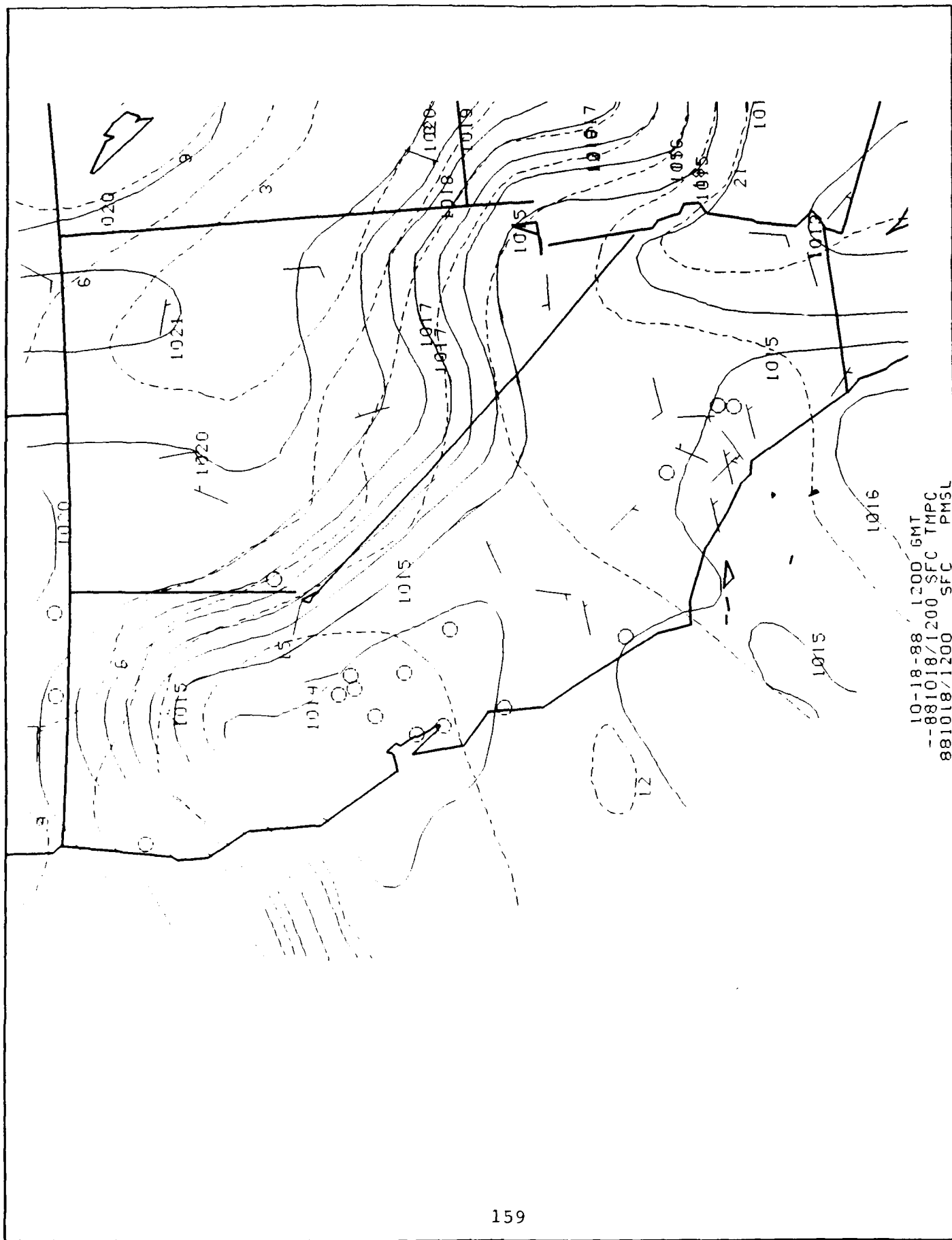


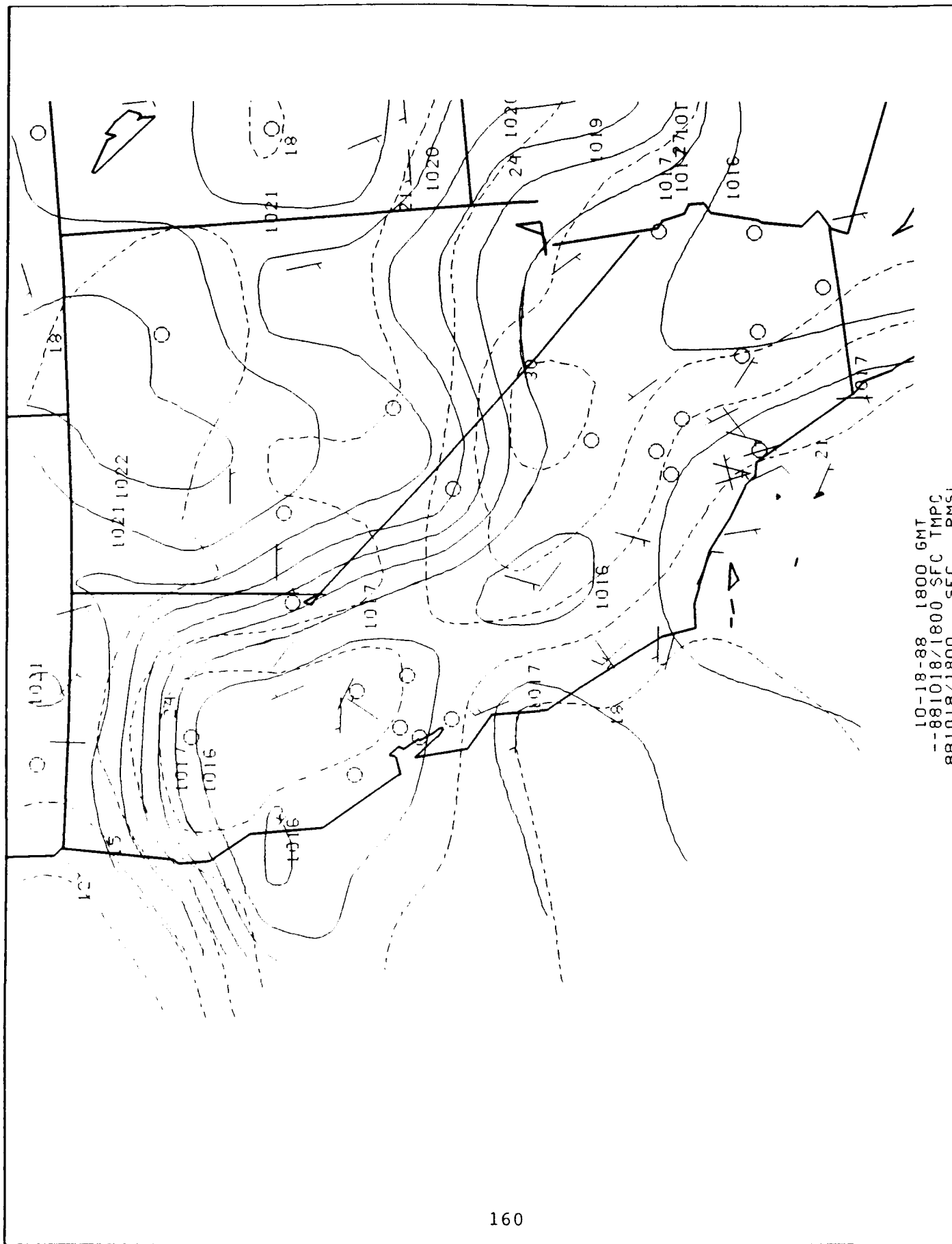
07-29-88 1400 GMT
 --880729/1400 SFC TMPC
 880729/1400 SFC PMSL

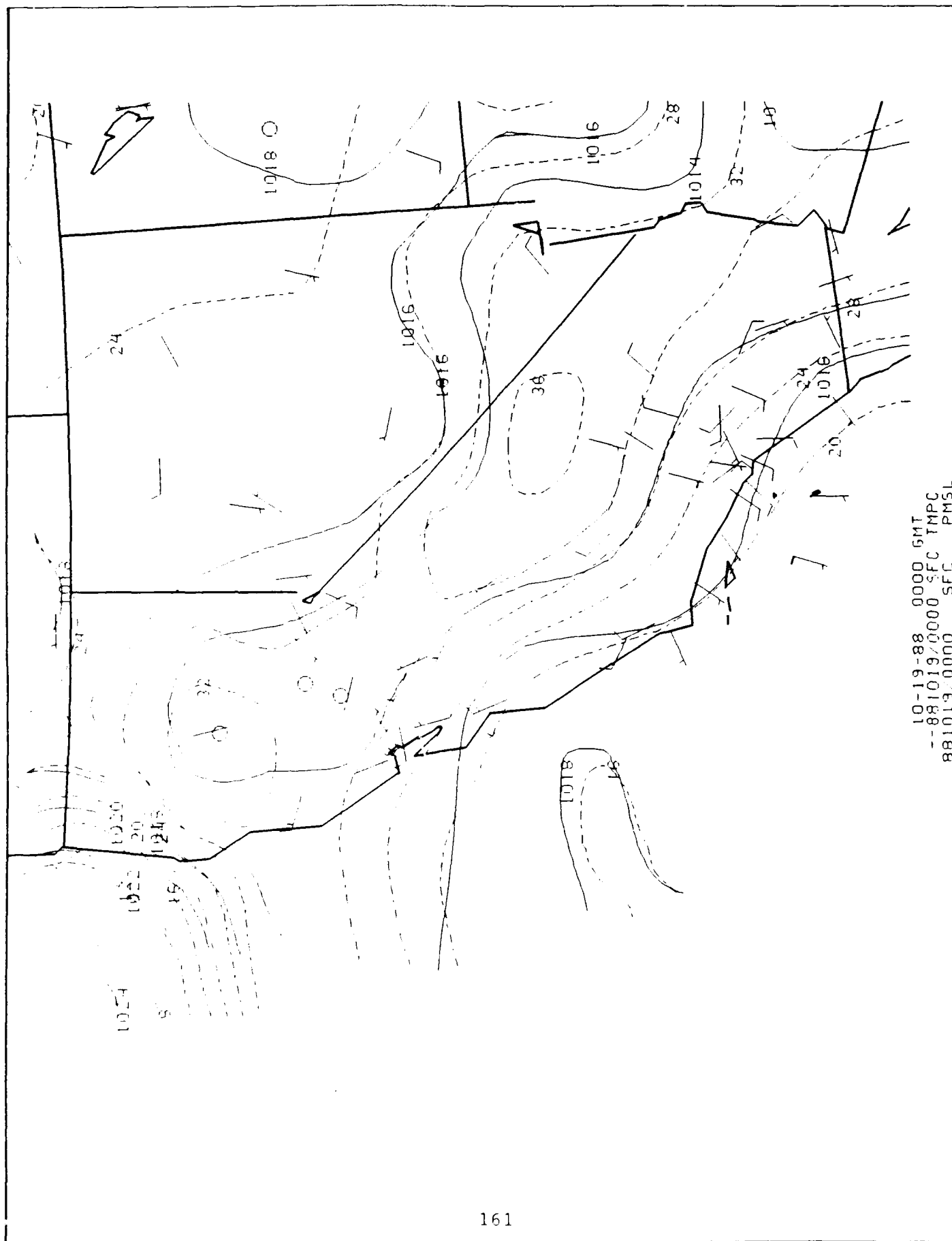


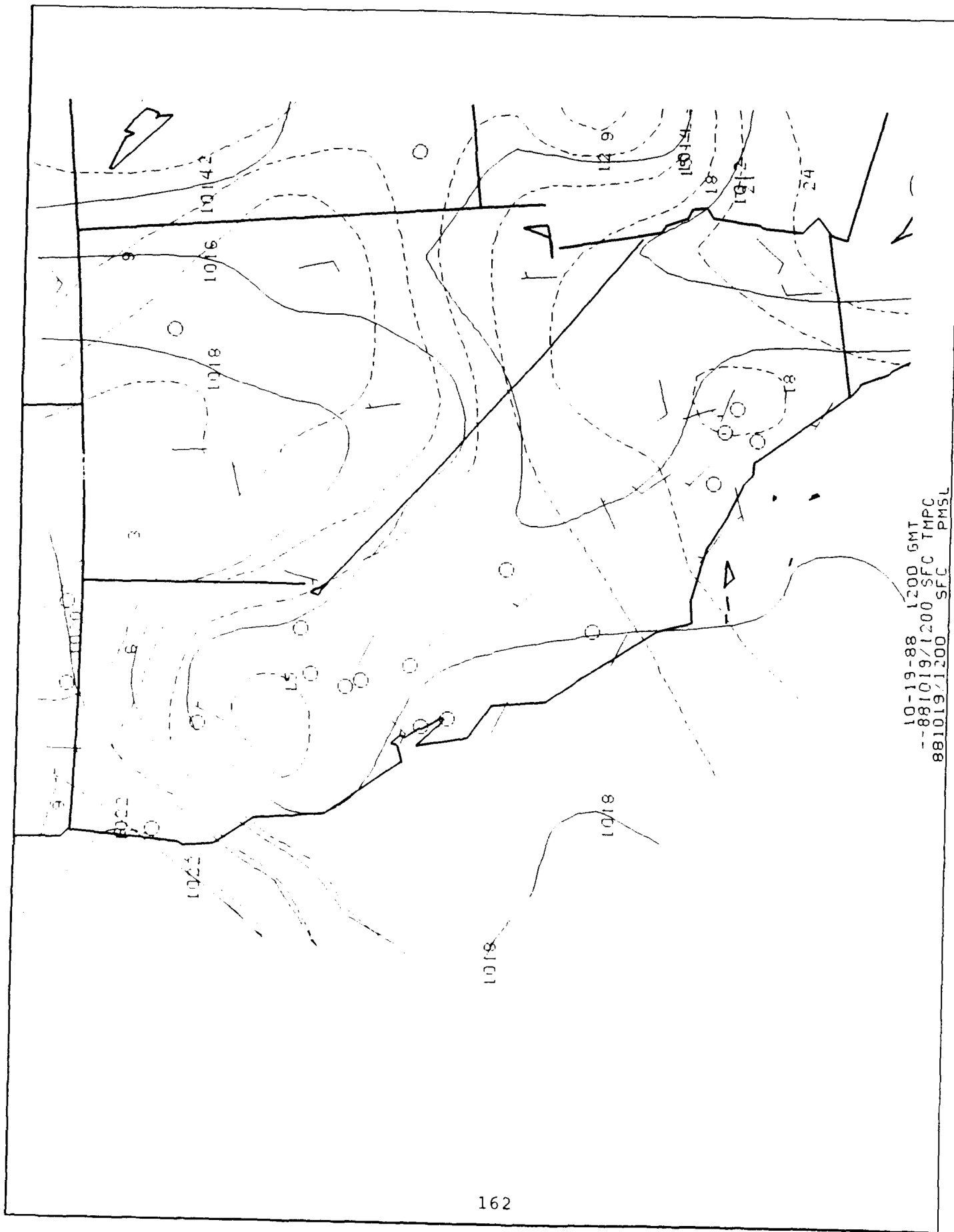


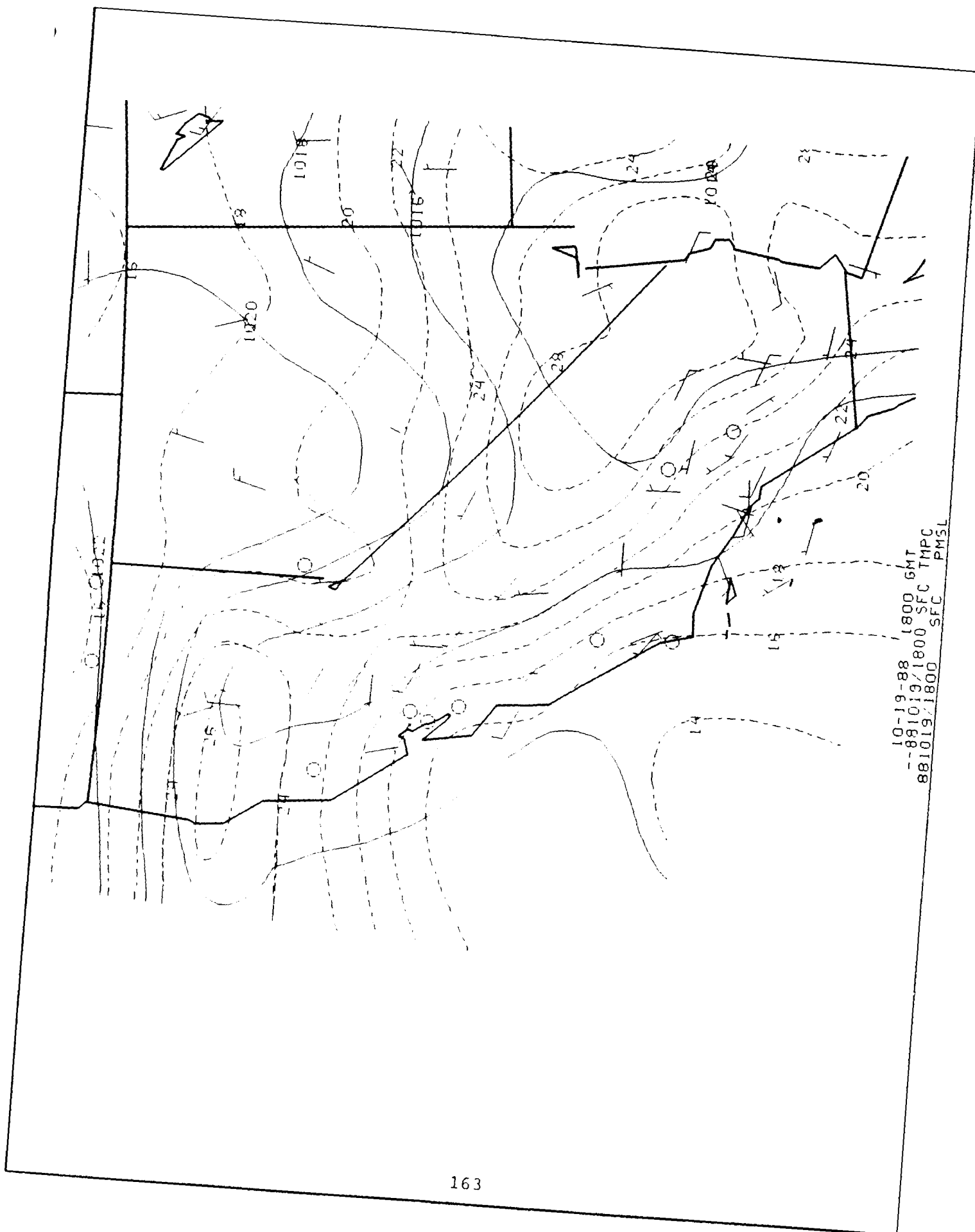












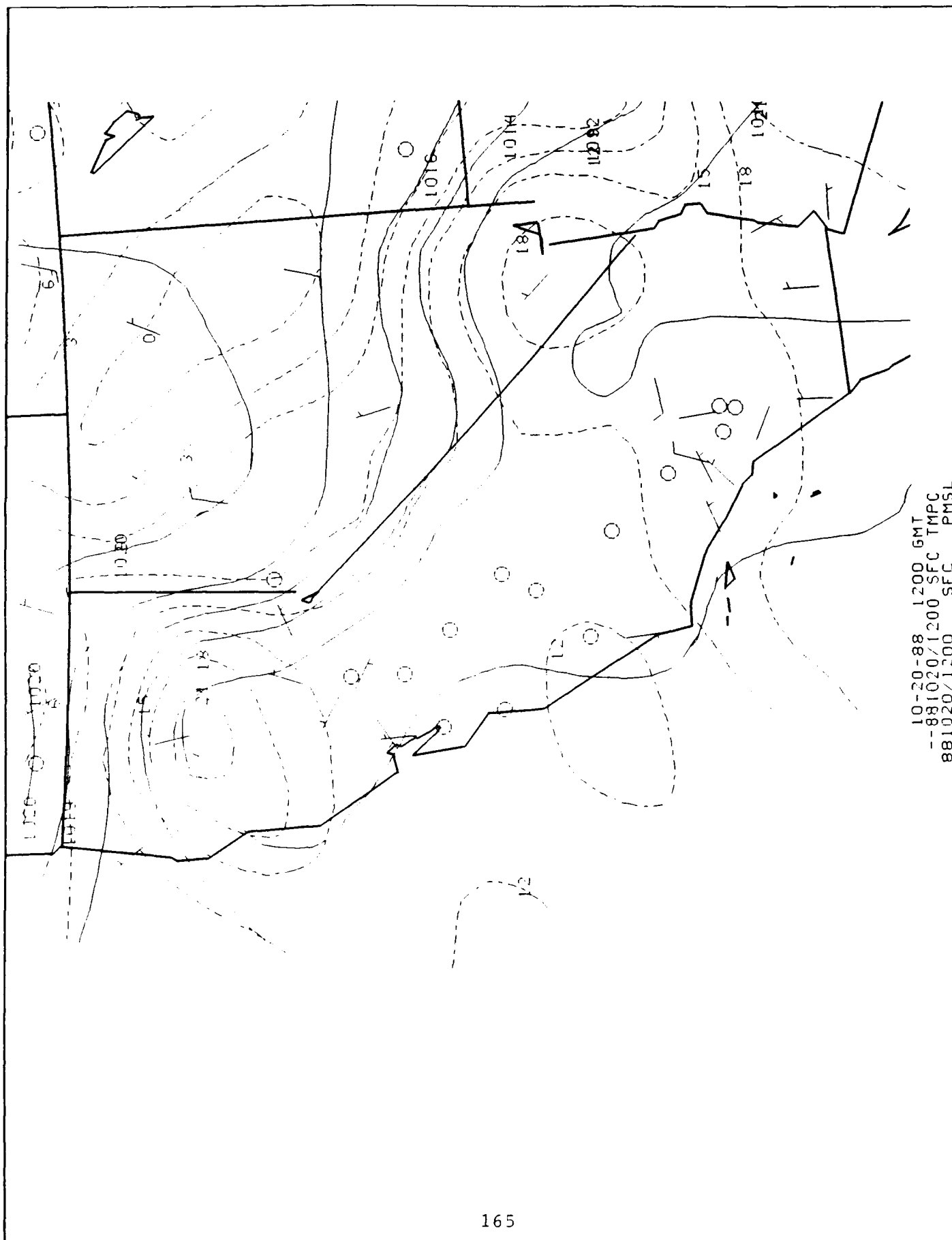


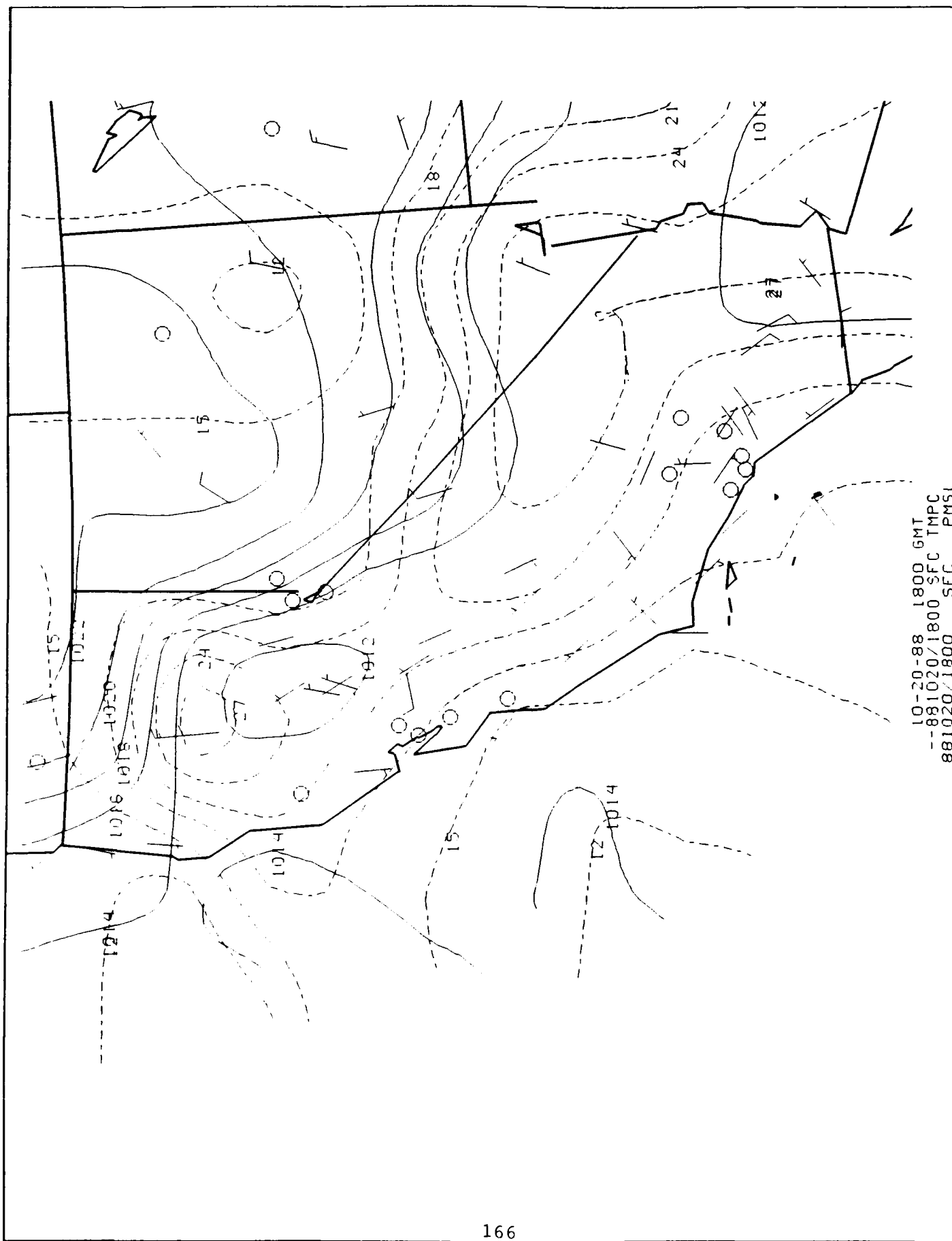
A

✓

A
--

10-20-88 0000 GMT





Regional Wind Field

The wind barbs (m/s) are hourly 12 ft averages from the Santa Barbara Air Quality Control District mesoscale network.

Day 1. The early morning charts show significant northwesterly winds only at the coastal sites, most likely reflecting the insulating effects of the nighttime surface inversion at inland locations. Remember, there was a northerly pressure gradient and no cloud cover on this night. This effect is reduced during the days, and the general pattern is more westerly winds near Santa Maria, with more northerly winds to the south of VBG.

Day 2. The morning winds (100, 700 LST) are extremely variable, with the exception of Pt. Arguello at 100. The strong 20 kt winds during clear conditions indicate that this anomaly which is often referenced is not exclusively a fog edge effect. The afternoon winds are consistent and westerly over the northern part of the region and in Lompoc, northerly at Pt. Arguello, and switch from onshore (south) to offshore (north) at the Santa Barbara Channel stations some time between 1300 and 1900.

Day 3. 100 and 700 maps are similar to day 2, including the strong 100 wind at Pt. Arguello. Coastal winds at 1300 are all onshore and inland winds are mostly westerly. The stations immediately at the coast most likely reflect local responses to the maximum heating which occurs at this time. The 1900 chart is still westerly in the north, but much more variable at other sites. Offshore flow is again suggested along the Santa Barbara Channel.

Day 4. 100 winds are light and variable with the exception of Pt. Arguello, as was the case during the spring. 1300 winds are near westerly at most stations. 1900 shows increased variability in the Santa Barbara Channel, and the onshore/offshore preference of days 2 and 3 is missing.

Day 5. Variable 100 winds become light and westerly in the northern areas by 700. The 1300 map has generally west winds everywhere, which become light and variable by 1900.

Day 6. Variable 100 winds gave way to consistent coastal onshore winds at 700 (west near Santa Maria, Pt. Concepcion and south in the Santa Barbara Channel). 1300 winds are slightly veered from their 700 directions and the 1900 flow is variable.

Day 7. Light and variable conditions dominate until 1300 when coastal sites are westerly. Inland sites remain variable all day.

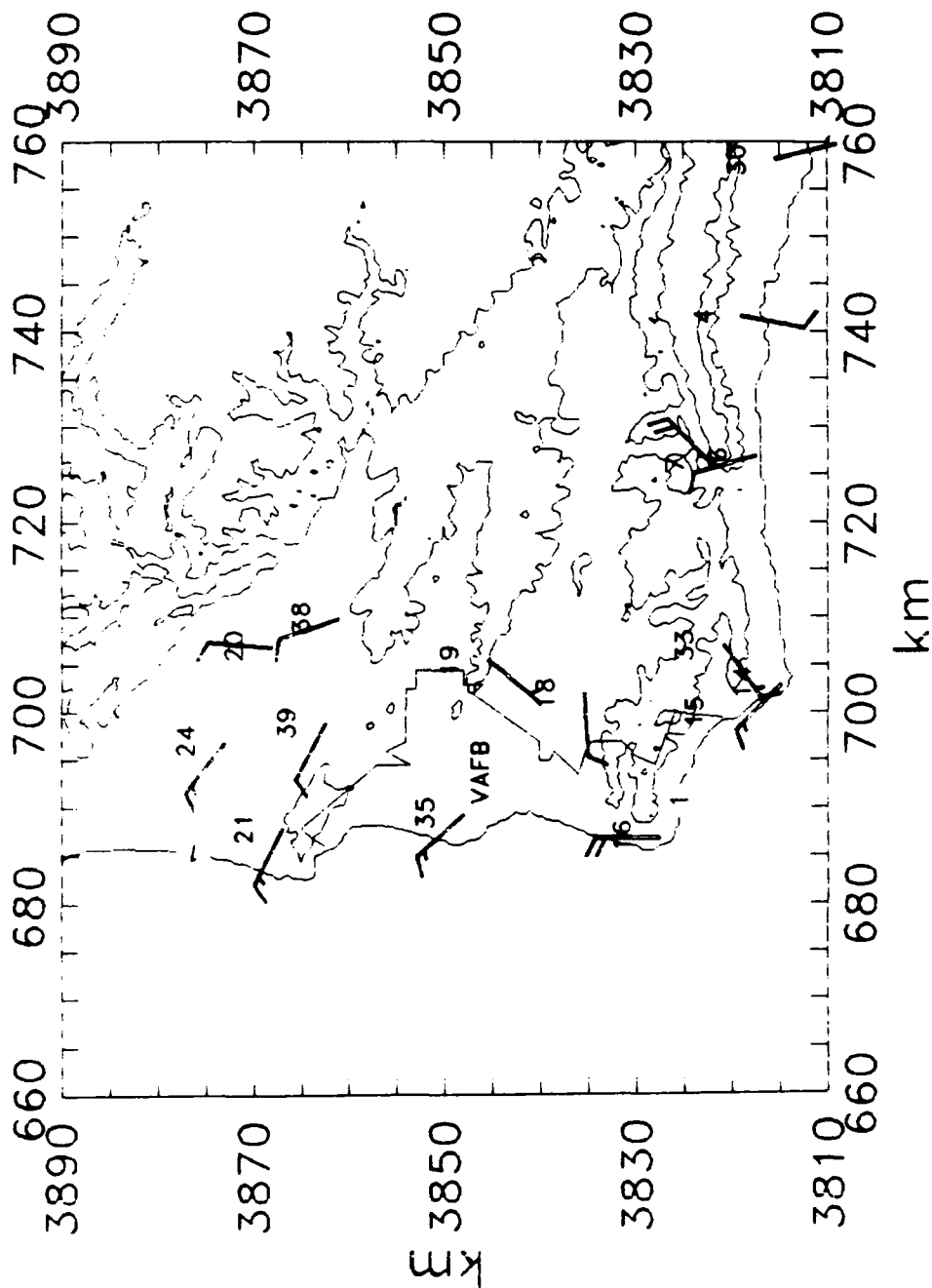
Day 8. The fall data is missing many of the Santa Maria area towers, but based on the previous data, the lone tower (#20) should be representative of the flow in that area. The early morning charts show easterly winds at all locations in the Channel. At 1300 those Channel stations were registering southerly winds; this included Pt. Arguello. Lompoc and Santa Maria were in northwesterlies. By 1900 the wind had reversed at Pt. Arguello to the north, veered to the north at Santa Maria and Lompoc, and become variable in the Santa Barbara Channel.

Day 9. At 100 the winds at most stations were decidedly northwesterly. At 700 the eastern Channel was experiencing southerly flow which continued through 1300, while the western locations were typically northwesterly. By 1900 most of the Channel towers showed offshore (northerly) flow, and inland stations were variable.

Day 10. Early morning was quite variable, except for northwesterlies near Pt. Arguello. At 1300 the typical pattern was established (west in Santa Maria/Lompoc, northwest at Pt. Arguello, southwest in the Channel). Again, at 1900 the Channel winds are more variable.

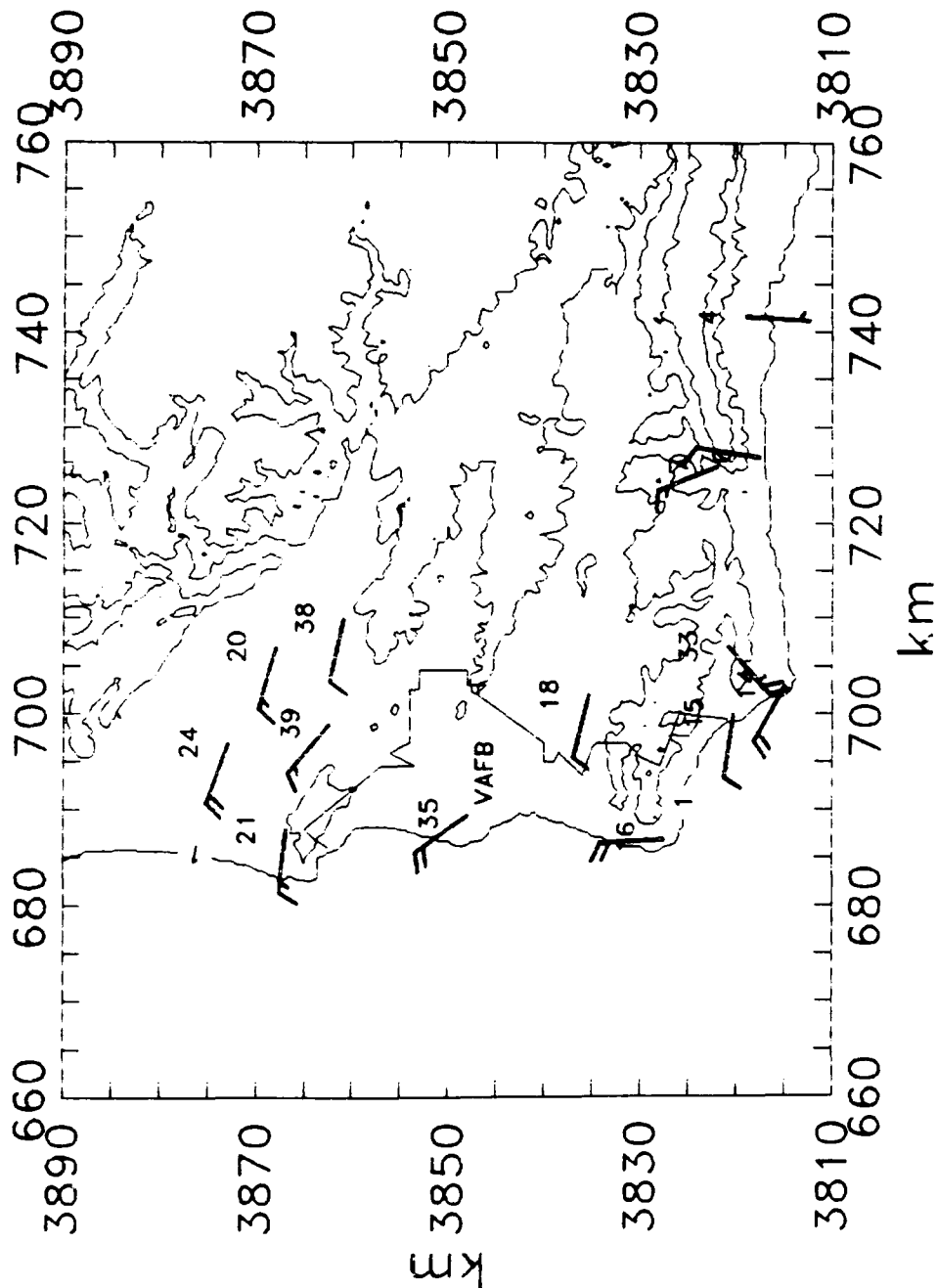
Day 11. Flow is light, but consistent and northerly at 100 in the southern areas. At 1300 winds are westerly in the Channel, and veer to the north by 1900 at most locations.

VANDENBERG REGION 5/18/88 07:00



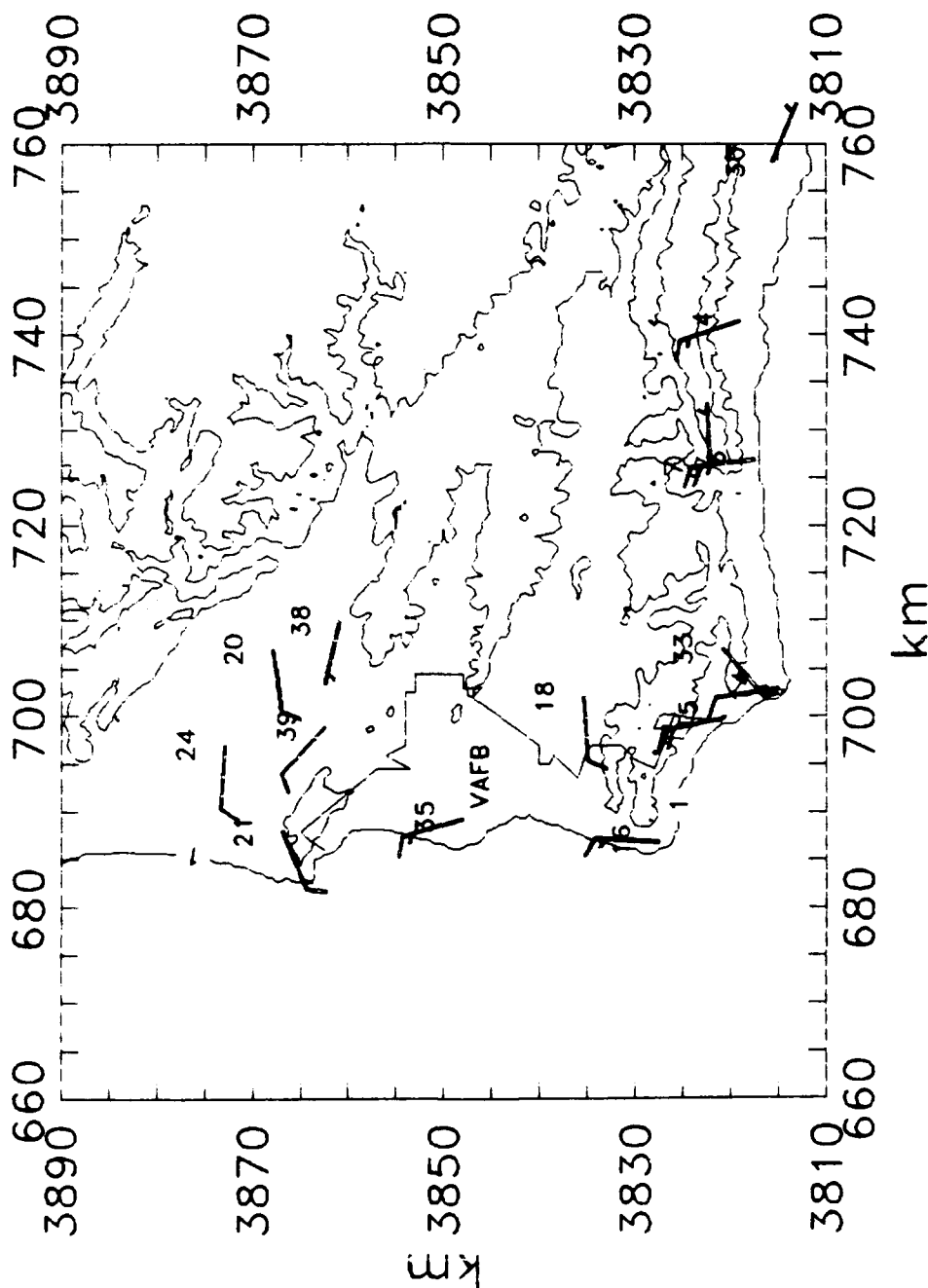
SCALE: 18 km = 1 inch
 CONTOUR interval = 200 m
 SANTA BARBARA AQMD SITES:
 4 Las Flores Canyon Site 4
 6 GTC Site A
 7 GTC Site B
 14 Point Conception
 15 Jalamia Beach
 16 Point Arguello
 18 H Street
 19 Lompoc HS&P
 20 Battles
 21 Casmallia Hills
 24 Bonita School
 30 Goleta
 33 Jalamia Road
 35 Watt Road VAFB
 38 Glacier Lane
 39 Briarwood

VANDENBERG REGION 5/18/88 13:00



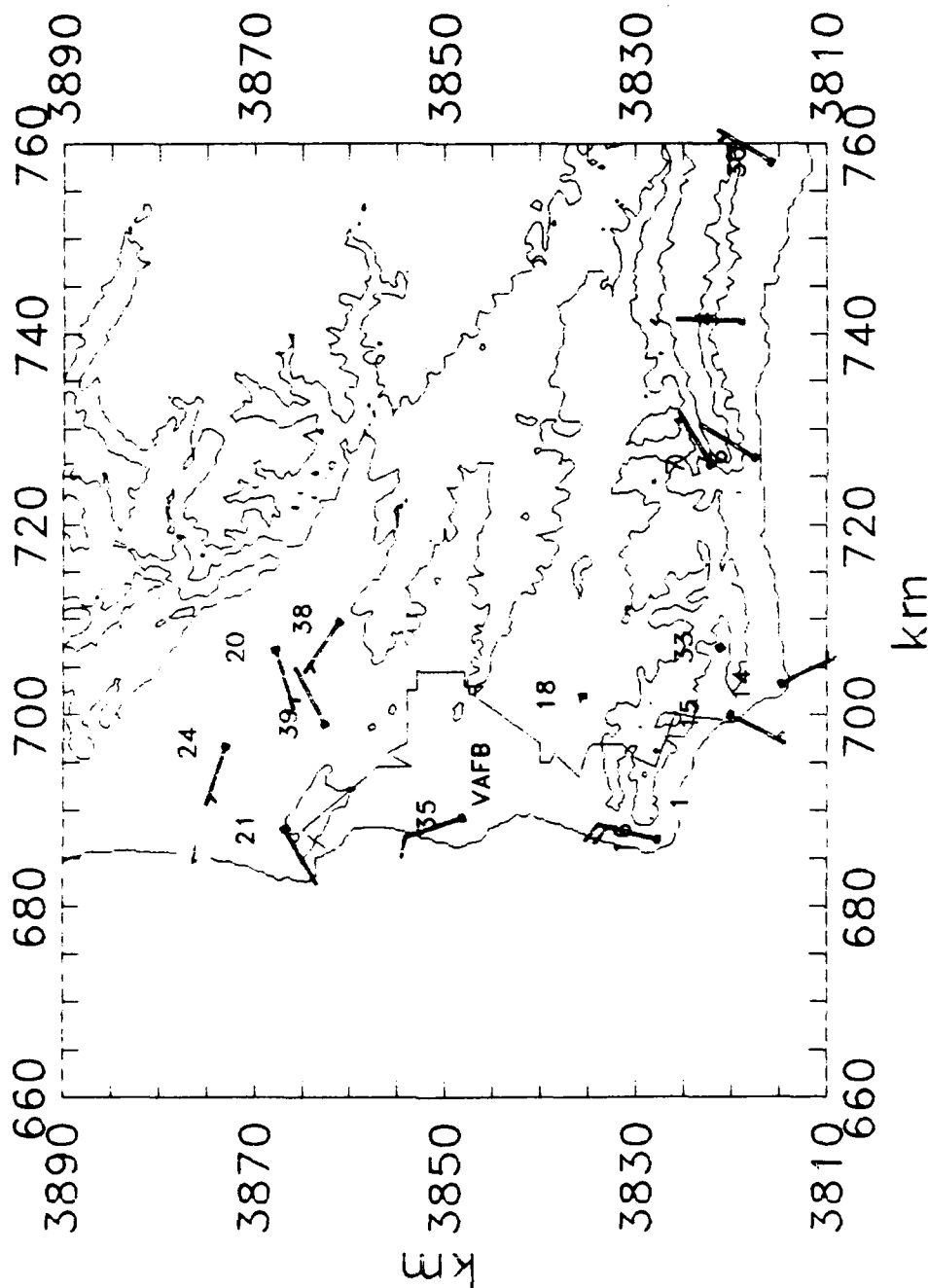
SCALE: 18 km = 1 inch
 CONTOUR interval = 200 m
 SANTA BARBARA AQMD SITES:
 4 Las Flores Canyon Site 4
 6 GTC Site A
 7 GTC Site B
 14 Point Conception
 15 Jalama Beach
 16 Point Arguello
 18 H Street
 19 Lompoc HS&P
 20 Battles
 21 Casmalia Hills
 24 Bonita School
 30 Goleta
 33 Jalama Road
 35 Watt Road VAFB
 38 Glacier Lane
 39 Briarwood

VANDENBERG REGION 5/18/88 19:00

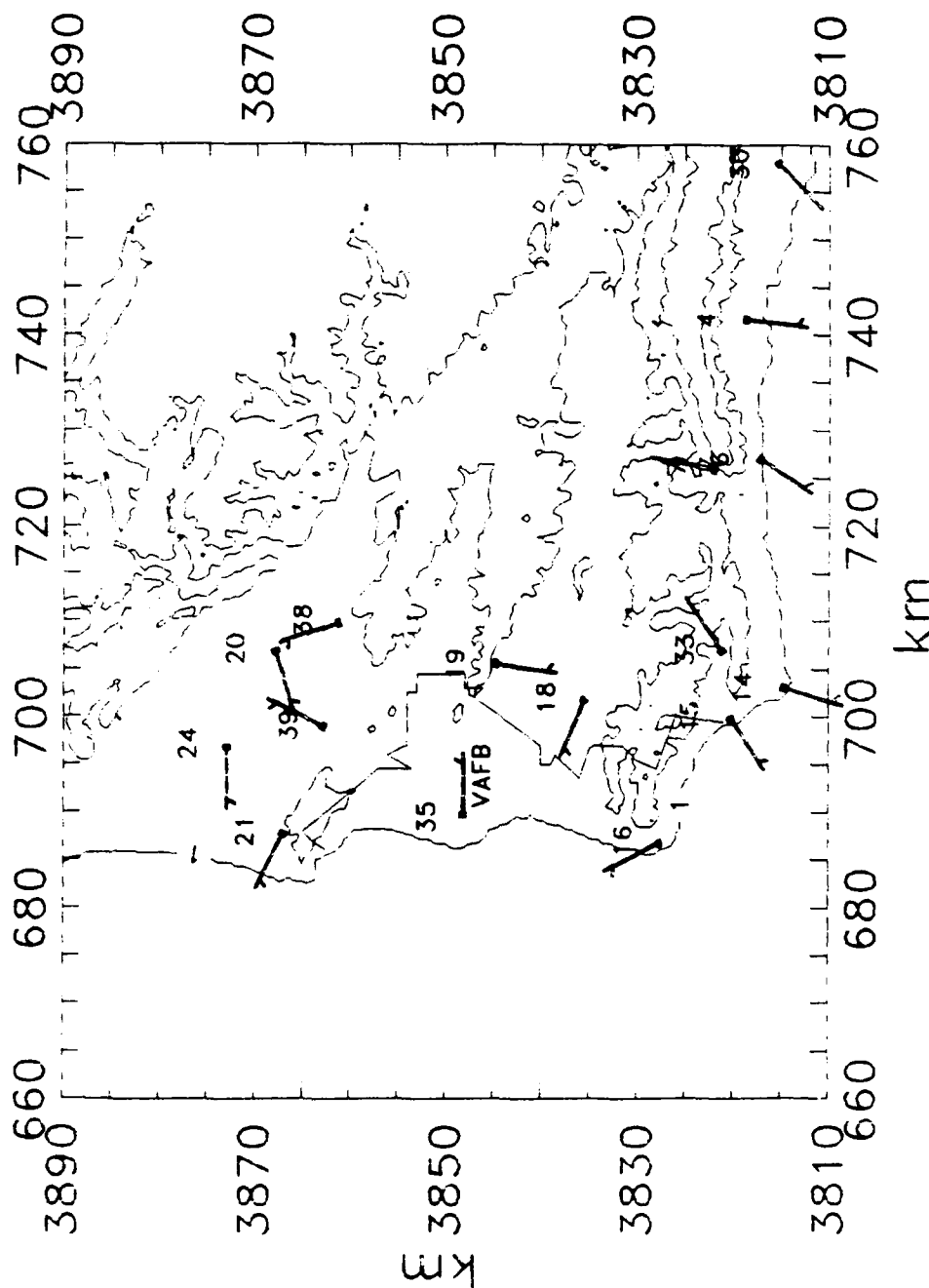


SCALE: 18 km = 1 inch
 CONTOUR interval = 200 m
 SANTA BARBARA AQMD SITES:
 4 Las Flores Canyon Site 4
 6 GTC Site A
 7 GTC Site B
 14 Point Conception
 15 Jalama Beach
 16 Point Arguello
 18 H Street
 19 Lompoc HS&P
 20 Battles
 21 Casmalia Hills
 24 Bonita School
 30 Goleta
 33 Jalama Road
 35 Watt Road VAFB
 38 Glacier Lane
 39 Briarwood

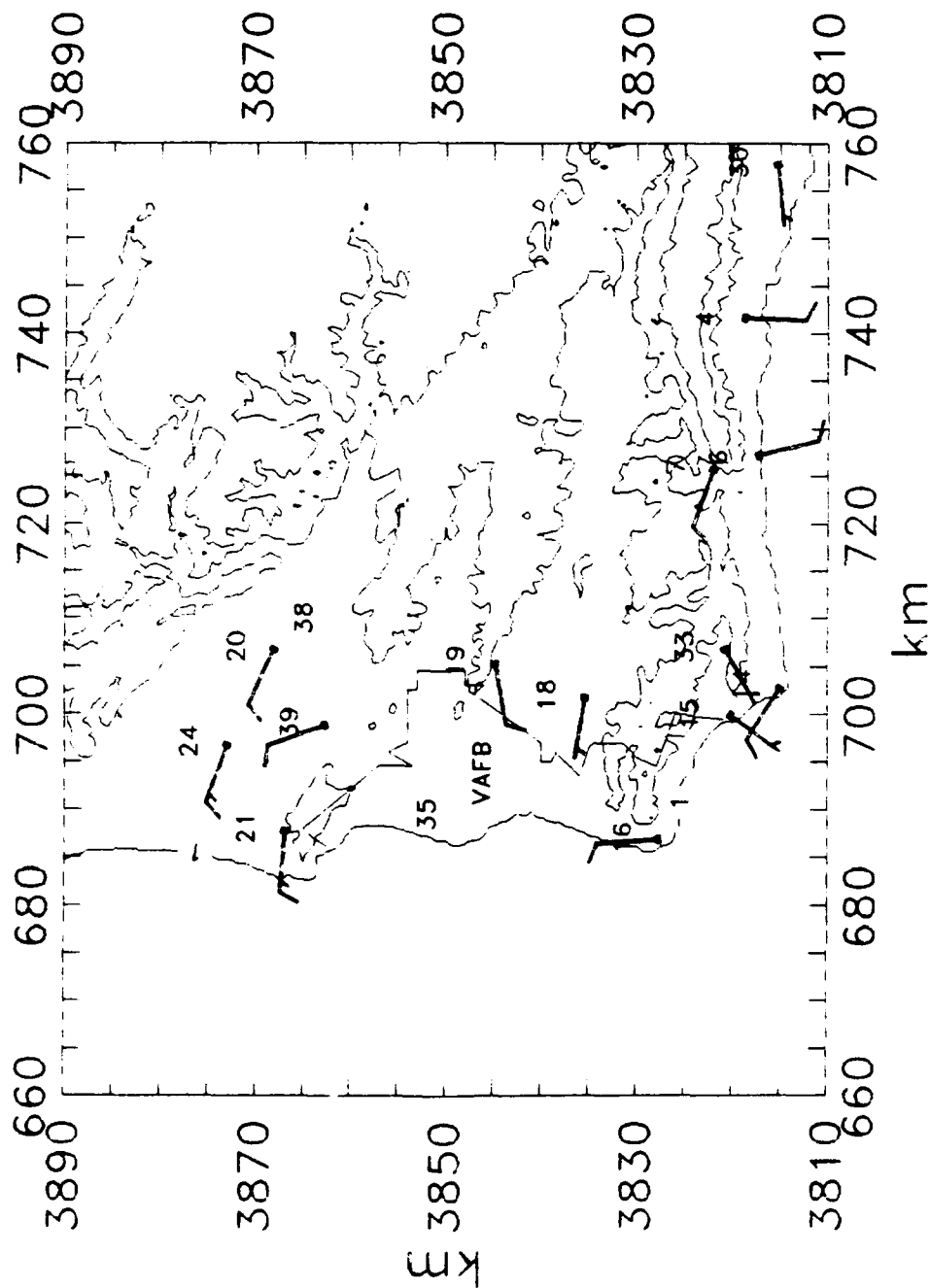
VANDENBERG REGION 5/19/88 01:00



VANDENBERG REGION 5/19/88 07:00

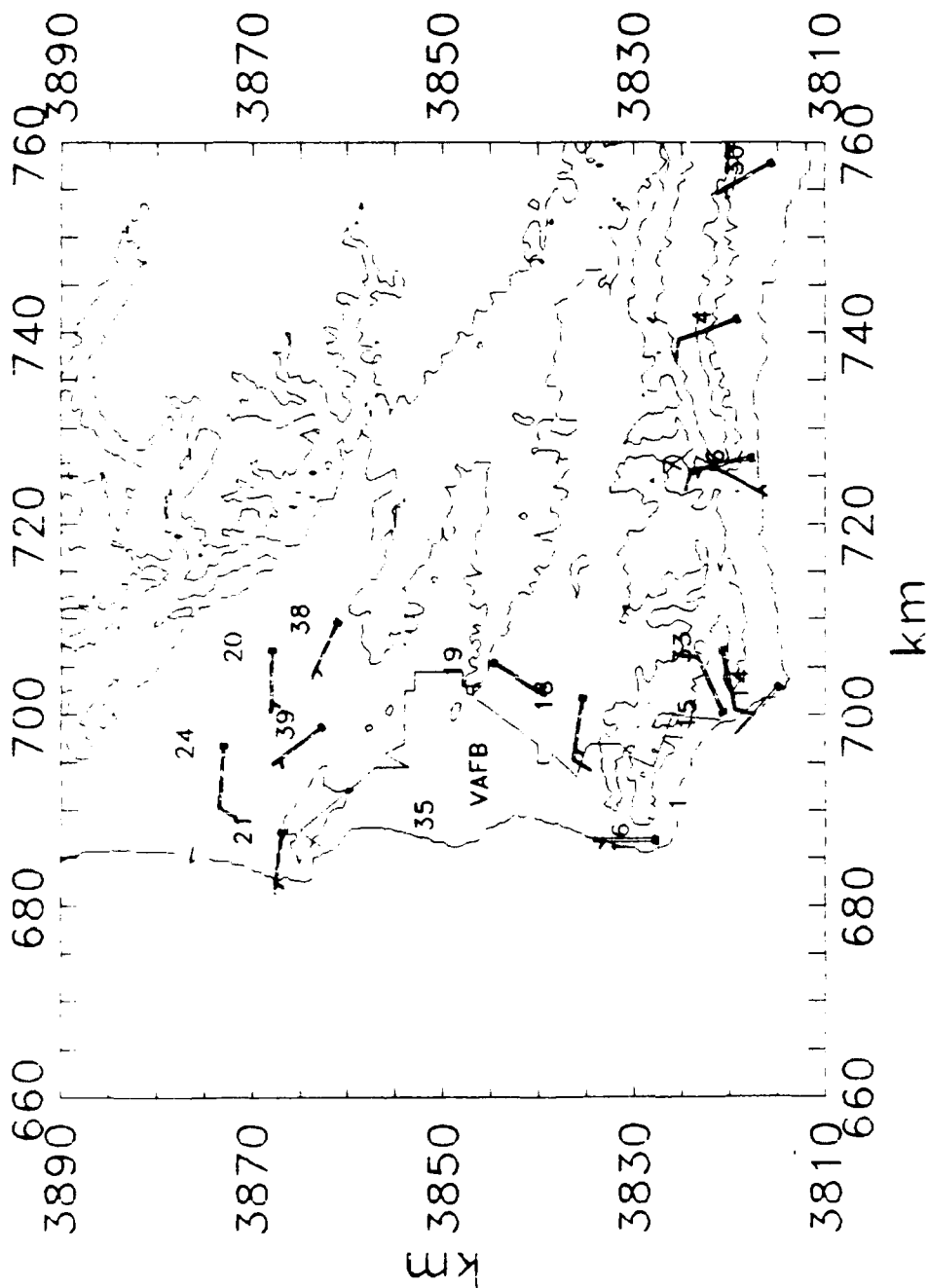


VANDENBERG REGION 5/19/88 13:00



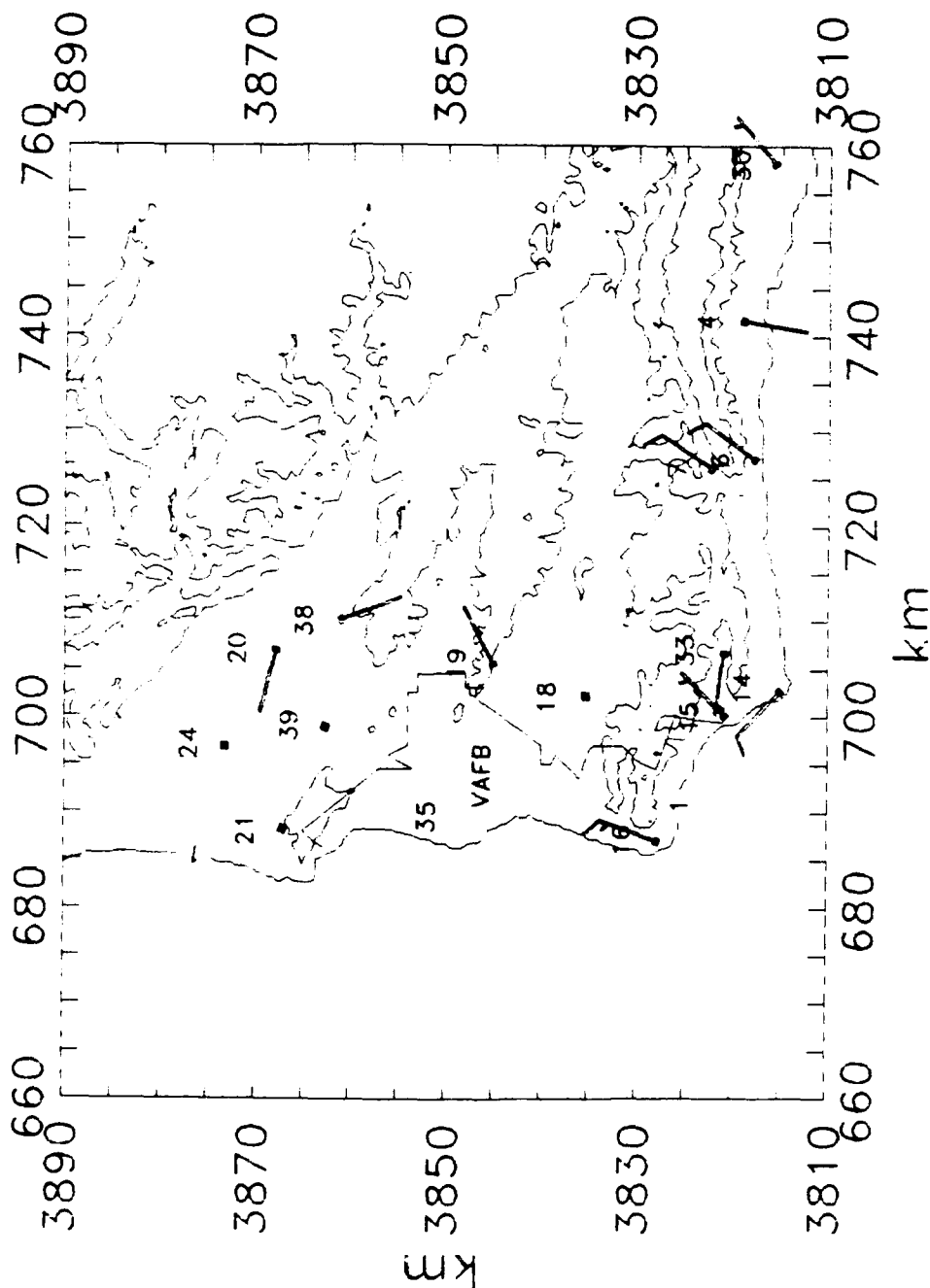
SCALE: 18 km = 1 inch
 CONTOUR interval = 200 m
 SANTA BARBARA AQMD SITES:
 4 Las Flores Canyon Site 4
 6 GTC Site A
 7 GTC Site B
 14 Point Conception
 15 Jalama Beach
 16 Point Arguello
 18 H Street
 19 Lompoc HS&P
 20 Battles
 21 Casmalia Hills
 24 Bonita School
 30 Goleta
 33 Jalama Road
 35 Watt Road VAFB
 38 Glacier Lane
 39 Briarwood

VANDENBERG REGION 5/19/88 19:00



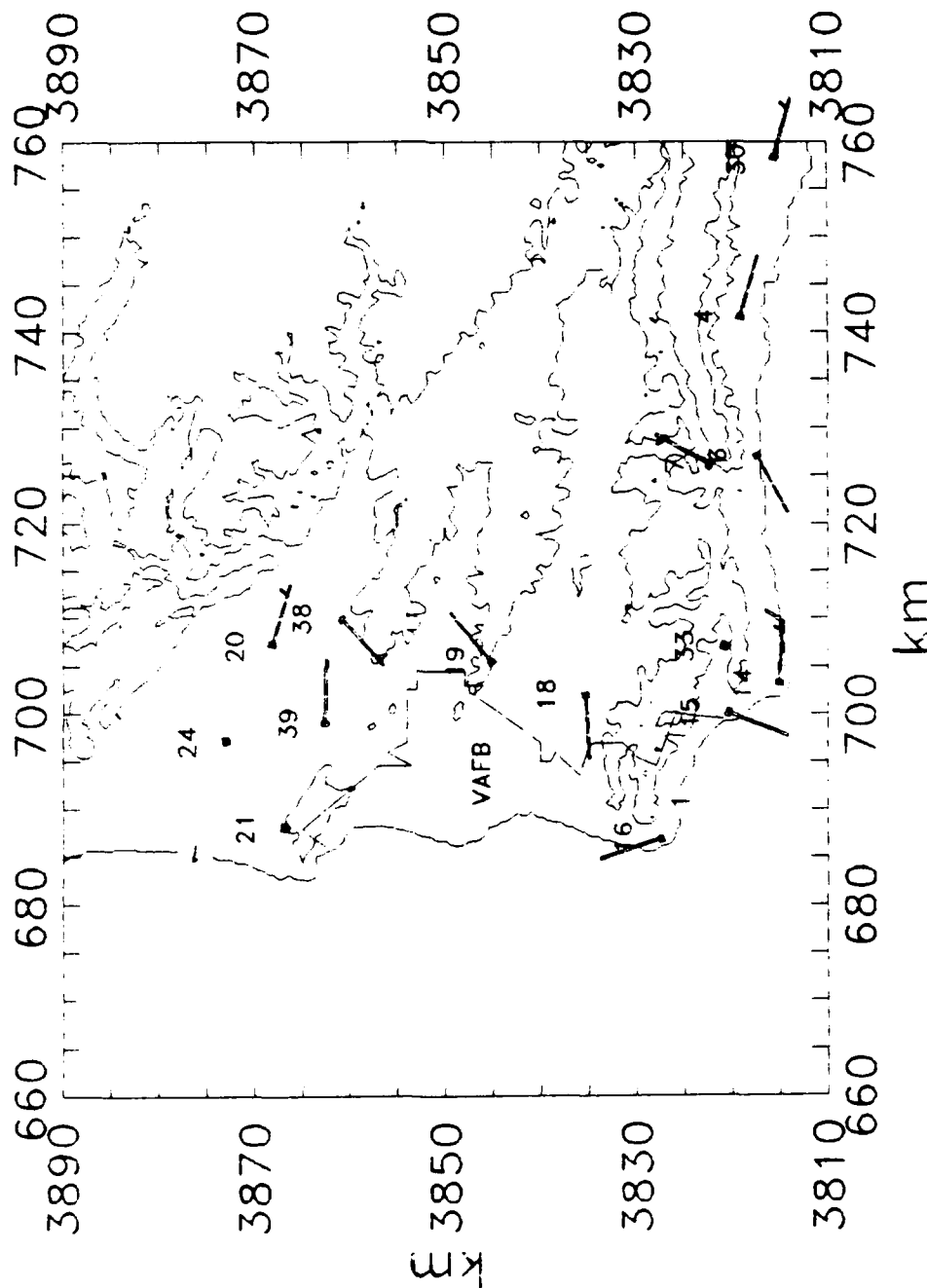
SCALE: 18 km = 1 inch
 CONTOUR interval = 200 m
 SANTA BARBARA AQMD SITES:
 4 Las Flores Canyon Site 4
 6 GTC Site A
 7 GTC Site B
 14 Point Conception
 15 Jalama Beach
 16 Point Arguello
 18 H Street
 19 Lompoc HS&P
 20 Battles
 21 Casmalia Hills
 24 Bonita School
 30 Goleta
 33 Jalama Road
 35 Watt Road VAFB
 38 Glacier Lane
 39 Briarwood

VANDENBERG REGION 5/20/88 01:00

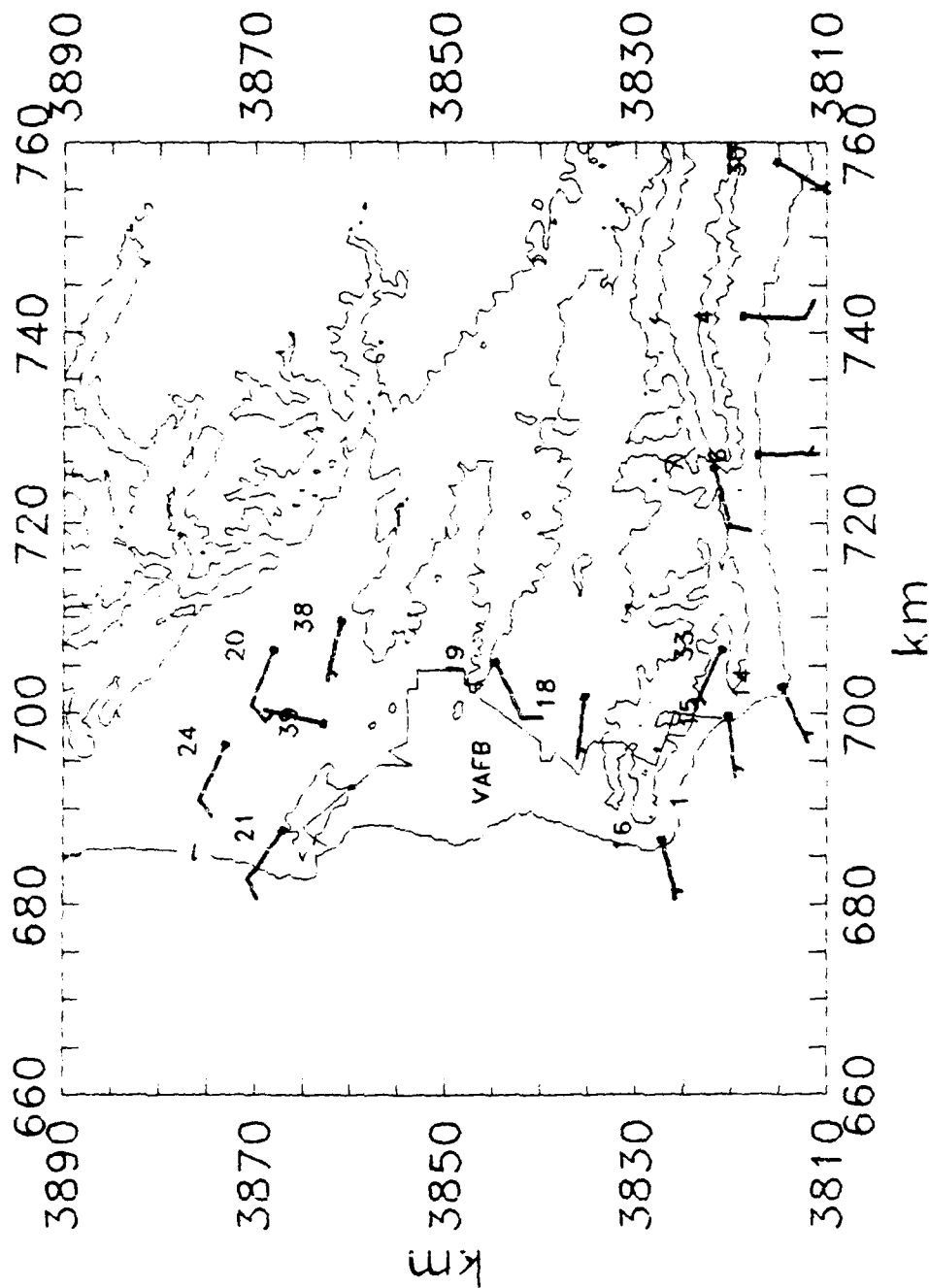


SCALE: 18 km = 1 inch
 CONTOUR interval = 200 m
 SANTA BARBARA AQMD SITES:
 4 Las Flores Canyon Site 4
 6 GTC Site A
 7 GTC Site B
 14 Point Conception
 15 Jalama Beach
 16 Point Arguello
 18 H Street
 19 Lompoc HS&P
 20 Battles
 21 Casmalia Hills
 24 Bonita School
 30 Goleta
 33 Jalama Road
 35 Watt Road VAFB
 38 Glacier Lane
 39 Briarwood

VANDENBERG REGION 5/20/88 07:00

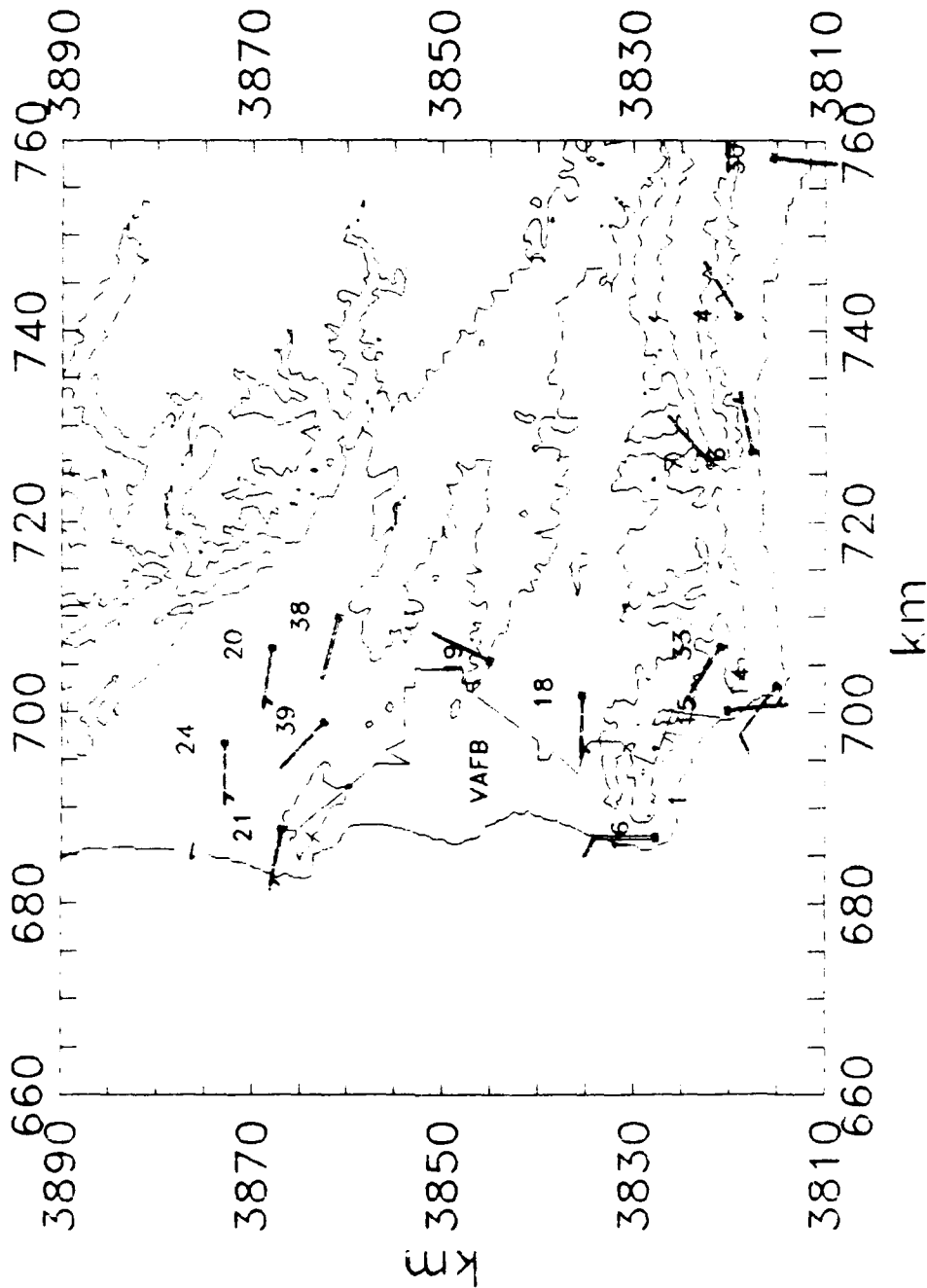


VANDENBERG REGION 5/20/88 13:00



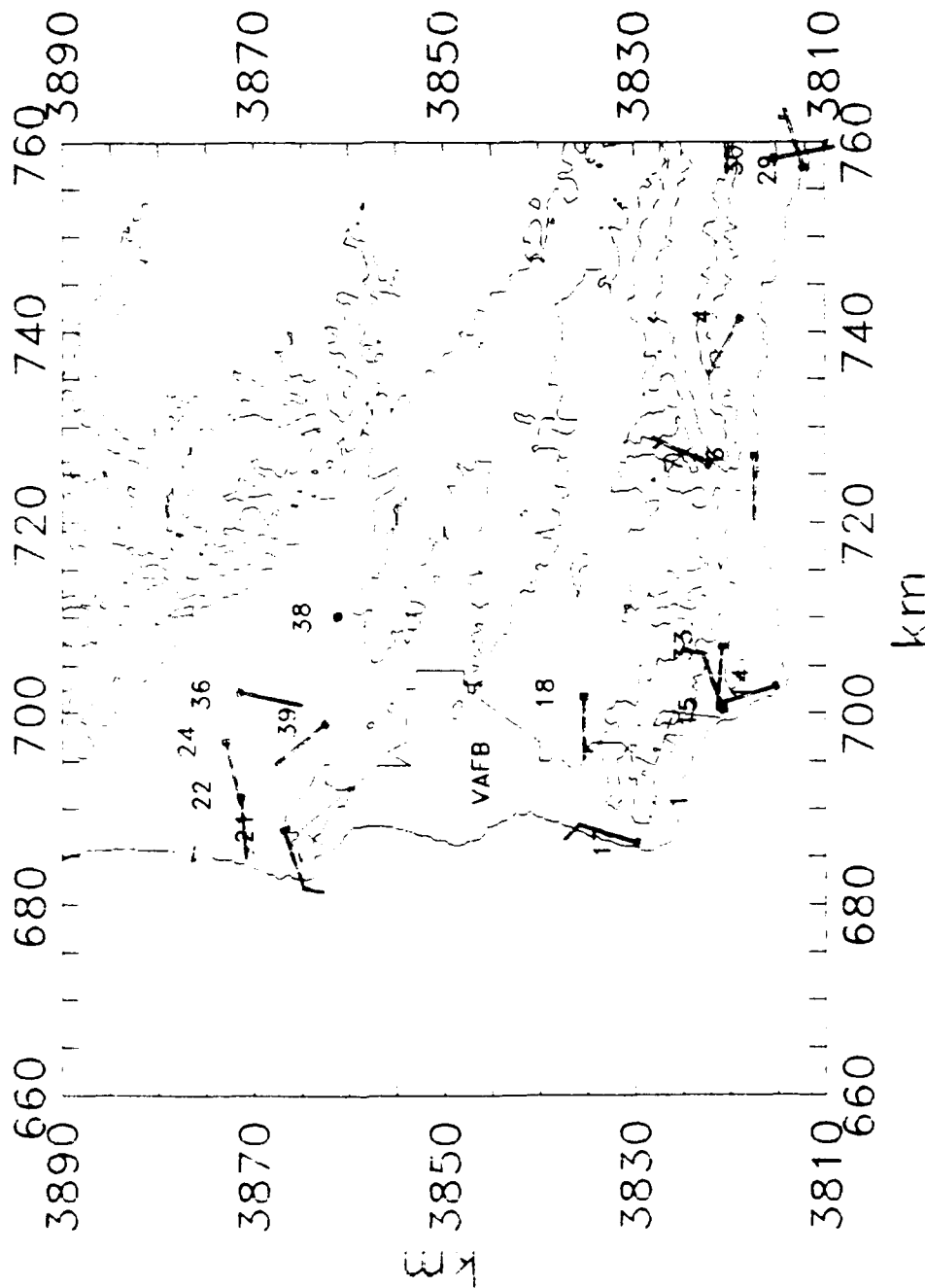
SCALE: 18 km = 1 inch
 CONTOUR interval = 200 m
 SANTA BARBARA AQMD SITES:
 4 Las Flores Canyon Site 4
 6 GTC Site A
 7 GTC Site B
 14 Point Conception
 15 Jalama Beach
 16 Point Arguello
 18 H Street
 19 Lompoc HS&P
 20 Battles
 21 Casmalia Hills
 24 Bonita School
 30 Goleta
 33 Jalama Road
 35 Watt Road VAFB
 38 Glacier Lane
 39 Briarwood

VANDENBERG REGION 5/20/88 19:00



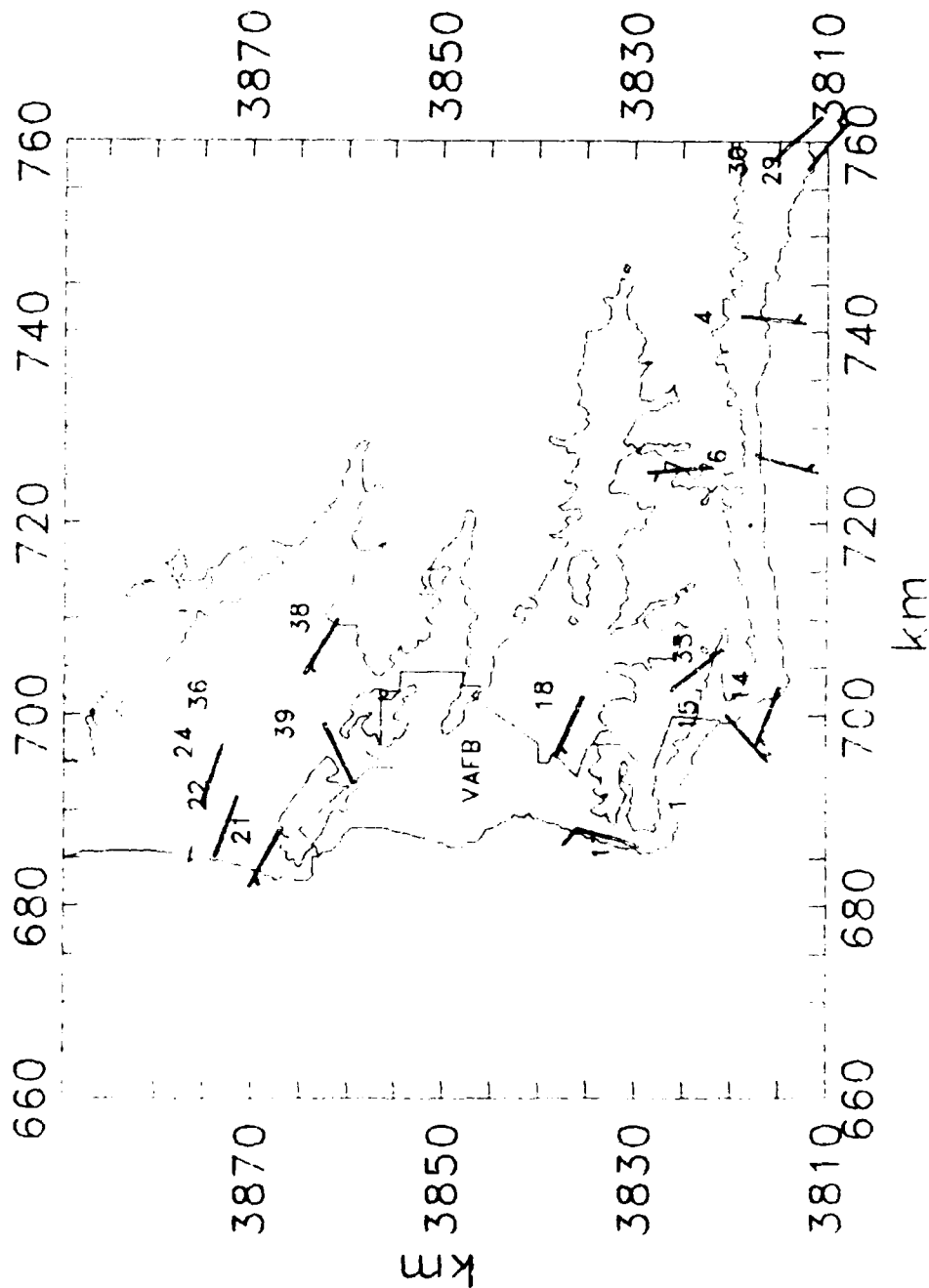
SCALE: 18 km = 1 inch
 CONTOUR interval = 200 m
 SANTA BARBARA AQMD SITE
 4 Las Flores Canyon Site
 6 GTC Site A
 7 GTC Site B
 14 Point Conception
 15 Jalama Beach
 16 Point Arguello
 18 H Street
 19 Lompoc HS&P
 20 Battles
 21 Casmalia Hills
 24 Bonita School
 30 Goleta
 33 Jalama Road
 35 Watt Road VAFB
 38 Glacier Lane
 39 Briarwood

VANDENBERG REGION 7/26/88 01:00

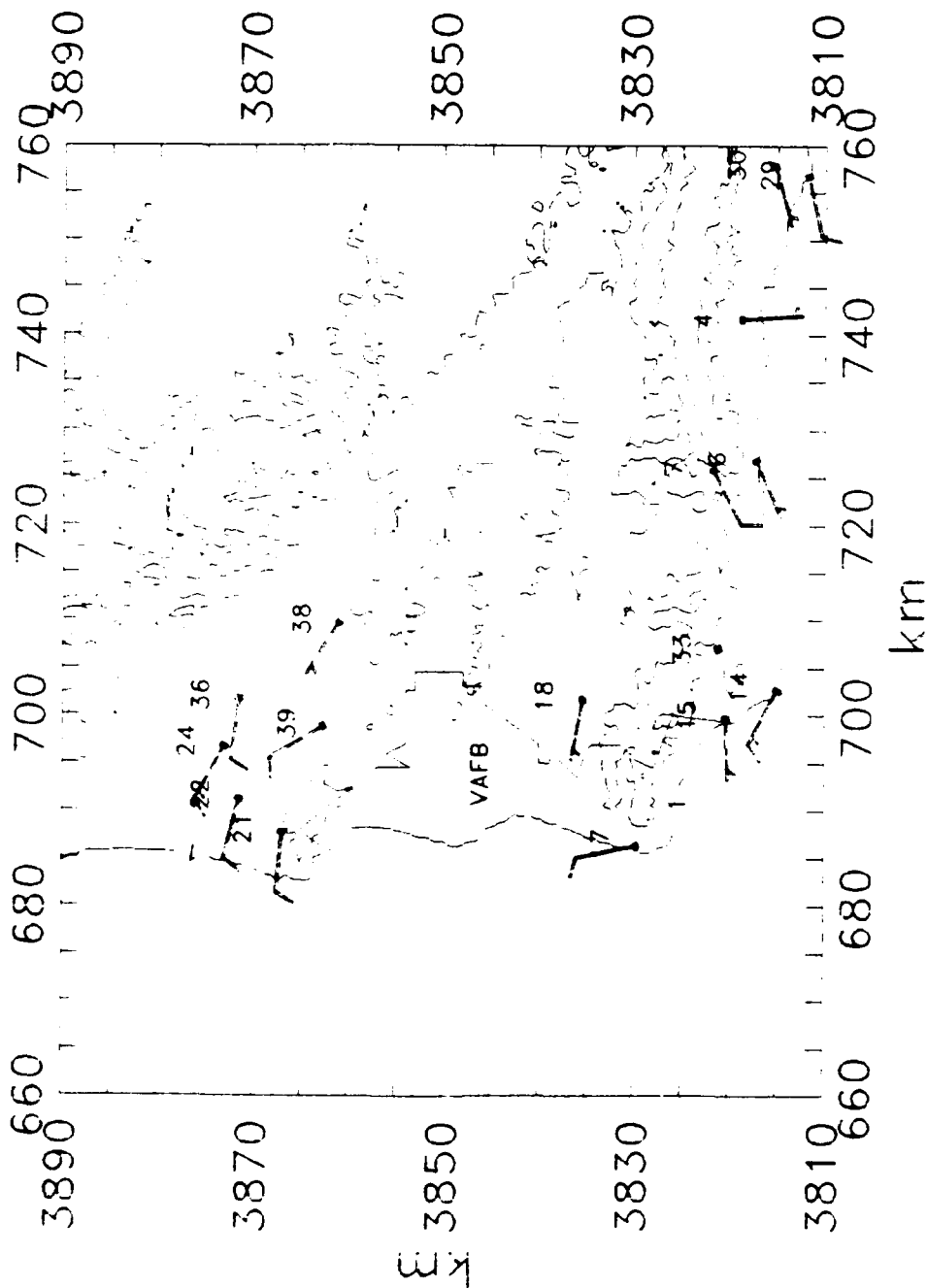


SCALE: 18 km = 1 inch
 CONTOUR interval = 200 m
 SANTA BARBARA AQMD SITES:
 4 Las Flores Canyon Site 4
 6 GTC Site A
 7 GTC Site B
 14 Point Conception
 15 Jalama Beach
 16 Point Arguello
 18 H Street
 19 Lompoc HS&P
 20 Battles
 21 Casmalia Hills
 24 Bonita School
 30 Goleta
 33 Jalama Road
 35 Watt Road VAFB
 38 Glacier Lane
 39 Briarwood

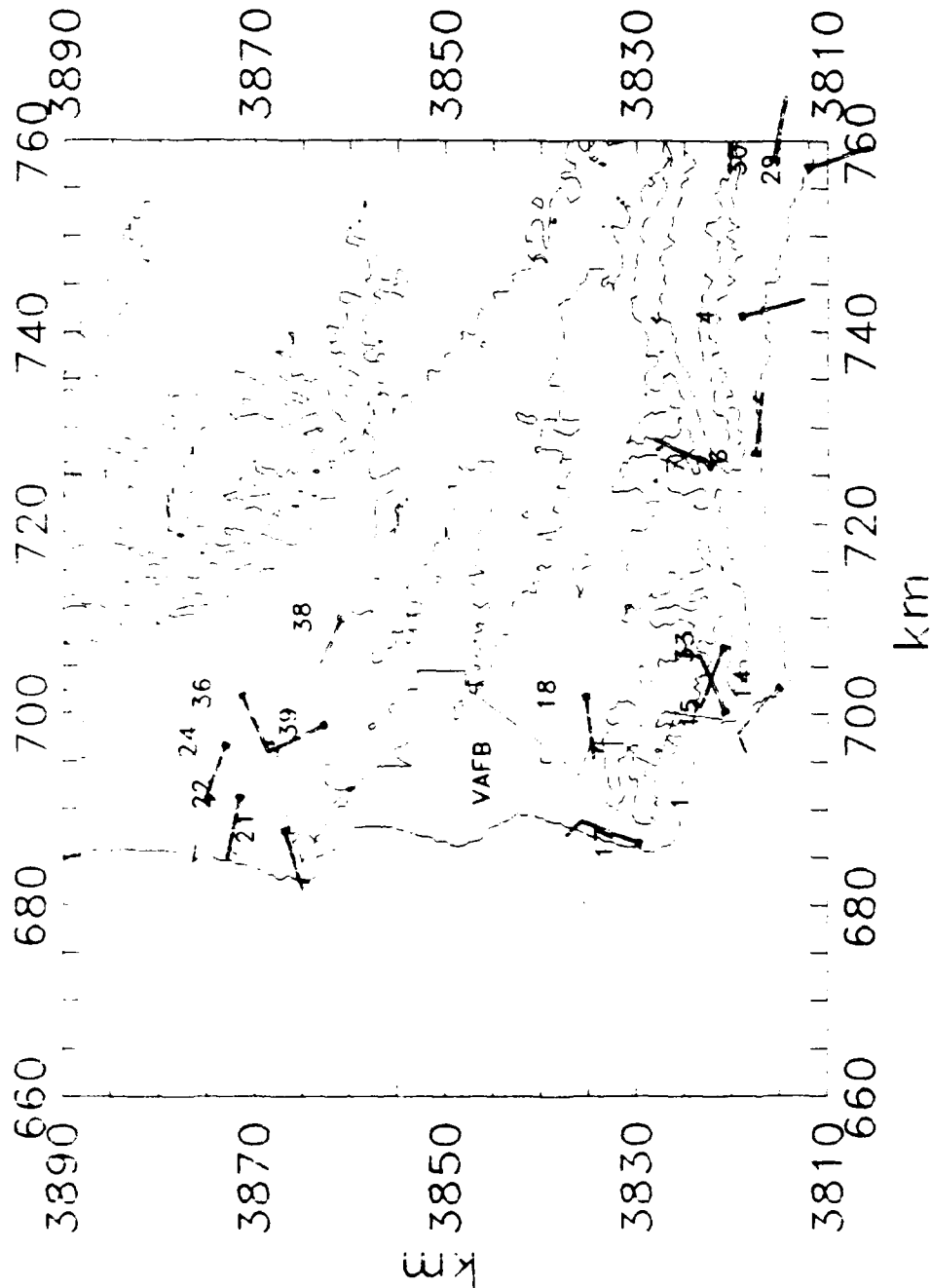
VANDENBERG REGION 7/26/88 07:00



VANDENBERG REGION 7/26/88 13:00

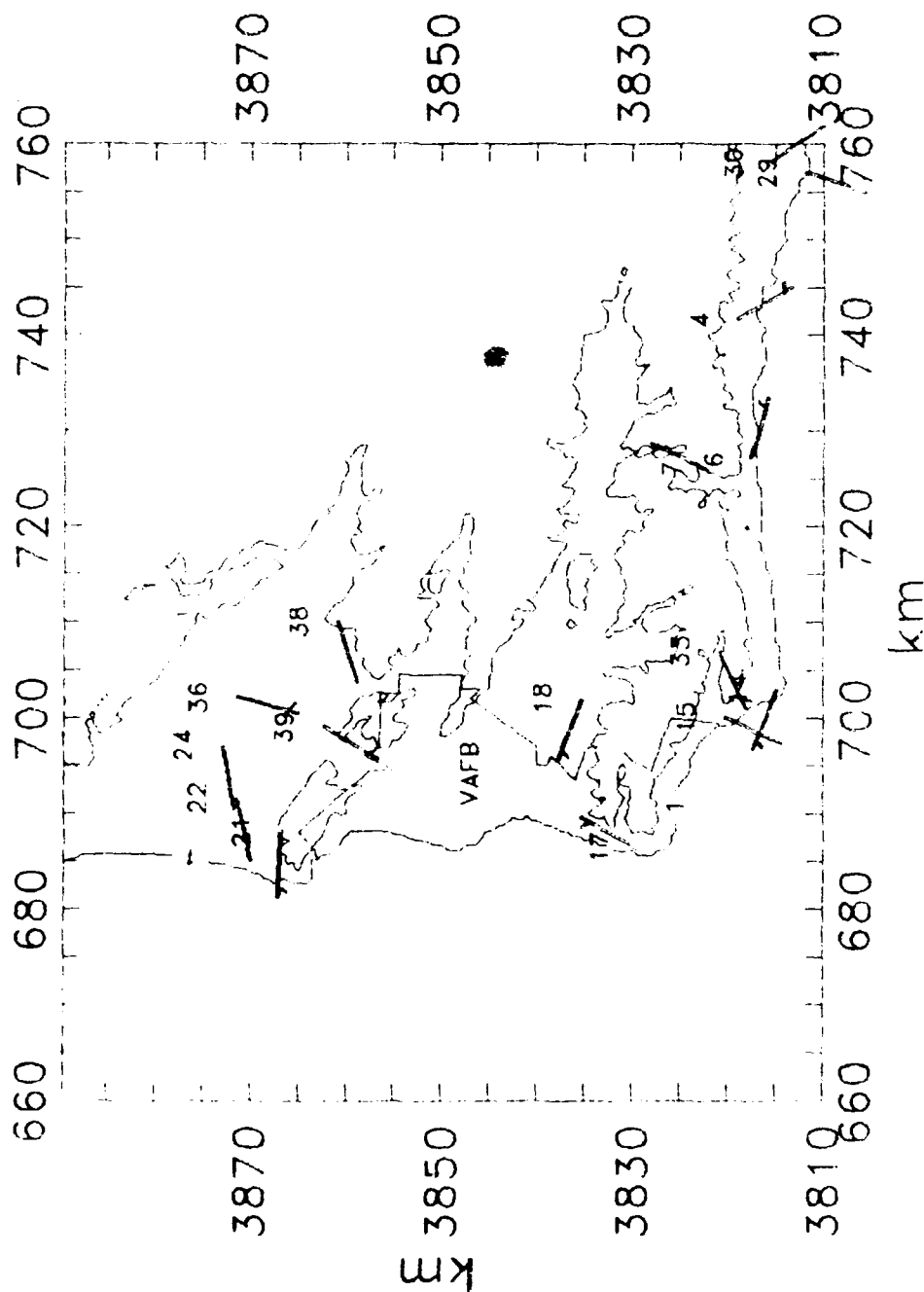


VANDENBERG REGION 7/26/88 19:00

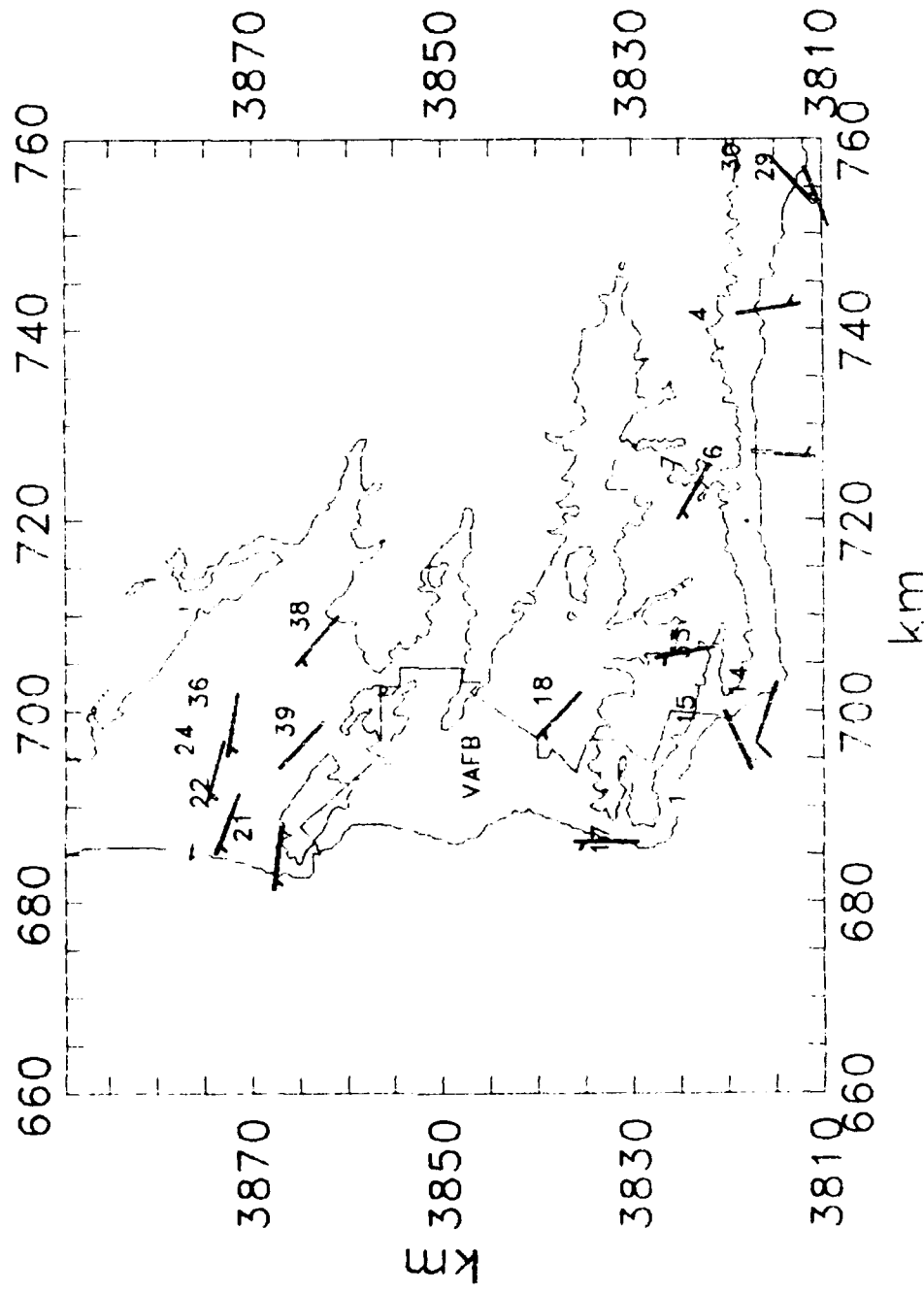


SCALE: 18 km = 1 inch
 CONTOUR interval = 200 m
 SANTA BARBARA AQMD SITES:
 4 Las Flores Canyon Site 4
 6 GTC Site A
 7 GTC Site B
 14 Point Conception
 15 Jalama Beach
 16 Point Arguello
 18 H Street
 19 Lompoc HS&P
 20 Battles
 21 Casmalia Hills
 24 Bonita School
 30 Goleta
 33 Jalama Road
 35 Watt Road VAFB
 38 Glacier Lane
 39 Briarwood

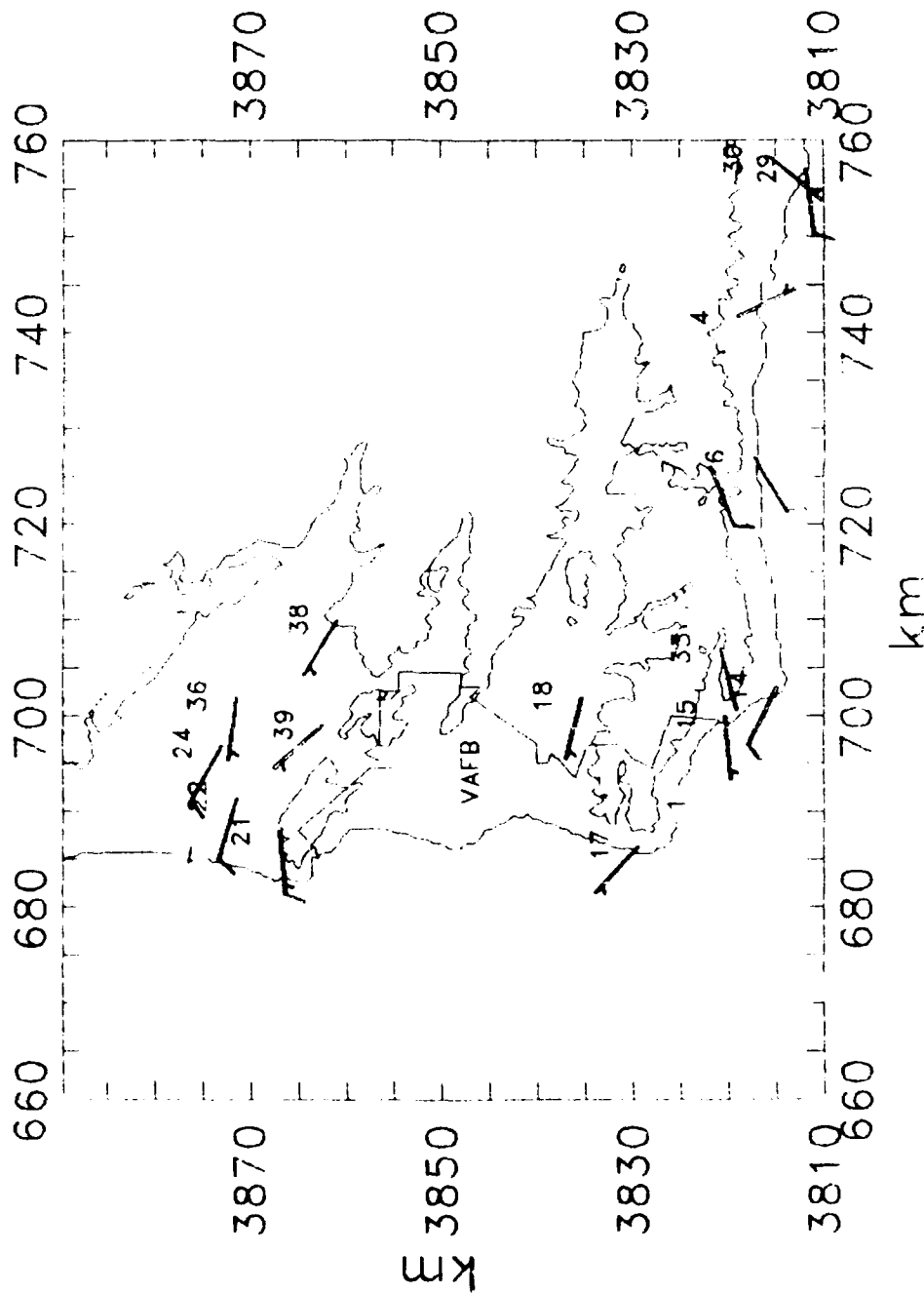
VANDENBERG REGION 7/27/88 01:00



VANDENBERG REGION 7/27/88 07:00

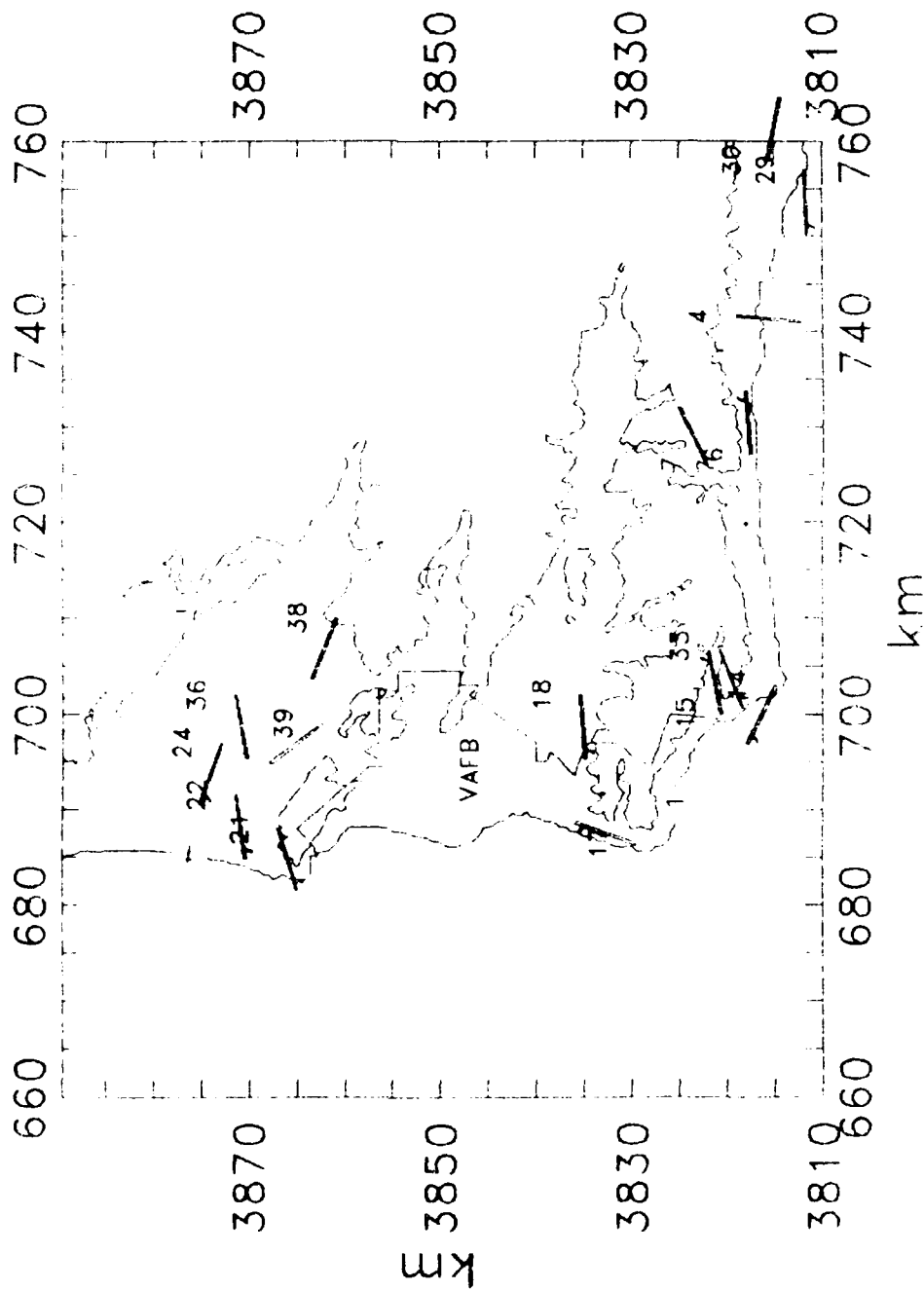


VANDENBERG REGION 7/27/88 13:00



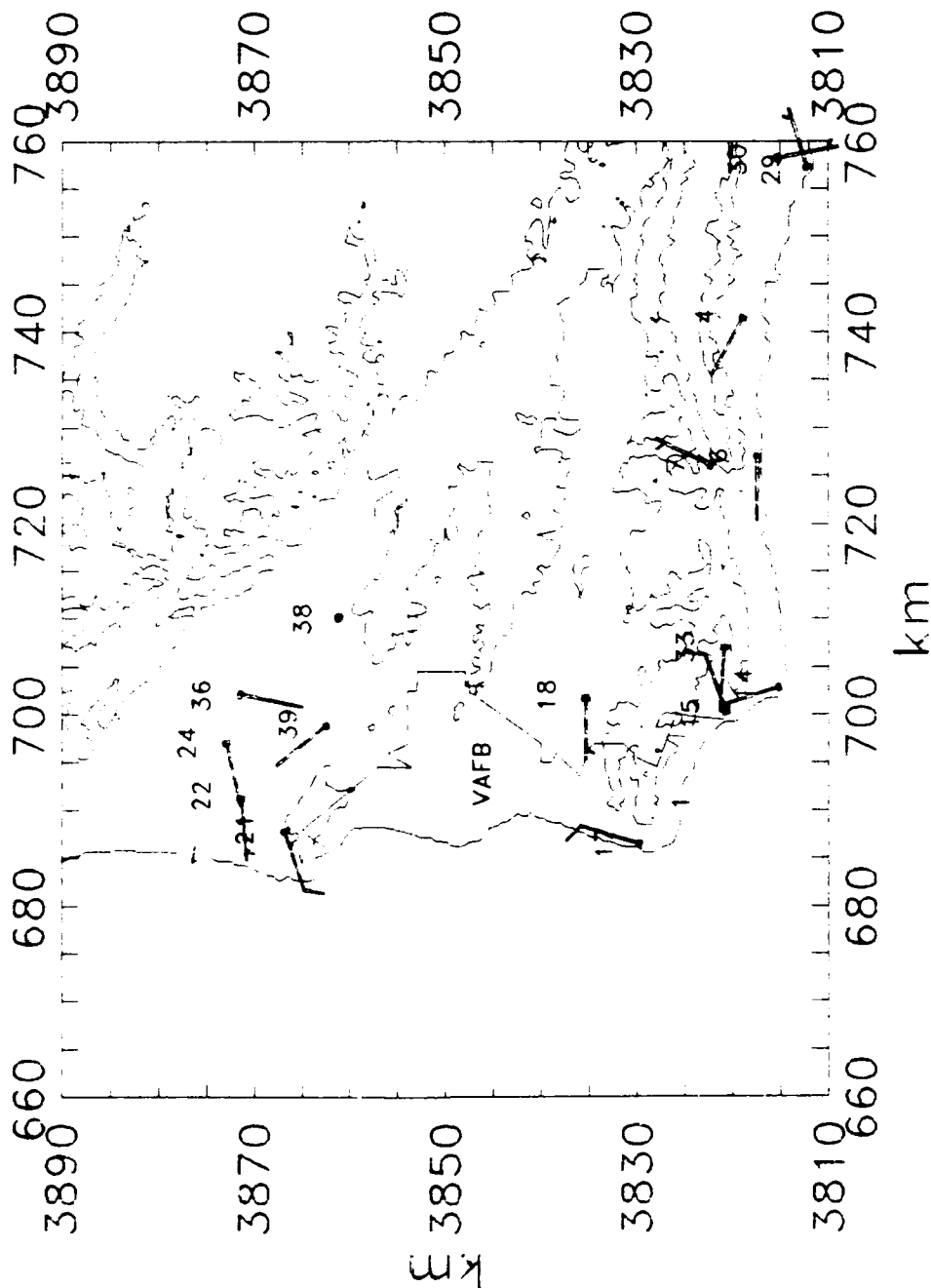
SCALE: 18 km = 1 inch
 CONTOUR interval = 200 m
 SANTA BARBARA AQMD SITES:
 4 Las Flores Canyon Site 4
 6 GTC SITE A
 7 GTC Site B
 14 Point Conception
 15 Jalama Beach
 17 Vandenberg STS
 18 H Street
 21 Casmall Hills
 22 Guadalupe
 24 Bonita School
 29 West Campus
 30 Goleta
 33 Jalama Road
 38 McClelland Street
 39 Briarwood

VANDENBERG REGION 7/27/88 19:00



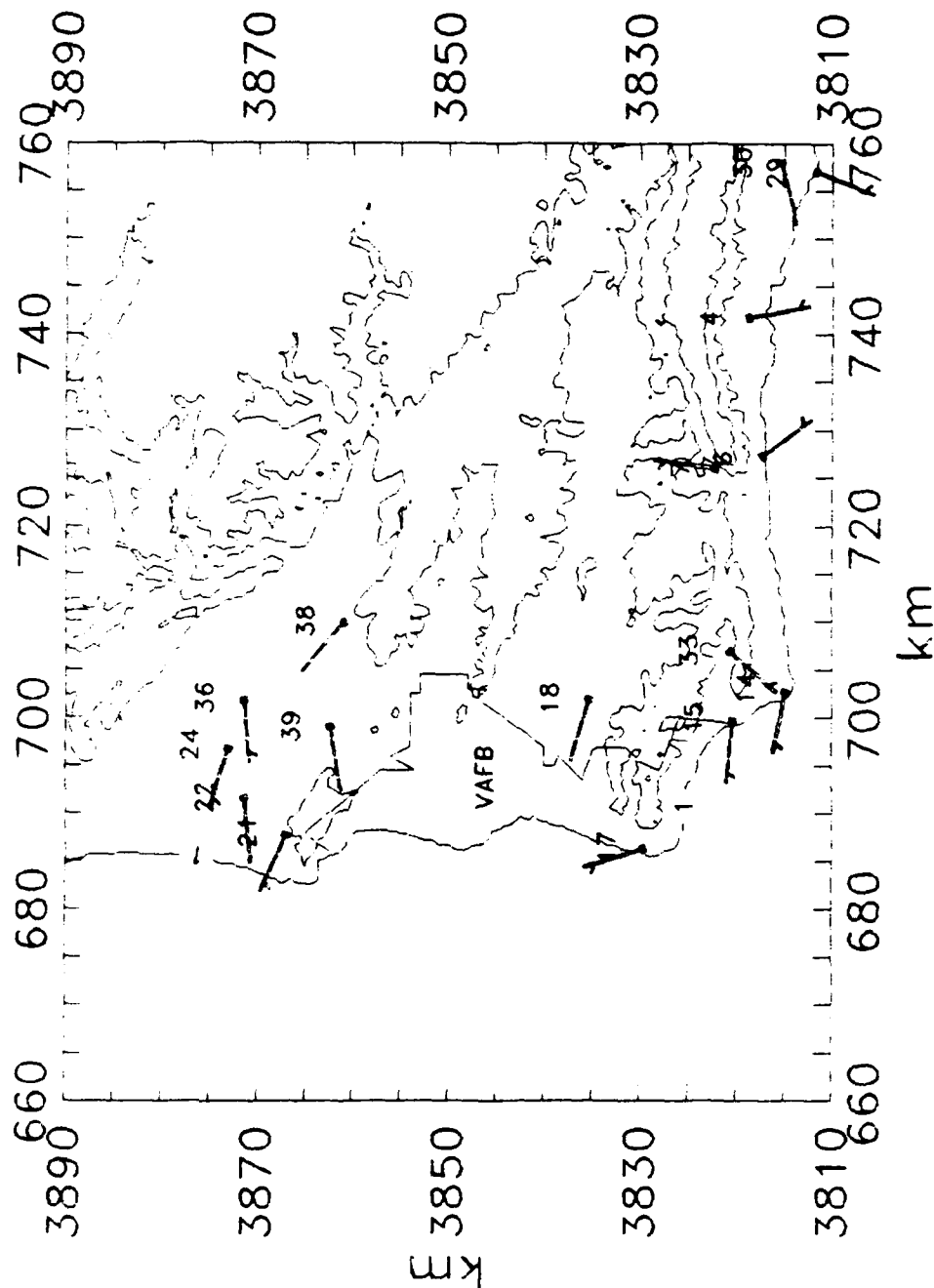
SCALE: 18 km = 1 inch
 CONTOUR interval = 200 m
 SANTA BARBARA AQMD SITES:
 4 Las Flores Canyon Site 4
 6 GTC SITE A
 7 GTC SITE B
 14 Point Conception
 15 Jalama Beach
 17 Vandenberg STS
 18 H Street
 21 Casmalia Hills
 22 Guadalupe
 24 Bonita School
 29 West Campus
 30 Goleta
 33 Jalama Road
 36 McClelland Street
 38 Glacier Lane
 39 Briarwood

VANDENBERG REGION 7/28/88 01:00

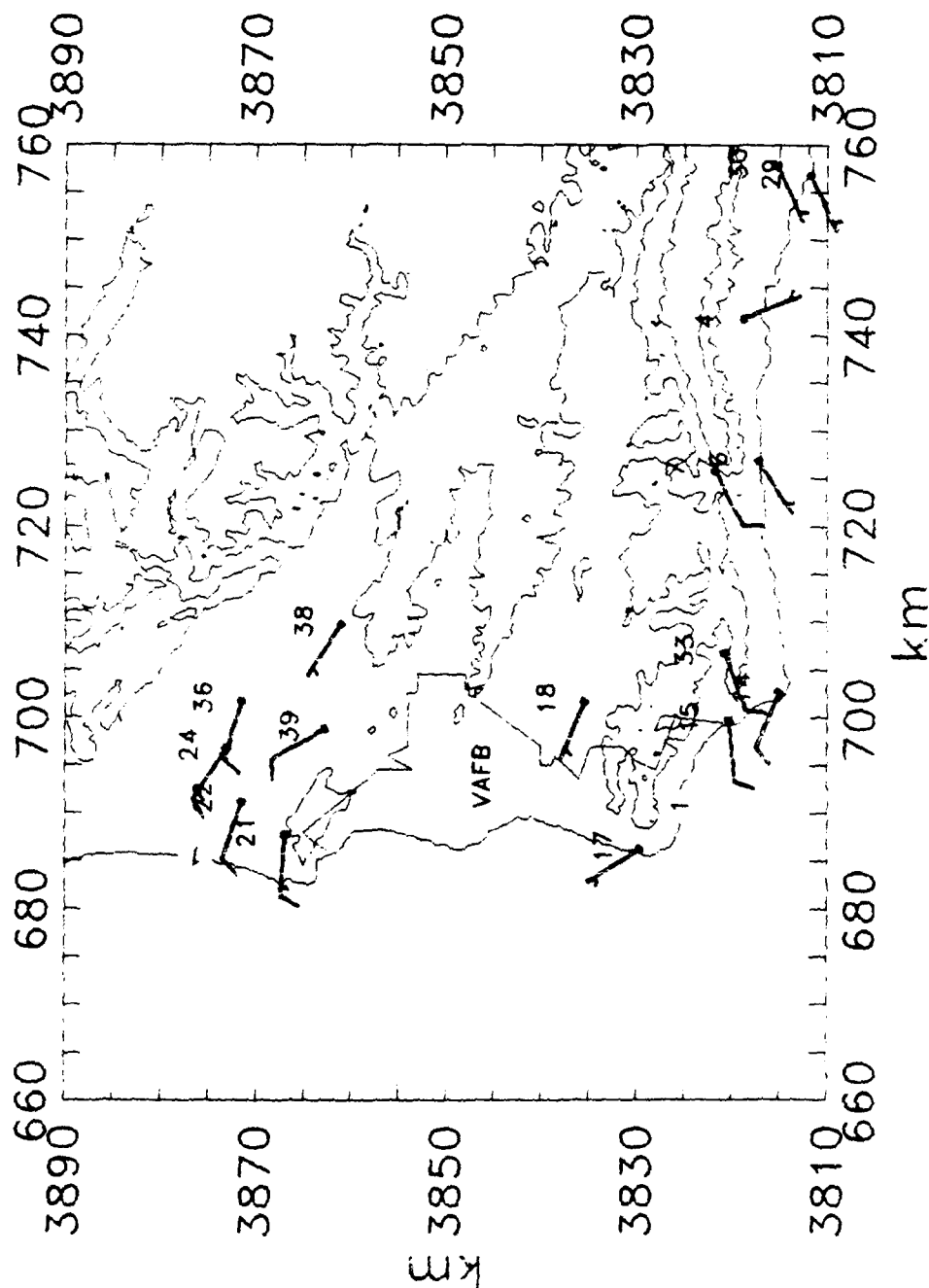


SCALE: 18 km = 1 inch
 CONTOUR interval = 200 m
 SANTA BARBARA AQMD SITES:
 4 Las Flores Canyon Site 4
 6 GTC Site A
 7 GTC Site B
 14 Point Conception
 15 Jalama Beach
 16 Point Arguello
 18 H Street
 19 Lompoc HS&P
 20 Battles
 21 Casmalia Hills
 24 Bonita School
 30 Goleta
 33 Jalama Road
 35 Watt Road VAFB
 38 Glacier Lane
 39 Briarwood

VANDENBERG REGION 7/28/88 07:00

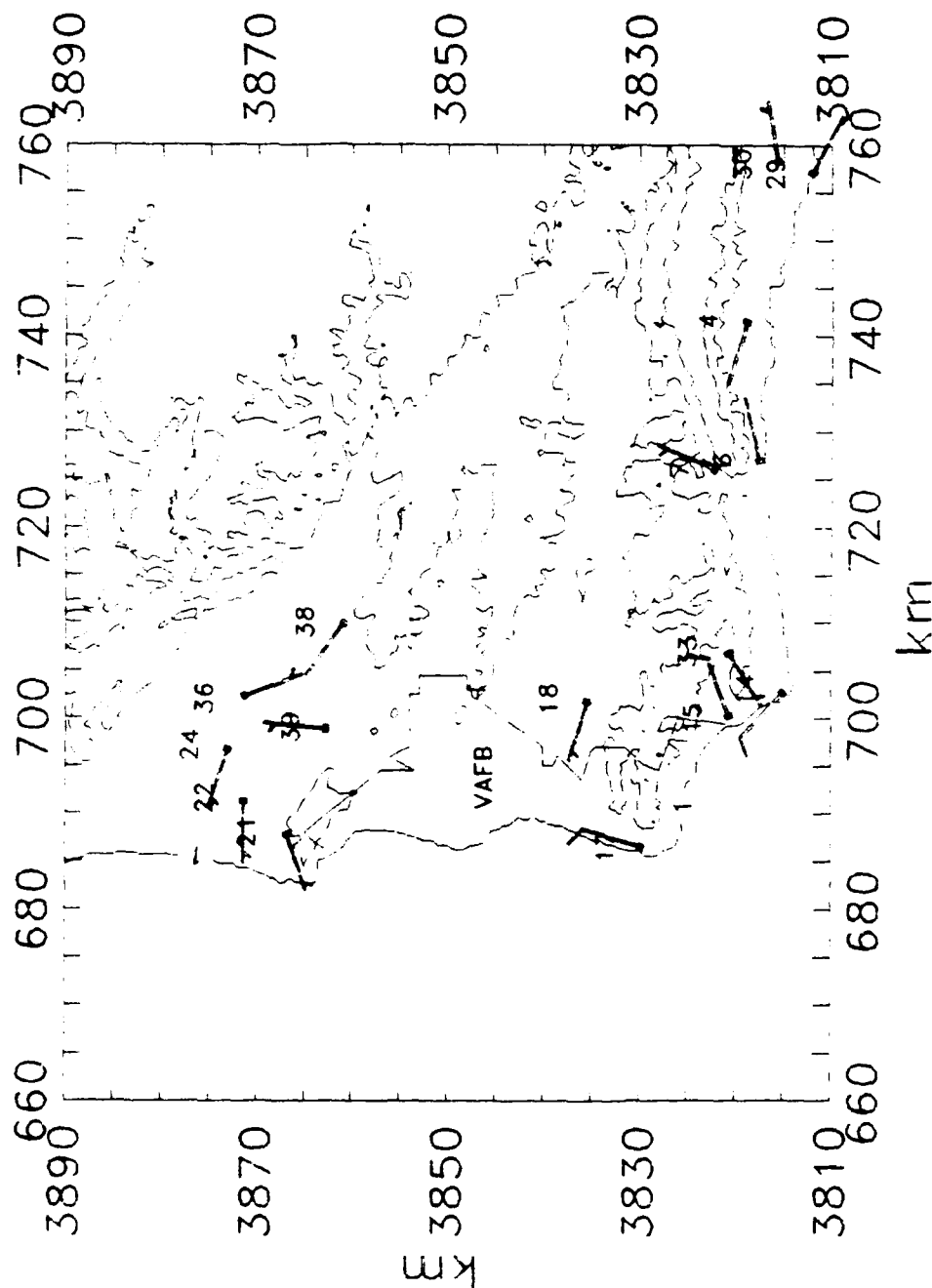


VANDENBERG REGION 7/28/88 13:00

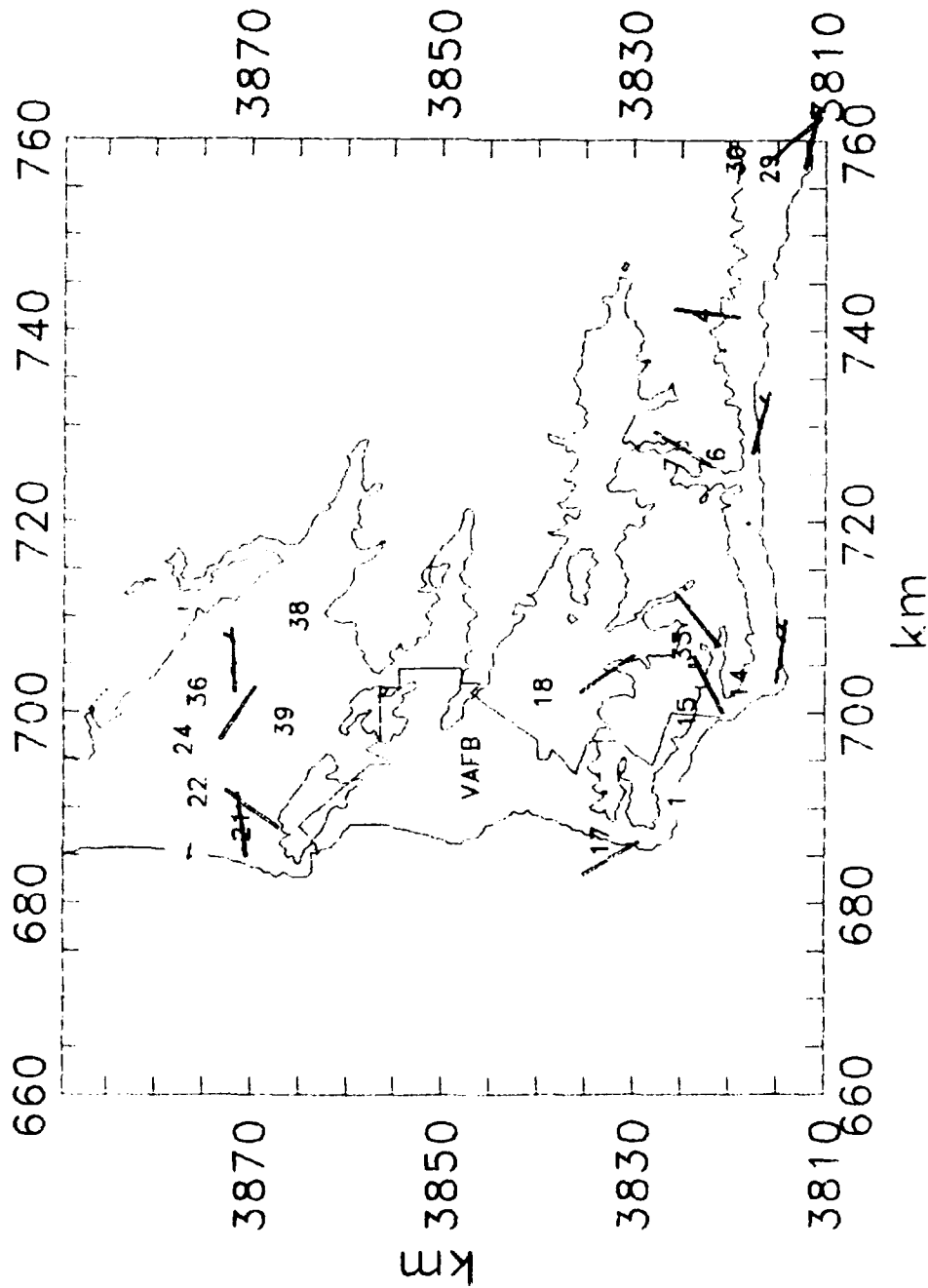


SCALE: 18 km = 1 inch
 CONTOUR interval = 200 m
 SANTA BARBARA AQMD SITES:
 4 Las Flores Canyon Site 4
 6 GTC Site A
 7 GTC Site B
 14 Point Conception
 15 Jajama Beach
 16 Point Arguello
 18 H Street
 19 Lompoc HS&P
 20 Battles
 21 Casmallia Hills
 24 Bonita School
 30 Goleta
 33 Jajama Road
 35 Watt Road VAFB
 38 Glacier Lane
 39 Briarwood

VANDENBERG REGION 7/28/88 19:00

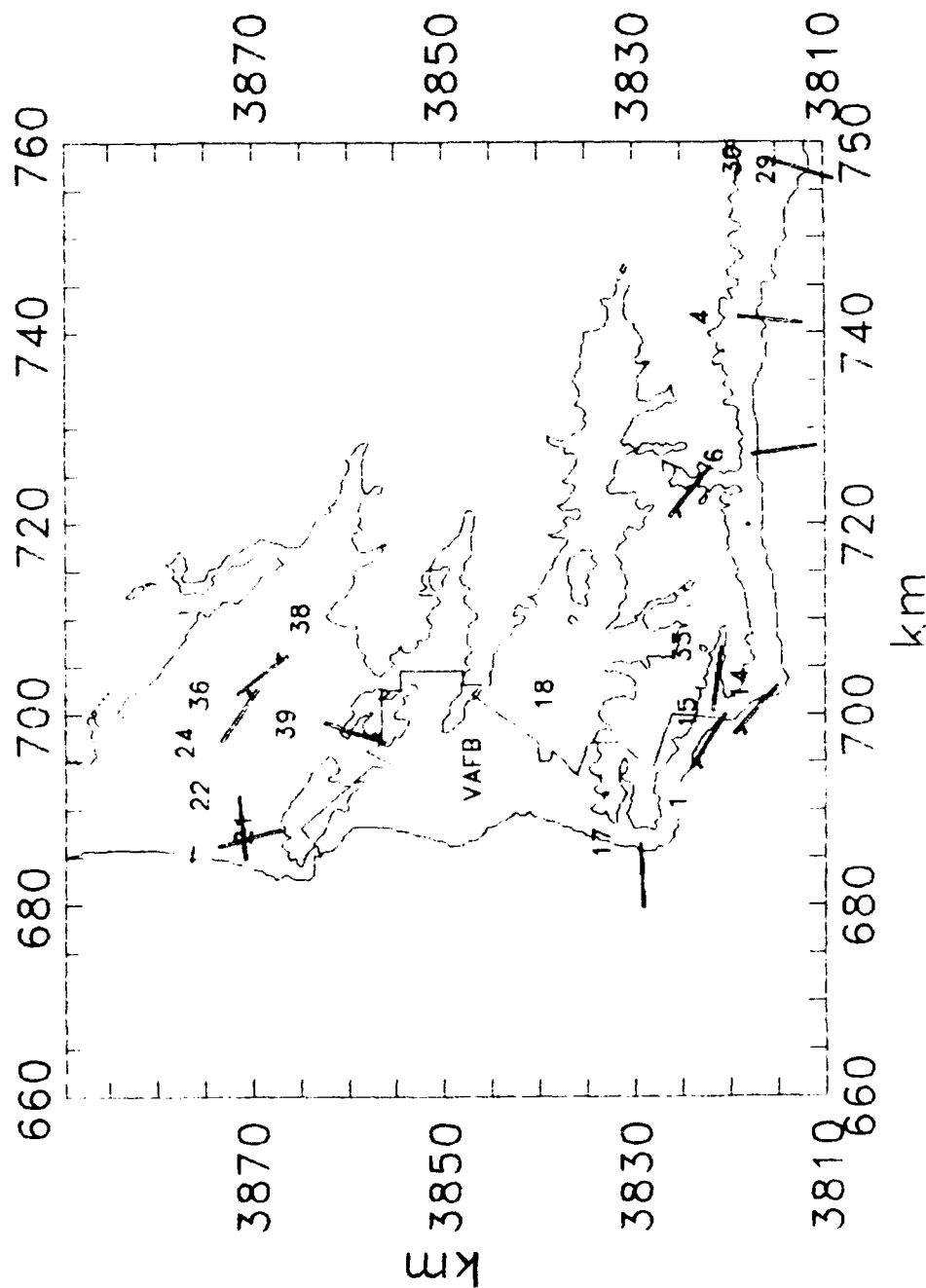


VANDENBERG REGION 7/29/88 01:00



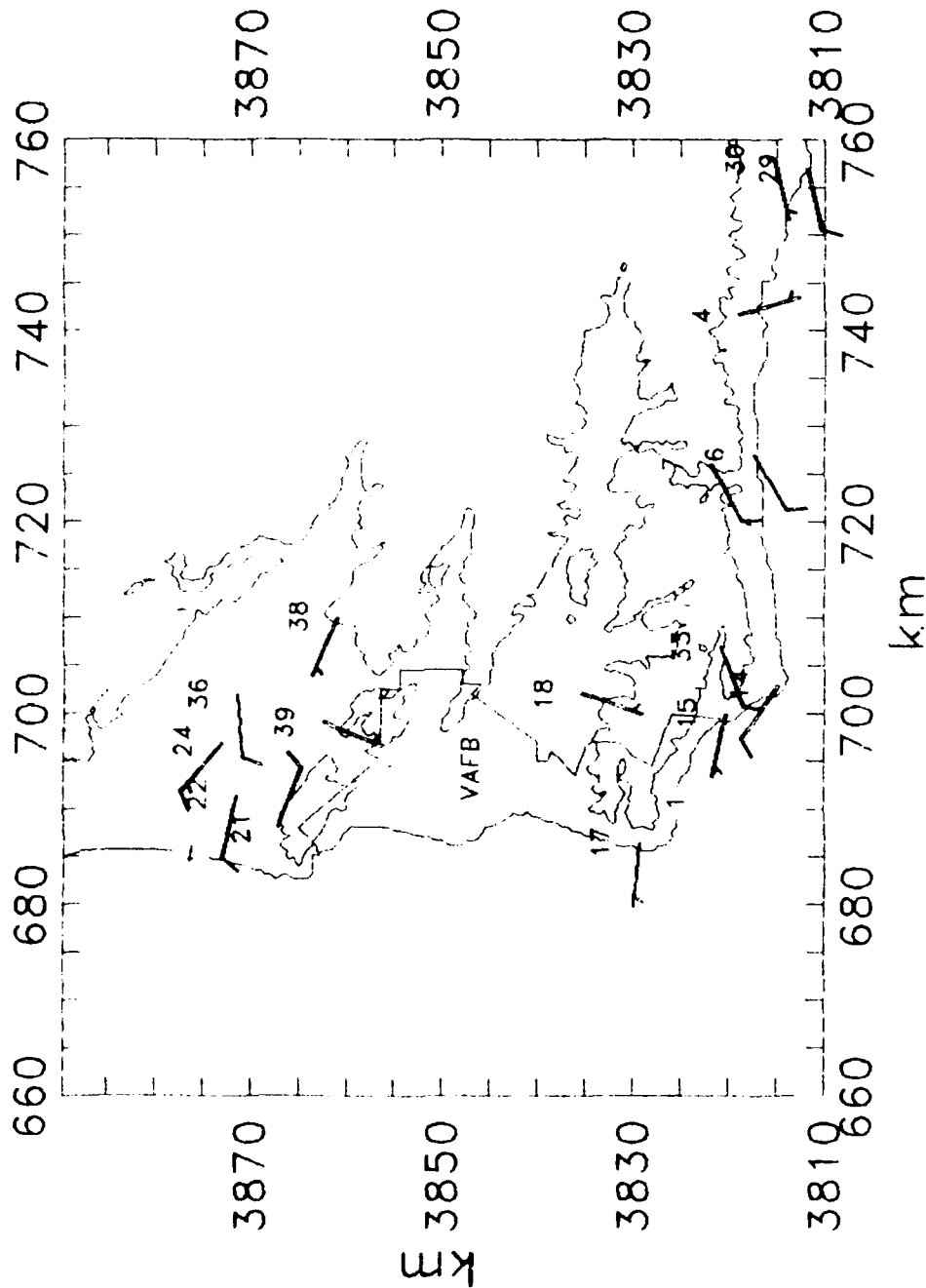
SCALE: 18 km = 1 inch
 CONTOUR interval = 200 m
 SANTA BARBARA AQMD SITES:
 4 Las Flores Canyon Site 4
 6 GTC SITE A
 7 GTC SITE B
 14 Point Conception
 15 Jalama Beach
 17 Vandenberg STS
 18 H Street
 21 Casmalia Hills
 22 Guadalupe
 24 Bonita School
 29 West Campus
 30 Goleta
 33 Jalama Road
 36 McClelland Street
 38 Glacier Lane
 39 Briarwood

VANDENBERG REGION 7/29/88 07:00



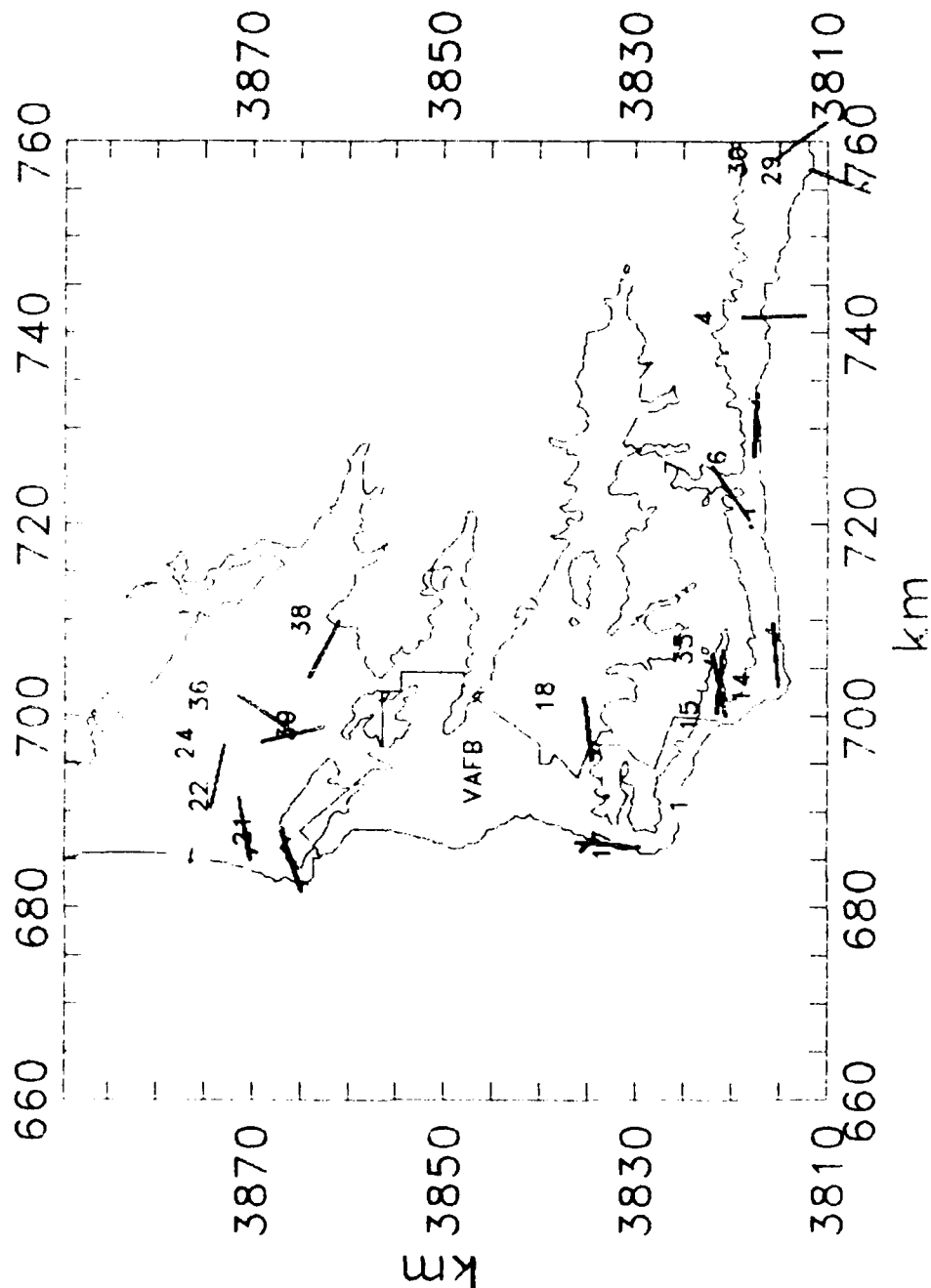
SCALE: 18 km = 1 inch
 CONTOUR interval = 200 m
 SANTA BARBARA AQMD SITES:
 4 Las Flores Canyon Site 4
 6 GTC SITE A
 7 GTC SITE B
 14 Point Conception
 15 Jalama Beach
 17 Vandenberg STS
 18 H Street
 21 Casmalia Hills
 22 Guadalupe
 24 Bonita School
 29 West Campus
 30 Goleta
 33 Jalama Road
 36 McClelland Street
 38 Glacier Lane
 39 Briarwood

VANDENBERG REGION 7/29/88 13:00



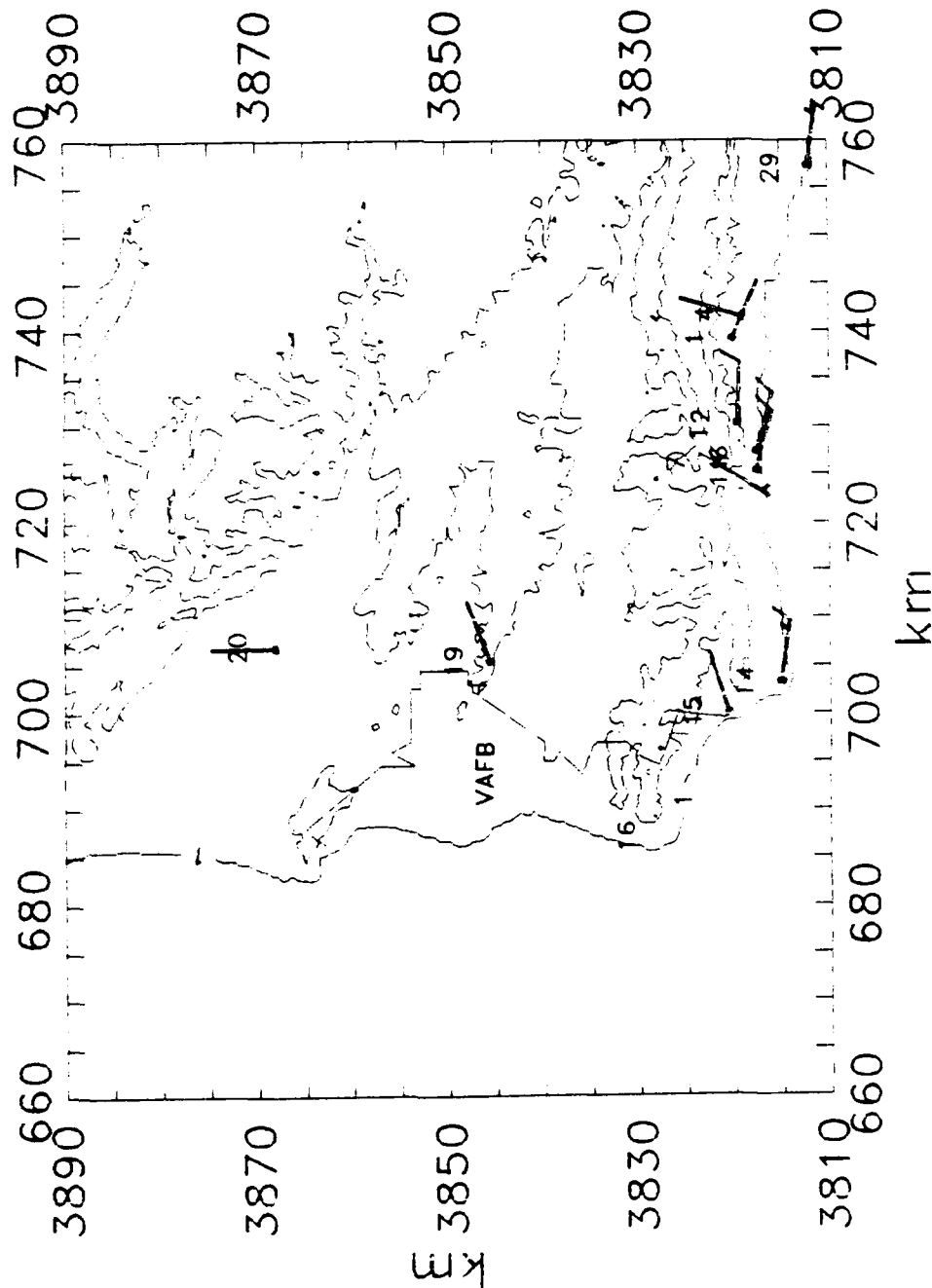
SCALE: 18 km = 1 inch
 CONTOUR interval = 200 m
 SANTA BARBARA AQMD SITES:
 4 Las Flores Canyon Site 4
 6 GTC SITE A
 7 GTC SITE B
 14 Point Conception
 15 Jalama Beach
 17 Vandenberg STS
 18 H Street
 21 Casmalia Hills
 22 Guadalupe
 24 Bonita School
 29 West Campus
 30 Goleta
 33 Jalama Road
 36 McClelland Street
 38 Glacier Lane
 39 Briarwood

VANDENBERG REGION 7/29/88 19:00



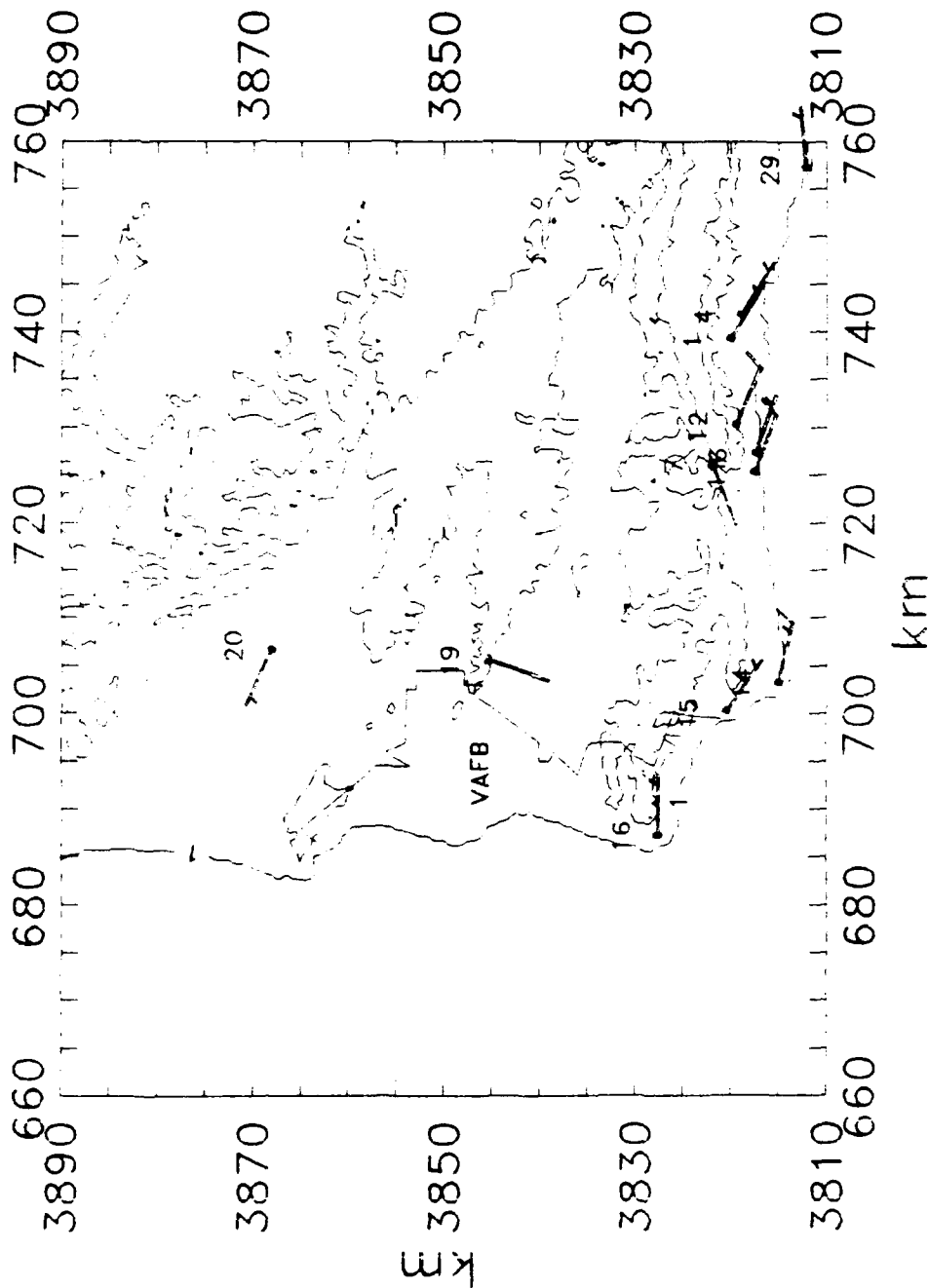
SCALE: 18 km = 1 inch
 CONTOUR interval = 200 m
 SANTA BARBARA AQMD SITES:
 4 Las Flores Canyon Site 4
 6 GTC SITE A
 7 GTC SITE B
 14 Point Conception
 15 Jalama Beach
 17 Vandenberg STS
 18 H Street
 21 Casmallia Hills
 22 Guadalupe
 24 Bonita School
 29 West Campus
 30 Goleta
 33 Jalama Road
 36 McClelland Street
 38 Glacier Lane
 39 Briarwood

VANDENBERG REGION 10/18/88 01:00



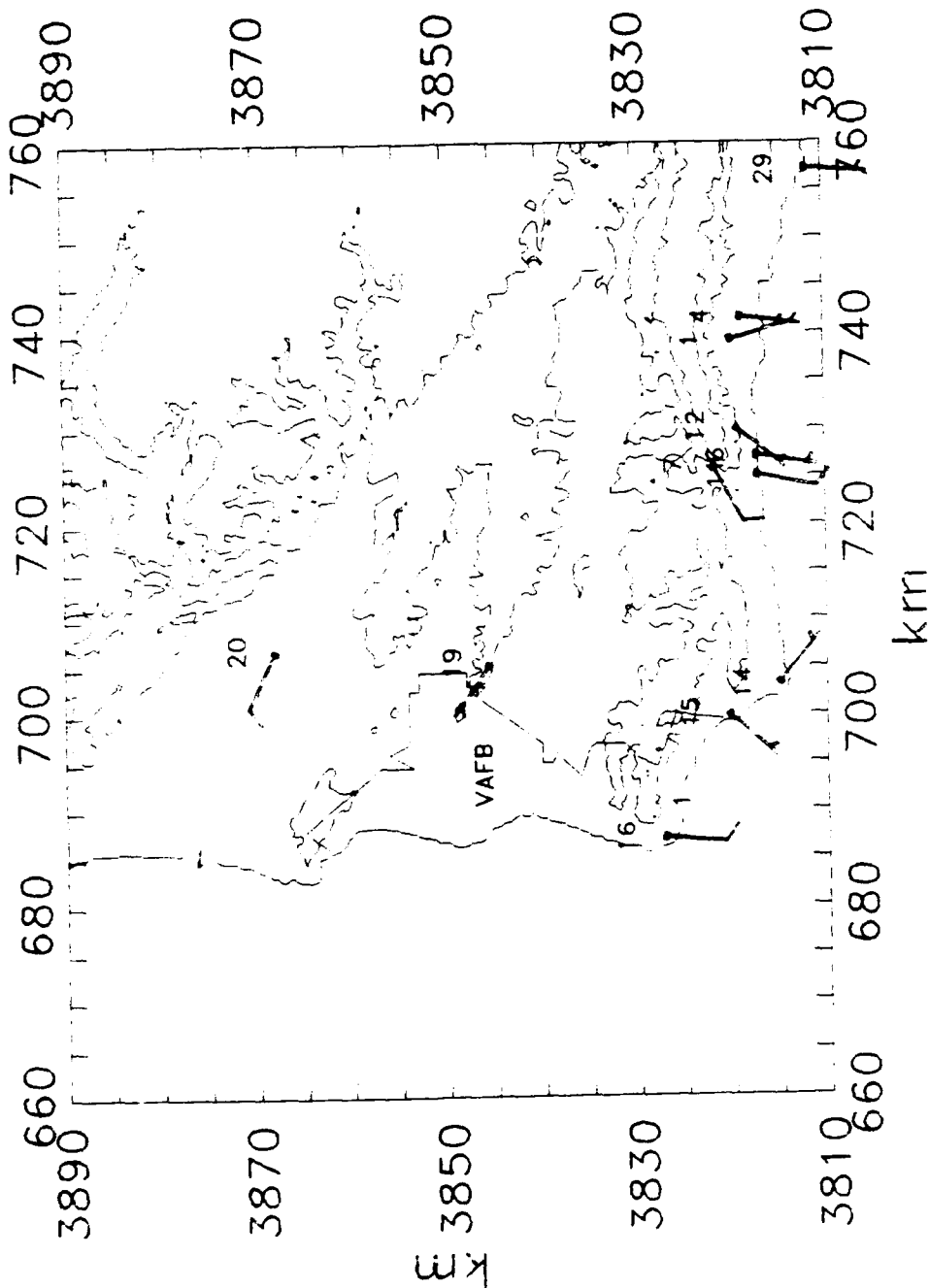
SCALE: 18 km = 1 inch
 CONTOUR interval = 200 m
 SANTA BARBARA AQMD SITES:
 1 Las Flores Canyon Site 1
 4 Las Flores Canyon Site 4
 6 GTC Site A
 7 GTC Site A
 11 Odor West
 12 Odor East
 14 Point Conception
 15 Jalama Beach
 16 Point Arguello
 19 Lompoc HS&P
 20 Battles
 29 West Campus

VANDENBERG REGION 10/18/88 07:00



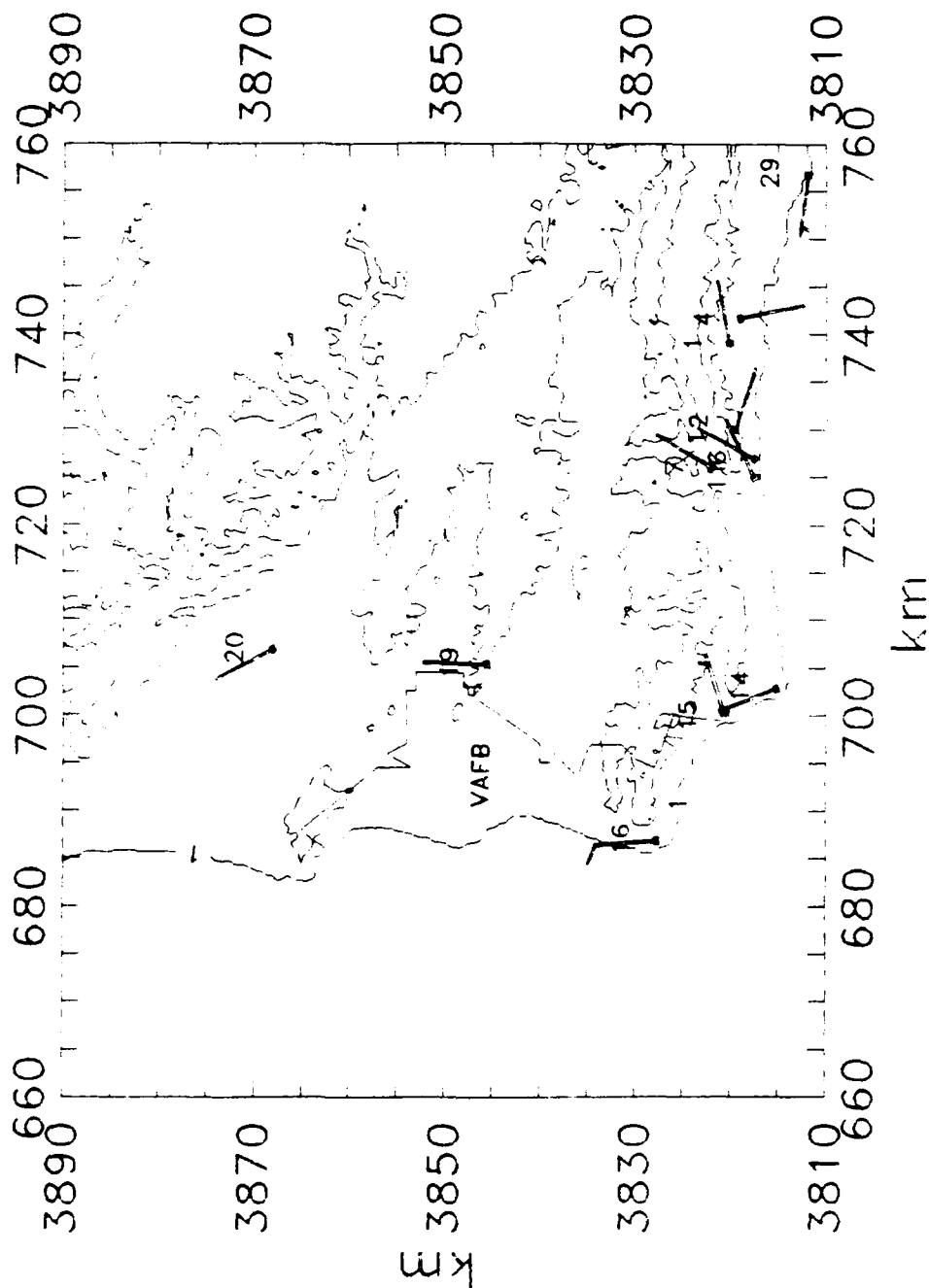
SCALE: 18 km = 1 inch
 CONTOUR interval = 200 m
 SANTA BARBARA AQMD SITES:
 1 Las Flores Canyon Site 1
 4 Las Flores Canyon Site 4
 6 GTC Site A
 7 GTC Site A
 11 Odor West
 12 Odor East
 14 Point Conception
 15 Jalama Beach
 16 Point Arguello
 19 Lompoc HS&P
 20 Battles
 29 West Campus

VANDENBERG REGION 10/18/88 13:00



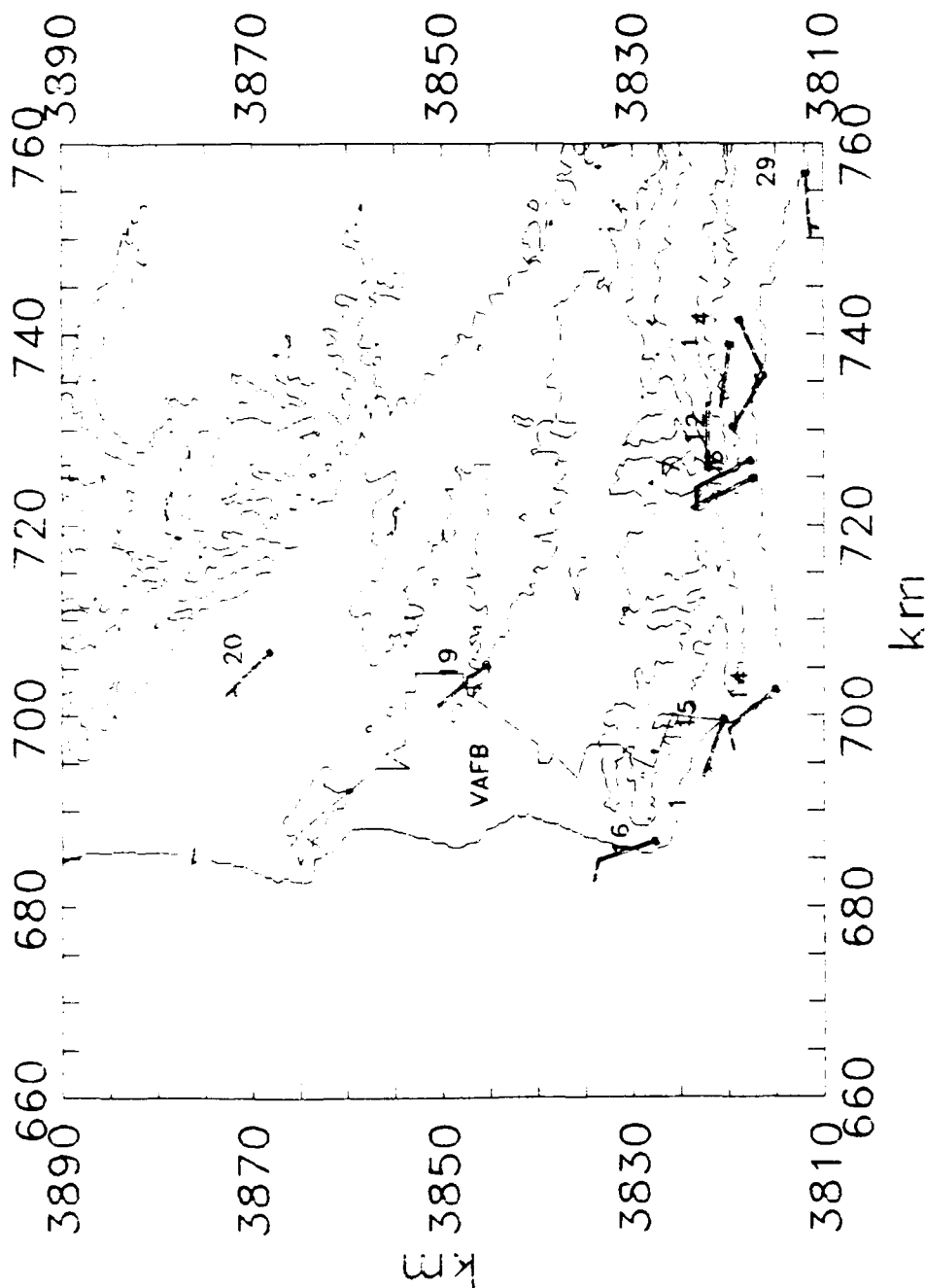
SCALE: 18 km = 1 inch
 CONTOUR interval = 200 m
 SANTA BARBARA AQMD SITES:
 1 Las Flores Canyon Site 1
 4 Las Flores Canyon Site 4
 6 GTC Site A
 7 GTC Site A
 11 Odor West
 12 Odor East
 14 Point Conception
 15 Jalama Beach
 16 Point Arguello
 19 Lompoc HS&P
 20 Battles
 29 West Campus

VANDENBERG REGION 10/18/88 19:00



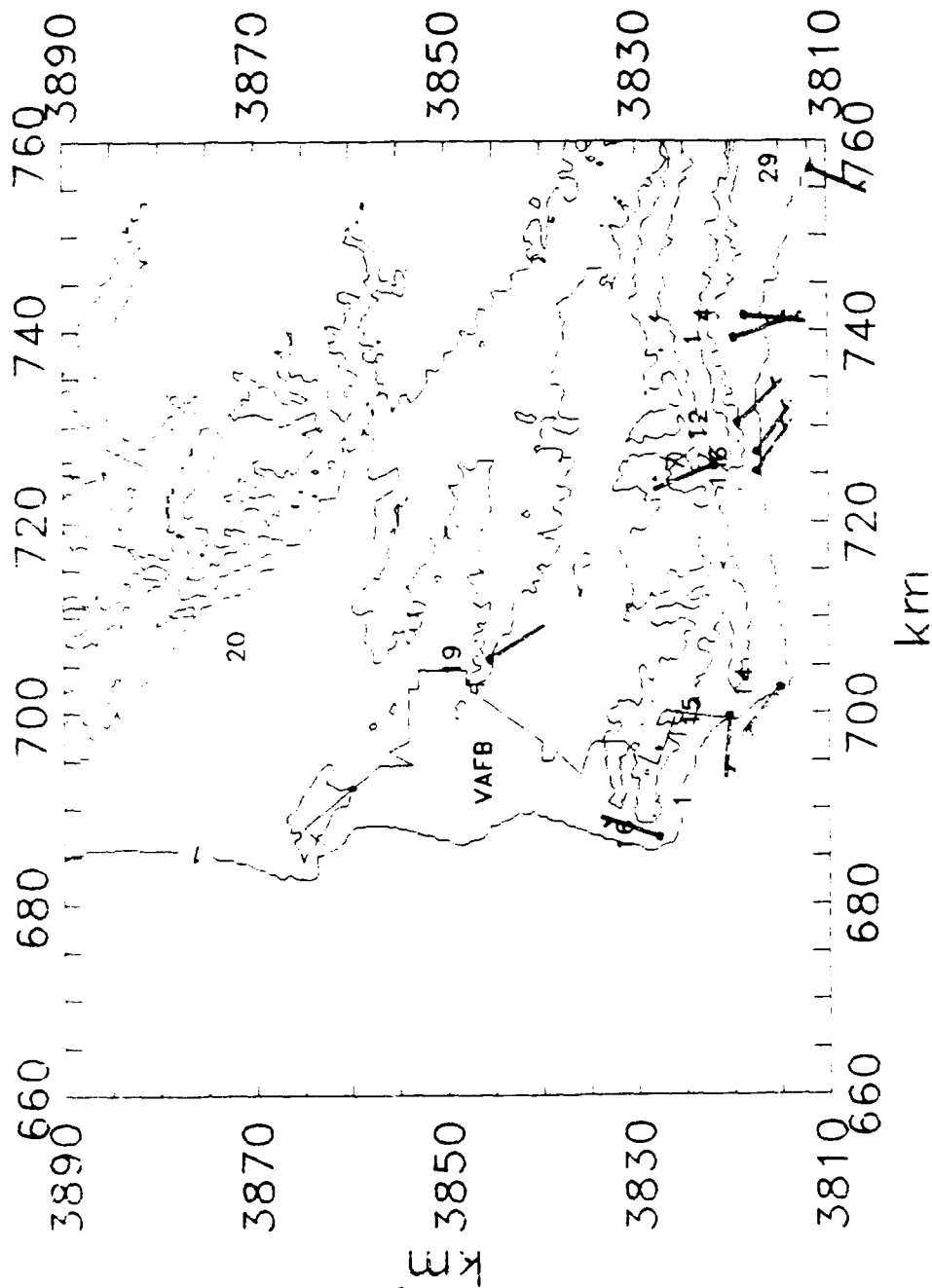
SCALE: 18 km = 1 inch
 CONTOUR interval = 200 m
 SANTA BARBARA AQMD SITES:
 1 Las Flores Canyon Site 1
 4 Las Flores Canyon Site 4
 6 GTC Site A
 7 GTC Site A
 11 Odor West
 12 Odor East
 14 Point Conception
 15 Jalama Beach
 16 Point Arguello
 19 Lompoc HS&P
 20 Battles
 29 West Campus

VANDENBERG REGION 10/19/88 01:00



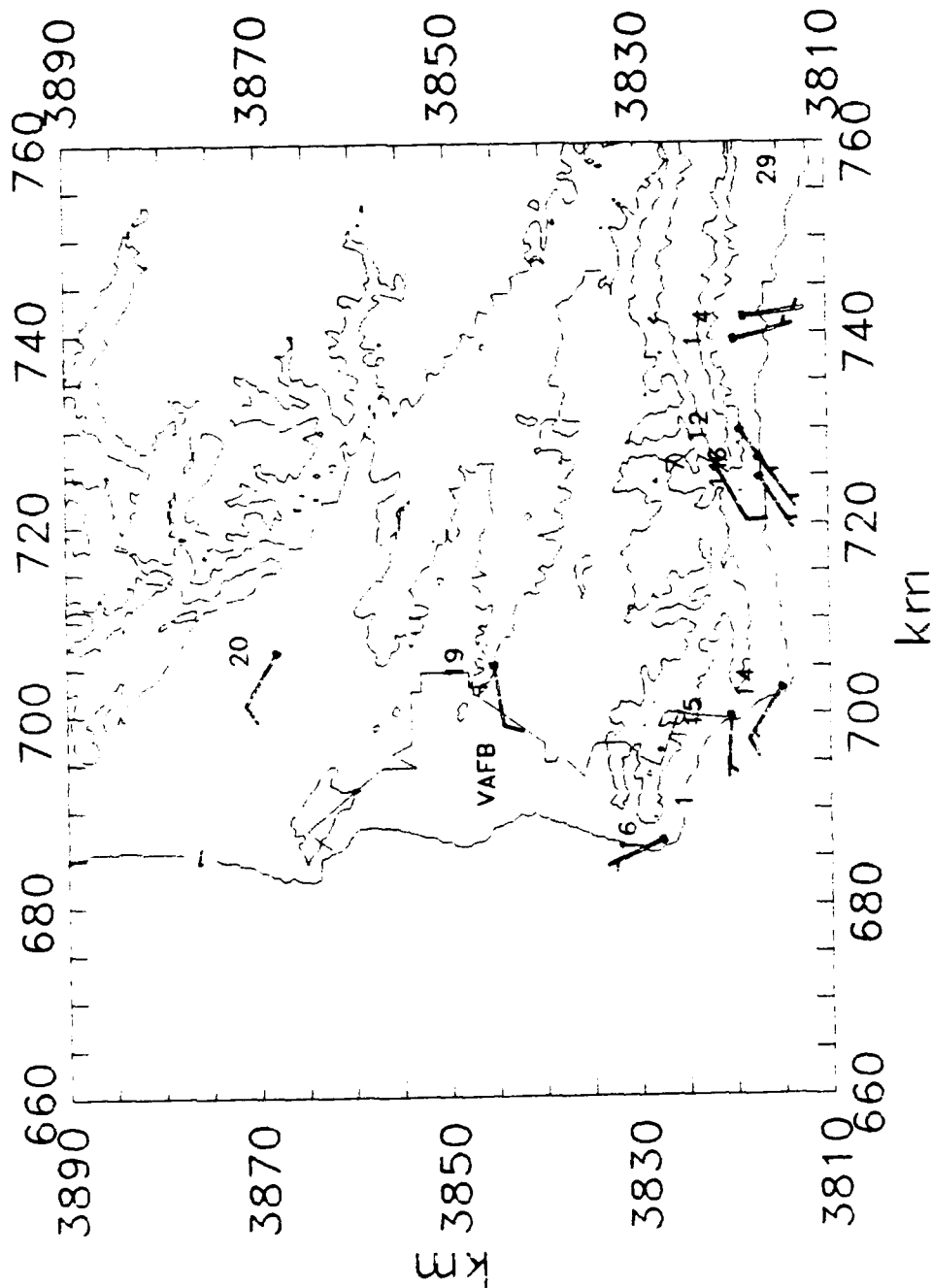
SCALE: 18 km = 1 inch
 CONTOUR interval = 200 m
 SANTA BARBARA AQMD SITES:
 1 Las Flores Canyon Site 1
 4 Las Flores Canyon Site 4
 6 GTC Site A
 7 GTC Site A
 11 Odor West
 12 Odor East
 14 Point Conception
 15 Jalama Beach
 16 Point Arguello
 19 Lompoc HS&P
 20 Battles
 29 West Campus

VANDENBERG REGION 10/19/88 07:00



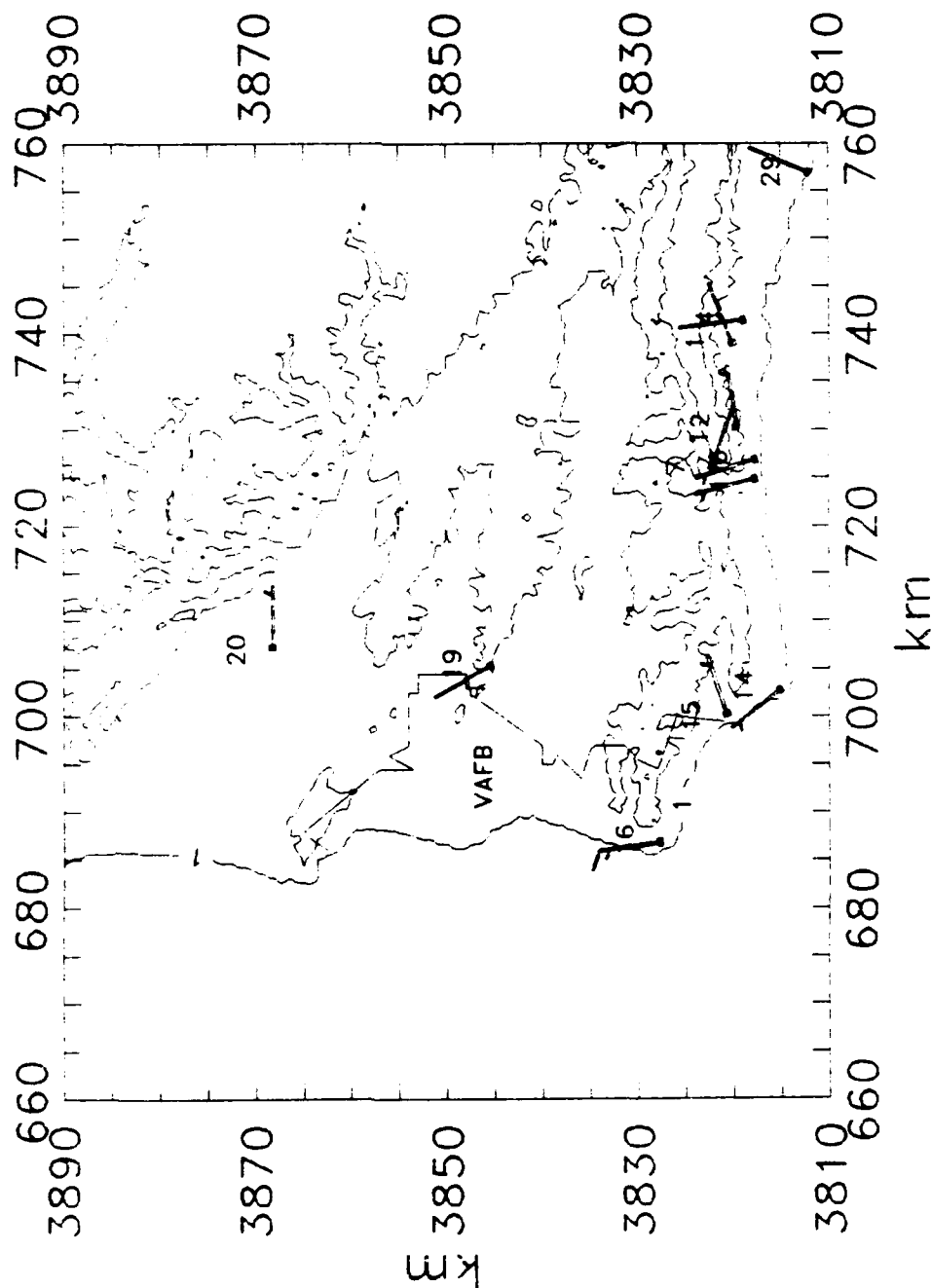
SCALE: 18 km = 1 inch
 CONTOUR interval = 200 m
 SANTA BARBARA AQMD SITES:
 1 Las Flores Canyon Site 1
 4 Las Flores Canyon Site 4
 6 GTC Site A
 7 GTC Site A
 11 Odor West
 12 Odor East
 14 Point Conception
 15 Jalama Beach
 16 Point Arguello
 19 Lompoc HS&P
 20 Battles
 29 West Campus

VANDENBERG REGION 10/19/88 13:00

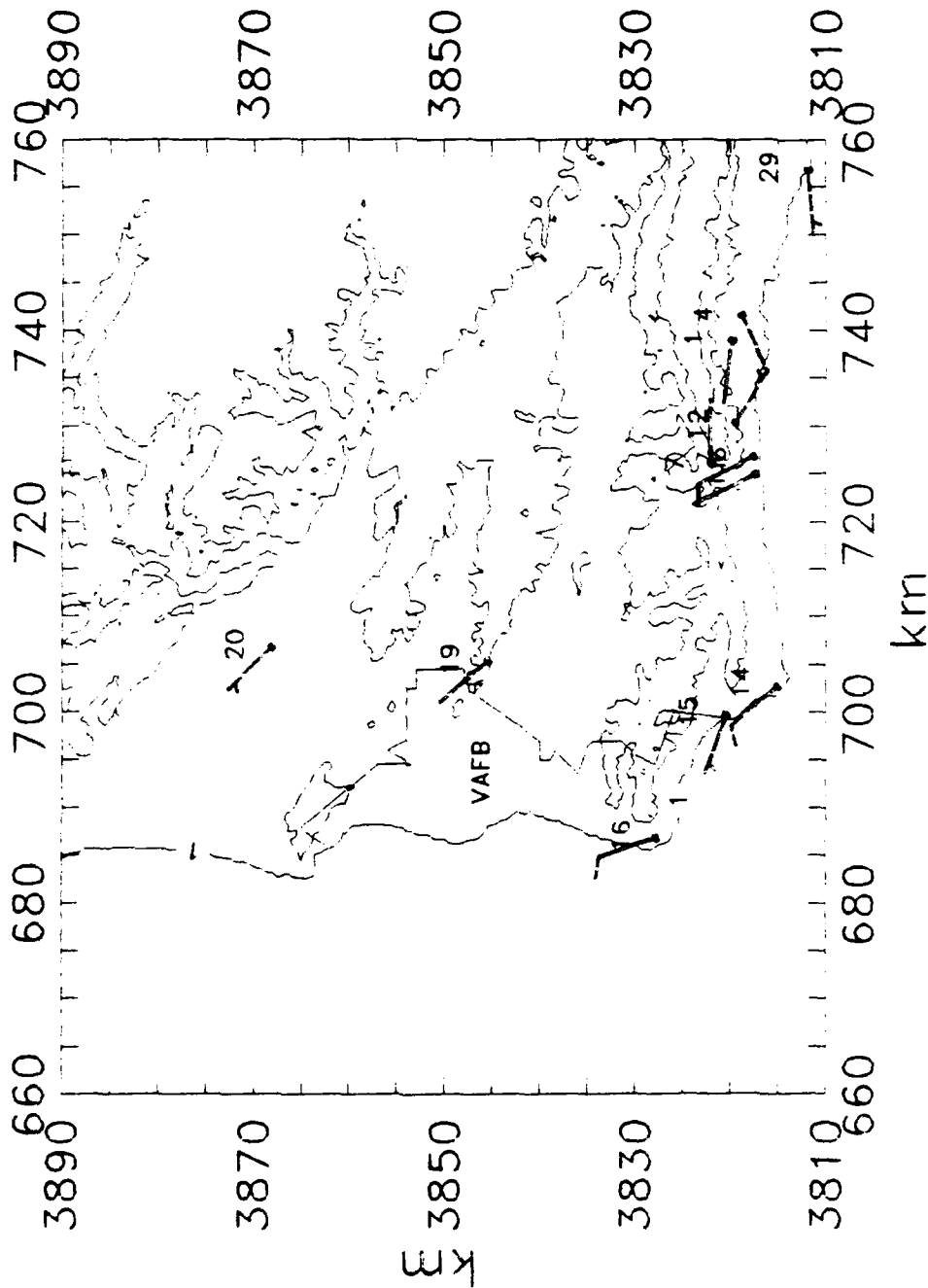


SCALE: 18 km = 1 inch
 CONTOUR interval = 200 m
 SANTA BARBARA AQMD SITES:
 1 Las Flores Canyon Site 1
 4 Las Flores Canyon Site 4
 6 GTC Site A
 7 GTC Site A
 11 Odor West
 12 Odor East
 14 Point Conception
 15 Jalama Beach
 16 Point Arguello
 19 Lompoc HS&P
 20 Battles
 29 West Campus

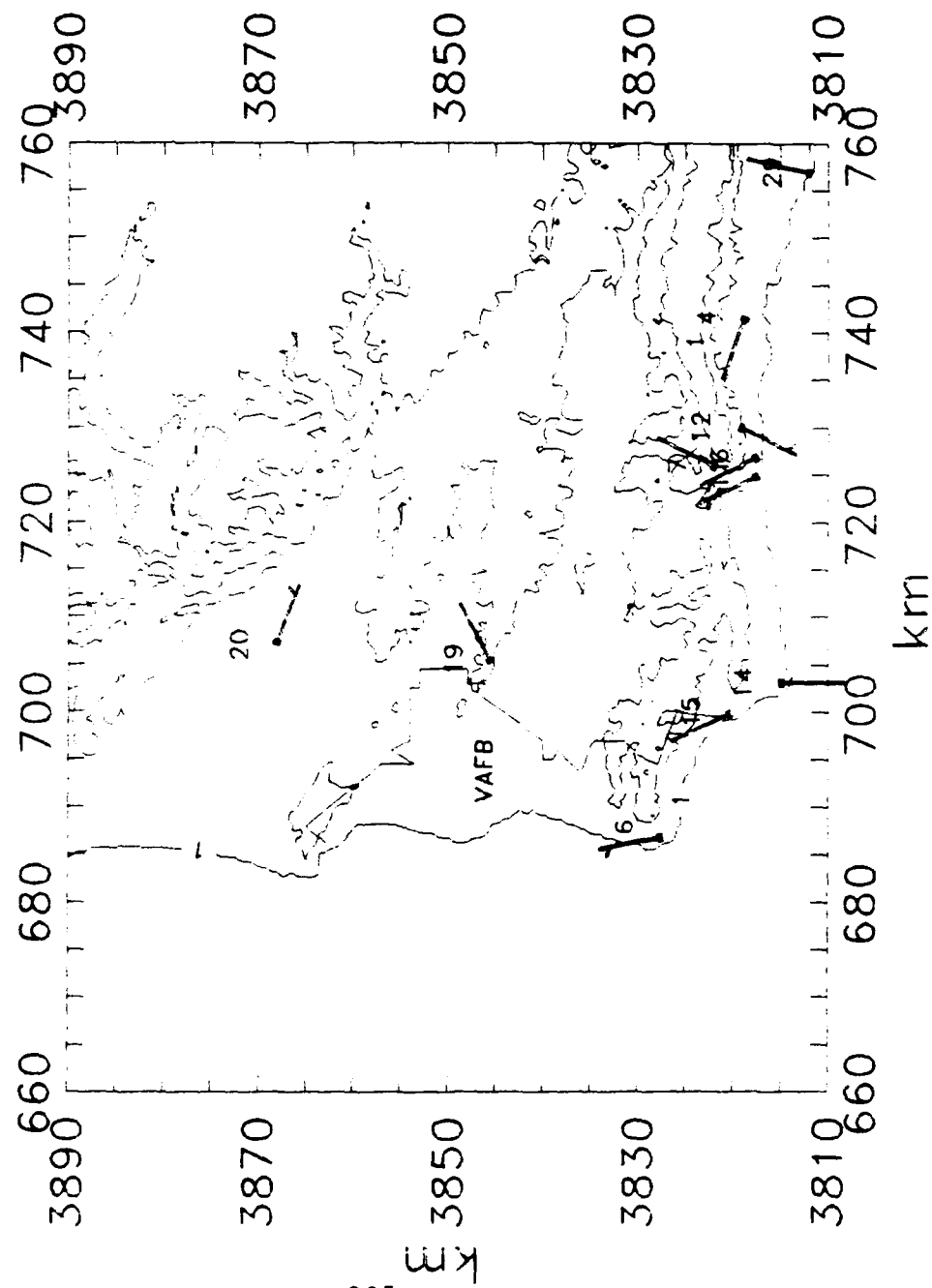
VANDENBERG REGION 10/19/88 19:00



VANDENBERG REGION 10/20/88 01:00

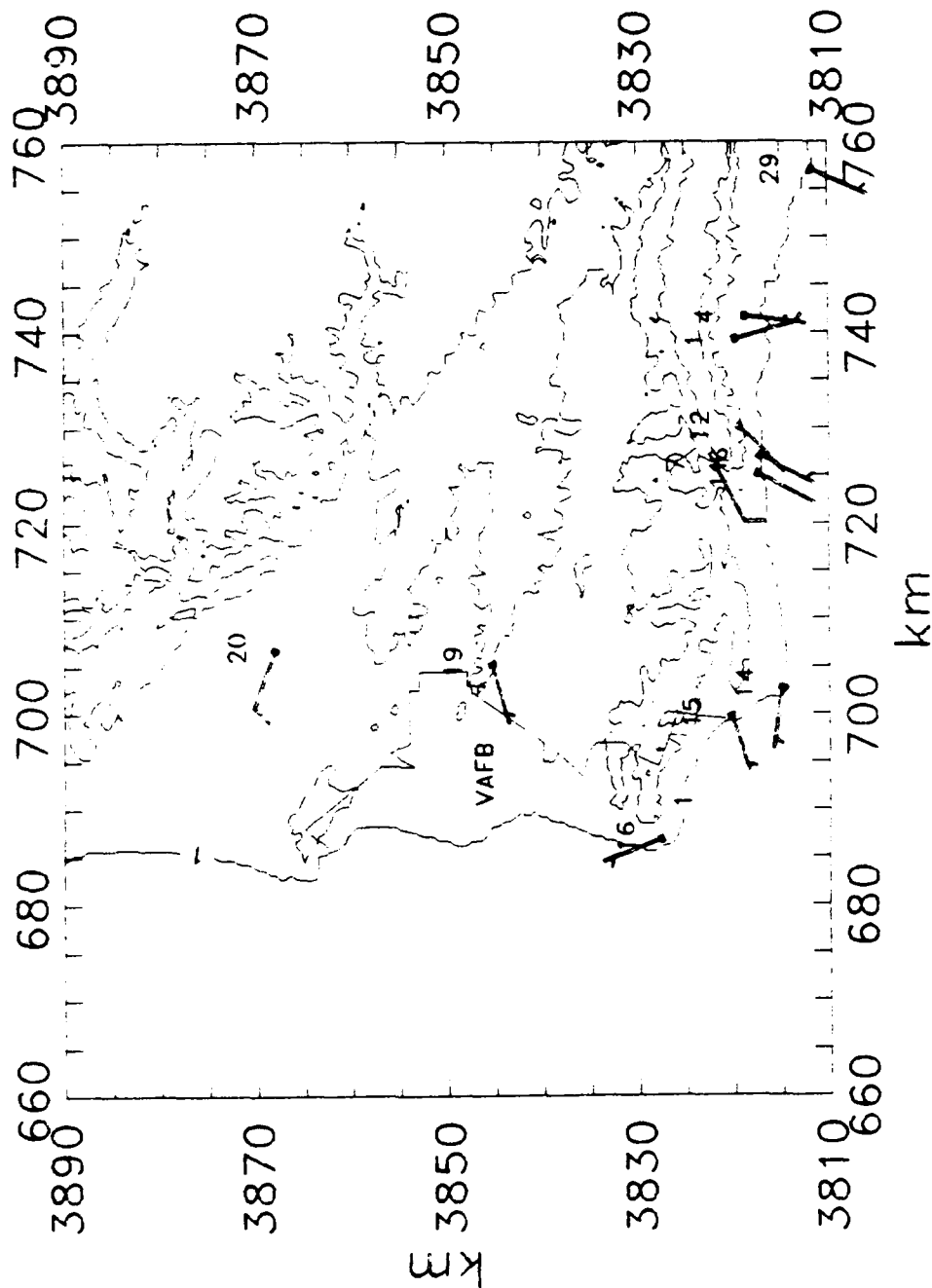


VANDENBERG REGION 10/20/88 07:00



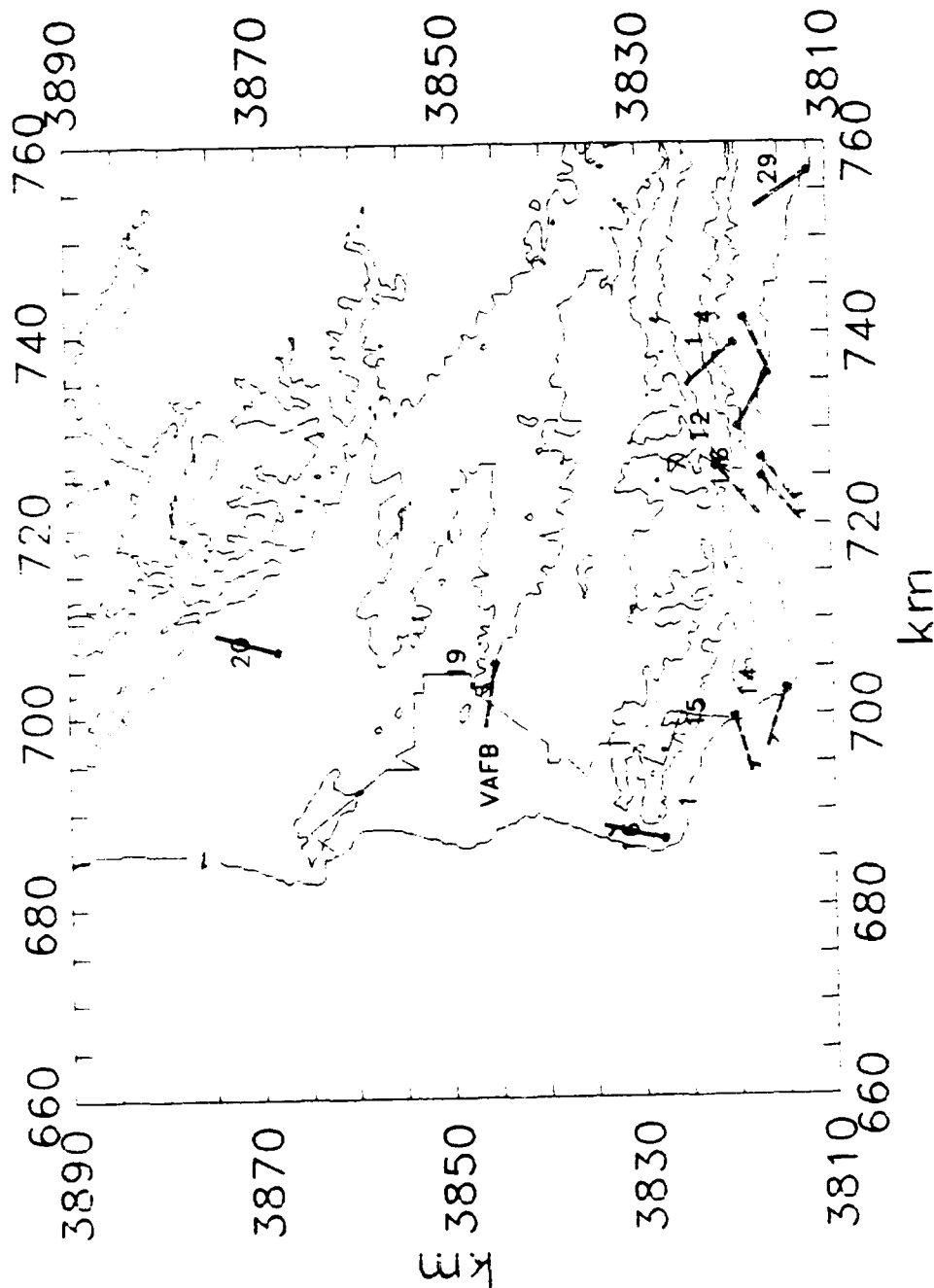
SCALE: 18 km = 1 inch
 CONTOUR interval = 200 m
 SANTA BARBARA AQMD SITES:
 1 Las Flores Canyon Site 1
 4 Las Flores Canyon Site 4
 6 GTC Site A
 7 GTC Site A
 11 Odor West
 12 Odor East
 14 Point Conception
 15 Jalama Beach
 16 Point Arguello
 19 Lompoc HS&P
 20 Battles
 29 West Campus

VANDENBERG REGION 10/20/88 13:00



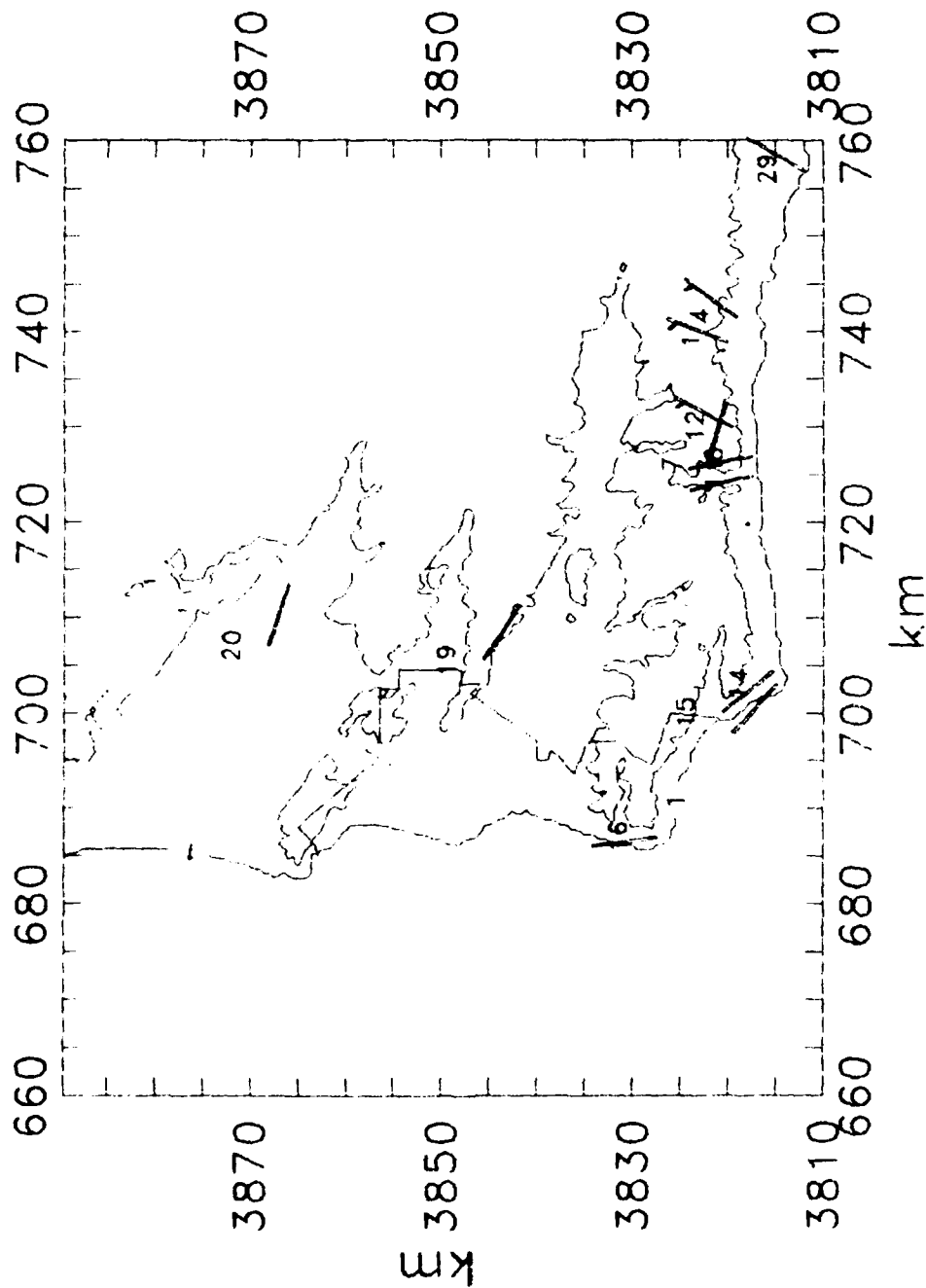
SCALE: 18 km = 1 inch
 CONTOUR interval = 200 m
 SANTA BARBARA AQMD SITES:
 1 Las Flores Canyon Site 1
 4 Las Flores Canyon Site 4
 6 GTC Site A
 7 GTC Site A
 11 Odor West
 12 Odor East
 14 Point Conception
 15 Jalama Beach
 16 Point Arguello
 19 Lompoc HS&P
 20 Battles
 29 West Campus

VANDENBERG REGION 10/20/88 19:00



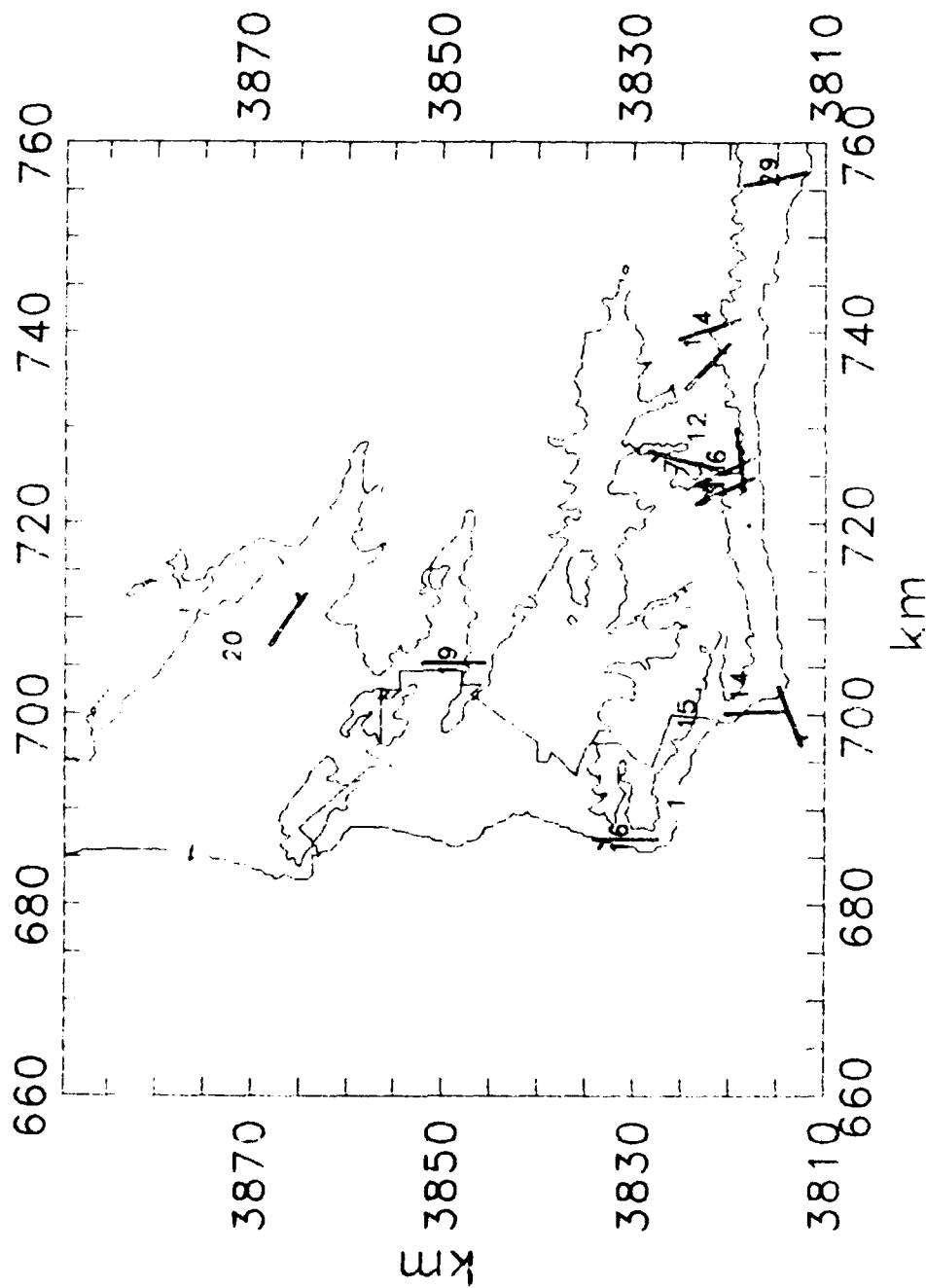
SCALE: 18 km = 1 inch
 CONTOUR interval = 200 m
 SANTA BARBARA AQMD SITES:
 1 Las Flores Canyon Site 1
 4 Las Flores Canyon Site 4
 6 GTC Site A
 7 GTC Site B
 11 Odor West
 12 Odor East
 14 Point Conception
 15 Jalama Beach
 16 Point Arguello
 19 Lompoc HS&P
 20 Battles
 29 West Campus

VANDENBERG REGION 10/21/88 01:00



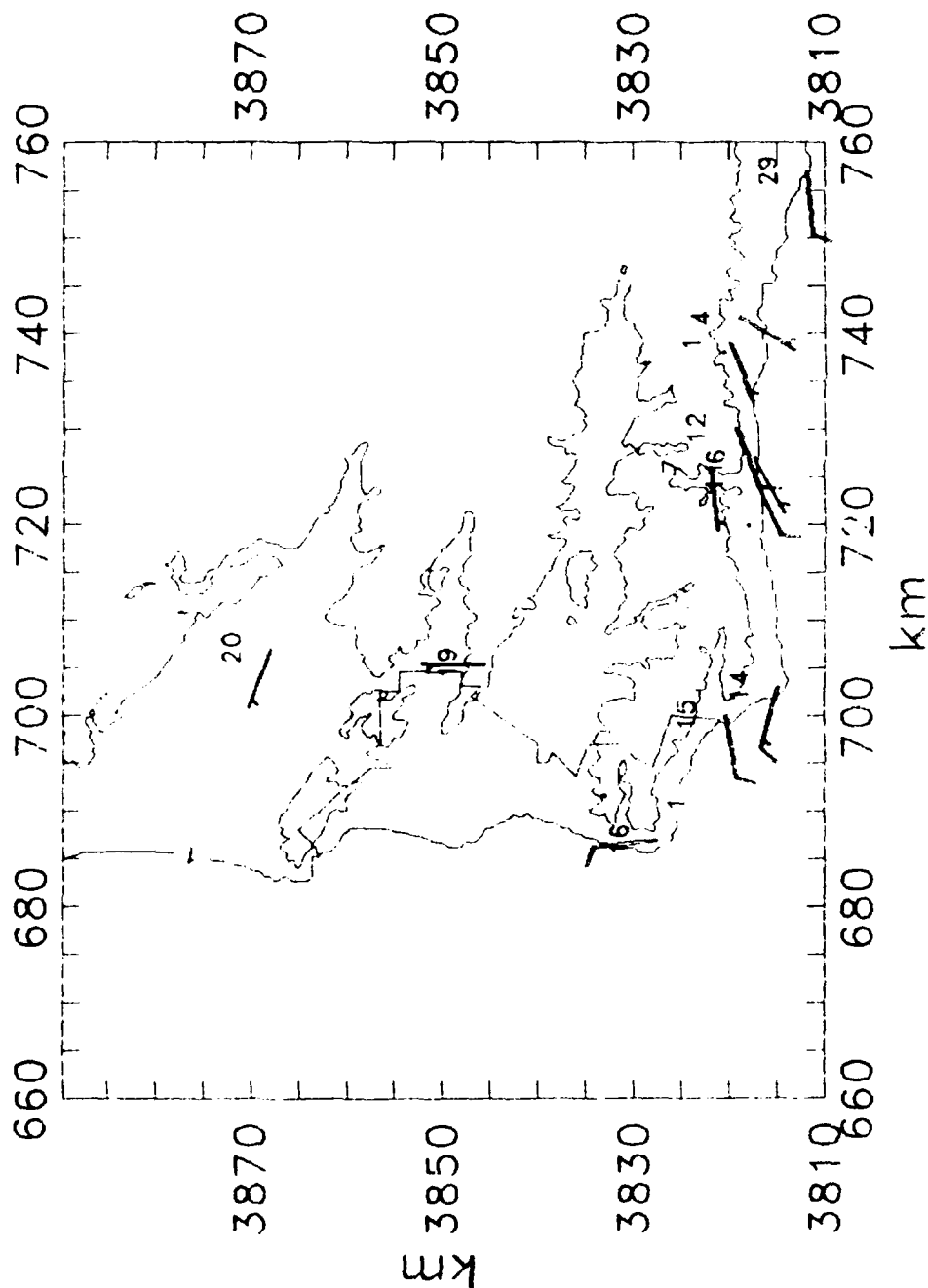
SCALE: 18 km = 1 inch
 CONTOUR interval = 200 m
 SANTA BARBARA AQMD SITES:
 1 Las Flores Canyon Site 1
 4 Las Flores Canyon Site 4
 6 GTC Site A
 7 GTC Site B
 11 Odor West
 12 Odor East
 14 Point Conception
 15 Jalama Beach
 16 Point Arguello
 19 Lompoc HS&P
 20 Battles
 29 West Campus

VANDENBERG REGION 10/21/88 07:00



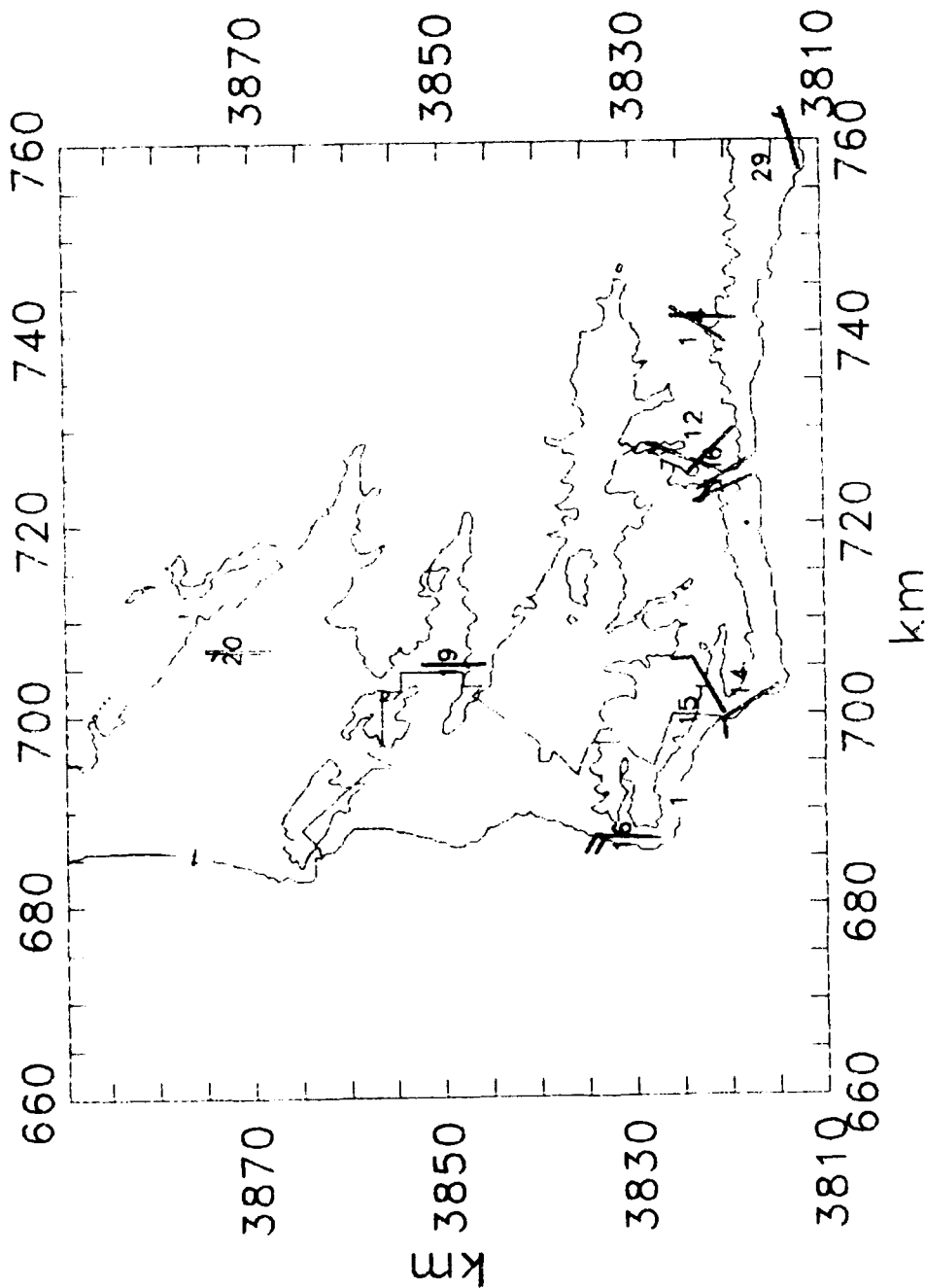
SCALE: 18 km = 1 inch
 CONTOUR interval = 200 m
 SANTA BARBARA AQMD SITES:
 1 Las Flores Canyon Site 1
 4 Las Flores Canyon Site 4
 6 GTC Site A
 7 GTC Site B
 11 Odor West
 12 Odor East
 14 Point Conception
 15 Jalama Beach
 16 Point Arguello
 19 Lompoc HS&P
 20 Battles
 29 West Campus

VANDENBERG REGION 10/21/88 13:00



SCALE: 18 km = 1 inch
 CONTOUR interval = 200 m
 SANTA BARBARA AQMD SITES:
 1 Las Flores Canyon Site 1
 4 Las Flores Canyon Site 4
 6 GTC Site A
 7 GTC Site B
 11 Odor West
 12 Odor East
 14 Point Conception
 15 Jalama Beach
 16 Point Arguello
 19 Lompoc HS&P
 20 Battles
 29 West Campus

VANDENBERG REGION 10/21/88 19:00



SCALE: 18 km = 1 inch
 CONTOUR interval = 200 m
 SANTA BARBARA AQMD SITES:
 1 Las Flores Canyon Site 1
 4 Las Flores Canyon Site 4
 6 GTC Site A
 7 GTC Site B
 11 Odor West
 12 Odor East
 14 Point Conception
 15 Jalama Beach
 16 Point Arguello
 19 Lompoc HS&P
 20 Battles
 29 West Campus

Base Wind Fields

The wind barbs (m/s) are hourly 12 ft averages from the VBG base WINDS network. When the stratus edge was observed, its location is given as a dashed line on the base maps.

Day 1. The frontal passage results in consistent north-northwesterly winds over the entire base during the morning, with slightly stronger winds over S. Base. Wind speeds increase at most towers starting at 1000, and there was a tendency for winds to be more westerly in the valley areas (near Towers 9 and 59), and more veered on the mountain tops later in the day (14, 19). This pattern was repeated on many occasions during the experiment and could be considered as the typical midday wind field. Speeds drop dramatically by 2200 and directions are much more variable, especially near Pt. Sal.

Day 2. Some early morning strong winds were measured at Pt. Arguello and at 014, by 700 winds were light and variable everywhere. At 1000 winds are coast-perpendicular, even near Pt. Sal and 53 where that makes them southwesterly. By 1300 flow is uniformly northwesterly everywhere except Pt. Arguello and 014 where it was slightly veered and stronger. This general pattern continued until 2200 when winds were more northerly, but lighter and more variable.

Day 3. Night winds were either northerly or easterly, especially at lower locations. By 1000 they had dramatically changed to roughly northerly at all towers, and then the typical weak westerly pattern at 1300. Towers 14 and 19 shift from north to south between these two time periods. By 1600 northwesterlies dominated the base. This was a very complicated day, since the trailer observed southwesterlies near the mouth of the Lompoc valley during midday.

Day 4. Night winds were light and north-northwesterly everywhere except near Pt. Sal (Towers 59 and 60), where the flow was contrary to the mean direction. (This feature was also observed on the evening of day 1.) The pattern changed very little until 2200 when the evening veering occurred.

Day 5. Flow began decidedly northeasterly along the S. Base coast and generally northwesterly elsewhere. The 1000 chart was actually more veered than at 1600 when all towers measured west-northwest flow. This trend reversed after that and by 2200 the typical evening pattern had established itself. To be specific that pattern is a) backed (northwest) in the lowest points of the valleys (Towers 50, 9), b) veered at higher locations (Towers 58, 14, 19), and

terrain following along the tall coastal bluffs
(17,60,18,300,200,301).

Day 6. The evening wind pattern of the previous day became generally northerly by 700. Maximum backing occurred near 1300. Significant veering did not occur until 1900, as on the previous day. All in all, very similar to day 5.

Day 7. Winds at 100 were again in the evening pattern, but by 1000 most towers were recording southwesterlies. They persisted through 1300, when the most backed winds were along the S. Base coast, and the lone "mountaintop" tower, 19, was northerly. Winds gradually veered through the day and were solidly northwesterly by 2200.

Day 8. Generally light easterly winds covered the base until 1000 when the sea breeze front was somewhere in the middle of the base with the coastal sites in westerlies and inland sites in easterlies. The typical midday pattern was established by 1300. By 1600 speeds were already dropping and the evening pattern had set in by 1900.

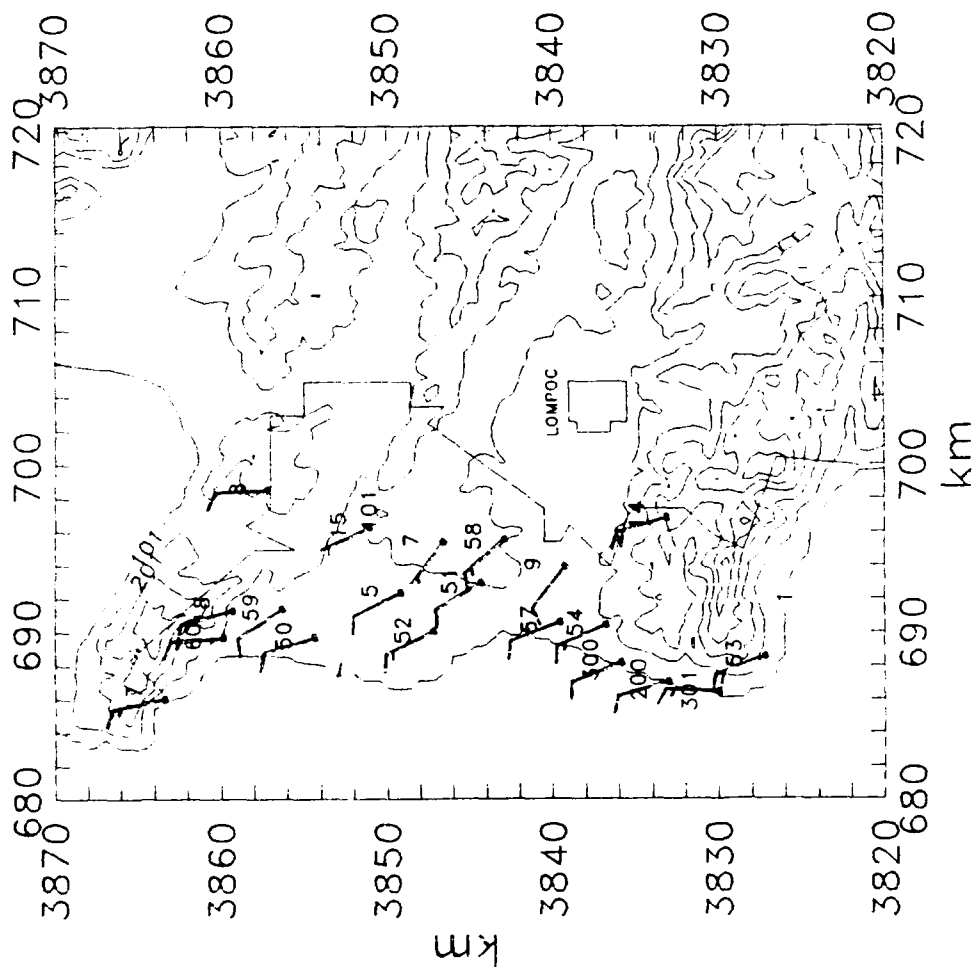
Day 9. At 100 flow was unusually westerly in the valleys, by 400 the evening pattern returned and lasted the rest of the morning. Winds stayed unusually northerly along the S. Base coast all day, and the evening pattern set in at 2200.

Day 10. Variable conditions were the rule until 700 when most towers measured easterlies. At 1000 there again was a convergence zone in the middle of the base. The 1300 and 1600 charts had low speeds and generally westerly directions. A rather rapid veering to the evening pattern occurred some time before the 1900 map.

Day 11. Variable 700 flow becomes north/northeast by 1000 at most towers. Light but uniform northwest flow is prevalent at 1300. Atypically, winds continue to back through the day and are southwest at some towers by 1600.

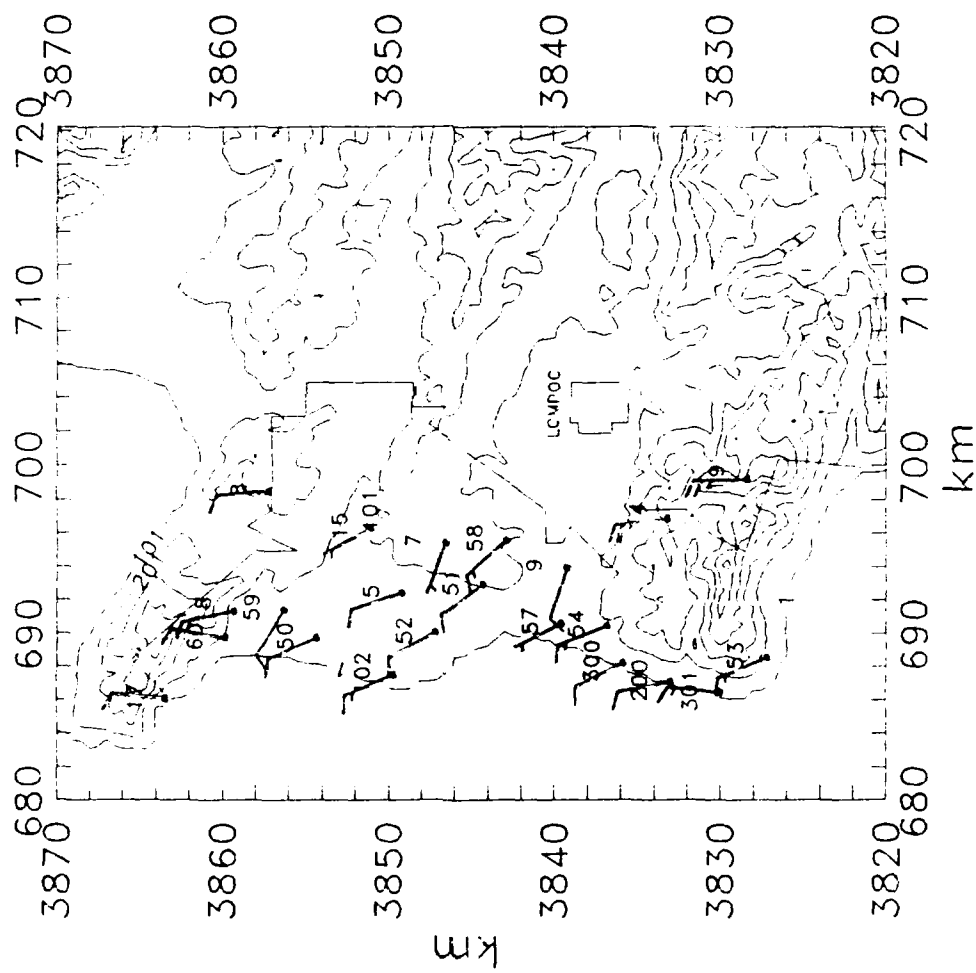
1 HOUR AVERAGES OF 12 FT. WINDS STANDARD NWS WIND BARBS

VANDENBERG AFB 5/18/88 1:00



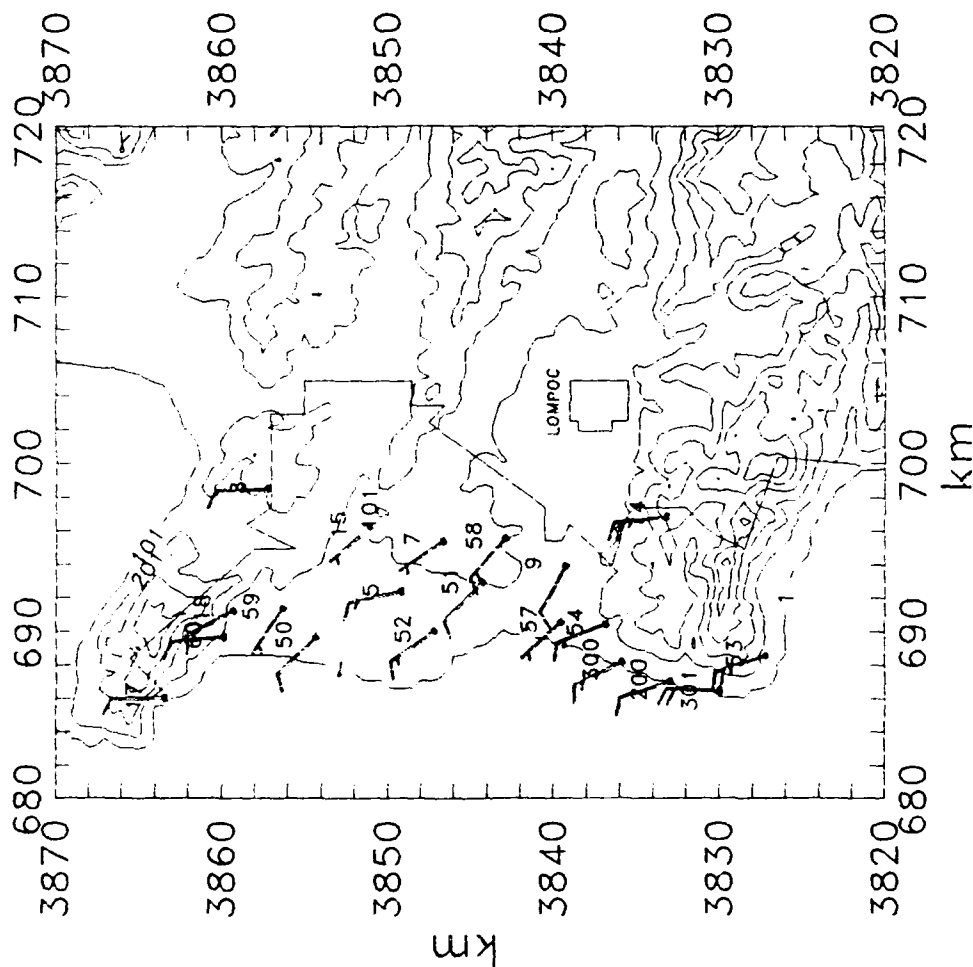
1 HOUR AVERAGES OF 12 FT. WINDS STANDARD NWS WIND BARBS

VANDENBERG AFB 5/18/88 04:00



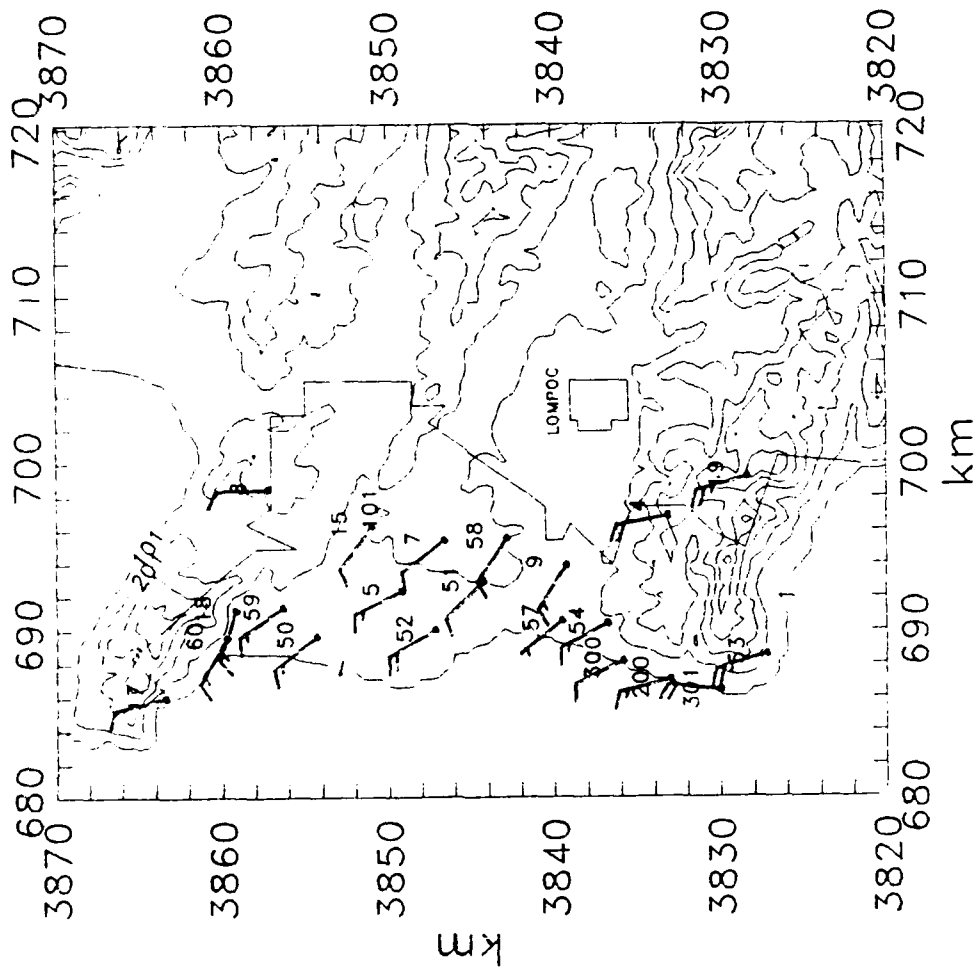
1 HOUR AVERAGES OF 12 FT. WINDS STANDARD NWS WIND BARBS

VANDENBERG AFB 5/18/88 07:00



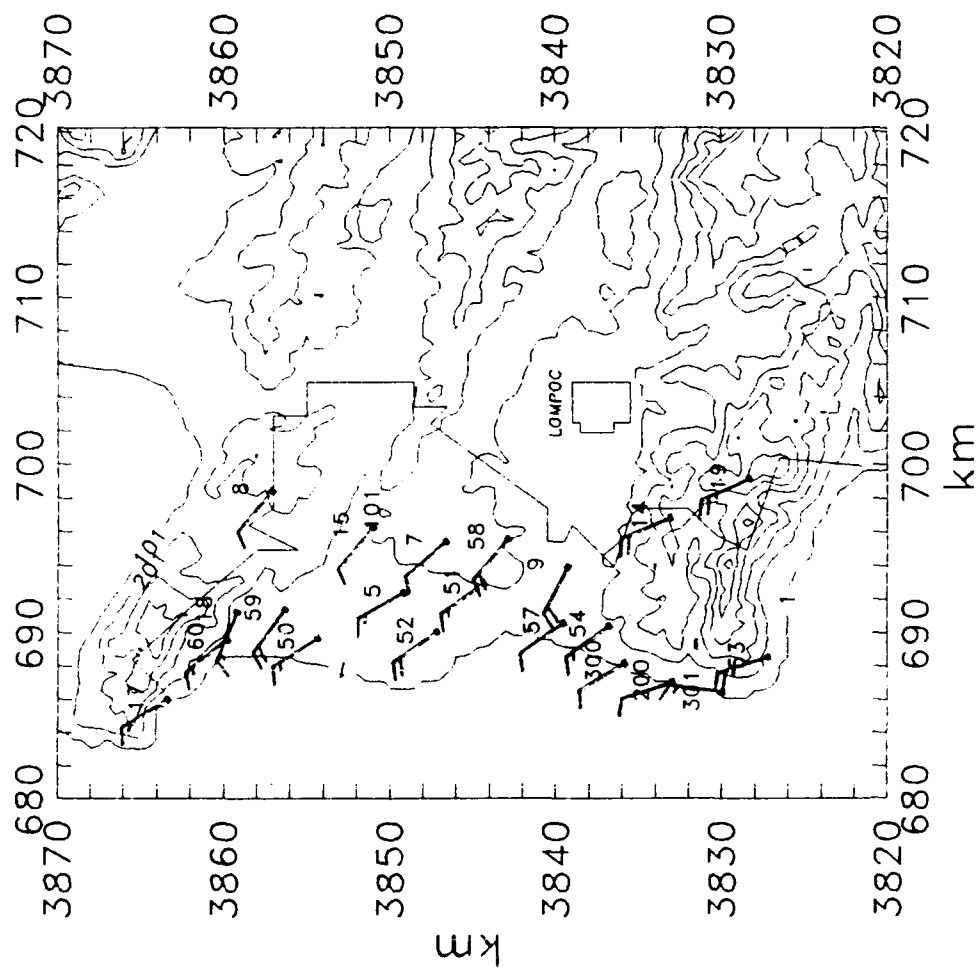
1 HOUR AVERAGES OF 12 FT. WINDS STANDARD NWS WIND BARBS

VANDENBERG AFB 5/18/88 10:00



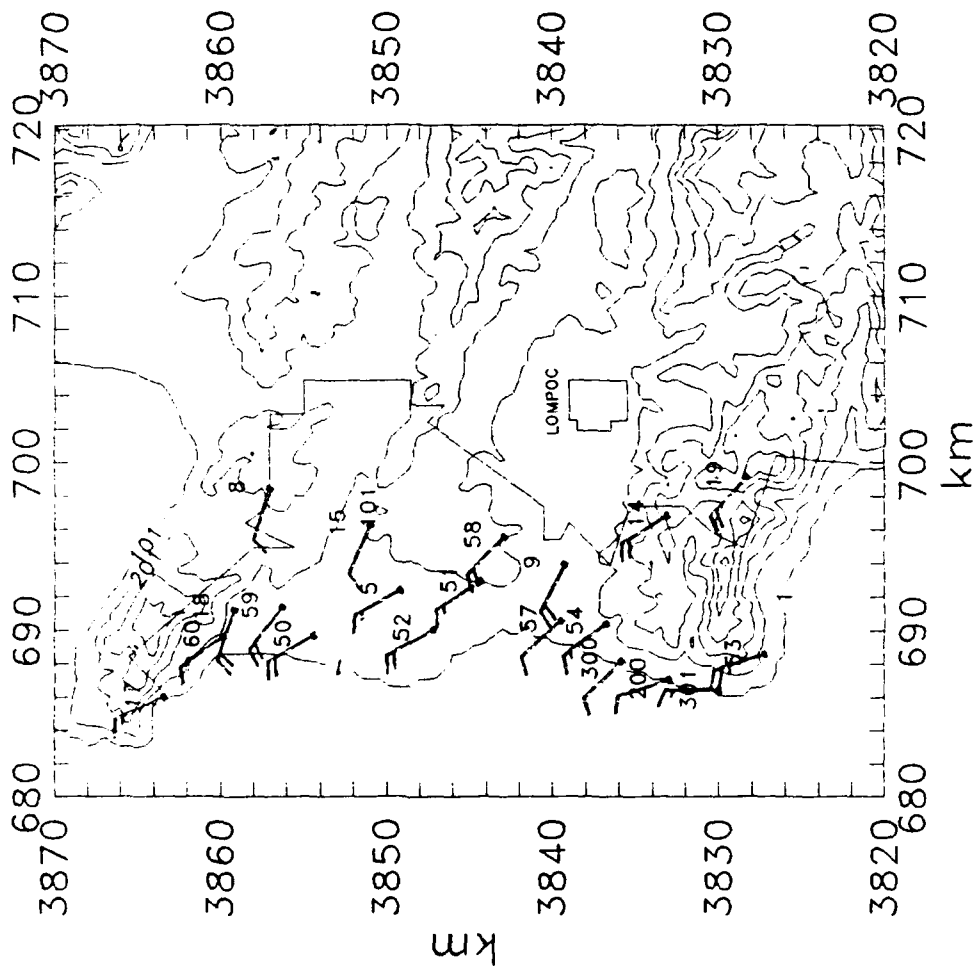
1 HOUR AVERAGES OF 12 FT. WINDS STANDARD NWS WIND BARBS

VANDENBERG AFB 5/18/88 13:00



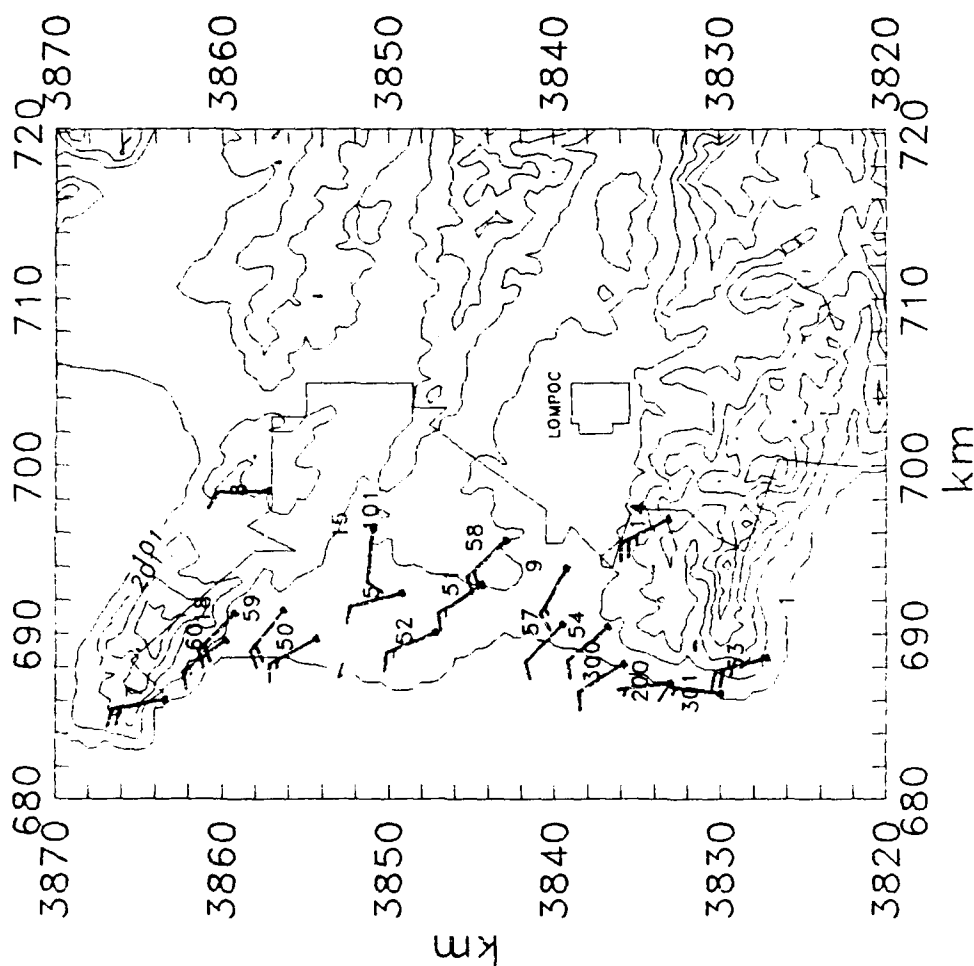
1 HOUR AVERAGES OF 12 FT. WINDS STANDARD NWS WIND BARBS

VANDENBERG AFB 5/18/88 16:00



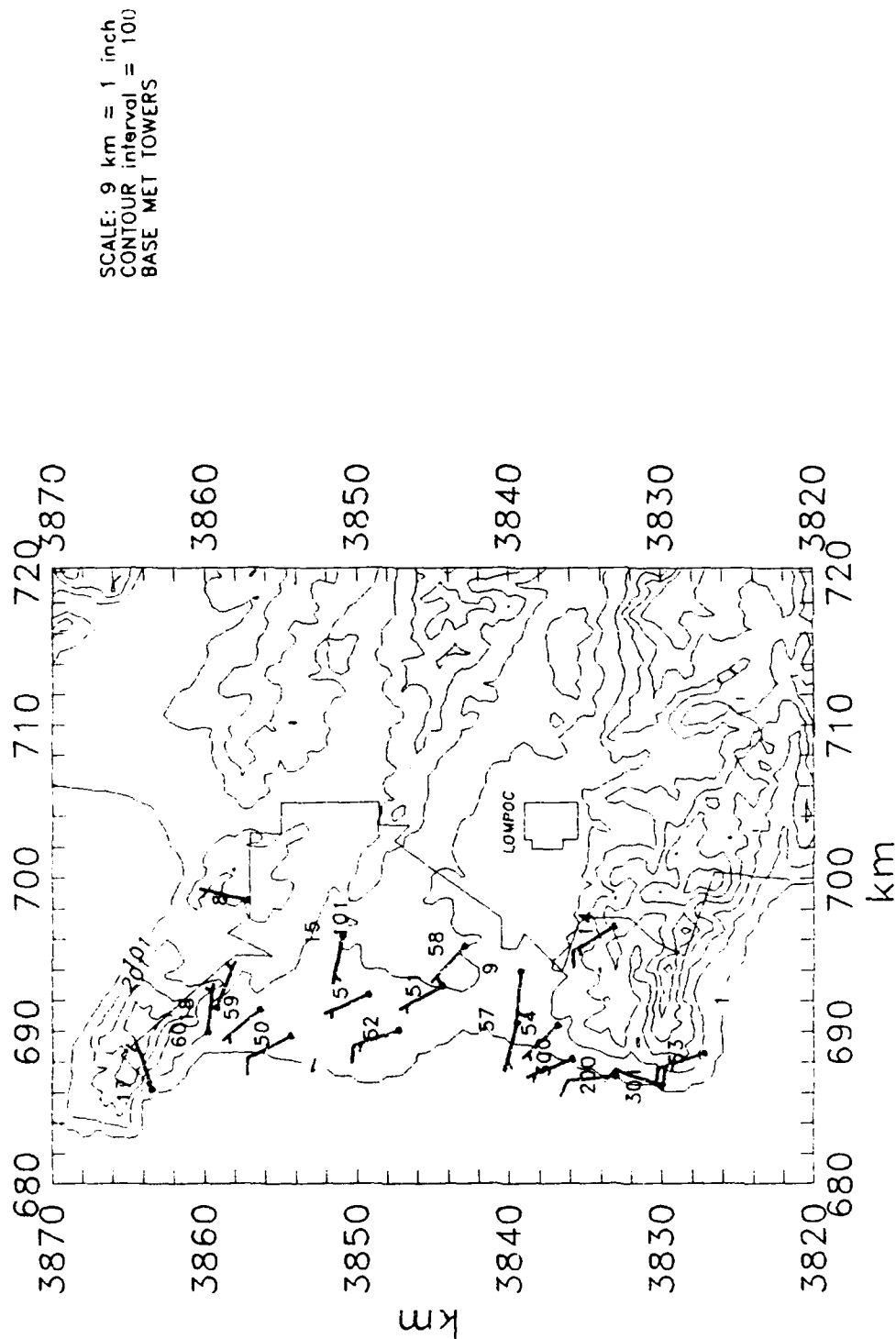
1 HOUR AVERAGES OF 12 FT. WINDS STANDARD NWS WIND BARBS

VANDENBERG AFB 5/18/88 19:00



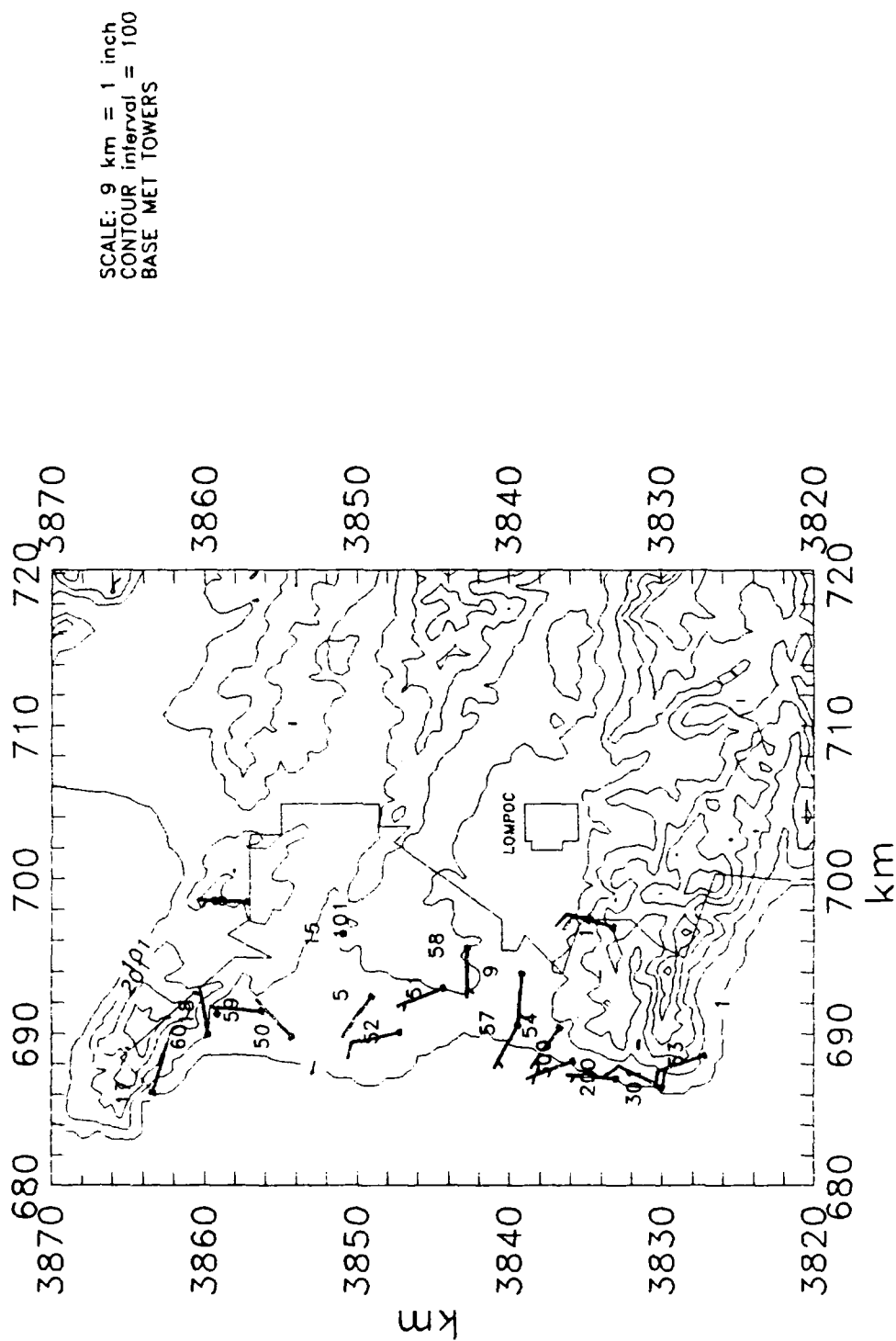
1 HOUR AVERAGES OF 12 FT. WINDS STANDARD NWS WIND BARBS

VANDENBERG AFB 5/18/88 22:00



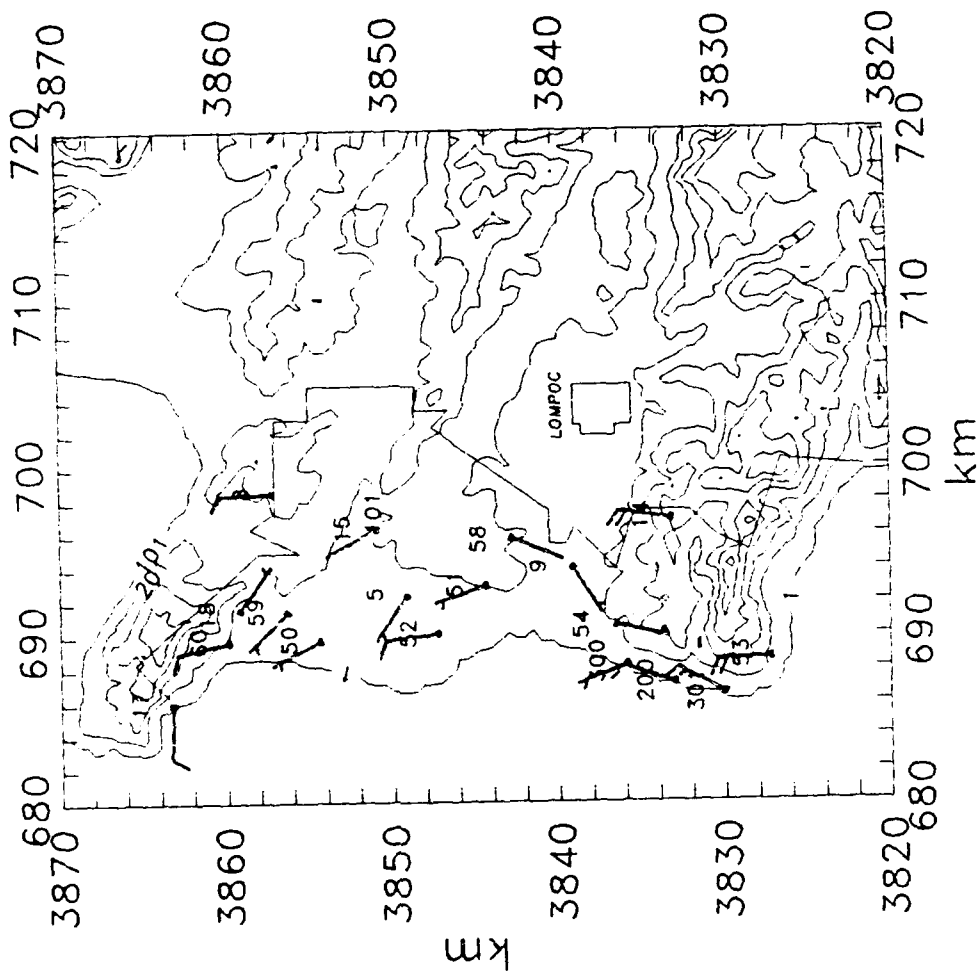
1 HOUR AVERAGES OF 12 FT. WINDS STANDARD NWS WIND BARBS

VANDENBERG AFB 5/19/88 01:00



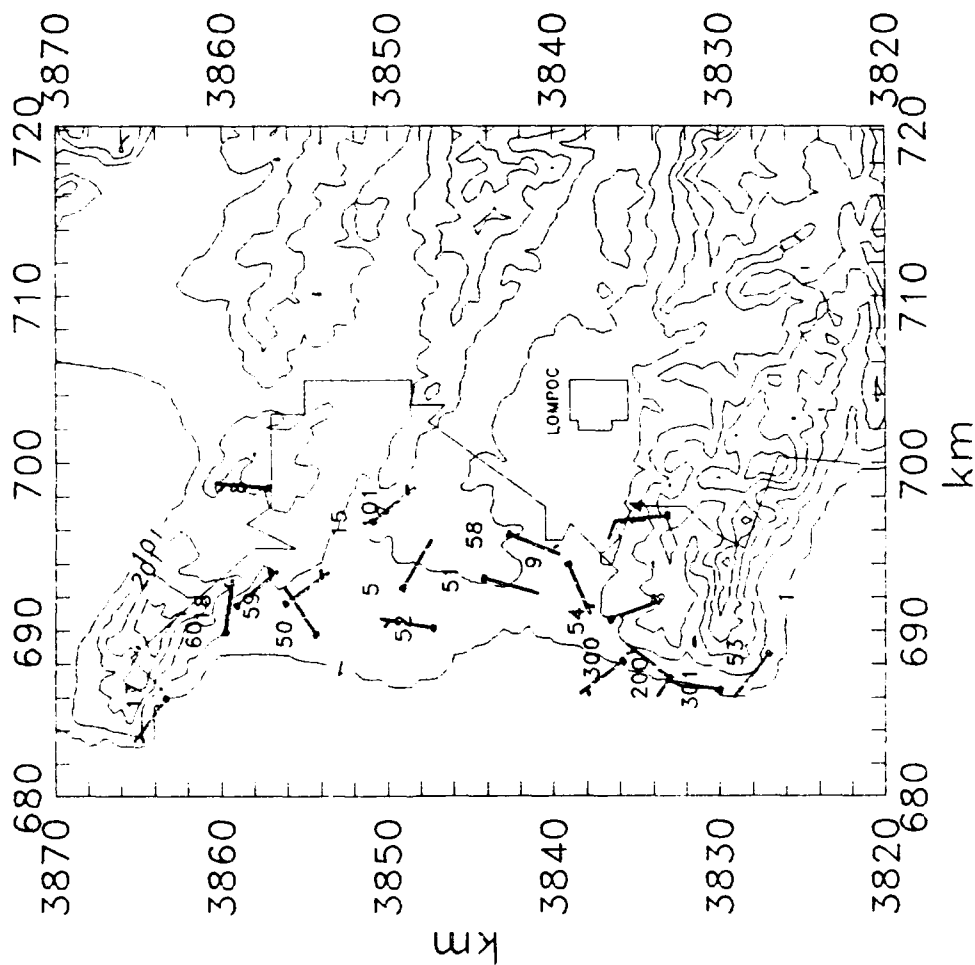
1 HOUR AVERAGES OF 12 FT. WINDS STANDARD NWS WIND BARBS

VANDENBERG AFB 5/19/88 04:00



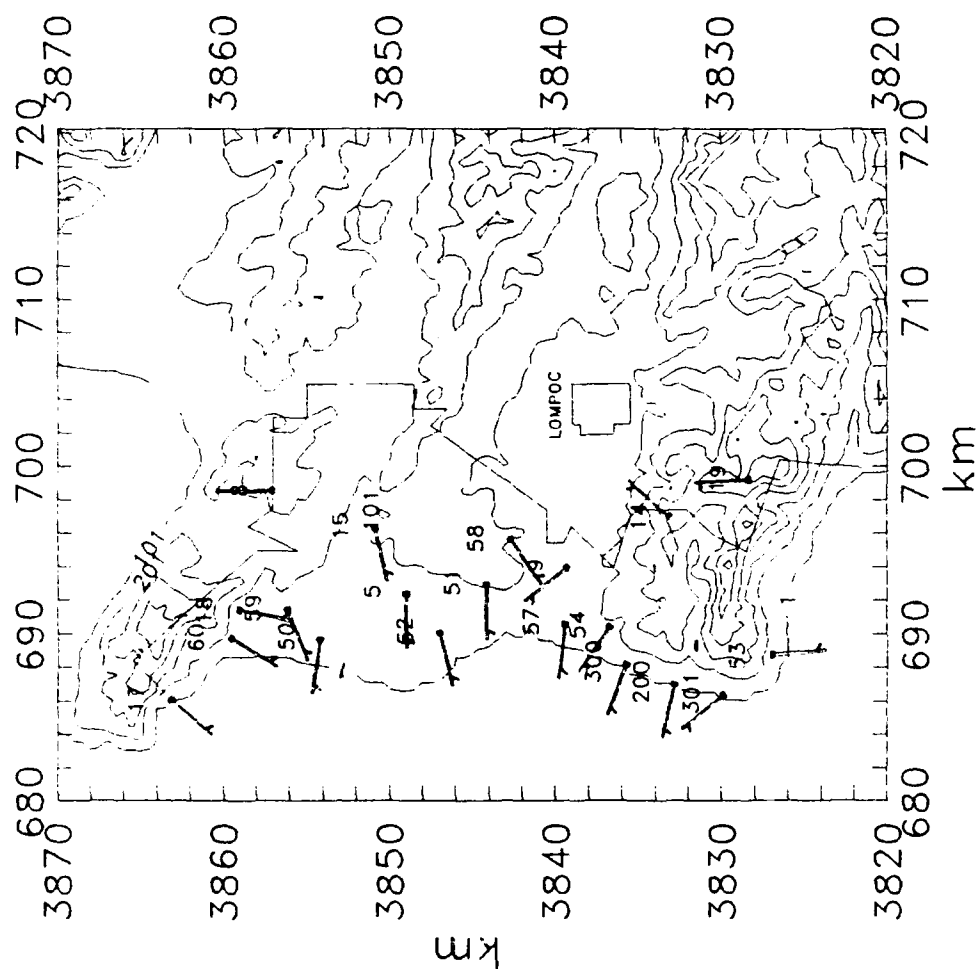
1 HOUR AVERAGES OF 12 FT. WINDS STANDARD NWS WIND BARBS

VANDENBERG AFB 5/19/88 07:00



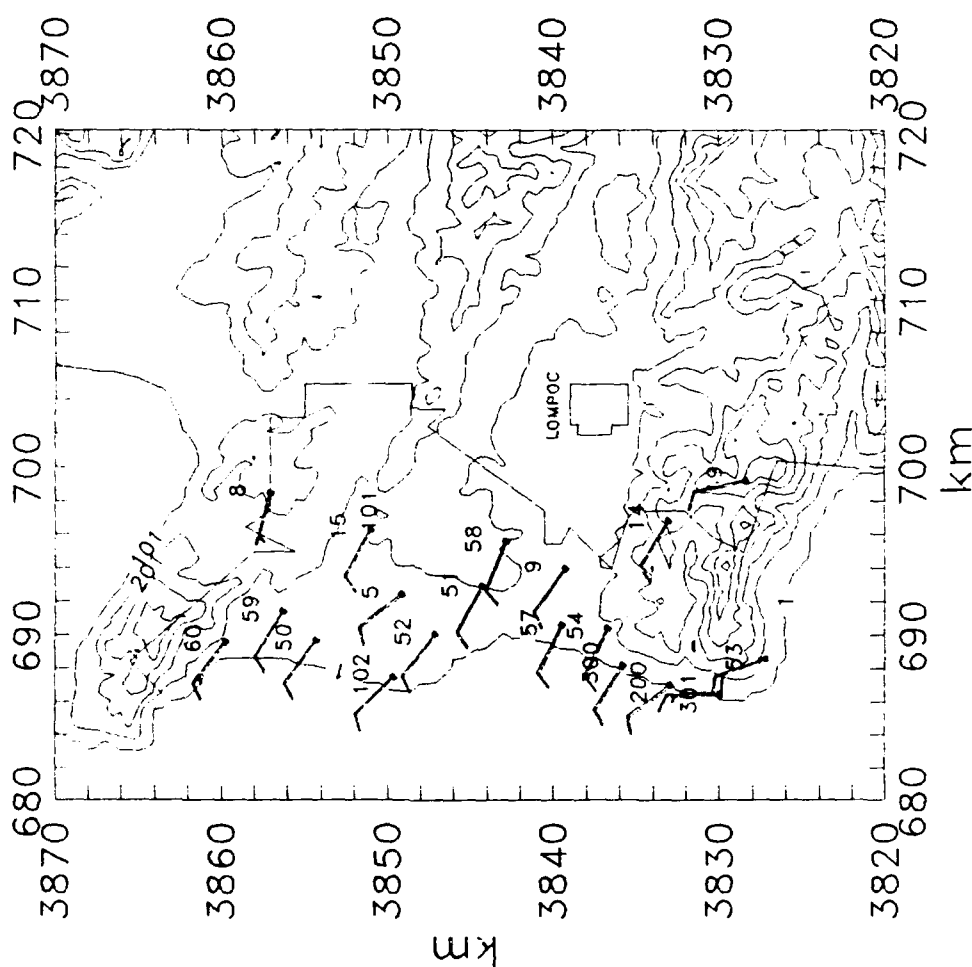
1 HOUR AVERAGES OF 12 FT. WINDS STANDARD NWS WIND BARBS

VANDENBERG AFB 5/19/88 10:00



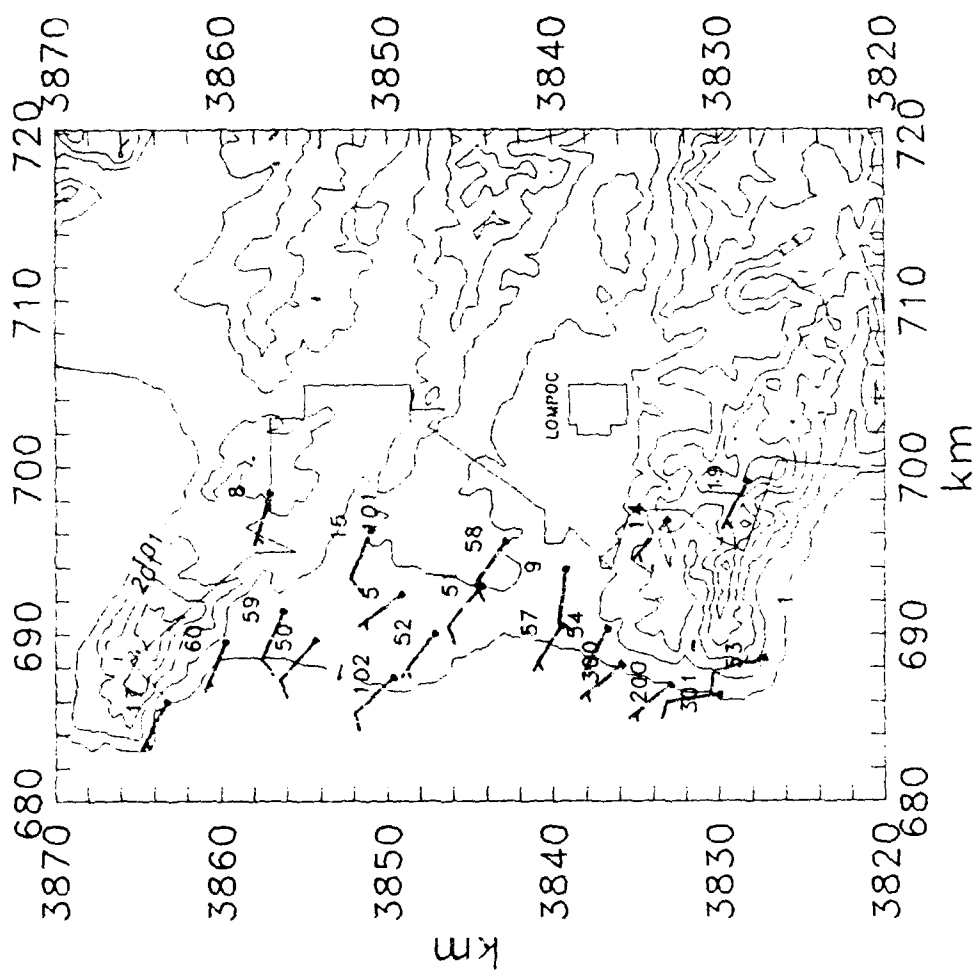
1 HOUR AVERAGES OF 12 FT. WINDS STANDARD NWS WIND BARBS

VANDENBERG AFB 5/19/88 13:00



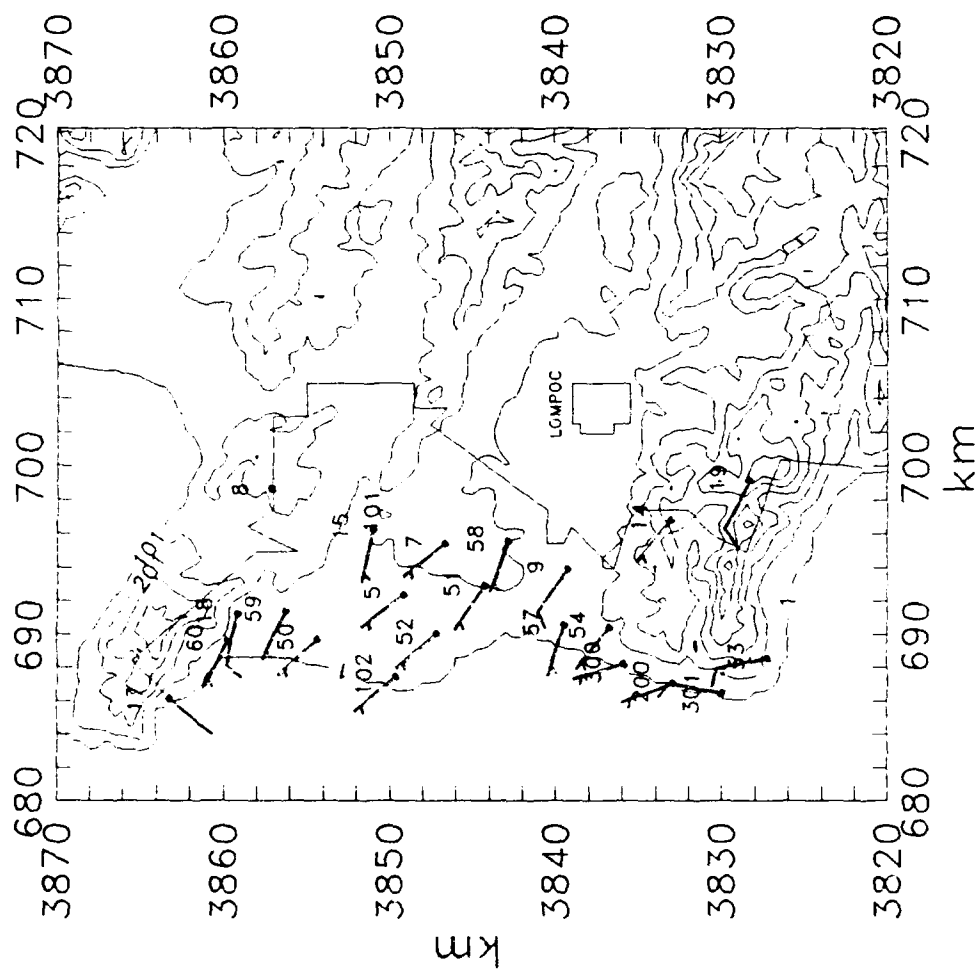
1 HOUR AVERAGES OF 12 FT. WINDS STANDARD NWS WIND BARBS

VANDENBERG AFB 5/19/88 16:00



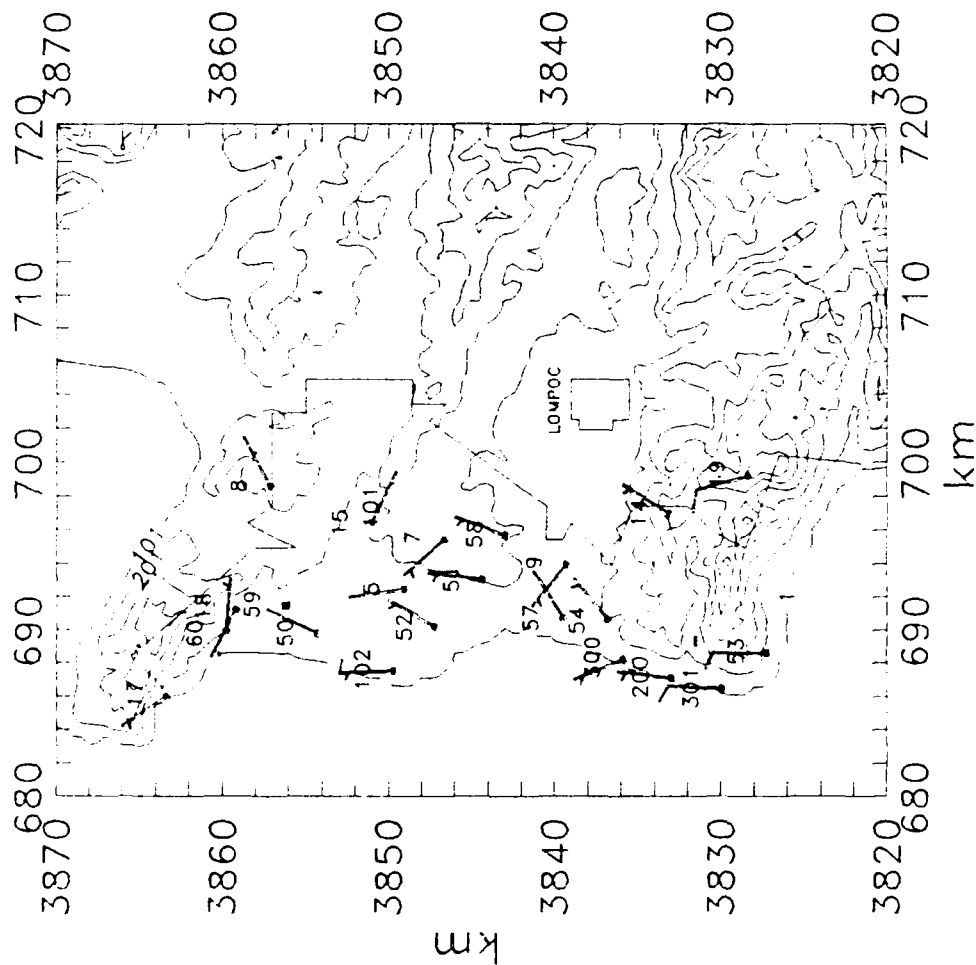
1 HOUR AVERAGES OF 12 FT. WINDS STANDARD NWS WIND BARBS

VANDENBERG AFB 5/19/88 19:00



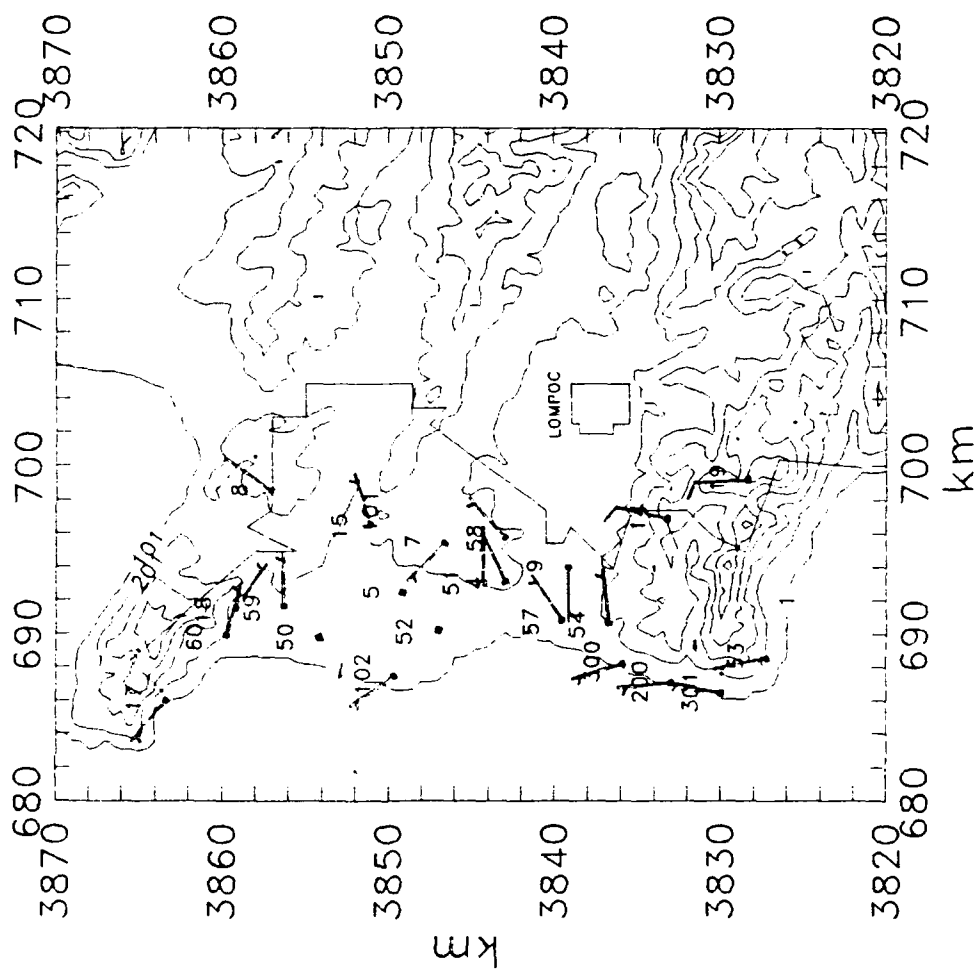
1 HOUR AVERAGES OF 12 FT. WINDS STANDARD NWS WIND BARBS

VANDENBERG AFB 5/19/88 22:00



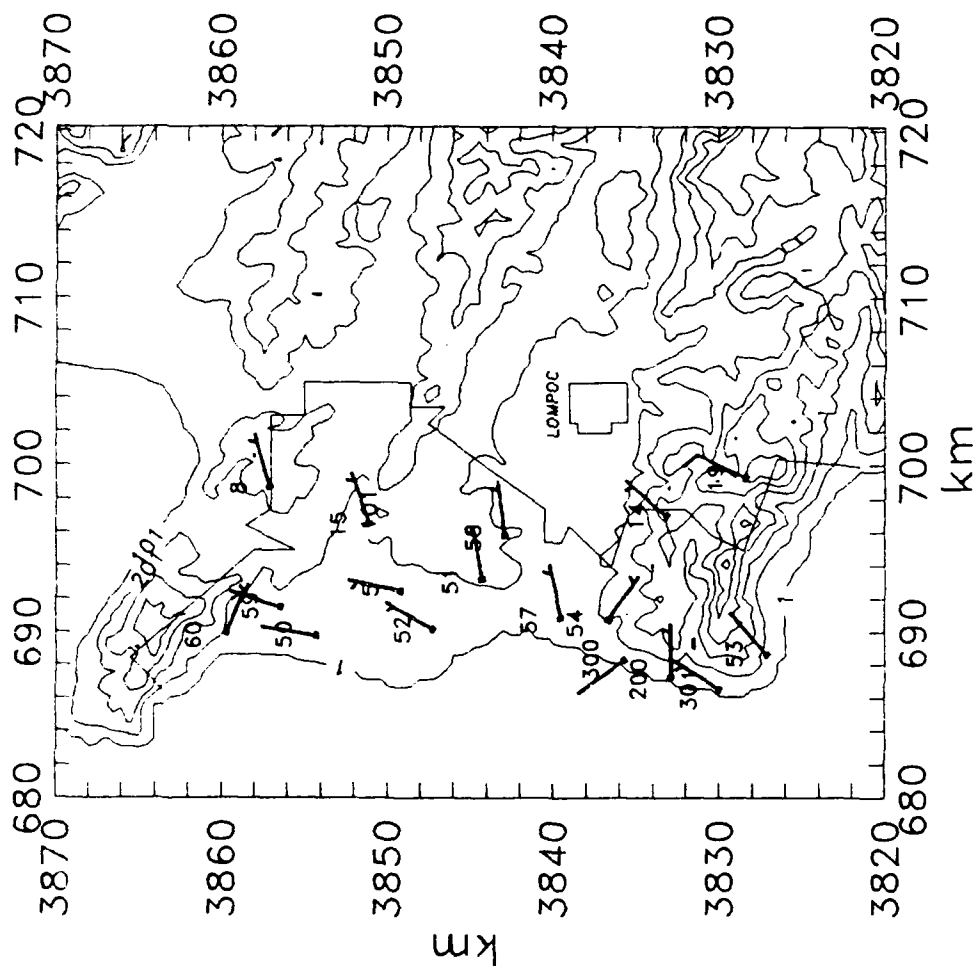
1 HOUR AVERAGES OF 12 FT. WINDS STANDARD NWS WIND BARBS

VANDENBERG AFB 5/20/88 01:00



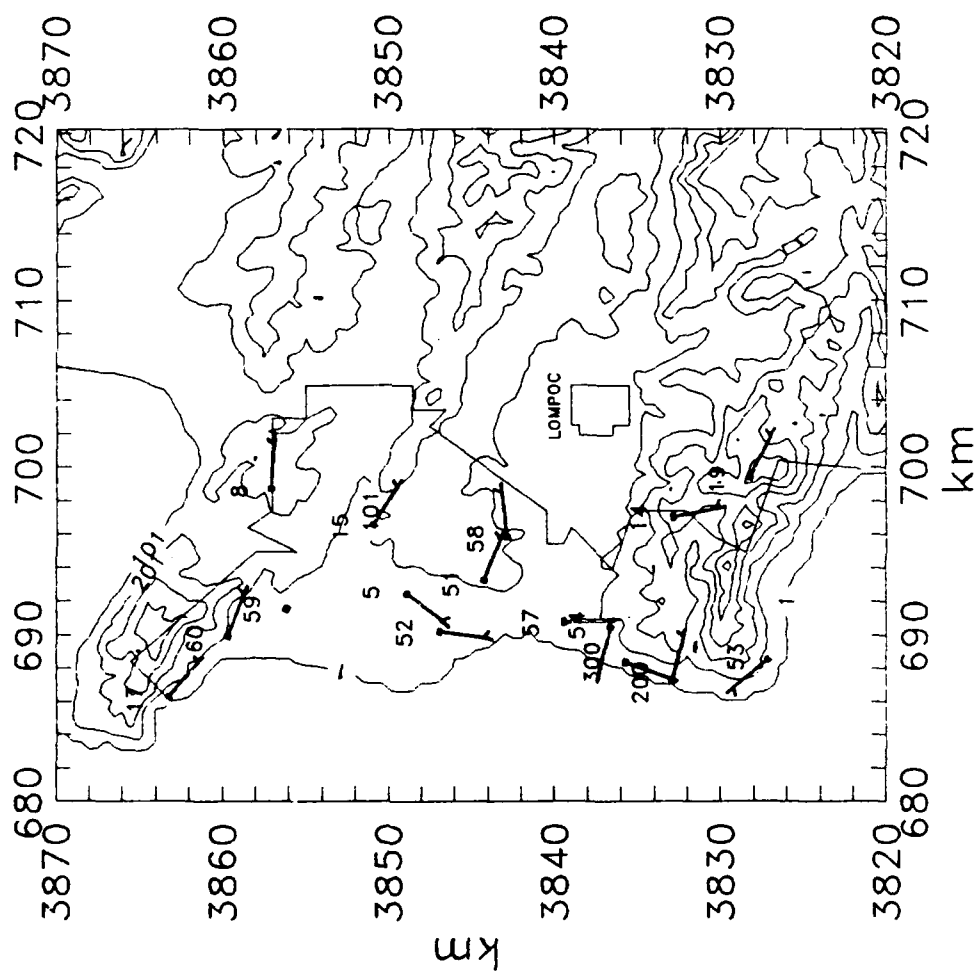
1 HOUR AVERAGES OF 12 FT. WINDS STANDARD NWS WIND BARBS

VANDENBERG AFB 5/20/88 04:00



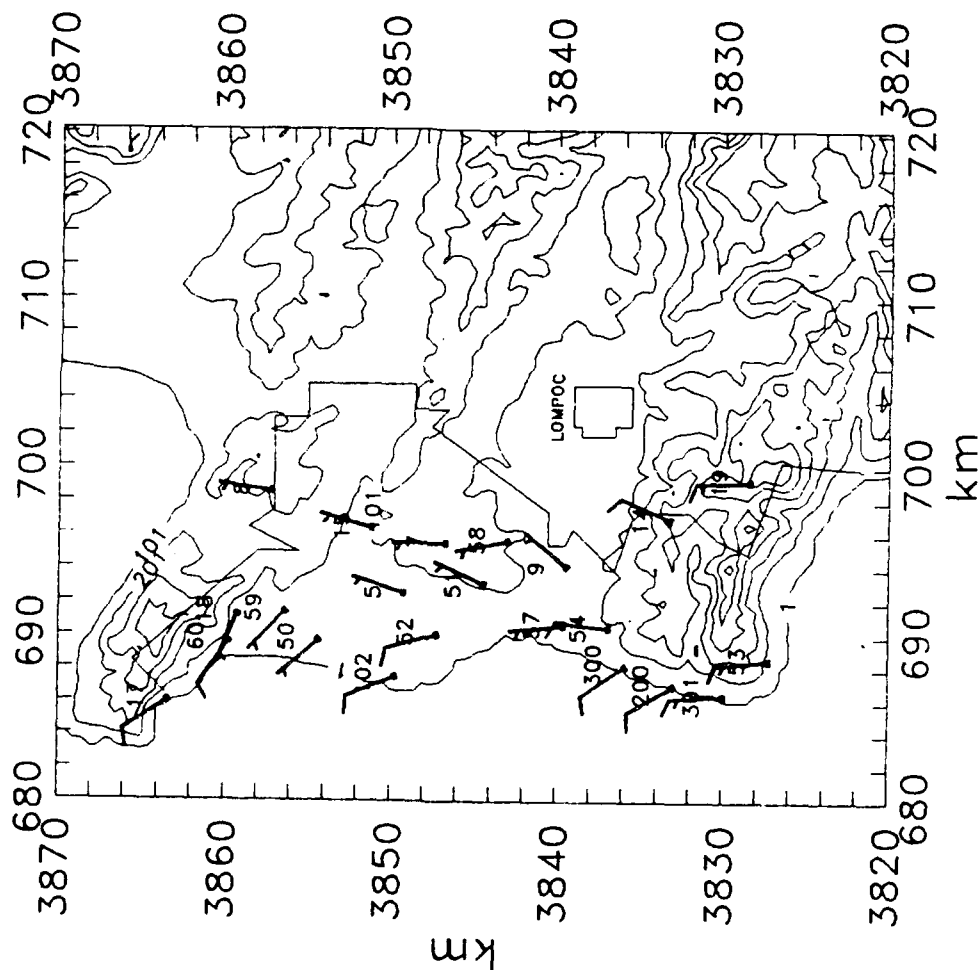
1 HOUR AVERAGES OF 12 FT. WINDS STANDARD NWS WIND BARBS

VANDENBERG AFB 5/20/88 07:00



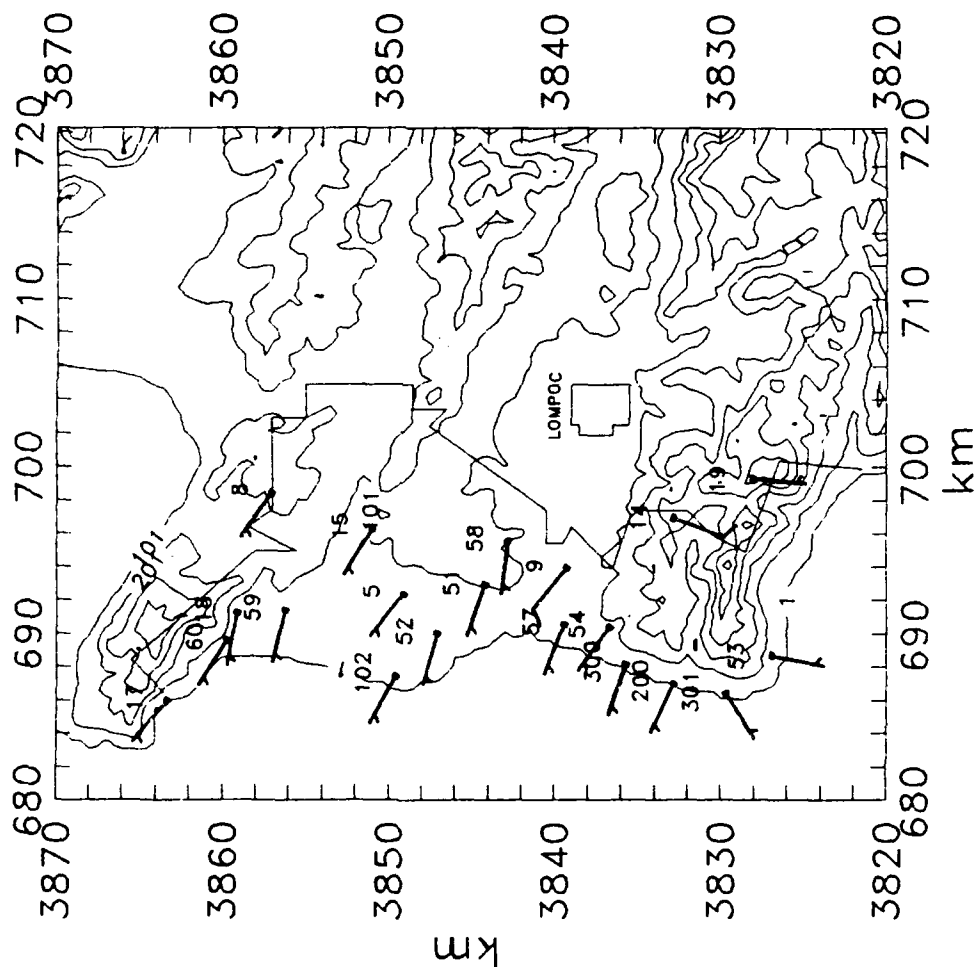
1 HOUR AVERAGES OF 12 FT. WINDS STANDARD NWS WIND BARBS

VANDENBERG AFB 5/20/88 10:00



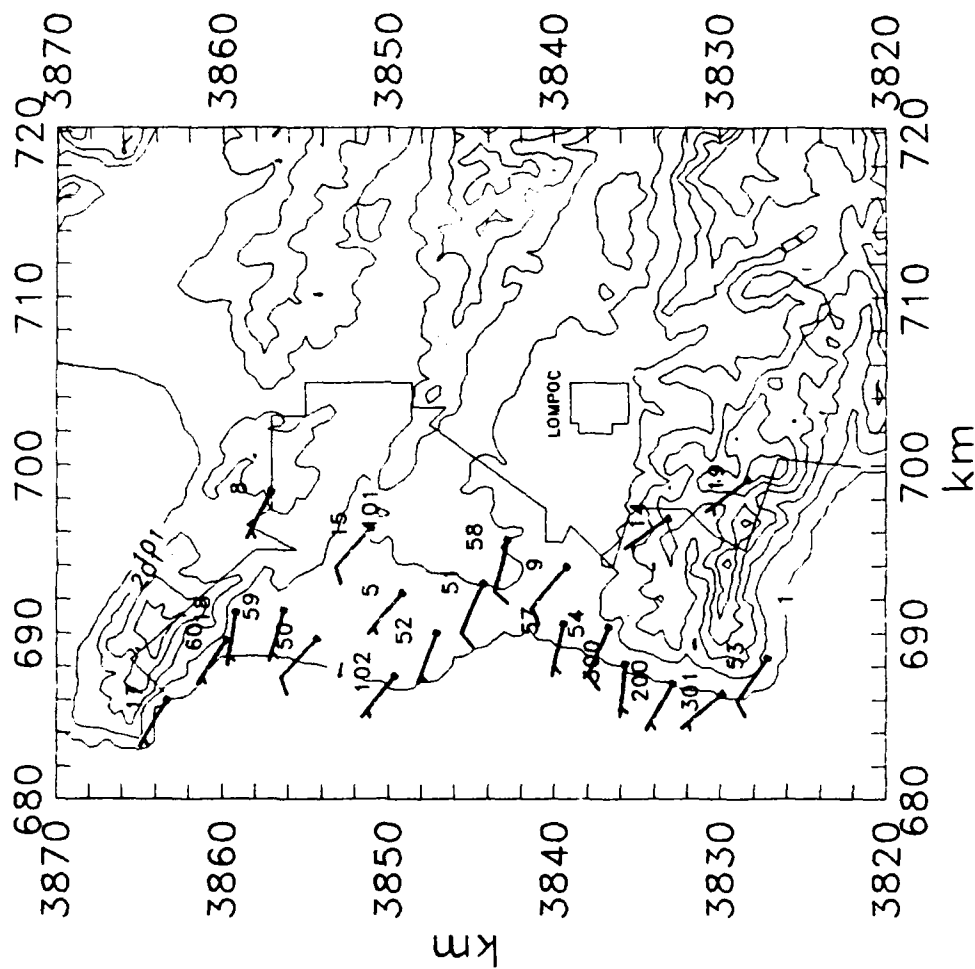
1 HOUR AVERAGES OF 12 FT. WINDS STANDARD NWS WIND BARBS

VANDENBERG AFB 5/20/88 13:00

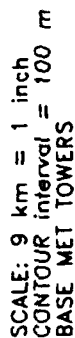


1 HOUR AVERAGES OF 12 FT. WINDS STANDARD NWS WIND BARBS

VANDENBERG AFB 5/20/88 16:00

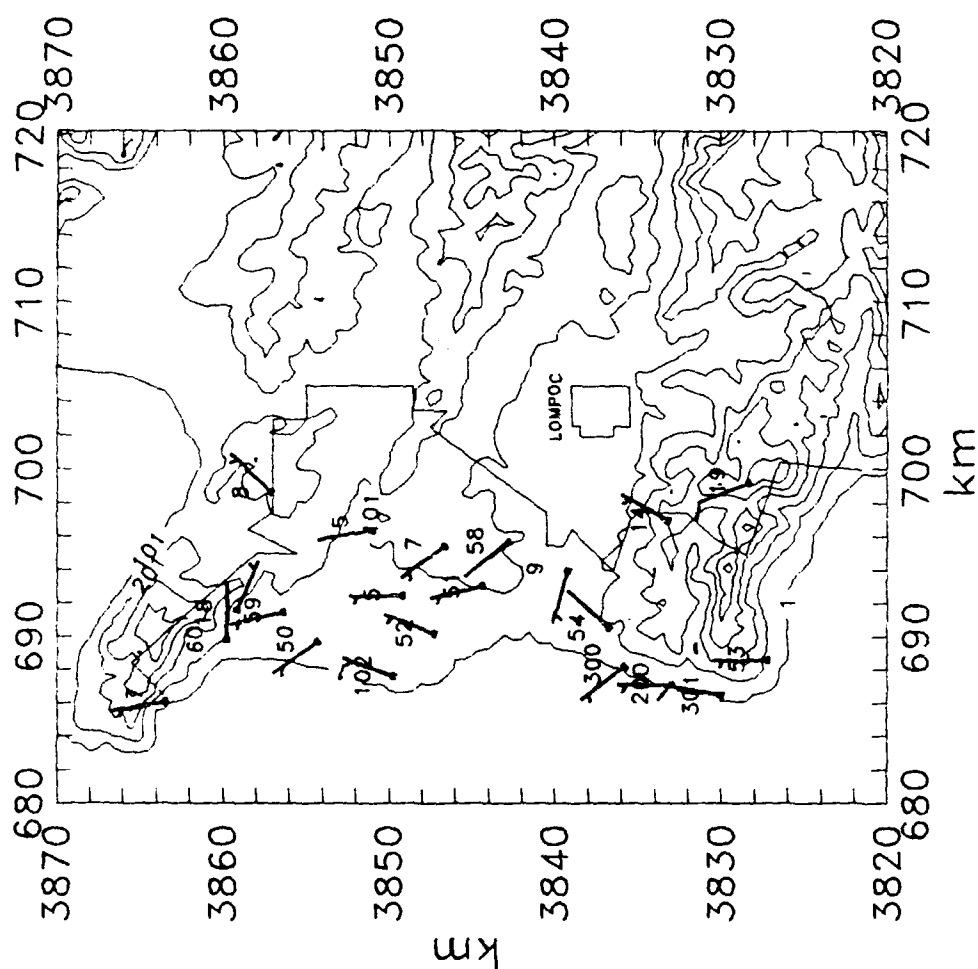


VANDENBERG AFB 5/20/88 19:00



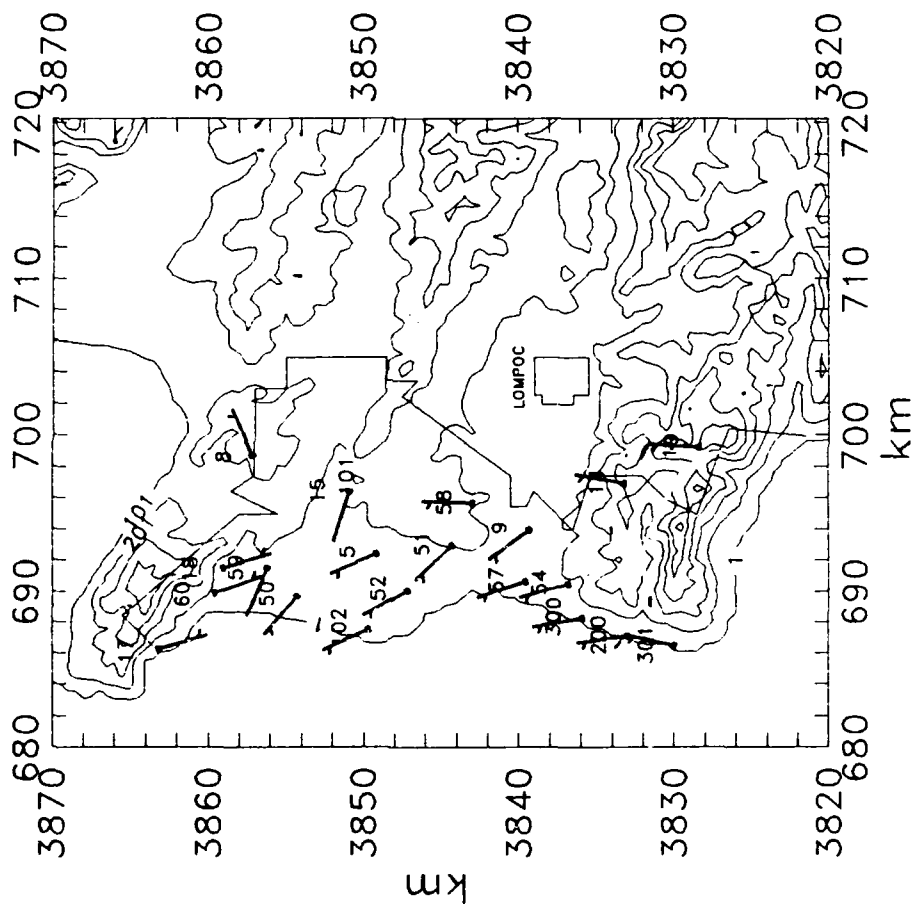
1 HOUR AVERAGES OF 12 FT. WINDS STANDARD NWS WIND BARBS

VANDENBERG AFB 5/20/88 22:00



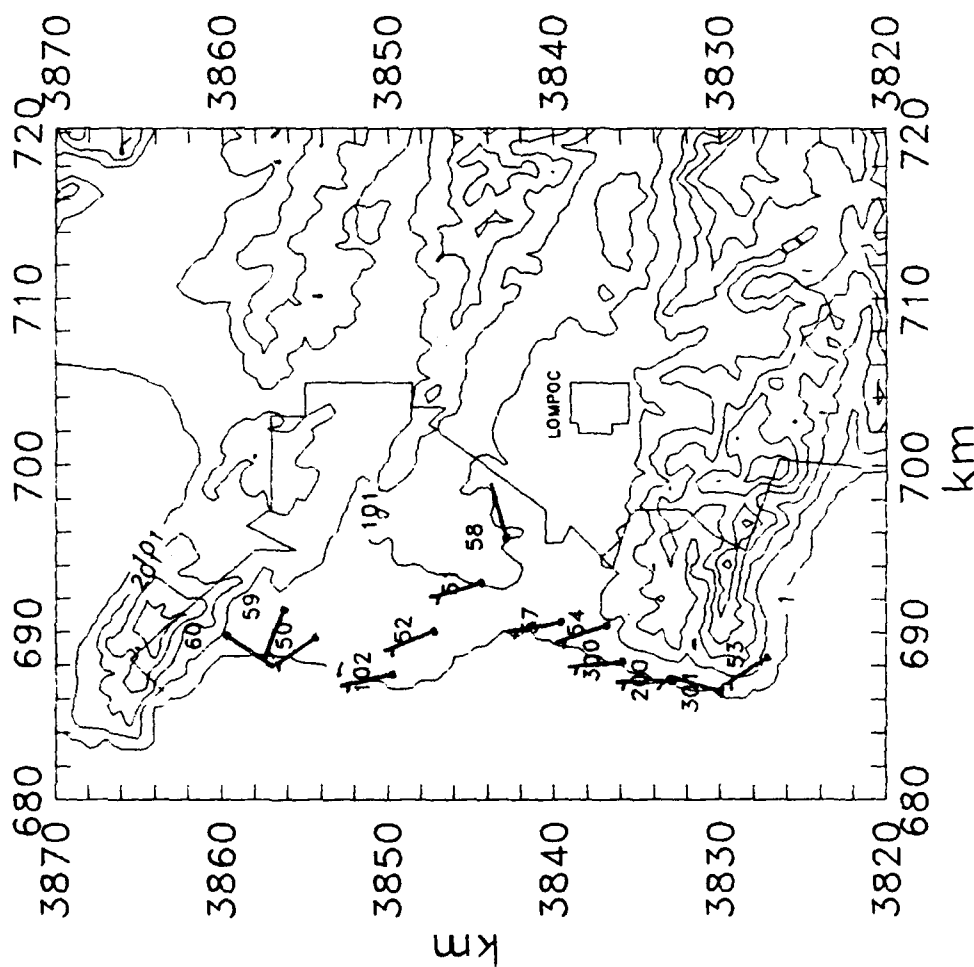
1 HOUR AVERAGES OF 12 FT. WINDS STANDARD NWS WIND BARBS

VANDENBERG AFB 7/26/88 01:00



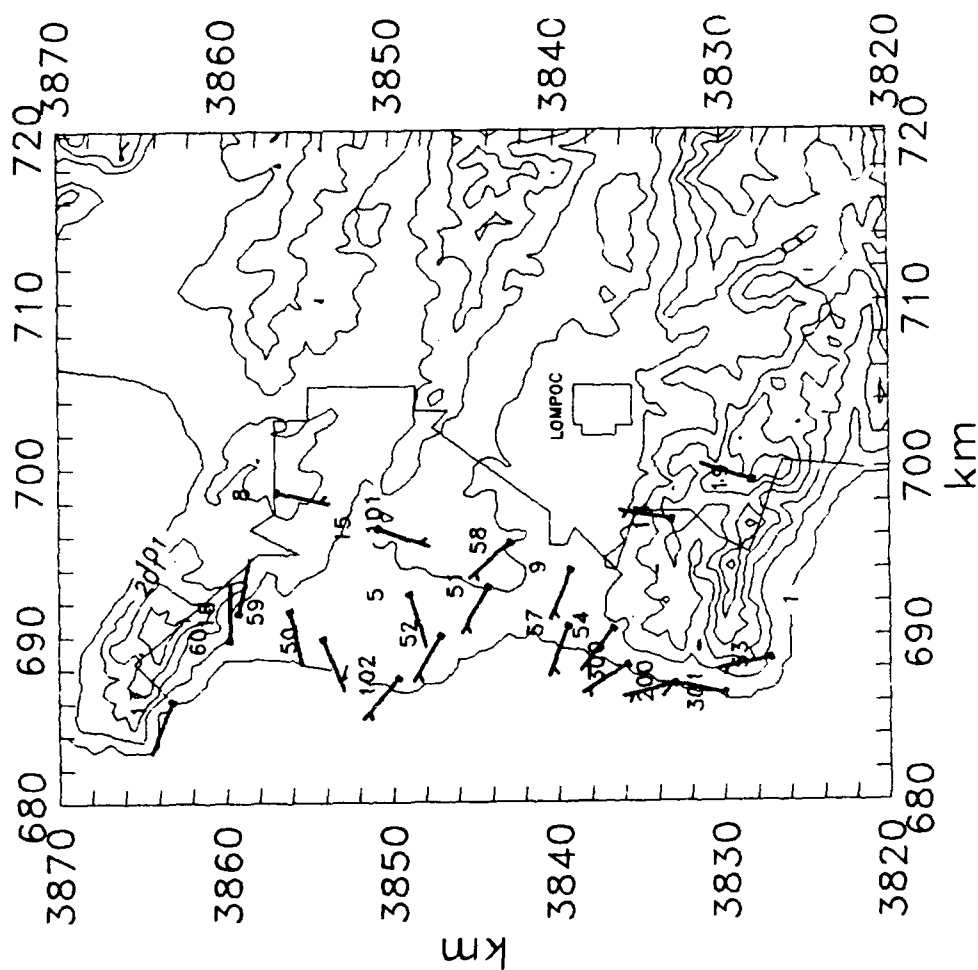
1 HOUR AVERAGES OF 12 FT. WINDS STANDARD NWS WIND BARBS

VANDENBERG AFB 7/26/88 04:00



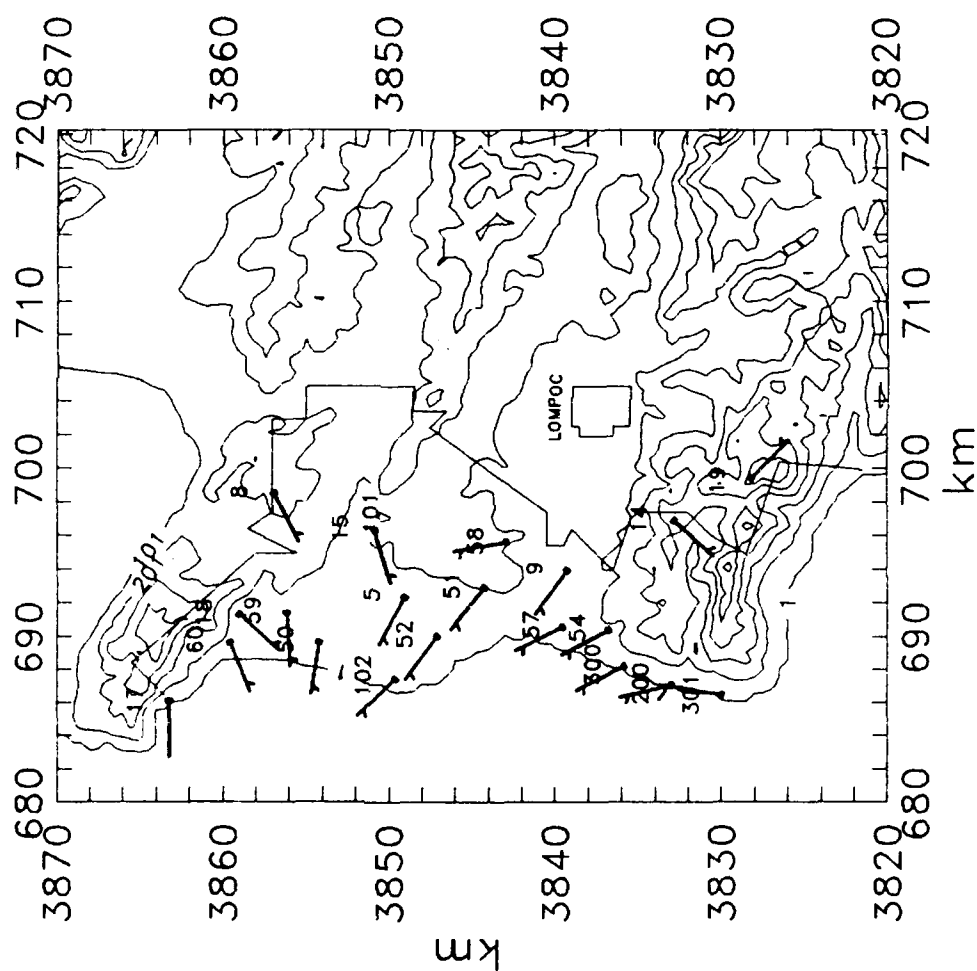
1 HOUR AVERAGES OF 12 FT. WINDS STANDARD NWS WIND BARBS

VANDENBERG AFB 7/26/88 07:00



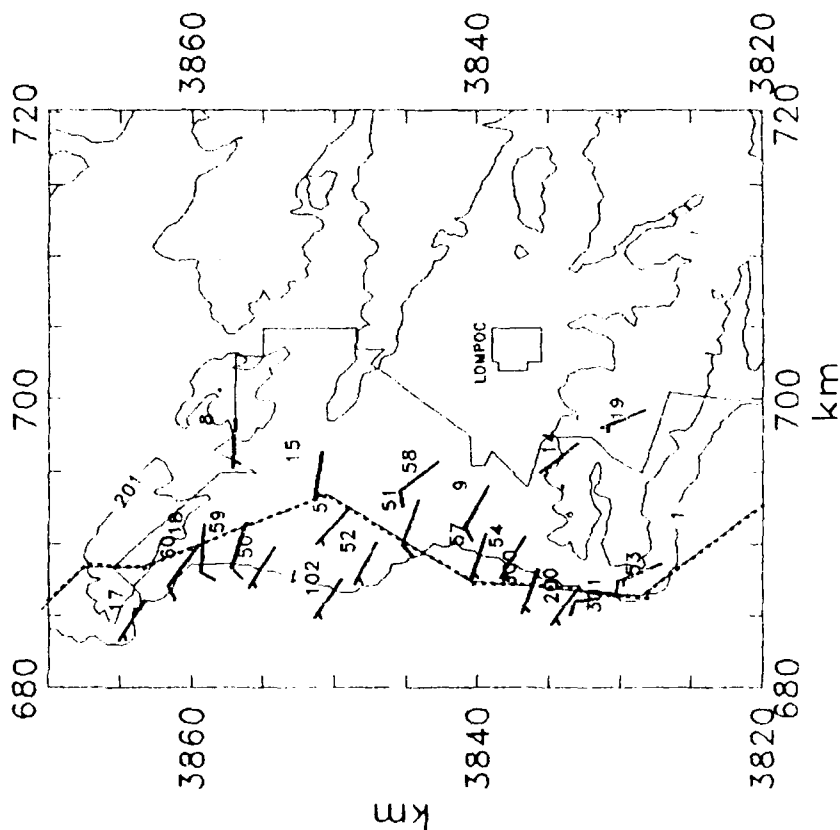
1 HOUR AVERAGES OF 12 FT. WINDS STANDARD NWS WIND BARBS

VANDENBERG AFB 7/26/88 10:00



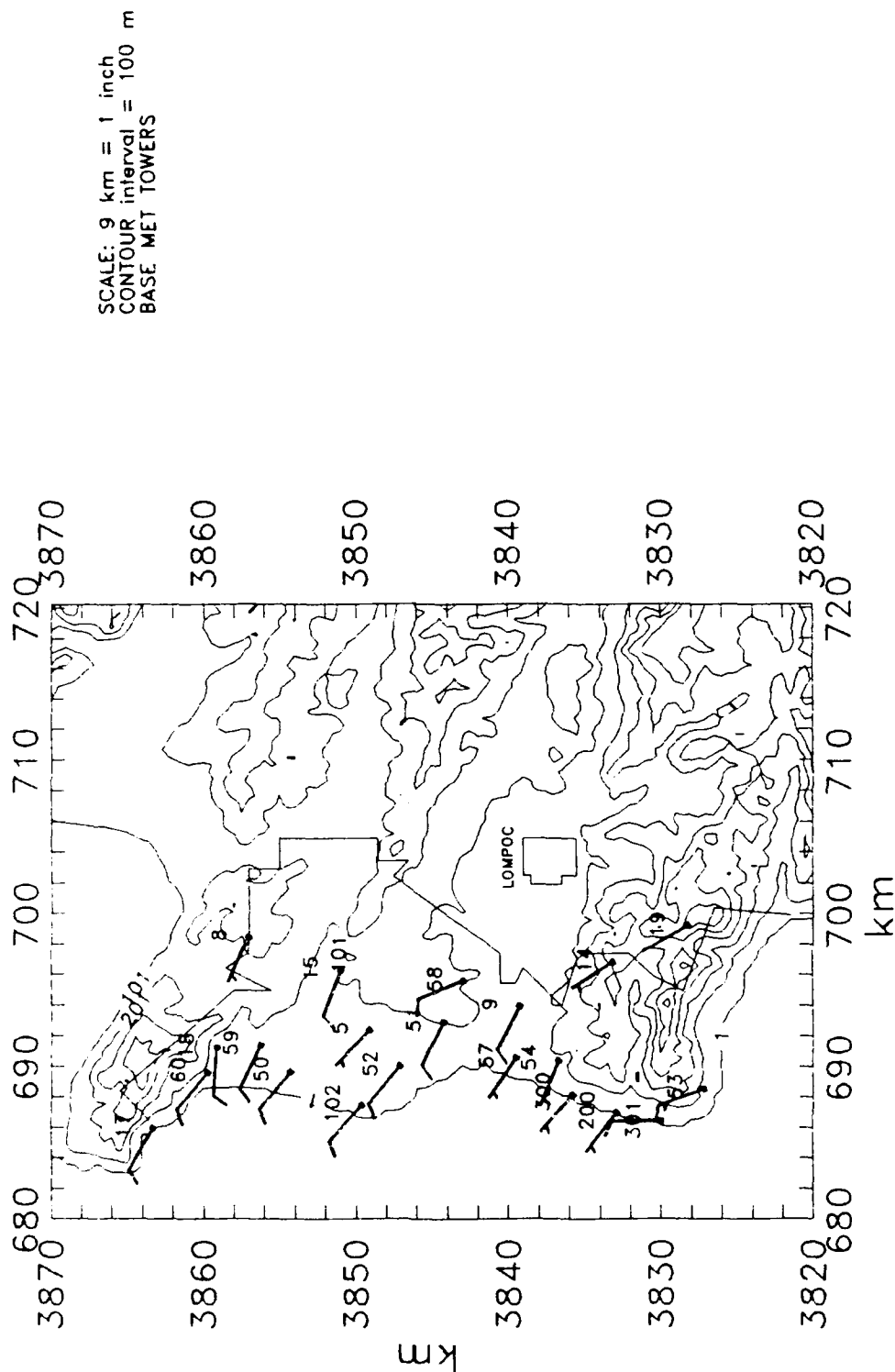
1 HOUR AVERAGES OF 12FT. WINDS WITH APPROXIMATED CLOUD EDGE STANDARD NWS WIND BARBS

VANDENBERG AFB 7/26/88 13:00



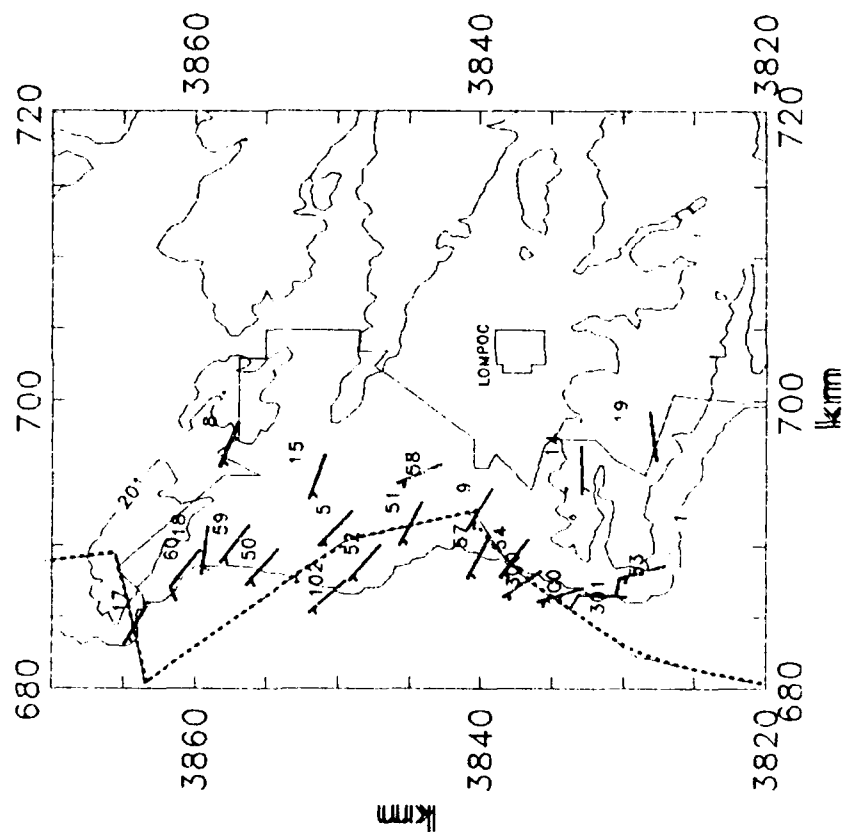
1 HOUR AVERAGES OF 12 FT. WINDS STANDARD NWS WIND BARBS

VANDENBERG AFB 7/26/88 16:00



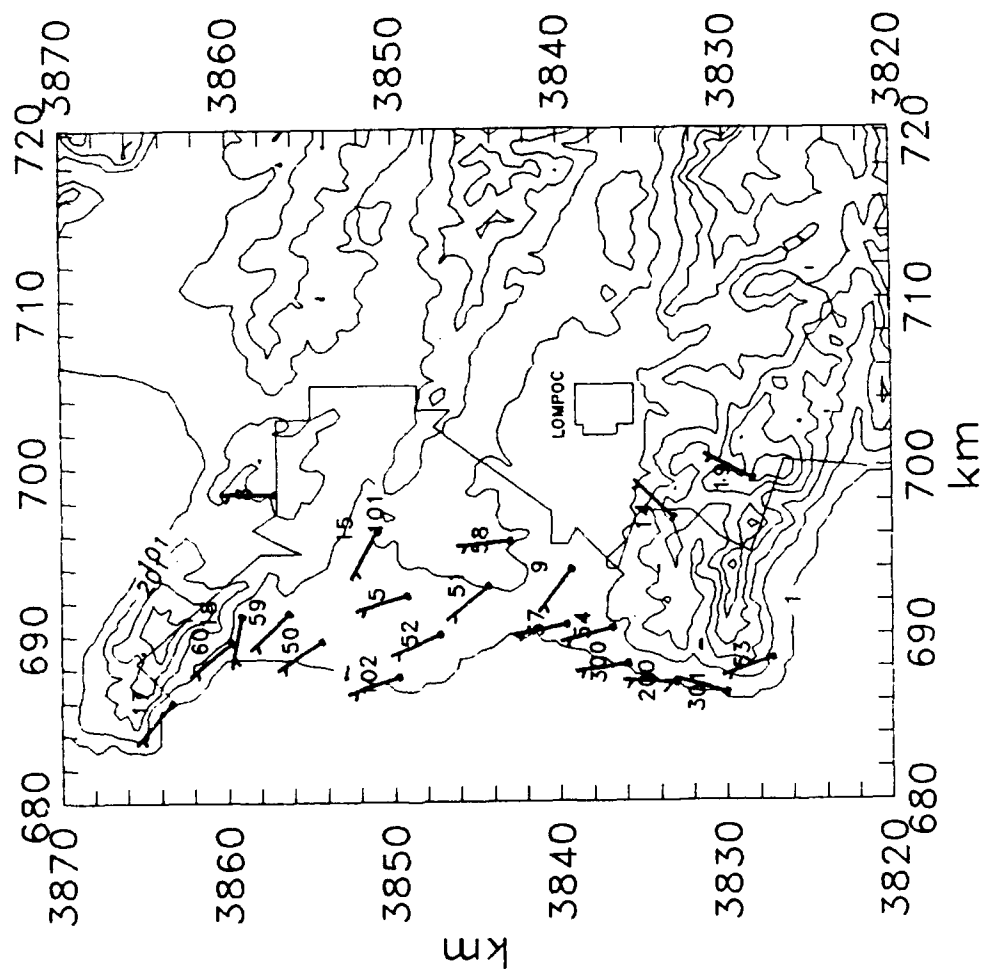
1 HOUR AVERAGES OF 12FT. WINDS WITH APPROXIMATED CLOUD EDGE STANDARD NWS WIND BARBS

VANDENBERG AFB 7/26/88 19:00



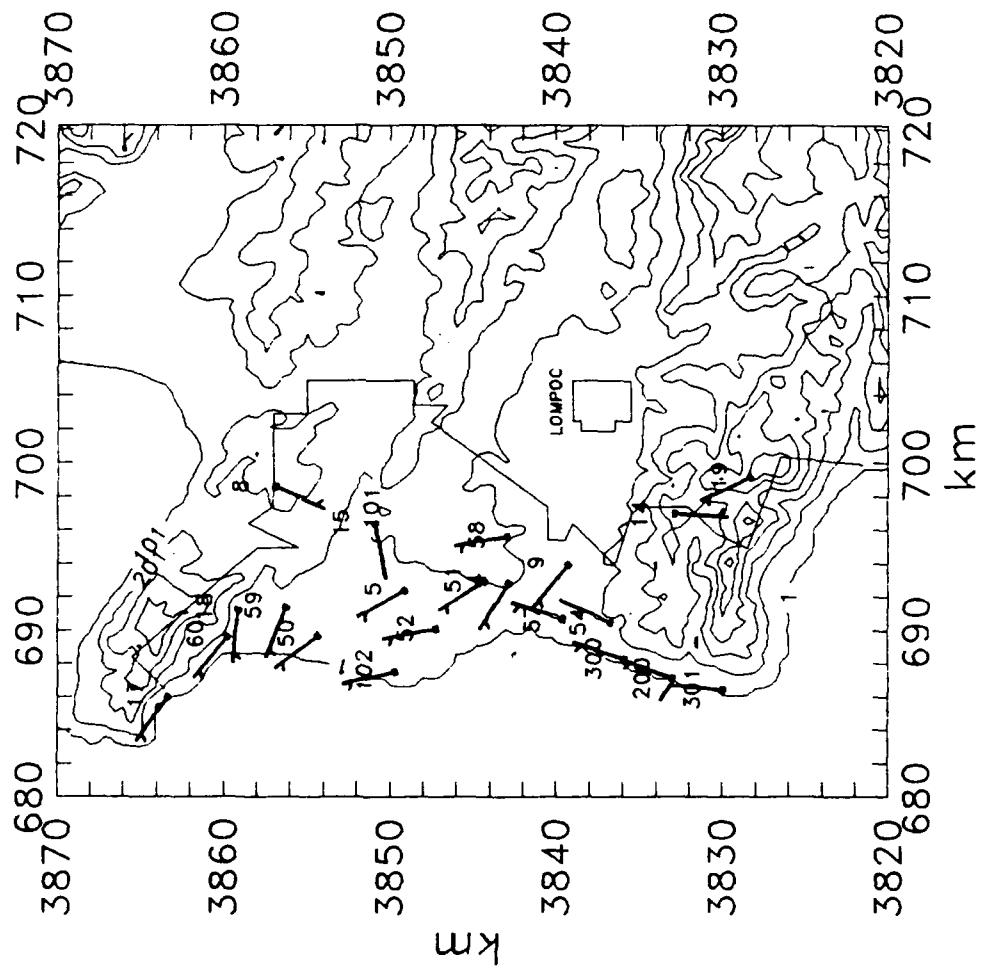
1 HOUR AVERAGES OF 12 FT. WINDS STANDARD NWS WIND BARBS

VANDENBERG AFB 7/26/88 22:00



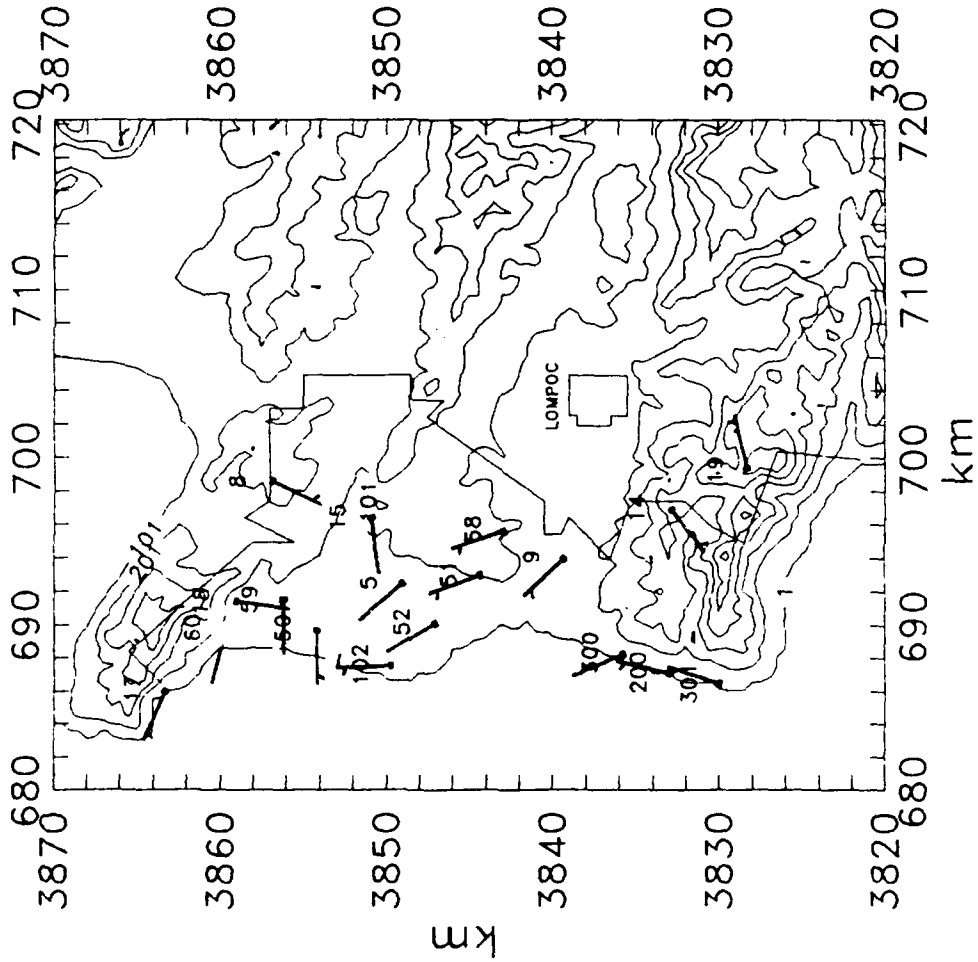
1 HOUR AVERAGES OF 12 FT. WINDS STANDARD NWS WIND BARBS

VANDENBERG AFB 7/27/88 01:00



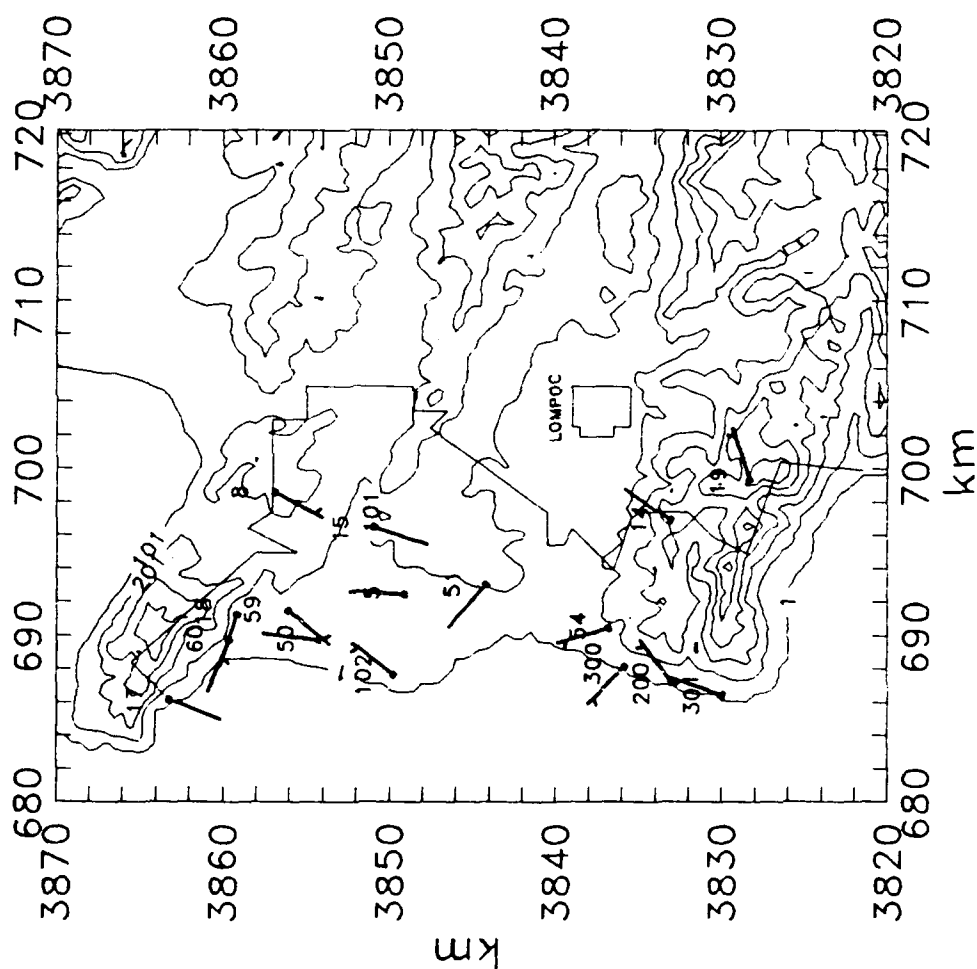
1 HOUR AVERAGES OF 12 FT. WINDS STANDARD NWS WIND BARBS

VANDENBERG AFB 7/27/88 04:00



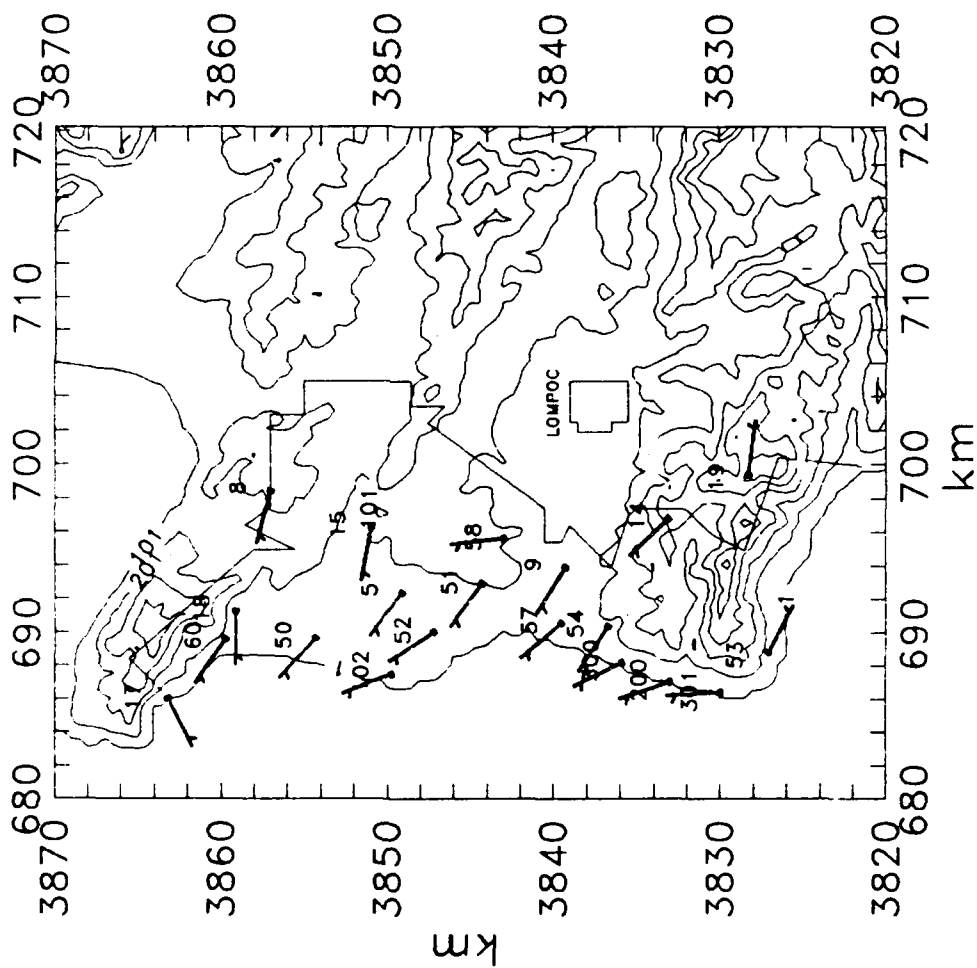
1 HOUR AVERAGES OF 12 FT. WINDS STANDARD NWS WIND BARBS

VANDENBERG AFB 7/27/88 07:00



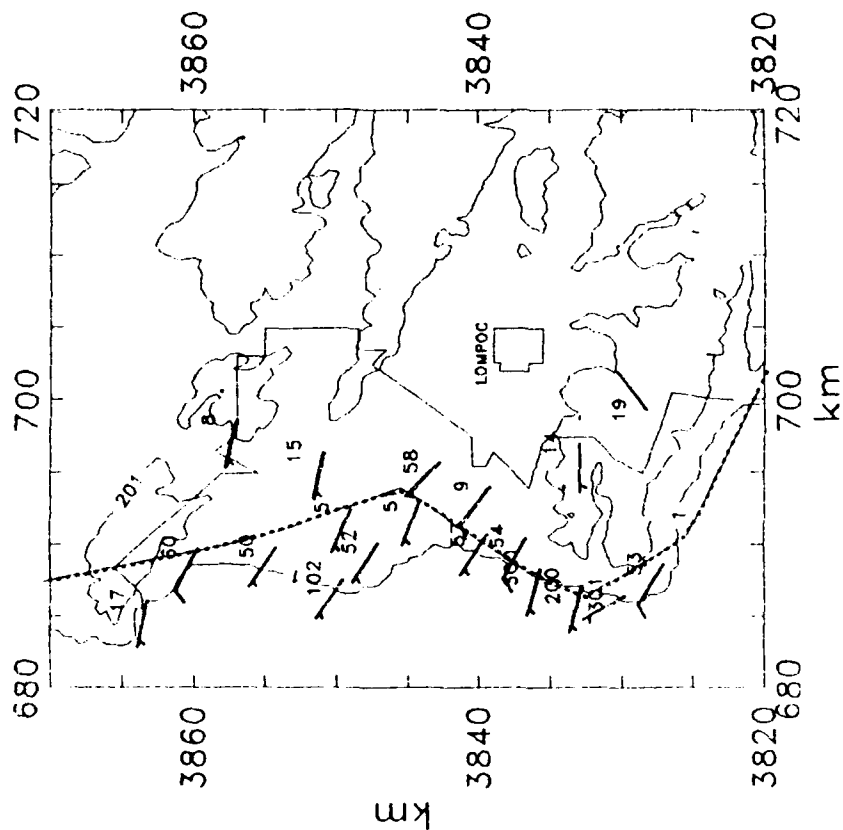
1 HOUR AVERAGES OF 12 FT. WINDS STANDARD NWS WIND BARBS

VANDENBERG AFB 7/27/88 10:00



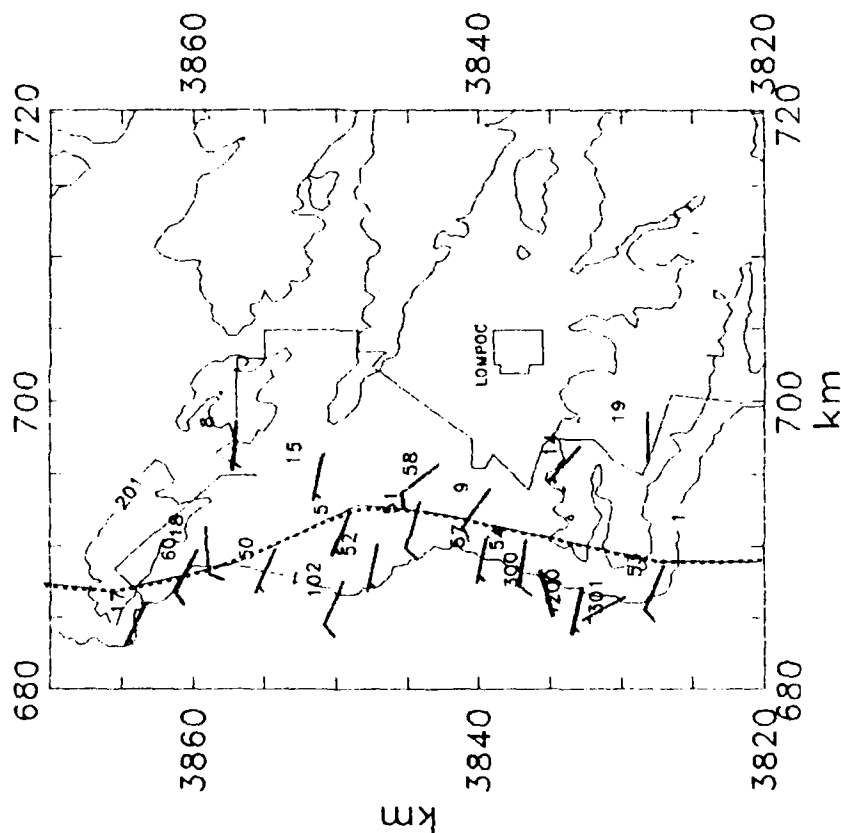
1 HOUR AVERAGES OF 12FT. WINDS WITH APPROXIMATED CLOUD EDGE STANDARD NWS WIND BARBS

VANDENBERG AFB 7/27/88 13:00



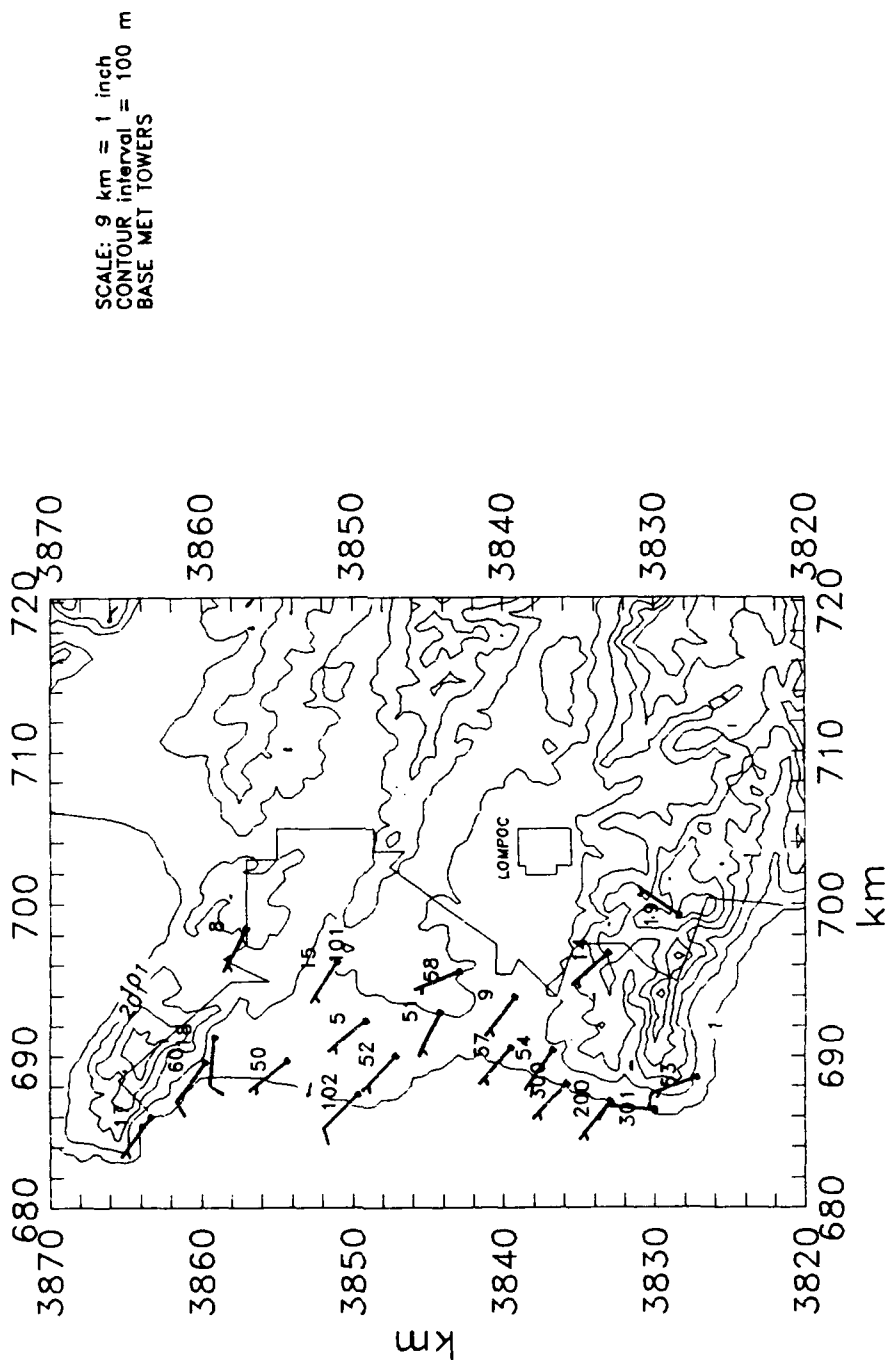
1 HOUR AVERAGES OF 12FT. WINDS WITH APPROXIMATED CLOUD EDGE STANDARD NWS WIND BARBS

VANDENBERG AFB 7/27/88 16:00



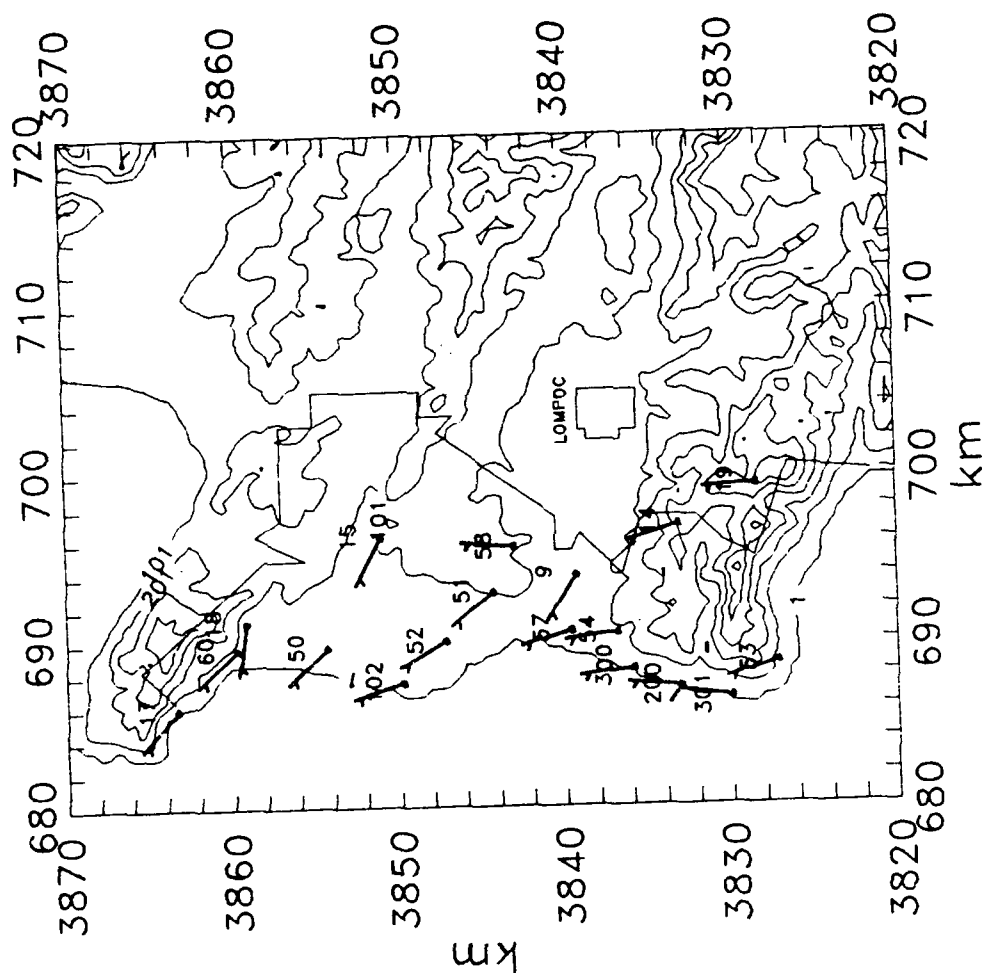
1 HOUR AVERAGES OF 12 FT. WINDS STANDARD NWS WIND BARBS

VANDENBERG AFB 7/27/88 19:00

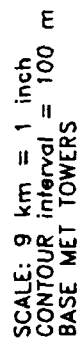


1 HOUR AVERAGES OF 12 FT. WINDS STANDARD NWS WIND BARBS

VANDENBERG AFB 7/27/88 22:00

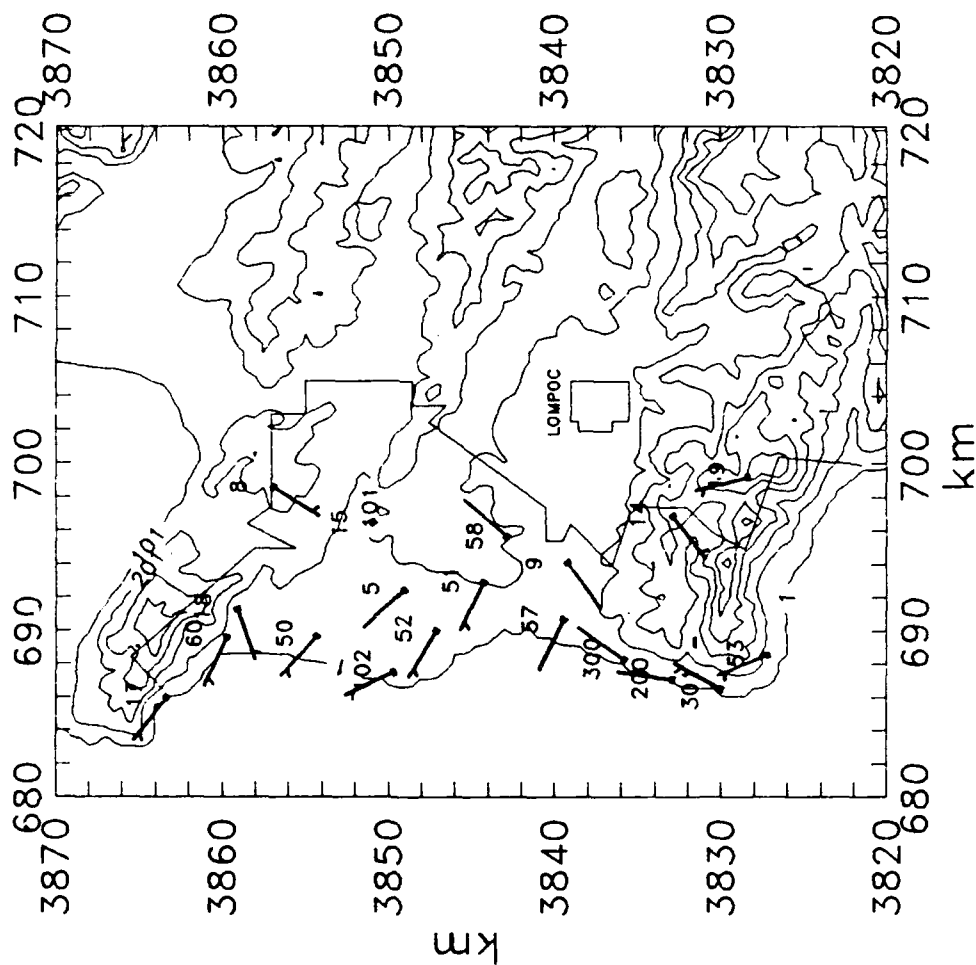


VANDENBERG AFB 7/28/88 01:00



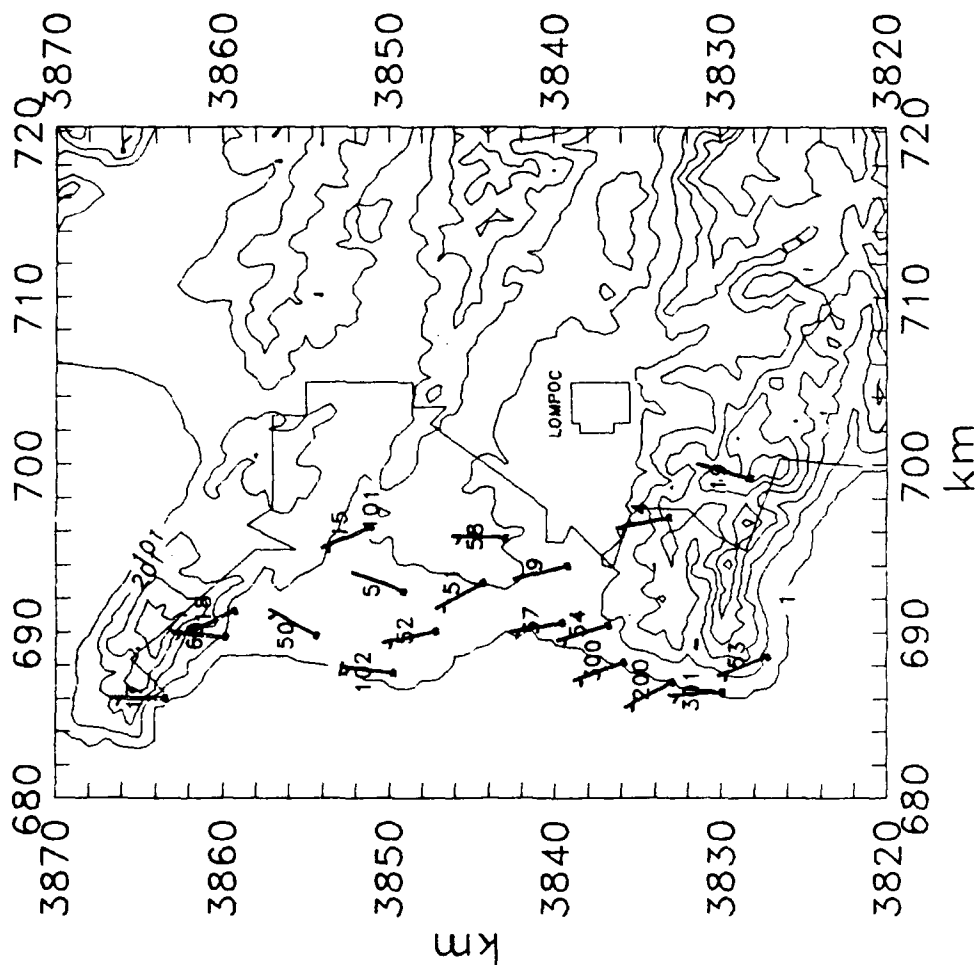
1 HOUR AVERAGES OF 12 FT. WINDS STANDARD NWS WIND BARBS

VANDENBERG AFB 7/28/88 04:00



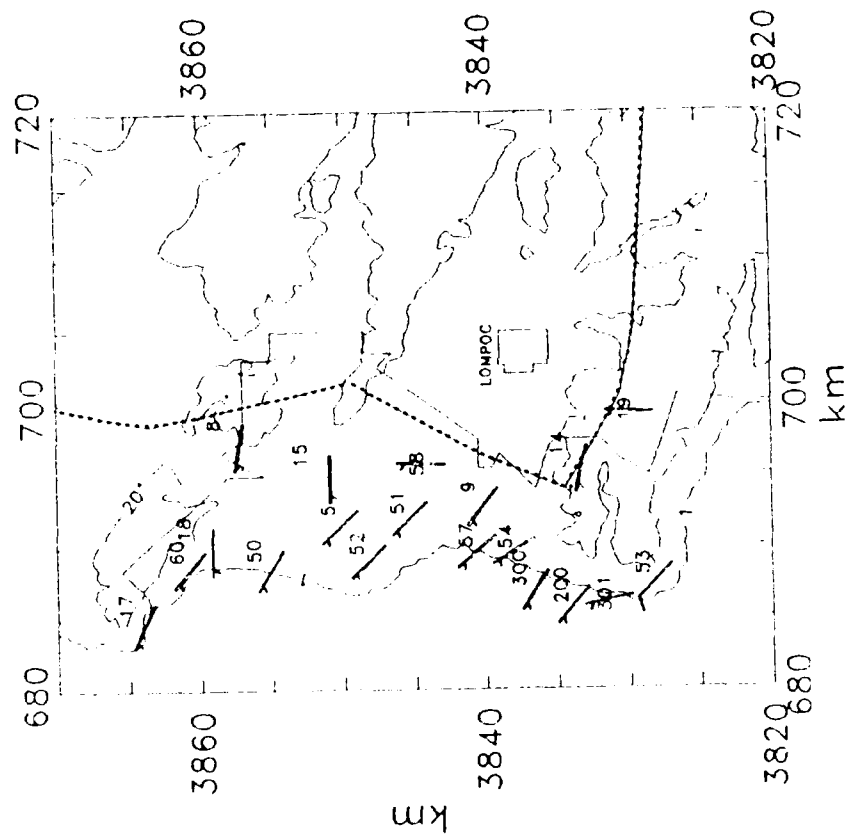
1 HOUR AVERAGES OF 12 FT. WINDS STANDARD NWS WIND BARBS

VANDENBERG AFB 7/28/88 07:00



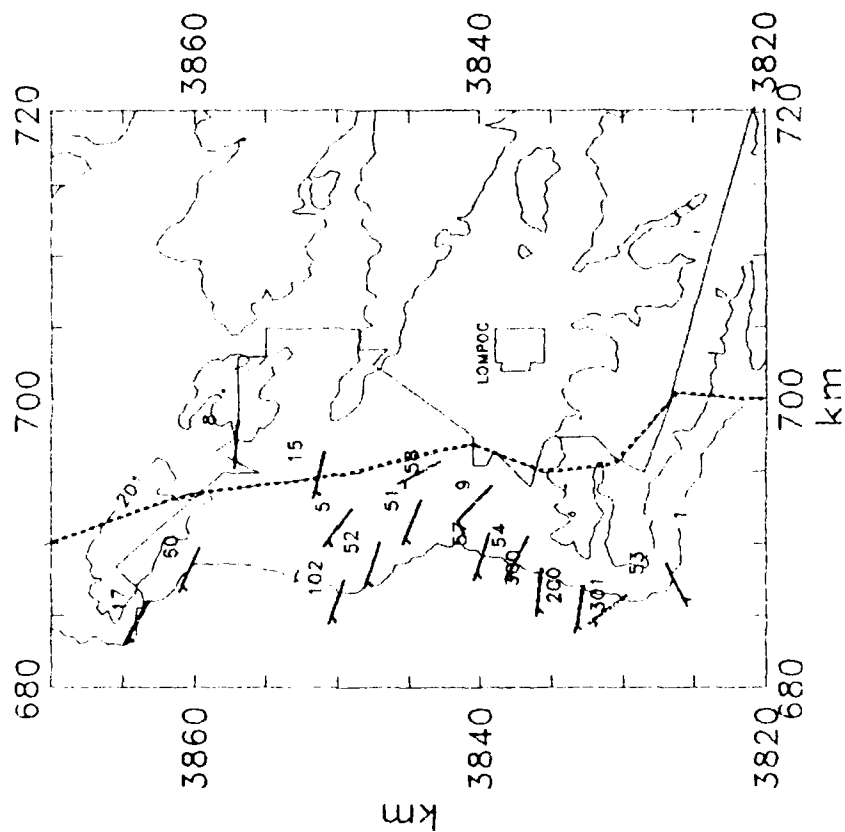
1 HOUR AVERAGES OF 12FT. WINDS WITH APPROXIMATED CLOUD EDGE STANDARD NWS WIND BARBS

VANDENBERG AFB 7/28/88 10:00



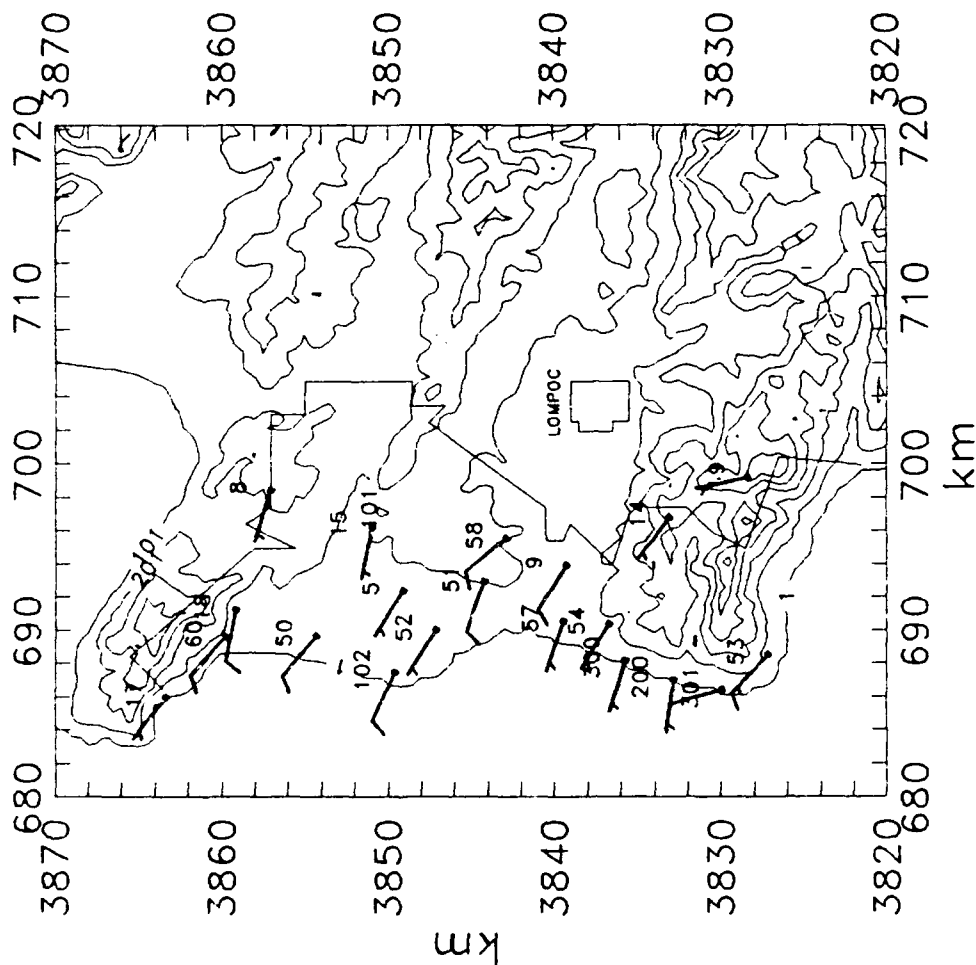
1 HOUR AVERAGES OF 12FT. WINDS WITH APPROXIMATED CLOUD EDGE STANDARD NWS WIND BARBS

VANDENBERG AFB 7/28/88 13:00



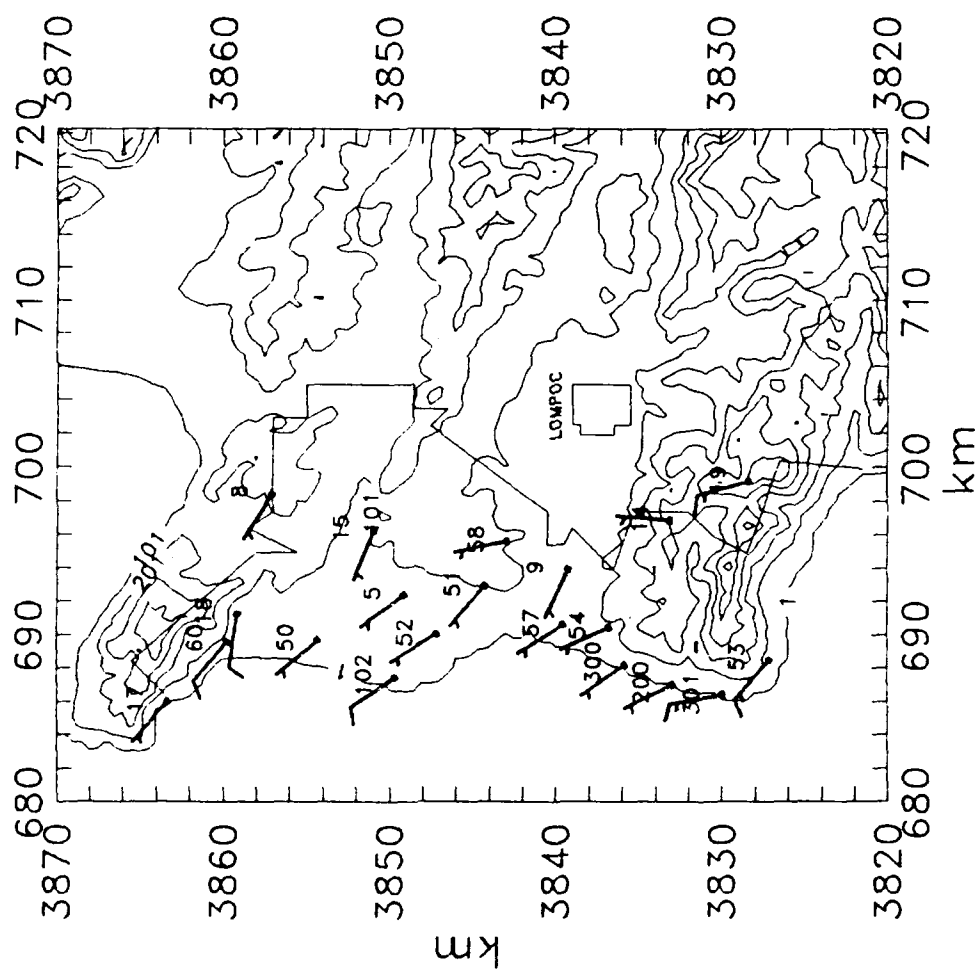
1 HOUR AVERAGES OF 12 FT. WINDS STANDARD NWS WIND BARBS

VANDENBERG AFB 7/28/88 16:00



1 HOUR AVERAGES OF 12 FT. WINDS STANDARD NWS WIND BARBS

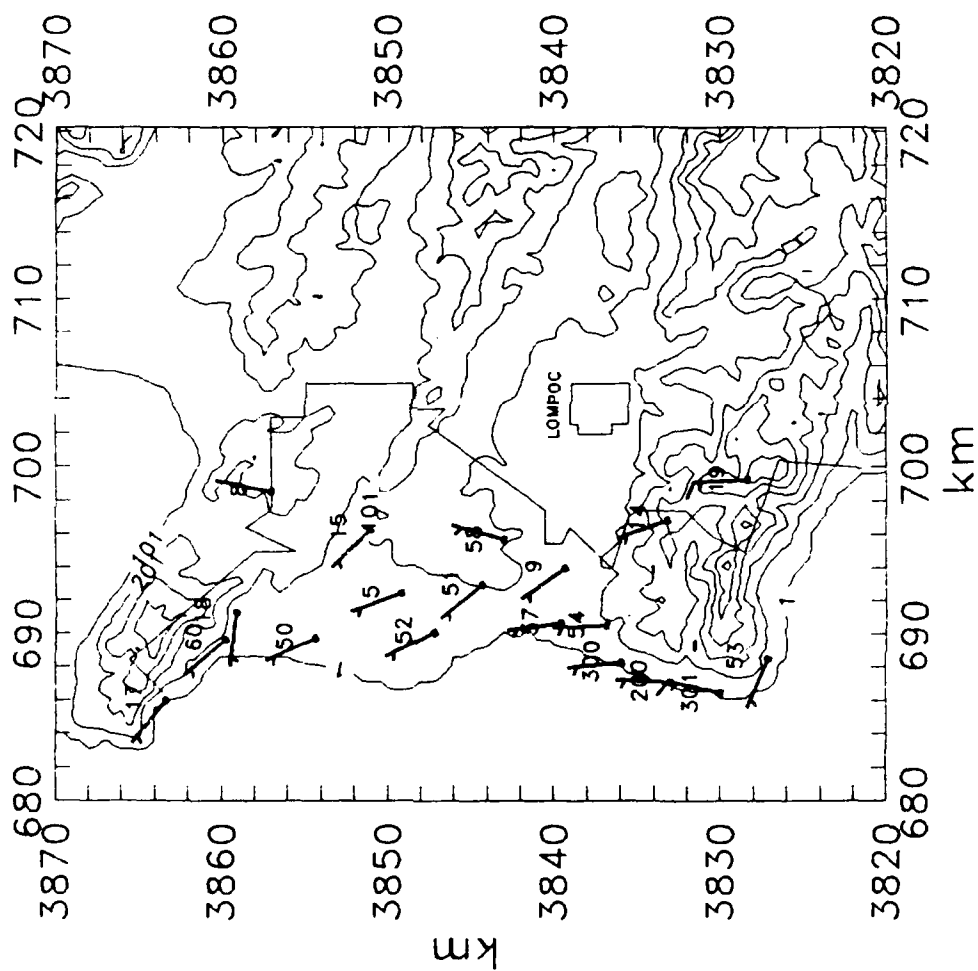
VANDENBERG AFB 7/28/88 19:00



SCALE: 9 km = 1 inch
CONTOUR interval = 100 m
BASE MET TOWERS

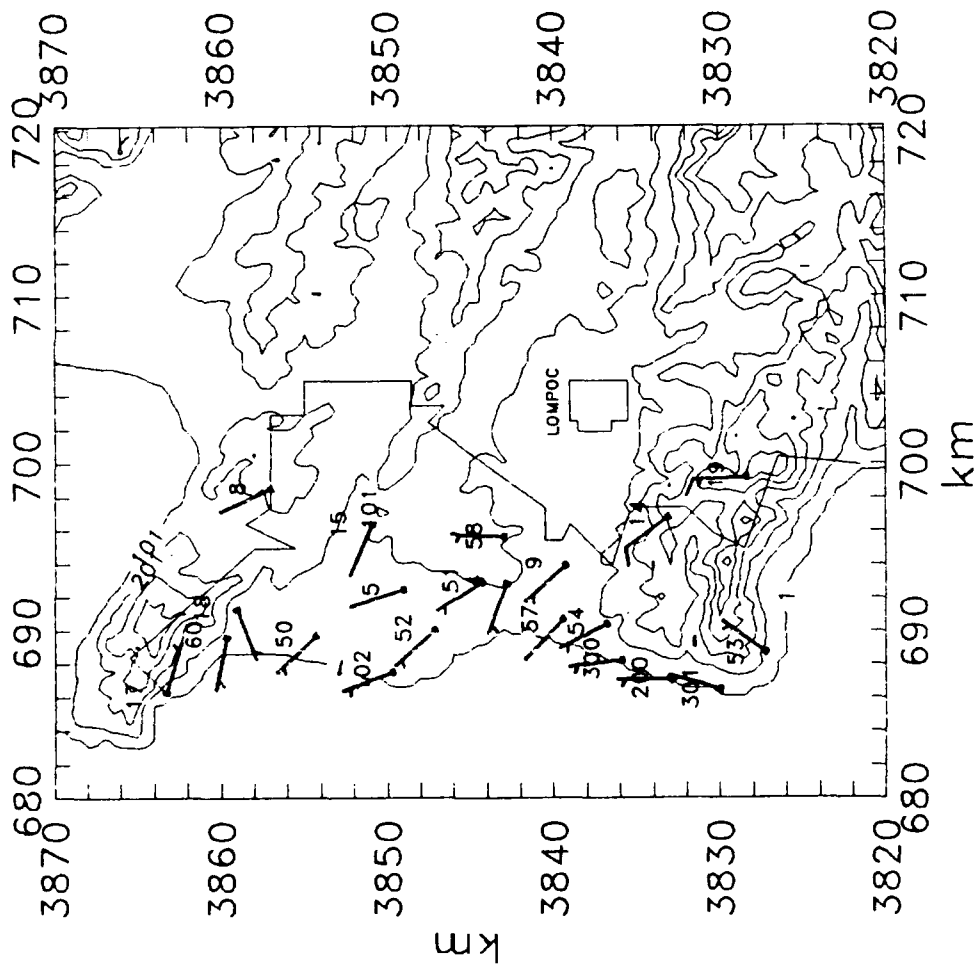
1 HOUR AVERAGES OF 12 FT. WINDS STANDARD NWS WIND BARBS

VANDENBERG AFB 7/28/88 22:00



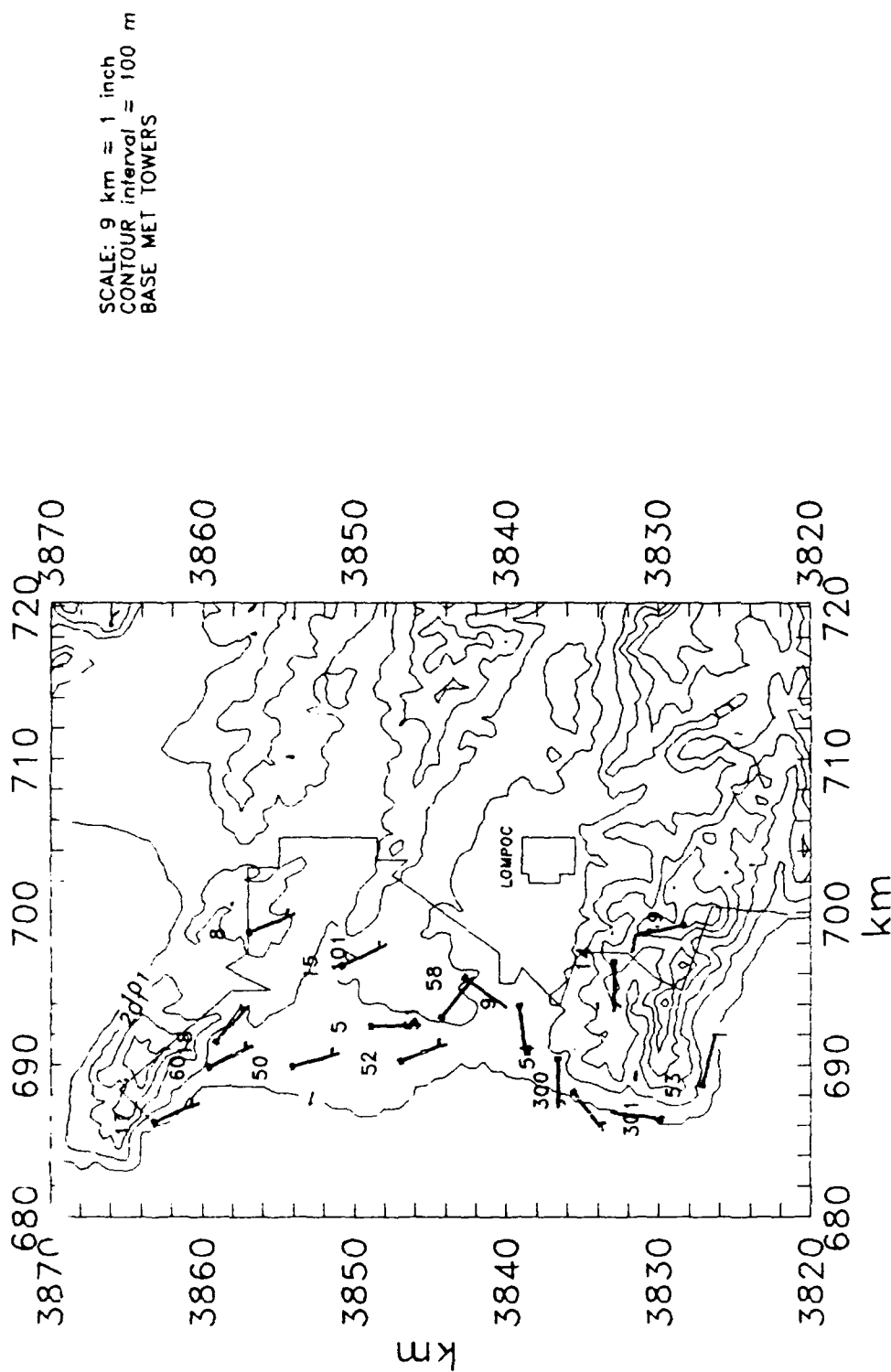
1 HOUR AVERAGES OF 12 FT. WINDS STANDARD NWS WIND BARBS

VANDENBERG AFB 7/29/88 01:00

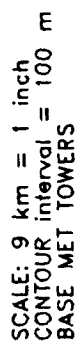


1 HOUR AVERAGES OF 12 FT. WINDS STANDARD NWS WIND BARBS

VANDENBERG AFB 7/29/88 04:00

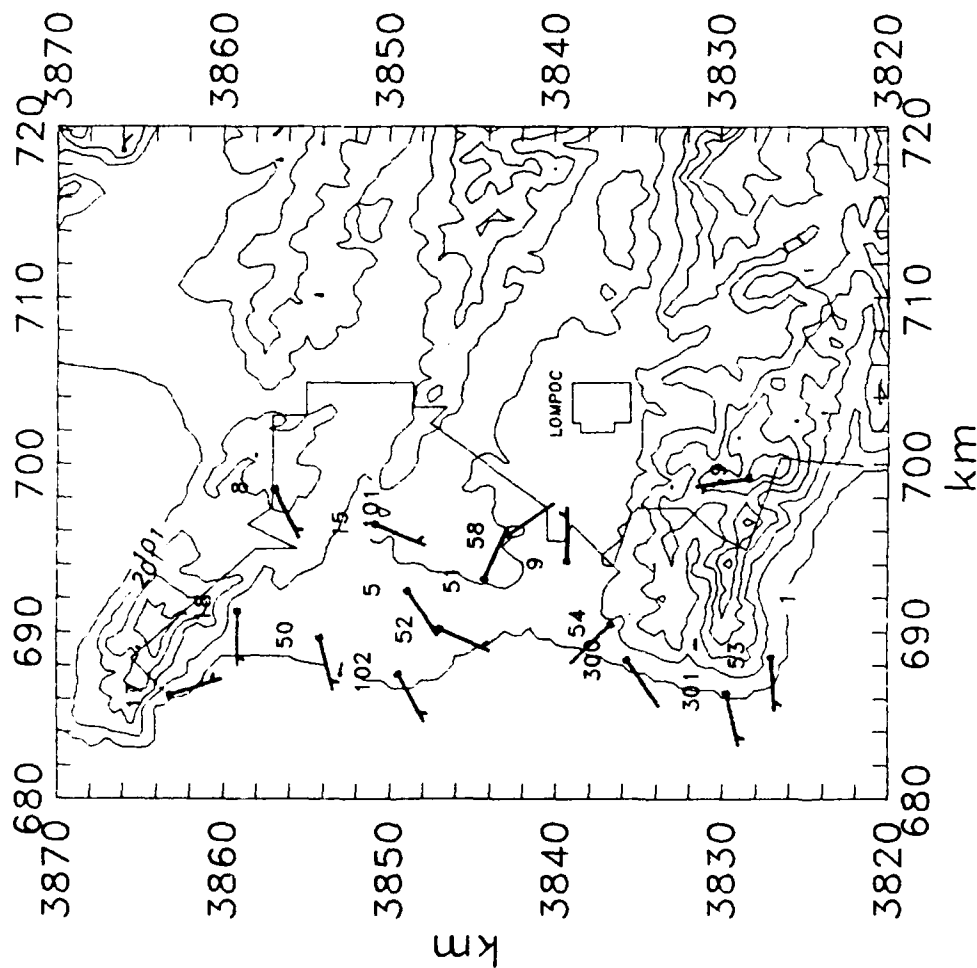


VANDENBERG AFB 7/29/88 07:00



1 HOUR AVERAGES OF 12 FT. WINDS STANDARD NWS WIND BARBS

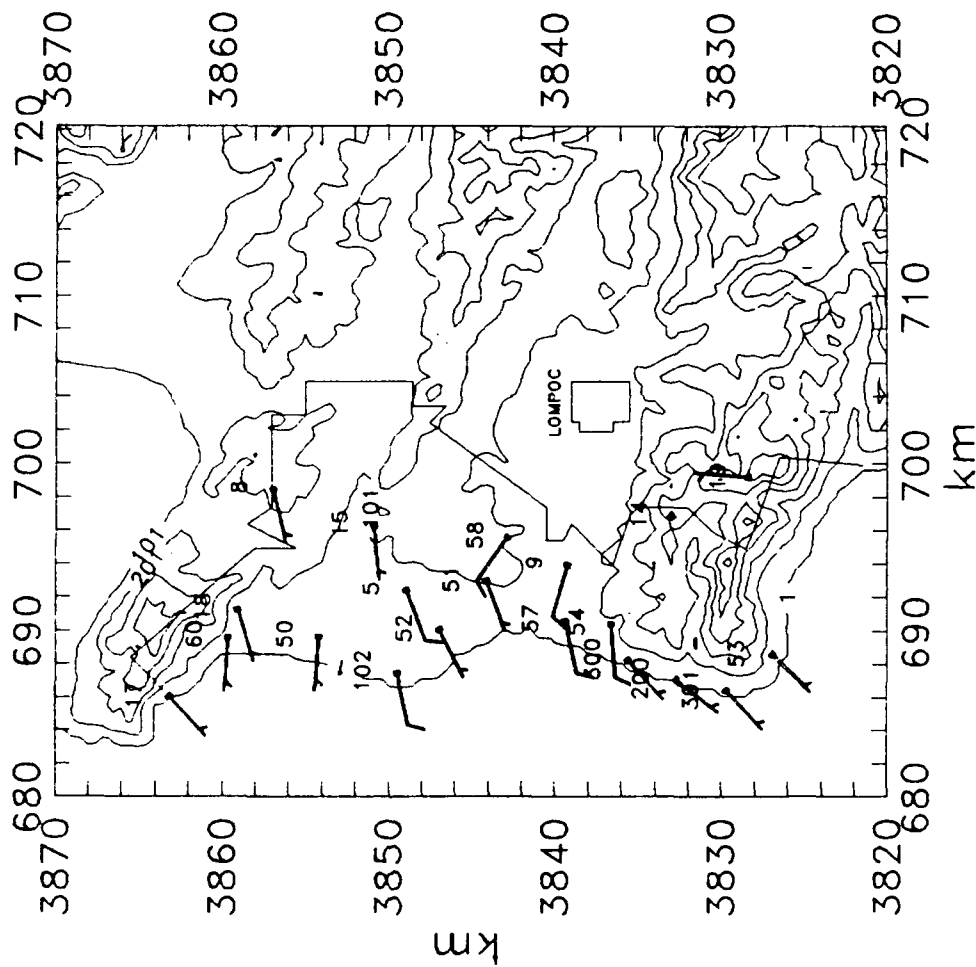
VANDENBERG AFB 7/29/88 10:00



SCALE: 9 km = 1 inch
CONTOUR interval = 100 m
BASE MET TOWERS

1 HOUR AVERAGES OF 12 FT. WINDS STANDARD NWS WIND BARBS

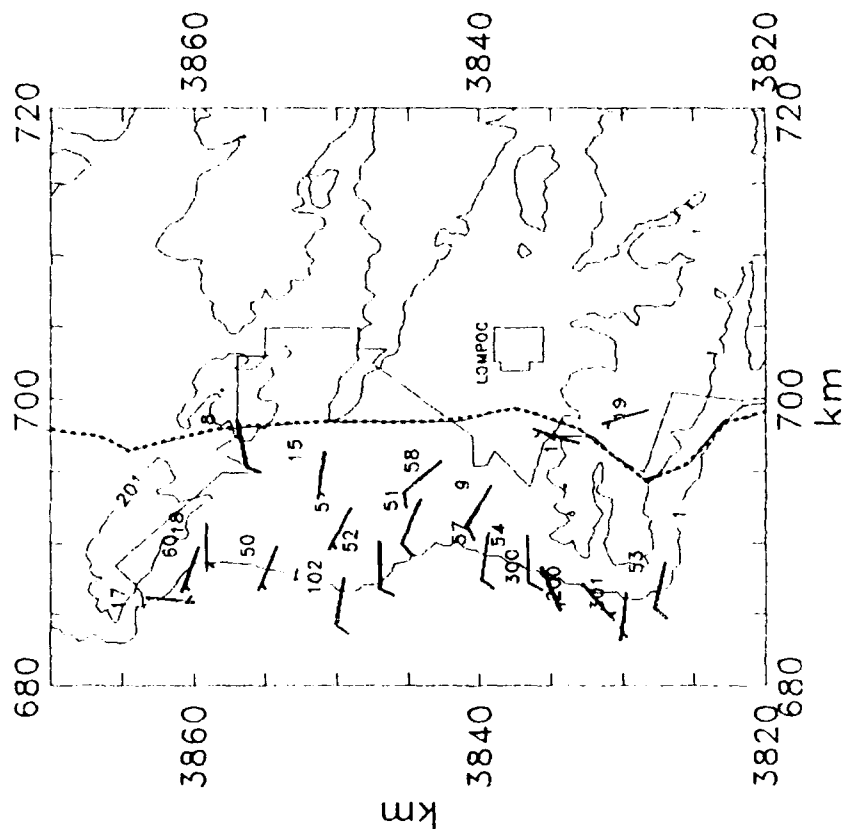
VANDENBERG AFB 7/29/88 13:00



SCALE: 9 km = 1 inch
CONTOUR interval = 100 m
BASE MET TOWERS

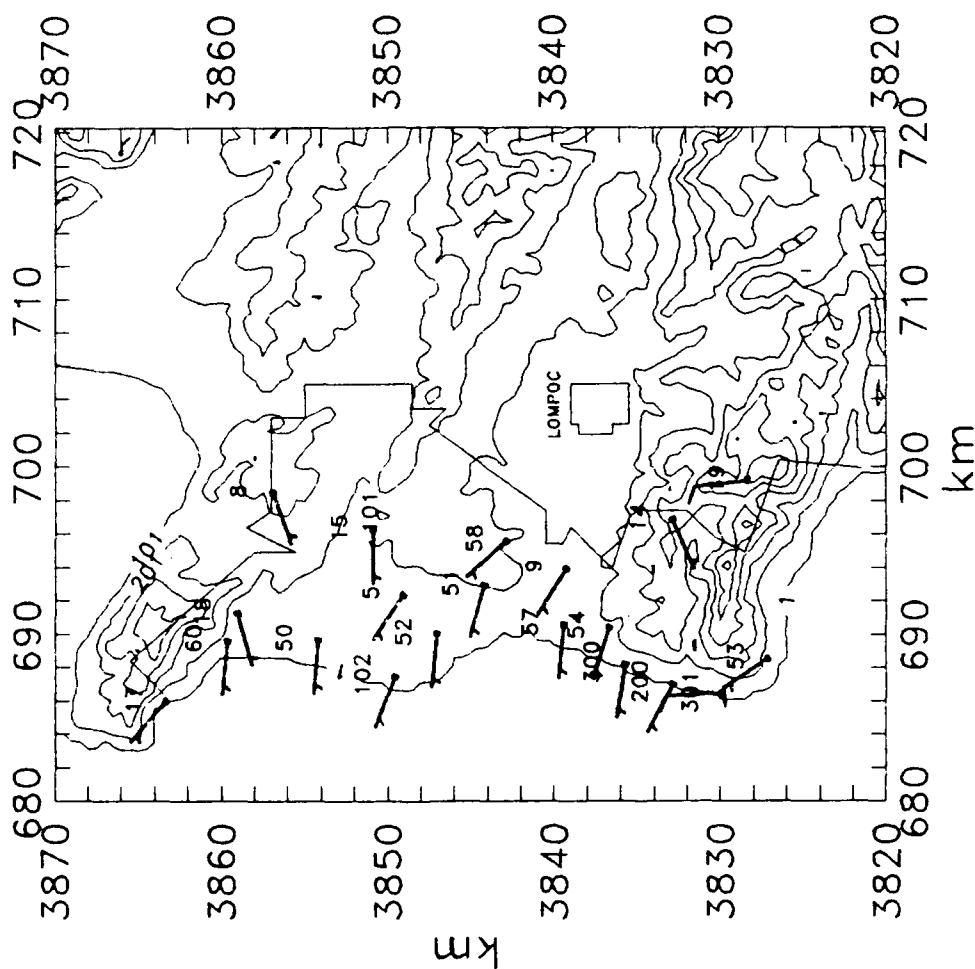
1 HOUR AVERAGES OF 12FT. WINDS WITH APPROXIMATED CLOUD EDGE STANDARD NWS WIND BARBS

VANDENBERG AFB 7/29/88 16:00

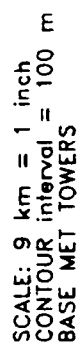


1 HOUR AVERAGES OF 12 FT. WINDS STANDARD NWS WIND BARBS

VANDENBERG AFB 7/29/88 19:00

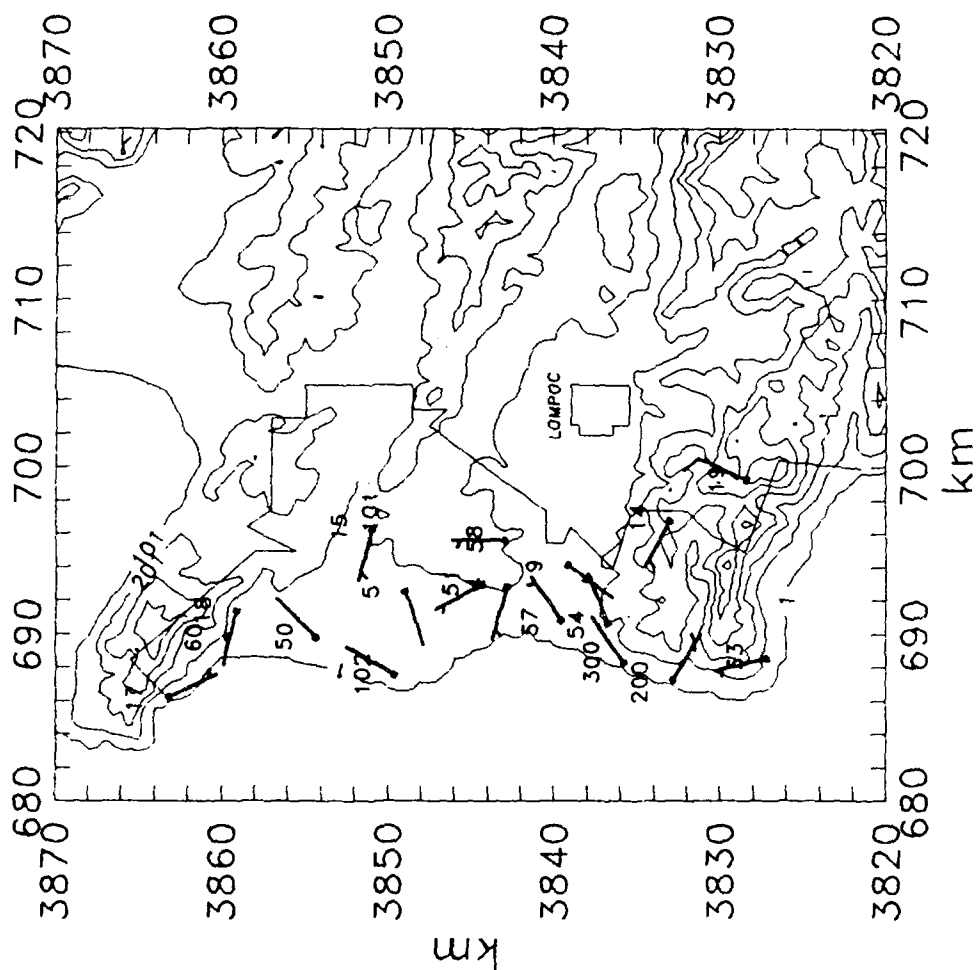


VANDENBERG AFB 7/29/88 22:00



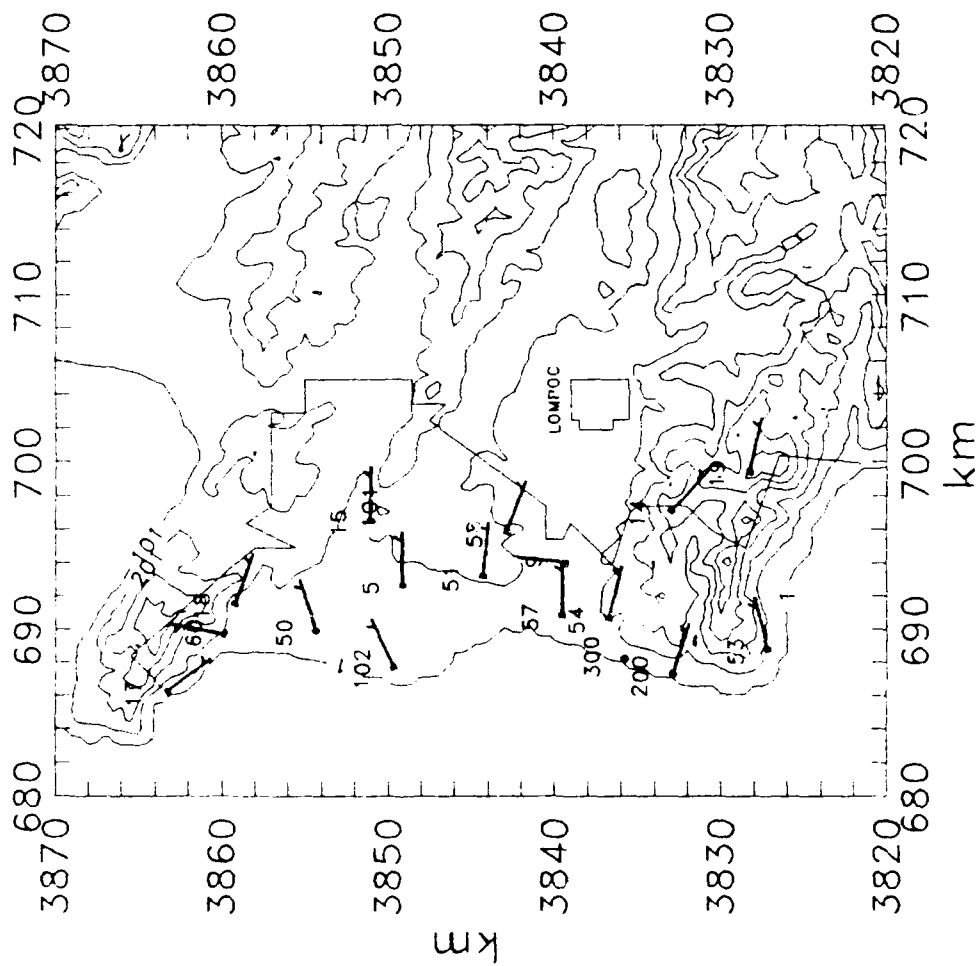
1 HOUR AVERAGES OF 12 FT. WINDS STANDARD NWS WIND BARBS

VANDENBERG AFB 10/18/88 01:00



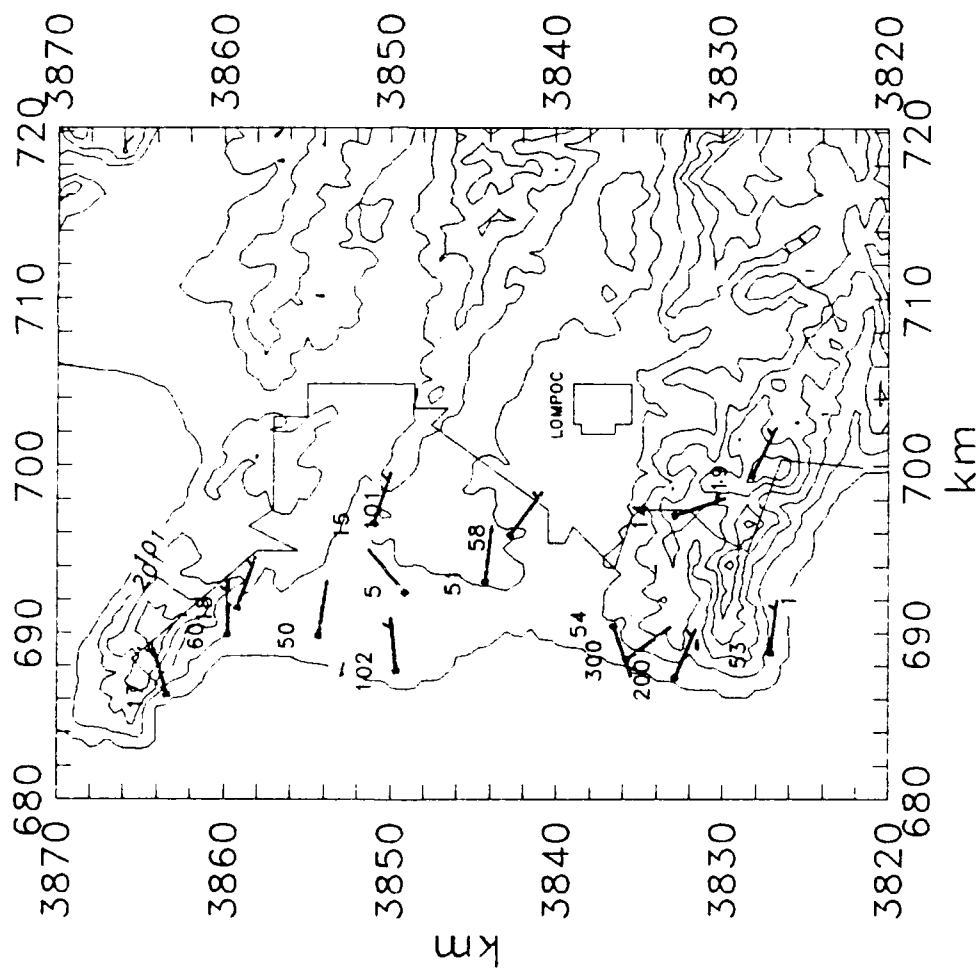
1 HOUR AVERAGES OF 12 FT. WINDS STANDARD NWS WIND BARBS

VANDENBERG AFB 10/18/88 04:00



1 HOUR AVERAGES OF 12 FT. WINDS STANDARD NWS WIND BARBS

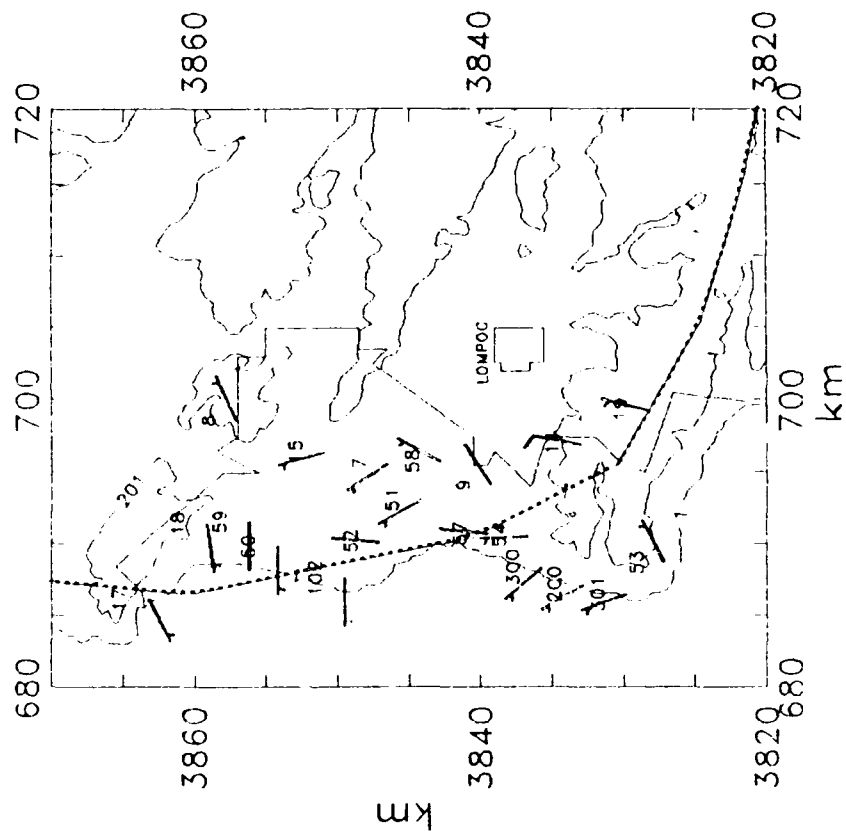
VANDENBERG AFB 10/18/88 07:00



SCALE: 9 km = 1 inch
CONTOUR interval = 100 m
BASE MET TOWERS

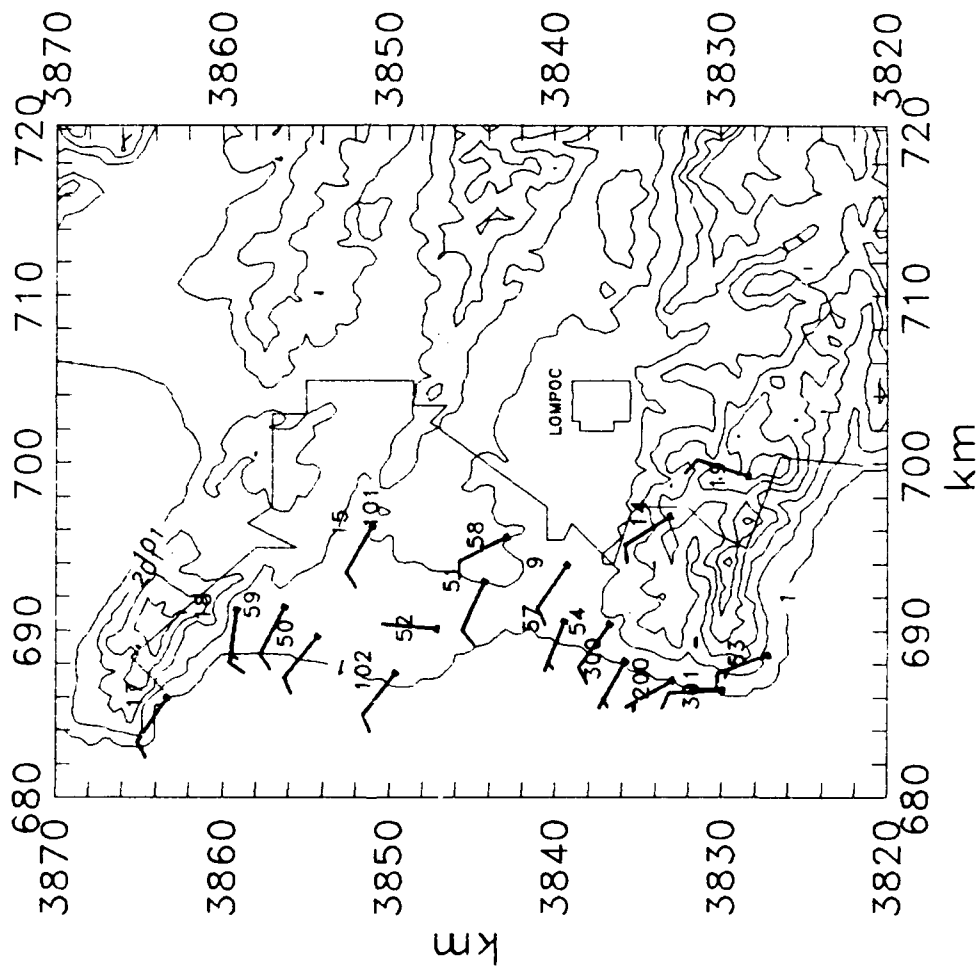
1 HOUR AVERAGES OF 12FT. WINDS WITH APPROXIMATED CLOUD EDGE STANDARD NWS WIND BARBS

VANDENBERG AFB 10/18/88 10:00



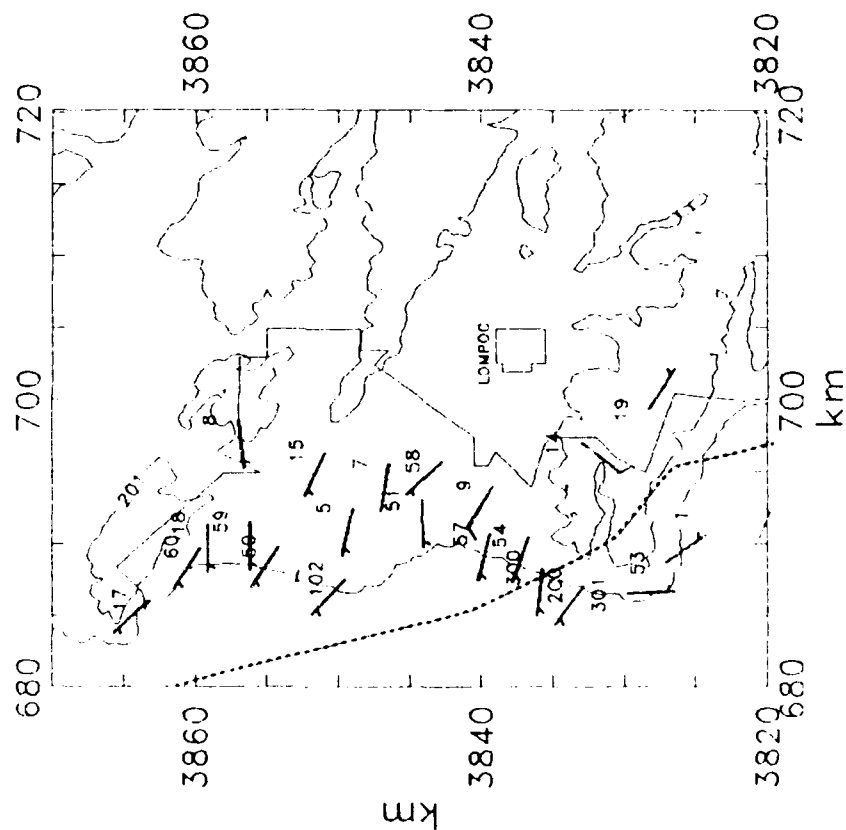
1 HOUR AVERAGES OF 12 FT. WINDS STANDARD NWS WIND BARBS

VANDENBERG AFB 10/18/88 13:00



1 HOUR AVERAGES OF 12FT. WINDS WITH APPROXIMATED CLOUD EDGE STANDARD NWS WIND BARBS

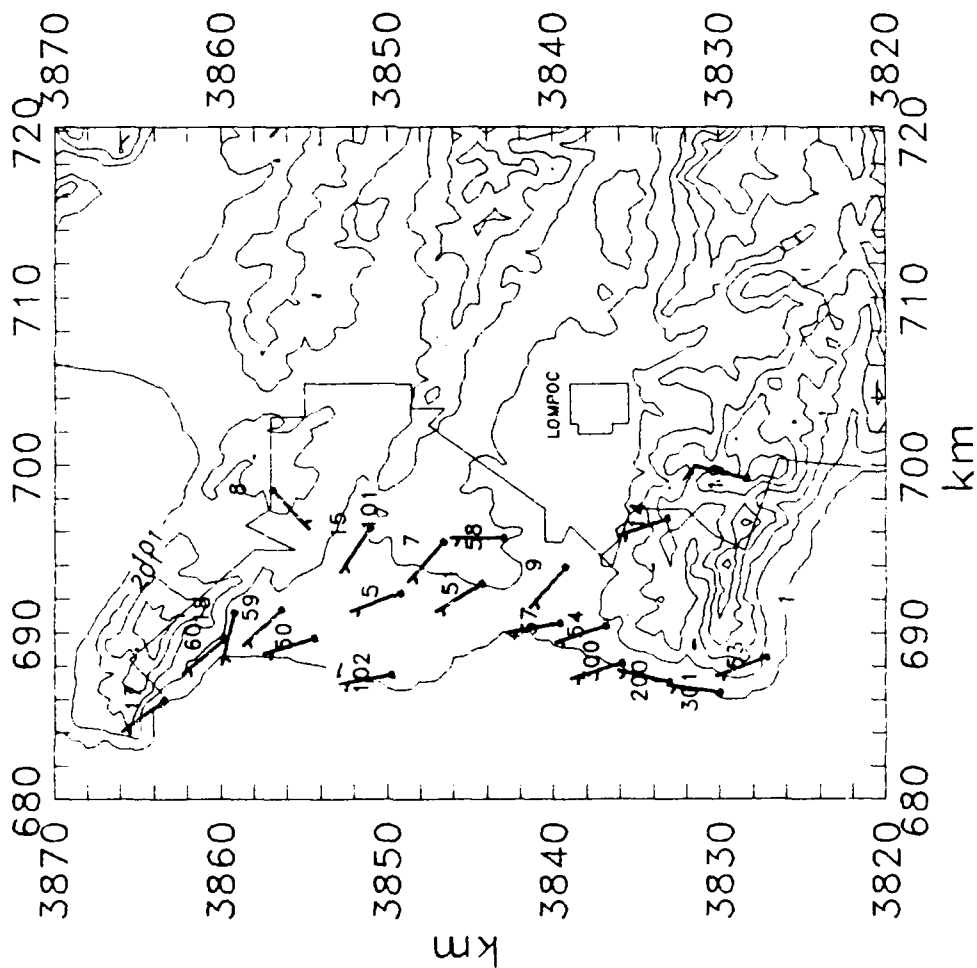
VANDENBERG AFB 10/18/88 16:00



SCALE: 18 km = 1 inch
CONTOUR interval = 200 m
BASE MET TOWERS

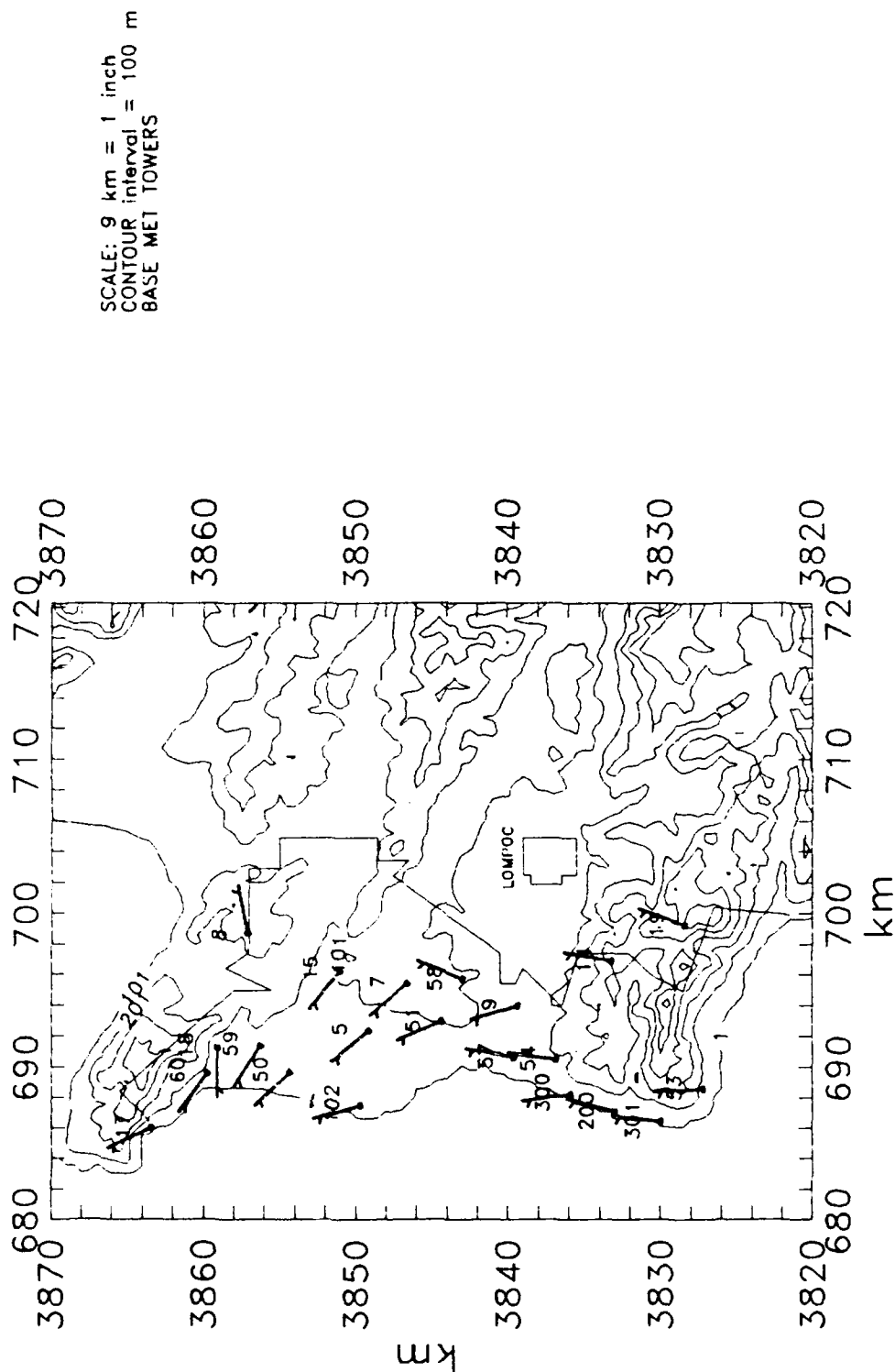
1 HOUR AVERAGES OF 12 FT. WINDS STANDARD NWS WIND BARBS

VANDENBERG AFB 10/18/88 19:00



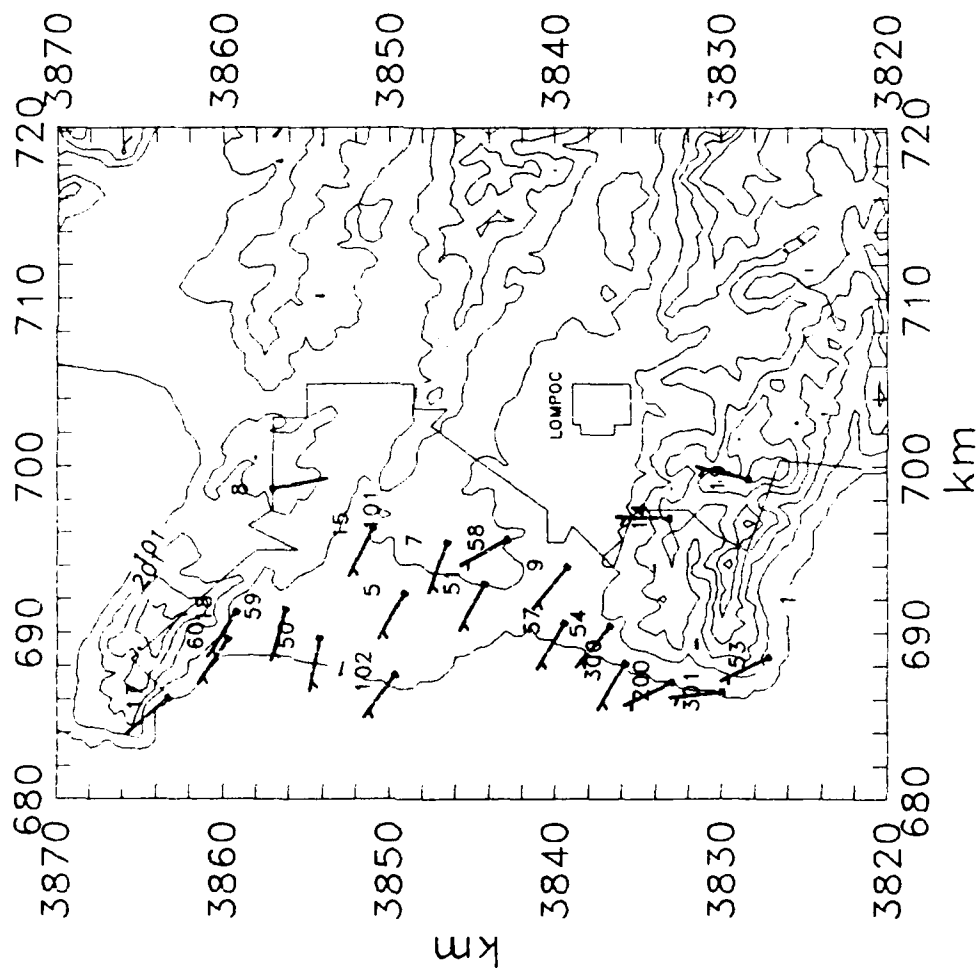
1 HOUR AVERAGES OF 12 FT. WINDS STANDARD NWS WIND BARBS

VANDENBERG AFB 10/18/88 22:00



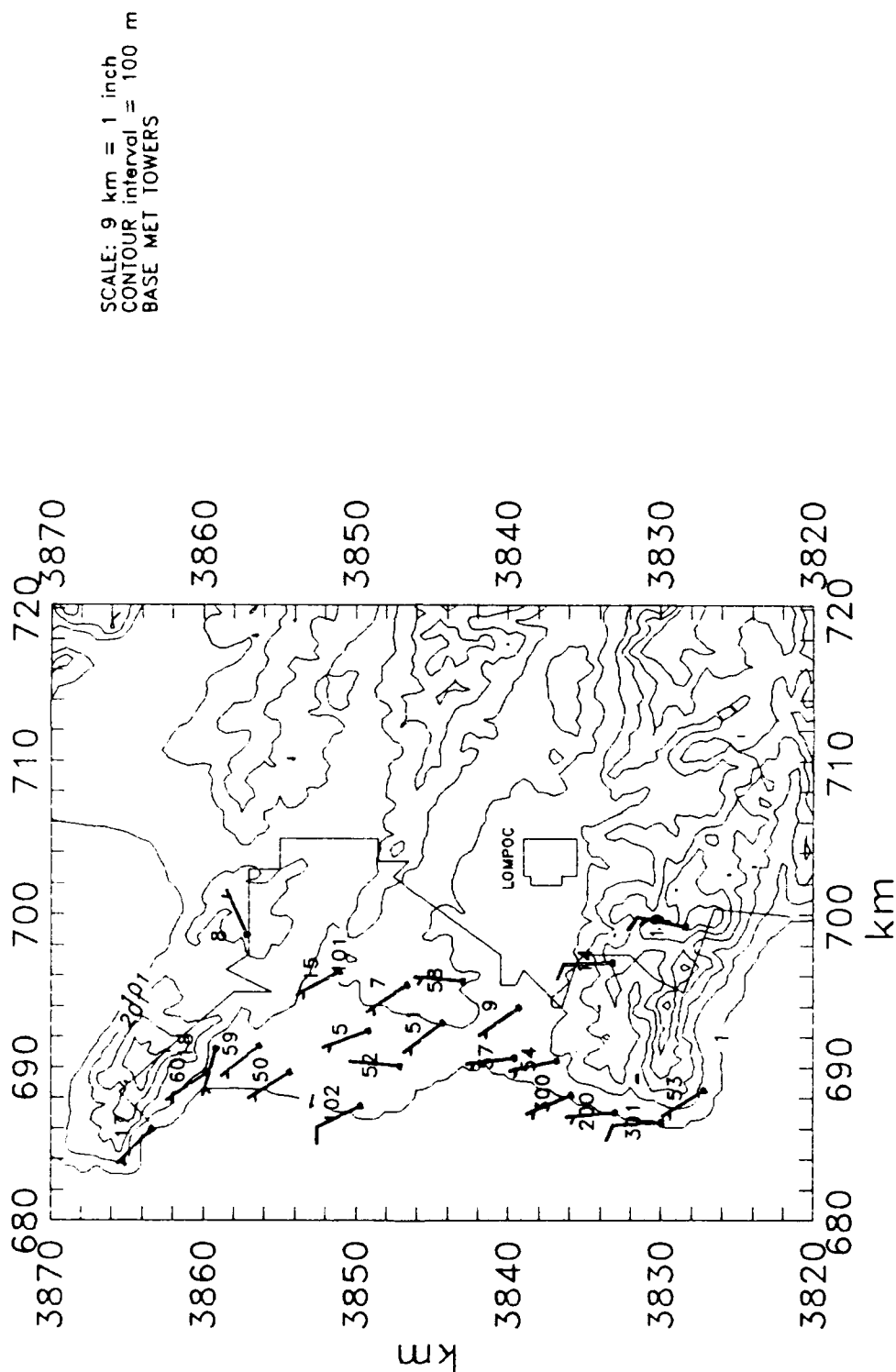
1 HOUR AVERAGES OF 12 FT. WINDS STANDARD NWS WIND BARBS

VANDENBERG AFB 10/19/88 01:00



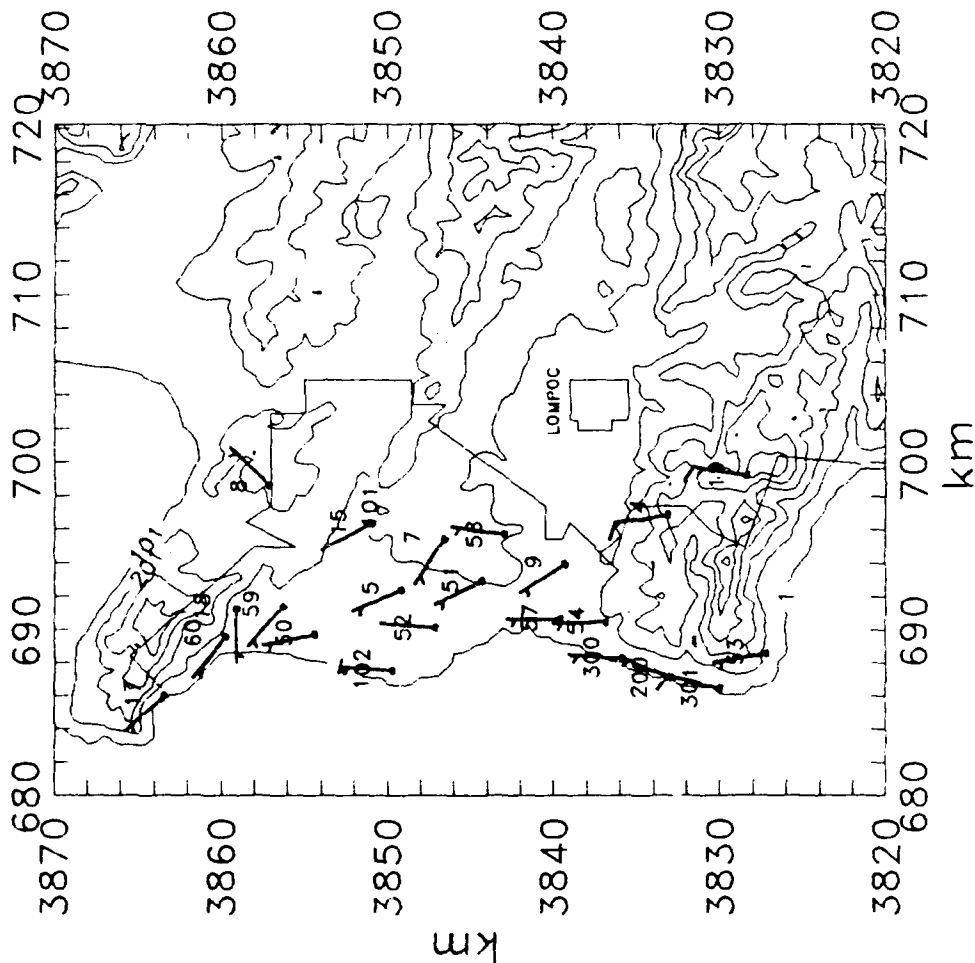
1 HOUR AVERAGES OF 12 FT. WINDS STANDARD NWS WIND BARBS

VANDENBERG AFB 10/19/88 04:00



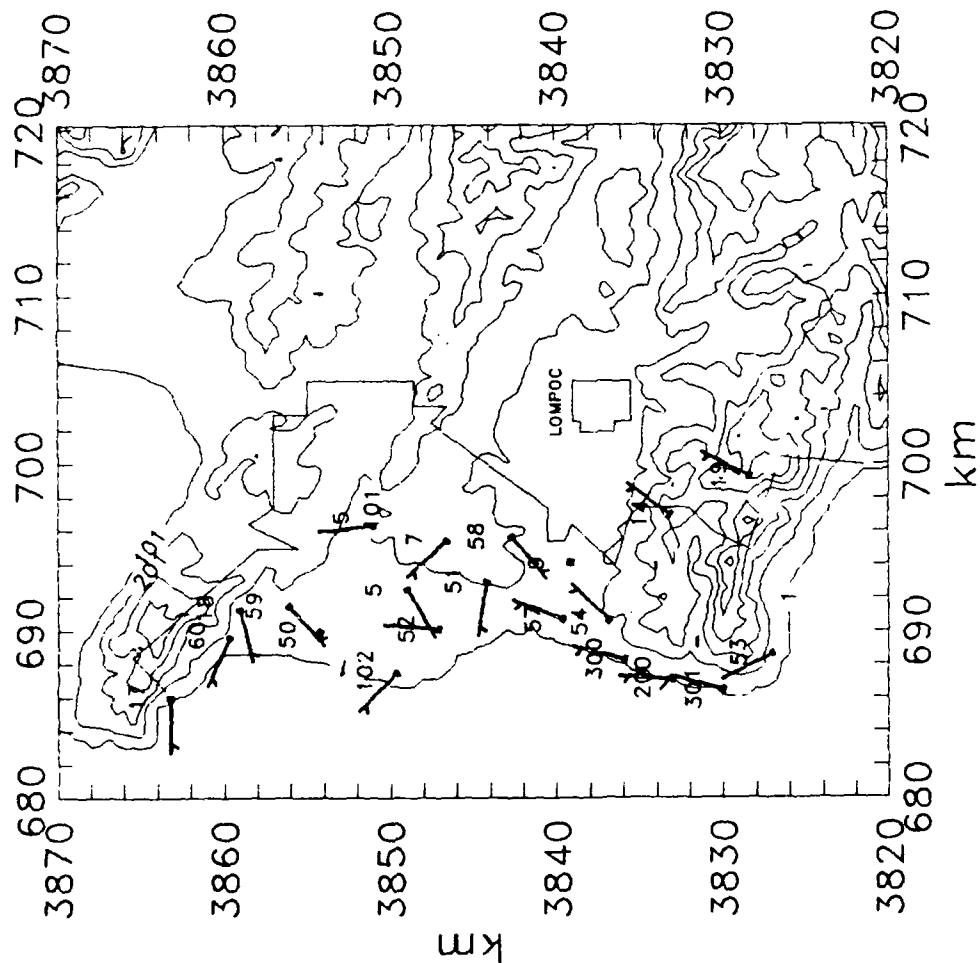
1 HOUR AVERAGES OF 12 FT. WINDS STANDARD NWS WIND BARBS

VANDENBERG AFB 10/19/88 07:00



1 HOUR AVERAGES OF 12 FT. WINDS STANDARD NWS WIND BARBS

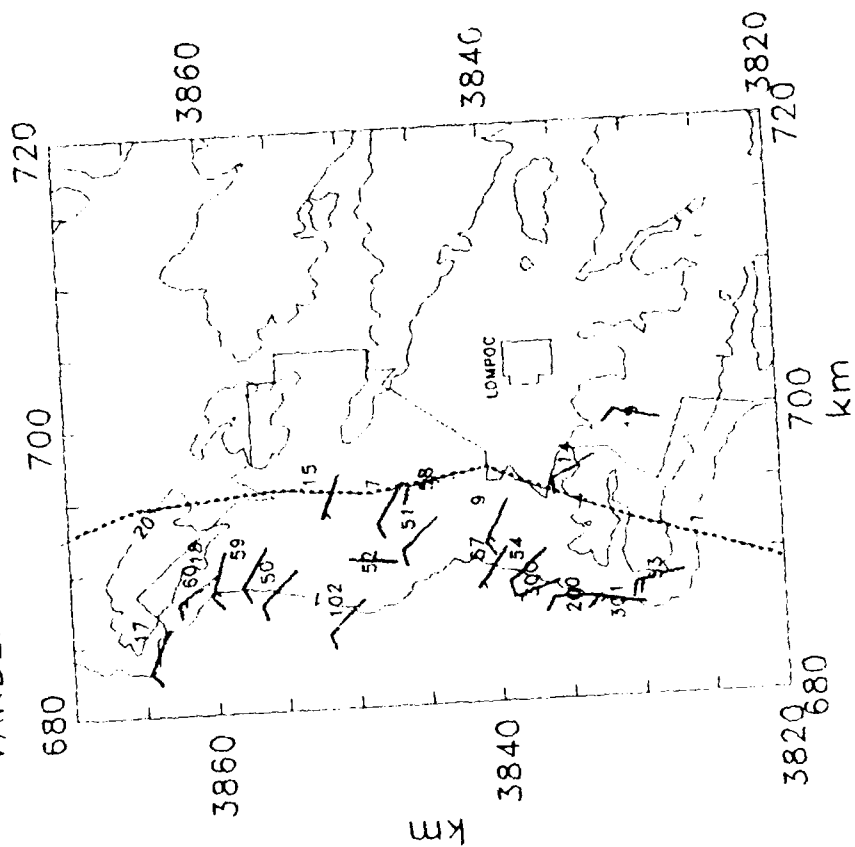
VANDENBERG AFB 10/19/88 10:00



SCALE: 9 km = 1 inch
CONTOUR interval = 100 m
BASE MET TOWERS

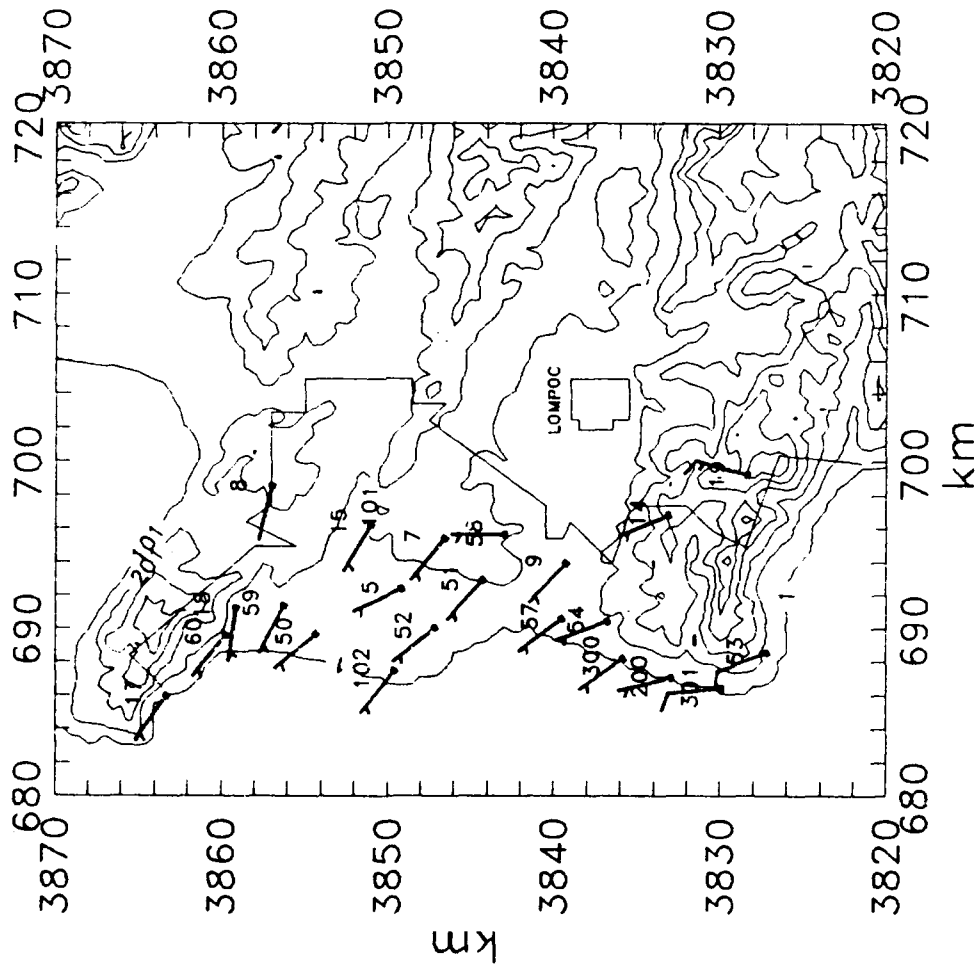
1 HOUR AVERAGES OF 12FT. WINDS WITH APPROXIMATED CLOUD EDGE STANDARD NWS WIND BARBS

VANDENBERG AFB 10/19/88 13:00



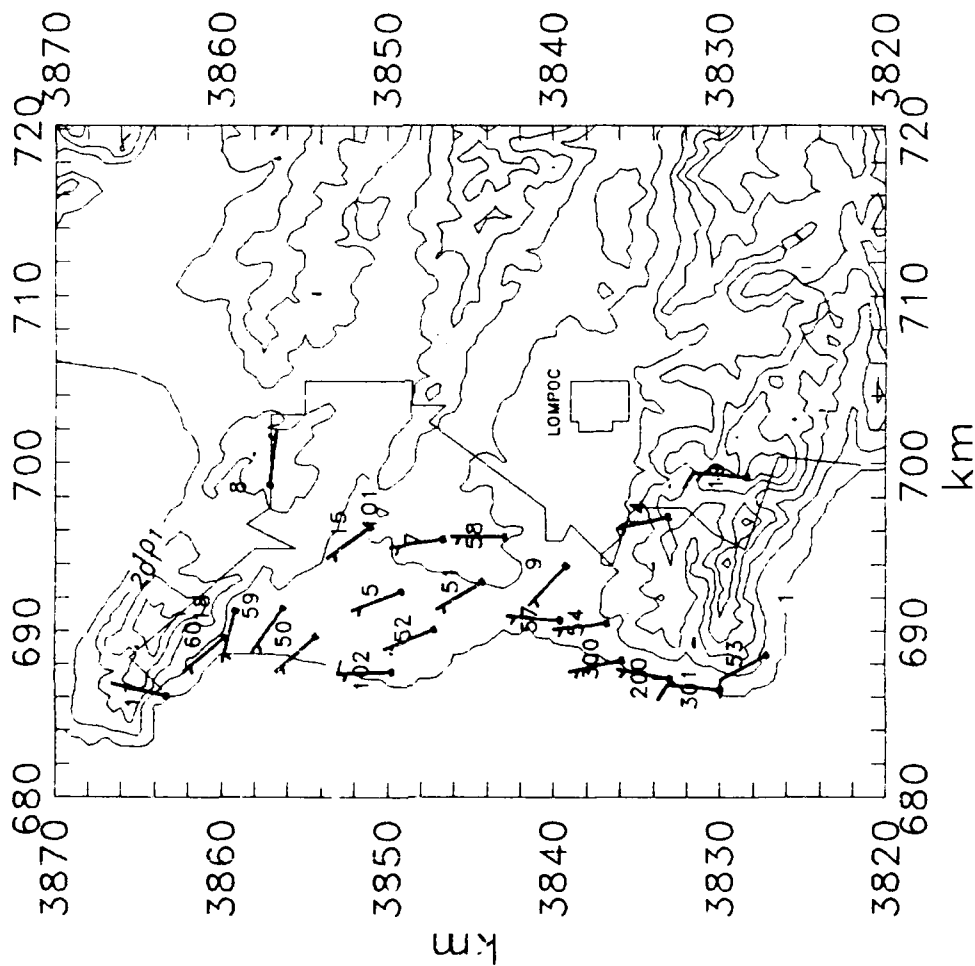
1 HOUR AVERAGES OF 12 FT. WINDS STANDARD NWS WIND BARBS

VANDENBERG AFB 10/19/88 19:00



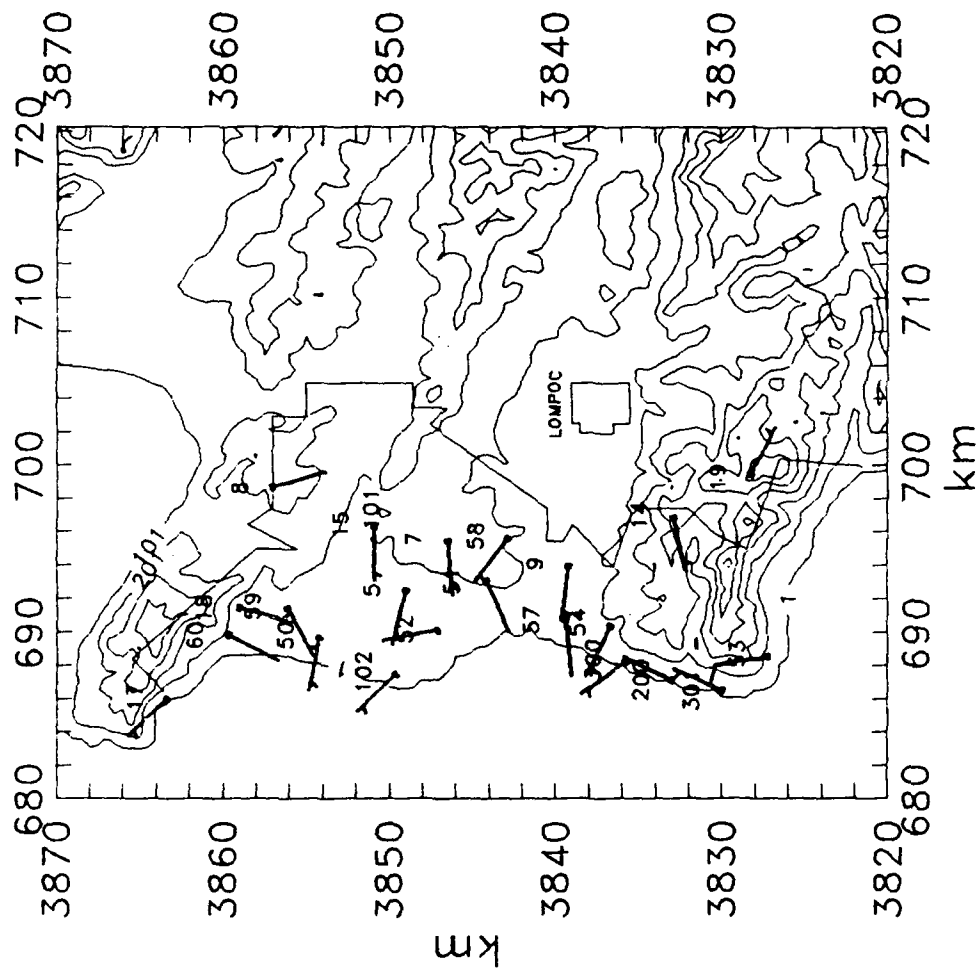
1 HOUR AVERAGES OF 12 FT. WINDS STANDARD NWS WIND BARBS

VANDENBERG AFB 10/19/88 22:00



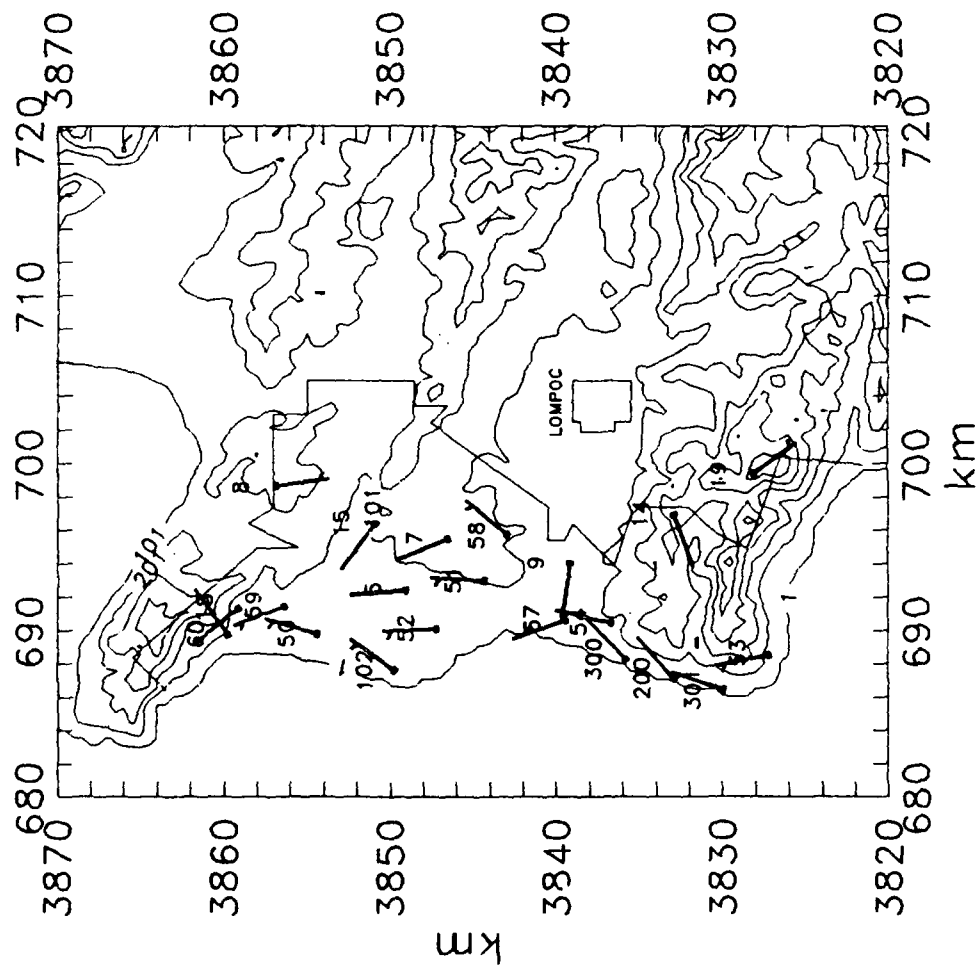
1 HOUR AVERAGES OF 12 FT. WINDS STANDARD NWS WIND BARBS

VANDENBERG AFB 10/20/88 01:00



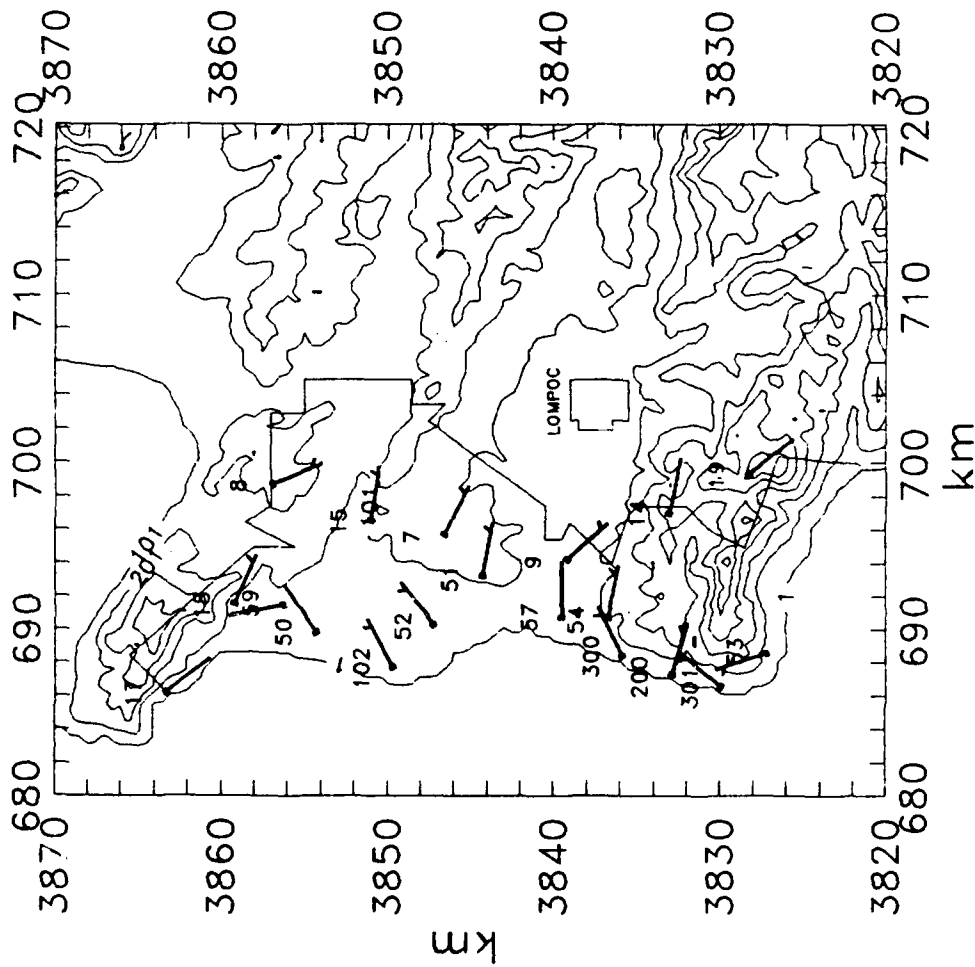
1 HOUR AVERAGES OF 12 FT. WINDS STANDARD NWS WIND BARBS

VANDENBERG AFB 10/20/88 04:00



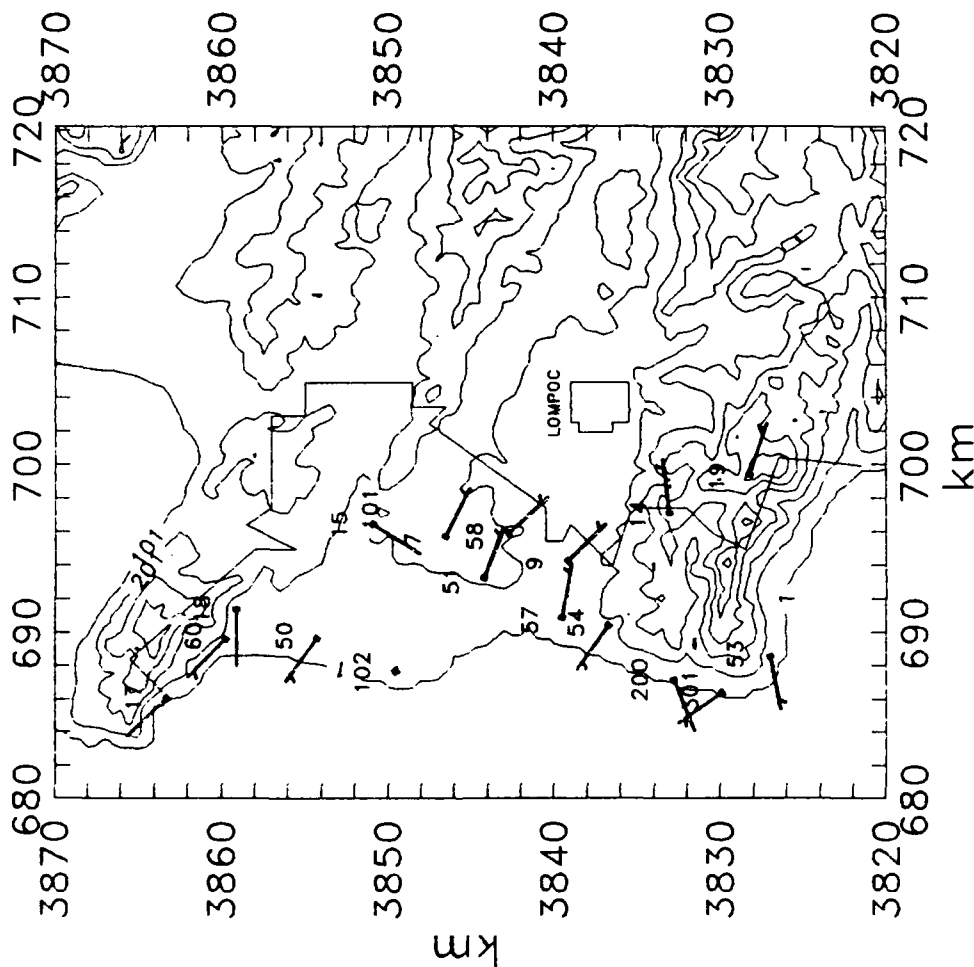
1 HOUR AVERAGES OF 12 FT. WINDS STANDARD NWS WIND BARBS

VANDENBERG AFB 10/20/88 07:00



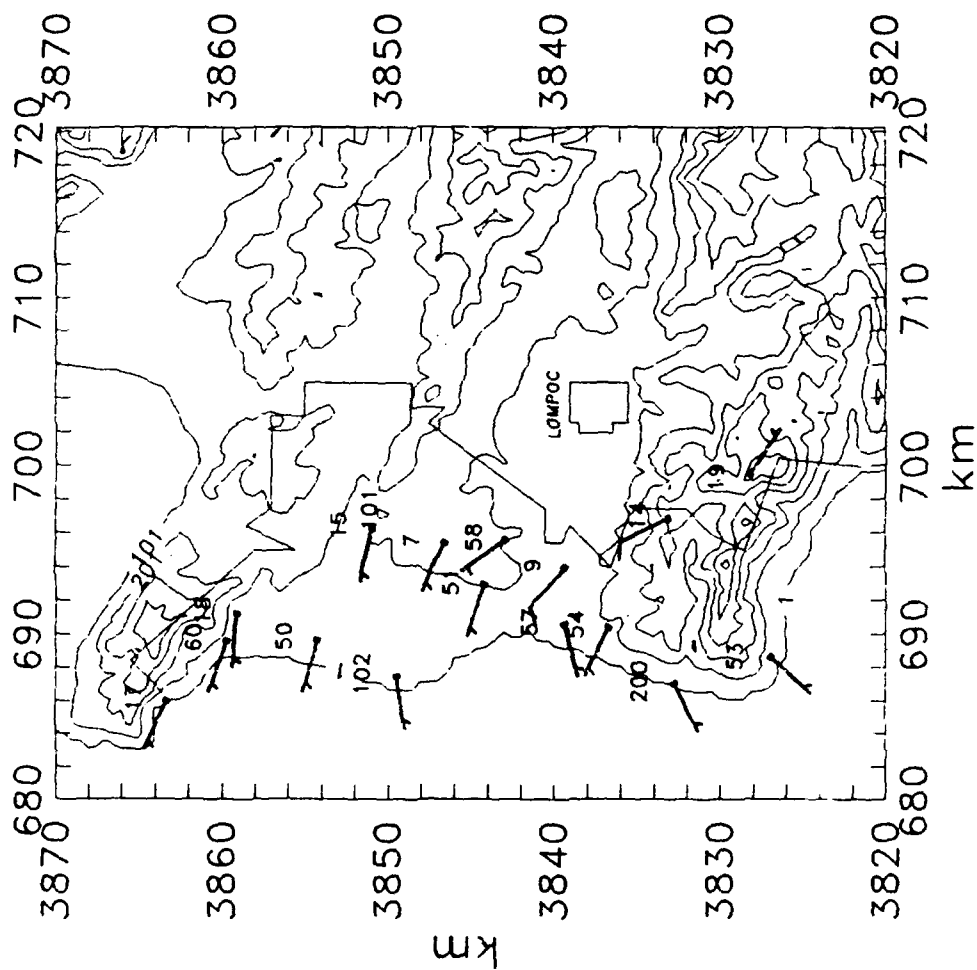
1 HOUR AVERAGES OF 12 FT. WINDS STANDARD NWS WIND BARBS

VANDENBERG AFB 10/20/88 10:00



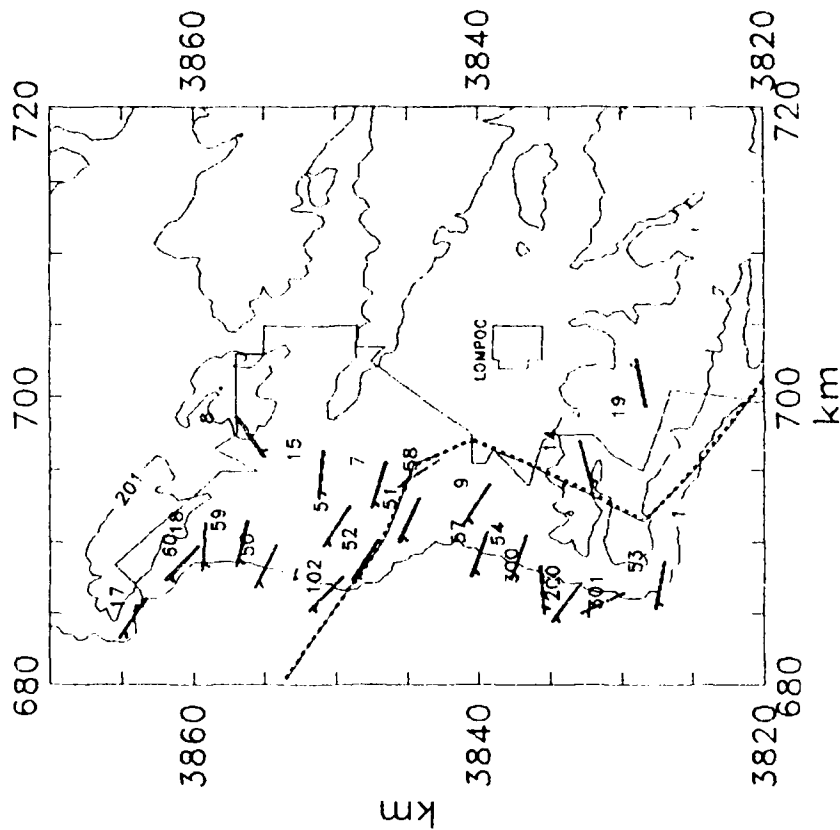
1 HOUR AVERAGES OF 12 FT. WINDS STANDARD NWS WIND BARBS

VANDENBERG AFB 10/20/88 13:00



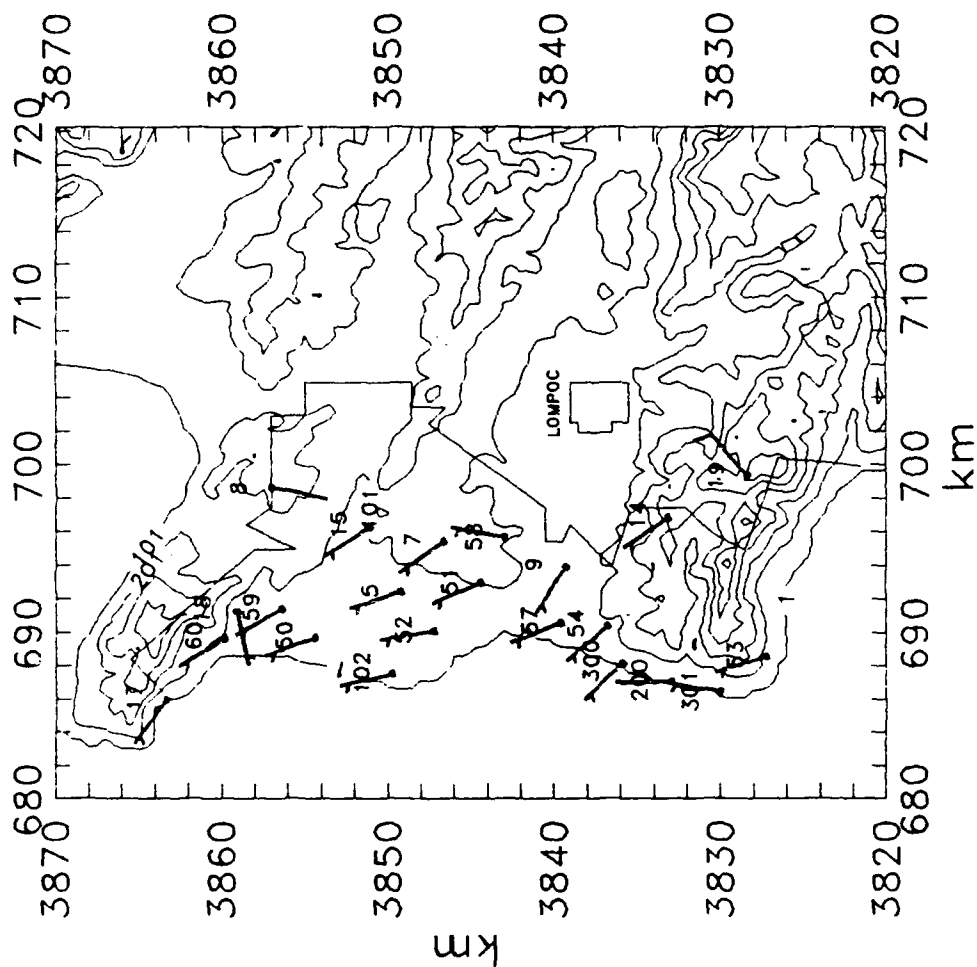
1 HOUR AVERAGES OF 12FT. WINDS WITH APPROXIMATED CLOUD EDGE STANDARD NWS WIND BARBS

VANDENBERG AFB 10/20/88 16:00



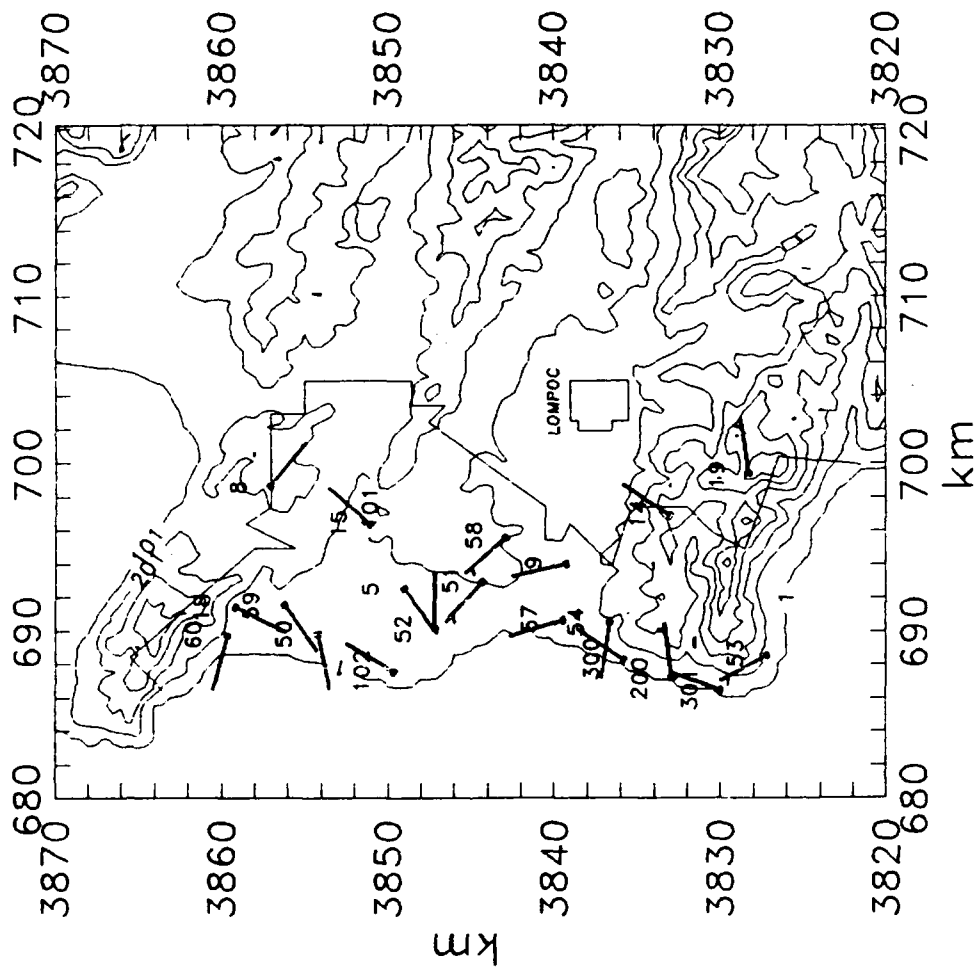
1 HOUR AVERAGES OF 12 FT. WINDS STANDARD NWS WIND BARBS

VANDENBERG AFB 10/20/88 19:00

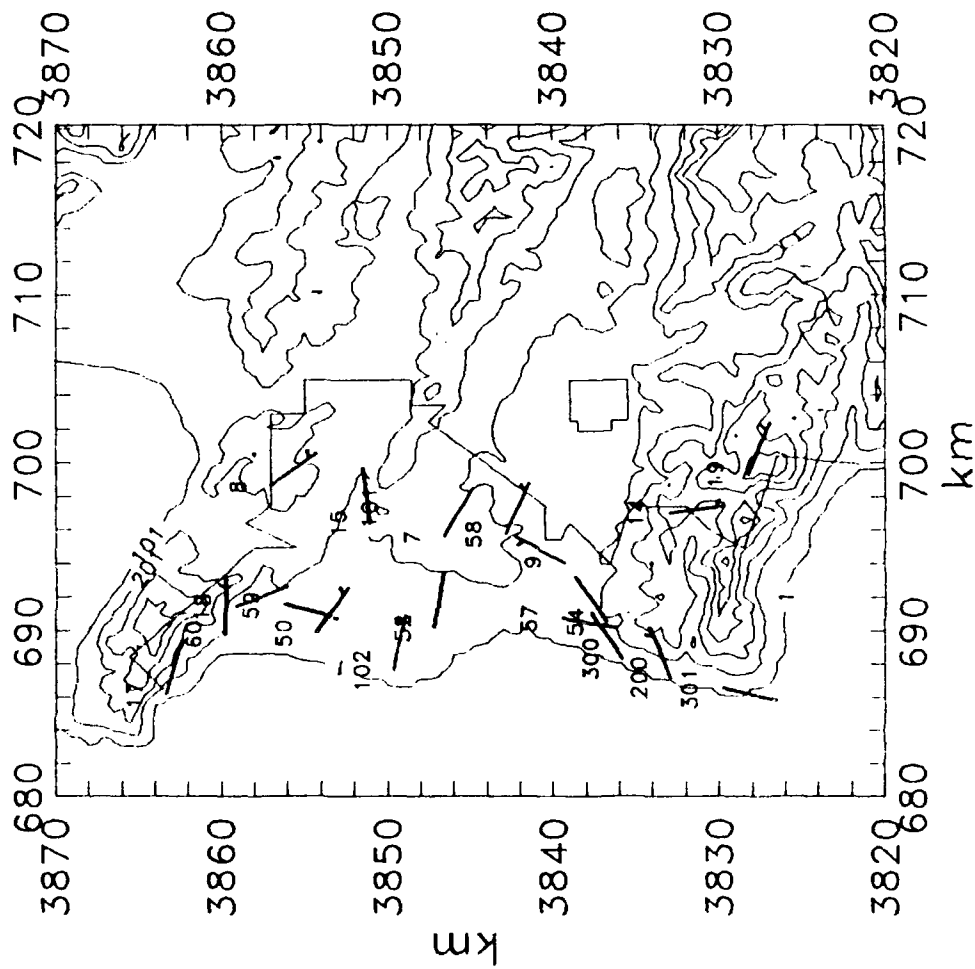


1 HOUR AVERAGES OF 12 FT. WINDS STANDARD NWS WIND BARBS

VANDENBERG AFB 10/20/88 22:00



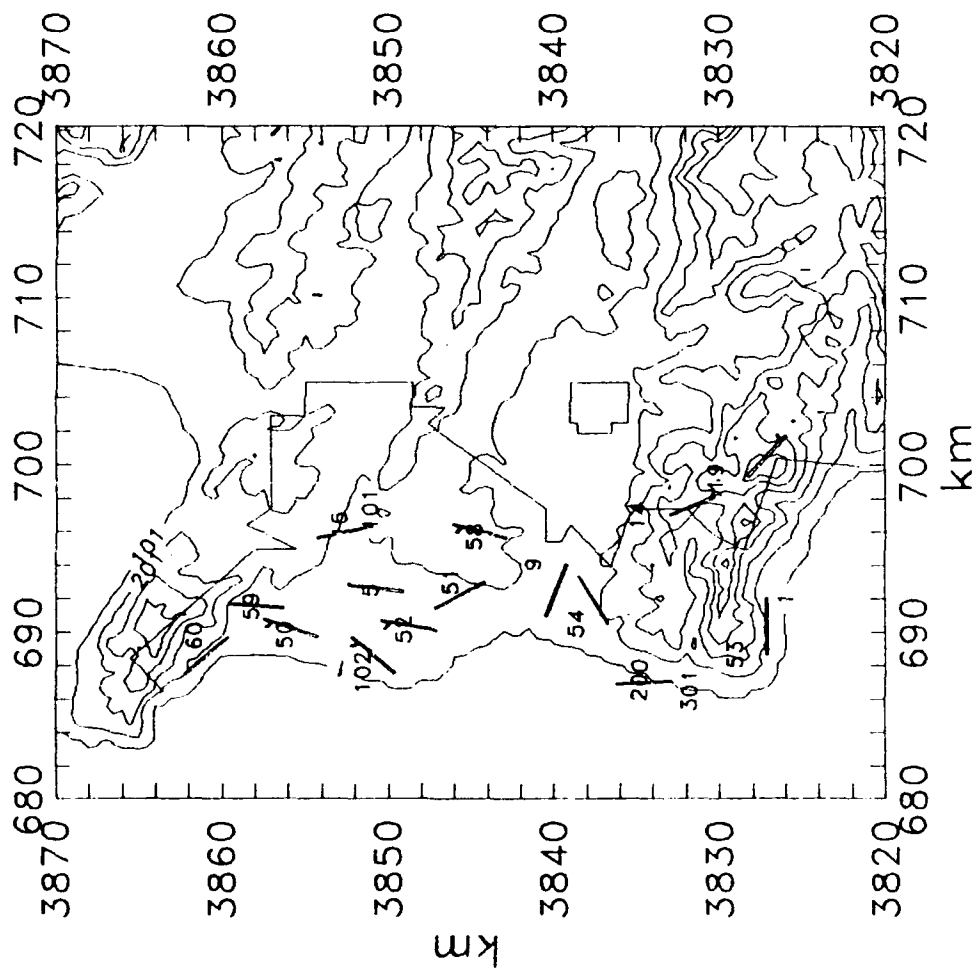
VANDENBERG AFB 10/21/88 01:00



SCALE: 18 km = 1 inch
CONTOUR Interval = 200
BASE MET TOWERS

1 HOUR AVERAGES OF 12FT.WINDS STANDARD NWS WIND BARBS

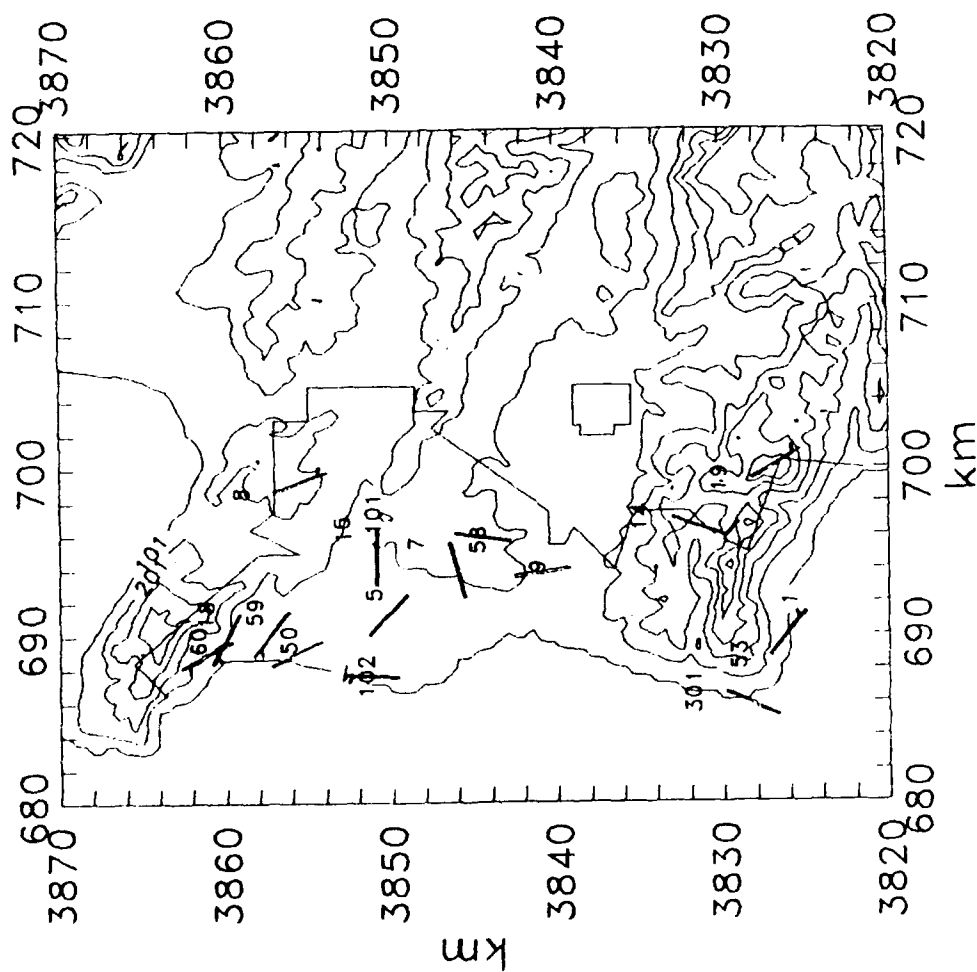
VANDENBERG AFB 10/21/88 04:00



SCALE: 18 km = 1 inch
CONTOUR Interval = 200
BASE MET TOWERS

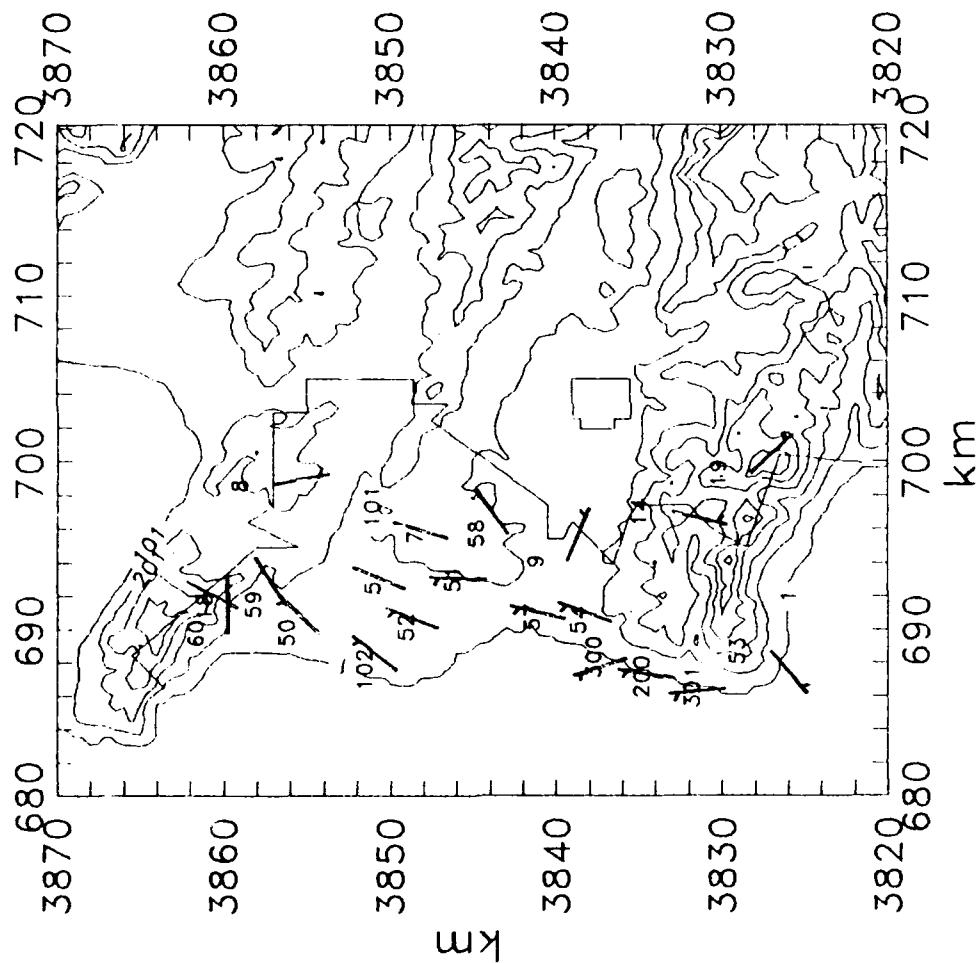
1 HOUR AVERAGES OF 12FT.WINDS STANDARD NWS WIND BARBS

VANDENBERG AFB 10/21/88 07:00



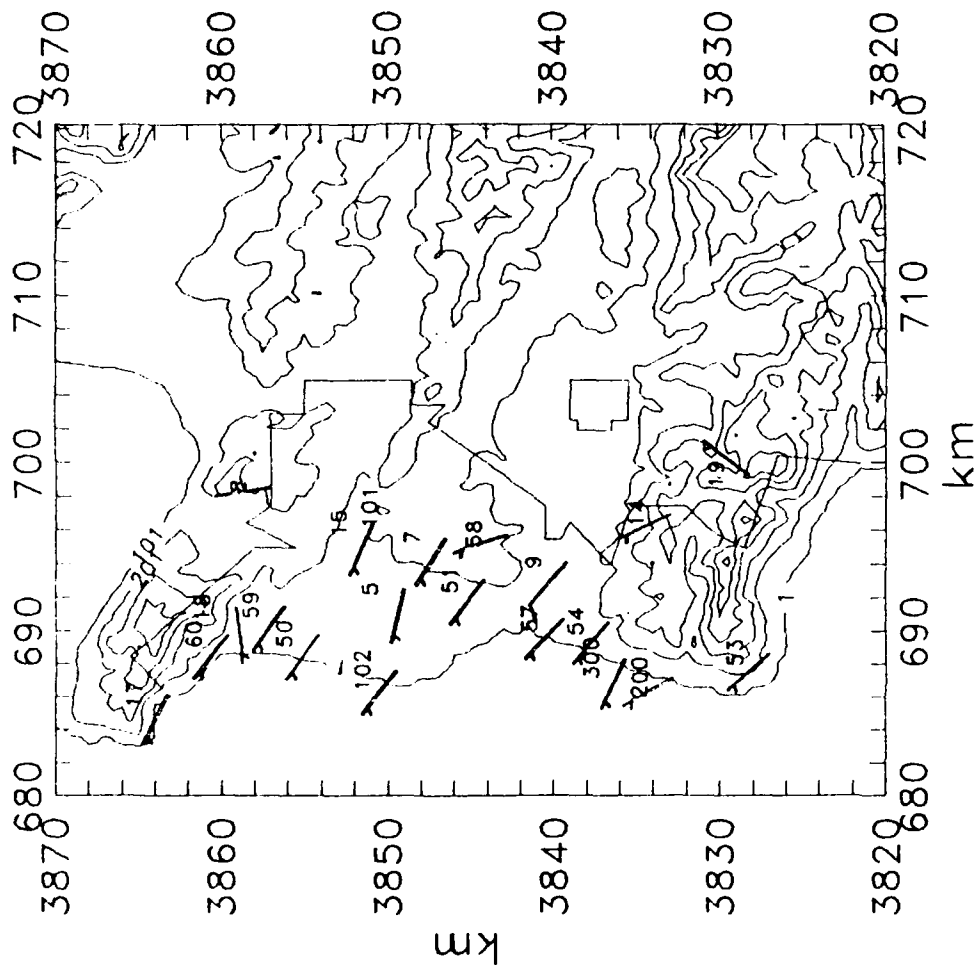
1 HOUR AVERAGES OF 12FT.WINDS STANDARD NWS WIND BARBS

VANDENBERG AFB 10/21/88 10:00



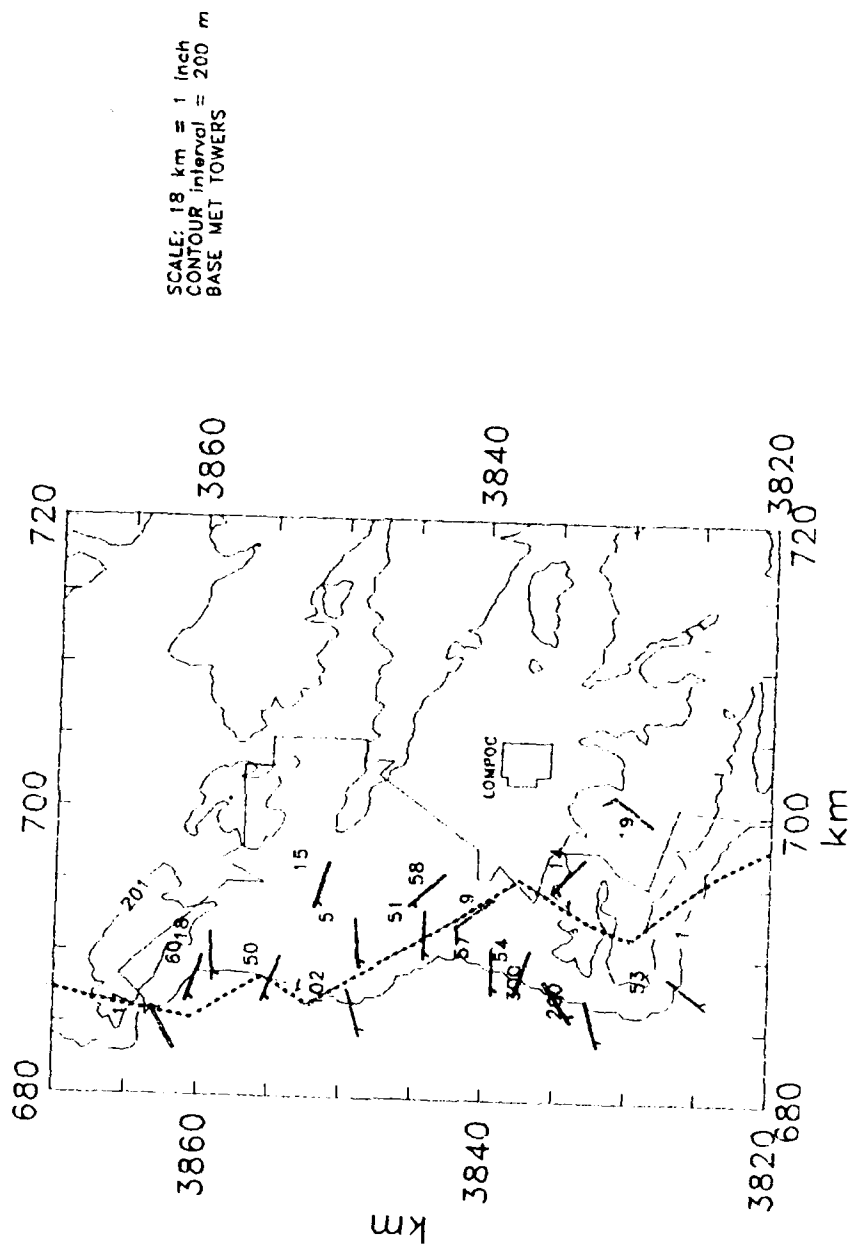
1 HOUR AVERAGES OF 12FT.WINDS STANDARD NWS WIND BARBS

VANDENBERG AFB 10/21/88 13:00



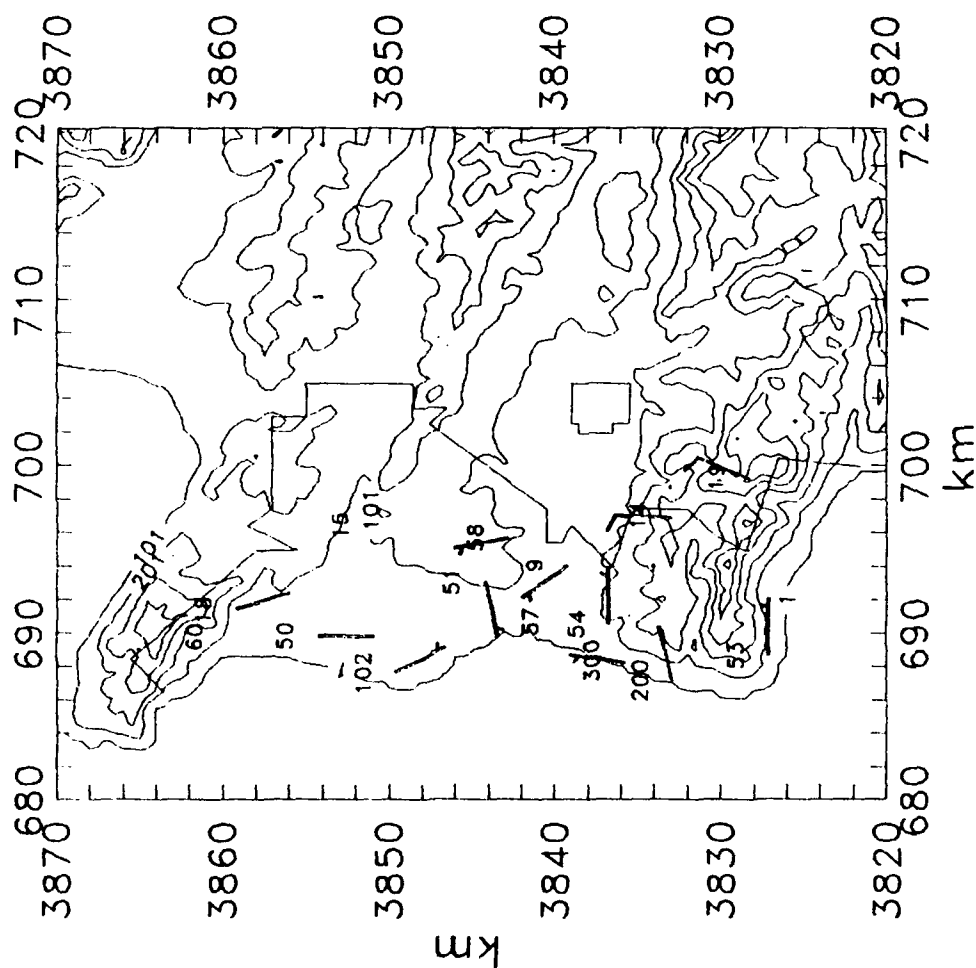
1 HOUR AVERAGES OF 12FT. WINDS WITH APPROXIMATED CLOUD EDGE STANDARD NWS WIND BARBS

VANDENBERG AFB 10/21/88 16:00



1 HOUR AVERAGES OF 12FT.WINDS STANDARD NWS WIND BARBS

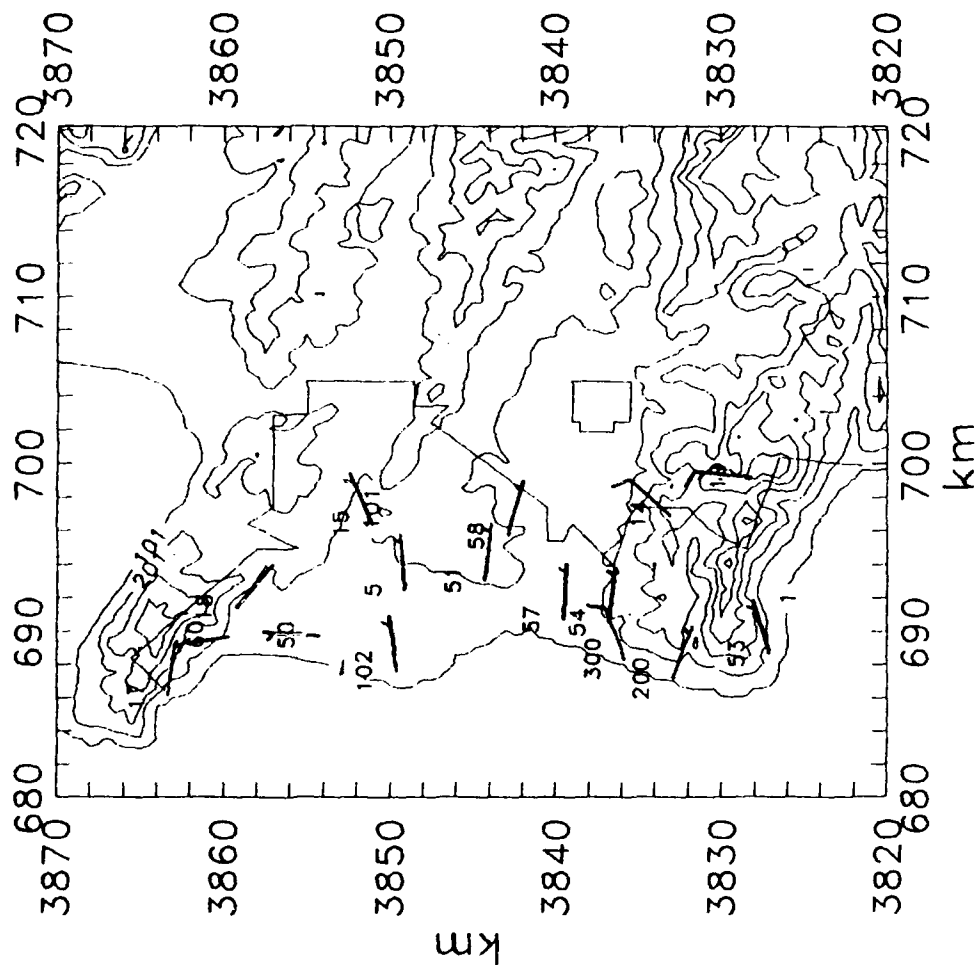
VANDENBERG AFB 10/21/88 19:00



SCALE: 18 km = 1 inch
CONTOUR Interval = 200 r
BASE MET TOWERS

1 HOUR AVERAGES OF 12FT.WINDS STANDARD NWS WIND BARBS

VANDENBERG AFB 10/21/88 22:00



APPENDIX C. RAWINSONDE SUMMARY

During each phase of VBLS, rawinsondes were launched from the NPS mobile laboratory to supplement the base 0Z and 12Z ascents. Some additional base soundes were launched at intermediate times (6,18Z) in support of VBLS. The NPS ascents occurred only during operations, and at times were staggered with the base launches (15,21,03Z). Several launches are missing for a variety of logistical reasons.

A summary of all launches is supplied in the following table. The traditional rawinsonde information has been compressed for this report into a few important quantities relative to the boundary layer. Complete rawinsonde files are available on request. For each ascent, a primary boundary layer scale inversion was identified based on 1) a strong temperature inversion, and 2) a large negative moisture gradient. The inversion bases and tops are identified in the table. In most cases, the inversion base was well-defined by the above criteria. A sharp change in the temperature gradient was not always apparent, and therefore the inversion thicknesses reported can be quite variable. In some instances a surface inversion was present and these ascents can be identified by 0 or very low inversion base heights (i.e. 10-17-88 458 LST). In a few cases, a very shallow surface fog layer resulted in artificially low boundary layers based on the above

definitions (i.e. 5-19-88 1616 LST) In this case we see strong winds through 800 m. The mean potential temperature gradient below, within, and above the inversion was determined by linear regression and those values are also reported in the table. Winds were averaged at several layers through and above the boundary layer and are also supplied in the table.

Day 1. The only evidence of pre-frontal conditions is southerly winds above the boundary layer on 5-16 and 5-17, and abnormally high boundary layer depths. The strongest post-frontal northwesterly winds are seen in the 0,12Z ascents of 5-18. Directions were close to due north through most of the morning, and boundary layer depths had dropped to about 200-300 m. Directions backed to the northwest by the afternoon, which is consistent with the tower observations. The temperature gradients reflect the typical characteristics seen in most of the ascents, namely, a) small positive gradient below the inversion b) a stronger gradient above the inversion, typically twice the value within the inversion, and c) a much stronger gradient within the inversion. Of course, when a surface inversion is present, these characteristics do not apply.

Day 2. Both morning ascents showed low inversions, but the earlier BLDG1764 launch measured strong northwesterly winds below northeasterly winds, while the later launch (near Ocean Park) saw lighter easterly winds through the entire boundary layer. The later launch was more characteristic of the base tower observations which were easterly at that time. Midday ascents are missing. The afternoon inversion depths are most likely artificially low due to an inversion associated with a shallow fog layer in the lower part of the marine boundary layer. The measured winds show fairly moderate flow from 300 deg at heights well above the estimated boundary layer depth listed in the table.

Day 3. Both morning ascents registered easterly winds. Midday ascents were again unsuccessful. The afternoon sonde shows moderate speed southwesterly winds above 100 m, but west-northwesterly below. The southwesterly winds observed by the trailer were evidently quite real.

Day 4. Inversion bases are consistently 300-350 m all day, with tops being much more variable. Winds below the inversion are predictably northwesterly while winds above the inversion are consistently northeasterly, except at 1838 when they were north-northwesterly.

Day 5. Boundary layer depths were similar to day 4. Winds below the inversion were again northwesterly (except at 817 LST), but light northeasterly winds above the inversion developed into strong northwesterly winds later in the afternoon.

Day 6. Inversion bases averaged around 400 m; a bit higher than on day 4 or 5. Winds above the boundary layer were northwesterly during the middle of the day, northeasterly early and late, but again noticeably strong late in the day.

Day 7. Strong speeds continued above the inversion. Some southwesterly flow is observed within the boundary layer, supporting the tower measurements.

Day 8. A surface-based inversion with substantial easterly winds gave way to boundary layer westerlies. Light east winds persisted above. Inversion layer heights were generally higher during all the October days (8-11).

Day 9. Confusingly, the 921 LST ascent shows northeasterly winds while other ascents show northwesterly flow in the boundary layer underneath northeasterly flow above the inversion.

Day 10. Winds above the boundary layer increased from the southeast during the day.

Day 11. Southeasterly flow above the boundary layer persisted in the morning, but backed to northeasterly in the afternoon.

RAWINDSONDE SUMMARY

KEY

time(LST) lat(min, add 45 deg) lon(min, add 45 deg) ID
altitude of inversion base (m) inversion top (m)
wind level 1: 50-100m [spd (m/s) dir(deg) # in ave]
wind level 2: 100-200m
wind level 3: 200-400m
wind level 4: 400-800m
wind level 5: inv base - inv top
wind level 6: inv top - 2000m
pot temp gradient layer 1: 50m-inv base [dK/dz (deg/m) #]
pot temp gradient layer 2: inv base-inv top
pot temp gradient layer 1: inv top- 2000 m

PHASE I

5-15-88

1701 39.90 34.60 BLDG900
436.6 680.5
1 6.2 308 1
2 5.7 307 2
3 3.9 297 3
4 3.9 177 6
5 3.8 181 5
6 2.7 168 21
1 0.002721505
2 0.054879535
3 0.006902346

5-16-88

416 39.90 34.60 BLDG900
680.5 924.3
1 2.1 337 1
2 3.6 346 2
3 5.1 348 3
4 4.5 328 6
5 2.8 277 5
6 4.3 210 17
1 0.002163185
2 0.044018336
3 0.007281816

1617 39.90 34.60 BLDG900
680.5 863.4
1 11.3 311 1
2 10.5 313 2
3 10.1 317 3
4 8.5 321 6
5 7.2 323 4
6 5.2 324 18
1 0.006311925
2 0.026504142
3 0.006058210

5-17-88

435 39.90 34.60 BLDG900
1351.0 1473.0
1 8.2 313 1
2 10.8 316 2
3 12.7 317 3
4 9.7 325 6
5 7.2 352 3
6 7.2 323 8
1 0.006040988
2 0.020580646
3 0.008613952

1715 39.90 34.60 BLDG900
436.6 558.6
1 15.9 316 1
2 19.8 321 2
3 20.2 322 3
4 17.2 326 6
5 18.5 324 3
6 13.9 355 23
1 -0.000410089
2 0.024916437
3 0.005563175

5-18-88

418 45.20 34.30 BLDG1764
204.8 326.7
1 14.9 347 1
2 14.9 352 1
3 15.0 5 4
4 15.7 19 6
5 14.9 3 3
6 15.5 13 27
1 0.018829813
2 0.019780723
3 0.008081360

5-19-88

855 48.00 37.00 NPS1
123.0 299.0
1 8.6 342 1
2 8.7 357 2
3 10.3 21 4
4 13.9 22 12
5 9.0 6 4
6 14.3 15 26
1 0.016234720
2 0.016464403
3 0.008281155

1310 37.00 33.00 NPS2
240.0 260.0
1 14.2 347 2
2 11.6 347 5
3 15.1 10 6
4 15.8 11 20
5 14.4 348 3
6 13.3 4 60
1 -99.000000000
2 0.139443204
3 0.005815701

1620 39.90 34.60 BLDG900
192.8 253.8
1 15.9 318 1
2 15.9 319 2
3 13.9 328 3
4 11.3 350 6
5 15.4 322 2
6 12.1 356 28
1 0.002348078
2 0.099089183
3 0.006814676

1929 37.00 37.00 NPS3
369.0 531.0
1 -99.0 -99 0
2 9.0 345 2
3 16.3 343 2
4 19.8 342 7
5 20.6 343 3
6 14.6 0 29
1 0.002342449
2 0.043756895
3 0.005509665

415 45.20 34.30 BLDG1764
21.9 143.8
1 8.2 345 1
2 8.7 358 1
3 10.8 24 4
4 12.3 37 6
5 6.8 349 3
6 9.6 45 30
1 -99.000000000
2 0.068167880
3 0.007891931

901 42.00 37.00 NPS4
134.0 259.0
1 1.8 43 1
2 2.5 40 2
3 5.0 42 3
4 3.2 70 7
5 3.2 39 3
6 4.3 123 33
1 0.009748494
2 0.051626459
3 0.006451678

1616 39.90 34.60 BLDG900
70.9 192.8
1 5.7 304 1
2 5.9 305 2
3 5.1 305 3
4 5.7 306 6
5 5.8 305 3
6 3.0 299 29
1 -99.000000000
2 0.049272105
3 0.003877331

1849 37.00 37.00 NPS6
0.0 278.0
1 2.7 352 1
2 2.7 352 1
3 4.2 346 3
4 4.4 304 6
5 3.3 351 5
6 3.9 302 10
1 -99.000000000
2 0.023571745
3 0.007703546

1617 39.90 34.60 BLDG900
 296.0 860.0
 1 5.7 301 1
 2 -99.0 -99 0
 3 3.4 300 3
 4 2.7 299 4
 5 2.7 306 7
 6 2.7 31 5
 1 0.003762733
 2 0.054732408
 3 0.020200744

817 42.00 37.00 NPS11
 382.0 834.0
 1 1.7 12 1
 2 1.7 12 1
 3 1.4 8 3
 4 1.8 26 4
 5 1.9 25 6
 6 1.2 34 15
 1 0.004108039
 2 0.037489880
 3 0.006158609

1838 40.00 24.00 NPS10
 295.0 461.0
 1 5.0 287 1
 2 5.0 287 1
 3 3.0 297 3
 4 3.4 301 6
 5 2.1 300 3
 6 4.6 349 27
 1 0.010068609
 2 0.036884766
 3 0.008214938

1115 45.20 34.30 BLDG1764
 326.0 505.0
 1 -99.0 -99 0
 2 -99.0 -99 0
 3 1.8 302 2
 4 1.8 21 5
 5 1.4 6 4
 6 2.2 3 8
 1 -99.000000000
 2 0.024095105
 3 0.010316370

2300 45.20 34.30 BLDG1764
 292.0 363.0
 1 -99.0 -99 0
 2 -99.0 -99 0
 3 3.1 338 4
 4 7.5 357 6
 5 2.6 334 2
 6 6.4 4 11
 1 0.002413410
 2 0.073837824
 3 0.024102438

1617 39.90 34.60 BLDG900
 278.0 769.0
 1 -99.0 -99 0
 2 5.7 291 1
 3 2.7 250 4
 4 4.5 300 3
 5 3.3 281 6
 6 5.9 333 5
 1 0.031069892
 2 0.033402637
 3 0.027121533

7-27-88

415 45.20 34.30 BLDG1764
 295.0 993.0
 1 -99.0 -99 0
 2 -99.0 -99 0
 3 1.4 318 3
 4 2.4 36 4
 5 2.0 26 7
 6 3.6 50 3
 1 0.002091930
 2 0.035676755
 3 0.019577375

1910 39.00 35.00 NPS12
 201.0 312.0
 1 1.6 291 1
 2 1.0 322 1
 3 1.8 25 4
 4 9.9 334 7
 5 1.5 39 3
 6 7.0 339 39
 1 0.002955826
 2 0.035193607
 3 0.009037850

PHASE II

5-20-88

415 45.20 34.30 BLDG1764
0.3 143.8
1 2.6 41 1
2 3.6 74 1
3 3.7 76 4
4 3.3 78 6
5 2.0 46 4
6 1.7 65 30
1 -99.000000000
2 0.107472859
3 0.002737669

843 42.00 37.00 NPS7
143.0 287.0
1 1.4 63 1
2 1.9 90 1
3 1.8 150 6
4 1.8 148 9
5 1.9 116 4
6 0.6 121 39
1 0.020232532
2 0.076009475
3 0.002460221

1619 39.90 34.60 BLDG900
70.9 253.8
1 4.1 290 1
2 4.1 242 2
3 2.7 241 3
4 2.0 241 6
5 3.6 254 4
6 3.0 205 28
1 -99.000000000
2 0.063837446
3 0.003349708

5-21-88 no ascents

5-22-88

417 45.20 34.30 BLDG1764
82.9 204.8
1 4.6 349 1
2 3.6 354 1
3 6.3 1 4
4 8.6 355 6
5 4.4 355 3
6 6.0 360 29
1 -99.000000000
2 0.112796374
3 0.005257996

7-26-88

415 45.20 34.30 BLDG1764
358.0 686.0
1 -99.0 -99 0
2 -99.0 -99 0
3 4.2 344 5
4 4.8 32 5
5 4.6 23 5
6 4.5 41 5
1 0.014670197
2 0.112909354
3 0.012839460

844 42.00 37.00 NPS8
365.0 618.0
1 -99.0 -99 0
2 -99.0 -99 0
3 -99.0 -99 0
4 -99.0 -99 0
5 -99.0 -99 0
6 -99.0 -99 0
1 0.005178778
2 0.032726314
3 0.021180848

1115 45.20 34.30 BLDG1764
292.0 1011.0
1 -99.0 -99 0
2 3.6 318 1
3 0.7 301 4
4 0.9 125 2
5 1.1 50 7
6 4.9 27 4
1 0.009303593
2 0.028639866
3 0.023484273

1438 47.00 36.00 NPS9
315.0 408.0
1 5.5 308 1
2 5.5 308 1
3 3.7 300 3
4 1.9 264 10
5 2.8 292 3
6 2.5 31 38
1 0.003475922
2 0.061543476
3 0.009059073

1617 39.90 34.60 BLDG900
 296.0 860.0
 1 5.7 301 1
 2 -99.0 -99 0
 3 3.4 300 3
 4 2.7 299 4
 5 2.7 306 7
 6 2.7 31 5
 1 0.003762733
 2 0.054732408
 3 0.020200744

1838 40.00 24.00 NPS10
 295.0 461.0
 1 5.0 287 1
 2 5.0 287 1
 3 3.0 297 3
 4 3.4 301 6
 5 2.1 300 3
 6 4.6 349 27
 1 0.010068609
 2 0.036884766
 3 0.008214938

2300 45.20 34.30 BLDG1764
 292.0 363.0
 1 -99.0 -99 0
 2 -99.0 -99 0
 3 3.1 338 4
 4 7.5 357 6
 5 2.6 334 2
 6 6.4 4 11
 1 0.002413410
 2 0.073837824
 3 0.024102438

7-27-88

415 45.20 34.30 BLDG1764
 295.0 993.0
 1 -99.0 -99 0
 2 -99.0 -99 0
 3 1.4 318 3
 4 2.4 36 4
 5 2.0 26 7
 6 3.6 50 3
 1 0.002091930
 2 0.035676755
 3 0.019577375

817 42.00 37.00 NPS11
 382.0 834.0
 1 1.7 12 1
 2 1.7 12 1
 3 1.4 8 3
 4 1.8 26 4
 5 1.9 25 6
 6 1.2 34 15
 1 0.004108039
 2 0.037489880
 3 0.006158609

1115 45.20 34.30 BLDG1764
 326.0 505.0
 1 -99.0 -99 0
 2 -99.0 -99 0
 3 1.8 302 2
 4 1.8 21 5
 5 1.4 6 4
 6 2.2 3 8
 1 -99.000000000
 2 0.024095105
 3 0.010316370

1617 39.90 34.60 BLDG900
 278.0 769.0
 1 -99.0 -99 0
 2 5.7 291 1
 3 2.7 250 4
 4 4.5 300 3
 5 3.3 281 6
 6 5.9 333 5
 1 0.031069892
 2 0.033402637
 3 0.027121533

1910 39.00 35.00 NPS12
 201.0 312.0
 1 1.6 291 1
 2 1.0 322 1
 3 1.8 25 4
 4 9.9 334 7
 5 1.5 39 3
 6 7.0 339 39
 1 0.002955826
 2 0.035193607
 3 0.009037850

2318 45.20 34.30 BLDG1764
 286.0 378.0
 1 -99.0 -99 0
 2 -99.0 -99 0
 3 3.4 358 3
 4 8.7 350
 5 3.6 360 2
 6 7.8 356 13
 1 0.003610925
 2 0.050068304
 3 0.034445703

7-28-88

422 45.20 34.30 BLDG1764
 423.0 500.0
 1 -99.0 -99 0
 2 -99.0 -99 0
 3 1.5 332 1
 4 4.8 12 7
 5 3.1 1 2
 6 4.4 18 10
 1 -99.000000000
 2 0.057748981
 3 0.038081255

612 45.20 34.30 BLDG1764
 398.0 608.0
 1 -99.0 -99 0
 2 -99.0 -99 0
 3 3.1 329 2
 4 3.8 353 5
 5 3.7 349 5
 6 2.7 358 7
 1 0.003812287
 2 0.066672966
 3 0.041158784

828 42.00 37.00 NPS13
 466.0 776.0
 1 1.5 287 1
 2 1.5 287 1
 3 1.2 328 3
 4 2.5 343 6
 5 2.5 343 6
 6 3.6 322 22
 1 0.005645065
 2 0.037096959
 3 0.006836438

1345 41.00 25.00 NPS14
 374.0 656.0
 1 -99.0 -99 0
 2 4.9 277 2
 3 1.9 303 3
 4 2.3 326 4
 5 2.0 326 5
 6 -99.0 -99 0
 1 0.012312022
 2 0.037374020
 3 0.003940130

1853 47.00 35.00 NPS15
 300.0 556.0

1 5.5 337 1
 2 5.5 337 1
 3 5.1 335 3
 4 9.5 325 6
 5 7.7 326 5
 6 7.9 359 24
 1 0.005754062
 2 0.057994936
 3 0.004316492

7-29-88

814 42.00 37.00 NPS16
 365.0 653.0
 1 -99.0 -99 0
 2 0.9 255 2
 3 1.7 278 2
 4 6.0 348 6
 5 4.7 338 5
 6 8.0 346 21
 1 0.005069630
 2 0.042208858
 3 0.007957227

1300 42.00 37.00 NPS17
 293.0 483.0
 1 4.3 234 1
 2 1.9 252 1
 3 1.7 9 3
 4 16.4 39 7
 5 7.1 33 4
 6 9.8 33 29
 1 0.004528219
 2 0.079094797
 3 0.004906616

PHASE III

10-17-88

458	45.20	34.30	BLDG1764
9.0	1437.0		
1	5.1	47	1
2	6.3	33	3
3	7.2	29	1
4	6.9	16	2
5	5.9	25	10
6	4.6	8	3
1	-99.0000000000		
2	0.125237554		
3	0.006467601		

1634	45.20	34.30	BLDG1764
97.0	667.0		
1	4.1	270	1
2	0.5	238	1
3	0.0	90	1
4	1.1	74	5
5	0.2	349	7
6	1.3	63	5
1	-99.0000000000		
2	0.017202253		
3	0.028624199		

1615	39.90	34.60	BLDG900
156.0	575.0		
1	-99.0	-99	0
2	5.1	291	3
3	6.3	311	3
4	6.3	312	3
5	5.6	306	7
6	3.2	353	5
1	-0.061457656		
2	0.007242643		
3	0.043639883		

10-19-88

415	45.20	34.30	BLDG1764
476.0	694.0		
1	-99.0	-99	0
2	-99.0	-99	0
3	5.7	342	1
4	4.9	359	8
5	5.0	0	6
6	4.7	342	7
1	0.003109308		
2	0.054500066		
3	0.032767098		

10-18-88

415	45.20	34.30	BLDG1764
114.0	964.0		
1	-99.0	-99	0
2	3.6	110	1
3	-99.0	-99	0
4	3.3	63	3
5	3.1	75	4
6	3.6	9	5
1	0.145750195		
2	0.013394055		
3	0.019030560		

921	70.00	60.00	NPS19
606.0	735.0		
1	2.7	13	1
2	4.8	17	2
3	6.7	19	3
4	3.7	13	6
5	2.4	5	2
6	6.5	2	20
1	0.004137570		
2	0.031811461		
3	0.014162015		

1352	75.00	42.00	NPS18
648.0	709.0		
1	-99.0	-99	0
2	4.8	337	2
3	6.1	13	4
4	4.6	37	6
5	2.6	60	1
6	1.2	90	30
1	0.009138033		
2	0.034084778		
3	0.008130382		

1448	73.00	43.00	NPS20
620.0	754.0		
1	-99.0	-99	0
2	3.3	342	2
3	4.5	349	3
4	4.6	343	8
5	4.0	322	2
6	8.1	20	33
1	0.002948154		
2	0.064862214		
3	0.006034677		

1615 39.90 34.60 BLDG900

436.0 732.0
1 5.1 318 1
2 -99.0 -99 0
3 4.1 325 1
4 7.0 344 5
5 7.0 344 5
6 8.5 12 5
1 0.003804461
2 0.027701532
3 0.054084536

1721 73.00 43.00 NPS21

829.0 876.0
1 -99.0 -99 0
2 2.2 290 2
3 6.2 318 3
4 12.6 341 8
5 9.4 328 1
6 8.1 12 30
1 0.014151054
2 0.047875557
3 0.005475321

10-20-88

854 67.00 60.00 NPS22

609.0 722.0
1 1.1 1 1
2 1.7 27 2
3 2.3 45 3
4 1.0 90 7
5 0.8 110 2
6 2.2 123 32
1 0.004488475
2 0.062435843
3 0.009417715

1432 62.00 60.00 NPS23

489.0 652.0
1 2.0 315 1
2 0.6 252 3
3 2.1 173 3
4 2.6 37 8
5 3.2 34 4
6 4.7 133 32
1 0.003655353
2 0.031780027
3 0.009253933

1702 39.90 34.60 BLDG900

595.0 1234.0
1 -99.0 -99 0
2 -99.0 -99 0
3 1.1 206 2
4 2.9 123 5
5 6.7 136 5
6 8.3 148 3
1 0.017604982
2 0.076762907
3 0.002678822

10-21-88

416 45.20 34.30 BLDG1764

466.0 1180.0
1 -99.0 -99 0
2 -99.0 -99 0
3 1.0 90 1
4 2.3 120 6
5 2.4 131 8
6 3.7 151 3
1 0.018747339
2 0.024288615
3 0.002488173

834 67.00 60.00 NPS24

686.0 769.0
1 1.2 249 1
2 1.6 233 2
3 2.2 216 3
4 3.1 86 6
5 5.4 68 1
6 3.6 112 29
1 0.003795173
2 0.053815290
3 0.008181449

1410 67.00 60.00 NPS25

720.0 835.0
1 -99.0 -99 0
2 2.6 315 2
3 3.2 333 3
4 2.7 345 6
5 1.0 342 2
6 2.3 46 27
1 -0.005126198
2 0.061560191
3 0.004228873

1615 45.20 34.30 BLDG1764

438.0 846.0
1 -99.0 -99 0
2 -99.0 -99 0
3 2.0 335 2
4 1.6 358 5
5 1.9 2 6
6 2.9 29 5
1 0.026466327
2 0.058049399
3 0.037502192

APPENDIX D. TRANSECT SUMMARY

The following tables are a condensation of the mobile laboratory data. The first table lists the locations sampled, coordinates, and location codes which are referred to in the following tables as "LC".

site code	MSL (m)	lat	lon	location
1	62	34.783	120.600	Abresa/13th
2	20	34.850	120.583	018 Pt Sal/Rancho Levy
3	41	34.800	120.597	WT050
4	5	34.772	120.583	El Rancho/Rancho Levy
5	100	34.753	120.570	WT005
6	137	34.733	120.583	WSMC HQ
7	90	34.775	120.490	#7 San Antonio/Vandenberg
8	110	34.762	120.453	#6 Site 6
9	110	34.758	120.428	#5 Old 1/site 5
10	270	34.735	120.438	#4 Old 1/below ridge
11	200	34.722	120.435	#3 Old 1/Oil fields
12	165	34.710	120.435	#2 Old 1/Rucker
13	324	34.728	120.442	#13 Old 1/just below ridge
14	324	34.727	120.442	#14 Old 1/just below ridge
15	85	34.683	120.452	#1 Old 1/hill base
16	43	34.677	120.445	#19 La Purisma by Lompoc/Casmalia Hwy
17	114	34.697	120.537	WT058 by 13th
18	6	34.690	120.600	Ocean Park
19	7	34.675	120.582	1/2 Park Gate
20	10	34.670	120.562	South Gate
21	9	34.665	120.553	WT009
22	11	34.662	120.535	Central/Union
23	18	34.660	120.502	Central/Leege
24	15	34.662	120.505	Douglas/246
25	22	34.638	120.482	Bailey/246
26	23	34.638	120.478	Lompoc City limit/246
27	28	34.637	120.458	Cypress/south I
28	33	34.645	120.430	River Park
29	40	34.622	120.428	Santa Rosa/Hwy 1
30	25	34.667	120.420	La Purisma shortcut
31	122	34.673	120.372	#20 246 past golf course
32	146	34.665	120.330	Campbell Rd West
33	171	34.652	120.313	Campbell Rd East
34	70	34.583	120.410	#27 Jalama W of Cabrillo
35	240	34.590	120.480	#28 Miguelito
36	140	34.595	120.467	#29 Miguelito upcanyon
37	146	34.567	120.365	#21 Cabrillo S of Jalama
38	210	34.527	120.412	#26 Jalama
39	330	34.528	120.390	#22 Jalama
40	100	34.510	120.453	#23 Jalama
41	80	34.517	120.472	#24 Jalama
42	100	34.512	120.463	#25 Jalama

43	10	34.510	120.500	Jalama Beach
44	329	34.612	120.563	WT101 turnout
45	442	34.608	120.527	WT014
46	135	34.645	120.585	SLC 3 Bear Creek
47	50	34.637	120.622	SLC 4 Surf
48	30	34.612	120.632	SLC 5
49	120	34.578	120.633	SLC 6
50	652	34.583	120.562	WT056
51	7	34.680	120.577	Bend in 246 OP-SG
52	120	34.618	120.403	Santa Rosa #1
53	200	34.608	120.338	Santa Rosa #2
54	150	34.640	120.572	Arguello/Bear Creek
55	70	34.563	120.625	Sudden Ranch Gate
56	60	34.562	120.612	Boathouse
57	40	34.562	120.558	VABM89 near BH
58	60	34.655	120.612	Bear Creek/Surf
59	130	34.660	120.560	VHF/Santa Ynez
60	11	34.655	120.537	Union/246
61	13	34.645	120.523	Bend in 246
62	25	34.650	120.470	Chestnut/Pine
63	220	34.613	120.615	OS62/Hilda (SLC5)
64	45	34.782	120.523	#8 San Antonio Rd/Canyon
65	45	34.672	120.448	La Purisma Flower Field
66	25	34.660	120.447	A St & Laurel
67	110	34.665	120.400	La Purisma Golf Course
68	130	34.665	120.367	Hapgoode & 246
69	130	34.635	120.287	Mail Rd & 246
70	12	34.662	120.526	Artesia/Central
71	22	34.662	120.482	Bailey/Central
72	25	34.660	120.455	H/Central
73	140	34.665	120.374	Tularisa/246 Ridge Top
74	20	34.842	120.588	Pt Sal/Rancho Levy
75	100	34.833	120.571	Astral/Rancho Levy
76	90	34.793	120.563	Arian/Rancho Levy
77	25	34.773	120.571	El Rancho Lateral
78	10	34.683	120.545	13th/Terra
79	25	34.777	120.566	Utah Gate
80	75	34.782	120.568	Umbra/Rancho Levy
81	92	34.815	120.542	Briesa/El Rancho
82	50	34.775	120.569	Fire Station/El Rancho 4
83	122	34.665	120.383	golf course/Hapgoode/246
84	110	34.620	120.250	Map edge/246
85	21	34.638	120.492	Between Bailey & Leege/246
86	320	34.710	120.278	#10 Drum Canyon (Mail)
87	170	34.730	120.280	#11 Drum Canyon
88	210	34.752	120.317	#12
89	100	34.767	120.423	San Antonio/Old Rte 1
90	260	34.730	120.441	#13 near Top of Route 1
91	270	34.728	120.441	#14 back of ridge Old Rte 1
92	23	34.662	120.473	Central/V
93	72	34.590	120.407	Jalama/Cabrillo (Rte 1)
94	180	34.528	120.343	Cabrillo/San Julian (Rte 1)
95	30	34.682	120.603	Tank Farm/Surf
96	80	34.605	120.633	Honda Cyn 1/2mile inland

97	260	34.689	120.294	Mail Rd #8
98	290	34.705	120.293	Mail Rd #9

The next table lists average values for each visit to a particular location. TIME is in Pacific Daylight. DT is the length of the visit (minutes). TP is the time period where 1 is before the "first transition" (before the sea breeze front has passed over all base towers), 2 is the semi-stationary sea breeze period, and 3 is after the "second transition" (after rapid veering occurs near dusk). Ubar is the surface wind speed (m/s) at 3.8 m for May or 4.9 m for July/October. Tbar is air temperature at 3.4 m. BL1 is "boundary layer #1" and BL2 is "boundary layer #2" (m). See VBLS Final Report - Results for further explanations.

5-18-88

LC	TIME	TP	DT	Ubar	Tbar	BL1	BL2
1	904	70	2	5.0	285.7	306.5	356.3
5	924	10	2	4.7	286.8	-99.0	389.8
6	954	30	2	3.4	287.8	271.1	352.5
17	1024	30	2	3.8	288.8	274.5	376.3
20	1054	30	2	4.9	288.6	147.3	407.3
44	1114	20	2	9.8	286.2	244.0	-99.0
45	1340	50	2	7.6	285.9	223.4	547.2
44	1410	20	2	6.0	287.0	334.2	-99.0
20	1500	40	2	5.5	288.8	114.6	371.4
46	1540	30	2	4.2	288.0	322.1	787.9
47	1610	20	2	-99.0	-99.0	67.8	324.7
48	1700	20	2	2.3	-99.0	127.2	-99.0
49	1730	20	2	-99.0	-99.0	191.6	515.3

5-19-88

LC	TIME	TP	DT	Ubar	Tbar	BL1	BL2
18	949	15	1	1.2	287.4	107.2	202.4
51	1008	10	1	2.9	290.6	193.6	302.3
24	1040	20	1	3.2	294.0	271.4	804.1
27	1055	5	1	1.6	-99.0	141.6	835.4
27	1100	5	2	1.4	-99.0	127.3	791.1
52	1130	10	2	-99.0	-99.0	182.0	730.3
53	1240	45	2	-99.0	-99.0	111.3	728.7
26	1451	10	2	5.7	296.4	259.2	327.2
24	1501	5	2	5.4	296.8	245.7	-99.0
21	1511	5	2	2.1	296.0	272.8	320.4
18	1526	10	2	2.2	-99.0	225.6	280.0
54	1550	10	2	2.6	294.5	193.1	-99.0
44	1605	5	2	3.6	296.9	183.0	-99.0
46	1620	10	2	1.9	290.5	240.6	-99.0
47	1635	10	2	1.3	289.1	176.2	-99.0

55	1700	5	2	4.5	295.6	162.7	-99.0
56	1720	15	2	6.3	297.9	154.2	266.4
57	1745	10	2	7.2	299.7	110.0	293.6
96	1855	30	2	-99.0	-99.0	324.9	412.6

5-20-88

LC	TIME	TP	DT	Ubar	Tbar	BL1	BL2
18	915	30	1	-99.0	-99.0	69.2	315.4
47	1000	5	2	1.4	287.8	262.5	-99.0
58	1010	5	2	1.3	288.1	287.5	-99.0
46	1020	5	2	1.4	289.0	212.5	-99.0
54	1030	5	2	2.6	290.2	262.5	-99.0
59	1040	5	2	1.9	291.3	162.5	-99.0
21	1055	10	2	3.9	289.1	395.4	-99.0
60	1105	10	2	3.8	291.7	174.5	293.4
61	1115	10	2	5.6	289.6	228.9	320.6
24	1125	10	2	5.8	289.5	238.2	-99.0
26	1135	10	2	-99.0	-99.0	223.8	-99.0
62	1230	5	2	2.2	-99.0	239.2	327.6
18	1320	35	2	2.3	289.5	73.1	300.4
47	1350	10	2	-99.0	-99.0	69.2	300.2
63	1430	25	2	-99.0	-99.0	240.8	228.7
54	1610	5	2	4.1	292.6	151.5	212.6
59	1620	5	2	2.9	292.9	163.8	233.1
21	1630	5	2	3.2	-99.0	261.7	-99.0
24	1640	5	2	-99.0	-99.0	225.0	245.4

7-26-88

LC	TIME	TP	DT	Ubar	Tbar	BL1	BL2
18	1005	90	1	2.2	287.3	91.5	478.9
21	1035	10	1	3.2	289.3	218.1	469.5
23	1055	10	1	-99.0	-99.0	282.0	424.6
66	1120	15	2	-99.0	-99.0	554.4	557.0
67	1145	10	2	-99.0	-99.0	561.7	592.2
68	1205	10	2	-99.0	-99.0	536.6	-99.0
1	1515	55	2	3.2	290.1	412.2	542.3
5	1540	10	2	-99.0	-99.0	429.7	633.4
17	1600	10	2	-99.0	-99.0	485.7	608.0
20	1620	15	2	3.9	291.2	386.8	516.1
54	1645	15	2	3.1	290.2	333.9	476.3
44	1705	10	2	-99.0	-99.0	266.7	353.3
18	1740	10	2	2.9	288.3	210.8	588.0
23	1805	10	2	5.3	290.3	515.0	672.5
67	1840	20	2	-99.0	-99.0	530.6	617.0
69	1900	10	2	-99.0	-99.0	638.5	694.6

7-27-88

LC	TIME	TP	DT	Ubar	Tbar	BL1	BL2
18	900	25	1	1.1	287.7	225.8	504.3
51	920	10	1	1.3	287.7	240.6	504.4
21	935	10	1	1.0	-99.0	179.7	510.1

70	950	10	1	1.6	288.0	144.4	505.9
23	1005	10	1	1.6	288.1	215.1	479.2
71	1025	15	1	2.1	288.5	169.3	452.1
72	1045	15	1	2.1	288.3	329.1	452.3
65	1055	5	1	-99.0	-99.0	498.0	-99.0
65	1105	10	2	3.0	292.0	501.3	557.3
30	1120	10	2	3.3	289.6	479.5	560.8
73	1145	15	2	-99.0	-99.0	532.7	577.7
68	1205	10	2	-99.0	-99.0	432.5	673.7
33	1245	10	2	3.4	-99.0	541.2	683.6
69	1305	15	2	5.9	-99.0	609.8	575.1
74	1445	10	2	3.6	-99.0	464.4	535.6
75	1510	20	2	3.7	289.5	407.8	509.4
76	1525	10	2	3.5	289.9	393.4	525.7
77	1545	15	2	-99.0	323.2	426.3	571.8
5	1600	10	2	3.0	292.6	433.2	565.9
6	1625	15	2	3.9	290.5	429.9	569.4
17	1640	10	2	4.2	289.5	520.3	643.8
78	1705	20	2	4.1	291.4	403.5	574.2
20	1730	20	2	3.9	289.7	373.8	509.6
54	1750	15	2	2.7	288.7	201.2	386.4
44	1810	10	3	3.0	288.3	243.7	453.7
45	1835	15	3	2.7	287.3	380.1	406.4
54	1915	25	3	1.9	287.7	176.3	415.0

7-28-88

LC	TIME	TP	DT	Ubar	Tbar	BL1	BL2
18	1030	55	1	1.6	287.6	120.5	549.8
24	1055	15	1	1.5	287.8	289.8	548.1
26	1110	10	2	-99.0	-99.0	307.1	552.1
27	1200	45	2	2.0	289.4	405.4	545.2
28	1230	20	2	-99.0	-99.0	506.4	684.8
30	1255	20	2	-99.0	-99.0	432.7	633.2
21	1530	45	2	5.3	287.5	556.3	644.2
20	1545	10	2	3.4	290.9	347.2	525.0
18	1605	15	2	-99.0	-99.0	103.8	550.4
79	1715	10	2	2.4	290.5	429.0	546.0
3	1740	10	2	3.2	289.6	241.0	393.6
80	1755	10	2	3.3	289.4	271.3	444.2
81	1825	15	3	-99.0	-99.0	154.8	474.9
82	1855	20	3	-99.0	-99.0	162.4	389.2

7-29-88

LC	TIME	TP	DT	Ubar	Tbar	BL1	BL2
18	825	30	1	1.9	286.9	239.7	537.0
21	845	10	1	1.5	287.3	139.1	533.7
23	900	10	1	-99.0	-99.0	154.4	494.4
28	925	15	1	-99.0	-99.0	270.2	525.8
67	945	10	1	-99.0	-99.0	274.2	495.3
83	1000	10	1	-99.0	-99.0	368.6	501.5
68	1015	10	1	1.5	290.0	388.4	439.3
32	1035	15	1	1.8	288.2	490.1	585.8

33	1050	10	1	2.2	289.3	393.9	652.6
84	1120	10	2	2.8	294.8	296.7	627.1
25	1205	15	2	2.9	292.5	433.0	595.8
21	1225	10	2	4.2	289.6	424.5	607.6
18	1305	30	2	3.8	290.1	134.3	569.1
46	1335	10	2	-99.0	-99.0	297.4	480.5
47	1400	10	2	7.1	287.9	424.8	536.6
48	1415	10	3	4.2	288.5	565.7	629.2
49	1430	10	3	2.6	288.3	317.5	466.2
56	1505	20	3	-99.0	-99.0	300.1	502.8

10-18-88

LC	TIME	TP	DT	Ubar	Tbar	BL1	BL2
18	1050	35	2	2.7	287.9	98.4	339.7
21	1115	15	2	4.7	289.4	314.3	375.2
23	1135	10	2	4.7	289.5	228.5	397.1
72	1150	10	2	5.1	292.7	-99.0	-99.0
12	1225	10	2	2.5	295.6	264.0	287.7
11	1250	20	2	3.6	291.2	162.3	226.3
10	1330	15	2	1.7	289.6	269.8	499.2
9	1405	35	2	5.1	293.7	260.6	401.2
7	1435	10	2	3.8	293.8	381.0	437.0
8	1450	10	2	2.4	290.4	274.4	366.2
64	1515	15	2	2.5	290.8	330.4	478.1
1	1545	15	2	1.9	292.0	281.0	352.3
5	1605	10	2	2.5	292.1	386.0	405.5
6	1620	10	2	1.4	292.2	206.2	243.5
17	1640	10	2	3.4	291.4	356.3	417.5
21	1655	10	2	4.2	290.8	131.5	273.7
24	1710	10	2	5.5	290.8	289.6	-99.0
25	1730	15	2	5.5	290.7	244.9	296.4

10-19-88

LC	TIME	TP	DT	Ubar	Tbar	BL1	BL2
18	930	50	1	1.1	-99.0	72.4	509.3
85	955	5	1	-99.0	-99.0	-99.0	-99.0
85	1000	5	2	-99.0	-99.0	172.6	376.2
67	1025	10	2	1.6	287.7	241.2	333.6
69	1050	10	2	2.6	288.0	416.5	692.5
97	1115	10	2	1.1	287.4	96.1	-99.0
98	1140	15	2	-99.0	-99.0	222.5	527.2
86	1200	15	2	1.5	289.1	425.3	614.8
87	1220	10	2	-99.0	-99.0	160.7	567.6
88	1255	20	2	-99.0	-99.0	257.0	646.1
89	1327	10	2	3.2	289.6	621.1	826.9
90	1347	10	2	-99.0	-99.0	238.6	494.8
91	1410	15	2	1.1	288.6	407.5	706.9
12	1450	30	2	2.5	291.3	317.6	598.3
92	1525	20	2	3.2	288.4	100.3	233.4
16	1550	15	2	3.5	289.3	306.5	470.4
30	1725	80	2	3.5	287.8	216.0	447.0

10-20-88

LC	TIME	TP	DT	Ubar	Tbar	BL1	BL2
18	910	25	1	1.4	286.4	77.7	739.7
21	930	10	1	-99.0	-99.0	67.7	-99.0
24	1000	20	1	-99.0	-99.0	117.9	245.7
27	1025	20	1	-99.0	-99.0	98.8	135.3
93	1055	15	1	-99.0	-99.0	87.5	158.6
93	1155	25	2	1.7	287.5	127.6	165.6
94	1220	10	2	2.2	287.8	262.2	319.9
37	1235	10	2	2.0	288.9	258.4	349.8
29	1305	20	2	-99.0	-99.0	261.1	606.0
1	1445	20	2	1.9	287.5	144.7	417.2
5	1505	10	2	-99.0	-99.0	132.0	274.7
17	1525	10	2	2.5	287.6	161.7	232.6
20	1545	10	2	2.3	287.8	126.8	269.4
54	1600	10	2	1.7	287.1	113.0	431.7
44	1615	10	2	1.5	285.9	141.8	319.7
95	1645	15	2	2.5	287.2	97.7	651.9
47	1700	5	2	1.8	286.8	70.8	549.8
47	1705	5	3	-99.0	-99.0	76.0	-99.0
48	1720	10	3	-99.0	-99.0	106.7	324.9
49	1735	10	3	1.4	286.7	75.0	641.7
46	1800	10	3	-99.0	-99.0	59.8	307.9

10-21-88

LC	TIME	TP	DT	Ubar	Tbar	BL1	BL2
18	840	35	1	1.1	287.2	86.8	553.7
21	855	10	1	-99.0	-99.0	60.6	259.3
24	920	10	1	-99.0	-99.0	132.0	448.0
27	940	10	1	-99.0	-99.0	126.9	300.0
93	1010	10	1	-99.0	-99.0	80.7	628.6
39	1035	15	1	-99.0	-99.0	137.3	425.3
40	1055	10	1	-99.0	-99.0	60.6	601.8
40	1100	5	2	-99.0	-99.0	103.3	601.8
41	1130	20	2	1.8	287.5	108.3	179.7
43	1220	45	2	2.4	289.1	103.1	184.5
41	1245	15	2	3.4	289.0	289.7	431.8
42	1305	10	2	2.8	-99.0	217.0	579.8
38	1325	10	2	-99.0	-99.0	339.1	553.3
34	1420	15	2	2.7	292.6	394.4	634.6
35	1510	15	2	1.8	288.7	169.1	498.6
36	1535	10	2	-99.0	-99.0	239.2	367.7
25	1605	15	2	5.4	288.2	266.3	504.1
20	1625	15	2	3.3	288.7	216.7	514.9

The following table lists some surface layer variables which correspond with the records in the last table. Again, these are averages for the visit to each location. Ustar is the surface friction velocity (m/s). Znot is the surface roughness length (m). H is heat flux (deg C * m/s). Tstar

is the surface layer temperature scale (deg C). L is the Monin-Obukhov length (m). L = 100 is missing data.

5-18-88

LC	ustar	znot	H	Tstar	L
1	0.661	0.1673	0.128	-0.194	-163.9
5	0.245	0.0007	0.214	-0.871	-5.1
6	0.258	0.0085	0.156	-0.603	-8.1
17	0.477	0.1255	0.144	-0.302	-55.4
20	0.384	0.0170	0.130	-0.340	-31.9
44	0.616	0.0057	0.181	-0.293	-94.6
45	0.624	0.0214	0.433	-0.694	-41.0
44	0.724	0.1134	0.384	-0.530	-72.4
20	0.623	0.0980	0.167	-0.268	-106.9
46	0.625	0.2098	0.233	-0.373	-76.8
47	-99.000	-99.0000	0.016	-99.000	100.0
48	-99.000	-99.0000	0.142	-99.000	100.0
49	-99.000	-99.0000	0.121	-99.000	100.0

5-19-88

LC	ustar	znot	H	Tstar	L
18	0.137	0.0280	0.071	-0.515	-2.7
51	0.279	0.0301	0.150	-0.538	-10.7
24	0.301	0.0313	0.159	-0.528	-12.9
27	-99.000	-99.0000	0.079	-99.000	100.0
27	-99.000	-99.0000	0.101	-99.000	100.0
52	-99.000	-99.0000	0.099	-99.000	100.0
53	-99.000	-99.0000	0.058	-99.000	100.0
26	0.347	0.0026	0.369	-1.065	-8.6
24	0.308	0.0017	0.253	-0.820	-8.8
21	0.241	0.0580	0.100	-0.415	-10.6
18	-99.000	-99.0000	0.294	-99.000	100.0
54	0.379	0.1759	0.147	-0.389	-27.7
44	0.245	0.0052	0.122	-0.500	-9.1
46	0.323	0.2523	0.090	-0.278	-27.8
47	0.078	0.0002	0.183	-2.339	-0.2
55	0.828	0.3866	0.202	-0.244	-211.5
56	0.797	0.1452	0.167	-0.209	-231.0
57	0.605	-99.0000	-99.000	-99.000	100.0
96	-99.000	-99.0000	0.220	-99.000	100.0

5-20-88

LC	ustar	znot	H	Tstar	L
18	-99.000	-99.0000	0.186	-99.000	100.0
47	0.229	0.1366	0.147	-0.643	-6.0
58	0.219	0.0992	0.231	-1.057	-3.3
46	0.211	0.0824	0.182	-0.862	-3.8
54	0.374	0.1574	0.178	-0.476	-21.7
59	0.287	0.1254	0.190	-0.660	-9.3
21	0.291	0.0102	0.131	-0.452	-13.8
60	0.131	0.0000	0.106	-0.813	-1.6

61	0.317	0.0020	0.110	-0.346	-21.5
24	0.431	0.0130	0.127	-0.294	-46.7
26	-99.000	-99.0000	0.136	-99.000	100.0
62	-99.000	-99.0000	0.137	-99.000	100.0
18	0.218	0.0197	0.197	-0.901	-3.9
47	-99.000	-99.0000	-99.000	-99.000	100.0
63	-99.000	-99.0000	0.501	-99.000	100.0
54	0.326	0.0126	0.269	-0.825	-9.6
59	0.215	0.0055	0.212	-0.989	-3.5
21	-99.000	-99.0000	0.118	-99.000	100.0
24	-99.000	-99.0000	0.109	-99.000	100.0

7-26-88

LC	ustar	znot	H	Tstar	L
18	0.991	1.9708	0.041	-0.042	-1725.1
21	0.183	0.0015	0.101	-0.551	-4.5
23	-99.000	-99.0000	-99.000	-99.000	100.0
66	-99.000	-99.0000	0.234	-99.000	100.0
67	-99.000	-99.0000	0.226	-99.000	100.0
68	-99.000	-99.0000	0.389	-99.000	100.0
1	0.532	0.3207	0.313	-0.588	-35.7
5	-99.000	-99.0000	0.359	-99.000	100.0
17	-99.000	-99.0000	0.310	-99.000	100.0
20	0.377	-99.0000	-99.000	-99.000	100.0
54	0.301	-99.0000	-99.000	-99.000	100.0
44	-99.000	-99.0000	-99.000	-99.000	100.0
18	0.391	0.2478	0.010	-0.025	-457.6
23	0.373	-99.0000	-99.000	-99.000	100.0
67	-99.000	-99.0000	0.201	-99.000	100.0
69	-99.000	-99.0000	0.154	-99.000	100.0

7-27-88

LC	ustar	znot	H	Tstar	L
18	0.168	-99.0000	-99.000	-99.000	100.0
51	0.275	-99.0000	-99.000	-99.000	100.0
21	-99.000	-99.0000	-99.000	-99.000	100.0
70	0.148	0.0284	0.025	-0.167	-9.6
23	0.201	0.1146	0.037	-0.183	-16.3
71	0.146	-99.0000	-99.000	-99.000	100.0
72	0.104	-99.0000	-99.000	-99.000	100.0
65	-99.000	-99.0000	-99.000	-99.000	100.0
65	0.294	0.0345	0.234	-0.795	-8.1
30	0.227	0.0034	0.339	-1.490	-2.6
73	-99.000	-99.0000	0.307	-99.000	100.0
68	-99.000	-99.0000	0.210	-99.000	100.0
33	0.306	0.0237	0.281	-0.919	-7.4
69	0.581	0.0567	0.518	-0.891	-27.8
74	0.331	0.0258	0.367	-1.109	-7.2
75	0.293	0.0101	0.398	-1.361	-4.7
76	0.340	0.0360	0.328	-0.964	-8.9
77	-99.000	-99.0000	0.390	-0.981	-13.3
5	0.298	0.0430	0.178	-0.598	-11.1

6	0.372	0.0401	0.281	-0.756	-13.6
17	0.413	0.0496	0.247	-0.598	-21.0
78	0.268	0.0046	0.147	-0.548	-9.8
20	0.339	0.0319	0.099	-0.293	-29.0
54	0.304	0.0927	0.064	-0.210	-32.5
44	0.173	0.0019	0.050	-0.289	-7.6
45	0.035	0.0000	0.072	-2.048	-0.0
54	0.266	0.1963	0.033	-0.123	-42.3

7-28-88

LC	ustar	znot	H	Tstar	L
18	0.174	0.0688	0.023	-0.133	-16.6
24	0.189	0.0896	0.067	-0.358	-7.3
26	-99.000	-99.0000	-99.000	-99.000	100.0
27	0.330	0.1989	0.240	-0.727	-11.1
28	-99.000	-99.0000	0.194	-99.000	100.0
30	-99.000	-99.0000	0.167	-99.000	100.0
21	0.156	0.0000	0.204	-1.306	-1.4
20	0.365	0.0778	0.140	-0.384	-25.7
18	-99.000	-99.0000	-99.000	-99.000	100.0
79	0.300	0.0883	0.201	-0.670	-9.9
3	0.344	0.0866	0.082	-0.239	-36.7
80	0.280	0.0307	0.045	-0.161	-36.1
81	-99.000	-99.0000	-99.000	-99.000	100.0
82	-99.000	-99.0000	-99.000	-99.000	100.0

7-29-88

LC	ustar	znot	H	Tstar	L
18	0.168	-99.0000	-0.008	-99.000	100.0
21	0.306	0.6085	0.022	-0.072	-94.4
23	0.118	-99.0000	-99.000	-99.000	100.0
28	-99.000	-99.0000	-99.000	-99.000	100.0
67	0.098	-99.0000	-99.000	-99.000	100.0
83	0.536	-99.0000	-99.000	-99.000	100.0
68	0.224	0.1154	0.142	-0.632	-5.9
32	0.289	0.1508	0.276	-0.956	-6.4
33	0.402	0.2922	0.343	-0.853	-14.0
84	0.387	0.1767	0.173	-0.448	-25.1
25	0.247	0.0173	0.192	-0.777	-5.9
21	0.409	0.0427	0.333	-0.815	-15.1
18	0.380	0.0546	0.161	-0.424	-25.2
46	-99.000	-99.0000	1.390	-99.000	100.0
47	0.367	0.0016	0.061	-0.167	-59.3
48	0.482	0.0986	0.262	-0.544	-31.5
49	0.401	0.2213	0.236	-0.589	-20.1
56	-99.000	-99.0000	-99.000	-99.000	100.0

10-18-88

LC	ustar	znot	H	Tstar	L
18	0.300	0.0772	0.104	-0.346	-19.2
21	0.362	0.0160	0.169	-0.467	-20.7

23	0.343	0.0117	0.155	-0.451	-19.3
72	0.317	0.0043	0.153	-0.484	-15.5
12	0.473	0.4413	0.194	-0.410	-41.2
11	0.399	0.0904	0.172	-0.432	-27.3
10	0.477	0.7604	0.285	-0.597	-28.2
9	0.240	0.0004	0.163	-0.678	-6.4
7	0.555	0.2433	0.201	-0.362	-63.6
8	0.327	0.1573	0.123	-0.376	-21.1
64	0.354	0.1494	0.233	-0.657	-14.1
1	0.234	0.0654	0.173	-0.741	-5.5
5	0.277	0.0681	0.117	-0.423	-13.5
6	0.340	0.5536	0.147	-0.432	-20.0
17	0.378	0.0868	0.127	-0.336	-31.6
21	0.287	0.0092	0.062	-0.216	-28.3
24	0.346	0.0059	0.087	-0.252	-35.4
25	0.275	0.0010	0.053	-0.193	-29.2

10-19-88

LC	ustar	znot	H	Tstar	L
18	0.133	-99.0000	-99.000	-99.000	100.0
85	0.089	-99.0000	-99.000	-99.000	100.0
85	-99.000	-99.0000	-99.000	-99.000	100.0
67	0.068	0.0000	0.030	-0.436	-0.8
69	0.277	0.0711	0.065	-0.236	-23.8
97	0.044	0.0000	0.037	-0.856	-0.2
98	-99.000	-99.0000	-99.000	-99.000	100.0
86	0.246	0.1542	0.171	-0.693	-6.4
87	-99.000	-99.0000	0.017	-99.000	100.0
88	-99.000	-99.0000	0.080	-99.000	100.0
89	0.298	0.0409	0.078	-0.261	-25.2
90	0.342	-99.0000	-99.000	-99.000	100.0
91	0.475	1.1859	0.323	-0.681	-24.3
12	0.440	0.3846	0.140	-0.318	-45.3
92	0.309	0.0500	0.077	-0.249	-28.1
16	0.376	0.0811	0.129	-0.343	-30.5
30	0.354	0.0648	0.091	-0.257	-35.9

10-20-88

LC	ustar	znot	H	Tstar	L
18	0.137	0.0407	0.012	-0.089	-15.5
21	-99.000	-99.0000	-99.000	-99.000	100.0
24	0.104	-99.0000	-99.000	-99.000	100.0
27	0.109	-99.0000	-99.000	-99.000	100.0
93	0.073	-99.0000	-99.000	-99.000	100.0
93	0.217	0.1078	0.068	-0.313	-11.1
94	0.280	0.1068	0.112	-0.399	-14.4
37	0.202	0.0468	0.042	-0.210	-14.3
29	-99.000	-99.0000	-99.000	-99.000	100.0
1	0.194	0.0430	0.048	-0.250	-11.0
5	-99.000	-99.0000	-99.000	-99.000	100.0
17	0.326	0.1510	0.074	-0.228	-34.3
20	0.322	-99.0000	-0.011	-99.000	100.0

54	0.180	0.0634	0.031	-0.171	-14.0
44	0.214	0.1748	0.036	-0.167	-20.1
95	0.207	0.0205	0.041	-0.199	-15.7
47	0.154	0.0246	0.016	-0.103	-16.9
47	-99.000	-99.0000	-99.000	-99.000	100.0
48	0.204	-99.0000	-99.000	-99.000	100.0
49	0.141	0.0482	0.019	-0.133	-11.0
46	-99.000	-99.0000	-99.000	-99.000	100.0

10-21-88

LC	ustar	znot	H	Tstar	L
18	0.196	0.3848	0.013	-0.064	-44.2
21	0.093	-99.0000	-99.000	-99.000	100.0
24	-99.000	-99.0000	-99.000	-99.000	100.0
27	0.065	-99.0000	-99.000	-99.000	100.0
93	0.169	-99.0000	-99.000	-99.000	100.0
39	0.152	-99.0000	-99.000	-99.000	100.0
40	-99.000	-99.0000	-99.000	-99.000	100.0
40	0.016	-99.0000	-99.000	-99.000	100.0
41	0.178	0.0365	0.043	-0.242	-9.6
43	0.414	0.4194	0.044	-0.106	-119.1
41	0.242	0.0087	0.104	-0.431	-10.0
42	-99.000	-99.0000	0.063	-99.000	100.0
38	-99.000	-99.0000	0.231	-99.000	100.0
34	0.338	0.1076	0.169	-0.499	-17.1
35	0.162	0.0187	0.056	-0.344	-5.6
36	-99.000	-99.0000	0.089	-99.000	100.0
25	0.086	0.0000	0.045	-0.525	-1.0
20	0.282	0.0336	0.040	-0.141	-41.4

The final table in this section lists some boundary layer average measures of the wind. C is the clocking variable, measuring the degree of rotation, and S is the speed up variable, measuring the degree of speed shear. See the VBLS Final Report - Results for more information. SIGV is the standard deviation of the lateral velocity component. SIGW is the standard deviation of the vertical velocity component. SPD is mean wind speed (m/s) and DIR is mean wind direction. All quantities have been averaged from .12_i to .82_i, or to the maximum altitude observed by the SODAR if that altitude was less than .82_i

5-18-88

LC	C	S	SIGV	SIGW	SPD(BL)	DIR(BL)
1	0.058	-0.142	0.23	0.56	13.4	320.0
5	0.053	-0.122	0.37	0.50	14.6	344.0
6	0.022	0.072	0.66	0.64	13.8	334.3
17	0.002	-0.044	0.81	0.49	13.4	336.7
20	0.023	0.054	0.48	0.58	12.8	302.5

44	0.072	0.177	0.53	0.64	13.5	331.3
45	0.020	0.001	0.44	0.49	12.7	325.1
44	-0.012	-0.041	0.47	0.59	14.4	314.7
20	0.177	2.346	0.00	-99.00	-99.0	-99.0
46	0.015	-0.193	0.82	1.03	9.6	317.8
47	-99.000	-99.000	0.00	-99.00	12.5	353.4
48	-99.000	-99.000	0.60	0.43	9.8	17.7
49	-0.052	-0.102	0.87	0.61	9.0	3.4

5-19-88

LC	C	S	SIGV	SIGW	SPD(BL)	DIR(BL)
18	-99.000	-99.000	0.73	0.20	1.7	291.5
51	-0.054	-0.191	0.98	0.22	4.1	306.2
24	0.067	-0.359	0.87	0.30	3.7	309.7
27	-99.000	-99.000	1.00	0.17	1.4	139.8
27	-99.000	-99.000	1.70	0.24	2.5	280.6
52	0.031	0.235	1.00	0.31	3.6	316.2
53	0.158	0.125	0.44	0.37	5.2	314.2
26	-0.053	0.066	0.43	0.37	8.8	285.2
24	0.012	-0.015	0.36	0.34	8.7	276.1
21	-0.007	0.051	0.30	0.32	8.8	291.6
18	0.022	0.109	0.31	0.23	10.1	330.5
54	0.031	0.036	0.99	0.27	4.0	280.6
44	-0.136	-0.004	0.80	0.24	5.5	316.6
46	0.004	0.088	0.25	0.21	8.3	300.4
47	-0.115	-0.055	1.08	0.39	7.0	0.3
55	-0.052	-0.158	0.20	0.30	19.1	333.5
56	-0.019	-0.087	0.23	0.55	16.8	335.2
57	-99.000	-99.000	0.15	0.29	13.4	299.8
96	0.138	0.261	1.00	0.28	2.9	272.2

5-20-88

LC	C	S	SIGV	SIGW	SPD(BL)	DIR(BL)
18	-0.209	-0.400	0.39	0.18	3.1	214.9
47	-0.317	0.163	0.62	0.22	2.2	256.9
58	0.091	-0.077	0.75	0.30	3.1	246.3
46	0.188	-0.562	0.47	0.30	4.5	265.1
54	-0.212	-0.491	0.46	0.19	2.3	246.4
59	0.090	0.451	1.20	0.44	4.0	280.5
21	-0.054	-0.146	0.68	0.27	8.1	279.0
60	-0.021	-0.044	0.68	0.42	8.7	290.1
61	-0.056	-0.091	0.59	0.37	9.2	285.1
24	-0.050	-0.212	0.48	0.37	8.7	289.7
26	0.007	-0.173	0.48	0.45	8.5	295.6
62	0.060	-0.115	1.36	0.27	3.3	280.8
18	-0.257	-0.075	0.00	-99.00	-99.0	-99.0
47	-0.018	0.168	0.00	-99.00	-99.0	-99.0
63	-0.108	0.370	0.93	0.30	3.6	159.6
54	-0.129	0.327	0.32	0.20	6.5	245.8
59	-0.188	-1.228	1.32	0.31	5.3	265.6
21	-0.008	-0.347	1.09	0.47	6.4	290.4
24	0.116	-0.334	0.56	0.44	9.0	306.0

7-26-88

LC	C	S	SIGV	SIGW	SPD(BL)	DIR(BL)
18	0.022	0.480	0.00	-99.00	-99.0	-99.0
21	-0.024	-0.022	0.00	-99.00	-99.0	-99.0
23	-0.033	0.034	0.00	-99.00	-99.0	-99.0
66	-0.045	-0.091	0.51	0.25	5.6	246.2
67	-0.024	-0.415	0.79	0.26	4.5	272.4
68	-0.025	-0.199	0.74	0.28	3.6	263.8
1	0.007	0.014	0.51	0.29	7.1	264.6
5	-0.015	-0.209	1.03	0.32	4.9	301.4
17	0.017	-0.001	1.13	0.37	5.4	320.2
20	0.021	0.049	0.71	0.30	5.6	285.6
54	-0.006	0.054	0.67	0.17	5.4	303.0
44	0.002	-0.332	0.94	0.15	1.9	336.0
18	0.068	-0.342	0.53	0.21	3.9	322.3
23	0.032	-0.067	0.37	0.21	7.8	266.6
67	0.005	0.054	0.64	0.29	5.6	264.8
69	0.001	-0.005	0.68	0.30	6.0	305.6

7-27-88

LC	C	S	SIGV	SIGW	SPD(BL)	DIR(BL)
18	-99.000	-99.000	0.00	-99.00	-99.0	-99.0
51	0.006	0.035	0.00	-99.00	-99.0	-99.0
21	0.172	0.331	0.00	-99.00	-99.0	-99.0
70	0.391	-0.792	0.00	-99.00	-99.0	-99.0
23	0.053	-0.103	0.00	-99.00	-99.0	-99.0
71	0.237	0.009	0.00	-99.00	-99.0	-99.0
72	-0.003	-0.052	0.00	-99.00	-99.0	-99.0
65	0.098	-0.183	0.62	0.22	4.1	224.7
65	0.061	-0.065	0.61	0.17	5.7	257.1
30	-0.004	0.192	0.52	0.19	6.3	249.0
73	-0.009	-0.095	0.77	0.25	3.7	288.4
68	-0.016	0.076	0.71	0.33	4.5	270.0
33	-0.011	0.082	0.70	0.30	4.8	276.7
69	-0.091	-0.081	0.87	0.39	5.5	308.0
74	0.092	0.028	0.64	0.24	5.6	286.5
75	0.012	-0.196	1.03	0.28	5.3	287.5
76	-0.012	-0.120	0.91	0.31	5.3	281.6
77	-0.024	0.020	0.82	0.29	5.1	295.9
5	0.032	0.133	1.24	0.31	4.7	295.7
6	-0.030	-0.045	0.95	0.33	5.5	294.8
17	0.015	0.026	0.55	0.21	7.1	291.4
78	0.035	0.014	0.50	0.27	6.5	277.8
20	0.006	0.055	0.61	0.30	6.2	288.7
54	0.028	-0.008	0.66	0.15	4.3	296.3
44	0.033	-0.620	0.77	0.13	2.1	318.1
45	-0.101	0.135	0.84	0.13	1.9	32.9
51	0.052	-0.049	0.91	0.19	3.1	304.6

7-28-88

LC	C	S	SIGV	SIGW	SPD(BL)	DIR(BL)
18	-0.027	-0.596	0.00	-99.00	-99.0	-99.0
24	0.073	-0.023	0.00	-99.00	-99.0	-99.0
26	0.147	0.047	0.00	-99.00	-99.0	-99.0
27	0.057	0.009	0.24	0.31	3.1	284.8
28	-0.010	-0.001	0.63	0.29	4.7	285.1
30	0.028	0.039	0.47	0.25	6.5	256.7
21	-0.022	0.034	0.75	0.33	8.0	285.2
20	-0.000	-0.050	0.90	0.31	6.0	300.2
18	-99.000	-99.000	1.15	0.23	2.8	293.8
79	0.165	-0.557	1.04	0.24	3.3	297.4
3	0.013	0.096	0.75	0.26	6.3	312.7
80	-0.002	0.121	0.72	0.23	6.4	310.9
81	0.024	0.123	0.62	0.13	3.7	299.9
82	-0.114	0.491	0.74	0.21	4.4	309.7

7-29-88

LC	C	S	SIGV	SIGW	SPD(BL)	DIR(BL)
18	0.214	-0.201	0.00	-99.00	-99.0	-99.0
21	-0.115	0.877	0.00	-99.00	-99.0	-99.0
23	0.083	0.543	0.00	-99.00	-99.0	-99.0
28	-99.000	-99.000	0.00	-99.00	-99.0	-99.0
67	-0.105	1.115	0.00	-99.00	-99.0	-99.0
83	0.021	0.452	0.00	-99.00	-99.0	-99.0
68	0.082	-0.483	0.00	-99.00	-99.0	-99.0
32	0.060	-0.166	1.00	0.22	2.3	263.4
33	-0.125	0.191	1.24	0.25	2.7	284.9
84	0.051	-0.110	0.65	0.21	4.7	275.3
25	-0.094	-0.112	0.65	0.17	2.6	278.6
21	-0.391	-0.379	0.64	0.14	3.1	270.0
18	-99.000	-99.000	0.10	0.12	5.2	235.8
46	-0.273	-0.618	0.39	0.28	6.4	211.1
47	-0.309	0.207	0.34	0.28	8.6	196.9
48	-0.178	0.412	0.30	0.43	9.3	196.4
49	-0.267	-0.188	0.49	0.21	4.6	188.6
56	-0.395	-0.447	0.86	0.26	3.8	217.1

10-18-88

LC	C	S	SIGV	SIGW	SPD(BL)	DIR(BL)
18	-0.164	-0.805	0.40	0.28	2.2	287.7
21	-0.042	-0.004	0.30	0.44	5.1	276.7
23	0.127	-0.545	0.65	0.37	5.1	296.6
72	-99.000	-99.000	0.00	-99.00	3.1	263.4
12	0.125	-0.339	1.14	0.30	3.2	302.8
11	0.006	0.284	1.13	0.20	2.1	270.0
10	0.380	-1.094	0.64	0.24	2.3	238.8
9	-0.030	-0.207	0.58	0.36	5.6	287.9
7	-0.011	-0.547	0.77	0.14	1.2	189.0
8	-0.024	-0.210	0.35	0.24	5.3	288.3
64	0.010	-0.114	1.05	0.33	3.7	254.2
1	-0.046	-0.044	0.64	0.29	3.9	274.5
5	-0.156	0.080	0.90	0.23	1.8	240.2

6	-0.110	0.402	0.65	0.41	4.8	267.2
17	0.082	0.276	0.20	0.51	4.3	322.8
21	-99.000	-99.000	0.35	0.75	1.4	193.2
24	-0.068	0.062	0.39	0.33	7.0	280.6
25	-0.046	-0.214	0.72	0.23	6.1	291.0

10-19-88

LC	C	S	SIGV	SIGW	SPD(BL)	DIR(BL)
18	-99.000	-99.000	0.00	-99.00	-99.0	-99.0
85	-99.000	-99.000	0.00	-99.00	-99.0	-99.0
85	-99.000	-99.000	0.00	-99.00	-99.0	-99.0
67	-99.000	-99.000	0.00	-99.00	-99.0	-99.0
69	-99.000	-99.000	0.00	-99.00	-99.0	-99.0
97	-99.000	-99.000	0.00	-99.00	-99.0	-99.0
98	-0.052	0.068	0.00	-99.00	-99.0	-99.0
86	-0.072	-0.039	0.00	-99.00	-99.0	-99.0
87	-99.000	-99.000	1.22	-99.00	-99.0	-99.0
88	-0.049	0.342	1.61	0.28	2.7	255.6
89	0.001	-0.019	0.65	0.63	3.6	201.0
90	-99.000	-99.000	0.47	0.21	2.5	298.3
91	0.004	-0.037	0.97	0.25	3.6	347.4
12	0.040	-0.143	0.69	0.44	4.3	312.1
92	-99.000	-99.000	0.35	0.26	6.3	270.0
16	-99.000	-99.000	0.43	0.22	6.0	273.2
30	-0.008	-0.096	0.76	0.26	4.5	279.1

10-20-88

LC	C	S	SIGV	SIGW	SPD(BL)	DIR(BL)
18	-99.000	-99.000	0.00	-99.00	-99.0	-99.0
21	-99.000	-99.000	0.00	-99.00	-99.0	-99.0
24	-99.000	-99.000	0.00	-99.00	-99.0	-99.0
27	-99.000	-99.000	0.00	-99.00	-99.0	-99.0
93	-99.000	-99.000	0.00	-99.00	-99.0	-99.0
93	0.170	0.463	0.00	-99.00	-99.0	-99.0
94	0.088	0.649	0.00	-99.00	-99.0	-99.0
37	-0.083	0.586	0.00	-99.00	-99.0	-99.0
29	0.009	-0.544	0.00	-99.00	-99.0	-99.0
1	0.189	-0.068	0.00	-99.00	-99.0	-99.0
5	-0.011	0.763	0.00	-99.00	-99.0	-99.0
17	-99.000	-99.000	0.00	-99.00	-99.0	-99.0
20	0.002	0.346	0.00	-99.00	-99.0	-99.0
54	0.095	0.934	0.00	-99.00	-99.0	-99.0
44	-99.000	-99.000	0.00	-99.00	-99.0	-99.0
95	-99.000	-99.000	0.00	-99.00	-99.0	-99.0
47	-99.000	-99.000	0.00	-99.00	-99.0	-99.0
47	-99.000	-99.000	0.00	-99.00	-99.0	-99.0
48	-99.000	-99.000	0.00	-99.00	-99.0	-99.0
49	-99.000	-99.000	0.00	-99.00	-99.0	-99.0
46	-99.000	-99.000	0.00	-99.00	-99.0	-99.0

10-21-88

LC	C	S	SIGV	SIGW	SPD(BL)	DIR(BL)
18	-99.000	-99.000	0.00	-99.00	-99.0	-99.0
21	-99.000	-99.000	0.00	-99.00	-99.0	-99.0
24	-99.000	-99.000	0.00	-99.00	-99.0	-99.0
27	-99.000	-99.000	0.00	-99.00	-99.0	-99.0
93	-99.000	-99.000	0.00	-99.00	-99.0	-99.0
39	-0.101	0.326	0.00	-99.00	-99.0	-99.0
40	-99.000	-99.000	0.00	-99.00	-99.0	-99.0
40	-99.000	-99.000	0.00	-99.00	-99.0	-99.0
41	0.462	0.443	0.00	-99.00	-99.0	-99.0
43	0.284	0.598	0.00	-99.00	-99.0	-99.0
41	0.016	-0.097	0.00	-99.00	-99.0	-99.0
42	-0.025	0.231	0.89	0.39	5.1	273.9
38	-0.008	-0.145	0.90	0.46	4.1	232.3
34	0.031	-0.016	1.10	0.31	3.4	29.5
35	0.418	0.978	1.15	0.16	0.6	356.1
36	0.081	0.572	1.94	0.19	1.6	289.9
25	-0.073	0.136	1.14	0.47	4.4	268.5
20	0.023	-0.052	0.71	0.28	2.6	308.6

APPENDIX E. BASE AVERAGE WINDS

The following table lists the hourly vector averaged winds measured at the 12 ft level from the following towers: WT004, 005, 007, 008, 009, 014, 015, 017, 018, 019, 050, 051, 052, 054, 057, 058, 059, 060, 101, 102, 200, 300. Because of anomalous flow at WT014, 053, and 301, these towers were not included in the average. Speeds are in m/s. Standard deviations of the hourly values across the base is listed below the means. For all data, the first row is hours 1 through 12, and the second row is hours 13 through 23.

5-18-88

spd	6.2	6.0	5.5	5.6	6.1	6.3	6.1	6.8	6.3	6.8	7.1
7.2											
	7.3	7.2	7.8	7.6	7.7	7.8	7.0	5.2	4.0	2.9	1.8
1.5											
sig	2.15	1.88	2.07	2.50	2.27	2.59	2.76	3.07	2.77	2.43	2.31
2.09											
	2.37	1.94	2.21	2.41	2.56	2.65	2.70	2.50	2.53	2.56	2.64
2.81											
dir	339	337	339	341	335	334	337	338	338	331	329
326											
	325	322	323	322	323	326	329	328	330	339	355
1											

sig	14.1	16.0	18.8	21.3	18.1	17.7	18.6	17.4	16.5	19.8	19.6
17.0											
	15.9	16.4	15.0	18.5	18.3	19.1	21.1	27.6	35.0	48.1	61.3
69.2											

5-19-88

spd	2.1	2.3	2.9	2.9	2.4	2.0	0.7	0.5	0.1	1.2	1.8
5.0											
	5.2	3.0	3.1	3.4	3.6	3.1	2.7	2.0	1.6	1.6	2.0
1.5											

sig	2.62	2.58	2.83	2.83	2.28	2.00	1.48	1.27	0.69	0.57	0.68
1.44											
	1.61	0.94	0.94	0.83	1.48	1.56	1.69	1.68	2.02	1.47	1.28
1.40											

dir	352	351	356	350	350	338	6	48	328	275	281
315											
	314	289	305	309	317	316	316	328	347	1	337
348											

sig	53.4	41.7	43.1	57.5	54.1	51.7	82.8	72.6	85.8	52.0	35.5
20.1											
	18.6	21.4	28.6	17.7	21.2	23.0	29.2	41.1	65.0	44.8	27.9
47.1											

5-20-88

spd	1.3	1.6	1.4	1.4	1.5	1.0	0.9	1.0	2.9	3.6	4.9
2.4											
	2.4	2.4	2.9	3.2	2.7	2.5	1.8	1.4	1.2	1.8	1.3
2.5											

sig	1.37	1.61	1.19	0.85	0.87	0.78	0.61	0.52	1.06	1.93	1.09
0.95											
	0.78	0.83	0.96	0.97	0.90	0.70	0.80	0.93	0.98	1.34	1.04
2.33											

dir	13	1	43	51	9	90	133	149	358	348	312
284											
	285	284	297	301	297	303	320	338	3	353	44
337											

sig	57.9	48.8	45.8	39.4	39.1	51.6	61.6	50.9	15.7	26.9	13.5
34.2											
	37.1	37.4	15.4	13.8	20.4	14.6	24.6	46.3	46.7	39.9	42.4
39.2											

7-26-88

spd	1.7	2.1	2.1	1.9	1.4	1.0	0.8	1.2	1.1	1.3	2.1
2.7											

1.7 3.3 3.6 3.7 3.7 3.8 3.6 2.8 2.7 2.2 2.1 1.8

sig 1.75 1.87 1.65 1.37 1.20 0.88 0.85 0.83 0.77 0.67 1.09
1.04

1.16 1.29 1.41 1.46 1.49 1.72 1.51 1.45 1.03 0.92 1.17
1.09

dir 352 349 346 350 353 333 319 305 313 303 308
305

306 311 310 312 313 316 316 323 340 342 344
337

sig 54.6 40.2 32.2 42.2 56.0 60.5 59.0 44.6 51.8 49.2 39.9
25.3

20.6 20.0 22.3 18.8 19.3 25.6 24.0 21.9 28.7 28.4 32.3
29.8

7-27-88

spd 1.1 1.0 0.9 0.7 0.9 0.8 0.4 1.1 1.0 1.1 1.5
2.4

2.9 3.2 3.3 3.2 3.3 3.2 3.1 2.4 2.2 2.0-99.0
2.3

sig 0.60 0.56 0.42 0.51 0.55 0.51 0.33 0.53 0.54 0.51 0.44
0.61

0.81 0.90 0.87 0.93 1.04 1.38 1.44 1.26 1.04 0.86 0.00
1.52

dir 331 300 309 321 340 16 350 348 325 318 305
302

299 290 289 291 302 311 318 323 328 338 -99
331

sig 47.8 41.9 42.4 56.9 46.4 50.8 70.9 39.5 43.7 45.3 36.3
21.7

26.3 17.6 19.1 17.8 19.3 19.1 24.2 26.7 24.3 24.5 0.0
23.6

7-28-88

spd 2.0 1.6 1.5 0.8 0.8 1.1 1.4 1.3 1.1 1.7 1.5
2.0

2.5 3.1 3.5 3.4 3.5 3.5 3.4 3.1 3.0 2.5 2.3
2.2

sig 1.17 0.93 0.85 0.57 0.41 0.39 0.59 0.54 0.54 0.81 0.65
0.37

0.60 0.69 0.85 1.07 1.30 1.26 1.61 1.48 1.89 1.81 2.02
1.62

dir 331 329 328 313 270 311 352 357 328 313 312
292

	293	290	289	303	311	317	323	334	335	344	356
348											
sig	21.4	28.3	33.6	50.6	46.9	37.1	16.2	20.4	45.6	25.6	37.4
23.5											
	19.9	22.9	21.1	18.2	17.2	19.1	20.4	25.3	20.0	26.2	24.0
26.1											

7-29-88

spd	1.5	1.0	0.6	0.4	0.8	1.0	0.9	0.9	0.8	0.8-99.0
1.9										
	2.9	3.8	3.6	2.9	2.7	2.9	2.3	1.8	1.9	2.1 0.9
0.7										
sig	1.52	1.44	1.42	1.19	1.03	0.89	0.82	0.76	0.67	0.57 0.00
0.42										
	1.10	1.38	1.29	1.19	0.84	1.02	1.36	1.30	1.64	1.30 0.81
0.60										
dir	340	349	359	186	192	215	211	206	230	244 -99
278										
	259	248	260	283	291	294	301	301	335	331 330
304										
sig	39.8	67.0	73.7	63.4	51.2	44.3	52.3	61.8	59.6	60.6 0.0
38.1										
	38.0	34.7	35.2	35.9	26.4	23.0	29.1	33.1	40.0	36.1 55.1
52.5										

10-18-88

spd	0.6	1.3	1.7	1.6	1.4	1.0	1.1	1.2	1.0	1.3	2.5
3.8											
	4.3	4.9	2.2	1.9	2.2	2.3	2.2	2.2	2.1	1.6	0.7
0.9											
sig	0.85	0.63	0.81	0.67	0.89	0.78	0.56	0.75	0.86	0.91 0.94	
1.53											
	1.44	1.87	0.69	0.76	0.74	0.48	0.73	1.01	0.73	0.64 0.39	
0.44											
dir	1	64	96	97	114	119	110	114	132	346 320	
322											
	315	320	294	280	280	314	338	348	349	348 349	
291											
sig	68.7	46.5	31.2	35.0	40.5	50.2	38.9	40.5	58.2	51.4 32.7	
31.1											
	26.3	26.3	49.5	46.3	39.2	26.1	30.2	33.3	27.9	34.5 59.3	
53.4											

10-19-88

spd	1.5	1.9	2.0	2.6	2.7	3.2	2.1	1.1	0.5	1.0	3.0
4.1											
	4.6	4.9	4.5	3.1	2.3	2.0	2.3	2.3	1.9	2.1	1.7
1.0											

sig	0.54	1.17	0.88	1.54	1.67	1.86	1.42	0.85	0.42	0.91	1.64
1.54											
	2.04	2.23	2.02	1.13	0.96	1.08	1.44	1.50	1.65	1.58	1.24
0.65											

dir	315	330	335	343	344	340	353	3	353	339	330
324											
	326	324	317	314	319	322	331	330	341	347	358
19											

sig	34.2	33.2	29.9	25.6	24.0	22.2	29.3	54.8	75.5	54.4	34.5
30.9											
	26.5	25.9	26.3	27.0	34.7	33.2	23.4	32.7	34.2	30.9	34.6
50.7											

10-20-88

spd	0.8	0.8	0.6	0.8	0.9	1.1	1.1	0.6	0.7	0.3	0.6
1.9											
	2.3	2.7	2.2	1.9	1.8	1.7	1.4	1.3	0.8	0.4	0.2
0.5											

sig	0.90	0.59	0.57	0.42	0.74	0.61	0.58	0.30	0.65	0.80	0.53
0.86											
	0.95	1.07	1.09	0.47	0.57	0.52	0.67	0.73	0.56	0.32	0.45
0.35											

dir	302	305	344	6	56	47	90	104	80	130	283
296											
	289	287	282	294	299	304	341	6	355	353	90
131											

sig	57.7	49.6	65.3	53.6	52.6	39.1	44.9	58.9	69.0	85.5	74.4
41.7											
	39.9	38.2	37.1	32.6	33.9	34.4	36.1	28.8	50.3	71.8	84.3
68.6											

10-21-88

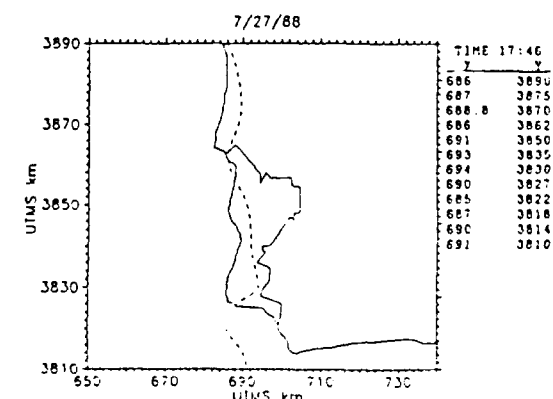
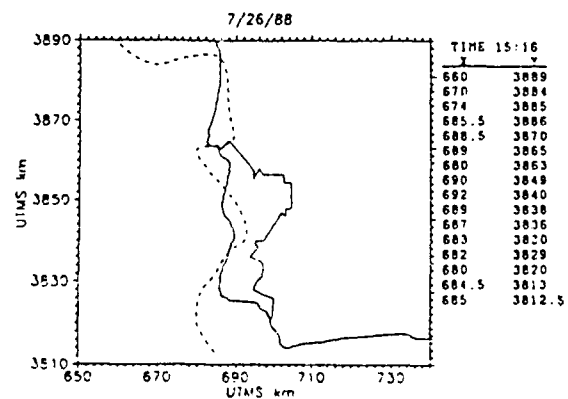
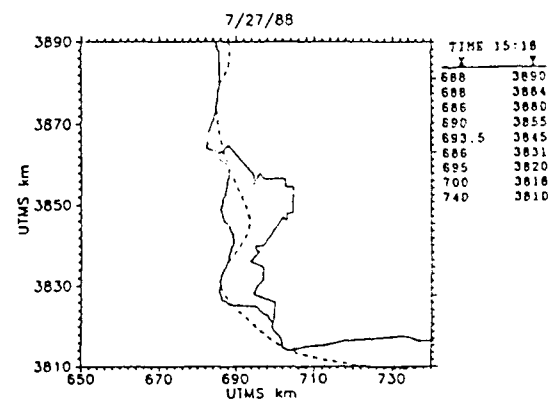
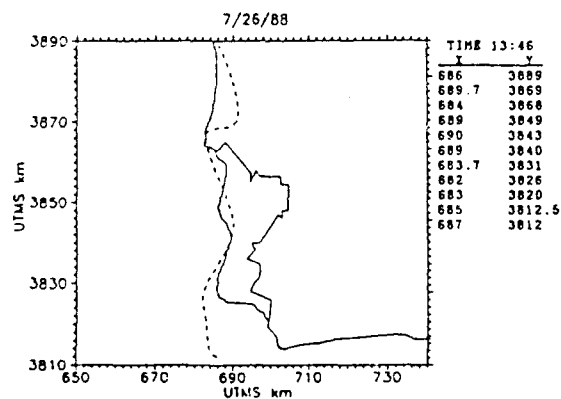
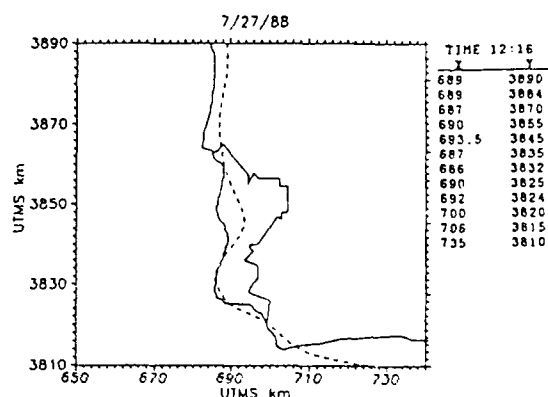
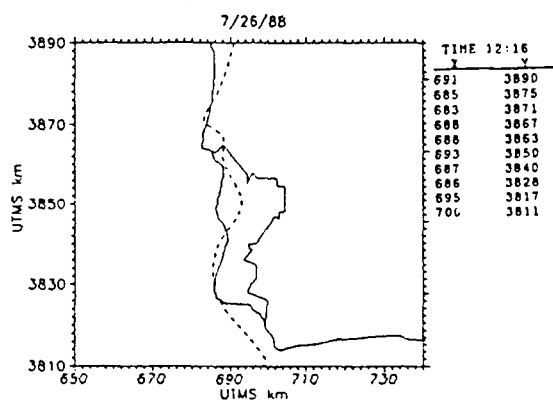
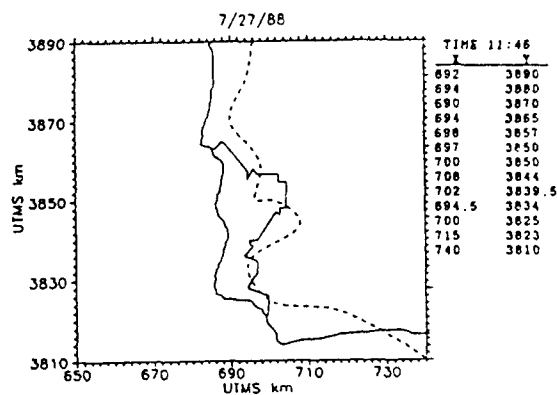
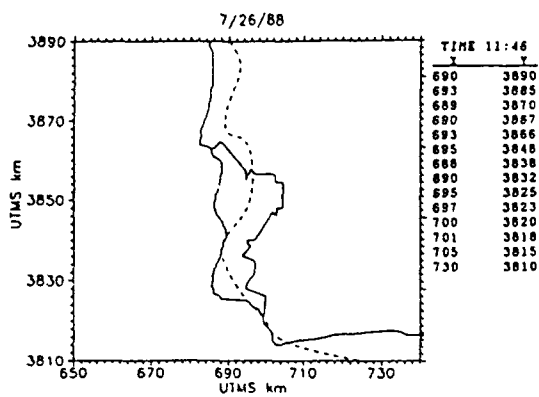
spd	0.8	0.7	1.0	0.6	0.7	0.8	0.3	0.1	0.6	0.7	0.7
1.5											
	2.4	2.4	2.4	2.0	1.9	1.4	0.8	1.3	1.3	1.8	0.6
0.2											

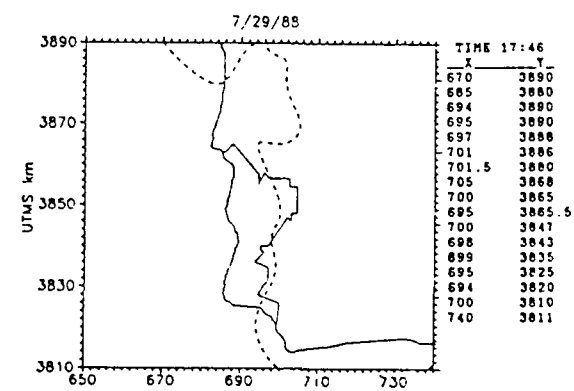
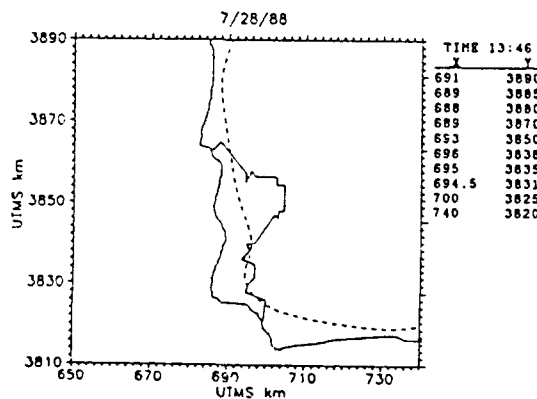
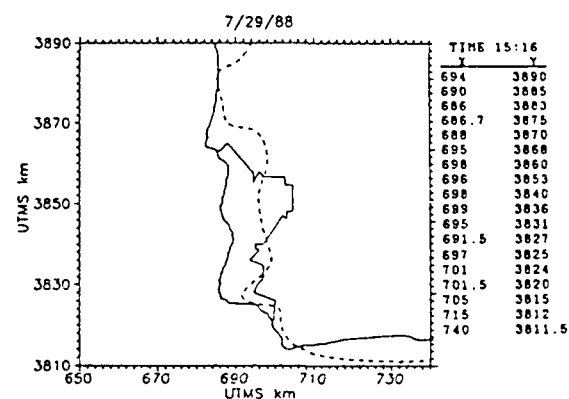
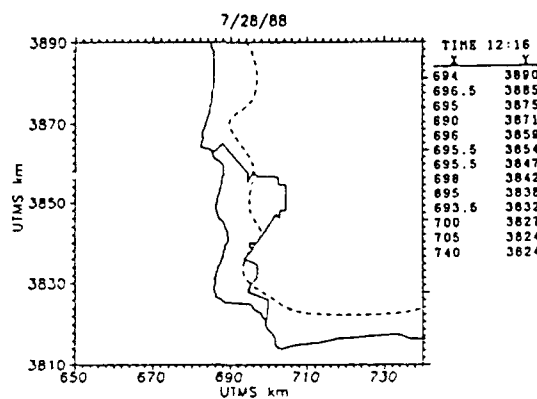
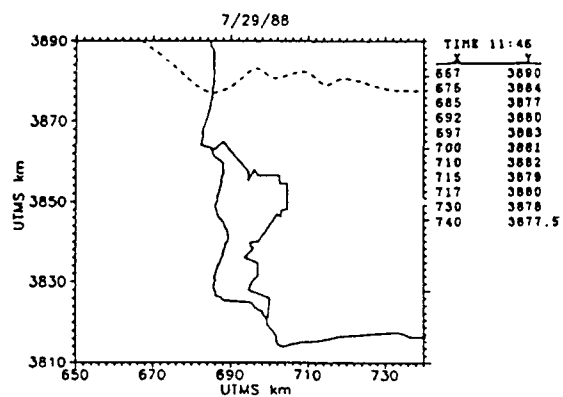
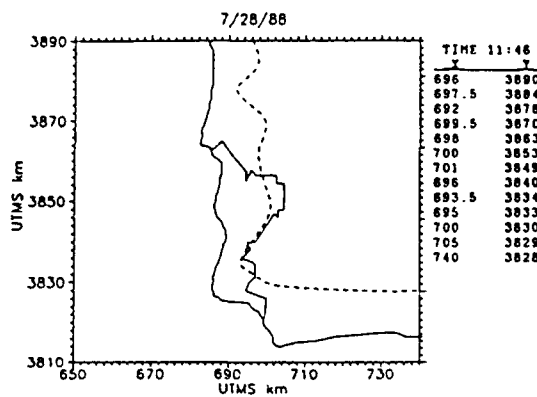
sig	0.36	0.50	0.77	0.39	0.45	0.65	0.80	0.83	0.48	0.44	0.48
0.58											
	0.78	1.02	1.10	0.90	0.91	1.17	1.58	1.55	1.58	1.44	1.25
0.98											

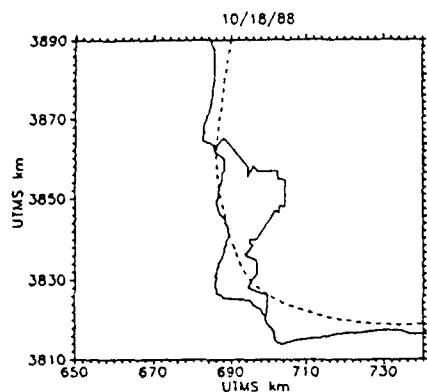
dir	112	110	76	24	35	152	270	209	358	36	337
313											
	310	307	282	288	301	317	23	47	55	62	46
333											
sig	46.5	55.5	48.2	60.7	52.6	58.7	71.6	81.8	60.2	57.9	62.0
36.5											
	26.0	38.3	45.1	38.0	31.2	44.6	72.3	46.7	44.4	38.8	73.7
85.3											

APPENDIX F. STRATUS EDGE BOUNDARIES

The approximate cloud edge for selected times is shown in the figures and tables below. X and Y coordinates for the cloud edge were obtained using the various landmarks in the VBG region in conjunction with actual cloud edge from GOES satellite photographs. A cubic spline, with tension factor two, was used to approximate the curvature of the cloud edge between the north-south data points. Only those days/times for which a cloud edge was present over the measurement domain are shown.

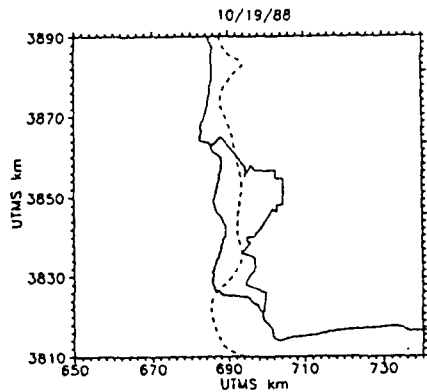






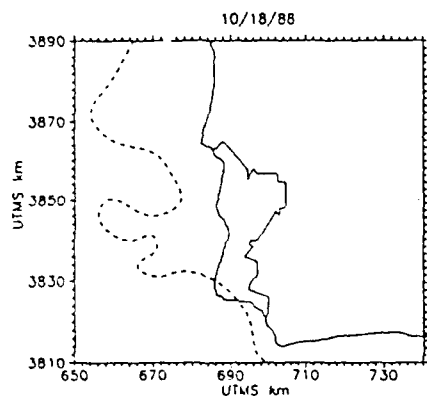
TIME 09:16

X	Y
690	3890
687	3870
686	3860
690	3840
695	3830
705	3824
715	3821
720	3820
740	3819



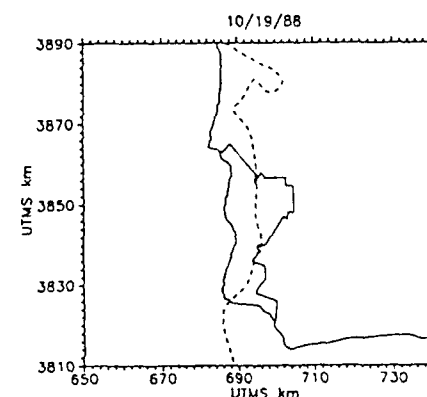
TIME 13:16

X	Y
687.5	3890
689.5	3886
694	3883
692	3881
688	3873
690.5	3867
692	3860
693.5	3854
692.5	3841
693.5	3836
693	3833
690	3829
686	3825
685.5	3821
689.5	3812
703	3810



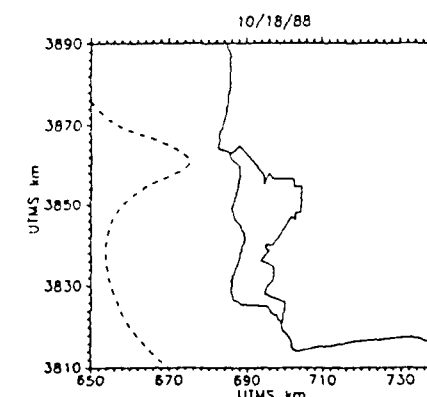
TIME 12:16

X	Y
665	3890
659	3880
654	3872
660	3865
670	3862
675.5	3855
677	3850
670	3846
658	3850
656	3846
665	3840
670	3841
671	3838
667	3835
666	3834
672	3831
675	3832
686	3830
695	3820
697	3812
700	3810



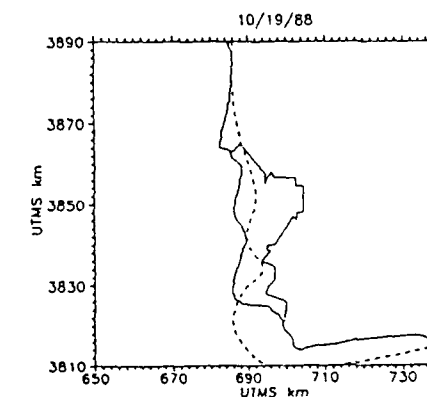
TIME 15:46

X	Y
687	3890
696	3885
700	3883
702	3880
698	3878
695	3881
691	3876
689	3873.5
692	3870
694	3865
695	3855
694.5	3848
695	3845
696	3840
695	3838
692	3830
686	3824
688	3812
689	3810



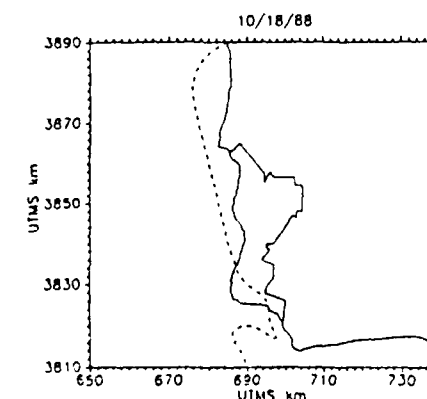
TIME 14:16

X	Y
650	3876
655	3871
670	3865
675	3861
665	3855
655	3845
654	3834
660	3820
670	3810



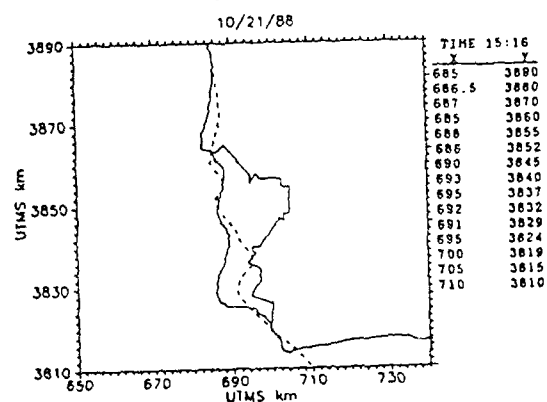
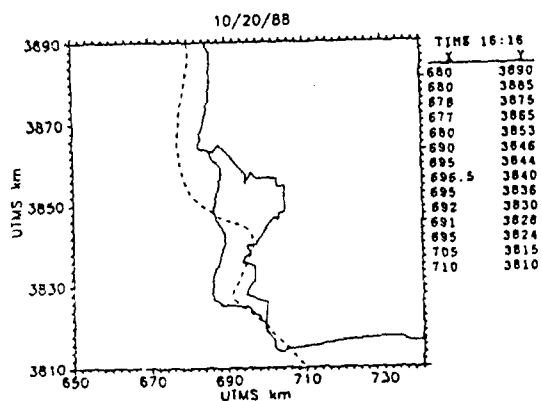
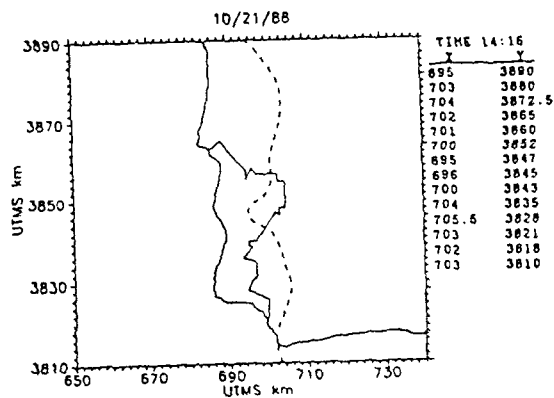
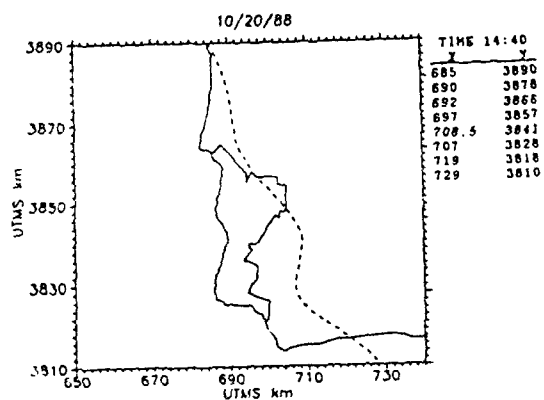
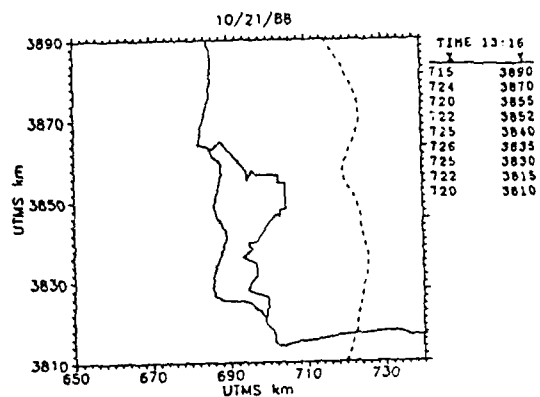
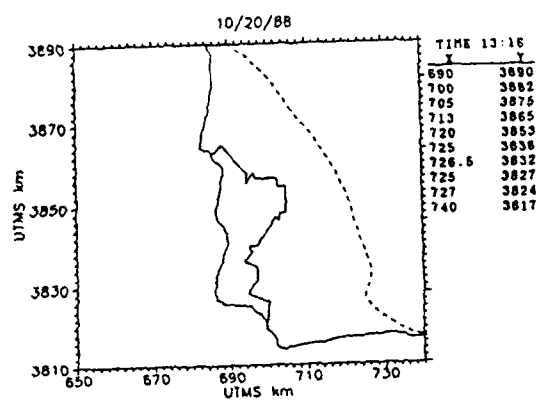
TIME 16:46

X	Y
686	3890
687	3870
690	3860
692	3850
690	3840
694	3834
690	3830
686	3820
695	3810
725	3812
740	3815



TIME 16:16

X	Y
685	3890
679	3886
676	3880
680	3860
685	3840
690	3830
695	3826
696	3821
697.5	3817
690	3820
686	3818
687.5	3815
690	3810



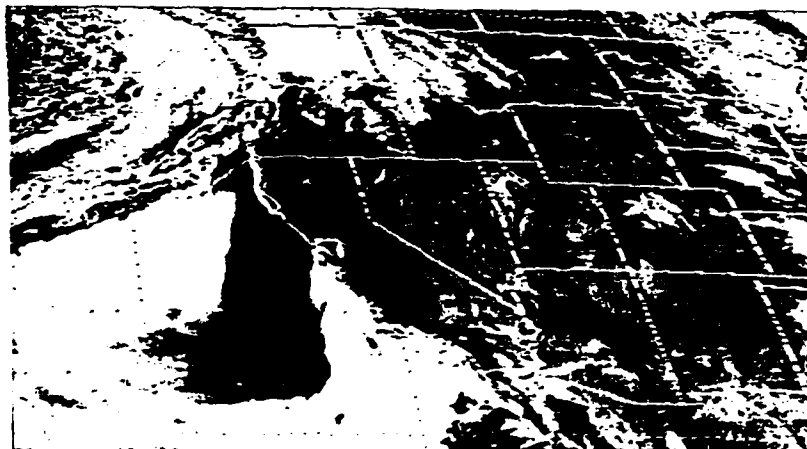
SAMPLE GOES VISUAL IMAGES



18 MAY 16:16Z



28 JULY 16:46Z



18 OCT 16:16Z

APPENDIX BIBLIGRAPHY

Grant, A.L.M., and R.D. Watkins, 1989: Errors in Turbulence Measurements with a Sonic Anemometer. *Boundary-Layer Meteor.*, **46**, 181-194.

Kaimal J.C., J.C. Wyngaard, Y. Izumi, and O.R. Cote, 1972: Spectral Characteristics of Surface-Layer Turbulence. *Quart. J. R. Met. Soc.*, **98**, 563-589.

Panofsky, H.A., and J.A. Dutton, 1984: *Atmospheric Turbulence*. New York, NY., John Wiley and Sons, Inc., pp. 209-210.

Schotanus, P., F.T.M. Nieuwstadt, H.A.R. De Bruin, 1983: Temperature Measurement with a Sonic Anemometer and its Application to Heat and Moisture Fluxes. *Boundary-Layer Meteor.*, **26**, 81-93.

Wyngaard, J.C., Y. Izumi, and S. A. Collins 1971: Behavior of the Refractive Index Structure Parameter Near the Ground. *J. Opt. Soc. Am.*, **61**, 1646-1650.

Wyngaard, J.C., 1973: On Surface-Layer Turbulence. Workshop on Micrometeorology. Ephrata, Pa., Science Press, pp 13-141.

DISTRIBUTION LIST

	No. copies
1. Defense Technical Information Center Cameron station Alexandria, VA 22314	2
2. Dudley Knox Library Naval Postgraduate School Monterey, CA 93943-5100	2
3. Director of Research (Code 012) Naval Postgraduate School Monterey, CA 93943-5100	1
4. Dr. Ray Kamada/061kd Naval Postgraduate School Monterey, CA 93943-5100	5
5. Dr. Bart Lundblad and Capt. Frank Smith Chemical Systems Directorate Space Launch Vehicle Operations Box 92957, Los Angeles, CA 90009-2957	5
6. Dr. Torben Mikkelsen Meteorology and Wind Energy Dept. RISO National Laboratory DK 4000 Roskilde, Denmark	2
7. Prof. Gordon Schacher Dean of Science and Engineering Naval Postgraduate School Monterey, CA 93943-5100	2
8. Dept. of Physics Naval Postgraduate School Monterey, CA 93943-5100	2
9. Capt. Mike Moss AFFTC/WE Tyndall Air Force Base, FL 32403-6001	1
10. Lt. Brad Larsen DET30, WSMC/WE Vandenberg AFB, CA 93437-5000	1
11. Col J. Hayes, Capt. Ken Carey, Mr. Steve Sambol, Mr. Glen Boire DET30, WSMC/WE Vandenberg AFB, CA 93437-5000	4
12. Mr. Darryl Dargitz WSMC/SE Vandenberg AFB, CA 93437-5000	1

DISTRIBUTION LIST (Cont.)

13. 1STRAT HOSP/SGB Attn: Lt. Col Keith Chandler Vandenberg, AFB, CA 93437-5000	1
14. Mr. Bill Boyd ESMC/SE Patrick AFB, FL 32925-5000	1
15. WSMC Attn: Col Smargie Vandenberg, AFB, CA 93437-5000	1
16. Lt. Dawn Stewart SD/WE and Maj Dan Berlinrut SD/SGX Los Angeles AFB, CA 90009-2960	2
17. 6595 ATG/TSLI Attn: Maj John Sigafoos Vandenberg, AFB, CA 93437-5000	1
18. AFFTC/WE Attn: Lt Col Myers Edwards AFB, CA 93523-5000	1
19. AFSTC/WE Attn: Lt Col Winston Crandall Kirkland AFB, NM 87117-6008	1
20. SD/WE Attn: Lt Col Paul Nipko Los Angeles AFB, CA 90009-2960	1
21. Wayne Bithell EG&G Box 5338 Vandenberg AFB, CA 93437	1
22. Dr. Ken Moe Box 92960 Worldway Postal Center Los Angeles, CA 90009-2960	1
TOTAL	39